Transition Metal Complexes with Fluorinated Ligand Systems

-

Investigation of the magnetic and (spectro-)electrochemical properties

Inaugural-Dissertation
to obtain the academic degree
Doctor rerum naturalium (Dr. rer. Nat.)

submitted to the Department of Biology, Chemistry and Pharmacy
of Freie Universität Berlin

by

Maite Maria Christa Nößler
from Berlin

Berlin, 2023

The doctoral studies presented herein were commenced in January 2019 at the Institute of Chemistry and Biochemistry of the Freie Universität Berlin under the supervision of Prof. Dr. Biprajit Sarkar. Intermitted by parental leave from June 2021 to March 2022. The work for this thesis was concluded in April 2023 at the Freie Universität Berlin.

1st Reviewer: Prof. Dr. Biprajit Sarkar, Universität Stuttgart
2nd Reviewer: Prof. Dr. Sebastian Hasenstab-Riedel, Freie Universität Berlin

Date of defense: 10.07.2023

“Per aspera ad astra”

Declaration

I hereby confirm that I have prepared this dissertation without the help of any impermissible sources. All citations are marked as such. The thesis has not been accepted in any previous doctorate degree procedure.

Maite Nößler
Berlin, April 2023

Parts of this dissertation have already been published as follows:

1. M. Nößler, D. Hunger, F. Reichert, M. Winkler, M. Reimann, J. Klein, S. Suhr, L. Suntrup, J. Beerhues, M. Kaupp, J. van Slageren, B. Sarkar, "Spin-state control of cobalt(II) and iron(II) complexes with click-derived tripodal ligands through mon-covalent and fluorine-specific interactions". *Dalton Trans.* **2021**, *50*, 18097–18106. DOI: 10.1039/D1DT03535E
2. M. Nößler, D. Hunger, N. I. Neuman, M. Reimann, F. Reichert, M. Winkler, J. Klein, T. Bens, L. Suntrup, S. Demeshko, J. Stubbe, M. Kaupp, J. van Slageren, B. Sarkar, "Fluorinated click-derived tripodal ligands drive spin crossover in both iron(II) and cobalt(II) complexes". *Dalton Trans.* **2022**, *51*, 10507–10517. DOI: 10.1039/D2DT01005D
3. F. Stein, M. Nößler, A. Singha Hazari, L. Böser, R. Walter, H. Liu, E. Klemm, B. Sarkar; "Ruthenium Complexes of Polyfluorocarbon Substituted Terpyridine and Mesoionic Carbene Ligands: An Interplay in CO_2 Reduction". *Chem. Eur. J.*, **2023**, 10.1002/chem.202300405 DOI: 10.1002/chem.202300405.
4. M. Nößler, R. Jäger, D. Hunger, M. Reimann, T. Bens, N. I. Neuman, A. Singha Hazari, M. Kaupp, J. van Slageren, B. Sarkar "Electrochemistry and Spin-Crossover Behavior of Fluorinated Terpyridine-Based Co(II) and Fe(II) Complexes", *Eur. J. Inorg. Chem.*, **2023**, 10.1002/ejic.202300091 DOI: 10.1002/ejic.202300091

Acknowledgements

First of all, I want to thank my supervisor Prof. Dr. Biprajit Sarkar for the opportunity to work on my thesis in his research group. I am especially grateful that I was able to complete this path in his research group from my bachelor's thesis to my doctorate, and that I was able to experience many wonderful moments, both in the lab and outside of it. I also thank him for the freedom he gave me that I sometimes needed as a mother.

I also want to thank Prof. Dr. Sebastian Hasenstab-Riedel for agreeing to be the second reviewer for this thesis, for giving me the opportunity to stay in Berlin over my thesis and welcoming me in his research group.

In this regard I thank Prof. Dr. Biprajit Sarkar, Prof. Dr. Sebastian Hasenstab-Riedel and Dr. Carsten Müller for the effort they put into making my pregnancy and parental leave possible during my doctorate and for supporting me in the best possible way to reconcile family and research.

I thank all former and present members of the Sarkar group from Berlin and Stuttgart for the nice years I have worked in this group during the last decade. Thank you for the time during corona and the sticking together as the last stand in Berlin. I thank you all for the laughs we had during the day, at barbecues, Pastenmittwoche and group trips.

A special thanks goes to the former and present members of the Riedel group, who welcomed me during the last years of my thesis and making my workdays fun. A special thanks goes to Marlon, Vossi, Paul, Jonas, Lili, Luise, Helen and Tyler. Thank you all for the big laughs, great music, Pastenmittwoche, cake and coffee breaks, Kaiserschmarrne and emotional moments we shared. Thank you for your support, the love and the family feeling.

I thank Sebastian Sobottka for the guidance during the start in the group, the introduction in electrochemistry and the fruitful discussions we had about research.

I also thank my students René Jäger and Lisa Böser, who contributed to this work. I thank Dr. Nicolás Neumann and Dr. Arijit Singha Hazari for help with the EPR measurements and Clemens Lücke for CV and UV/Vis-SEC measurements.

I also want to thank David Hunger from the group of Prof. Dr. Joris van Slageren for the successful cooperations.

I also thank Dr. Simon Steinhauer for the help on NMR spectroscopy and X-ray diffraction. Dr. Günther Thiele is thanked for the help on the measurement and solving of crystal structures. I also thank the members of the Core Facility BioSupraMol at Freie Universität Berlin for the various measurements.

Dr. Tyler Gully, Tobias Bens, Marlon Winter, Patrick Voßnacker, Dr. Sebastian Sobottka, Jonas R. Schmid and Dr. Merlin Kleoff are kindly acknowledged for proof reading parts of this thesis.

I also want to thank my family for the support throughout the years, especially my mother, who I can always rely on and talk to, and my father who took care of my daughters before they went to kindergarten and for all of his help with technical issues. Without your support I would never have been able to walk this path to the end.
My infinite gratitude goes to my husband Robin, who supported me through my studies and the thesis and who helped me with simulations. Thank you for your love, laughter and the last decade we spent together. Also, thank you for your patience and everything you have done for me.
Finally, I want to thank my two daughters Emilia and Alba, who bring as much joy into my life as possible. Even the darkest day becomes brighter when I come home to you.

Abstract

This thesis presents the synthesis metal complexes with a variety of fluorinated ligand systems, featuring tripodal, terpiridine and azobenzene ligands. The resulting compounds thereof show various characteristics and therefore were investigated in terms of their geometric and electronic structures by single crystal X-ray diffraction, cyclic voltammetry, superconducting quantum interference device (SQUID) magnetometry and/or (spectro-)electrochemical methods.

The first part of this thesis addresses new compounds of the form $[M(L)_2](BF_4)_2$ (M = cobalt(II), iron(II); L = fluorinated tripodal ligand) and the influence of fluorine specific interactions in the secondary coordination sphere on the spin state of the central metal ion. For this purpose, a combined study by single X-ray diffraction analysis and SQUID magnetometry measurements was performed to investigate the spin states of the metal centers. It could be shown, that for the ligand, which contains either a pentrafluoro-benzyl or a 4-fluorobenzyl substituents, an effect of the fluorine specific interactions was observed. The complexes bearing the pentafluorobenzyl substituents do not display the expected $\pi \cdots \pi$ interactions, but an edge-to-face interaction. However, this leads to a change of the spin state for the iron(II) complex, while the corresponding cobalt(II) complexes remain in the low spin state. For the other substituent a partial spin crossover (SCO) behavior was observed for one cobalt(II) complex, depending on the co-crystallizing solvent, while the iron(II) complex displays a complete SCO. These results were obtained by a combination of X-ray diffraction analysis, SQUID magnetometry, electron paramagnetic resonance (EPR) spectroscopy and theoretical calculations.

In the second part terpyridine ligands bearing different fluorinated backbones were implemented with cobalt(II) and iron(II) and the differences within the complexes were investigated primarily by SQUID magnetometry and EPR studies. The cobalt(II) complexes, where the tpy ligands bear a long fluorinated alkyl chain, show fluorine specific interactions that have an impact on the EPR spectra. Furthermore, ruthenium(II) complexes combining a mesoionic carbene and a terpyridine ligand were employed for electrocatalytic reduction of CO_2. The complexes show a high selectivity towards CO and a faradaic efficiency of 92%.

The final part deals with a series of platinum(II) donor-acceptor complexes bearing different azobenzene and bridging quinone ligands. The complexes exhibit strong electrochromic behavior and were studied towards the influence of different (perfluorinated) alkyl chains on the azobenzene ligands on the electrochemical behavior.

In the present thesis the impact of fluorine on different ligand systems and its influence on the physical and electrochemical properties of the resulting metal complexes are highlighted, which can be useful for estimating the properties of potential target compounds.

Kurzzusammenfassung

In dieser Arbeit wird die Synthese einer Vielzahl von fluorierten Ligandensystemen mit tripodalen, terpyridin und azobenzol Liganden vorgestellt. Die daraus resultierenden Verbindungen weisen verschiedene Eigenschaften auf und wurden daher hinsichtlich ihrer physikalischen und elektrochemischen Eigenschaften mittels Röntgenstrukturanalyse, SQUID-Magnetometrie und/oder (spektro-)elektrochemischer Methoden untersucht.

Der erste Teil dieser Arbeit befasst sich mit neuen Verbindungen der Form $[M(L)_2](BF_4)_2$ (M = Cobalt(II), Eisen(II); L = fluorierter tripodaler Ligand) und dem Einfluss von fluorspezifischen Wechselwirkungen in der sekundären Koordinationssphäre. Zu diesem Zweck wurde eine kombinierte Studie mittels Einkristall-Röntgenstrukturanalyse und SQUID-Magnetometriemessungen durchgeführt, um die Spinzustände der Metallzentren zu untersuchen.

Es konnte gezeigt werden, dass für den Liganden, der entweder eine Pentrafluorbenzyl- oder eine 4-Fluorbenzyl-Einheit enthält, ein Effekt der fluorspezifischen Wechselwirkungen beobachtet wurde. Die Komplexe mit den Pentafluorbenzyl-Substituenten zeigen nicht, wie erwartet, π···π-Wechselwirkungen, sondern eine Kante-zu-Fläche-Wechselwirkung. Dies führt zu einem Wechsel des Spinzustands für den Eisen(II)-Komplex, während die entsprechenden Cobalt(II)-Komplexe im low spin Spinzustand bleiben. Für den anderen Substituenten wurde für einen Cobalt(II)-Komplex ein teilweises Spin-Crossover-Verhalten (SCO) beobachtet, das vom ko-kristallisierenden Lösungsmittel abhängt, während der Eisen(II) Komplex ein vollständiges SCO zeigt. Diese Ergebnisse wurden durch eine Kombination aus Röntgenstrukturanalyse, SQUID-Magnetometrie, EPR-Spektroskopie und theoretischen Berechnungen erzielt.

Im zweiten Teil wurden terpyridin Liganden mit unterschiedlichen fluorierten Rückgraten mit Cobalt(II) und Eisen(II) umgesetzt und die Unterschiede innerhalb der Komplexe wurden vor allem durch SQUID-Magnetometrie und EPR-Studien hervorgehoben. Die Cobalt(II)-Komplexe, bei denen eine lange fluorierte Alkylkette am terpyridin Liganden vorhanden ist, zeigen fluorspezifische Wechselwirkungen, die sich auf die EPR-Spektren auswirken. Darüber hinaus wurden Ruthenium(II)-Komplexe, die ein mesoionisches Carben und einen terpyridin Liganden kombinieren, zur elektrokatalytischen Reduktion von CO_2 eingesetzt. Die Komplexe weisen eine hohe Selektivität gegenüber CO und einen faradayschen Wirkungsgrad von 92% auf.

Der letzte Teil befasst sich mit einer Reihe von Platin(II)-Donor-Akzeptor-Komplexen, die aus verschiedene azobenzol und verbrückende chinon Liganden bestehen. Die Komplexe

zeigen ein starkes elektrochromes Verhalten und wurden auf den Einfluss verschiedener (perfluorierter) Alkylketten an den azobenzol Liganden auf das elektrochemische Verhalten untersucht.

In der vorliegenden Arbeit werden die Auswirkungen von Fluor auf verschiedene Ligandensysteme und sein Einfluss auf die physikalischen und elektrochemischen Eigenschaften beleuchtet, was für die Einschätzung der Eigenschaften potenzieller Zielverbindungen hilfreich sein kann.

Contents

List of Abbreviations & Acronyms

abpy	2,2'-azobispyridine
acac	acetylacetonate
adc-R	azodicarbonyls
ATRP	atom transfer radical polymerization
bpy	2,2′-bipyridine
Cat	catecholate
CuAAC	copper(I)-catalyzed azide-alkyne cycloaddition
CV	cyclic voltammetry
dhbq	2,5-dihydroxy-1,4-benzoquinone
DSSC	dye-sensitized solar cells
EC′	one-electron, one substrate electrocatalytic reaction
EPR	electron praramagnetic resonance
HS	high-spin
IR	infrared
LS	low-spin
LFSE	ligand field stabilization energy
LLCT	ligand-to-ligand charge transfer
LC	liquid crystals
LIESST	light-induced excited-spin-state trapping
MIC	mesoionic carbene
MMA	methyl methacrylate
NCI	noncovalent interactions
NIR	near infrared
NMR	nuclear magnetic resonance
OTTLE cell	optically transparent thin layer electrochemical cell
OTf	trifluoromethanesulfonate
pap	2-phenylazopyridine
PFC	perfluorocarbon
ph	phenyl
phen	1,10-phenantroline
pimp	phenyliminiomethylpyridine
Q	*o*-benzoquinone
ROP	ring-opening polymerization

SCO	spin-crossover
SEC	spectroelectrochemistry
SS-NMR	solid-state nuclear magnetic resonance
SQ	semiquinonate
tbta	tris(benzyltriazolylmethyl)amine
(TD)DFT	time-dependent density functional theory
tmima	tris(2-(1-methylimidazolyl)methyl)amine
tpa	tris-(2-pyridylmethyl)amine
tpy	2,2':6',2''-terpyridine
tren	tris(2-aminoethyl)amine
TS	transition state
UV	ultra violet
VT	valence tautomerism
ZFS	zero-field splitting

1. Introduction

In nature, coordination compounds play an important role in living systems. They are present in the active sites of enzymes and act as highly efficient catalysts in biological transformations. Additionally, coordination compounds have found many applications, e.g. as alizarin dyes, already centuries before the term coordination chemistry was established.[1] Alfred Werner created the basis for the understanding of transition metal complexes formed by ligand substitution reactions, and is therefore known as the father of coordination chemistry.[2]

The properties of metal complexes result from an interplay of the properties of the central atom and the ligands. Since the choice of the central atom is limited by the periodic table and the design of organic ligands is almost unlimited, the latter are of great importance to design and synthesize complexes that exhibit specific properties. In order to tune these properties, it is important to understand and predict the interactions of the metal center and its surrounding ligands in the first and the second coordination sphere. In this regard a number of powerful tools have been developed to modify the ligand backbone of individual molecules, which leads to increasingly complex molecules.[3] In addition to fundamental studies, the investigation of particular complex properties led to the development of research areas such as bioinorganic chemistry or supramolecular chemistry.

In recent decades, fluorinated compounds have become of increasing interest in life science as they are used in many commodities in daily life, for example dental products, crop protection agents, or pharmaceuticals.[4] By the replacement of hydrogen atoms by fluorine the physical and chemical properties of compounds can be strongly altered due to their differences in electronegativity, bond strength and polarizability. This in turn leads to a great influence on inter- and intramolecular interactions.[4]

In this thesis the influence of fluorine on the ligand system regarding the electrochemical and magnetic properties of metal complexes will be studied. In this context the introduction focuses on the ligands presented in figure 1, which are known for a long time and various metal complexes thereof have been described in literature. Additionally, the fundamentals of spin-crossover and electrocatalysis will be introduced.

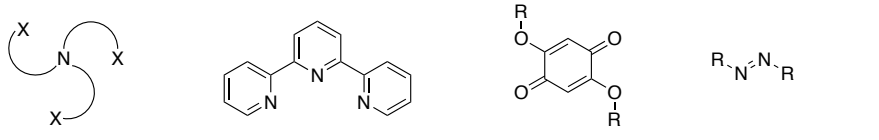

amine anchored tripodal ligands | 2,2′:6′,2″-terpyridines | substituted quinones | azo-group containing ligands

Figure 1: General structure of ligands used in this thesis.

1.1. Ligand Systems

1.1.1. Tripodal Ligands

Since the first report of the amine anchored tripodal ligand tris(2-aminoethyl)amine (tren) in 1896[5] the class of tripodal ligands gained interest in coordination chemistry. Tripodal ligands are tri- or tetradentate ligands consisting of a central donor atom with three coordinated arms, that contain at least one methylene group and a donor atom.[5] In 1967, Anderegg described another prominent example of these ligands, tris-(2-pyridylmethyl)amine (tpa).[6] Complexes containing these two ligands dominate the literature.[5] Since then, tripodal ligands were widely used in coordination chemistry.[6b] Tpa can be coordinated to a variety of transition metals[6b] including metals from group 1 to 13 of the periodic table.[7] It is a fascinating chelator ligand because of its properties associated with its π-accepting pyridyl groups and σ-donating tertiary amine groups.[7-8] Typically, it coordinates in a tetradentate fashion but, through dissociation of a pyridyl arm, tridentate coordination could be observed.[7] Other famous tripodal ligands are those containing imidazolyl (e.g., tris(2-(1-methylimidazolyl)methyl)amine, tmima)[9] or pyrazolyl (e.g., tris[2-(3,5-dimethyl-1-pyrazolyl)ethyl]amine)[10] donors (figure 2).

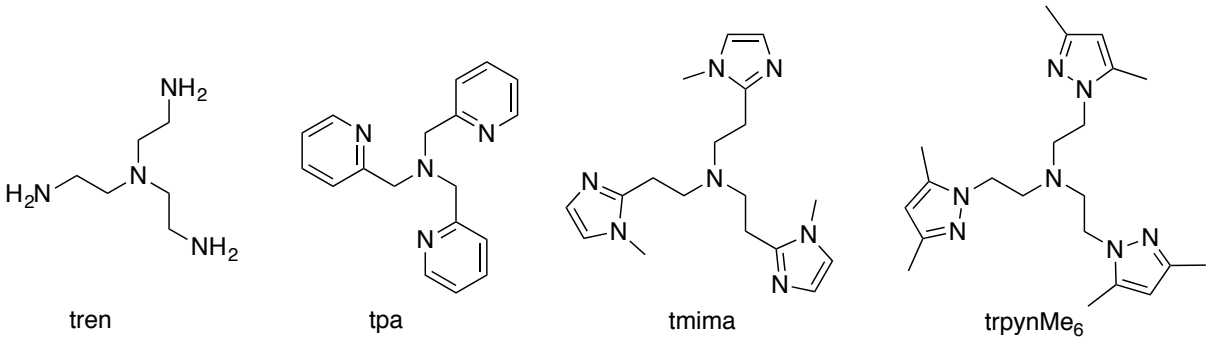

Figure 2: Structures of different tripodal ligands.[5-6, 9-10]

Functional enzyme models,[6b, 11] spin-crossover,[6b, 12] catalysis,[7, 13] and C-H and O-O activation of small molecules[7, 14] are only a few examples, in which complexes containing tripodal ligands have been applied. The tuning of these ligands is rather straightforward and possible by varying not only the lengths of the arms but also exchanging the donor atoms (e.g., P, O, S or N).[6b, 15] Furthermore, the concept of replacing the arms to achieve mixed tripodal ligands became more important. This leads to a better understanding of the influence of the different donor groups, e.g., regarding the stabilization of the copper (II) oxidation state.[7] Based on tpa, Britosek *et al.* replaced the arms with dimethylamine arms resulting in Me_6-tren (a tren derivative) (figure 3).

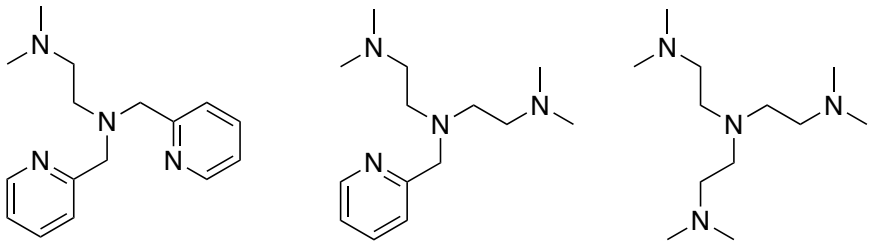

Figure 3: Mixed tripodal ligands yielding in Me_6-tren derivatives.[14b]

Coordinated to an iron(II)-center with either two acetonitrile or triflate (OTf) ligands lead to the formation of the complexes $[Fe(L)(OTf)_2]^{2+}$ and $[Fe(L)(CH_3CN)_2]^{2+}$ (L = tripodal ligands).[14b] Several changes could be observed due to the different nature of the ligands:[14b]

(I) By increasing the number of dimethylamine arms, the coordination sphere changes from a five- to sixfold coordination,

(II) The iron(II)-center in $[Fe(tpa)(CH_3CN)_2]^{2+}$ is a low-spin iron(II), whereas the other complexes are high-spin at room temperature,

(III) All complexes catalyze the oxidation of cyclohexane with H_2O_2, but the catalytic activity increases as a function of the total number of pyridines.

The difference between efficiency and selectivity is based on the number of pyridine donors in the ligands. If at least two pyridine donors are present, the complexes show a Fenton-type reactivity, which involves a radical chain auto-oxidation mechanism, whereas the complexes that contain less pyridine units probably form oxo-bridged iron(III) molecules. This makes the complexes less stable, causing them to degrade more quickly under the reaction conditions.[14b]

1.1.2. The Rise of "Click" Chemistry

Although the synthesis of triazoles was discovered in the early 20th century by O. Dimroth[16] and further investigated by Huisgen *et al.*,[17] the modern conception of the so-called "Click" chemistry began in 2001. This term was proposed by Sharpless *et al.*[18] and enables molecules to be easily synthesized from smaller units. In 2022, Barry Sharpless, Morten Meldal and Carolyn Bertozzi are awarded with the Nobel Prize for their work in the field of Click chemistry. This shows that even after two decades this concept is still of utmost importance.

Click chemistry is defined as reactions that “must be of wide scope, giving consistently high yields with a variety of starting materials”.[19] Furthermore, the reaction should work under aerobic conditions, easy to perform, the starting materials must be readily available, and the work-up conditions must be simple.[19]

Often the Cu(I)-catalyzed azide-alkyne cycloaddition (CuAAC) is used as synonym for click chemistry.[20] The CuAAC was discovered in 2002 by two independent groups (the group of Sharpless and the group of Meldal)[21] and fulfills the criteria of the click reaction defined by Sharpless.[22] For the synthesis of triazoles, the [3+2] cycloaddition of azide and alkyne is a powerful tool and belongs to the most important reactions in click chemistry.[23] Due to their modular synthesis and versatile coordination motifs, the interest in 1,2,3-triazoles increased over the past decades (figure 4).[24]

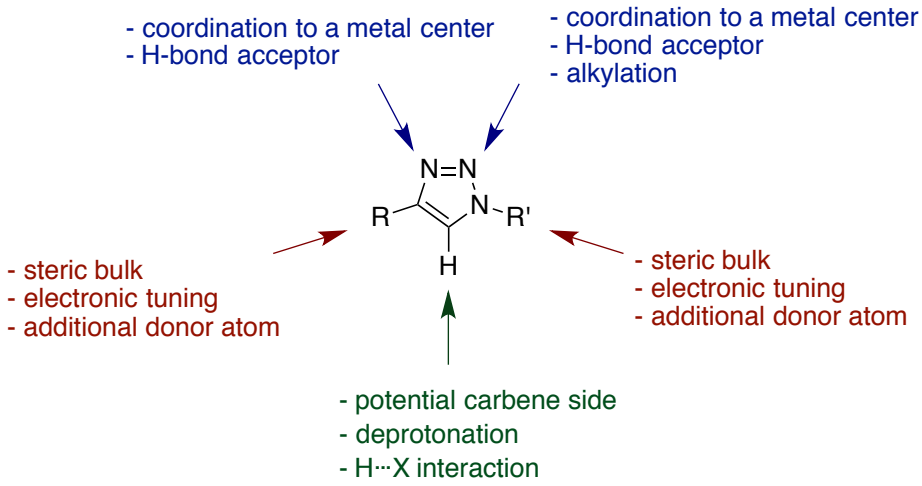

Figure 4: 1,4-Disubstituted 1,2,3-triazole, characteristics/functionalities of the heterocycle (Adapted from Sarkar *et al.*).[22a]

While the uncatalyzed 1,3-dipolar cycloaddition of azides and alkynes results in the two possible regioisomers (1,4-regioisomer and 1,5-regioisomer), a regioselectivity can be obtained in a metal catalyzed reaction.[25] The CuAAC forms exclusively the 1,4-disubstituted 1,2,3-triazoles, whereas the other regioisomer can be obtained by e.g. varying the metal, for instance, ruthenium or zinc (scheme 1).[22b, 25]

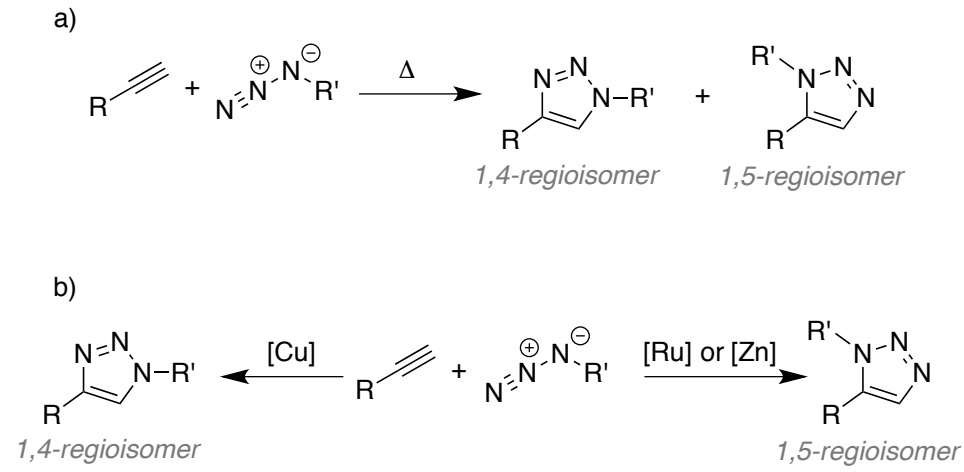

Scheme 1: a) Thermal synthesis of 1,2,3-triazoles in a Huisgen cycloaddition; b) Transition metal catalyzed cycloaddtion of 1,2,3-triazoles.[17, 22a, 25]

The free energy profile for the non-catalytic cycloaddition of phenylacetylene and azidobenzene is depicted in figure 5. The activation free energy of corresponding transition states are found to be close to one another, which explains the aforementioned non-selectivity of this reaction.[25-26] These observations are supported experimentally, where a 1:1 mixture of the two isomers is usually found.[26]

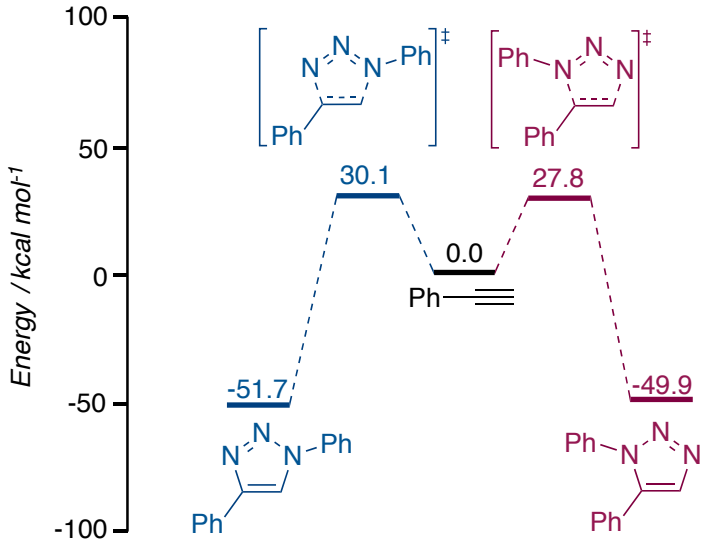

Figure 5: DFT-based energy profile of non-catalyzed Huisgen cycloaddition.[25]

Due to all its advantages, the CuAAC reactions became popular in various fields such as polymer and material science,[27] drug discovery,[22b, 27b] bioorganic chemistry,[27b] and polymer science.[27c]

The reactivity of the conventional method of *in situ* generation of an active copper(I) species by reaction of copper(II) sulfate with sodium ascorbate in aqueous solution is limited.[27b] A more modern approach incorporates highly active copper(I) (pre-)catalysts.[21, 22b] In this regard, catalysts, which contain tetradentate ligands can be used to enhance reaction rates, by providing higher yields or larger rate constants.[21] One early example is a catalyst with the tren ligand.[28] Shortly after, the 1,2,3-triazole containing ligand tris(benzyltriazolylmethyl)amine (tbta) was found to even better stabilize the copper(I) oxidation state (figure 6).[29] A di-copper complex derived from tbta and [Cu(MeCN)](BF_4) was than isolated by the group of Williams. This dinuclear complex showed the same catalytic reactivity as in situ generation of a Cu^I catalyst derived from a copper(II) salt and tbta, while sodium ascorbate is present, which lead to the conclusion, that the catalytically active species has to be the dimer.[29a]

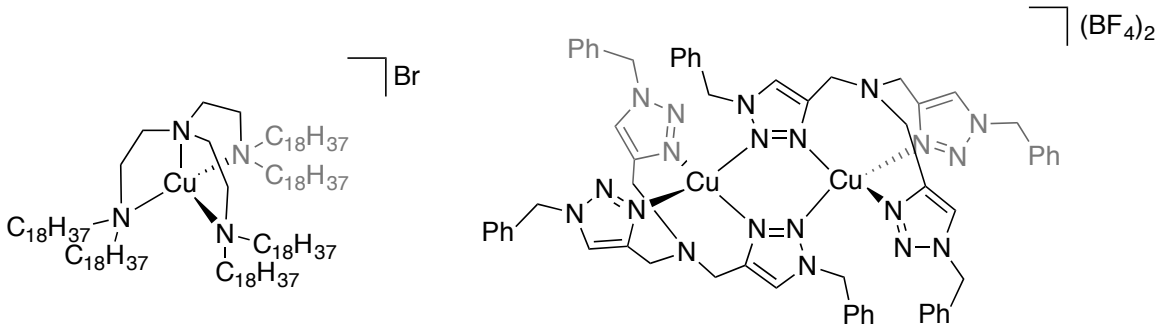

Figure 6: Copper(I) catalysts derived from tripodal ligands.[28-29]

1.1.2.1. Triazole-Based Tripodal Ligands and Their Complexes

The use of "click" chemistry for the synthesis of tripodal ligands leads to numerous ways to tune this ligand-class. One famous example is the aforementioned tbta (figure 7), which is synthesized by a Cu(I)-catalyzed azide-alkyne cycloaddition.[30] This ligand was used in different metal complexes to investigate their magnetic properties.[31] In these complexes, the effect of weak interactions (T- or π-stacking) in the solid state can be studied, which are useful in understanding spin-crossover (SCO) compounds.[31c]

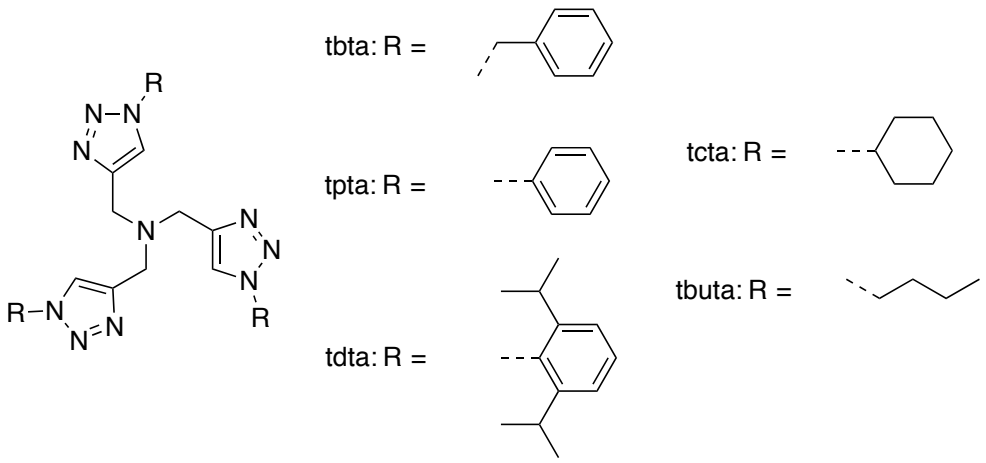

Figure 7: Selected examples of click-derived tripodal ligands.[31c, 32]

In principle, octahedral metal complexes with a d^4-d^7 electronic configuration can exist in two spin states: high spin (HS) or low spin (LS).[31c, 33] Depending on the interplay between the spin pairing energy and the ligand field stabilization energy (LFSE), one of the spin states is stabilized.[33] The d-orbitals in an octahedral ligand field are split into the e_g and t_{2g} levels and separated by the LFSE.[34] In the case of a d^6-configuration, a weak field induces a higher spin pairing energy than the LFSE, which stabilizes the $t_{2g}^4e_g^2$ configuration, while in a strong ligand field the $t_{2g}^6e_g^0$ configuration is stabilized as the spins are forced to pair (scheme 2).[34]

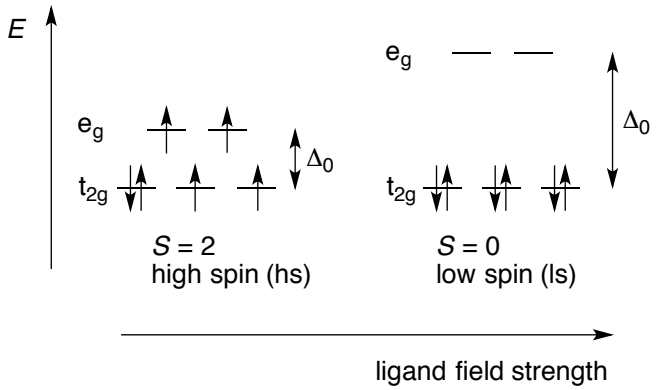

Scheme 2: Examples for high spin and low spin configuration in d^6 octahedral complexes.[34]

Furthermore, these systems in principle provide the possibility of magnetic bistability (the existence of two distinct magnetic states)[35] and the two spin states can be switched by applying external stimuli such as temperature, pressure, light, electric fields, and analytes.[33, 36] Materials that show bistability can potentially be applied in sensors,[36b, c] memory devices[36b, c] and switches.[36b]

The switching between the LS and HS states can be observed in SCO complexes. A variety of metal complexes have been investigated for SCO, with most containing aromatic *N*-heterocycles.[34, 37] The most common examples of SCO complexes contain either an iron(II) or cobalt(II) metal center, whereas iron complexes are better studied, due to the use of Mössbauer spectroscopy in combination with iron.[36b, c, 38] One of the first studied compounds was the iron(II) complex $[Fe(phen)_2(NCS_2)]$ (phen: 1,10-phenantroline),[39] and in the case of cobalt(II) compounds, first reports date back to 1961 with the compound $[Co(PdAdH)_2]I_2$ (PdAdH: bis-(2,6-pyridindialihydrazone).[40]

There are two primary differences in regard to cobalt(II) and iron(II) SCO compounds, (I) the spin state of cobalt(II) changes from $S = 1/2$ to $S = 3/2$, with $\Delta S = 1$, while Fe(II) changes with $\Delta S = 2$. Due to the single electron in the e_g level a Jahn-Teller distortion is induced, strongly affecting the bond lengths around the cobalt(II) center.[41] The transition temperature of a SCO compound can be investigated through temperature-dependent measurements of the magnetic moment, as the magnetic moment depends on the spin state. And (II) the bond lengths around the metal center change depending on the spin state. The bonds are elongated in the HS state in comparison to the LS state, due to the electrons in the e_g level. Therefore, temperature-dependent X-ray diffraction studies can give more information about the spin state. There are different classifications of the spin-state changes, which can be for example described as (a) gradual, (b) abrupt, (c) with hysteresis, (d) with steps or (e) incomplete (figure 8).[34]

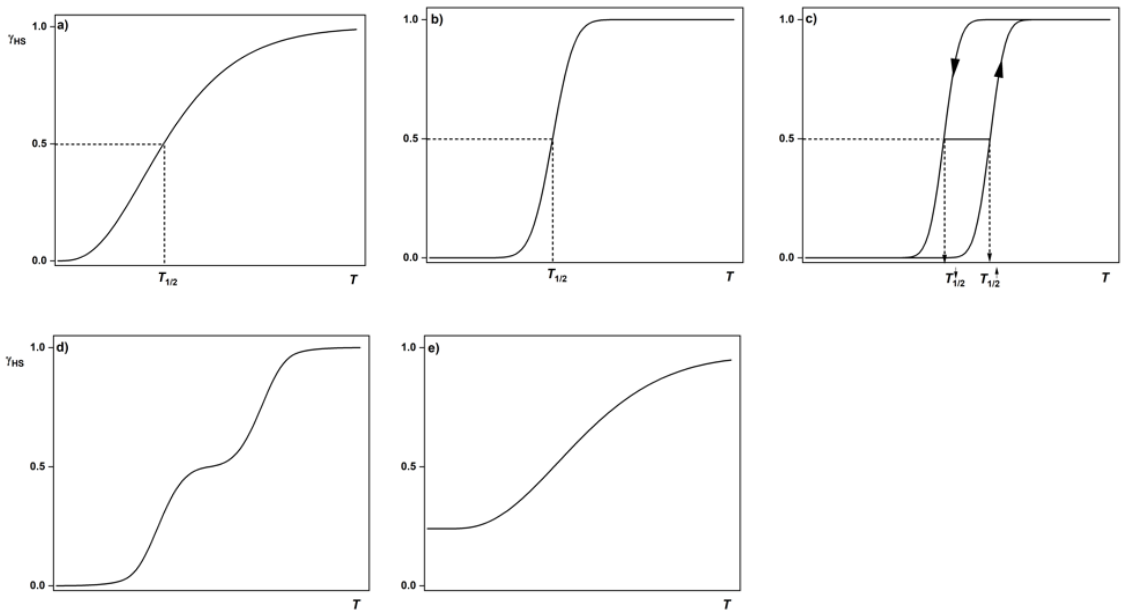

Figure 8: Spin transition curves of SCO systems in the solid state: (a) gradual, (b) abrupt, (c) with hysteresis, (d) with steps, or (e) incomplete (Adapted from Gütlich *et al.*).[34]

However, it is still challenging to predict the noncovalent interactions (NCIs) like halogen bonding or $\pi \cdots \pi$ interactions, which have an effect on the magnetic properties, even though there are several examples in the literature.[33, 42] In this regard, the group of Sarkar used click-derived 1,2,3-triazole tripodal ligands to further investigate the impact of NCIs on SCO.[31c] They presented four new cobalt(II) complexes, which were investigated towards "the effect of soft-donor click ligands on the magnetic state".[31c] In this work, SCO was observed for the homoleptic $[Co(tbta)_2](ClO_4)_2$ complex at high temperatures, while the effect of the functional groups and different coordination modes revealed an impact of the intra- and intermolecular stacking interactions.[31c] Later, iron(II) analogues of the $[Co(tbta)_2](ClO_4)_2$ complex were synthesized to show the importance of the NCIs.[33] Additionally, the influence of solvent molecules could be identified through the characterization of the $[Fe(tbta)_2](BF_4)_2 \bullet 2$ EtOH and $[Fe(tbta)_2](BF_4)_2$ complexes. Two tbta ligands directly coordinate either to the cobalt(II) or iron(II) metal center via the central amine as well as with two arms through triazole donors. One arm remains uncoordinated, which is then responsible for intra- and intermolecular non-covalent interactions. The resulting T-stacking motif is caused by intramolecular C-H $\cdots \pi$ interactions between the benzyl ring of an uncoordinated arm and the benzyl hydrogen atom of a coordinated arm (left complex in figure 9).[33] However, co-crystallizing solvent molecules can prevent this interaction in the secondary coordination sphere and inhibit any SCO by locking the molecule in the HS state.[33] The importance of NCIs is further supported by the use of tpta. The tpta

ligand does not allow C-H ⋯ π interactions due to the shorter phenyl ring on the triazole unit. Hence no SCO is observed within the investigated temperature range (right complex in figure 9).[31b]

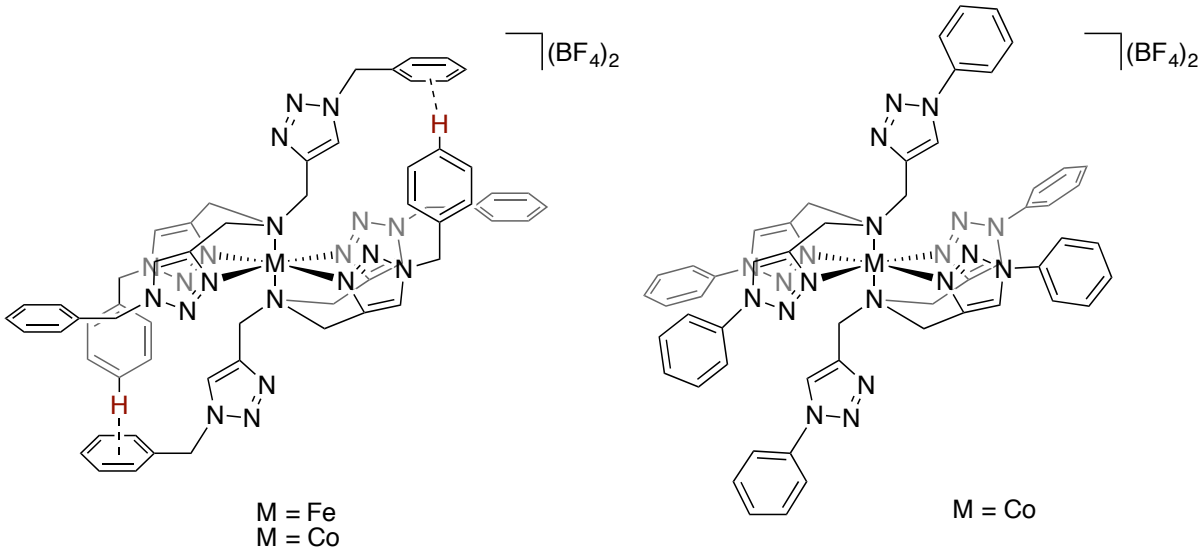

Figure 9: Iron(II) and cobalt(II) complexes with tripodal ligands, left: with tbta, right: with tpta.[31b, 33]

Apart from SCO complexes, tripodal "click" ligands can also be used for synthesizing blue light emitting cerium(III) complexes[43] or to support copper-catalyzed atom transfer radical polymerization (ATRP) of methyl methacrylate (MMA).[44] Here, the substituents have a dramatic effect on the well-controlled nature of polymerization and the activity of the copper catalysts.[44] Moreover, the cobalt complex with the tpta ligand, which is bridged over two μ-hydroxide ligands (and NO_3^- as counterion) can be used in electrochemical water oxidation. Unfortunately, the complex decomposed during electrochemical water oxidation, forming a highly active cobalt oxide on the electrode surface.[45]

The functionality of the aforementioned mixed tripodal ligands was tuned with click chemistry (figure 10) to develop fluorescent probes for the detection of NO and HNO,[46] or for zinc(II).[47] Additionally, the catalytic oxidation of benzene into phenol can be performed using iron(III) complexes of these ligands.[48] Furthermore, cobalt(III) complexes with hybrid pyrazolyl-triazolyl ligands were synthesized for the potential use in the development of new catalysts.[49]

Sarkar *et al.* further investigated ruthenium(II) complexes with mixed tripodal ligands with respect to their redox properties,[8] reactivity[8] and catalytic activity.[50] The ligands were synthesized starting from tpa and the stepwise replacement of the pyridine arms. The investigations revealed that an increasing number of triazole units do not only increase the

electron density at the metal center, which finally affects the redox- and photoreactivity of the complexes, but also has an influence on the oxidation of cyclooctane to cyclooctanone.[50] Increasing the number of the triazole arms results in a higher yield during catalytic oxidation.[50]

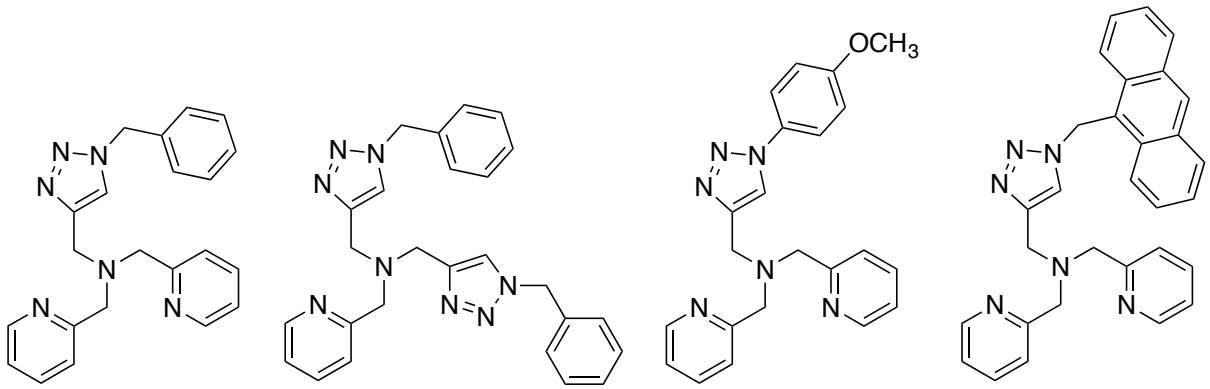

Figure 10: Selected examples of „click“ derived mixed tripodal ligands.[46a]

Additionally, several non-tpa based, click-derived tripodal ligands can be found in the literature, such as azatriquinane based ligands,[51] the carbon anchored tris(1-benzyl-1H-1,2,3-triazol-4-yl)methanol,[52] and the phosphorous anchored ligand tris(1-benzyl-1H-1,2,3-triazol-4-yl)phosphine oxide (figure 11).[53]

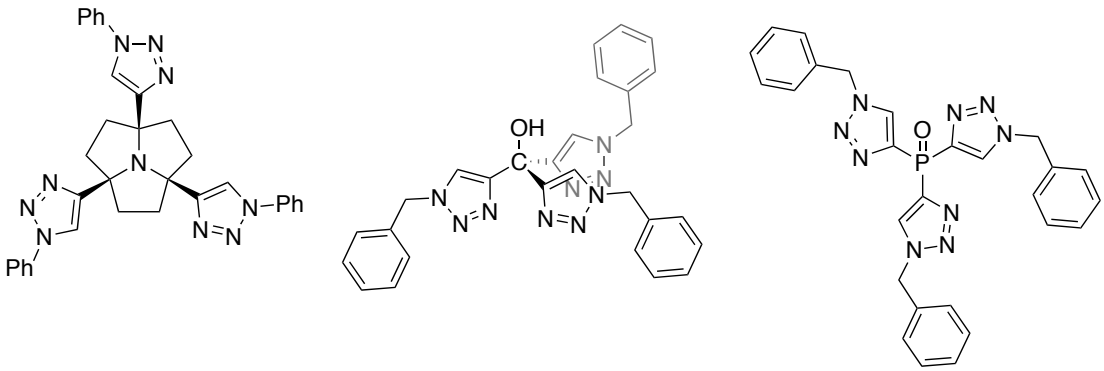

Figure 11: Different non-tpa based tripodal ligands.[51, 52b, 54]

1.1.3. Terpyridines

Since the first report of 2,2’: 6’,2’’-terpyridine (tpy) in 1932 by Morgan and Burstall[55] a huge variety of articles containing tpy and its derivatives have been published so far (figure 12). In recent decades, the ligand tpy has gained increasing interest since it finds application in a huge variety of fields. In the early 1970’s, complexes of tpy were of great importance, as platinum tpy complexes can bind to DNA through intercalation.[56] In this regard, [(tpy)-Pt(S(CH$_2$)$_2$OH]$^+$ was found to inhibit the binding of ethidium bromide, an intercalating dye, to calf thymus DNA.[56]

In addition, tpy compounds have found numerous applications as electrocatalysts for proton and CO_2 reduction,[57] as catalysts for C–C bond formation reactions,[58] as gel systems,[59] as photosensitizers,[60] in supramolecular chemistry[60a, 61] and as redox shuttles for dye-sensitized solar cells (DSSC).[60a, 62]

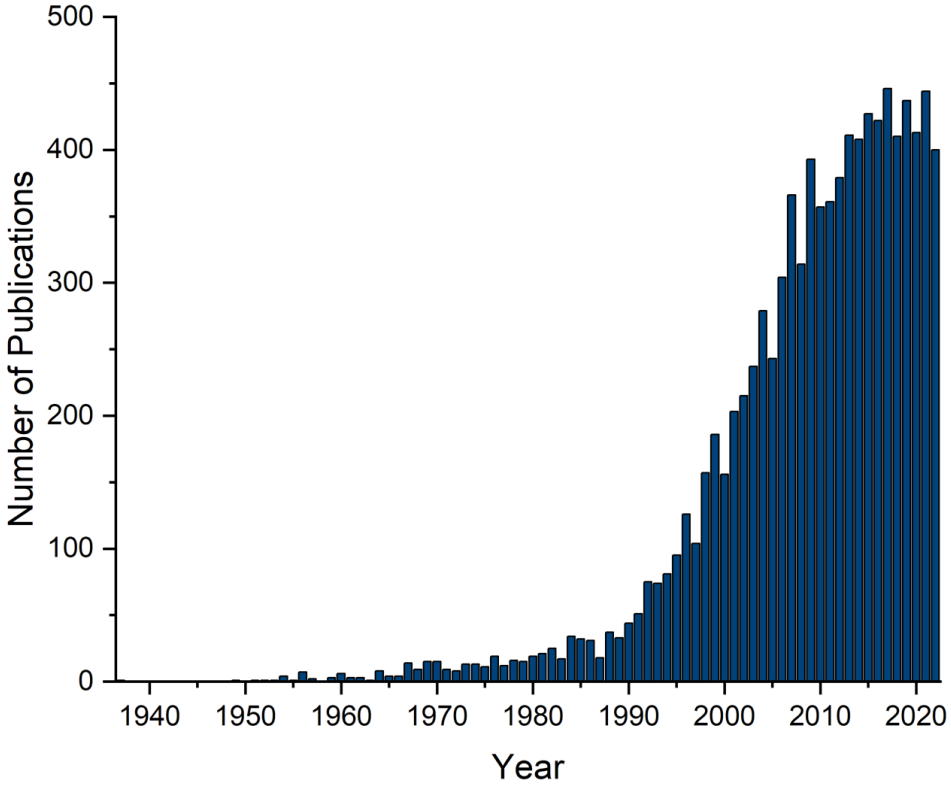

Figure 12: Data Base Search in Scifinder@ based on the keyword "terpyridine".

As the tpy molecule contains three nitrogen atoms it can act as a tridentate ligand.[63] In this regard, there are two possible cases, the mono-tpy and the bis-tpy complexes (scheme 3), where the ligand is bound in a nearly planar geometry.[58a] The complex stability of $[M(tpy)_2]$ complexes is strongly linked to the metal cations with the binding affinity towards the transition metal as follows: $Cd^{2+} < Zn^{2+} < Fe^{2+} < Os^{2+} < Ru^{2+}$.[58a, 64]

Originally, Moss and Mellon[65] proposed tpy as a colorimetric reagent for iron, but since then various complexes with different metal centers have been synthesized, including e.g. Fe,[55] Ni,[66] Os,[66] Ru,[67] Pt,[56, 68] and Zn.[69] The ability of tpy to coordinate with various different metal centers makes it an excellent ligand in coordination chemistry.

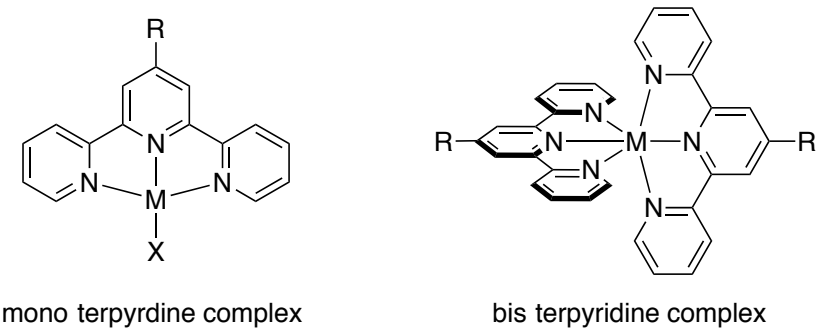

Scheme 3: Two possible complex structures of tpy-based metal complexes.[58a]

As mentioned above, the original synthesis of 2,2':6',2''-terpyridine was developed by Morgan and Burstall in 1932[55] and included the oxidative coupling of pyridines. Another typical synthesis starts from 2-acetylpyridine, proceeding via a ketoenamine and subsequent generation of a diketone, followed by a ring closure with a suitable nitrogen-source (scheme 4).[63c, 70] Since then, several new synthetic procedures, in particular including Pd-based coupling reactions (Hiyama-coupling,[71] Stille-coupling,[71] or Negishi-coupling[72]) or traditional ring closure methods,[73] have been established. Furthermore, the introduction of different substituents on the tpy ligand has received significant interest in order to tune the molecular properties (e.g., the electronic properites) of the ligand.[60a, 74]

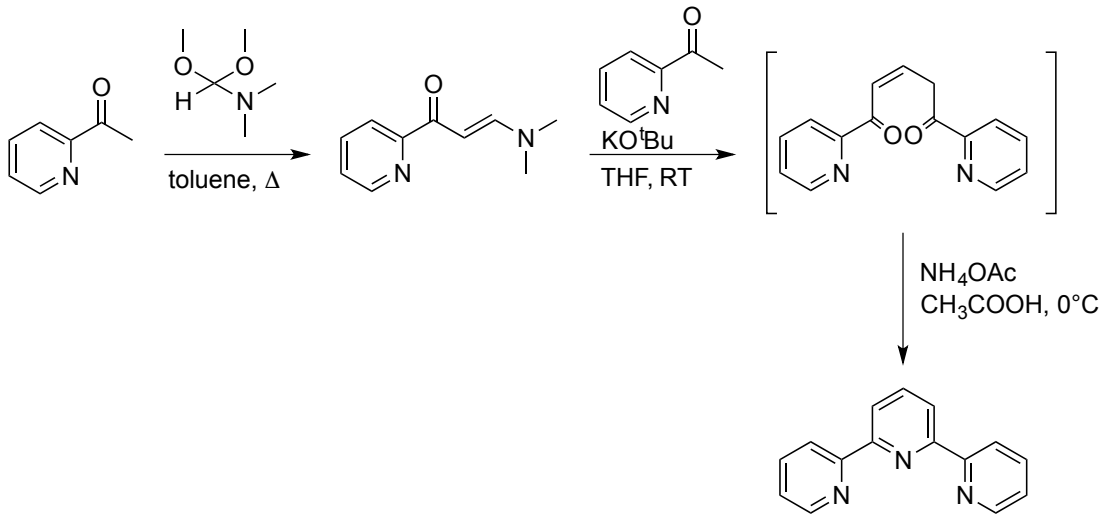

Scheme 4: Synthetic route of 2,2':6',2''-terpyridine starting from 2-acetylpyridine.[70]

At the C(4') position, prominent functionalities are hydroxyl-groups,[75] chloro-[75] or bromo[76] substituents or a methanesulfonyl group (figure 13).[77] However, for particular substitution patterns the synthesis can still be challenging. The Reißig group developed a strategy to synthesis tpy ligands, which contain dimethylamino substituents at different positions (figure 13).[78]

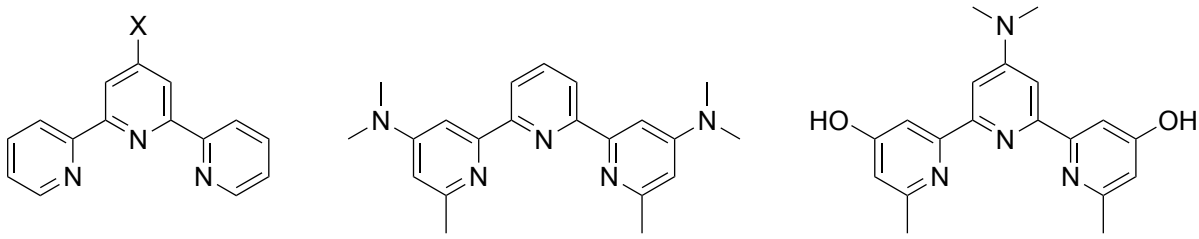

X = OH, Cl, Br, SO_2CH_3

Figure 13: Examples of different substituted tpy ligands. [75-78]

The 2,2':6',2''-terpyridine is a redox-active ligand, which can be reduced several times. The metal complexes based upon this ligand display fascinating electrochemical properties.[79] Additionally, the electronic nature of the ligand can be influenced. In this regard, the presented dimethylamine substituted tpy-based ligands are attractive as redox-active substituents, since disubstituted amines can be oxidized to the corresponding aminium radical cations.

Based upon the above properties, the Sarkar group studied different ruthenium complexes that contain tpy ligands with different numbers of dimethylamino (NMe_2) substituents (figure 14).[80] Here, the oxidation of ruthenium could be tuned up to 1 V in comparison to $[Ru(tpy)_2]^{2+}$.[80] In addition, up to four chemically reversible reduction steps were observed, which shows the applicability of such tpy ligands for tuning redox potentials of metal centers.[80] The influence on the electrochemical behavior of NMe_2 groups on tpy was also investigated in cobalt complexes. In the work of Fontecave *et al.* the redox potential of Co^{III}/Co^{II}, Co^{II}/Co^{I} and $Co^{I}/Co^{I}(tpy)^{\bullet-}$ couples can be modulated over 1 V, depending on the substituents.[60a] More cathodic values are observed for the Co^{III}/Co^{II} redox potential when larger numbers of amino substituents are introduced to the tpy ligand.[60a] In the aforementioned study, the effect of one electron-donating group (NMe_2) at the 4-position of the central ring can be compensated by two electron-withdrawing groups (CF_3) at the 4-position of the outer rings (figure 14).[60a] Regarding the ligands with NMe_2 groups there were two main conclusions: complexes with NMe_2 at the position on the central pyridyl moiety lead to similar redox potential values as for one on each of the outer rings and the most electron-rich ligand can be generated by introducing a NMe_2 group on each ring.[60a] These properties make the presented complexes good candidates in redox flow battery applications or in dye sensitized solar cell applications.[60a]

Moreover, terpyridine complexes can potentially be used as photosensitizers,[76] which was investigated by the Damraur group regarding an iron complex, and the Berlinguette group using ruthenium complexes.[81]

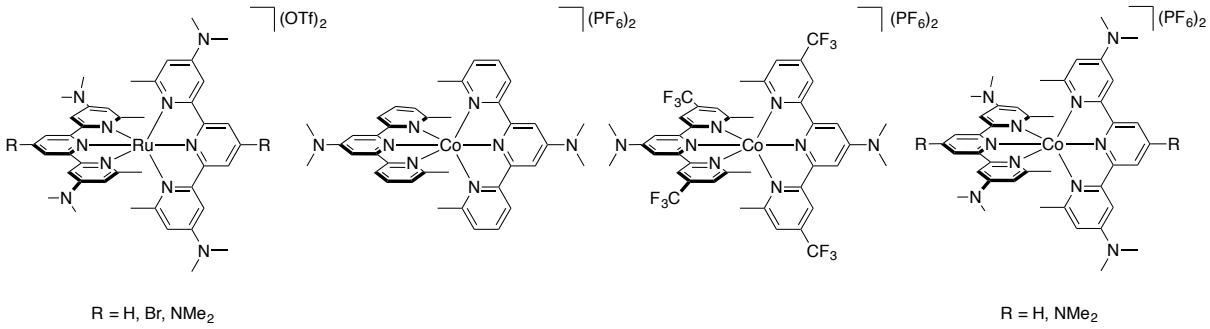

Figure 14: Selected ruthenium und cobalt complexes with NMe_2 substituted tpy ligands.[60a, 80]

1.1.3.1. Alkyl-Chain Based Terpyridine Complexes

Lately, the design of molecules that could be used in information storage and processing has increased notably. These materials usually should display bistability. One example is the application of soft materials,[82] where weak interactions between individual structural elements are reflected.[83] This is due to their inherent internal degree of freedom, which is why they tend to show a high responsiveness to external stimuli.[83] One method to obtain soft metal complexes is the introduction of long alkyl chains onto the ligand.[84]

In this regard tpy-based complexes that display the aforementioned phenomenon of SCO may play a role, if the metal center has a configuration of d^4-d^7.[38] As the $[Co(tpy)_2]X_2\ n\ H_2O$ (X = halide, pseudohalide, NO_3^-, ClO_4^-; n = 0–5) shows incomplete or gradual SCO behavior,[85] complexes bearing long alkyl chains are expected to show liquid-crystal properties as well as unique physical properties.[86] Therefore, the group of Hayami published several cobalt(II) complexes with different tpy ligands, which display interesting magnetic and liquid crystalline properties.[36a, 38, 86-87] The complexes $[Co(Cn\text{-tpy})_2]^{2+}$ were synthesized and investigated (figure 15), where compounds with n = 12–16 exhibit a reverse spin transition between the HS and LS state with a thermal hysteresis.[86]

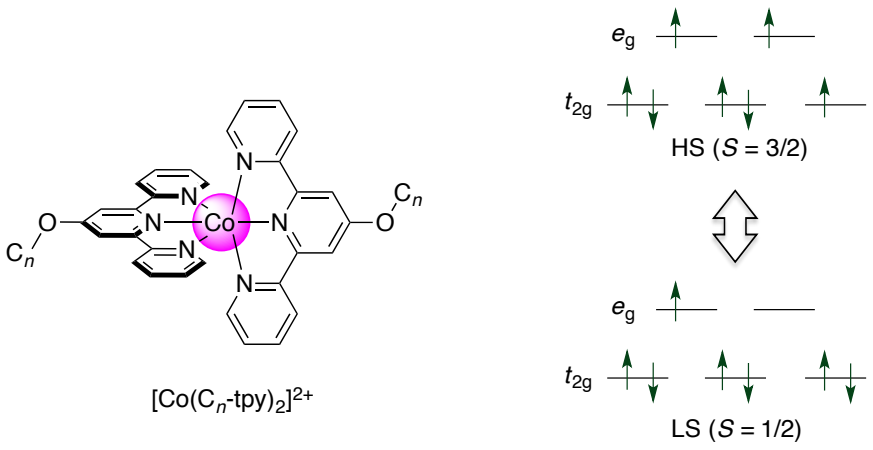

Figure 15: Schematic representation of the SCO behavior between LS and HS states in a tpy-based cobalt(II) complex bearing long alkyl chains. Figure adapted from Akiyoshi *et al*.[84]

In addition, liquid crystalline properties were observed for the complex $[Co(C_{16}\text{-tpy})_2](BF_4)_2$.[86] The complex $[Co(C_{12}\text{-tpy})_2](BF_4)_2$ exhibits a multi phase transition with a wide thermal hysteresis loop, while the solvated compound $[Co(C_{12}\text{-tpy})_2](BF_4)_2 \cdot EtOH \cdot 0.5H_2O$ shows a magnetic behavior that is described as a "re-entrant SCO."[88] The unusual SCO behavior is assumed to be induced by the thermal motion of the long alkyl chains.[84] In addition, the group of Hayami synthesized complexes with branched alkyl chain (figure 16) to increase the mesophase transition temperature of the metallomesogen (transition metal complexes that exhibit liquid crystal behavior).[87a] In the case of the cobalt(II) compound $[Co(C_5C_{12}C_{10}\text{-tpy})_2](BF_4)_2$ the spin transition was directly related to the mesophase transition and triggered by a crystal-to-mesophase transition.[87a] Thus, the design and synthesis of soft material complexes give rise to new metal-complex based soft materials, which may be important for the development of functional devices in the future.[84]

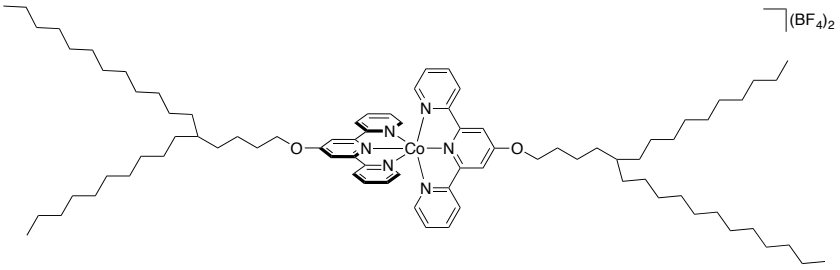

Figure 16: Chemical structure of $[Co(C_5C_{12}C_{10}\text{-tpy})_2](BF_4)_2$.[87a]

More recently, the group of Hayami published cobalt(II) and zinc(II) complexes with fluorine substituents on an additional phenyl ring on the central pyridine ring (figure 17).[89] In these complexes, a flip-flop motion of the fluorophenyl ring was observed in single crystal X-ray structures, at several temperatures, and solid-state ^{19}F NMR (SS NMR) spectroscopy.[89] The cobalt complex shows an incomplete SCO, where the increase is in accordance with the thermally induced flip-flop motion from the SS NMR spectra.[89] Due to the flip-flop motion, the LS cobalt state is destabilized and the magnitude of rotation can be controlled by an electric field, which provides new insight for molecule-based magnetoelectric materials.[89]

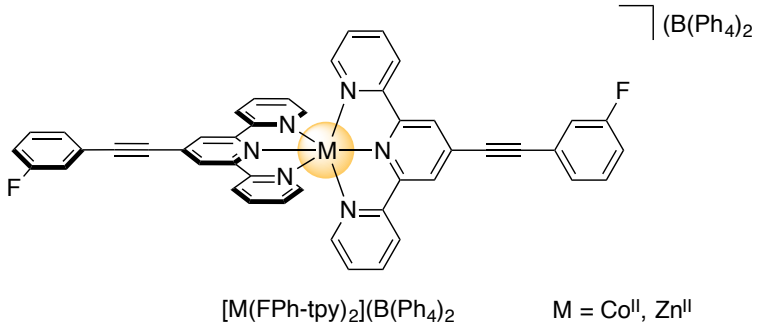

Figure 17: $[M(FPh\text{-}tpy)_2](BPh_4)_2$ complexes, that exhibit a flip-flop motion.[89]

Not only mononuclear complexes can be found that exhibit interesting SCO behavior. Zhu *et al.* demonstrated that increasing the core number could improve the cooperativity of spin transition leading to thermal hysteresis loops that occurs in the high-temperature region.[90] An effective approach was presented for the direct preparation of multinuclear SCO compounds from tpy ligands, through tpy-ligand complementary pairing (figure 18).[90]

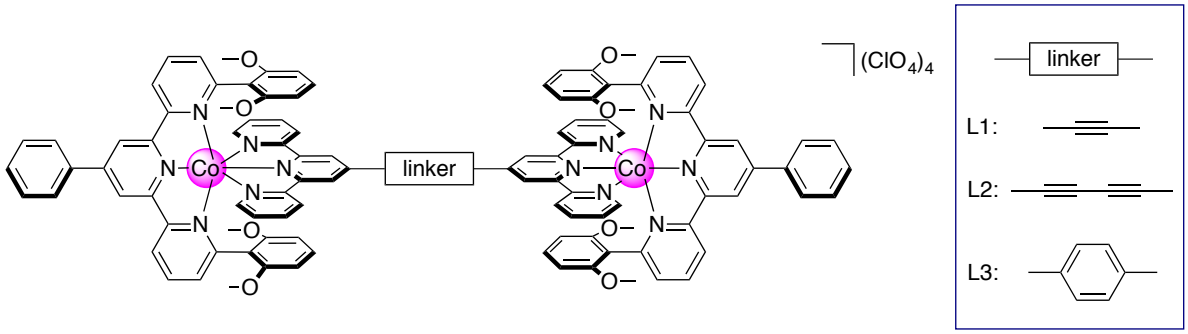

Figure 18: Dinuclear cobalt(II) compounds from the ditopic tpy ligands and 2,6-dimethoxyphenyl substituted tpy ligand.[90]

Only a few examples of tpy ligands bearing a fluorinated tail can be found in the literature (figure 19),[59, 91] even though complexes bearing perfluorocarbon (PFC) tails are of interest, as they can find applications in catalysis, supramolecular chemistry, and separation technologies.[91b] In addition, a contribution to the understanding of the physicochemical fundamentals based on fluorine chemistry and solid-state structure data may be important for this type of compounds.[91b] Therefore, the group of Haukka synthesized ruthenium complexes bearing one or two tpy units with a C_8F_{17} tag.[91b] They were able to obtain single crystals of good quality for complexes bearing one, two or three perfluorinated tags.[91b] Through X-ray data analysis the tendency of fluorinated pendants to segregate into fluorous domains in the solid state was revealed.[91b] The ruthenium complexes bearing a tpy ligand with a PFC tail and a bipyridine unit all show an octahedral environment, where the metal center is coordinated by the bipyridine through NN and tpy through NNN, respectively, and by a chloride ion.[91b] In the packing, parallel-displaced $\pi \cdots \pi$ stacking interactions of the tpy rings, edge-to-face $\pi \cdots \pi$ stacking of the tpy edge and the bipyridine face, anion π

interactions and halogen bonds were observed.[91b] Regarding F···F interactions, type I C–F ··· F–C interchain geometries were found within the lattice with C–F ··· F angles in the range of 120 – 158 deg.[91b] Other examples of tpy ligands bearing PFC tails in literature study the self-assembly into gels of *d*-block metal complexes (figure 19),[59, 91c] where the fluorine-fluorine interactions play a role in gel formation.[91c]

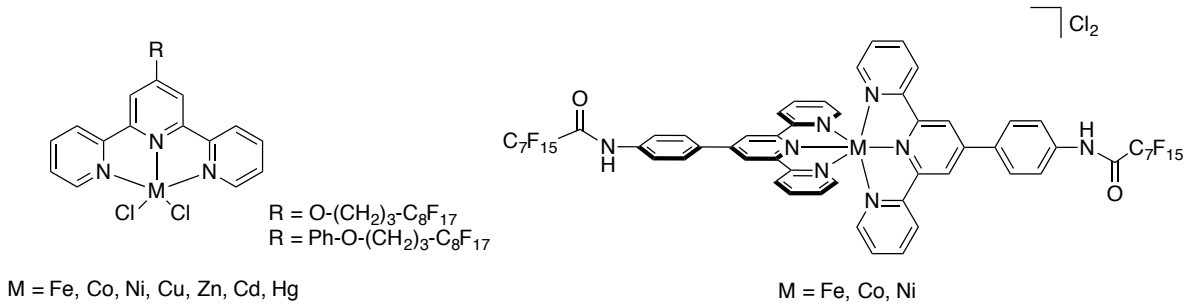

Figure 19: Examples of tpy-based metal complexes bearing a PFC tag.[59, 91c]

1.1.4. Redox-Active Ligands

In coordination chemistry redox-active ligands are well established.[92] They can coordinate to a metal ion and participate in its redox chemistry.[93] With the ligands serving as electron reservoirs they mediate multielectron reactions together with metal centers, that would not be possible otherwise.[92, 94] Moreover, complexes containing redox-active ligands, in many cases, impart intriguing electronic and optical properties, which will be discussed in the following.

These ligands have already been distinguished in several classes (figure 20), e.g.,

(I) As actor by forming bonds as a reactant,

(II) As spectator, where through standard ligand effects the metal is modified or,

(III) As spin isomers where a spin isomer is involved as the reactive form of the complex.[95]

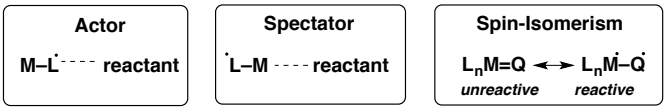

Figure 20: Selected types of redox-active ligands.[95]

In this context the term "non-innocence" is often used. If a ligand can also undergo electron transfer its oxidation state is not *a priori* obvious, which leads to a change of the “ligand oxidation state”.[96] Typical examples of this type of ligands are $O_2/O_2^{\bullet-}/O_2^{2-}$ or $NO^+/NO^{\bullet}/NO^-$, which were classified by Jørgensen in 1966 as “suspect” or “non-innocent”.[97] In contrast Jørgensen defines innocent ligands as ligands that allow “oxidation

states of the central atoms to be defined". Later Ward and McCleverty further defined the class of non-innocent ligands. They characterized the behavior of non-innocent ligands as ambi-valent since it could also depend on the metal center.[96, 98]

In the following sections two classes of redox active ligands will be discussed, quinone and azo-containing ligands.

1.1.4.1.Quinone Ligands

Quinones are naturally occurring redox active molecules that function in vital electron-transport processes, often in conjugation with a transition-metal center.[99] Important roles of *p*-quinones are in respiration, information-transfer processes and photosynthesis.[100]

The simplest example of quinone ligands functioning as an electron reservoir is *o*-benzoquinone (Q).[101] Through two reversible one-electron reductions the monoanionic, radical semiquinonate (SQ) and the fully reduced dianionic catecholate (Cat), forms of Q can be generated.[102] In general, the different binding modalities can be chemically or electrochemically induced, since the redox potentials of the three quinone oxidation states are within the metal-centered valence changes.[103] Overall, the ligands most commonly bind to the metal center as semiquinonate anions or catecholate dianions (scheme 5).[104]

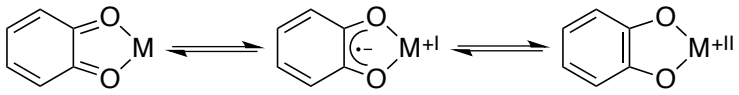

Scheme 5: Possible formal charge distributions between ligand and metal in isoelectronic forms (adapted from Kaim and Schwederski).[96]

In recent years, substituted *p*-quinones have been widely used as ligands in coordination chemistry.[105] The noteworthy properties that such ligands impart onto their metal complexes make such compounds useful in a broad range of fields, including homogeneous catalysis,[106] coordination polymers,[107] supramolecular chemistry,[105b, 108] and as bridging ligands in combination with redox active metal centers such as ruthenium.[109]

In this regard, the ligand 2,5-dihydroxy-1,4-benzoquinone (dhbq) is widely used as it is capable of bridging two or more metal centers.[105c, 107a, 110] Furthermore its redox chemistry is of great interest, as there are five different redox forms possible (scheme 6).

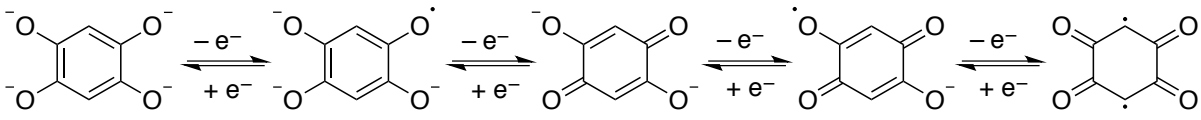

Scheme 6: Scheme of deprotonated dhbq and its possible redox forms.

The possible combination with a variety of metal centers leads to properties that have been studied for various purposes, with some prominent examples being valence tautomerism (VT, or redox isomerism),[110b, f] spin-spin coupling[107a, 111] or sensors based on supramolecular assemblies.[110c, 112] One possible way of modification of dhbq is the substitution of the "H" atoms on the C-H group by "Cl" or "^{t}butyl-group". Furthermore, the [O] donors can be exchanged by isoelectronic [NR] moieties, which enable the tuning of electronic and steric properties of the ligands and their metal centers. One such [NR] group can be e.g. the 2,6-diisopropylaniline, which leads to the ligands H_2Q_{Dipp} (figure 23). In this regard a possible synthesis for the exchange of one or two of the [O]-groups was investigated (scheme 7).[113]

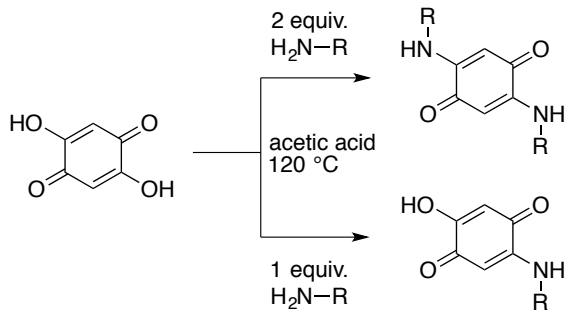

Scheme 7:Possible synthetic route of quinone ligands with [NR] group (adapted from Sarkar *et al.*).[113]

In the past few decades, an unprecedented variety of ligands in coordination chemistry has been revealed through the characterization of quinone complexes.[104b]

Various complexes have been reported, in which 1,2-dihydroxybenzene and its derivatives (e.g. 2,4-di-*tert*-butyl-6-(phenylamino)phenol) have been used. As with dhbq, this ligand can undergo a number of oxidations or reductions resulting in three different oxidation states: the fully oxidized *o*-iminoquinone, the *o*-iminosemiquinonate, and the fully reduced *o*-amidophenolate. Complexes with this type of ligand gained interest in the last two decades through the research of the groups of Wieghardt,[114] Rauchfuss,[115] Abakumov[116] and Kaim.[117] The nature of these compounds and their electronic structure have been elucidated by various spectroscopic, electrochemical, and theoretical methods.[118] Homoleptic complexes with a platinum, palladium, nickel and copper metal center have been published by the group of Wieghardt, which are antiferromagnetically coupled to an *o*-iminosemiquinone.[114] Later, Nasibipour *et al.* published a nickel(II) complex with the radical *o*-iminosemiquinone form, that showed catalytic activity towards the homocoupling of terminal alkynes with good reactivity, good reaction time, mild conditions and low catalyst amounts (figure 21).[119] The catalytic activity is due to the capability of the ligand to switch its oxidation state from iminobenzosemiquinone to iminobenzoquinone and *vice versa*.[119]

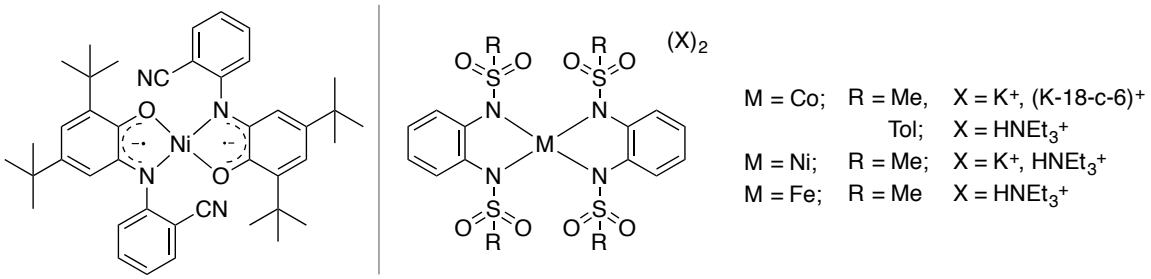

Figure 21: Homoleptic nickel(II) complex with 2,4-di-*tert*-butyl-6-(phenylimino)semiquinonate.(left), homoleptic complexes of 1,2-bis(sulfonamido)benzenes (right).[119-120]

Balch and Holm described metal complexes with *o*-phenylenediamine and its derivatives in 1966.[121] Due to their intriguing properties and significant potential as solid-state materials and chemotherapeutic agents, they utilized various metal(II) centers such as platinum(II) or palladium(II), but focused on the magnetic properties and electronic structures in their study.[122] Furthermore, they were able to elucidate the redox chemistry of these complexes by various spectroscopic and theoretical methods as ligand-based redox processes.[123]

In combination with certain transition metal centers 1,2-diamidobenzenes are typical examples of redox-active ligands known to exhibit non-innocent behavior.[121, 124] Due to their unusual electronic structures and electrochemical properties, their metal complexes have traditionally been studied.[121, 124-125] The homoleptic complexes with the bis(sulfonamide)benzene ligands presented in figure 21 (right) were synthesized to evaluate the utility of these ligands to induce large zero-field splitting (ZFS, D) in metal complexes that may act as single-ion magnets.[120] Such bis(sulfonamide)benzene ligands with cobalt form robust systems for the formation of complexes for slow relaxation of magnetization as well as with large negative ZFS, whereas for the nickel complex a very large positive ZFS was observed. In the future, such compounds will most likely provide more robust systems for single-molecule magnet research.[120]

With copper as a metal center, quinone ligands play an important role in catalysis, biochemistry and optically/magnetically switchable materials.[126] The consequences for catalytic reactivity[127] can be seen in biochemical systems like the enzyme tyrosinase.[128] In regard of magnetic systems, the metal-ligand interactions play a role in phenomena like bridge-mediated spin-spin coupling[105c, 110g, 129] or redox isomerism.[130] Concerning this, the group of Sarkar published the first example of a fully unreduced form of a di-*o*-quinone type ligand in a dicopper(I) complex.[126]

Moreover, complexes that contain the aforementioned bridging quinonoid ligands with unsymmetrically substituted donor groups were characterized.[131] This resulted in a

modification of chloranilic acid by substitution of one [O] group to one [NR] group. This enables studies on the preferential coordination of metal centers at one of the binding sites.
The presented complexes bear the potentially bridging quinone ligand in combination with a tripodal ligand. The mononuclear cobalt(II) complex exhibits redox-induced spin-state switching and yields a LS-cobalt(III) complex, when a reversible one-electron-transfer step is performed, whereas the mononuclear iron(II) complex shows SCO in the solid and in solution. The spin state of the latter can be switched by varying the pressure or temperature and the complex shows a light-induced spin-state trapping (LIESST) effect with a thermal relaxation at 42 K.[131] Moreover, diiron complexes with a symmetrical and unsymmetrical substituted quinonoid bridging ligands and tpa as stopper ligand were synthesized to probe multiple bistability in theses systems. This study showed, that the unsymmetrically-substituted bridge could stabilize the spin states of the iron(II) centers in a site-selective manner. Moreover, they showed that the symmetry of the bridge plays a crucial role in determining the electronic, electrochemical and magnetic coupling of such metal complexes. For generating large hysteresis loops in SCO processes the unsymmetrically substituted bridge seems to be of particular benefit.[132] Moreover, ruthenium complexes of this type have been studied in order investigate the effect on the redox and electronic properties of different bridges. The oxidation of such complexes leads to mixed-valent systems with strong absorptions in the NIR region. The properties of the NIR bands can be controlled through substitution on the bridging ligand.[133] Complexes with the combination of quinonoid bridging ligands and tripodal ligands are depicted in figure 22.

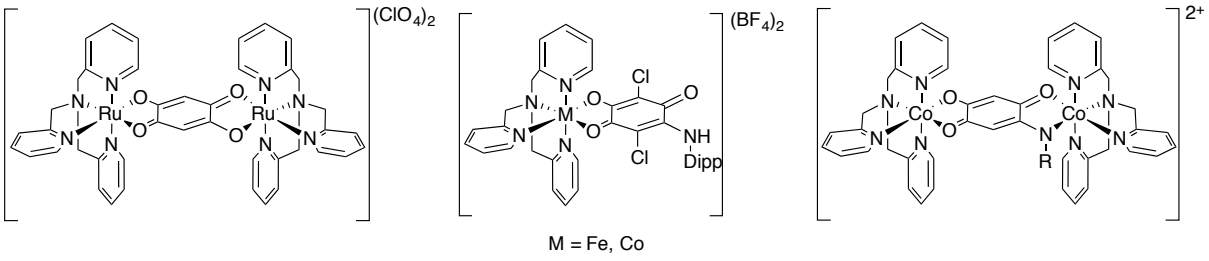

Figure 22: Examples of complexes with quinones and tripodal ligands.[131, 133-134]

Another interesting class of bridging ligands, related to the dhbq, are the tetraazalenes, that have attracted interest as bridging ligands in dinuclear complexes.[129]
An increasing number of articles and communications have been published on similar systems since Cheng *et al.* reported on dinuclear copper and nickel complexes bridged by a sulfonated tetraazalene.[135] Furthermore, the all-nitrogen-donating-ligand azophenine (figure 23) has been known since 1875,[136] but was only sporadically used for metal complexes.[137]

A previously discovered molecule was rediscovered through the work of Kaim and co-workers on the coordination-induced tautomerization of azophenine,[137c] leading to the publication of several mono- and binuclear complexes with related ligands. Several of the azophenine containing transition metal complexes exhibit interesting magnetic properties[137e, 138] and catalytic activity.[139]

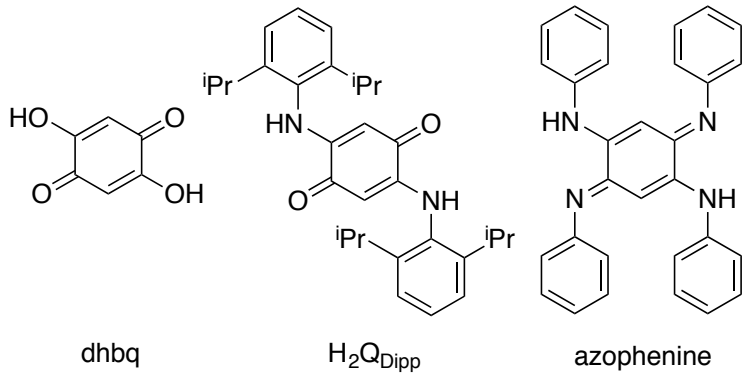

Figure 23:Ligand dhbq and related ligands with isolectronic [NR] groups.

Two examples of azophenine containing complexes are shown in figure 24. The depicted nickel(II) complex was reported by the group of Braunstein in 2006 and shows a complete delocalization of the π system of two separate N–C3–N moieties. Furthermore this complex shows a moderate catalytic activity in ethylene oligomerization.[140]

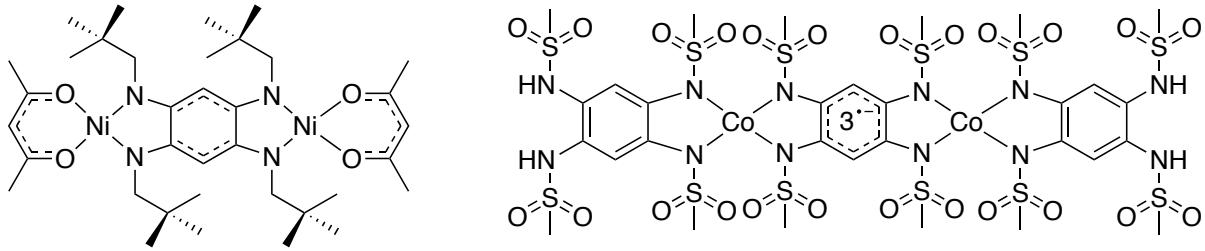

Figure 24: Examples of tetraazalene-bridged dinuclear transition metal complexes. [140-141]

The presented cobalt(II) complex shows that a strongly anisotropic, four-coordinated cobalt(II) building block enables the preparation of a radical-bridged dinuclear metal complex that substantially suppresses the Raman relaxation process and thus prolongs the relaxation time of the magnetization by a factor of 350. The hyperfine coupling seemed to limit the strength of the coercive field and thus also the magnetic bistability of the complex.[141]

All in all, the synthesis and investigation of complexes with quinonoidal ligands is still an integral part of modern research. In this thesis only bridging quinone ligands have been used.

1.1.4.2. Azo-Containing Ligands

Azo-containing ligands are a well-established class of non-innocent ligands in coordination chemistry.[142] These ligands are extensively incorporated in a wide range of applications such as molecular devices,[143] food additives,[144] therapeutic agents,[144a] or liquid crystalline materials,[145] but also in the textile industry[146] and cosmetic industry.[147]

Some well-known examples of azo ligands, depicted in figure 25, are 2,2'-azobispyridine (abpy),[148] 2-phenylazopyridine (pap)[149] and azodicarbonyls (adc-R)[150] with pyridyl or carbonyl moieties as additional donors bound to the azo moiety. While abpy and adc-R were usually used as symmetric bridges that bind to two metal centers, the pap ligand was often functionalized on the phenyl ring to increase its denticity.[151] Within coordination chemistry a less researched class of ligand are the azocarboxamides.[152] This versatile ligands offer many different coordination modes and several functionalities.[153]

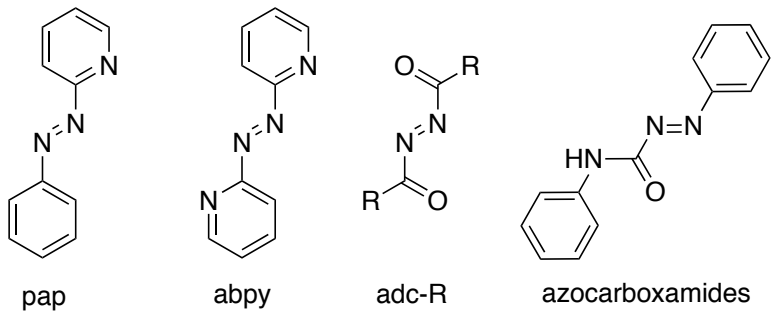

Figure 25: Structure of different azo containing ligands. [148-150, 152]

Abpy is of interest, as it possesses the functional azo group and two pyridyl groups that are able to coordinate to metals.[154] Formally, abpy is related to the 2,2'-bipyridine ligand and is known to form complexes with a variety of metal centers, e.g. Pt,[155] Os or Ru[156] but also complexes with less common metal centers e.g. with Au and Ag can be found.[154] Due to the small size of the π system, and the low-lying π^* orbital, abpy is a unique ligand.[157] Its ability to bridge two metal centers about 5 Å apart makes it ideal for investigating metal–metal interactions over an unsaturated bis-chelating molecular bridge.[157] Complexes with abpy are used as cytotoxic agents,[158] as components in switchable materials[159] or as magnetic resonance imaging probes.[160] Moreover, abpy can undergo *E/Z* photoisomerism leading to different possible coordination modes (figure 26).[148c] The abpy ligand may be present in its unreduced form, but copper, ruthenium and osmium complexes have also been reported, in which the abpy is present as an anion radical.[156a, b, 161]

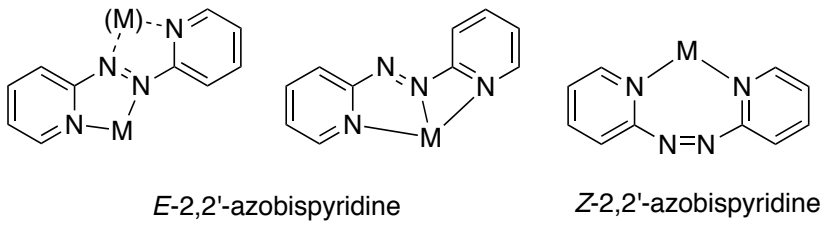

Figure 26: Possible coordination modes of 2,2'-abpy.[148c]

Ruthenium and osmium complexes with pap, for example, display cytotoxic properties against cancer cells.[158a, 162] Furthermore, the protonation of the cobalt complex leads to a hydrogen atom, proton and hydride donor (figure 27).[163] Pap is a strong π-accepting and weak σ-donating ligand, which was found to stabilize metals in low oxidation states.[164] But through modification of the pap ligand the position of the π*-orbital can be influenced. The introduction of a chloride on the fifth position on the pyridine ring lead to the derivative Clpap that is a better π acceptor.[165] In combination with ruthenium(II) this can lead to complexes that have a higher binding affinity to DNA.[165]

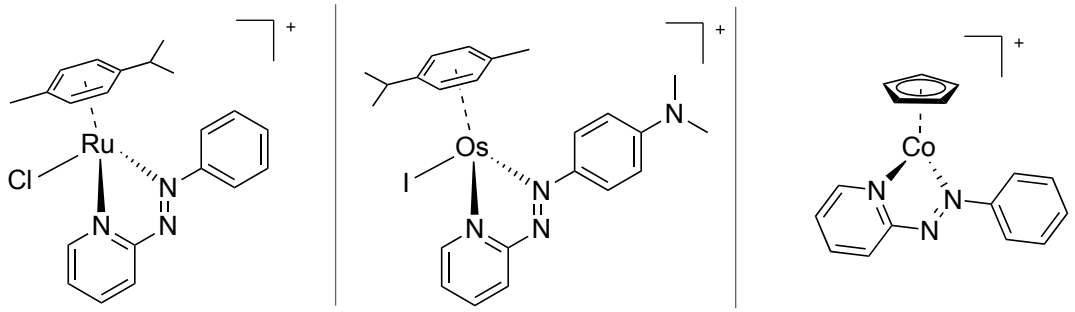

Figure 27: Different known metal complexes containing the pap ligand. (Left) with ruthenium, (middle) with osmium, and (right) with cobalt.[158a, 162d, 163]

1.1.4.2.1. Azobenzene

Another prominent example of azo-containing ligands are the azobenzenes. Azobenzene was discovered in 1834 by Mitscherlich[143] and exhibit unique photochromic behavior[143] and photoactivity.[166] These properties will be described in the following section.

A particular property of azobenzene is its ability to exist in either the *trans* or *cis* form, in which case the ligand is isomerized by UV light (figure 28),[143, 166] thermal stimulus,[167] electrostatic stimulation[168] or mechanical stress.[167-168] The *trans* isomer is thermodynamically more stable, such that *cis* → *trans* isomerization occurs in the absence of light at room temperature.[167-168]

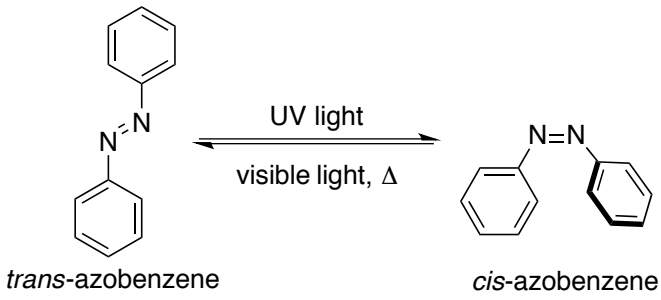

Figure 28: *Trans-cis* isomerisation of azobenzene.[143, 168]

Azo-containing molecules are very good π-acceptor ligands, due to the relatively low-lying azo-centered π^*-molecule orbital, which can be chemically and electrochemically reduced, leading to occupation by one or two electrons (figure 29).[149a, 156c] When azobenzene is reduced with one or two electrons, a radical anion is generated as intermediate, after a one-electron reduction, which can be then further reduced to the 1,2-disubstituted hydrazide dianion.[149a, 156c]

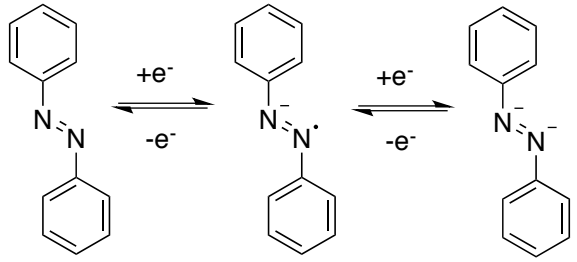

Figure 29: Possible redox forms of azobenzene.

There is a broad range of methods to synthesize azobenzene compounds, for example the oxidative coupling of anilines or aromatic amines, with the use of oxidants in stoichiometric amounts.[144b, 169] However, new synthetic approaches need to be developed,[143-144] as the above-mentioned oxidizing agents[144b, 169] or various metal containing compounds that are used for the synthesis[169] are either environmentally unfavorable[144b, 170] or generate an undesirably high amount of waste.[143-144] In this context, Zhang and Jiao developed a synthetic pathway in which azobenzenes are converted from anilines by Cu-catalyzed oxidative dehydrogenation with air as an oxidant.[144a, 170] Acceptorless dehydrogenation reactions appear to be a promising attempt in which H_2 is released.[144a] The reaction starts from a hydrazobenzene derivative, which is reacted with a photoredox, proton reduction catalyst, leading to the corresponding azobenzene under production of H_2.[144a] This leads to environmentally friendly reaction conditions, where the main advantage is, that no external oxidant is required, which leads to a reduction in toxic waste.[144a] Four possible synthetic approaches are depicted in figure 30.[144a]

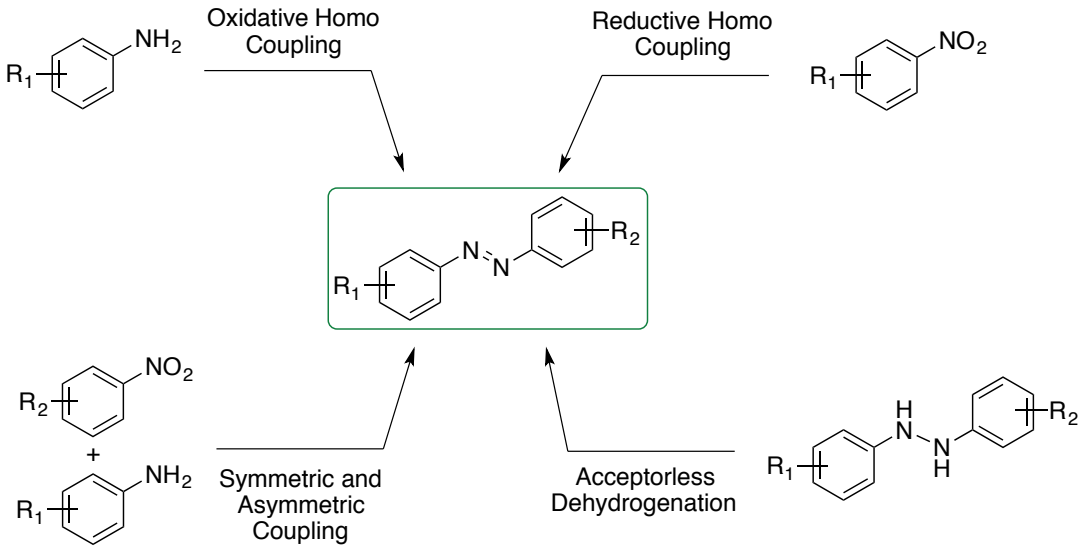

Figure 30: Literature-known approaches of the synthesis of azobenzene derivatives adapted from Sahoo *et al.*[144a]

The bidentate azobenzene normally coordinates to a transition metal in a chelating manner, where it is C-H activated by the metal center and binds as an anion.[171] The first examples of orthometallation were platinum(II) and palladium(II) complexes with azobenzene.[171b, 172] In its doubly orthometallated form it can also act as a bridging ligand. However, only very few azobenzene-bridged transition metal complexes are known to date.[173]

1.1.4.2.2. Azobenzene-Based Metal Complexes

Since its discovery a broad range of metal complexes with azobenzene have been reported. Already in 1965 Cope and Siekman observed the formation of platinum(II) and palladium(II) complexes with a carbon-to-metal σ bond.[171b] Later Barberio *et al.* attached alkyl chains on the phenyl rings to obtain liquid crystalline materials (figure 31).[174]

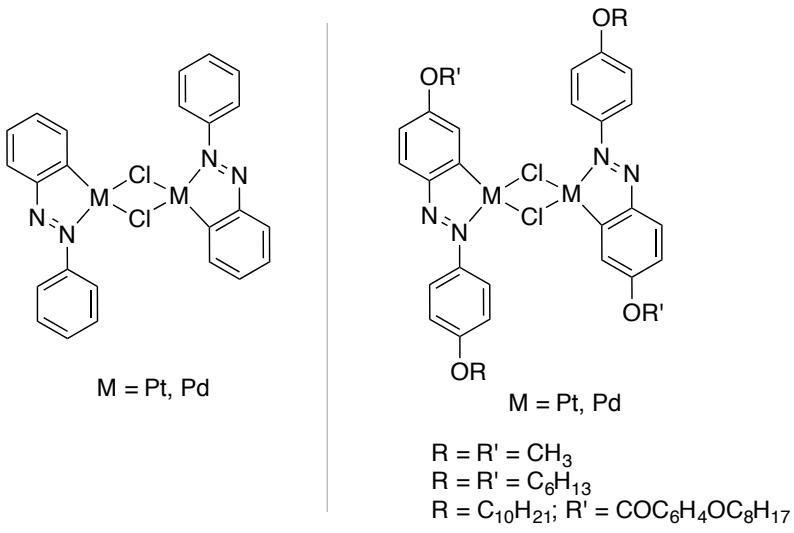

Figure 31: Known complexes with azobenzene.[171b, 174]

In regard of the targeted synthesis of liquid crystals azobenzene is extensively used as a ligand. Liquid crystals (LC) are non-isotropic liquids that have two refractive indexes.[175] The so called mesophase is an intermediate phase formed of the LC, which is situated in between the crystalline solid and an isotropic liquid.[176] The *cis* isomers of azobenzene are bent and usually not mesogenic, whereas the rod-shaped azobenzene units in *trans*-configuration are typical mesogens,[177] which is why the LCs of the latter case exhibit photochemical phase transition behavior.[178] Therefore, azobenzene LCs can be used in photocontrolled information storage, display devices and photoelectric sensors.[179] A typical way to design molecules that readily form an LC phase is to attach at least one flexible electron-donating group, such as alkyl or alkoxy groups.[179f, 180] The metallomesogens are metal containing liquid crystals, where the chemical or physical properties can be fine tuned by the use of different metal centers, e.g. platinum or palladium.[174]

Few examples of metal catalysts with an azobenzene unit for photocontrolled ring-opening polymerization (ROP) have been reported. Jones *et al*. synthesized different aluminium(III) and zinc(II) complexes (figure 32), that were investigated towards their potential use in ROP. Under variable light conditions, selective incorporation of monomers should be possible, resulting in polymers with different structures.[181] However, the photoisomerization of azobenzene can also be used in a huge variety of different application areas. For example in rhodium(II) complexes that intercalate into DNA, where upon light exposure the azobenzene moiety can stabilize the DNA double-helix and modulate DNA transcription due to its *cis*-form. Therefore it might be used as photoswitchable DNA molecular locks to regulate gene transcription.[182] Furthermore, azobenzene is widely used as a photochromic unit in photoswitchable catalysis.[168] It is important that such a catalyst has a difference in activity or selectivity for the “on” and “off” states, where irradiation with light can increase the selectivity or activity towards a single monomer, which can then incorporate into a chain.[181] Upon irradiation, a geometrical change must be induced, which can lead to a steric,[183] cooperative[184] or electronic effect[185] and which makes a catalyst effective. The aforementioned *trans*-*cis* isomerization of azobenzene makes it an excellent candidate for such purpose. In 1981 Ueno, Takahashi and Osa reported one of the earliest examples of photoswitchable catalysis, which is based on the conformational change of the isomerization of azobenzene.[183a]

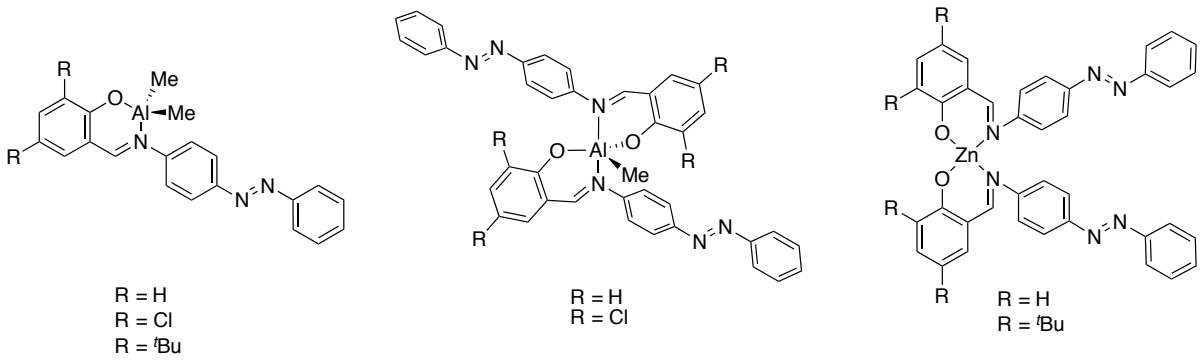

Figure 32: Aluminium(III) and zinc(II) complexes bearing azobenzene units.[181]

The fields mentioned above are only a small part of the possible applications of azobenzene. Due to its isomerization under UV-light and the wide range of possible incorporation into various building blocks azobenzene is still of interest in modern research.

1.1.4.3. Complexes with Redox-Active Ligands

Since humanity's need of energy increases, it is important to focus on renewable sources. One such source may be the sun, as it generates more energy per unit time than needed.[186] In this regard the development of devices that make this energy available is of great interest.[186] A focus of the development of alternative energy sources has already been on quinones, since they can be used in solar cells to harness solar energy in combination with an acceptor ligand and a metal center such as platinum(II).[187]

Platinum(II) complexes have been investigated intensively, since square planar platinum complexes (figure 33) are of great interest due to their mesomorphic properties,[188] possible use as antitumor agents[188] and photophysical properties.[188-189] The 2,2′-bipyridine (bpy) containing luminescent [Pt(bpy)Cl_2] is one of the first examples of square planar platinum complexes.[190] Regarding the potential application in efficient olefin polymerization reactions or C–H bond activation other -diimine ligands were used also.[191] Compared to the coordinatively saturated d^6 metal ion complexes, with ruthenium(II) or iridium(III) metal centers,[192] a further interesting feature of these d^8 platinum(II) systems is their potential reactivity through axial interaction.[193]

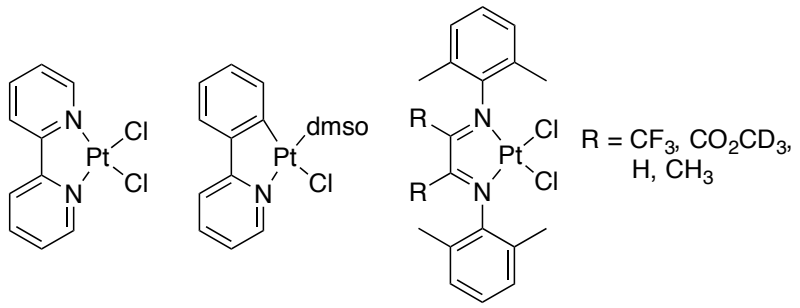

Figure 33: Square planar platinum(II) complexes with different acceptor ligands.[188, 190-191]

Bpy has been combined with a cobalt center and quinone ligands, which generated a complex that exhibits valence tautomerism, electronic isomers, that have different distributions of charge due to intramolecular electron transfer, which is triggered by external stimuli.[194] The Co complex, containing the 3,5-di-tert-butyl-o-benzoquinone (DB) in the cat (DB_{cat}) or sq (DB_{sq}) form, [Co^{III}(3,5-DB_{cat})(3,5-DB_{sq})(bpy)] is the first example of such a valence tautomer and was presented by Buchanan and Pierpont (figure 34).[195] An electron of the 3,5-DB_{cat} can be transferred to the LS cobalt(III) under thermal stimuli, resulting in a spin inversion to a HS cobalt(II), which is then coordinated to two 3,5-DB_{sq} ligands.[195]

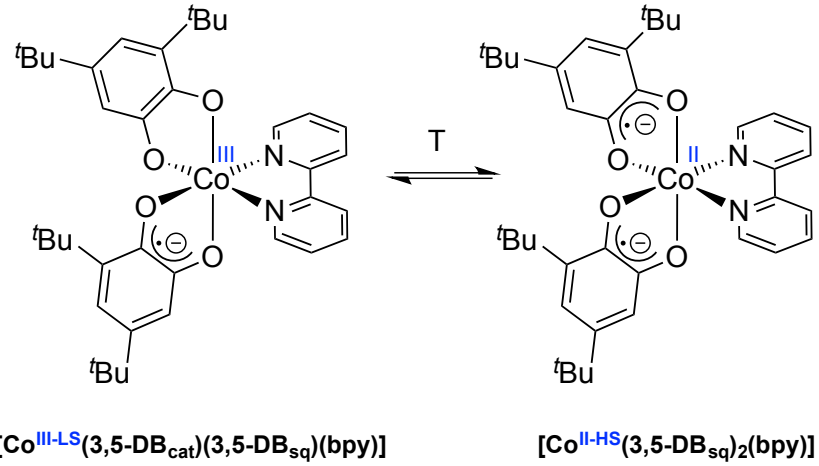

Figure 34: Valence tautomeric cobalt complex (Adapted from Buchanan and Pierpont).[195]

The combination of the aforementioned π-donor and π-acceptor ligands with different metal centers lead to stable systems,[196] which usually undergo intense ligand-to-ligand charge transfers (LLCTs) resulting in unique photophysical and photochemical properties on the metal complexes.[197] This makes them excellent candidates for application in small molecule activation,[198] dye-sensitized solar cells[199] and catalysis.[200] In order to synthesize donor-acceptor complexes bpy, pap, and phenyliminiomethylpyridine (pimp) have been applied as acceptor ligands for such systems.[196c, 201]

Weinstein *et al.* worked intensively on the characterization of the photophysical properties of donor-acceptor complexes and subsequently used them for the hydrogen production from water and harvesting of solar energy.[197a] The usually very intense LLCT transition of donor-acceptor complexes and their modular synthesis make them excellent candidates for solar energy applications, as the requirements for harnessing solar energy are the use of a strong chromophore and efficient charge separation.[202] In this regard, the challenges are the stabilization of the donor-acceptor complexes in long-term use and the use of expensive platinum or palladium.[199]

Subsequent work from Sarkar *et al.* used the asymmetric pap and pimp ligands as acceptor and the asymmetric catecholates and amidophenolates as donor ligands, which lead to different possible regioisomers. The pap and pimp isomers could be separated for two cases and via time-resolved infrared spectroscopy the strong charge-transfer character of the pap containing complexes examined.[187a, 201c] In addition, it was possible to show the redox-induced reactivity towards small molecules of isomeric platinum(II) based donor-acceptor systems (figure 35). The Lewis acidity at the metal center increases due to redox steps at the non-innocent ligands, which makes the platinum(II) center reactive for activating H_2 and towards PPh_3.[198]

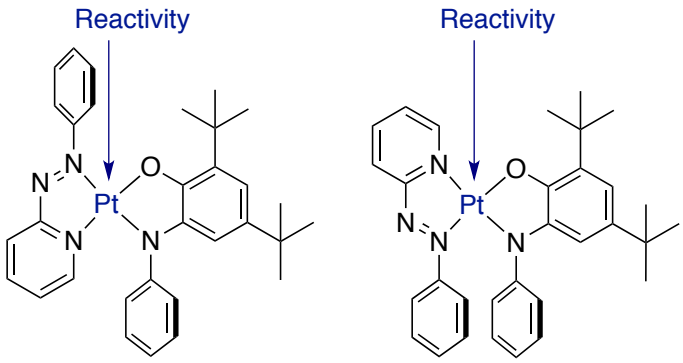

Figure 35: Platinum(II) complexes suitable for activation of small molecules.[198]

For the complexes with pimp as acceptor ligand different coordination motifs ([O,O]; [O,N] and [N,N]) were used for the quinone ligands (figure 36). Additionally, two asymmetric ligands were used, which can, as previously discussed, lead to the possible formation of two regioisomers, but for both cases only one isomer was isolated.[201c] This phenomenon might be explained by the *trans*- influence of the imino and pyridine fragment of the precursor and used ligand, which makes one isomer energetically more favorable by 0.2 eV, already showing that the use of an imino group instead of an azo group, as used in the pap ligand, can significantly affect the stereochemistry of such compounds.[201c] In addition, for the complexes with phenylenediamine ligands interesting redox-driven linkage isomerism was observed during the oxidation in UV/Vis-NIR spectroelectrochemical experiments, which results in stunning modifications in the NIR region of the spectrum of the isomers.[201c] Furthermore, some of these complexes can be applied in catalysis in the cross-dehydrogenative coupling of nucleophiles to *N*-phenyltetrahydroisoquinoline.[201c]

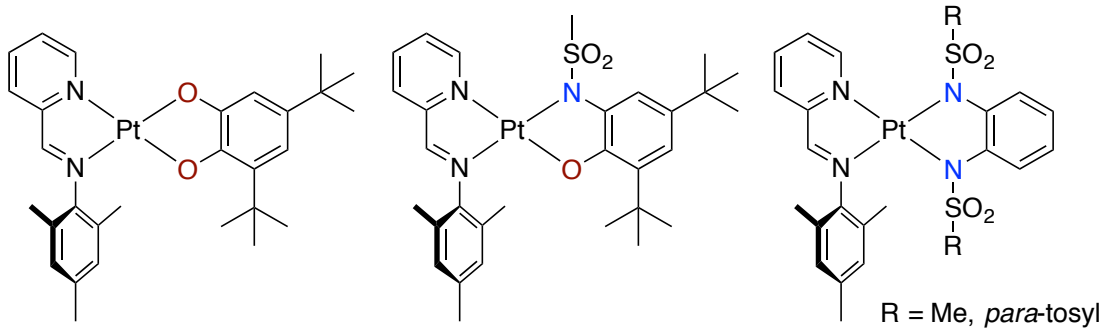

Figure 36: Examples of donor-acceptor complexes with pimp.[201c]

The intensive use of azobenzene in coordination and organometallic chemistry has already been mentioned. It has been used as a chelating ligand,[171a, 203] but azobenzene as a bis-chelating bridging ligand with metal centers is less reported.[172-173, 173e, 204] However, synthesis of a dinuclear platinum(II) complex bridged over azobenzene with two quinone ligands was performed. In comparison to the mononuclear complex the site of the reduction can be shifted by either changing the metal center or by varying the number of metal centers.[205] Furthermore, mononuclear complexes that combine an azobenzene and a quinone ligand were subsequently published. The mononuclear azobenzene complexes were investigated towards their non-innocent nature by a combination of electrochemical and UV/Vis-NIR spectroelectrochemical methods.[206] The palladium(II) complexes, depicted in figure 37, show a double redox activity of both ligands.[206]

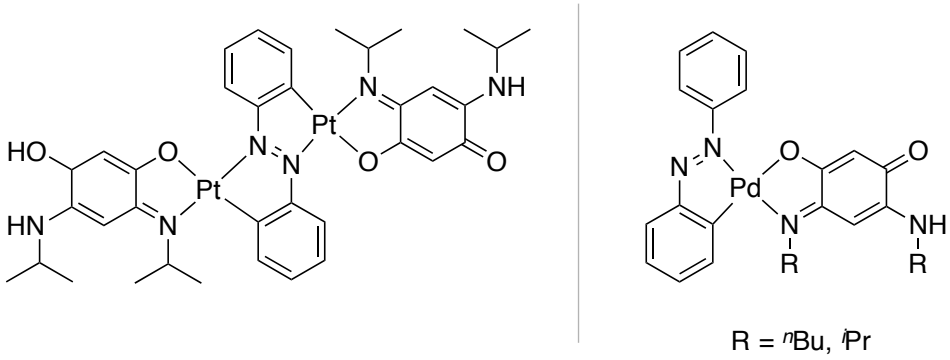

Figure 37: Known metal complexes bearing azobenzene and quinone ligands.[205-206]

Furthermore, dinuclear complexes bridged over a quinone ligand have been reported, for example with ruthenium(II),[110a, 207] palladium(II),[208] and platinum(II).[208] They are of interest as they can be used as linker in metal-organic frameworks,[209] in new organometallic supramolecular architectures[210] or as anticancer reagents.[211]

Moreover, ruthenium complexes with [O,N,O,N] substituted quinone were investigated towards their electrochemical behavior.[207a] By changing the substituents on the bridge the redox potentials of the ligand can be altered.[207a] Furthermore, for the complexes with bpy

(figure 38), a switchable NIR absorption was observed, where an one-electron transfer leads to NIR bands that can be switched on and off.[207a] In addition, mixed-valent species were detected in the ruthenium complex with acetylacetonato (acac) ligands, where upon oxidation a ruthenium(III)–ruthenium(IV) species was obtained while reduction leads to a ruthenium(III)– ruthenium(III) quinonoid radical-containing species.[207b]

Using similar bridging ligands, a platinum complex, a palladium complex, as well as a platinum complex with azophenine as a bridge were studied, with all complexes containing two additional azobenzene units.[208] The electrochemical investigations showed the dependency of the metal center as well of the bridge.[208] The metal complexes display strong electrochromic behavior, as upon stepwise reduction the complexes show absorption bands in the NIR region, and their position and intensity can be controlled by the redox state of the compounds.[208] Moreover, the platinum(II) complex with the [O,N,O,N] donor set has an extinction coefficient of more than 180000 $M^{-1}cm^{-1}$ in its doubly reduced form.[208] For such transitions in metal complexes this is one of the largest values observed. In these metal complexes a strongly delocalized nature of the frontier orbitals was revealed through a combination of EPR spectroscopy and (TD)DFT calculations.[208] The occurrence of NIR bands of high intensity and strong electrochromic behavior in these metal complexes is probably brought by this delocalization and the resulting extended π-systems.[208] In this study, they showed how the combination of multiple redox-active ligands with square-planar metal centers could generate new compounds that are highly electrochromic and redox-rich.[208]

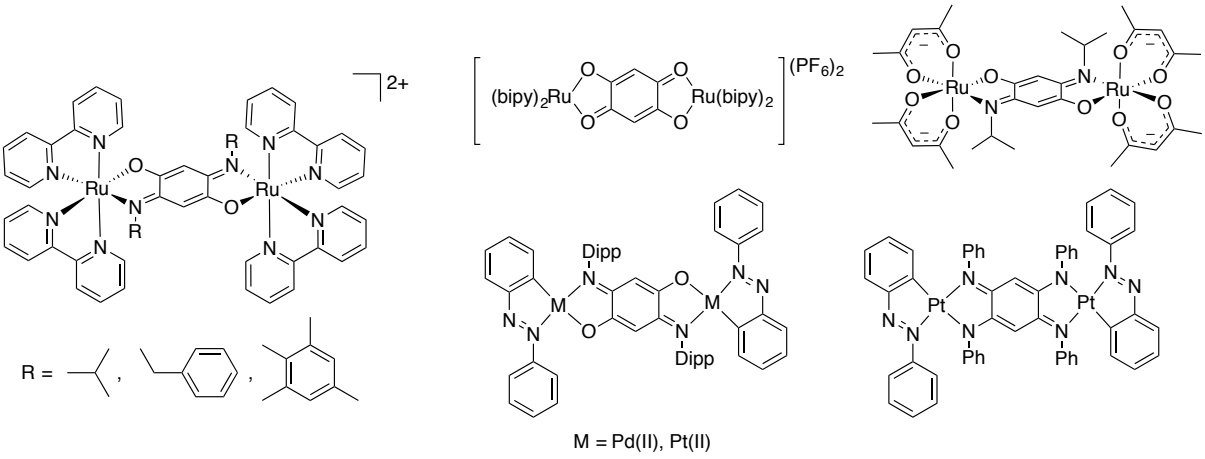

Figure 38: Known metal complexes bridged over a quinone ligand.[110a, 207-208]

1.2. Electrochemistry

In this work, electrochemical and spectroelectrochemical techniques have been used to characterize various molecular redox properties. Therefore, these methods will be briefly discussed with respect to their advantages, limitations, and challenges. In principle, electrochemistry is about the transfer of electrons during chemical changes and it provides valuable tools for both, the preparative and analytical chemist and to analyze reactions that involve electron transmission.[212]

For the analysis of such electron transfer processes and chemical reactions cyclic voltammetry (CV) is a standard technique.[213] The setup consists of a cell with a three-electrode system, which includes a working-electrode, a reference-electrode and a counter electrode. CV can be used to investigate a variety of redox processes, for example, the kinetics of electron transfer[214] or the reversibility of an electrochemical reaction.[215] In this context, metal complexes can be evaluated regarding the influence of substituents of redox-active ligands and their respective metal centers on the redox behavior. Furthermore, the study of electron transfer-initiated chemical reactions also includes catalytic reactions.[212] Hence, the basics of electrocatalysis and the spectroelectrochemical techniques will be discussed below.

1.2.1. Electrocatalysis

In consideration of the threat of climate change, the constantly growing population and the associated problems such as rising demand for energy or chemical products, it is important to develop new catalysts that facilitate chemical reactions[216] and to further develop energy sources. Therefore, the study of molecular electrocatalysts and subsequent reactions gained importance for new technologies,[217] i.e., water oxidation or oxygen, proton, or CO_2 reduction, as they involve the storage or release of energy.[218] CO_2 has attracted interest, as it is the most important gas contributing to the greenhouse effect. Furthermore, it is an important source of carbon and can be electrochemically reduced to fuels.[219]

Because of the high overpotential of the reductive cathodic process, selective electrochemical CO_2 reduction is still a subject of research, even after the concept was developed decades ago.[218b, 220] The electronic properties of the various applied ligands, e.g. *N*-heterocyclic carbenes or tpy, can be tuned by introducing a stronger electron-donating ligand, which increases the CO_2 activation rate.[221] However, since a stronger electron donating ligand usually leads to a more negative reduction potential, an unwanted increase in the overpotential is induced.[221] The design of a catalyst, in which two different ligands were introduced, is one possibility to solve this problem.[221] In such a system one ligand controls

the reduction potentials, whereas the other controls the kinetics of chemical steps.[221] In this regard, the group of Miller examined ruthenium(II) complexes bearing a bidentate and a tpy ligand, which also affects the *trans* effect in electrocatalysis.[221-222]

The use of a catalyst lowers the energy of a reaction transition state (TS) in the conversion of substrates to the desired product (figure 39). With the use of a catalyst the reaction conditions are less drastic and require lower temperatures, for example.

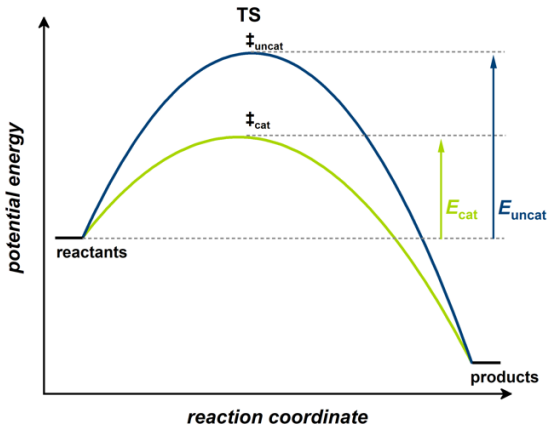

Figure 39: Energy diagram for a single-step reaction with (green) and without (black) a catalyst.

In contrast to a "standard" homogeneous catalysis, in which the substrates and the catalysts are in the same phase,[223] electrocatalysis is used for the electrochemical generation of the active form of a catalyst, and can be heterogeneous. In the latter case the solid electrode acts as the electron donor (or acceptor) of the outer sphere to the liquid electrolyte.[219, 223]

In an electrochemical reaction a species, A, with charge z can be reduced or oxidized at the electrode leading to compound B with a charge of z–1 or z+1. However, if an electrochemical catalyst is involved, the pre-catalyst, P, has to be reduced at the electrode to form the active catalyst Q. Q catalyzes the reaction from A to product B, by transferring an electron to A, while P is regenerated. When P is reduced a second time, the catalysis process is repeated until A is either fully converted or the potential is reset to a potential, where P cannot be further reduced or decomposes. The direct electrochemical reaction and the reaction, applying a catalyst are depicted in figure 40.

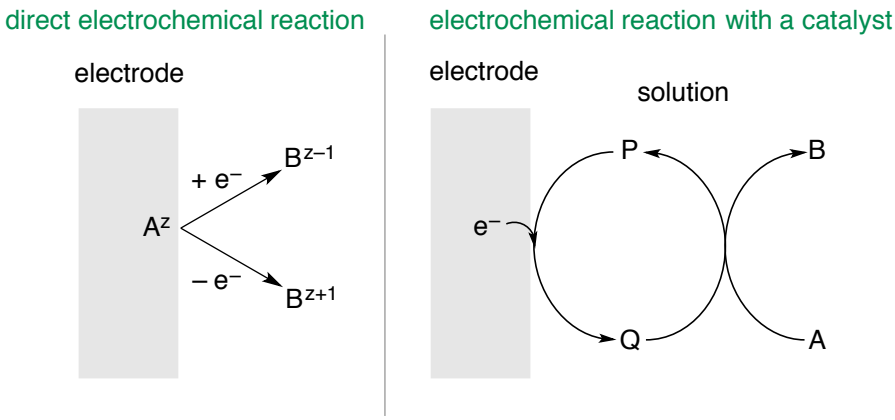

Figure 40: Representation of a direct and a catalyzed electrochemical reaction (adapted from Savéant).[219]

In regards to CV and electrocatalysis, the kinetic zone diagram needs to be mentioned. This diagram was introduced by Savéant and Su and is used for electrocatalytic systems and their voltammetric responses.[224] It is of interest for electrochemical reactions to obtain mechanistic insight into molecular catalysts that can be derived from current-potential curves, which are obtained with CV.[224a] A simple one-electron, one substrate electrocatalytic reaction (EC′) was described mathematically by Savéant and Su.[224b] In the kinetic zone diagram nine 'zones' are classified and various waveforms have been determined on the basis of dimensionless parameters. However, there is no catalyst that exhibits waveforms corresponding to all nine zones. But examples of catalysts with a voltammetric response equivalent to two or three adjacent zones in the EC′-zone diagram have been reported.[224a] Regarding the aforementioned one-electron reduction of a substrate, A to B, the possible waveforms of the CV are described pictorially as a function of the two dimensionless parameters λ (the kinetic factor) and γ (the excess factor) (eq. 3 and 4).[225]

$$P + e^- \rightleftharpoons Q \tag{1}$$

$$Q + A \xrightarrow{k_e} P + B \tag{2}$$

$$\lambda = \left(\frac{RT}{F}\right)\left(\frac{k_e C_P^0}{v}\right) \tag{3}$$

$$\gamma = \frac{C_A^0}{C_P^0} \tag{4}$$

These equations include the homogeneous electron transfer rate k_e, the scan rate v, as well as the ignition concentrations of substrate A C_A^0 and catalyst P C_P^0. An important application of the homogeneous electrocatalytic EC′-zone diagram is to identify the zone of the obtained CV and tune the kinetic (λ) and excess (γ) parameters to provide access to other zones.[225-226] Furthermore, the overpotential η and the kinetic rate contant (k_{obs}) can be used to evaluate the quality of the catalyst.[225] The overpotential η, a thermodynamic parameter, is the difference

between the standard potential $E^0_{\mathrm{A/B}}$ and the applied potential E_{cat} of the catalyzed reaction of compound A to B (eq. 5), which is defined as the driving force of a reaction.[225-226]

$$\eta = E_{\mathrm{cat}} - E^0_{\mathrm{A/B}} \tag{5}$$

But for quantitative and direct comparison of catalysts, the overpotential should not be a general method, as there are several possible ways to determine η.[225] If the same conditions for the measurements of a series of catalyst are used, the overpotential can be used in order to compare these catalysts.[225]

For the reaction described in eq. 2 the parameter k_{obs} (defined by eq. 6) is the rate of the formation of P from Q through a homogeneous reaction.[225]

$$k_{obs} = k_e C_A^0 \tag{6}$$

Considering a CV experiment with an S-shaped curve, which corresponds to an ideal catalytic reaction, the current (i) of the curve can be described by eq 7,

$$i = \frac{nFAC_P^0\sqrt{Dk_{\mathrm{obs}}}}{1+\exp\left[\frac{nF}{RT}\left(E - E^0_{\mathrm{P/Q}}\right)\right]} \tag{7}$$

where n is the number of transferred electrons, F is the Faraday constant, A is the electrode surface, D is the diffusion coefficient, R is the gas constant, T is the temperature, C_P^0 is the bulk concentration of the pre-catalyst P, E is the applied potential and $E^0_{\mathrm{P/Q}}$ is the standard potential in absence of substrate of the redox couple P/Q.[225]

If a catalytic plateau current is observed, eq. 7 simplifies to

$$i_c = nFAC_P^0\sqrt{Dk_{\mathrm{obs}}} \tag{8}$$

and after applying the Randles-Sevcik equation, eq. 9,[227] which describes for a reversible redox process the dependence of the peak current i_{p} and the scan rate v, the relationship depicted in eq. 10 is obtained.[225]

$$i_p = 0.4633\, nFAC_P^0\sqrt{\frac{nFvD}{RT}} \tag{9}$$

$$\frac{i_c}{i_p} = 2.24\sqrt{\frac{RT}{nFv}k_{\mathrm{obs}}} \tag{10}$$

As eq. 10 does not require an independent measurement of D, A and C_P^0 it is more favored in experimental settings. The discussed equations have been applied for the estimation of the catalytic rates of more complex systems, although they require approximations.[225]

1.2.2. Spectroelectrochemistry

The first publications, which concern spectroelectrochemistry (SEC), the combination of spectroscopic and electrochemical methods,[228] date back more than half a century.[229] However, the first SEC experiment was performed by Kuwana et al. in 1964.[230] One major

drawback of electrochemical methods is, that they indicate redox processes, but do not allow determining the involved species. To determine the involved species additional experimental techniques need to be applied.[231] Therefore, experiments were developed, where the electrochemical measurements are combined with several spectroscopic methods, e.g, infrared (IR),[231] Raman,[231] EPR,[232] NMR,[233] or UV/Vis/NIR spectroscopies.[234] SEC has been growing as a useful tool in inorganic chemistry since it can help in characterizing the site of a redox process as metal- or ligand-based.[235]

The setup for UV/Vis/NIR SEC measurements typically utilizes an optically transparent thin layer electrochemical cell (OTTLE cell) with a three-electrode setup (a working electrode (e.g. Au or Pt), a counter electrode (Pt) and a reference electrode (Ag)) can be applied. A major drawback is the longer electrolysis time, which requires robust systems. In general, it is possible to perform *ex-situ* and *in-situ* experiments. In the case of the *ex-situ* measurement, a sample with a long-lived intermediate is required since the solution is electrolyzed outside of the spectrometer. But a major advantage is the use of non-specialized equipment for the spectroscopic and electrochemical setup. For the *in-situ* measurements, a specialized cell (e.g., the OTTLE cell) needs to be built, but the benefit of spectroscopic tracking of the (electro)chemical conversion is very beneficial.[236]

If a paramagnetic metallic species or ligand is present, EPR SEC measurements can be performed, to get further information on the electrochemically generated species. A drawback of this technique are the EPR tubes, which act as the electrochemical cell and usually only offer a low volume and poor electrode geometry, which may lead to high resistance inside the cell.[232] In addition, many cells operate only near or at room temperature, as it is very difficult for typical electrochemical cells to operate at low temperatures in the cavity.[237] For the setup for EPR SEC measurements a three-electron setup is used, where thin metal wires (of approximately 0.1mm and coated with polytetrafluoroethylene) are used, which are placed into a usual EPR tube. The counter electrode needs to be sufficiently removed from the EPR measurement cavity, but simultaneously near to the working electrode, to prevent the detection of paramagnetic side products yet allow detection of the desired species at the working electrode. Due to these challenges the samples are typically generated *ex-situ* where the paramagnetic intermediate is electrogenerated outside the spectrometer and afterward transferred to a conventional EPR tube, which can then be cooled or frozen if desired.[238] To assign if the respective redox process is ligand-centered or metal-based, EPR SEC is a powerful tool.[235]

1.3. References

[1] V. Bhatt in *Chapter 1 - Basic Coordination Chemistry*, (Ed. V. Bhatt), Academic Press, **2016**, pp. 1-35.
[2] J. Klein, U. Albold, L. Suntrup and B. Sarkar, *ChemPhotoChem* **2018**, *2*, 357-361.
[3] J.-F. Ayme and J.-M. Lehn in *Chapter One - From Coordination Chemistry to Adaptive Chemistry*, *Vol. 71* Eds.: R. van Eldik and R. Puchta), Academic Press, **2018**, pp. 3-78.
[4] K. Reichenbächer, H. I. Süss and J. Hulliger, *Chem. Soc. Rev.* **2005**, *34*, 22-30.
[5] A. G. Blackman, *Polyhedron* **2005**, *24*, 1-39.
[6] a) G. Anderegg and F. Wenk, *Helv. Chim. Acta* **1967**, *50*, 2330-2332; b) A. G. Blackman, *Eur. J. Inorg. Chem.* **2008**, *2008*, 2633-2647.
[7] A. Kaur, T. G. Ribelli, K. Schröder, K. Matyjaszewski and T. Pintauer, *Inorg. Chem.* **2015**, *54*, 1474-1486.
[8] F. Weisser, S. Hohloch, S. Plebst, D. Schweinfurth and B. Sarkar, *Chem. Eur. J.* **2014**, *20*, 781-793.
[9] R. H. Fish, M. S. Konings, K. J. Oberhausen, R. H. Fong, W. M. Yu, G. Christou, J. B. Vincent, D. K. Coggin and R. M. Buchanan, *Inorg. Chem.* **1991**, *30*, 3002-3006.
[10] T. N. Sorrell and D. L. Jameson, *Inorg. Chem.* **1982**, *21*, 1014-1019.
[11] a) H. G. Jang, D. D. Cox and L. Que, *J. Am. Chem. Soc.* **1991**, *113*, 9200-9204; b) A. Nanthakumar, S. Fox, N. N. Murthy, K. D. Karlin, N. Ravi, B. H. Huynh, R. D. Orosz, E. P. Day, K. S. Hagen and N. J. Blackburn, *J. Am. Chem. Soc.* **1993**, *115*, 8513-8514; c) K. D. Karlin, A. Nanthakumar, S. Fox, N. N. Murthy, N. Ravi, B. H. Huynh, R. D. Orosz and E. P. Day, *J. Am. Chem. Soc.* **1994**, *116*, 4753-4763.
[12] K. S. Min, A. DiPasquale, A. L. Rheingold and J. S. Miller, *Inorg. Chem.* **2007**, *46*, 1048-1050.
[13] a) K. Chen, M. Costas, J. Kim, A. K. Tipton and L. Que, *J. Am. Chem. Soc.* **2002**, *124*, 3026-3035; b) K. Chen, M. Costas and J. L. Que, *J. Chem. Soc., Dalton Trans.* **2002**, 672-679; c) J. Y. Ryu, J. Kim, M. Costas, K. Chen, W. Nam and L. Que Jr, *Chem. Commun.* **2002**, 1288-1289; d) J. Xia and K. Matyjaszewski, *Macromolecules* **1999**, *32*, 2434-2437; e) J.-W. Wang, H.-H. Huang, J.-K. Sun, T. Ouyang, D.-C. Zhong and T.-B. Lu, *ChemSusChem* **2018**, *11*, 1025-1031.
[14] a) M. Yamaguchi, H. Kousaka, S. Izawa, Y. Ichii, T. Kumano, D. Masui and T. Yamagishi, *Inorg. Chem.* **2006**, *45*, 8342-8354; b) G. J. P. Britovsek, J. England and A. J. P. White, *Inorg. Chem.* **2005**, *44*, 8125-8134.
[15] Z. Dai and J. W. Canary, *New J. Chem.* **2007**, *31*, 1708-1718.
[16] O. Dimroth, *Justus Liebigs Ann. Chem.* **1909**, *364*, 183-226.
[17] R. Huisgen, *Proc. Chem. Soc.* **1961**, 357-396.
[18] Z.-G. Wu, X.-J. Liao, L. Yuan, Y. Wang, Y.-X. Zheng, J.-L. Zuo and Y. Pan, *Chem. Eur. J.* **2020**, *26*, 5694-5700.
[19] H. C. Kolb and K. B. Sharpless, *Drug Discov. Today* **2003**, *8*, 1128-1137.
[20] B. Schulze and U. S. Schubert, *Chem. Soc. Rev.* **2014**, *43*, 2522-2571.
[21] L. Liang and D. Astruc, *Coord. Chem. Rev.* **2011**, *255*, 2933-2945.
[22] a) D. Schweinfurth, L. Hettmanczyk, L. Suntrup and B. Sarkar, *Z. Anorg. Allg. Chem.* **2017**, *643*, 554-584; b) M. S. Singh, S. Chowdhury and S. Koley, *Tetrahedron* **2016**, *72*, 5257-5283.

[23] Q. Zhu, S. Chen, F. Xu and J. Zhu, *Inorg. Chem.* **2020**.
[24] D. Schweinfurth, S. Strobel and B. Sarkar, *Inorg. Chim. Acta* **2011**, *374*, 253-260.
[25] Y. Li, X. Qi, Y. Lei and Y. Lan, *RSC Adv.* **2015**, *5*, 49802-49808.
[26] F. Himo, T. Lovell, R. Hilgraf, V. V. Rostovtsev, L. Noodleman, K. B. Sharpless and V. V. Fokin, *J. Am. Chem. Soc.* **2005**, *127*, 210-216.
[27] a) L. Zhang, X. Chen, P. Xue, H. H. Y. Sun, I. D. Williams, K. B. Sharpless, V. V. Fokin and G. Jia, *J. Am. Chem. Soc.* **2005**, *127*, 15998-15999; b) R. Berg, J. Straub, E. Schreiner, S. Mader, F. Rominger and B. F. Straub, *Adv. Synth. Catal.* **2012**, *354*, 3445-3450; c) J. E. Hein, J. C. Tripp, L. B. Krasnova, K. B. Sharpless and V. V. Fokin, *Angew. Chem. Int. Ed.* **2009**, *48*, 8018-8021.
[28] N. Candelon, D. Lastécouères, A. K. Diallo, J. Ruiz Aranzaes, D. Astruc and J.-M. Vincent, *Chem. Commun.* **2008**, 741-743.
[29] a) P. S. Donnelly, S. D. Zanatta, S. C. Zammit, J. M. White and S. J. Williams, *Chem. Commun.* **2008**, 2459-2461; b) T. R. Chan, R. Hilgraf, K. B. Sharpless and V. V. Fokin, *Org. Lett.* **2004**, *6*, 2853-2855.
[30] D. Schweinfurth, J. Klein, S. Hohloch, S. Dechert, S. Demeshko, F. Meyer and B. Sarkar, *Dalton Trans.* **2013**, *42*, 6944-6952.
[31] a) D. Schweinfurth, J. Krzystek, M. Atanasov, J. Klein, S. Hohloch, J. Telser, S. Demeshko, F. Meyer, F. Neese and B. Sarkar, *Inorg. Chem.* **2017**, *56*, 5253-5265; b) D. Schweinfurth, S. Demeshko, M. G. Sommer, S. Dechert, F. Meyer and B. Sarkar, *Eur. J. Inorg. Chem.* **2016**, *2016*, 2581-2585; c) D. Schweinfurth, F. Weisser, D. Bubrin, L. Bogani and B. Sarkar, *Inorg. Chem.* **2011**, *50*, 6114-6121.
[32] a) M. G. Sommer, R. Marx, D. Schweinfurth, Y. Rechkemmer, P. Neugebauer, M. van der Meer, S. Hohloch, S. Demeshko, F. Meyer, J. van Slageren and B. Sarkar, *Inorg. Chem.* **2017**, *56*, 402-413; b) A. L. Ward, L. Elbaz, J. B. Kerr and J. Arnold, *Inorg. Chem.* **2012**, *51*, 4694-4706.
[33] D. Schweinfurth, S. Demeshko, S. Hohloch, M. Steinmetz, J. G. Brandenburg, S. Dechert, F. Meyer, S. Grimme and B. Sarkar, *Inorg. Chem.* **2014**, *53*, 8203-8212.
[34] P. Gütlich, Y. Garcia and H. A. Goodwin, *Chem. Soc. Rev.* **2000**, *29*, 419-427.
[35] S. Venkataramani, U. Jana, M. Dommaschk, F. D. Sönnichsen, F. Tuczek and R. Herges, *Science* **2011**, *331*, 445-448.
[36] a) S. Hayami, R. Moriyama, Y. Shigeyoshi, R. Kawajiri, T. Mitani, M. Akita, K. Inoue and Y. Maeda, *Inorg. Chem.* **2005**, *44*, 7295-7297; b) D. Shao, L. Shi, L. Yin, B.-L. Wang, Z.-X. Wang, Y.-Q. Zhang and X.-Y. Wang, *Chem. Sci.* **2018**, *9*, 7986-7991; c) V. García-López, M. Palacios-Corella, V. Gironés-Pérez, C. Bartual-Murgui, J. A. Real, E. Pellegrin, J. Herrero-Martín, G. Aromí, M. Clemente-León and E. Coronado, *Inorg. Chem.* **2019**, *58*, 12199-12208.
[37] H. Toftlund, *Coord. Chem. Rev.* **1989**, *94*, 67-108.
[38] S. Hayami, Y. Komatsu, T. Shimizu, H. Kamihata and Y. H. Lee, *Coord. Chem. Rev.* **2011**, *255*, 1981-1990.
[39] E. Koenig and K. Madeja, *Inorg. Chem.* **1967**, *6*, 48-55.
[40] R. C. Stoufer, D. H. Busch and W. B. Hadley, *J. Am. Chem. Soc.* **1961**, *83*, 3732-3734.
[41] P. Gütlich and H. A. Goodwin, *Spin Crossover in Transition Metal Compounds I, II, and III*, Springer, Berlin, Germany, **2004**.

[42] M. A. Halcrow, *Chemical Society Reviews* **2011**, *40*, 4119-4142.
[43] A. Baschieri, A. Mazzanti, S. Stagni and L. Sambri, *Eur. J. Inorg. Chem.* **2013**, *2013*, 2432-2439.
[44] P. Sangtrirutnugul, P. Maisopa, L. Chaicharoenwimolkul, A. Sunsin, E. Somsook and V. Reutrakul, *J. Appl. Polym. Sci.* **2013**, *127*, 2757-2763.
[45] S. Nestke, J. Stubbe, R. Koehler, E. Ronge, U. Albold, W. Vioel, C. Jooss, B. Sarkar and I. Siewert, *Z. Anorg. Allg. Chem.* **2022**, *648*, e202200119.
[46] a) Y. Zhou, K. Liu, J.-Y. Li, Y. Fang, T.-C. Zhao and C. Yao, *Org. Lett.* **2011**, *13*, 1290-1293; b) J. Rosenthal and S. J. Lippard, *J. Am. Chem. Soc.* **2010**, *132*, 5536-5537.
[47] S. Huang, R. J. Clark and L. Zhu, *Org. Lett.* **2007**, *9*, 4999-5002.
[48] B. Xu, W. Zhong, Z. Wei, H. Wang, J. Liu, L. Wu, Y. Feng and X. Liu, *Dalton Trans.* **2014**, *43*, 15337-15345.
[49] J. R. Cubanski, M. E. Reish, A. G. Blackman, P. J. Steel, K. C. Gordon, D. A. McMorran and J. D. Crowley, *Aust. J. Chem.* **2015**, *68*, 1160-1170.
[50] F. Weisser, H. Stevens, J. Klein, M. van der Meer, S. Hohloch and B. Sarkar, *Chem. Eur. J.* **2015**, *21*, 8926-8938.
[51] M. Jevric, T. Zheng, N. K. Meher, J. C. Fettinger and M. Mascal, *Angew. Chem. Int. Ed.* **2011**, *50*, 717-719.
[52] a) P. Etayo, C. Ayats and M. A. Pericàs, *Chem. Commun.* **2016**, *52*, 1997-2010; b) S. Özçubukçu, E. Ozkal, C. Jimeno and M. A. Pericàs, *Org. Lett.* **2009**, *11*, 4680-4683.
[53] B. Li, A. Hagenbach and U. Abram, *Inorg. Chem.* **2019**, *58*, 7925-7930.
[54] E. T. Papish, T. M. Donahue, K. R. Wells and G. P. A. Yap, *Dalton Trans.* **2008**, 2923-2925.
[55] G. T. Morgan and F. H. Burstall, *J. Chem. Soc.* **1932**, 20-30.
[56] K. W. Jennette, S. J. Lippard, G. A. Vassiliades and W. R. Bauer, *PNAS USA* **1974**, *71*, 3839-3843.
[57] a) N. Elgrishi, M. B. Chambers, V. Artero and M. Fontecave, *Phys. Chem. Chem. Phys.* **2014**, *16*, 13635-13644; b) N. Elgrishi, S. Griveau, M. B. Chambers, F. Bedioui and M. Fontecave, *Chem. Commun.* **2015**, *51*, 2995-2998.
[58] a) C. Wei, Y. He, X. Shi and Z. Song, *Coord. Chem. Rev.* **2019**, *385*, 1-19; b) K. M. M. Huihui, R. Shrestha and D. J. Weix, *Org. Lett.* **2017**, *19*, 340-343.
[59] R. Tatikonda, S. Bhowmik, K. Rissanen, M. Haukka and M. Cametti, *Dalton Trans.* **2016**, *45*, 12756-12762.
[60] a) S. Aroua, T. K. Todorova, P. Hommes, L.-M. Chamoreau, H.-U. Reissig, V. Mougel and M. Fontecave, *Inorg. Chem.* **2017**, *56*, 5930-5940; b) J. P. Sauvage, J. P. Collin, J. C. Chambron, S. Guillerez, C. Coudret, V. Balzani, F. Barigelletti, L. De Cola and L. Flamigni, *Chem. Rev.* **1994**, *94*, 993-1019.
[61] R. A. Fallahpour, *Synthesis* **2003**, *2*, 155–184.
[62] S. A. Sapp, C. M. Elliott, C. Contado, S. Caramori and C. A. Bignozzi, *J. Am. Chem. Soc.* **2002**, *124*, 11215-11222.
[63] a) W. R. McWhinnie and J. D. Miller, *Adv. Inorg. Chem. Radiochem.* **1969**, *12*, 135-215; b) E. C. Constable, *Adv. Inorg. Chem. Radiochem.* **1986**, *30*, 69-121; c) U. S. Schubert, H. Hofmeier and G. R. Newkome, *Modern Terpyridine Chemistry*, Wiley-VCH, Weinheim, **2006**, p.

[64] J. M. Ludlow, Z. Guo, A. Schultz, R. Sarkar, C. N. Moorefield, C. Wesdemiotis and G. R. Newkome, *Eur. J. Inorg. Chem.* **2015**, 5662–5668.
[65] M. L. Moss and M. G. Mellon, *Ind. Eng. Chem., Anal. Ed.* **1942**, *14*, 862-865.
[66] D. B. Taylor, K. P. Callahan and I. Shaikh, *J. Med. Chem.* **1975**, *18*, 1088-1094.
[67] G. Ciantelli, P. Legittimo and F. Pantani, *Anal. Chim. Acta* **1971**, *53*, 303-308.
[68] M. Howe-Grant, K. C. Wu, W. R. Bauer and S. J. Lippard, *Biochem.* **1976**, *15*, 4339-4346.
[69] H. Wang, F. Cai, D. Feng, L. Zhou, D. Li, Y. Wei, Z. Feng, J. Zhang, J. He and Y. Wu, *J. Mol. Struct.* **2019**, *1194*, 157-162.
[70] D. L. Jameson, L. E. Guise, C. A. Bessel and K. Takeuchi, *Inorganic Syntheses*, **1998**, p. 46–50.
[71] Y. Yamamoto, T. Tanaka, M. Yagi and M. Inamoto, *Heterocycles* **1996**, 189–194.
[72] F.-Q. Fang and G. S. Hanan, *Synlett* **2003**, *6*, 852–854.
[73] a) F. Kröhnke, *Synthesis* **1976**, 1–24; b) I. Eryazici, C. N. Moorefield, S. Durmus and G. R. Newkome, *J. Org. Chem.* **2006**, *71*, 1009-1014; c) J. Sauer, D. K. Heldmann and G. R. Pabst, *Eur. J. Org. Chem.* **1999**, 313–321; d) G. Onodera, Y. Shimizu, J.-n. Kimura, J. Kobayashi, Y. Ebihara, K. Kondo, K. Sakata and R. Takeuchi, *J. Am. Chem. Soc.* **2012**, *134*, 10515-10531.
[74] a) N. Elgrishi, M. B. Chambers and M. Fontecave, *Chem. Sci.* **2015**, *6*, 2522-2531; b) J. Chambers, B. Eaves, D. Parker, R. Claxton, P. S. Ray and S. J. Slattery, *Inorg. Chim. Acta* **2006**, *359*, 2400-2406.
[75] E. C. Constable and M. D. Ward, *J. Chem. Soc., Dalton Trans.* **1990**, 1405-1409.
[76] V. Grosshenny and R. Ziessel, *J. Organomet. Chem.* **1993**, *453*, C19-C22.
[77] K. Potts, *Bull. Soc. Chim. Belg.* **1990**, *99*, 741.
[78] P. Hommes, C. Fischer, C. Lindner, H. Zipse and H.-U. Reissig, *Angew. Chem. Int. Ed.* **2014**, *53*, 7647-7651.
[79] J. England, C. C. Scarborough, T. Weyhermüller, S. Sproules and K. Wieghardt, *Eur. J. Inorg. Chem.* **2012**, *2012*, 4605-4621.
[80] J. Klein, A. Stuckmann, S. Sobottka, L. Suntrup, M. van der Meer, P. Hommes, H.-U. Reissig and B. Sarkar, *Chem. Eur. J.* **2017**, *23*, 12314-12325.
[81] a) S. G. Shepard, S. M. Fatur, A. K. Rappé and N. H. Damrauer, *J. Am. Chem. Soc.* **2016**, *138*, 2949-2952; b) D. G. Brown, N. Sanguantrakun, B. Schulze, U. S. Schubert and C. P. Berlinguette, *J. Am. Chem. Soc.* **2012**, *134*, 12354-12357.
[82] P.-G. d. Gennes, *Angew. Chem. Int. Ed.* **1992**, *31*, 842–845.
[83] a) M. Daoud and C. E. Williams, *Soft Matter Physics*, Springer Verlag, Berlin, **1993**, p; b) I. W. Hamley, *Introduction to Soft Matter*, Wiley, Chichester, **2000**, p; c) M. Kleman and O. D. Lavrentovich, *Soft Matter Physics: An Introduction*, Springer, **2003**, p.
[84] R. Akiyoshi, R. Ohtani, L. F. Lindoy and S. Hayami, *Dalton Trans.* **2021**, *50*, 5065-5079.
[85] a) J. S. Judge and W. A. Baker, *Inorg. Chim. Acta* **1967**, *1*, 68-72; b) S. Kremer, W. Henke and D. Reinen, *Inorg. Chem.* **1982**, *21*, 3013-3022.
[86] S. Hayami, Y. Shigeyoshi, M. Akita, K. Inoue, K. Kato, K. Osaka, M. Takata, R. Kawajiri, T. Mitani and Y. Maeda, *Angew. Chem. Int. Ed.* **2005**, *44*, 4899-4903.

[87] a) S. Hayami, R. Moriyama, A. Shuto, Y. Maeda, K. Ohta and K. Inoue, *Inorg. Chem.* **2007**, *46*, 7692-7694; b) S. Hayami, K. Murata, D. Urakami, Y. Kojima, M. Akita and K. Inoue, *Chem. Commun.* **2008**, 6510-6512; c) S. Hayami, D. Urakami, Y. Kojima, H. Yoshizaki, Y. Yamamoto, K. Kato, A. Fuyuhiro, S. Kawata and K. Inoue, *Inorg. Chem.* **2010**, *49*, 1428-1432; d) Y. Komatsu, K. Kato, Y. Yamamoto, H. Kamihata, Y. H. Lee, A. Fuyuhiro, S. Kawata and S. Hayami, *Eur. J. Inorg. Chem.* **2012**, *2012*, 2769-2775; e) S. Hayami, M. Nakaya, H. Ohmagari, A. S. Alao, M. Nakamura, R. Ohtani, R. Yamaguchi, T. Kuroda-Sowa and J. K. Clegg, *Dalton Trans.* **2015**, *44*, 9345-9348.
[88] S. Hayami, K. Kato, Y. Komatsu, A. Fuyuhiro and M. Ohba, *Dalton Trans.* **2011**, *40*, 2167-2169.
[89] R. Akiyoshi, Y. Komatsumaru, M. Donoshita, S.Dekura, Y. Yoshida, H. Kitagawa, Y. Kitagawa, L. F. Lindoy and S. Hayami, *Angew. Chem. Int. Ed.* **2021**, *60*, 12717–12722.
[90] S.-Y. Zhang, H.-Y. Sun, R.-G. Wang, Y.-S. Meng, T. Liu and Y.-Y. Zhu, *Dalton Trans.* **2022**, *51*, 9888-9893.
[91] a) V. Madhu, Y. Diskin-Posner and R. Neumann, *Eur. J. Inorg. Chem.* **2011**, 1792–1796; b) R. Tatikonda, M. Cametti, E. Kalenius, A. Famulari, K. Rissanen and M. Haukka, *Eur. J. Inorg. Chem.* **2019**, *2019*, 4463-4470; c) L. Arnedo-Sánchez, Nonappa, S. Bhowmik, S. Hietala, R. Puttreddy, M. Lahtinen, L. De Cola and K. Rissanen, *Dalton Trans.* **2017**, *46*, 7309-7316.
[92] J. Chirik Paul and K. Wieghardt, *Science* **2010**, *327*, 794-795.
[93] S. A. Pattenaude, K. C. Mullane, E. J. Schelter, M. G. Ferrier, B. W. Stein, S. E. Bone, J. S. Lezama Pacheco, S. A. Kozimor, P. E. Fanwick, M. Zeller and S. C. Bart, *Inorg. Chem.* **2018**, *57*, 6530-6539.
[94] P. J. Chirik, *Inorg. Chem.* **2011**, *50*, 9737-9740.
[95] O. R. Luca and R. H. Crabtree, *Chem. Soc. Rev.* **2013**, *42*, 1440-1459.
[96] W. Kaim and B. Schwederski, *Coord. Chem. Rev.* **2010**, *254*, 1580-1588.
[97] C. K. Jørgensen, *Coord. Chem. Rev.* **1966**, *1*, 164-178.
[98] M. D. Ward and J. A. McCleverty, *J. Chem. Soc., Dalton Trans.* **2002**, 275-288.
[99] S. D. Thomson, *Naturally Occuring Quinones: IV*, Springer, Amsterdam, **1996**, p.
[100] a) Y. Izumi, H. Sawada, N. Sakka, N. Yamamoto, T. Kume, H. Katsuki, S. Shimohama and A. Akaike, *J. Neurosci. Res.* **2005**, *79*, 849 – 860; b) M. He, P. J. Sheldon and D. H. Sherman, *Proc. Natl. Acad. Sci. USA* **2001**, *98*, 926-931.
[101] D. L. J. Broere, R. Plessius and J. I. van der Vlugt, *Chem. Soc. Rev.* **2015**, *44*, 6886-6915.
[102] P. Zanello and M. Corsini, *Coord. Chem. Rev.* **2006**, *250*, 2000-2022.
[103] a) N. A. Ketterer, H. Fan, K. J. Blackmore, X. Yang, J. W. Ziller, M.-H. Baik and A. F. Heyduk, *J. Am. Chem. Soc.* **2008**, *130*, 4364-4374; b) C. G. Pierpont and R. M. Buchanan, *Coord. Chem. Rev.* **1981**, *38*, 45-87.
[104] a) C. G. Pierpont, *Coord. Chem. Rev.* **2001**, *95*, 216–217; b) C. G. Pierpont, *Coord. Chem. Rev.* **2001**, *219-221*, 415-433.
[105] a) S. Scheuermann, H. V. T. Kretz, J. W. Bats, M. Bolte, H.-W. Lerner and M. Wagner, *Chem. Eur. J.* **2008**, *14*, 2590–2601; b) W.-G. Jia, Y.-F. Han, Y.-J. Lin, L.-H. Weng and G.-X. Jin, *Organometallics* **2009**, *28*, 3459-3464; c) J. S. Miller and K. S. Min, *Angew. Chem. Int. Ed.* **2009**, *48*, 262 – 272.

[106] D. Zhang and G.-X. Jin, *Organometallics* **2003**, *22*, 2851-2854.
[107] a) S. Kitagawa and S. Kawata, *Coord. Chem. Rev.* **2002**, *224*, 11-34; b) G. Margraf, T. Kretz, F. F. de Biani, F. Laschi, S. Losi, P. Zanello, J. W. Bats, B. Wolf, K. Remović-Langer, M. Lang, A. Prokofiev, W. Assmus, H.-W. Lerner and M. Wagner, *Inorg. Chem.* **2006**, *45*, 1277-1288.
[108] J. Mattsson, P. Govindaswamy, A. K. Renfrew, P. J. Dyson, P. Štěpnička, G. Süss-Fink and B. Therrien, *Organometallics* **2009**, *28*, 4350-4357.
[109] a) D. Kumbhakar, B. Sarkar, S. Maji, S. M. Mobin, J. Fiedler, F. A. Urbanos, R. Jiménez-Aparicio, W. Kaim and G. K. Lahiri, *J. Am. Chem. Soc.* **2008**, *130*, 17575-17583; b) S. Kar, B. Sarkar, S. Ghumaan, D. Janardanan, J. van Slageren, J. Fiedler, V. G. Puranik, R. B. Sunoj, W. Kaim and G. K. Lahiri, *Chem. Eur. J.* **2005**, *11*, 4901-4911.
[110] a) M. D. Ward, *Inorg. Chem.* **1996**, *35*, 1712-1714; b) C. Carbonera, A. Dei, J.-F. Letard, C. Sangregorio and L. Sorace, *Angew. Chem. Int. Ed.* **2004**, *43*, 3136 –3138; c) Y.-F. Han, W.-G. Jia, W.-B. Yu and G.-X. Jin, *Chem. Soc. Rev.* **2009**, *38*, 3419-3434; d) F.-L. Yang, W.-H. Wu, Y.-Q. Wang, X. Chen, B.-B. Liang, H.-L. Mi, G.-L. Zhang, X.-Y. Chen and Y. Shi, *Cryst. Growth Des.* **2021**, *21*, 6671-6683; e) H. Dong, H. Gao, J. Geng, X. Hou, S. Gao, S. Wang and S. Chou, *J. Phys. Chem. C* **2021**, *125*, 20814-20820; f) J. Tao, H. Maruyama and O. Sato, *J. Am. Chem. Soc.* **2006**, *128*, 1790-1791; g) O. Sato, A. Cui, R. Matsuda, J. Tao and S. Hayami, *Acc. Chem. Res.* **2007**, *40*, 361-369; h) O. Sato, J. Tao and Y.-Z. Zhang, *Angew. Chem. Int. Ed.* **2007**, *46*, 2152-2187.
[111] P. Chaudhuri and K. Oder, *J. Chem. Soc., Dalton Trans.* **1990**, 1597-1605.
[112] B. Therrien, G. Süss-Fink, P. Govindaswamy, A. K. Renfrew and P. J. Dyson, *Angew. Chem. Int. Ed.* **2008**, *47*, 3773–3776.
[113] D. Schweinfurth, H. S. Das, F. Weisser, D. Bubrin and B. Sarkar, *Inorg. Chem.* **2011**, *50*, 1150-1159.
[114] a) P. Chaudhuri, C. N. Verani, E. Bill, E. Bothe, T. Weyhermüller and K. Wieghardt, *J. Am. Chem. Soc.* **2001**, *123*, 2213-2223; b) X. Sun, H. Chun, K. Hildenbrand, E. Bothe, T. Weyhermüller, F. Neese and K. Wieghardt, *Inorg. Chem.* **2002**, *41*, 4295-4303.
[115] a) M. R. Ringenberg, S. L. Kokatam, Z. M. Heiden and T. B. Rauchfuss, *J. Am. Chem. Soc.* **2008**, *130*, 788-789; b) J. L. Boyer, T. R. Cundari, N. J. DeYonker, T. B. Rauchfuss and S. R. Wilson, *Inorg. Chem.* **2009**, *48*, 638-645; c) M. R. Ringenberg, M. J. Nilges, T. B. Rauchfuss and S. R. Wilson, *Organometallics* **2010**, *29*, 1956-1965.
[116] A. I. Poddel'sky, V. K. Cherkasov and G. A. Abakumov, *Coord. Chem. Rev.* **2009**, *253*, 291-324.
[117] a) R. Hübner, S. Weber, S. Strobel, B. Sarkar, S. Záliš and W. Kaim, *Organometallics* **2011**, *30*, 1414-1418; b) S. Ye, B. Sarkar, F. Lissner, T. Schleid, J. van Slageren, J. Fiedler and W. Kaim, *Angew. Chem. Int. Ed.* **2005**, *44*, 2103-2106.
[118] S. Kokatam, T. Weyhermüller, E. Bothe, P. Chaudhuri and K. Wieghardt, *Inorg. Chem.* **2005**, *44*, 3709-3717.
[119] M. Nasibipour, E. Safaei, M. S. Masoumpour and A. Wojtczak, *RSC Adv.* **2020**, *10*, 24176-24189.
[120] H. Bamberger, U. Albold, J. Dubnická Midlíková, C.-Y. Su, N. Deibel, D. Hunger, P. P. Hallmen, P. Neugebauer, J. Beerhues, S. Demeshko, F. Meyer, B. Sarkar and J. van Slageren, *Inorg. Chem.* **2021**, *60*, 2953-2963.

[121] A. L. Balch and R. H. Holm, *J. Am. Chem. Soc.* **1966**, *88*, 5201-5209.
[122] G. A. Fox and C. G. Pierpont, *Inorg. Chem.* **1992**, *31*, 3718-3723.
[123] a) V. Bachler, G. Olbrich, F. Neese and K. Wieghardt, *Inorg. Chem.* **2002**, *41*, 4179-4193; b) W. Jacques, C. Daul, A. Van Zelewsky, A. Goursot and E. Penigault, *Chem. Phys. Lett.* **1982**, *88*, 78-83.
[124] a) M. M. Khusniyarov, K. Harms, O. Burghaus, J. Sundermeyer, B. Sarkar, W. Kaim, J. van Slageren, C. Duboc and J. Fiedler, *Dalton Trans.* **2008**, 1355-1365; b) D. Herebian, E. Bothe, F. Neese, T. Weyhermüller and K. Wieghardt, *J. Am. Chem. Soc.* **2003**, *125*, 9116-9128; c) K. Chłopek, E. Bothe, F. Neese, T. Weyhermüller and K. Wieghardt, *Inorg. Chem.* **2006**, *45*, 6298-6307.
[125] S. Pascal and O. Siri, *Coord. Chem. Rev.* **2017**, *350*, 178-195.
[126] U. Albold, C. Hoyer, N. I. Neuman, S. Sobottka, A. S. Hazari, G. K. Lahiri and B. Sarkar, *Inorg. Chem.* **2019**, *58*, 3754-3763.
[127] W. Kaim and B. Schwederski, *Bioinorganic Chemistry: Inorganic Elements in the Chemistry of Life*, Wiley-VCH: Chichester, UK, , **1994**, p.
[128] a) H. Decker, T. Schweikardt and F. Tuczek, *Angew. Chem. Int. Ed.* **2006**, *45*, 4546-4550; b) J. N. Hamann, B. Herzigkeit, R. Jurgeleit and F. Tuczek, *Coord. Chem. Rev.* **2017**, *334*, 54-66; c) A. Hoffmann, C. Citek, S. Binder, A. Goos, M. Rübhausen, O. Troeppner, I. Ivanović-Burmazović, E. C. Wasinger, T. D. P. Stack and S. Herres-Pawlis, *Angew. Chem. Int. Ed.* **2013**, *52*, 5398–5401.
[129] B. Sarkar, D. Schweinfurth, N. Deibel and F. Weisser, *Coord. Chem. Rev.* **2015**, *293-294*, 250-262.
[130] a) D. N. Hendrickson and C. G. Pierpont, *Top. Curr. Chem.* **2004**, *234*, 63–95; b) J. Rall, M. Wanner, M. Albrecht, F. M. Hornung and W. Kaim, *Chem. Eur. J.* **1999**, *5*, 2802–2809; c) A. Dei, D. Gatteschi, C. Sangregorio and L. Sorace, *Acc. Chem. Res.* **2004**, *37*, 827-835.
[131] M. van der Meer, Y. Rechkemmer, F. D. Breitgoff, S. Dechert, R. Marx, M. Dorfel, P. Neugebauer, J. van Slageren and B. Sarkar, *Dalton Trans.* **2016**, *45*, 8394-8403.
[132] M. van der Meer, Y. Rechkemmer, F. D. Breitgoff, R. Marx, P. Neugebauer, U. Frank, J. van Slageren and B. Sarkar, *Inorg. Chem.* **2016**, *55*, 11944-11953.
[133] F. Weisser, R. Huebner, D. Schweinfurth and B. Sarkar, *Chem. Eur. J.* **2011**, *17*, 5727-5736.
[134] M. van der Meer, Y. Rechkemmer, U. Frank, F. D. Breitgoff, S. Hohloch, C.-Y. Su, P. Neugebauer, R. Marx, M. Dörfel, J. van Slageren and B. Sarkar, *Chem. Eur. J.* **2016**, *22*, 13884-13893.
[135] H.-Y. Cheng, G.-H. Lee and S.-M. Peng, *Inorg. Chim. Acta* **1992**, *191*, 25–27.
[136] C. Kimich, *Ber. Dtsch. Chem. Ges.* **1875**, *8*, 1026–1032.
[137] a) O. Siri, J.-p. Taquet, J.-P. Collin, M.-M. Rohmer, M. Bénard and P. Braunstein, *Chem. Eur. J.* **2005**, *11*, 7247-7253; b) Y. Su, Y. Zhao, J. Gao, Q. Dong, B. Wu and X.-J. Yang, *Inorg. Chem.* **2012**, *51*, 5889-5896; c) J. Rall, A. F. Stange, K. Hübler and W. Kaim, *Angew. Chem. Int. Ed.* **1998**, *37*, 2681-2682; d) O. Siri, P. Braunstein, M.-M. Rohmer, M. Bénard and R. Welter, *J. Am. Chem. Soc.* **2003**, *125*, 13793-13803; e) I.-R. Jeon, J. G. Park, D. J. Xiao and T. D. Harris, *J. Am. Chem. Soc.* **2013**, *135*, 16845-16848; f) S. Frantz, J. Rall, I. Hartenbach, T. Schleid, S. Záliš and W. Kaim, *Eur. J. Chem.* **2004**, *10*, 149-154.

[138] J. A. DeGayner, I.-R. Jeon and T. D. Harris, *Chem. Sci.* **2015**, *6*, 6639-6648.
[139] a) K. Ohno, A. Nagasawa and T. Fujihara, *Dalton Trans.* **2015**, *44*, 368-376; b) Y.-B. Huang, G.-R. Tang, G.-Y. Jin and G.-X. Jin, *Organometallics* **2008**, *27*, 259-269.
[140] J.-p. Taquet, O. Siri, P. Braunstein and R. Welter, *Inorg. Chem.* **2006**, *45*, 4668-4676.
[141] Uta Albold, Heiko Bamberger, P. P. Hallmen, J. v. Slageren and B. Sarkar, *Angew. Chem. Int. Ed.* **2019**, *58*, 9802–9806.
[142] a) B. Sarkar, S. Patra, J. Fiedler, R. B. Sunoj, D. Janardanan, G. K. Lahiri and W. Kaim, *J. Am. Chem. Soc.* **2008**, *130*, 3532-3542; b) B. Sarkar, S. Patra, J. Fiedler, R. B. Sunoj, D. Janardanan, S. M. Mobin, M. Niemeyer, G. K. Lahiri and W. Kaim, *Angew. Chem. Int. Ed.* **2005**, *44*, 5655-5658.
[143] T. H. L. Nguyen, N. Gigant and D. Joseph, *ACS Catal.* **2018**, *8*, 1546-1579.
[144] a) M. K. Sahoo, K. Saravanakumar, G. Jaiswal and E. Balaraman, *ACS Catal.* **2018**, *8*, 7727-7733; b) M. Wang, J. Ma, M. Yu, Z. Zhang and F. Wang, *Catal. Sci. Technol.* **2016**, *6*, 1940-1945.
[145] J. Arias, M. Bardají, P. Espinet, C. L. Folcia, J. Ortega and J. Etxebarría, *Inorg. Chem.* **2009**, *48*, 6205-6210.
[146] S. Benkhaya, S. M' rabet and A. El Harfi, *Inorg. Chem. Commun.* **2020**, *115*, 107891.
[147] S. K. Kyei, O. Akaranta and G. Darko, *Sci. Afr.* **2020**, *8*, e00406.
[148] a) N. Doslik, T. Sixt and W. Kaim, *Angew. Chem. Int. Ed.* **1998**, *37*, 2403-2404; b) M. Krejcik, S. Zalis, J. Klima, D. Sykora, W. Matheis, A. Klein and W. Kaim, *Inorg. Chem.* **1993**, *32*, 3362-3368; c) J. Long, D. Kumar, C. Deo, P. Retailleau, G. V. Dubacheva, G. Royal, J. Xie and N. Bogliotti, *Chem. Eur. J.* **2021**, *27*, 9563-9570.
[149] a) S. Samanta, P. Ghosh and S. Goswami, *Dalton Trans.* **2012**, *41*, 2213-2226; b) M. Shivakumar, K. Pramanik, P. Ghosh and A. Chakravorty, *Inorg. Chem.* **1998**, *37*, 5968-5969; c) K. M. Waldie, S. Ramakrishnan, S.-K. Kim, J. K. Maclaren, C. E. D. Chidsey and R. M. Waymouth, *J. Am. Chem. Soc.* **2017**, *139*, 4540-4550; d) B. Sarkar, R. Hubner, R. Pattacini and I. Hartenbach, *Dalton Trans.* **2009**, 4653-4655; e) D. Sengupta, P. Ghosh, T. Chatterjee, H. Datta, N. D. Paul and S. Goswami, *Inorg. Chem.* **2014**, *53*, 12002-12013.
[150] a) W. Kaim and V. Kasack, *Inorg. Chem.* **1990**, *29*, 4696-4699; b) R. Jana, B. Sarkar, D. Bubrin, J. Fiedler and W. Kaim, *Inorg. Chem. Commun.* **2010**, *13*, 1160-1162; c) S. Roy, B. Sarkar, H.-G. Imrich, J. Fiedler, S. Záliš, R. Jimenez-Aparicio, F. A. Urbanos, S. M. Mobin, G. K. Lahiri and W. Kaim, *Inorg. Chem.* **2012**, *51*, 9273-9281; d) S. Mondal, B. Schwederski, W. Frey, J. Fiedler, S. Záliš and W. Kaim, *Inorg. Chem.* **2018**, *57*, 3983-3992.
[151] a) M. Panda, S. Das, G. Mostafa, A. Castiñeiras and S. Goswami, *Dalton Trans.* **2005**, 1249-1255; b) N. D. Paul, T. Krämer, J. E. McGrady and S. Goswami, *Chem. Commun.* **2010**, *46*, 7124-7126; c) D. Sengupta, N. Saha Chowdhury, S. Samanta, P. Ghosh, S. K. Seth, S. Demeshko, F. Meyer and S. Goswami, *Inorg. Chem.* **2015**, *54*, 11465-11476.
[152] a) M. G. Sommer, S. Marinova, M. J. Krafft, D. Urankar, D. Schweinfurth, M. Bubrin, J. Košmrlj and B. Sarkar, *Organometallics* **2016**, *35*, 2840-2849; b) M. G. Sommer, P. Kureljak, D. Urankar, D. Schweinfurth, N. Stojanović, M. Bubrin, M. Gazvoda, M. Osmak, B. Sarkar and J. Košmrlj, *Chem. Eur. J.* **2014**, *20*, 17296 – 17299.
[153] J. Klein, J. Beerhues, D. Schweinfurth, M. van der Meer, M. Gazvoda, G. K. Lahiri, J. Kosmrlj and B. Sarkar, *Chem. Eur. J.* **2018**, *24*, 18020–18031.

[154] M. Bardají, M. Barrio and P. Espinet, *Dalton Trans.* **2011**, *40*, 2570-2577.
[155] A. Dogan, B. Sarkar, A. Klein, F. Lissner, T. Schleid, J. Fiedler, S. Záliš, V. K. Jain and W. Kaim, *Inorg. Chem.* **2004**, *43*, 5973-5980.
[156] a) A. Das, T. M. Scherer, S. M. Mobin, W. Kaim and G. K. Lahiri, *Chem. Eur. J.* **2012**, *18*, 11007-11018; b) K. Pramanik, M. Shivakumar, P. Ghosh and A. Chakravorty, *Inorg. Chem.* **2000**, *39*, 195-199; c) W. Kaim, *Coord. Chem. Rev.* **2001**, *219-221*, 463-488; d) M. Heilmann, S. Frantz, W. Kaim, J. Fiedler and C. Duboc, *Inorg. Chim. Acta* **2006**, *359*, 821-829.
[157] W. Kaim and S. Kohlmann, *Inorg. Chem.* **1987**, *26*, 68-77.
[158] a) S. J. Dougan, M. Melchart, A. Habtemariam, S. Parsons and P. J. Sadler, *Inorg. Chem.* **2006**, *45*, 10882-10894; b) A. H. Velders, H. Kooijman, A. L. Spek, J. G. Haasnoot, D. de Vos and J. Reedijk, *Inorg. Chem.* **2000**, *39*, 2966-2967; c) A. C. G. Hotze, M. Bacac, A. H. Velders, B. A. J. Jansen, H. Kooijman, A. L. Spek, J. G. Haasnoot and J. Reedijk, *J. Med. Chem.* **2003**, *46*, 1743-1750.
[159] a) K. i. Aoki, M. Nakagawa and K. Ichimura, *J. Am. Chem. Soc.* **2000**, *122*, 10997-11004; b) K. Han, W. Su, M. Zhong, Q. Yan, Y. Luo, Q. Zhang and Y. Li, *Macromol. Rapid Commun.* **2008**, *29*, 1866-1870; c) H. Ren, P. Yang and F. M. Winnik, *Polym. Chem.* **2020**, *11*, 5955-5961.
[160] M. Dommaschk, M. Peters, F. Gutzeit, C. Schütt, C. Näther, F. D. Sönnichsen, S. Tiwari, C. Riedel, S. Boretius and R. Herges, *J. Am. Chem. Soc.* **2015**, *137*, 7552-7555.
[161] A.-L. Barra, L.-C. Brunel, F. Baumann, M. Schwach, M. Moscherosch and W. Kaim, *J. Chem. Soc., Dalton Trans.* **1999**, 3855-3857.
[162] a) S. J. Dougan, A. Habtemariam, S. E. McHale, S. Parsons and P. J. Sadler, *Proc. Natl. Acad. Sci. USA* **2008**, *105*, 11628-11633; b) P. C. A. Bruijnincx and P. J. Sadler in *Controlling platinum, ruthenium, and osmium reactivity for anticancer drug design*, *Vol. 61* Eds.: R. van Eldik and C. D. Hubbard), Academic Press, **2009**, pp. 1-62; c) G. Gasser, I. Ott and N. Metzler-Nolte, *J. Med. Chem.* **2011**, *54*, 3-25; d) I. Romero-Canelón and P. J. Sadler, *Inorg. Chem.* **2013**, *52*, 12276-12291.
[163] E. A. McLoughlin, K. M. Waldie, S. Ramakrishnan and R. M. Waymouth, *J. Am. Chem. Soc.* **2018**, *140*, 13233-13241.
[164] a) D. Datta and A. Chakravorty, *Inorg. Chem.* **1983**, *22*, 1085-1090; b) R. A. Krause and K. Krause, *Inorg. Chem.* **1982**, *21*, 1714-1720; c) S. Goswami, A. R. Chakravarty and A. Chakravorty, *Inorg. Chem.* **1981**, *20*, 2246-2250; d) M. N. Ackermann, W. G. Fairbrother, N. S. Amin, C. J. Deodene, C. M. Lamborg and P. T. Martin, *J. Organomet. Chem.* **1996**, *523*, 145-151.
[165] A. Ratanaphan, T. Nhukeaw, P. Temboot and K. Hansongnern, *Transition Met. Chem.* **2012**, *37*, 207-214.
[166] K. Yadav, T. Halbritter, A. Heckel and T. G. Gopakumar, *J. Phys. Chem. C* **2018**, *122*, 15330-15337.
[167] X. Jing-Jing, S. Dong, Z. Zhi-Gang and W. Xiao-Qian, *Chin. Phys. B* **2016**, *25*, 096401.
[168] H. M. D. Bandara and S. C. Burdette, *Chem. Soc. Rev.* **2012**, *41*, 1809-1825.
[169] R. Zhao, C. Tan, Y. Xie, C. Gao, H. Liu and Y. Jiang, *Tetrahedron Lett.* **2011**, *52*, 3805-3809.
[170] C. Zhang and N. Jiao, *Angew. Chem. Int. Ed.* **2010**, *49*, 6174-6177.

[171] a) S. Roy, I. Hartenbach and B. Sarkar, *Eur. J. Inorg. Chem.* **2009**, 2553–2558; b) A. C. Cope and R. W. Siekman, *J. Am. Chem. Soc.* **1965**, *87*, 3272-3273.
[172] A. R. Siedle, *J. Organomet. Chem.* **1981**, *208*, 115-123.
[173] a) R. Bennett, M. Bruce, B. Goodall and F. Stone, *Aust. J. Chem.* **1974**, *27*, 2131-2133; b) M. Ćurić, D. Babić, A. Višnjevac and K. Molčanov, *Inorg. Chem.* **2005**, *44*, 5975-5977; c) D. Cinčić, M. Juribašić, D. Babić, K. Molčanov, P. Šket, J. Plavec and M. Ćurić, *Chem. Commun.* **2011**, *47*, 11543-11545; d) C. H. Zambrano, P. R. Sharp and C. L. Barnes, *Organometallics* **1995**, *14*, 3607-3610; e) M. Bruce, M. Liddell, M. Snow and E. Tiekink, *Aust. J. Chem.* **1988**, *41*, 1407-1415; f) J. M. Hoover, J. Freudenthal, F. E. Michael and J. M. Mayer, *Organometallics* **2008**, *27*, 2238-2245.
[174] M. Ghedini, D. Pucci, A. Crispini and G. Barberio, *Organometallics* **1999**, *18*, 2116-2124.
[175] a) Z. Jamain, M. Khairuddean, T. Guan-Seng and A. B. A. Rahman, *Macromol. Res.* **2021**, *29*, 331-341; b) R. Brightman, *Dictionary of Chemistry in Nature*, Mc-Graw Hill: New York, NY, USA, **1954**, p.
[176] S. Yildiz, M. C. Cetinkaya, H. Ozbek, V. Tzitzios and G. Nounesis, *J. Mol. Liq.* **2020**, *298*, 112029.
[177] a) T. Ikeda, S. Kurihara, D. B. Karanjit and S. Tazuke, *Macromolecules* **1990**, *23*, 3938-3943; b) O. Tsutsumi, T. Shiono, T. Ikeda and G. Galli, *J. Phys. Chem. B* **1997**, *101*, 1332-1337; c) X. Lu, S. Guo, X. Tong, H. Xia and Y. Zhao, *Adv. Mater.* **2017**, *29*, 1606467; d) S.-Q. Han, Y.-Y. Chen, B. Xu, J. Wei and Y.-L. Yu, *Chin. J. Polym. Sci.* **2020**, *38*, 806-813; e) H.-B. Cheng, S. Zhang, J. Qi, X.-J. Liang and J. Yoon, *Adv. Mater.* **2021**, *33*, 2007290.
[178] a) K. Arai and Y. Kawabata, *Macromol. Rapid Commun.* **1995**, *16*, 875-880; b) S. Kadota, K. Aoki, S. Nagano and T. Seki, *J. Am. Chem. Soc.* **2005**, *127*, 8266-8267; c) M. Hoshino, E. Uchida, Y. Norikane, R. Azumi, S. Nozawa, A. Tomita, T. Sato, S.-i. Adachi and S.-y. Koshihara, *J. Am. Chem. Soc.* **2014**, *136*, 9158-9164; d) H. Sasaki, K. Abe, M. Sagisaka and A. Yoshizawa, *J. Mater. Chem. C* **2021**, *9*, 12928-12937.
[179] a) T. Ikeda and O. Tsutsumi, *Science* **1995**, *268*, 1873-1875; b) C. Hsu, Z. Xu and X. Wang, *Adv. Funct. Mater.* **2018**, *28*, 1802506; c) J. Tian, L. Fu, Z. Liu, H. Geng, Y. Sun, G. Lin, X. Zhang, G. Zhang and D. Zhang, *Adv. Funct. Mater.* **2019**, *29*, 1807176; d) S. O. Hacioglu, *Chin. J. Polym. Sci.* **2020**, *38*, 109-117; e) C. Hsu, Z. Xu and X. Wang, *Adv. Funct. Mater.* **2019**, *29*, 1806703; f) T. Ikeda, M. Nakano, Y. Yu, O. Tsutsumi and A. Kanazawa, *Adv. Mater.* **2003**, *15*, 201-205.
[180] a) P.-C. Yang, C.-Y. Li, H. Wu and J.-C. Chiang, *J. Taiwan Inst. Chem. Eng.* **2012**, *43*, 480-490; b) Y. Xiao, C. He, Z.-F. Yang, E.-Q. Chen, H.-J. Lu, X.-H. Li and Y.-F. Tu, *Chin. J. Polym. Sci.* **2022**, *40*, 584-592.
[181] S. Kaler, P. McKeown, B. D. Ward and M. D. Jones, *Inorg. Chem. Front.* **2021**, *8*, 711-719.
[182] M. Lin, S. Zou, T. Li, J. Karges, Y. Chen, Y. Zhao, L. Ji and H. Chao, *Chem. Commun.* **2022**, *58*, 4324-4327.
[183] a) A. Ueno, K. Takahashi and T. Osa, *J. Chem. Soc., Chem. Commun.* **1981**, 94-96; b) H. Sugimoto, T. Kimura and S. Inoue, *J. Am. Chem. Soc.* **1999**, *121*, 2325-2326; c) L. Osorio-Planes, C. Rodríguez-Escrich and M. A. Pericàs, *Org. Lett.* **2014**, *16*, 1704-1707.

[184] a) R. Cacciapaglia, S. Di Stefano and L. Mandolini, *J. Am. Chem. Soc.* **2003**, *125*, 2224-2227; b) F. Würthner and J. Rebek Jr, *Angew. Chem. Int. Ed.* **1995**, *34*, 446-448.
[185] a) D. Wilson and N. R. Branda, *Angew. Chem. Int. Ed.* **2012**, *51*, 5431-5434; b) B. M. Neilson and C. W. Bielawski, *J. Am. Chem. Soc.* **2012**, *134*, 12693-12699.
[186] F. S. Peter Gruss, *Die Zukunft der Energie: Die Antwort der Wissenschaft*, Verlag C. H. Beck, München, **2008**, p.
[187] a) N. Deibel, D. Schweinfurth, J. Fiedler, S. Zalis and B. Sarkar, *Dalton Trans.* **2011**, *40*, 9925-9934; b) N. Deibel, D. Schweinfurth, S. Hohloch, M. Delor, I. V. Sazanovich, M. Towrie, J. A. Weinstein and B. Sarkar, *Inorg. Chem.* **2014**, *53*, 1021-1031.
[188] N. Godbert, T. Pugliese, I. Aiello, A. Bellusci, A. Crispini and M. Ghedini, *Eur. J. Inorg. Chem.* **2007**, *2007*, 5105-5111.
[189] J. Brooks, Y. Babayan, S. Lamansky, P. I. Djurovich, I. Tsyba, R. Bau and M. E. Thompson, *Inorg. Chem.* **2002**, *41*, 3055-3066.
[190] C. Gourlaouen and C. Daniel, *Dalton Trans.* **2014**, *43*, 17806-17819.
[191] M. Lersch, A. Krivokapic and M. Tilset, *Organometallics* **2007**, *26*, 1581-1587.
[192] J. S. Per-Inge Kvam, *Acta Chem. Scand.* **1995**, *49*, 313-324.
[193] J. A. G. Williams, A. Beeby, E. S. Davies, J. A. Weinstein and C. Wilson, *Inorg. Chem.* **2003**, *42*, 8609-8611.
[194] a) E. Evangelio and D. Ruiz-Molina, *Eur. J. Inorg. Chem.* **2005**, *2005*, 2957-2971; b) E. Evangelio, D. N. Hendrickson and D. Ruiz-Molina, *Inorg. Chim. Acta* **2008**, *361*, 3403-3409.
[195] R. M. Buchanan and C. G. Pierpont, *J. Am. Chem. Soc.* **1980**, *102*, 4951-4957.
[196] a) G. K. Rauth, S. Pal, D. Das, C. Sinha, A. M. Z. Slawin and J. D. Woollins, *Polyhedron* **2001**, *20*, 363-372; b) A. B. P. Lever, P. R. Auburn, E. S. Dodsworth, M. A. Haga, W. Liu, M. Melnik and W. A. Nevin, *J. Am. Chem. Soc.* **1988**, *110*, 8076-8084; c) R. Roy, P. Chattopadhyay, C. Sinha and S. Chattopadhyay, *Polyhedron* **1996**, *15*, 3361-3369.
[197] a) P. A. Scattergood, P. Jesus, H. Adams, M. Delor, I. V. Sazanovich, H. D. Burrows, C. Serpa and J. A. Weinstein, *Dalton Trans.* **2015**, *44*, 11705-11716; b) W. B. Connick, D. Geiger and R. Eisenberg, *Inorg. Chem.* **1999**, *38*, 3264-3265; c) S. D. Cummings and R. Eisenberg, *J. Am. Chem. Soc.* **1996**, *118*, 1949-1960; d) J. A. Weinstein, M. T. Tierney, E. S. Davies, K. Base, A. A. Robeiro and M. W. Grinstaff, *Inorg. Chem.* **2006**, *45*, 4544-4555.
[198] N. Deibel, D. Schweinfurth, S. Hohloch, J. Fiedler and B. Sarkar, *Chem. Commun.* **2012**, *48*, 2388-2390.
[199] S. Archer and J. A. Weinstein, *Coord. Chem. Rev.* **2012**, *256*, 2530-2561.
[200] a) J. Jacquet, P. Chaumont, G. Gontard, M. Orio, H. Vezin, S. Blanchard, M. Desage-El Murr and L. Fensterbank, *Angew. Chem. Int. Ed.* **2016**, *55*, 10712-10716; b) J. L. Boyer, J. Rochford, M.-K. Tsai, J. T. Muckerman and E. Fujita, *Coord. Chem. Rev.* **2010**, *254*, 309-330.
[201] a) S. Reinhardt and K. Heinze, *Z. Anorg. Allg. Chem.* **2006**, *632*, 1465–1470; b) K. Heinze and S. Reinhardt, *Chem. Eur. J.* **2008**, *14*, 9482–9486; c) S. Sobottka, M. Nößler, A. L. Osterichter, G. Hermann, N. Z. Subat, J. Beerhues, M. B.-v. d. Meer, L. Suntrup, U. Albold, S. Hohloch, J. C. Tremblay and B. Sarkar, *Chem. Eur. J.* **2020**, *26*, 1314–1327.
[202] a) J. Yang, D. K. Kersi, L. J. Giles, B. W. Stein, C. Feng, C. R. Tichnell, D. A. Shultz and M. L. Kirk, *Inorg. Chem.* **2014**, *53*, 4791-4793; b) Y.-M. Zhang, F. Meng, J.-H. Tang, Y.

Wang, C. You, H. Tan, Y. Liu, Y.-W. Zhong, S. Su and W. Zhu, *Dalton Trans.* **2016**, *45*, 5071-5080.
[203] a) T. Yutaka, I. Mori, M. Kurihara, J. Mizutani, N. Tamai, T. Kawai, M. Irie and H. Nishihara, *Inorg. Chem.* **2002**, *41*, 7143-7150; b) S. Kume and H. Nishihara, *Dalton Trans.* **2008**, 3260-3271; c) M. E. Moustafa, M. S. McCready and R. J. Puddephatt, *Organometallics* **2012**, *31*, 6262-6269.
[204] Y. Yamamoto and H. Yamazaki, *J. Org. Chem.* **1977**, *42*, 4136-4139.
[205] N. Deibel, S. Hohloch, M. G. Sommer, D. Schweinfurth, F. Ehret, P. Braunstein and B. Sarkar, *Organometallics* **2013**, *32*, 7366-7375.
[206] N. Deibel, D. Schweinfurth, R. Huebner, P. Braunstein and B. Sarkar, *Dalton Trans.* **2011**, *40*, 431-436.
[207] a) H. S. Das, D. Schweinfurth, J. Fiedler, M. M. Khusniyarov, S. M. Mobin and B. Sarkar, *Chem. Eur. J.* **2014**, *20*, 4334-4346; b) H. S. Das, F. Weisser, D. Schweinfurth, C.-Y. Su, L. Bogani, J. Fiedler and B. Sarkar, *Chem. Eur. J.* **2010**, *16*, 2977-2981.
[208] N. Deibel, M. G. Sommer, S. Hohloch, J. Schwann, D. Schweinfurth, F. Ehret and B. Sarkar, *Organometallics* **2014**, *33*, 4756-4765.
[209] a) S. Halis, A. K. Inge, N. Dehning, T. Weyrich, H. Reinsch and N. Stock, *Inorg. Chem.* **2016**, *55*, 7425-7431; b) M. E. Ziebel, L. E. Darago and J. R. Long, *J. Am. Chem. Soc.* **2018**, *140*, 3040-3051.
[210] A. A. Adeyemo, A. Shettar, I. A. Bhat, P. Kondaiah and P. S. Mukherjee, *Dalton Trans.* **2018**, *47*, 8466-8475.
[211] H. Jung, A. Dubey, H. J. Koo, V. Vajpayee, T. R. Cook, H. Kim, S. C. Kang, P. J. Stang and K.-W. Chi, *Chem. Eur. J.* **2013**, *19*, 6709-6717.
[212] N. Elgrishi, K. J. Rountree, B. D. McCarthy, E. S. Rountree, T. T. Eisenhart and J. L. Dempsey, *J. Chem. Educ.* **2018**, *95*, 197-206.
[213] J. Heinze, *Angew. Chem.* **1984**, *96*, 823-840.
[214] S. H. DuVall and R. L. McCreery, *Anal. Chem.* **1999**, *71*, 4594-4602.
[215] A. M. Bond and S. W. Feldberg, *J. Phys. Chem. B* **1998**, *102*, 9966-9974.
[216] J. I. van der Vlugt, *Eur. J. Inorg. Chem.* **2012**, *2012*, 363-375.
[217] a) J. L. Dempsey, A. J. Esswein, D. R. Manke, J. Rosenthal, J. D. Soper and D. G. Nocera, *Inorg. Chem.* **2005**, *44*, 6879-6892; b) K. J. Lee, N. Elgrishi, B. Kandemir and J. L. Dempsey, *Nat. Rev. Chem.* **2017**, *1*, 0039.
[218] a) S. Lewis Nathan and G. Nocera Daniel, *Proc. Natl. Acad. Sci.* **2006**, *103*, 15729-15735; b) E. E. Benson, C. P. Kubiak, A. J. Sathrum and J. M. Smieja, *Chem. Soc. Rev.* **2009**, *38*, 89-99; c) M. D. Kärkäs, O. Verho, E. V. Johnston and B. Åkermark, *Chem. Rev.* **2014**, *114*, 11863-12001; d) J. R. McKone, S. C. Marinescu, B. S. Brunschwig, J. R. Winkler and H. B. Gray, *Chem. Sci.* **2014**, *5*, 865-878.
[219] J.-M. Savéant, *Chem. Rev.* **2008**, *108*, 2348-2378.
[220] a) J. Qiao, Y. Liu, F. Hong and J. Zhang, *Chem. Soc. Rev.* **2014**, *43*, 631-675; b) R. Francke, B. Schille and M. Roemelt, *Chem. Rev.* **2018**, *118*, 4631-4701.
[221] S. Gonell, E. A. Assaf, K. D. Duffee, C. K. Schauer and A. J. M. Miller, *J. Am. Chem. Soc.* **2020**, *142*, 8980-8999.
[222] S. Gonell, M. D. Massey, I. P. Moseley, C. K. Schauer, J. T. Muckerman and A. J. M. Miller, *J. Am. Chem. Soc.* **2019**, *141*, 6658-6671.

[223] R. Poli, *Comments Inorg. Chem.* **2009**, *30*, 177-228.
[224] a) D. J. Martin, B. D. McCarthy, E. S. Rountree and J. L. Dempsey, *Dalton Trans.* **2016**, *45*, 9970-9976; b) J. M. Savéant and K. B. Su, *J. Electroanal. Chem.* **1984**, *171*, 341-349.
[225] E. S. Rountree, B. D. McCarthy, T. T. Eisenhart and J. L. Dempsey, *Inorg. Chem.* **2014**, *53*, 9983-10002.
[226] C. Costentin and J.-M. Savéant, *ChemElectroChem* **2014**, *1*, 1226-1236.
[227] P. Zanello, *Inorganic Electrochemistry: Theory, Practice and Application*, The Royal Society of Chemistry, Cambridge, **2003**, p.
[228] W. Kaim and J. Fiedler, *Chem. Soc. Rev.* **2009**, *38*, 3373-3382.
[229] A. B. Winterbottom, *Trans. Faraday Soc.* **1946**, *42*, 487-495.
[230] T. Kuwana, R. K. Darlington and D. W. Leedy, *Anal. Chem.* **1964**, *36*, 2023-2025.
[231] J. Souza Garcia, C. A. Angelucci, L. S. Parreira and P. V. B. Santiago in *Spectroelectrochemistry Applied to Electrocatalytic Processes*, (Ed. K. Wandelt), Elsevier, Oxford, **2018**, pp. 486-495.
[232] František Hartl, R. P. Groenestein and T. Mahabiersing, *Collect. Czech. Chem. Commun.* **2001**, *66*, 52-66.
[233] J. A. Richards and D. H. Evans, *Anal. Chem.* **1975**, *47*, 964-966.
[234] H. L. S. R. Domingos, F. van Anrooij, H. J. Sanders, B. H. Bakker, W. J. Buma, F. Hartl, S. Woutersen, *Rev. Sci. Instrum.* **2013**, *84*, 033103.
[235] J. A. Crayston in *1.45 - Spectroelectrochemistry*, Eds.: J. A. McCleverty and T. J. Meyer), Pergamon, Oxford, **2003**, pp. 775-789.
[236] P. Zanello, F. Fabrizi de Biani and C. Nervi, *Inorganic electrochemistry. Theory, practice and application*, RSC The Royal Soc. of Chemistry, Cambridge, **2012**, p.
[237] a) D. Lexa, M. Momenteau, J. Mispelter and J. M. Saveant, *Inorg. Chem.* **1989**, *28*, 30-35; b) W. Kaim, S. Ernst and V. Kasack, *J. Am. Chem. Soc.* **1990**, *112*, 173-178; c) M. T. Barton, N. M. Rowley, P. R. Ashton, C. J. Jones, N. Spencer, M. S. Tolley and L. J. Yellowlees, *J. Chem. Soc., Dalton Trans.* **2000**, 3170-3175.
[238] a) F. D'Souza, P. Boulas, A. M. Aukauloo, R. Guilard, M. Kisters, E. Vogel and K. M. Kadish, *J. Phys. Chem.* **1994**, *98*, 11885-11891; b) C. Holliger, A. J. Pierik, E. J. Reijerse and W. R. Hagen, *J. Am. Chem. Soc.* **1993**, *115*, 5651-5656.

2. Scope of this Work

Within this thesis, different fluorinated ligand systems will be synthesized and investigated towards their fluorine specific interactions and its impact on the properties of the resulting metal complexes. For the investigation of the properties, a combination of single crystal X-ray diffraction, SQUID magnetometric, (spectro-)electrochemical, EPR spectroscopic measurements and quantum chemical calculations have been applied.

In the first part, metal complexes containing fluorinated tripodal ligands will be explored. New cobalt(II) and iron(II) complexes will be synthesized and investigated towards the fluorine specific interactions in the secondary coordination sphere through a combination of the aforementioned methods. For this purpose, a variety of tripodal ligands are used to achieve a better understanding of the interactions of the different arms and the resulting influence on the magnetic properties of the complexes (figure 41).

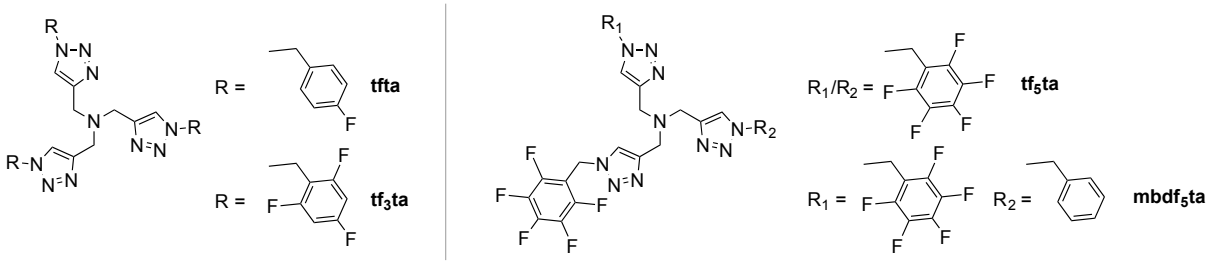

Figure 41: Tripodal ligands used in this work.

The second part deals with tpy ligands bearing different fluorinated backbones and metal complexes thereof (figure 42). The aim is to synthesize cobalt(II) and iron(II) complexes that show interesting spin crossover properties in combination with liquid crystalline behavior. Furthermore, the electrochemistry will be investigated and EPR studies will be performed to study the influence of the ligand backbone on the redox behavior and magnetic properties. The synthesis of ruthenium(II) complexes combining a MIC and different fluorinated tpy ligands will be performed and the focus will be on the possible application in electrocatalysis for CO_2 reduction.

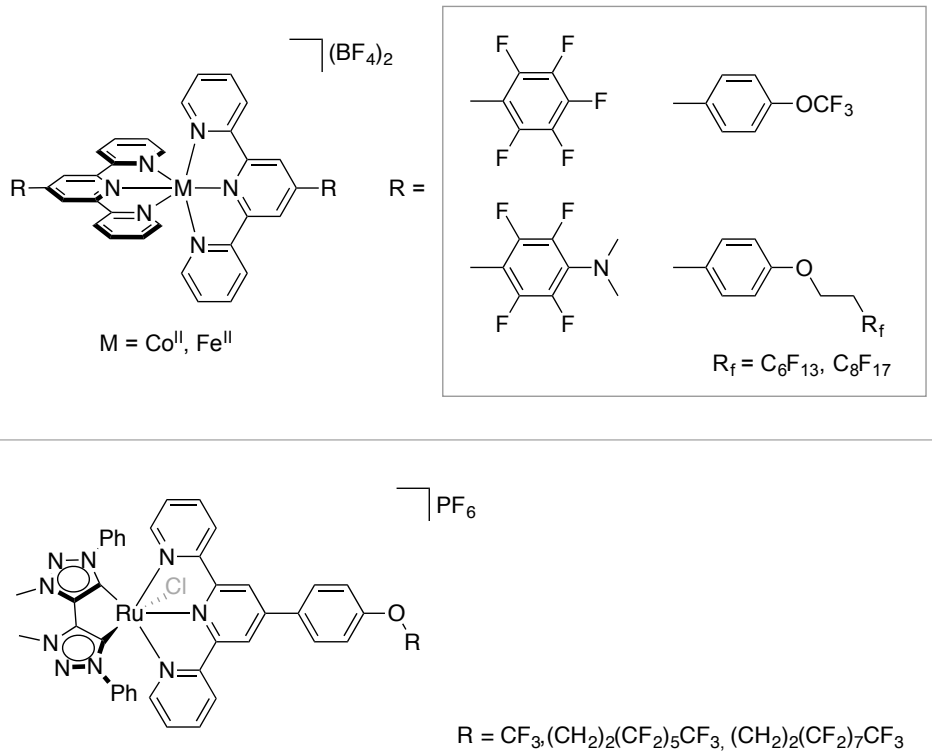

Figure 42: Used tpy ligands and complexes thereof (top: homoleptic cobalt(II) and iron(II) complexes, bottom: ruthenium(II) complexes for application in electrocatalysis).

In the last part, the focus will be on dinuclear platinum(II) donor-acceptor complexes with bridging quinone ligands and varying azobenzene stoppers (figure 43). Two bridging ligands one with an [O, N, O, N] and one with an [N, N, N, N] substitution pattern will be used. The focus will be on the different azobenzene ligands bearing (fluorinated) alkyl chains and the impact on the electrochemical properties. Furthermore, the complexes will be studied for the potential application as redox active liquid crystalline material. Therefore, a combined study of cyclic voltammetry, UV/Vis/NIR and EPR spectroelectrochemistry will be performed as these compounds usually show a strong electrochromic behavior. These results will be compared to known complexes bearing the same bridging ligands and unsubstituted azobenzene stoppers.

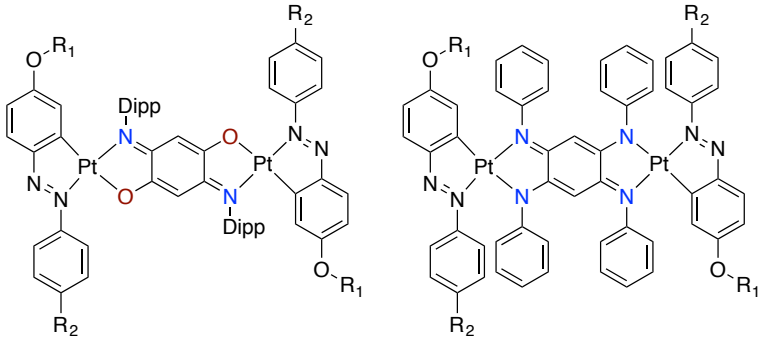

Figure 43: Coordination motif of platinum(II) complexes with different bridgine quinone and azobenzene ligands.

3. Results and Discussion

3.1. Tripodal-based Fe and Co complexes

3.1.1. Spin-state control of cobalt(II) and iron(II) complexes with click-derived tripodal ligands through non-covalent and fluorine-specific interactions

Maite Nößler,[a],⊥ David Hunger,[b],⊥ Felix Reichert,[b] Mario Winkler,[b] Marc Reimann,[c] Johannes Klein,[a] Simon Suhr,[d] Lisa Suntrup, [a] Julia Beerhues,[d] Martin Kaupp,[c] Joris van Slageren[b] and Biprajit Sarkar[a,d]**

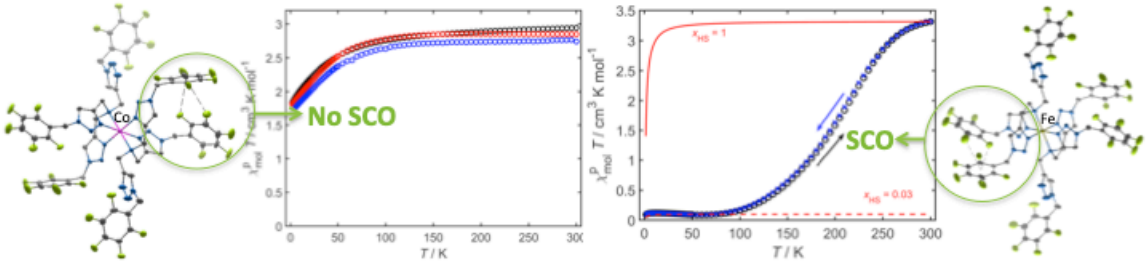

[a] Institut für Chemie und Biochemie, Anorganische Chemie
Freie Universität Berlin, Fabeckstraße 34-36, 14195, Berlin (Germany)
[b] Institut für Physikalische Chemie,
Universität Stuttgart, Pfaffenwaldring 55, D-70569 Stuttgart, Germany
[c] Institut für Theoretische Chemie
Technische Universität Berlin, Straße des 17. Juni 135, 10623 Berlin (Germany)
[d] Lehrstuhl für Anorganische Koordinationschemie
Universität Stuttgart, Pfaffenwaldring 55, 70569 Stuttgart (Germany)
⊥ Equal contribution

This article was published and is reprinted with the permission of the Royal Society of Chemistry:

M. Nößler, D. Hunger, F. Reichert, M. Winkler, M. Reimann, J. Klein, S. Suhr, L. Suntrup, J. Beerhues, M. Kaupp, J. van Slageren, B. Sarkar, *Dalton Trans.* **2021**, *50*, 18097–18106.
DOI: https://doi.org/10.1039/D1DT03535E

Author contribution: The project was designed by Biprajit Sarkar, Johannes Klein and Maite Nößler. The ligands and complexes were synthesized and characterized by Maite Nößler, Johannes Klein, Jessica Stubbe (during her research internship supervised by Johannes Klein) and Simon Suhr. The SQUID experiments, high-frequency EPR and Mössbauer spectroscopy measurements were performed by David Hunger, Felix Reichert and Mario Winkler. Marc Reimann performed the quantum chemical calculations. X-Ray diffraction analysis was carried out by Maite Nößler, Lisa Suntrup and Julia Beerhues. The paper was written by Maite Nößler, David Hunger, Biprajit Sarkar and Joris van Slageren

3.1.2. Fluorinated Click-Derived Tripodal Ligands Drive Spin Crossover in both Iron(II) and Cobalt(II) Complexes

Maite Nößler,[a],⊥ David Hunger,[c],⊥ Nicolás I. Neuman,[a, b, f] Marc Reimann,[d] Felix Reichert,[c] Mario Winkler,[c] Johannes Klein,[a] Tobias Bens,[b] Lisa Suntrup,[a] Serhiy Demeshko,[e] Jessica Stubbe,[a] Martin Kaupp,[d] Joris van Slageren[c] and Biprajit Sarkar[a,b]**

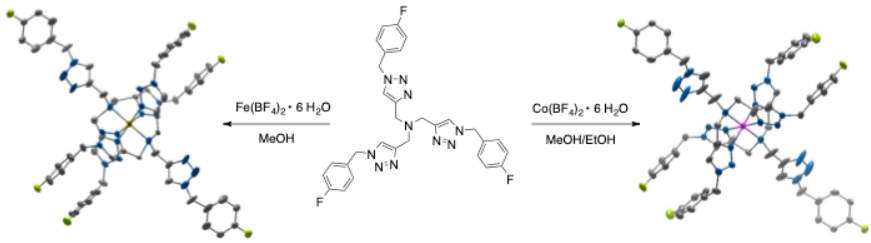

[a] Institut für Chemie und Biochemie, Anorganische Chemie, Freie Universität Berlin, Fabeckstraße 34-36, 14195, Berlin (Germany)

[b] Lehrstuhl für Anorganische Koordinationschemie, Universität Stuttgart, Pfaffenwaldring 55, D-70569 Stuttgart, Germany

[c] Institut für Physikalische Chemie, Universität Stuttgart, Pfaffenwaldring 55, D-70569 Stuttgart, Germany

[d] Institut für Theoretische Chemie
Technische Universität Berlin, Straße des 17. Juni 135, 10623 Berlin (Germany)

[e] Institut für Anorganische Chemie, Universität Göttingen, Tammanstraße 4, D-37077, Göttingen, Germany

[f] Instituto de Desarrollo Tecnológico para la Industria Química, INTEC, UNL-CONICET Paraje El Pozo, Santa Fe, Argentina

⊥ Equal contribution

This article was published and is reprinted with the permission of the Royal Society of Chemistry:

M. Nößler, D. Hunger, Nicolás I. Neuman, M. Reimann, F. Reichert, M. Winkler, J. Klein, T. Bens, L. Suntrup, S. Demeshko, J. Stubbe, M. Kaupp, J. van Slageren, B. Sarkar, *Dalton Trans.* **2022**, *51*10507-10517.

Doi: https://doi.org/10.1039/D2DT01005D

Author contribution: The project was designed by Biprajit Sarkar, Johannes Klein and Maite Nößler. The ligands and complexes were synthesized and characterized by Maite Nößler, Johannes Klein and Jessica Stubbe (during her research internship supervised by Johannes Klein). Serhiy Demeshko performed preliminary SQUID experiments The SQUID experiments, high-frequency EPR and Mössbauer spectroscopy measurements were performed by David Hunger, Felix Reichert and Mario Winkler. Marc Reimann performed the quantum chemical calculations. EPR measurements were performed by Maite Nößler and Nicolás I. Neuman. Simulation of the EPR spectra were performed by Nicolás I. Neuman and Tobias Bens. X-Ray diffraction analysis was carried out by Maite Nößler and Lisa Suntrup. The paper was written by Maite Nößler, David Hunger, Biprajit Sarkar and Joris van Slageren.

3.2. Terpyridine-based Metal Complexes

3.2.1. Electrochemistry and Spin-Crossover Behavior of Fluorinated Terpyridine-Based Co(II) and Fe(II) Complexes

Maite Nößler,[a] René Jäger,[a] David Hunger,[c] Marc Reimann,[d] Tobias Bens,[b] Nicolás I. Neuman,[b, e] Arijit Singha Hazari,[b] Martin Kaupp,[d] Joris van Slageren[b] and Biprajit Sarkar[a ,b]**

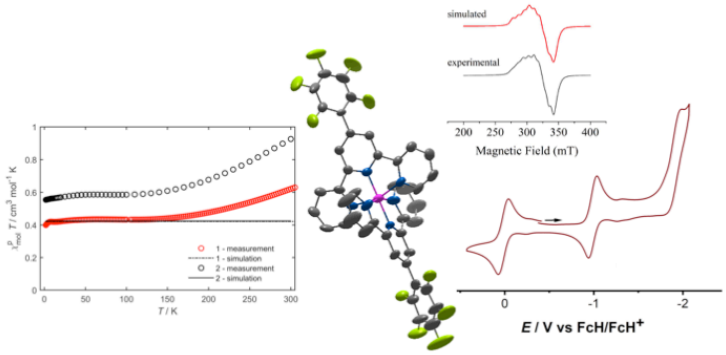

[a] Institut für Chemie und Biochemie, Anorganische Chemie
Freie Universität Berlin, Fabeckstraße 34-36, 14195, Berlin (Germany)
[b] Institut für Anorganische Chemie,
Universität Stuttgart, Pfaffenwaldring 55, 70569 Stuttgart (Germany)
[c] Institut für Physikalische Chemie,
Universität Stuttgart, Pfaffenwaldring 55, 70569 Stuttgart, Germany
[d] Technische Universität Berlin, Institut für Chemie, Theoretische Chemie/Quantenchemie, Sekr C7,
Straße des 17. Juni 135, D-10623 Berlin, Germany
[e] Instituto de Desarrollo Tecnológico para la Industria Química,
INTEC, UNL-CONICET Paraje El Pozo, Santa Fe, Argentina

This article was published and is reprinted with the permission from WILEY-VCH:

Maite Nößler,[a] René Jäger,[a] David Hunger,[c] Marc Reimann,[d] Tobias Bens,[b] Nicolás I. Neuman,[b, e] Arijit Singha Hazari,[b] Martin Kaupp,[d] Joris van Slageren[b]* and Biprajit Sarkar[a ,b]*, *Eur. J. Inorg. Chem.* **2023,** e202300091.

DOI: https://doi.org/10.1002/ejic.202300091 (© WILEY-VCH Verlag GmbH & Co. KGaA, Weinheim)

Author contribution: The project was designed by Biprajit Sarkar and Maite Nößler. The ligands and complexes were synthesized and characterized by Maite Nößler. René Jäger worked in this project during a research internship. Cyclic voltammetric and UV/Vis/NIR-spectroelectrochemical measurements were performed by René Jäger and Maite Nößler. The SQUID experiments were performed by David Hunger. X-Ray diffraction analysis was carried out by Maite Nößler. DFT calculations were performed by Marc Reimann. EPR measurements were performed by Maite Nößler and Nicolás I. Neuman, subsequent simulation of the spectra was performed by Tobias Bens, Nicolás I. Neuman and Arijit Singha Hazari. The manuscript was written by Maite Nößler, David Hunger, Nicolas Neumann, Marc Riemann, Martin Kaupp, Joris van Slageren and Biprajit Sarkar.

EurJIC
European Journal of Inorganic Chemistry

Chemistry Europe
European Chemical Societies Publishing

Accepted Article

Title: Electrochemistry and Spin-Crossover Behavior of Fluorinated Terpyridine-Based Co(II) and Fe(II) Complexes

Authors: Maite Nößler, René Jäger, David Hunger, Marc Reimann, Tobias Bens, Nicolás I. Neuman, Arijit Singha Hazari, Martin Kaupp, Joris van Slageren, and Biprajit Sarkar

To be cited as: *Eur. J. Inorg. Chem.* **2023**, e202300091

Link to VoR: https://doi.org/10.1002/ejic.202300091

WILEY-VCH

European Journal of Inorganic Chemistry 10.1002/ejic.202300091

Electrochemistry and Spin-Crossover Behavior of Fluorinated Terpyridine-Based Co(II) and Fe(II) Complexes

Maite Nößler,[a] René Jäger,[a] David Hunger,[c] Marc Reimann,[d] Tobias Bens,[b] Nicolás I. Neuman,[b, e] Arijit Singha Hazari,[b] Martin Kaupp,[d] Joris van Slageren[b] and Biprajit Sarkar[a ,b]**

[a] M. M. C. Nößler, R. Jäger, Prof. Dr. B. Sarkar
Institut für Chemie und Biochemie, Freie Universität Berlin, Fabeckstraße 34-36, D-14195, Berlin, Germany. URL: https://www.iac.uni-stuttgart.de/en/research/aksarkar/
E-mail: biprajit.sarkar@iac.uni-stuttgart.de

[b] T. Bens, Dr. A. Singha Hazari, Dr. N. I. Neuman, Prof. Dr. B. Sarkar
Institut für Anorganische Chemie, Universität Stuttgart, Pfaffenwaldring 55, D-70569 Stuttgart, Germany

[c] D. Hunger, Prof. Dr. J. van Slageren
Institut für Physikalische Chemie, Universität Stuttgart, Pfaffenwaldring 55, 70569 Stuttgart, Germany. URL: https://www.ipc.uni-stuttgart.de/slageren/

[d] M. Reimann, Prof. Dr. M. Kaupp
Technische Universität Berlin, Institut für Chemie, Theoretische Chemie/Quantenchemie, Sekr C7, Straße des 17. Juni 135, D-10623 Berlin, Germany

[e] Dr. N. I. Neuman
Instituto de Desarrollo Tecnológico para la Industria Química, INTEC, UNL-CONICET Paraje El Pozo, Santa Fe, Argentina

European Journal of Inorganic Chemistry 10.1002/ejic.202300091

Abstract

Due to their ability to form stable molecular complexes that have tailor-made properties, terpyridine ligands are of great interest in chemistry and material science. In this regard, we prepared two terpyridine ligands with two different fluorinated phenyl rings on the backbone. The corresponding Co^{II} and Fe^{II} complexes were synthesized and characterized by single-crystal X-ray structural analysis, electrochemistry and temperature-dependent SQUID magnetometry. Single crystal X-ray diffraction analyses at 100 K of these complexes revealed Co–N and Fe–N bond lengths that are typical of low spin Co^{II} and Fe^{II} centers. The metal centers are coordinated in an octahedral fashion and the fluorinated phenyl rings on the backbone are twisted out of the plane of the terpyridine unit. The complexes were investigated with cyclic voltammetry and UV/Vis-NIR spectroelectrochemistry. All complexes show a reversible oxidation and several reduction processes. Temperature dependent SQUID magnetometry revealed a gradual thermal SCO behavior in two of the complexes. EPR spectroscopy was also performed on the complexes.

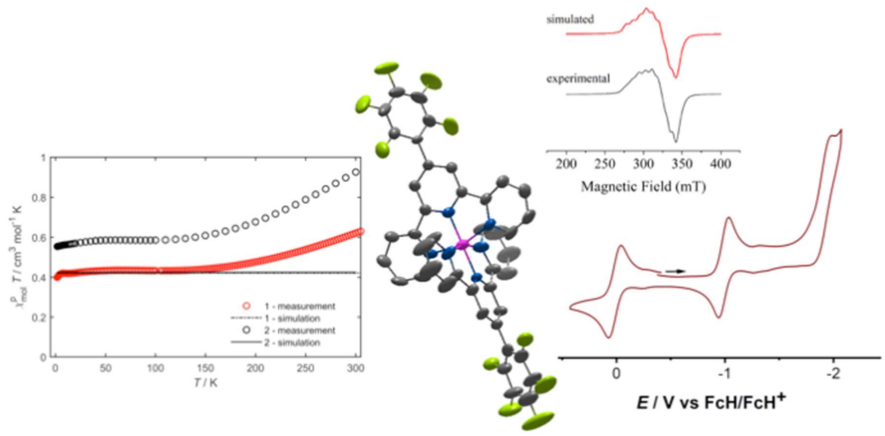

European Journal of Inorganic Chemistry 10.1002/ejic.202300091

Introduction

An important class of chelating ligands are the 2,2′:6′,2′′--terpyridines (TPYs). These ligands coordinate to different transition-metal ions of various oxidation states and form stable complexes.[1] Since the initial synthesis of terpyridine in 1932[2] several different synthetic methods have been developed for its synthesis. These include, amongst others, a Pd(0)-catalyzed pyridine coupling,[3] Hiyama,[4] Stille[5] or Suzuki cross-coupling or oxidation of diacetylpyridine and condensation with an aldehyde[6]. But there are still limitations regarding the efficient synthesis of structurally diverse terpyridine ligands and those bearing electronically different substituents.[7] There is a wide range of applications of metal complexes containing one or two terpyridine ligands: electrocatalysis for proton[8] or CO_2 reduction[8a, 9] and water oxidation,[10] photosensitizers,[11] redox shuttles for dye sensitized solar cells (DSSC),[12] supramolecular polymers,[13] nonlinear optics,[14] ion sensors[15] or anolytes for redox flow batteries[16] to name only a few examples. Furthermore, a high potential in clinical applications for complexes bearing a tpy unit has been reported.[17] The complexes are able to intercalate with DNA and for example the cytotoxicity of $Ru(TPY)Cl_2$ was investigated, which exhibits activity against certain leukemia cells in between the activity of cisplatin and carboplatin.[17b]

Terpyridine complexes can behave as spin-crossover systems and are hence of great interest for their potential use as sensors,[18] switches and memory devices.[19] Spin-crossover (SCO), known as the reversible switching between a low-spin (LS) and a high-spin (HS) state of a molecule, occurs typically in octahedrally coordinated transition-metal complexes with a d^4-d^7 electronic configuration. The SCO can be stimulated by external stimuli such as pressure, light, temperature or electric fields.[19b, 19c] Most commonly Co^{II} and Fe^{II} complexes have been studied, with $Fe^{II/III}$-based SCO complexes being an overwhelming majority.[20]

Over recent years materials that exhibit synergistic coexistence of two or more properties (multifunctional molecular materials) have received attention due to their potential applications in sensors, electrooptic devices, information storage and spintronics.[21] In such applications, the more attractive multifunctional molecule-based materials are SCO compounds, which are coupled for example with electrical conductivity,[22] liquid crystalline behavior,[23] non-linear optical (NLO)[24] and/or luminescence properties.[25] More recently, the group of Hayami investigated a Co^{II} complex bearing a terpyridine unit with a ((3-fluorophenyl)ethynyl) substituent in the para position of the central pyridine ring (FPh-terpy), that exhibit SCO behavior that is dependent on the degree of motion of the fluorophenyl ring. A ferroelectric

European Journal of Inorganic Chemistry 10.1002/ejic.202300091

hysteresis loop and spontaneous polarization is induced due to an electrically reversible dipole moment which results from the motion.[26]

The SCO properties of a bulk sample can be dramatically influenced by tuning the interactions between the SCO molecules the sample is based on.[27] In order to design new materials that might be applicable in information technology, it is important to understand the cooperative behavior in SCO transition.[27] One possible way to influence this behavior is to increase the flexibility of the ligands by attaching long alkyl groups.[27-28] In this regard the group of Hayami extensively studied Co^{II} complexes containing terpyridine ligands with long alkyl chains with respect to their SCO behavior.[27, 29] Moreover, these complexes also exhibit liquid crystalline properties.

The investigation presented in this work includes the synthesis of two Co^{II} and two Fe^{II} complexes with terpyridine ligands containing fluorinated substituents (Scheme 1). These substituents were introduced to either tune the properties of the metal complexes (fluorine as the most electronegative element, possible F-specific interactions), or to introduce additional functionalities (for example the redox-active dimethyl-amino group). Both of the aforementioned substituents are expected to affect the electrochemical and the spectroscopic properties of the metal complexes. Additionally, the fluorinated substituents can potentially engage in fluorine-specific interactions which can influence the magnetic properties of the resulting metal complexes. The complexes were characterized through crystallographic methods, cyclic voltammetry as well as UV/Vis/NIR spectroelectrochemistry and EPR spectroscopy. Additionally, the SCO behavior was investigated through temperature dependent SQUID magnetometry.

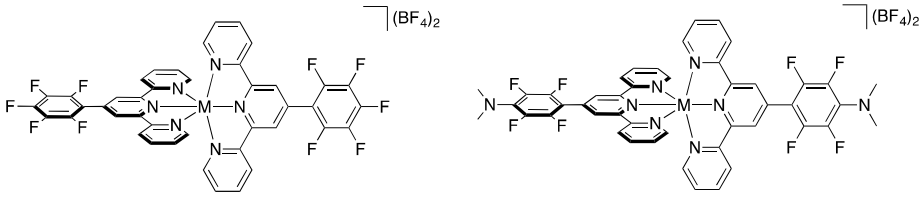

1: M = Co
3: M = Fe

2: M = Co
4: M = Fe

Scheme 1: New Co^{II} and Fe^{II} terpyridine complexes presented in this work.

Results and Discussion

Synthesis and Structural Characterization

European Journal of Inorganic Chemistry 10.1002/ejic.202300091

2,3,4,5,6-pentafluorobenzaldehyde was reacted with 2-acetylpyridine to yield ligand **1** according to a published procedure (Scheme 2).[30] Ligand **2** was synthesized by stirring 4'-(perfluorophenyl)-2,2':6',2''-terpyridine in *N*-*N*-dimethylformamide. The corresponding homoleptic complexes containing two of these ligands were synthesized by reacting the metal salt ($Co(BF_4)_2 \cdot 6\ H_2O$ or $Fe(BF_4)_2 \cdot 6\ H_2O$) with the ligands in a stoichiometric ratio of 1:2 in methanol at room temperature (See Experimental Section). All complexes were easily purified by dissolution of the complex in acetonitrile and suspension in diethylether. The resulting precipitates were filtered and the newly synthesized complexes were characterized by mass spectrometry, elemental analysis and, in case of complexes **1**-**3**, by X-ray diffraction. The cobalt complexes are paramagnetic, which was confirmed with ^{1}H-NMR spectra showing peaks up to 55 ppm, whereas the iron complexes are diamagnetic at room temperature, yielding diamagnetic ^{1}H NMR spectra in *d^3-acetonitrile* (See Supporting Information). This observation of low-spin Fe^{II} centers under ambient conditions was also reported with other Fe^{II} terpyridine-based complexes.[31]

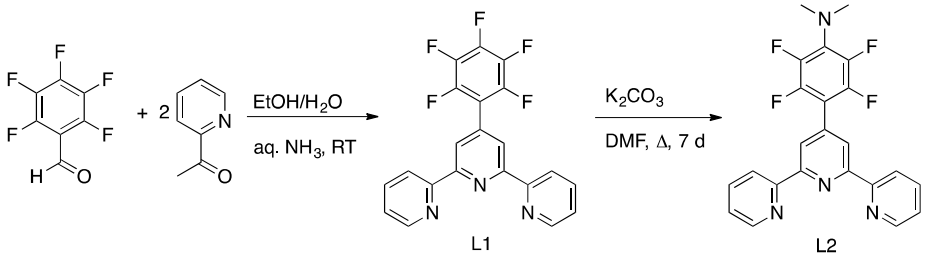

Scheme 2: Synthesis of ligands **1** and **2**.

It was possible to obtain suitable single crystals of three of the complexes by slow diffusion of diethylether in acetonitrile solutions. All the complexes crystallize in the orthorhombic Fdd2 space group and show the expected coordination motif. The metal center is coordinated in an octahedral fashion through the three nitrogen atoms of each ligand (Figure 1). The Co-N6 octahedron is highly distorted as can be seen from the shorter Co-N distance to the central pyridyl-N atoms compared the distances to the peripheral pyridyl-N atoms (Table 1). The fluorinated phenyl rings on the backbone are twisted out of the plane of the terpyridine unit. The bond lengths between 1.880 (7) and 2.152 (4) Å indicate a LS center for the Co^{II} complexes **1** and **2**[19c] and the bond lengths between 1.862 (7) and 1.980 (4) Å also point towards a LS center for the Fe^{II} complex **3** at the measured temperature of 100 K.[32]

European Journal of Inorganic Chemistry 10.1002/ejic.202300091

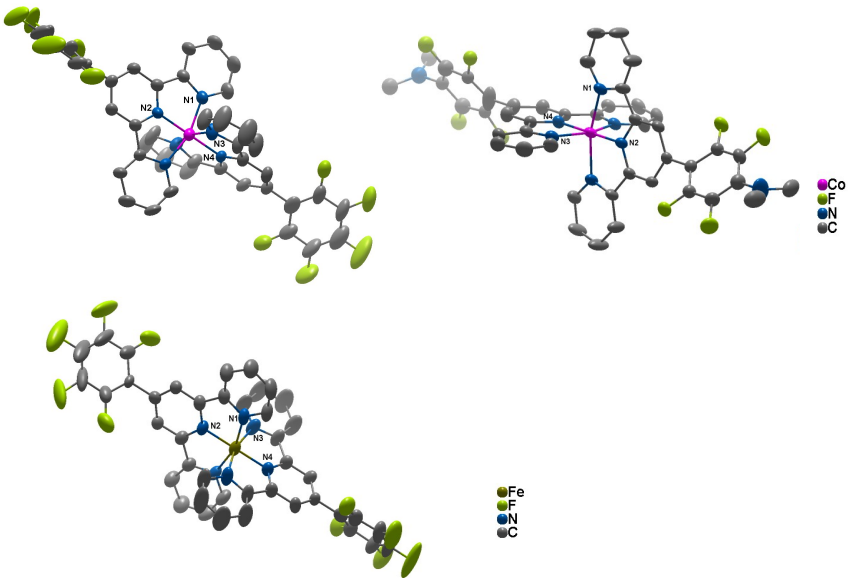

Figure 1: Perspective view of cobalt complexes **1** and **2** and iron complex **3** (disordered atoms were deleted, for a complete representation see Figure S12). Ellipsoids are at a probability level of 50%. H atoms, anions and solvent molecules are omitted for clarity.

The bond angles in and between the terpyridine rings and the metal center are similar for **1** and **3**. The angles of **2** show a larger distortion in the bond angles for one terpyridine unit with a difference up to 6° in comparison to **1** (for the N3-M-N3 angle). Selected bond angles of the complexes are depicted in table 2. The longer bond distances of Co-N3 of 0.2 Å support this observation. It appears that the introduction of the NMe_2 groups has an influence on the N-M-N angles, since the values differ from those of the complexes with the pentafluorophenyl ring. The angle between the planes of the tridentate ligands are nearly perpendicular to one another with values of 89.1° for complex **1**, 87.9° for complex **2** and 88.9° for complex **3**. The contact bond of 7.123 (2) Å between two nearest-neighbors of complex **1** is rather long, and similar values are also observed for the other two complexes. No specific fluorine specific interactions were observed. Nevertheless, the packing of the molecules is as expected (figure 2). The terpyridine units are face to face to one another and the BF_4^- anions and solvent molecules are arranged between the sheets (see Supporting Information).

European Journal of Inorganic Chemistry 10.1002/ejic.202300091

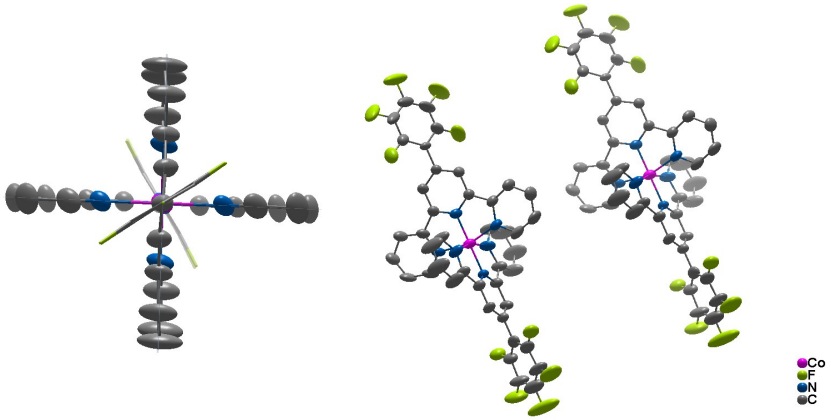

Figure 2: Orthogonality and depiction of neighboring atoms of complex **1**.

Table 1: Selected bond lengths of complexes **1**-**3**.

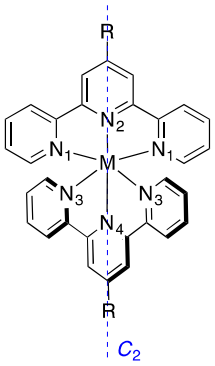

	M – N1	M – N2	M – N3	M – N4
1	1.968 (4)	1.880 (7)	1.976 (4)	1.894 (6)
2	2.022 (3)	1.891 (5)	2.152 (4)	1.949 (5)
3	1.966 (6)	1.86 (1)	1.979 (6)	1.90 (1)
$Co[TPYOC_{14}H_{29}]_2(BF_4)_2$[29f], [a]	2.137(4)/ 2.114(4)	1.910(3)	1.977(4)/ 1.976(4)	1.844(3)
$Fe[N_3P_3(OPh)_5(OPhTPY)]_2(PF_6)_2$[32], [b]	1.886 (3)	1.987 (3)	1.995 (3)	1.976 (3)

[a] Complex with a LS Co^{II} center:. [b]Complex with a LS Fe^{II} center.

Table 2: Selected bond angles of complexes **1**-**3**.

European Journal of Inorganic Chemistry 10.1002/ejic.202300091

	1	2	3
N1-M-N1	160.9 (3)	160.8 (2)	161.3 (3)
N1-M-N2	80.4 (2)	80.4 (1)	80.6 (2)
N1-M-N3	90.9 (2), 92.0 (2)	91.0 (2), 92.8 (2)	90.3 (2), 92.5 (2)
N1-M-N4	99.5 (2)	99.5 (2)	99.3 (2)
N2-M-N3	98.7 (2)	101.63 (9)	98.8 (2)
N2-M-N4	180.0	180.0	180.0
N3-M-N3	162.4 (3)	156.7 (2)	162.3 (3)
N3-M-N4	81.2 (2)	78.37 (9)	81.1 (2)

Cyclic Voltammetry

In order to investigate the influence of the metal center and the substituents on the terpyridine ligands on the redox properties of the complexes, cyclic voltammograms were recorded in anhydrous dichloromethane and acetonitrile solutions. The redox potentials for selected processes are given in table 3.

Cyclic voltammetry reveals that all complexes show at least one reversible oxidation for the M^{II}/M^{III} redox couple (in a 0.1 M NBu_4PF_6 dichloromethane solution).[33] In case of **2** and **3** a second irreversible oxidation is observed (see Supporting Information).

Both the cobalt complexes display a large peak-to-peak separation for the oxidation waves with ΔE_p of 164 mV for **1** and 104 mV for **2** for the first oxidation, whereas values of 88 mV and 83 mV were obtained for the iron complexes **3** and **4** (in CH_2Cl_2 at a scan rate of 0.1 V). This has been observed earlier for similar systems[34] and is probably related to the slow kinetics for electron transfer for such cobalt complexes which have to undergo a large structural reorganization because of their change from a HS Co(II) (predominant form at ambient temperatures) to a LS Co(III) form. The oxidation potentials of the iron complexes **3** and **4** are shifted to more positive potentials compared to their cobalt analogues. This fact is likely related to the removal of an electron from a e_g orbital in a HS Co(II) case in comparison to the removal of an electron from a t_{2g} orbital in a LS Fe(II) case. Our calculations at the B97-D/def2-TZVP level clearly support the low-spin nature of both d^6 compounds. For the Co(II) compound, however, both relative energies and the form of the calculated spectrum rather suggest the presence of a low-spin (doublet) ground state (see Section S6 of the SI). This is consistent with the structures obtained experimentally at 100 K. The effect of the substituents on the ligand on the oxidation potentials of the metal complexes is negligible.

All complexes display two reduction steps. For the cobalt complex **1** the first reduction is

European Journal of Inorganic Chemistry 10.1002/ejic.202300091

reversible, whereas for complex **2** both the first and the second reduction steps are irreversible (Figure 3). At this point it is not completely clear as to why the reversibility of the first reduction step is different for the complexes **1** and **2**. A possible reason could be the presence of the additional basic dimethylamino groups on the backbone of the substituted terpyridine ligands in complex **2**. Such basic groups might become more susceptible to follow-up reactions on reduction of the complex. In contrast, the iron complexes **3** and **4** both display two reversible reduction steps. Furthermore, the first reduction step for the iron complexes is negatively shifted by about 400 mV compared to those of the cobalt complexes (Figure 3 and Table 3). We attribute these differences to a predominantly ligand centered reduction step for the iron complexes, and to a more complex electronic situation for the reduced forms of the cobalt complexes (see below). This phenomenon has been observed earlier in different metal complexes with terpyridine ligands,[35] but also for e.g. bis(pyridine-2.6-diimine) cobalt, zinc and iron complexes,[36] where it had been assigned to a metal-centered reduction of Co^{II} to Co^{I}. The potentials of the redox processes observed in both dichloromethane and acetonitrile solvents only differ slightly (see table 3). However, in an acetonitrile solution additional redox processes can be observed for complexes **2**-**4**. The additional reduction processes are all irreversible (see Supporting Information). This might be due to disconnection of the ligand and addition of an acetonitrile molecule.[37]

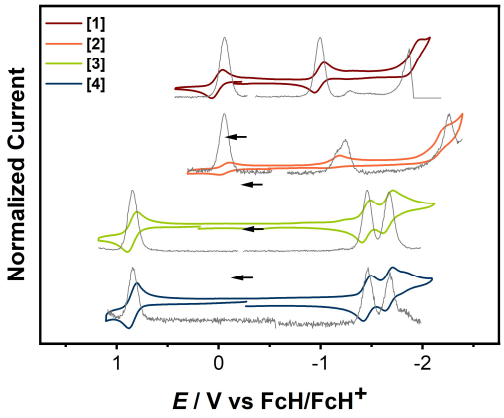

Figure 3: Cyclic voltammograms and differential pulse voltammograms of complexes **1**-**4** in CH_2Cl_2/NBu_4PF_6 measured with a glassy carbon working electrode (FcH = ferrocene; FcH^+ = ferrocenium).

Table 3: Redox potentials vs. FcH/FcH^+ measured in CH_2Cl_2 at 100 mVs^{-1} with 0.1 M Bu_4NPF_6 at room temperature.[a]

	$E_{1/2}^{Ox1}$	$E_{1/2}^{Red1}$	$E_{1/2}^{Red2}$

European Journal of Inorganic Chemistry 10.1002/ejic.202300091

1	-0.06	-0.99	-1.99[b]
2	-0.05	-1.10[b]	-2.24[b]
3	0.85	-1.45	-1.66
4	0.84	-1.46	-1.68

[a] All measured with a glassy carbon electrode. [b] Peak potential for irreversible processes.

UV/Vis/NIR spectroelectrochemistry

The interplay of the electrochemical and optical properties was probed with UV/Vis/NIR spectroelectrochemistry using an optically transparent thin layer electrochemical (OTTLE) cell. Therefore, we concentrated on the first oxidation of all the complexes, the first reduction for **1** and **2** and the first two reductions for **3** and **4**. Due to strong adsorption of complex **4** on the gold working electrode, which inhibited any optical observations, the complex was measured with a platinum working electrode. In the UV/Vis spectra (shown in figure S8) it is evident that the variations of the ligand backbone do not have a strong effect on the absorption spectrum. Since the complexes with both ligands showed a similar behavior, TD- DFT calculations at the B97-D/def2-TZVP level were performed only for complexes **1** and **3** (for Details, see Section S6 of the Supporting Information). The measured UV/Vis spectra are in good agreement with the calculated ones (see figures S17 and S18 in the Supporting Information).

Figure 4 shows the results of UV/Vis/NIR spectroelectrochemistry for complexes **1** (in CH_2Cl_2) and **2 (**in CH_3CN). Upon oxidation of complex **1** (Figure 4a) and **2** (Figure S10e) a decrease in the extinction coefficient was observed (in CH_2Cl_2).

Upon reduction of **1** and **2** the band at 500 nm increases in intensity and a new band at around 1300 nm arises (Figure 4b and d). This feature is very different from what is observed for the reduced forms of the iron complexes (see below). DFT (B97-d/def2-TZVP) calculations suggest a distribution of the spin density over both the ligands and the metal, pointing to a complex electronic situation (see Supporting Information, section S6 for details). Regarding previous studies on terpyridine-based cobalt complexes of the group of Wieghardt, the bands at 500 nm and 1300 nm might be assigned to metal-to-ligand $3d^8 \rightarrow 3d^7\,\pi^{*1}$ charge-transfer transitions.[38] Since the second reduction of **1** and **2** were irreversible during CV they were not investigated any further. As the native spectra and the end spectrum after reduction of **1** is similar to the native spectrum the process seems to be reversible, while for **2** is irreversible, which is in accordance with the data obtained from cyclo voltammetric measurements.

European Journal of Inorganic Chemistry 10.1002/ejic.202300091

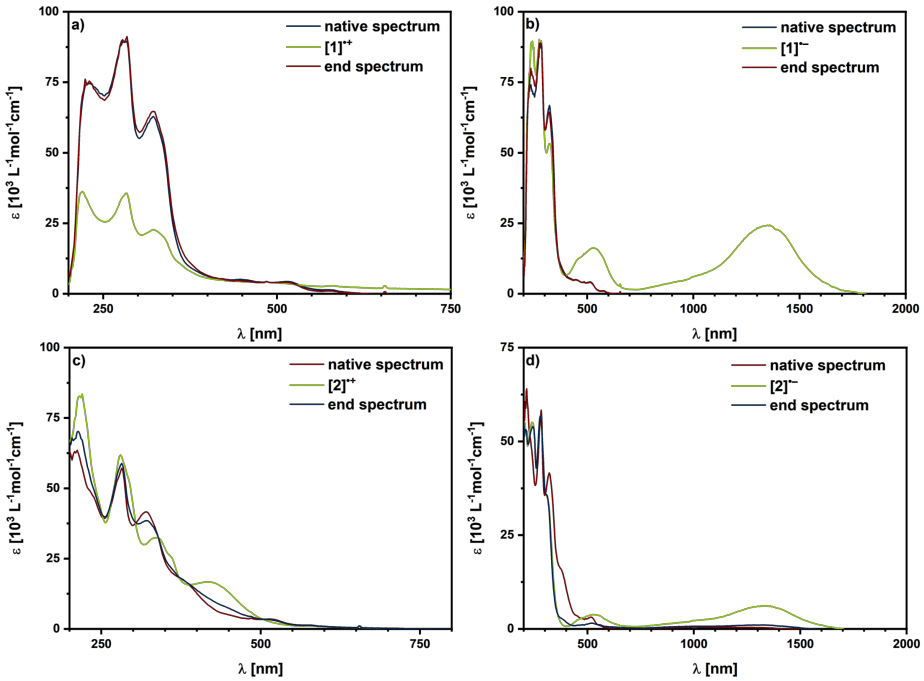

Figure 4: UV/Vis SEC spectra of complex **1** top, left: oxidation, right: reduction in CH_2Cl_2/NBu_4PF_6 measured with a gold working electrode; bottom UV/Vis/NIR spectrum of complex **2** during the oxidation in CH_3CN/NBu_4PF_6 measured with a gold working electrode.

As the spectra for both iron complexes are similar, only the spectra of **3** will be discussed in detail (figure 5a-c). In the native form, **3** and **4** exhibit $\pi-\pi*$ transitions below 350 nm and a MLCT band at 560 nm. Additionally, shoulders are observed at around 630 nm which are consistent with iron-centered d-d transitions in related systems.[32] Upon oxidation, the band at 560 nm decreases and increases again after re-reduction (figure 5a), showing a reversible oxidation for **3,** which corresponds to an Fe^{II} to Fe^{III} oxidation, as confirmed by calculated natural population analysis (NPA) charges obtained at the DFT level (see Supporting Information, section S6). During the reduction, the MLCT band at 560 nm shifts to higher wavelengths and the appearance of additional shoulders can be observed (figure 5b), which is clearly reproduced by theory (Fig. S17 of the Supporting Information).

Overall, the oxidation and first reduction process of **3** are fully reversible, as the native and the end spectrum after the second reduction show a loss in the extinction coefficient (figure 5c). This might be due to structural changes upon reduction or decomposition of the complexes.

European Journal of Inorganic Chemistry 10.1002/ejic.202300091

The reduction overall takes place at the ligand, as is supported by NPA charges (see section S6 of the Supporting Information).

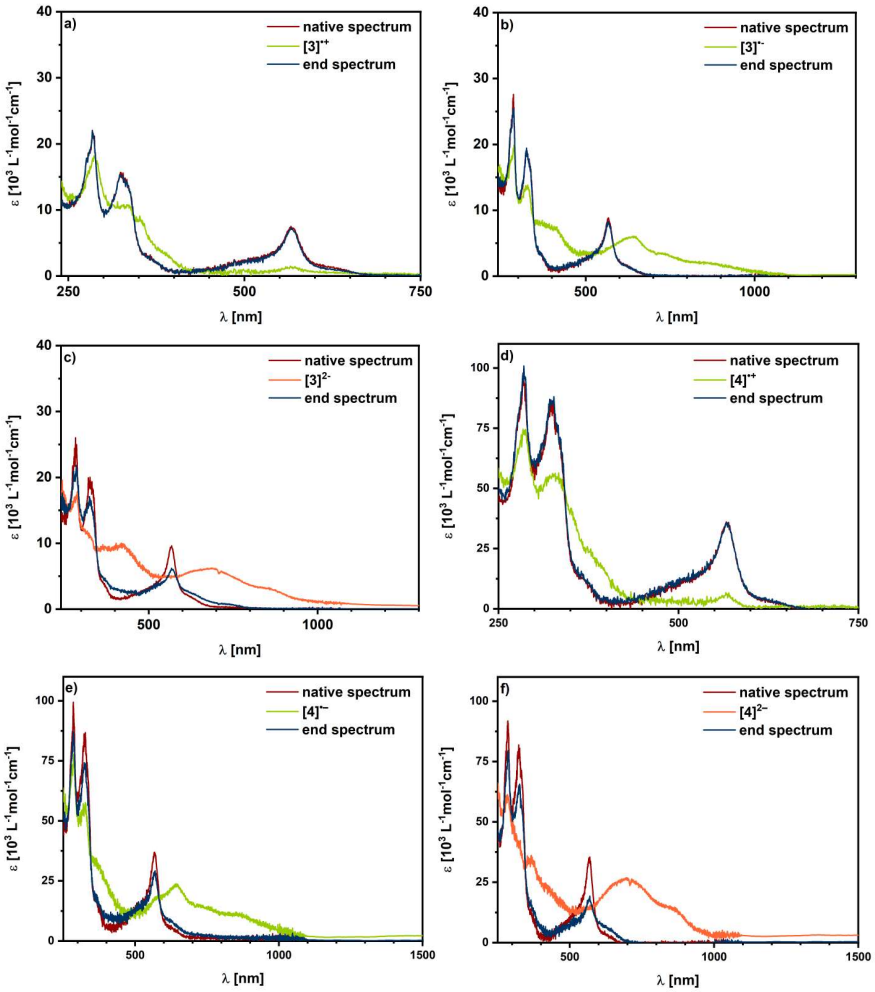

Figure 5: UV/Vis SEC spectra of complex **3** (a) oxidation, b) first reduction c) second reduction) in CH_2Cl_2/NBu_4PF_6 measured with a gold working electrode; UV/Vis SEC spectra of complex **4** (d) oxidation, e) first reduction f) second reduction) in CH_2Cl_2/NBu_4PF_6 measured with a platinum working electrode.

EPR Spectroscopy

Both Co^{II} complexes **1** and **2** display anisotropic EPR signals in solution and in the solid state at 93 K, with partially resolved hyperfine splittings arising from interaction of the electron spin with the ^{59}Co nucleus (I = 7/2). The EPR spectra obtained from powdered samples of **1** and **2**

European Journal of Inorganic Chemistry 10.1002/ejic.202300091

were simulated with rhombic **g**- and **A**-matrices (values given in Table 4). The *g*-values in the 2.00-2.20 range are consistent with a low-spin Co^{II} center[39] and in agreement with the Co-N distances determined from X-ray diffraction. The rhombic ***g***-matrices, deviating from the free-electron value of 2, as well as the large hyperfine splittings, clearly indicate a metal centered spin. In a perfectly octahedral environment, the unpaired electron would reside in the degenerate e_g orbitals. Jahn-Teller distortions lift this degeneracy, which can result in the unpaired electron being either on a $d_{x^2-y^2}$ or d_{z^2} orbital, or a mixture of the two, with the *z*-axis being that of the axial Jahn-Teller distortion.[39-40] The rhombic nature of the *g*-values in complexes **1** and **2** indicate that the magnetic orbital is an admixture of the $d_{x^2-y^2}$ or d_{z^2} orbitals.

The spectra recorded in the solid state and in solution have similar *g*- and *A*-values for **1** but show different *A*-values for **2**. Additionally, the hyperfine coupling in solution for **2** shows a better resolution (figure 6). These differences are consistent with small changes in the solution and solid-state structures, likely arising from packing effects in the latter.

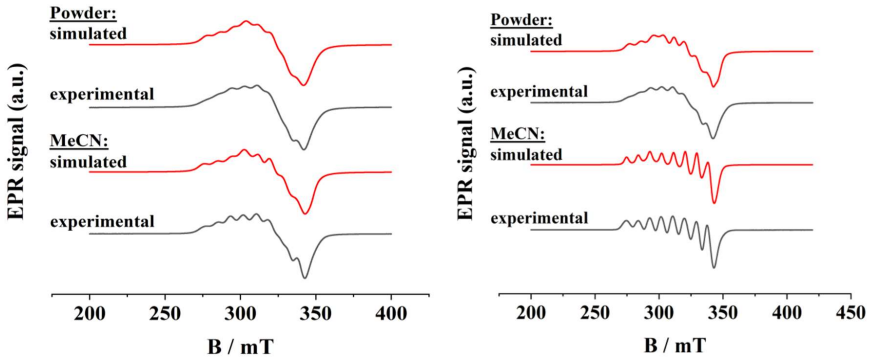

Figure 6: Experimental (grey) and simulated (red) EPR spectra of: left: $Co(TPYF_5Ph)_2(BF_4)_2$ **1** of powdered sample at –180°C and in CH_3CN at −179°C, right: $Co(TPYPhF_4NMe_2)_2(BF_4)_2$ **2** of powdered sample at −179°C and in CH_3CN at –180°C.

Table 4: Simulation parameters of **1** and **2**. *g*-values, hyperfine *A*-values (MHz), anisotropic Gaussian broadening HS (MHz) and isotropic Gaussian and Lorentzian broadenings (mT).

	1		**2**	
	Powder	**CH_3CN**	**Powder**	**CH_3CN**
g_x	2.022	2.004	2.009	2.033
g_y	2.147	2.159	2.178	2.144

European Journal of Inorganic Chemistry 10.1002/ejic.202300091

g_z	2.191	2.199	2.192	2.199
A_x / MHz	52.3	42.3	42.0	75.9
A_y / MHz	84.6	82.9	91.7	173.4
A_z / MHz	271.6	281.7	279.4	287.2
HS_x / MHz	276.7	4.2	0.2	152.0
HS_y / MHz	219.8	60.8	123.7	208.7
HS_z / MHz	89.5	146.2	171.9	81.1
lwpp / mT	[2.79 3.88]	3.61	[0 2.05]	[0.81 1.04]

In addition to the native state of complexes **1** and **2**, the one-electron reduced form of complexes **3** and **4** were investigated with EPR spectroelectrochemical measurements. For both complexes a signal, without hyperfine coupling, could be observed after electrolysis at temperatures below 0 °C (Figure 7). The *g*-values of 1.983 for both complexes are close to the *g*-values of the free electron (table 5),[41] which indicates a ligand-centered spin. These measurements support the assignment of the first reduction being located on the terpyridine ligand. The Fe nucleus has no nuclear spin, but the ^{14}N nuclei in the terpyridine ligands have $I = 1$. Using the same intrinsic line width (~2 mT) as for the Co complexes resulted in a much too narrow simulated resonance, which did not adequately reproduce the experimental spectra. For this reason, we included in the simulation the (unresolved) hyperfine interaction to three ^{14}N nuclei, which improved the simulations. The spectra are depicted in figure 7.

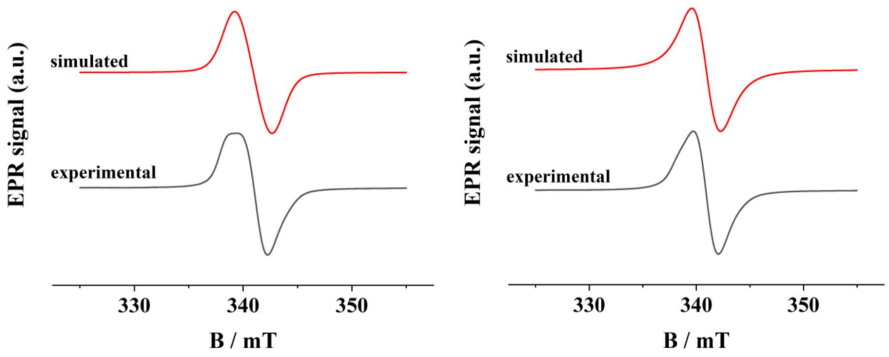

Figure 7: Experimental (grey) and simulated (red) EPR spectra of $Fe(TPYPhF5)_2(BF_4)_2$ **3** (left) and $Fe(TPYPhF_4NMe_2)_2(BF_4)_2$ **4** right during EPR SEC measurements of the first reduction in a CH_2Cl_2/NBu_4PF_6 measured with a platinum working electrode.

Table 5: Simulation parameters for one-electron reduced states of **3** and **4** in a frozen solution of CH_2Cl_2.

European Journal of Inorganic Chemistry 10.1002/ejic.202300091

Parameters	**3**	**4**
	Frozen solution	Frozen solution
g	1.983	1.983
A_N/ MHz	10.0	9.0
Line width for isotropic broadening / mT	[2.00]	[1.45]

Magnetic Measurements

As the complexes contain M^{II} ions in a d^6 or d^7 electronic configuration the metal centers can occur in two spin states (high spin and low spin) and might be reversibly switched between these states by an external stimulus. In this regard, an excellent method for probing the temperature dependent SCO behavior of Fe^{II} and Co^{II} compounds is SQUID magnetometry. If the energy difference from the LS state (S = 0 or S = $^1/_2$) to the HS state (S = 2 or S = $^3/_2$) is provided by thermal energy, a change in the magnetic behavior can be observed.[42] For this, complexes **1-3** were investigated by the means of SQUID magnetometry in the temperature [T] range of 1.8 to 300 K. The T dependence of the χT product is depicted, where χ is the molar static magnetic susceptibility, which can be approximated at low fields as the ration between the molar magnetization and the applied magnetic field.

For the cobalt complexes a gradual thermal SCO behavior is observed from 150 K on with increasing temperature. Due to no strong intermolecular interactions between the SCO units this gradual SCO is expected. The $\chi_M T$ value for complex **1** increases from 0.39 cm^3Kmol^{-1} at 1.8 K to 0.42 cm^3Kmol^{-1} at 7 K and remains almost constant at 0.44 cm^3Kmol^{-1} up to 150 K. From 150 K the start of the SCO is observed with a gradual increase of the χ_MT value from 0.44 cm^3Kmol^{-1} at 150 K to 0.63 cm^3Kmol^{-1} at 300 K.

Complex **2** displays a similar SCO behavior as complex **1**. In this case the $\chi_M T$ value remains almost constant at 0.59 cm^3Kmol^{-1} until it starts increasing upon heating at 150 K. The curve is gradually increasing up to 300 K with a $\chi_M T$ value of 0.92 cm^3Kmol^{-1}.

Spin-Hamiltonian simulations of the temperature dependence of $\chi_M T$ based on the parameters obtained by powder EPR of the low spin species of **1** and **2** are shown in figure 8. While for **1**, the measured $\chi_M T$ values between 5 and 100 K are in good accordance with the simulation, a strong deviation in the case of **2** is found. In both cases, the measured curves also show a bending to smaller $\chi_M T$ values below 5 K, hinting towards an interaction, which is not covered by the simulation. An explanation for this is a residual of HS species at low temperatures, which is significantly higher in the case of **2**. This will result in a way higher $\chi_M T$ in the temperature range, where only the LS system is expected, than the $\chi_M T$ value based on the EPR parameters.

European Journal of Inorganic Chemistry 10.1002/ejic.202300091

In the case of **3**, no SCO and a minor $\chi_M T$ value was observed from 1.8 K up to 300 K. The LS state of Fe^{II} is S = 0 and hence not possessing any magnetic moment. Nevertheless with 0.08 cm^3Kmol^{-1}, a non-zero value of $\chi_M T$ is found at 300 K. This is even lower than the theoretical value for a S = $^1/_2$ system with $g = 2$ (0.375 cm^3Kmol^{-1}). As in the case of both Co^{II} compounds, this moment is attributed to a minor Fe^{II} HS amount of 2% in the sample (Figure S1).

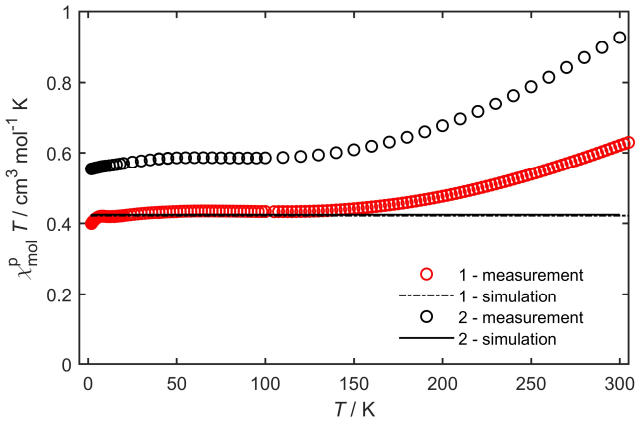

Figure 8: Temperature dependency of the $\chi_M T$ product for **1** and **2** in an applied magnetic field of 1000 Oe as well as the corresponding LS spin Hamiltonian simulations.

Conclusion

We successfully synthesized a new terpyridine ligand and a series of new terpyridine ligand based homoleptic Co^{II} and Fe^{II} complexes. The complexes were characterized and investigated through cyclic voltammetry, UV/Vis/NIR spectroelectrochemistry and EPR spectroscopy. The cyclic voltammogram revealed, that the change of the para-F on the backbone to the NMe_2 group only has a marginal influence on the redox-potentials, but the different metal centers show redox processes at different potentials. Furthermore, the change of the solvent from CH_2Cl_2 to CH_3CN leads to additional processes, which might be due to reaction with CH_3CN molecules during the measurement or an increased solvent window. The solid-state structure of complexes **1**-**3** was revealed by single crystal X-ray diffraction analysis. For complexes **1**-**3** the bond distances point towards a LS center at 100 K. Additionally, the SCO behavior was investigated through SQUID magnetometric measurements. Complexes **1** and **2** show a gradual SCO whereas complex **3** remains in the LS state over the measured temperature range. Furthermore, the ^{1}H NMR spectra of complex **3** indicates that the Fe^{II} center is in its LS state at room temperature.

European Journal of Inorganic Chemistry 10.1002/ejic.202300091

EPR measurement of complexes **1** and **2** show partially resolved hyperfine splittings that arise from interactions of the electron spin with the ^{59}Co nucleus. This pattern was observed in the solid state and solution sample. The first reduction process of complexes **3** and **4** were investigated with EPR spectroelectrochemical measurements. The obtained signals show *g* values that are close to the one of the free electron, which supports the observation of a terpyridine-based process for the iron complexes. In contrast, the first reduction process of the Co complexes is of a more mixed nature, which was confirmed by UV/Vis SEC measurements and quantum chemical calculations of complex **1**. Finally, all complexes were probed with polymerized optical microscopy regarding their liquid crystalline properties. Unfortunately, all complexes remained solid over the measured temperature range and thus no phase transitions could be observed.

Experimental Section

General Remarks and Instrumentation. If noted, reactions were carried out using standard Schlenk-line techniques under an inert atmosphere of argon (Linde, HiQ Argon 5.0, purity ≥99.999%). Compounds: Ligands **1** was synthesized following published procedures.[30] Commercially available chemicals were used without further purification. Dry DMF was available from Acros Organics (99.8% extra dry) and was used as received. Other dry solvents were available from MBRAUN MB-SPS- 800 solvent system and degassed by standard techniques prior to use. Column chromatography was conducted using aluminum oxide (Aluminum Oxide basic, Macherey-Nagel, 50−200 μm). ^{1}H NMR, proton decoupled ^{13}C and ^{19}F NMR were recorded on JEOL ECS 400 spectrometer and JEOL ECZ 400R spectrometer. Chemical shifts are reported in ppm (relative to the TMS signal) with reference to the residual solvent peaks.[43] Multiplets are reported as follows: singlet (s), duplet (d), triplet (t), quartet (q), quintet (quint), septet (sept), and combinations thereof. Mass spectrometry was performed on an Agilent 6210 ESI-TOF. Elemental analysis was performed on a Perkin Elmer Analyser 240.

Cyclic voltammograms were recorded with a PAR VersaStat 4 potentiostat (Ametek) by working in anhydrous and degassed acetonitrile or dichloromethane with 0.1 M NBu_4PF_6 (dried, > 99.0%, electrochemical grade, Fluka) as supporting electrolyte. Concentrations of the complexes were about $1 \cdot 10^{-4}$ M. A three-electrode setup was used with a glassy carbon working electrode, a coiled platinum wire as counter electrode and a coiled silver wire as a pseudoreference electrode. The ferrocene/ferrocenium or

European Journal of Inorganic Chemistry 10.1002/ejic.202300091

decamethylferrocene/decamethylferrocenium couples were used as internal reference.

UV/Vis spectra were recorded with an Avantes spectrometer consisting of a light source (AvaLight-DH-S-Bal), a UV/VIS detector (AcaSpec-ULS2048), and an NIR detector (AvaSpec-NIR256-TEC) or on a J&M Tidas UV- Vis-NIR spectrophotometer. Spectroelectrochemical measurements were carried out in an optically transparent thin-layer electrochemical (OTTLE) cell (CaF_2 windows) with a gold or platinum working electrode, a platinum mesh counter electrode, and a silver-foil pseudoreference electrode.[44] Anhydrous and degassed acetonitrile or dichloromethane with 0.1 M NBu_4PF_6 as supporting electrolyte was used as solvent. An Autolab PGSTAT101 potentiostat (Metrohm) was used for all spectro-electrochemical measurements.

Electron paramagnetic resonance

EPR spectra at X-band frequency (ca. 9.5 GHz) were obtained with a Magnettech MS-5000 benchtop EPR spectrometer equipped with a rectangular TE 102 cavity and TC HO4 temperature controller. The measurements were carried out in synthetic quarz glass tubes. For EPR spectro-electrochemistry a three-electrode setup was employed using two Teflon-coated platinum wires as working and counter electrodes and a Teflon-coated silver wire as pseudo-reference electrode. Spectral simulations were performed with EasySpin 5.1.4[7] and MatLab R2012a.

X-ray diffraction

X-ray data were collected on a Bruker Smart AXS or Bruker D8 Venture system at 100(2) K, respectively, using graphite-monochromated Moα radiation (λ_α = 0.71073 Å). Using the Smart software or using the APEX2 software, respectively, evaluated the strategy for the data collection. The data were collected by the standard omega scan or omega + phi scan techniques, and were scaled and reduced using Saint + and SADABS software. Direct methods or intrinsic phasing using SHELXT-2014/7 solved the structures. Structures were refined by full matrix least-squares using OLEX2,[45] refining on F2. Non-hydrogen atoms were refined anisotropically.[46] Deposition numbers 2150337 (for **1**), 2150346 (for **2**), 2150345 (for **3**), contain the supplementary crystallographic data for this paper. These data are provided free of charge by the joint Cambridge Crystallographic Data Centre and Fachinformationszentrum Karlsruhe.

SQUID Magnetometry

European Journal of Inorganic Chemistry 10.1002/ejic.202300091

All susceptibility measurements were carried out on a Quantum Design MPMS3 SQUID magnetometer. The measurements at a constant magnetic field of 1000 Oe in a temperature range from 1.8 K to 50 K and at 10 000 Oe in a temperature range from 40 K to 300 K. The measured data in the intersection of the temperature ranges served to compensate for possible ferromagnetic impurities. Samples were pounded with little pressure and mixed with eicosane. The mixture was melted in a capsule with a hot air gun maximized to a temperature of 50°C (323.15 K) and the capsule was then fixed in a plastic tube. The temperature dependent measurements were limited to a temperature of 300 K due to the melting of the used eicosane matrix (melting point of eicosane: 311 K). Data were corrected for the diamagnetic contribution to the susceptibility by means of Pascal's constants.[47]

Computational Details

All calculations have been performed using the TURBOMOLE program package, version 7.5.1 [TURBOMOLE V7.4 2019, a Development of University of Kalsruhe and Forschungszentrum Karlsruhe GmbH, 1989-2007, TURBOMOLE GmbH, since 2007; Available from http://www.turbomole.com.].[48] Structures were optimized using the TPSS functional,[49] def2-TZVP basis sets,[50] including Grimme's D3 dispersion corrections[51] with Becke-Johnson damping[52] and the COSMO solvation model[53] with a dielectric constant of 8.94 for CH_2Cl_2. All calculations employed *gridsize* 3 and the multipole accelerated RIJ[54] approach in combination with the respective auxiliary basis sets.[55] Based on the excellent performance of the B97-D functional[56] in the recent benchmark study on SCO energies in Fe(II) complexes,[57] additional energy and TDDFT calculations were performed at the B97-D/def2-TZVP level.

For TDDFT spectra calculations, the ground-state SCF was converged until the energy changes were below 10^{-8} Hartree, and the changes in the density matrix were below 10^{-7}. A sufficient number of excitations were calculated so that the largest excitation energy covered was above 4.9 eV, which corresponds to λ=250 nm. The excitation energies were converged until the remaining residue was below 10^{-4}.

Synthesis

TPY-PhF$_5$ L1

European Journal of Inorganic Chemistry 10.1002/ejic.202300091

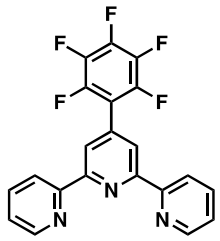

The synthesis was performed according to a literature known procedure.[1]
2,3,4,5,6-pentafluorobenzaldehyde (586.3 mg, 3.0 mmol) was dissolved in ethanol (20 mL), 2-acetylpyridine (848.0 mg, 0.7 mmol) and KOH (390.0 mg, 7.0 mmol) were added. 25 mL of concentrated ammonia solution was added and the mixture was stirred at room temperature over night. The resulting solid was filtered and washed with cold water and ethanol yielding in the desired product as yellow solid (199.8 mg, 0.5 mmol, 71%).
The ^{1}H NMR spectrum is similar to the spectrum literature (recorded in $CDCl_3$).[58]
^{1}H-NMR (DMSO, 400 MHz, 21 °C): δ = 8.73 (dq, ^{3}J = 9.2, 1.1 Hz, 2H), 8.70 – 8.65 (m, 4H), 7.93 (td, J = 7.7, 1.8 Hz, 2H), 7.44 – 7.34 (m, 2H) ppm.
^{19}F (DMSO, 400 MHz, 21 °C): δ = –142.80, –145.82, –156.45, –157.99, –164.16 ppm.

TPY-PhF$_4$NMe$_2$ L2

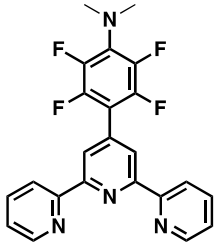

4'-(perfluorophenyl)-2,2':6',2"-terpyridine (199.6 mg, 0.5 mmol) and K_2CO_3 (276.4 g, 2.0 mmol) were dissolved in dry *N*,*N*-dimethylformamide (10 mL). The mixture was stirred at 90°C for one week. After cooling to room temperature CH_2Cl_2 (30 mL) was added and extracted with water and brine (30 mL). The crude product was purified by column chromatography (basic Al_2O_3, CH_2Cl_2). The solvent was evaporated, the resulting solid dissolved in CH_2Cl_2 and precipitated in *n*-pentane. After filtration the solvent was evaporated yielding in a yellow solid (86.0 mg, 0.2 mmol, 41%).
^{1}H-NMR ($CDCl_3$, 400 MHz, 24 °C): δ = 8.70 (d, ^{3}J = 4.8 Hz, 2H), 8.66 (dd, ^{3}J = 8.0, 4.3 Hz, 2H), 8.57 (s, 2H), 7.93 – 7.84 (m, 2H), 7.41 – 7.29 (m, 2H), 4.43 – 4.35 (m, 3H), 1.47 (t, ^{3}J = 7.0 Hz, 3H) ppm.

European Journal of Inorganic Chemistry 10.1002/ejic.202300091

^{19}F-NMR (CDCl3, 376 MHz, 23 °C): δ = –141.99 (dd, J = 22.7, 7.7 Hz), –143.26 – (–144.01) (m), –144.45 – (145.17) (m), –151.51 (d, J = 12.3 Hz), –153.02 (t, J = 21.3 Hz), –156.68 – (–156.86) (m), –161.17 (dd, J = 21.2, 7.6 Hz) ppm.

^{13}C-NMR ($CDCl_3$, 101 MHz, 27 °C) δ = 15.5, 43.3, 71.1, 121.4, 122.2, 124.1, 124.1, 137.0, 149.4, 155.8, 156.1 ppm.

HRMS (ESI): calcd. For $[C_{23}H_{17}F_4N_4]^+$ $[M - H]^+$: 425.1384 *m/z*; found 425.1385.

$[Co(TpyPhF_5)_2](BF_4)_2$ 1

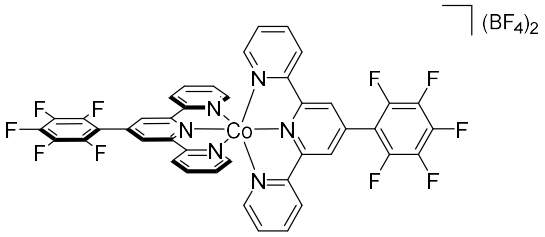

$Co(BF_4)_2$ • 6 H_2O (170.3 mg, 0.5 mmol) was dissolved in 30 mL MeOH and 4'-(perfluorophenyl)-2,2':6',2''-terpyridine (399.0 mg, 1.0 mmol) was added. The mixture was stirred for two days, the solvent was evaporated and the crude product was dissolved in acetonitrile and precipitated in ethanol, yielding in a red solid (399.0 mg, 0.4 mmol, 76%). Crystals suitable for X-Ray diffraction were grown by slow diffusion of diethylether in an acetonitrile solution of the complex.

HRMS (ESI): calcd. For $[C_{42}H_{20}CoF_{10}N_6]^{2+}$: *m/z* 428.5455; found 428.5488.

Anal. Calcd for $C_{42}H_{20}B_2CoF_{18}N_6$: C, 48.92; H, 1.96; N, 8.15. Found: C, 48.94; H, 2.00; N, 8.17.

$[Co(TpyPhF_4NMe_2)_2](BF_4)_2$ 2

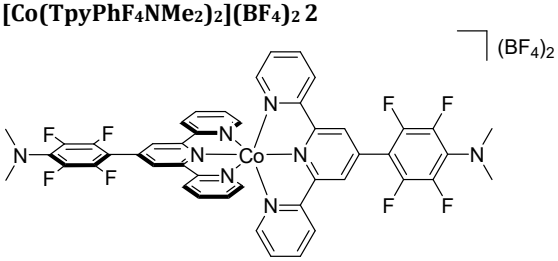

$Co(BF_4)_2$ • 6 H_2O (49.40 mg, 0.15 mmol) was dissolved in 5 mL MeOH and 4-([2,2':6',2''-terpyridin]-4'-yl)-2,3,5,6-tetrafluoro-*N*,*N*-dimethylaniline (121.3 mg, 0.29 mmol) was added. The mixture was stirred for one week, the solvent was evaporated and the crude product was dissolved in acetonitrile and precipitated in diethylether, yielding in a red

European Journal of Inorganic Chemistry 10.1002/ejic.202300091

solid (100.10 mg, 0.09 mmol, 62%). Crystals suitable for X-Ray diffraction were grown by slow diffusion of diethylether in an acetonitrile solution of the complex.

HRMS (ESI): calcd. For $[C_{46}H_{32}CoF_8N_8]^{2+}$: *m/z* 453.5972; found 453.6017.

Anal. Calcd for $C_{46}H_{32}B_2F_{16}CoN_8$: C, 51.09; H, 2.98; N, 10.36. Found: C, 51.23; H, 3.25; N, 10.66.

$[Fe(TpyPhF_5)_2](BF_4)_2$ 3

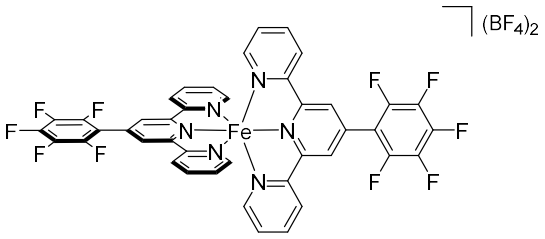

$Fe(BF_4)_2$ • 6 H_2O (168.7 mg, 0.5 mmol) was dissolved in 10 mL MeOH and 4'-(perfluorophenyl)-2,2':6',2''-terpyridine (399.0 mg, 1.0 mmol) was added. The mixture was stirred for four days, the solvent was evaporated and the crude product was dissolved in acetonitrile and precipitated in ethanol, yielding in a purple solid (439.5 mg, 0.4 mmol, 85%). Crystals suitable for X-Ray diffraction were grown by slow diffusion of diethylether in an acetonitrile solution of the complex.

^{1}H-NMR (CD_3CN, 400 MHz, 21 °C): δ = 9.06 (s, 4H), 8.50 (s, 4H), 7.92 (s, 4H), 7.15 (d, ^3J = 20.7 Hz, 8H) ppm.

^{19}F-NMR (CD_3CN, 377 MHz, 19 °C): δ = –142.6, –144.8, –151.7, –152.8, –157.9, –162.8 ppm.

^{13}C-NMR (CD_3CN, 151 MHz, 25 °C): δ = 161.5, 161.3, 158.3, 158.2, 154.2, 139.9, 128.6, 128.5, 125.3, 125.1, 72.4, 15.7 ppm.

HRMS (ESI): calcd. For $[C_{42}H_{20}CoF_{10}N_6]^{2+}$: *m/z* 427.0464; found 427.0491.

Anal. Calcd for $C_{42}H_{20}B_2F_{18}FeN_6 \cdot 1.65\ H_2O \cdot 0.15\ C_2H_3N$: C, 47.75; H, 2.25; N, 8.10. Found: C, 47.61; H, 2.09; N, 8.24.

$[Fe(TpyPhF_4NMe_2)_2](BF_4)_2$ 4

European Journal of Inorganic Chemistry 10.1002/ejic.202300091

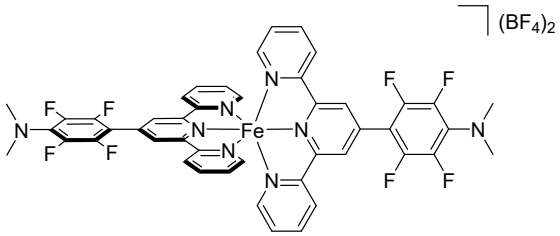

$Fe(BF_4)_2 \bullet 6\ H_2O$ (47.8 mg, 0.14 mmol) was dissolved in 5 mL MeOH and 4-([2,2':6',2''-terpyridin]-4'-yl)-2,3,5,6-tetrafluoro-*N*,*N*-dimethylaniline (120.4 mg, 0.28 mmol) was added. The mixture was stirred for one week, the solvent was evaporated and the crude product was dissolved in acetonitrile and precipitated in diethylether, yielding in a purple solid (74.80 mg, 0.07 mmol, 50%).

^{1}H-NMR (CD_3CN, 401 MHz, 19 °C): δ = 9.06 (s, 4H), 8.46 (t, ^3J = 8.3 Hz, 4H), 7.87 (m, 4H), 7.14 (d, ^3J = 5.6 Hz, 4H), 7.08 (d, ^3J = 5.9 Hz, 8H), 4.53 (q, ^3J = 7.0 Hz, 4H), 1.48 (t, ^3J = 7.0 Hz, 4H) ppm.

^{19}F-NMR (CD_3CN, 377 MHz, 19 °C): δ = –144.73, –151.17, –157.36 ppm.

^{13}C-NMR (CD_3CN, 151 MHz, 25 °C): δ = 161.5, 158.4, 154.3, 140.0, 128.6, 128.3, 125.3, 125.1, 111.0, 72.5, 15.8 ppm.

Anal. Calcd for $C_{46}H_{32}B_2F_{16}FeN_8 \cdot 0.55\ C_4H_{10}O \cdot 0.3\ CH_2Cl_2$: C, 50.90; H, 3.36; N, 9.79. Found: C, 51.28; H, 2.97; N, 9.39.

Supporting Information

Additional references cited within the Supporting Information.[59-64]

Deposition Numbers

<urlhref="https://www.ccdc.cam.ac.uk/services/structures?id=doi:10.1002/###.2022 0XXX"> 2150337 (for **1**), 2150346 (for **2**), 2150345 (for **3**), </url> contain(s) the supplementary crystallographic data for this paper. These data are provided free of charge by the joint Cambridge Crystallographic Data Centre and Fachinformationszentrum Karlsruhe <url href="http://www.ccdc.cam.ac.uk/structures">Access Structures service</url>.

Acknowledgments

We would like to thank Prof. Dr. Sabine Laschat and Eugen Wuckert for the POM measurements of the complexes. We would like to thank Fridolin Hennhöfer for the help with

European Journal of Inorganic Chemistry 10.1002/ejic.202300091

the EPR SEC measurements. We would like to acknowledge the assistance of the Core Facility BioSupraMol supported by the DFG. Funded by the Deutsche Forschungsgemeinschaft [DFG, German Research Foundation – Project-ID 387284271 – SFB 1349].

Keywords: cobalt, iron, fluorinated terpyridine, electrochemistry, spin crossover

References

[1] a) U. S. Schubert, H. Hofmeier, G. R. Newkome, *Modern Terpyridine Chemistry*, Wiley-VCH, Weinheim, **2006**; b) H. Hofmeier, U. S. Schubert, *Chem. Soc. Rev.* **2004**, *33*, 373-399.

[2] G. T. Morgan, F. H. Burstall, *J. Chem. Soc.* **1932**, 20-30.

[3] a) P. E. Rosevear, W. H. F. Sasse, *J. Heterocycl. Chem.* **1971**, *8*, 483–485; b) M. T. Robo, M. R. Prinsell, D. J. Weix, *J. Org. Chem.* **2014**, *79*, 10624-10628.

[4] a) T. Hiyama, *Metal-Catalyzed Cross-Coupling Reactions*, Wiley-VCH, Weinheim, Germany, **1998**; b) T. Hiyama, Y. Hatanaka, *Pure Appl. Chem.* **1994**, *66*, 1471–1478; c) T. Hiyama, *J. Organomet. Chem.* **2002**, *653*, 58–61.

[5] a) R.-A. Fallahpour, *Synthesis* **2000**, 1665–1667; b) R. García-Lago, J. Alonso-Gómez, C. C. Sicre, M., *Heterocycles* **2008**, *75*; c) M. Benaglia, S. Toyota, C. R. Woods, J. S. Siegel, *Tetrahedron Lett.* **1997**, *38*.

[6] I. Sasaki, J. C. Daran, G. G. A. Balavoine, *Synthesis* **1999**, *1999*, 815–820.

[7] a) S. Aroua, T. K. Todorova, P. Hommes, L.-M. Chamoreau, H.-U. Reissig, V. Mougel, M. Fontecave, *Inorg. Chem.* **2017**, *56*, 5930-5940; b) P. Hommes, C. Fischer, C. Lindner, H. Zipse, H.-U. Reissig, *Angew. Chem. Int. Ed.* **2014**, *53*, 7647-7651; c) J. R. Colombe, S. Bernhardt, C. Stathakis, S. L. Buchwald, P. Knochel, *Org. Lett.* **2013**, *15*, 5754-5757.

[8] a) N. Elgrishi, S. Griveau, M. B. Chambers, F. Bedioui, M. Fontecave, *Chem. Commun.* **2015**, *51*, 2995-2998; b) N. Elgrishi, M. B. Chambers, M. Fontecave, *Chem. Sci.* **2015**, *6*, 2522-2531.

[9] N. Elgrishi, M. B. Chambers, V. Artero, M. Fontecave, *Phys. Chem. Chem. Phys.* **2014**, *16*, 13635-13644.

[10] R. Tatikonda, M. Cametti, E. Kalenius, A. Famulari, K. Rissanen, M. Haukka, *Eur. J. Inorg. Chem.* **2019**, *2019*, 4463-4470.

[11] a) S. G. Shepard, S. M. Fatur, A. K. Rappé, N. H. Damrauer, *J. Am. Chem. Soc.* **2016**, *138*, 2949-2952; b) D. G. Brown, N. Sanguantrakun, B. Schulze, U. S. Schubert, C. P. Berlinguette, *J. Am. Chem. Soc.* **2012**, *134*, 12354-12357; c) H.-W. Lin, Y.-S. Wang, Z.-Y. Huang, Y.-M. Lin, C.-W. Chen, S.-H. Yang, K.-L. Wu, Y. Chi, S.-H. Liu, P.-T. Chou, *Phys. Chem. Chem. Phys.* **2012**, *14*, 14190-14195.

[12] a) J.-H. Yum, E. Baranoff, F. Kessler, T. Moehl, S. Ahmad, T. Bessho, A. Marchioro, E. Ghadiri, J.-E. Moser, C. Yi, M. K. Nazeeruddin, M. Grätzel, *Nat. Commun.* **2012**, *3*, 631; b) S. A. Sapp, C. M. Elliott, C. Contado, S. Caramori, C. A. Bignozzi, *J. Am. Chem. Soc.* **2002**, *124*, 11215-11222.

[13] a) Z. Zheng, L. Opilik, F. Schiffmann, W. Liu, G. Bergamini, P. Ceroni, L.-T. Lee, A. Schütz, J. Sakamoto, R. Zenobi, J. VandeVondele, A. D. Schlüter, *J. Am. Chem. Soc.* **2014**, *136*, 6103-6110; b) G. Gröger, W. Meyer-Zaika, C. Böttcher, F. Gröhn, C. Ruthard, C. Schmuck, *J. Am. Chem. Soc.* **2011**, *133*, 8961-8971; c) U. S. Schubert, C.

European Journal of Inorganic Chemistry 10.1002/ejic.202300091

Eschbaumer, *Angew. Chem. Int. Ed.* **2002**, *41*, 2892-2926; d) F. Chen, Y.-K. Tian, Y. Chen, *Chem. Asian J.* **2018**, *13*, 3169-3172.

[14] J. Tan, R. Li, D. Li, Q. Zhang, S. Li, H. Zhou, J. Yang, J. Wu, Y. Tian, *Dalton Trans.* **2015**, *44*, 1473-1482.

[15] A. Fermi, G. Bergamini, M. Roy, M. Gingras, P. Ceroni, *J. Am. Chem. Soc.* **2014**, *136*, 6395-6400.

[16] C. S. Sevov, S. L. Fisher, L. T. Thompson, M. S. Sanford, *J. Am. Chem. Soc.* **2016**, *138*, 15378-15384.

[17] a) S. J. Lippard, *Acc. Chem. Res.* **1978**, *11*, 211-217; b) P. M. van Vliet, S. M. S. Toekimin, J. G. Haasnoot, J. Reedijk, O. Nováková, O. Vrána, V. Brabec, *Inorg. Chim. Acta* **1995**, *231*, 57-64; c) I. Eryazici, C. N. Moorefield, G. R. Newkome, *Chem. Rev.* **2008**, *108*, 1834-1895.

[18] K. Senthil Kumar, M. Ruben, *Coord. Chem. Rev.* **2017**, *346*, 176-205.

[19] a) O. Sato, *Nat. Chem.* **2016**, *8*, 644-656; b) M. A. Halcrow, *Spin-crossover materials. Properties and application*, Wiley, Chichester, **2013**; c) P. Gütlich, H. A. Goodwin, *Spin Crossover in Transition Metal Compounds I, II, and III*, Springer, Berlin, Germany, **2004**.

[20] D. Shao, L. Shi, F.-X. Shen, X.-Q. Wei, O. Sato, X.-Y. Wang, *Inorg. Chem.* **2019**, *58*, 11589-11598.

[21] a) P. Silva, S. M. F. Vilela, J. P. C. Tomé, F. A. Almeida Paz, *Chem. Soc. Rev.* **2015**, *44*, 6774-6803; b) C.-L. Ho, Z.-Q. Yu, W.-Y. Wong, *Chem. Soc. Rev.* **2016**, *45*, 5264-5295; c) M. Castellano, R. Ruiz-García, J. Cano, J. Ferrando-Soria, E. Pardo, F. R. Fortea-Pérez, S.-E. Stiriba, W. P. Barros, H. O. Stumpf, L. Cañadillas-Delgado, J. Pasán, C. Ruiz-Pérez, G. de Munno, D. Armentano, Y. Journaux, F. Lloret, M. Julve, *Coord. Chem. Rev.* **2015**, *303*, 110-138; d) M. K. Singh, Y. Yang, C. G. Takoudis, *Coord. Chem. Rev.* **2009**, *253*, 2920-2934; e) E. Chelebaeva, J. Larionova, Y. Guari, R. A. S. Ferreira, L. D. Carlos, F. A. A. Paz, A. Trifonov, C. Guérin, *Inorg. Chem.* **2009**, *48*, 5983-5995; f) J. Long, J. Rouquette, J. M. Thibaud, R. A. Ferreira, L. D. Carlos, B. Donnadieu, V. Vieru, L. F. Chibotaru, L. Konczewicz, J. Haines, Y. Guari, J. Larionova, *Angew. Chem. Int. Ed.* **2015**, *54*, 2236–2240.

[22] a) C. Faulmann, K. Jacob, S. Dorbes, S. Lampert, I. Malfant, M.-L. Doublet, L. Valade, J. A. Real, *Inorg. Chem.* **2007**, *46*, 8548-8559; b) K. Takahashi, H.-B. Cui, Y. Okano, H. Kobayashi, H. Mori, H. Tajima, Y. Einaga, O. Sato, *J. Am. Chem. Soc.* **2008**, *130*, 6688-6689; c) M. Nihei, N. Takahashi, H. Nishikawa, H. Oshio, *Dalton Trans.* **2011**, *40*, 2154-2156; d) S. M. B. H. Phan, E. Steven, J. S. Brooks, M. Shatruk, *Angew. Chem. In. Ed.* **2015**, *54*, 823–827.

[23] a) S. Hayami, R. Moriyama, A. Shuto, Y. Maeda, K. Ohta, K. Inoue, *Inorg. Chem.* **2007**, *46*, 7692-7694; b) M. Seredyuk, A. B.Gaspar, V. Ksenofontov, Y. Galyametdinov, J. Kusz, P. Gütlich, *Adv. Funct. Mater.* **2008**, *18*, 1089–2101; c) M. Seredyuk, A. B. Gaspar, V. Ksenofontov, Y. Galyametdinov, J. Kusz, P. Gütlich, *J. Am. Chem. Soc.* **2008**, *130*, 1431-1439; d) A. B. Gaspar, M. Seredyuk, P. Gütlich, *Coord. Chem. Rev.* **2009**, *253*, 2399-2413; e) R. Akiyoshi, Y. Hirota, D. Kosumi, M. Tsutsumi, M. Nakamura, L. F. Lindoy, S. Hayami, *Chem. Sci.* **2019**, *10*, 5843-5848.

[24] a) A. B. Gaspar, V. Ksenofontov, M. Seredyuk, P. Gütlich, *Coord. Chem. Rev.* **2005**, *249*, 2661-2676; b) S. Bonhommeau, P. G. Lacroix, D. Talaga, A. Bousseksou, M. Seredyuk, I. O. Fritsky, V. Rodriguez, *J. Phys. Chem. C* **2012**, *116*, 11251-11255; c) W. Liu, X. Bao, L.-L. Mao, J. Tucek, R. Zboril, J.-L. Liu, F.-S. Guo, Z.-P. Ni, M.-L. Tong, *Chem. Commun.* **2014**, *50*, 4059-4061.

[25] a) I. Suleimanov, O. Kraieva, J. Sánchez Costa, I. O. Fritsky, G. Molnár, L. Salmon, A. Bousseksou, *J. Mater. Chem. C* **2015**, *3*, 5026-5032; b) A. Santoro, L. J. Kershaw

European Journal of Inorganic Chemistry 10.1002/ejic.202300091

Cook, R. Kulmaczewski, S. A. Barrett, O. Cespedes, M. A. Halcrow, *Inorg. Chem.* **2015**, *54*, 682-693; c) C. F. Wang, R. F. Li, X. Y. Chen, R. J. Wei, L. S. Zheng, J. Tao, *Angew. Chem. In. Ed.* **2015**, *54*; d) M. Estrader, J. S. Uber, L. A. Barrios, J. Garcia, P. Lloyd-Williams, O. Roubeau, S. J. Teat, G. Aromi, *Angew. Chem. In. Ed.* **2017**, *56*, 15622–15627; e) J.-Y. Ge, Z. Chen, L. Zhang, X. Liang, J. Su, M. Kurmoo, J.-L. Zuo, *Angew. Chem. In. Ed.* **2019**, *58*; f) B. Benaicha, K. Van Do, A. Yangui, N. Pittala, A. Lusson, M. Sy, G. Bouchez, H. Fourati, C. J. Gómez-García, S. Triki, K. Boukheddaden, *Chem. Sci.* **2019**, *10*, 6791-6798.

[26] R. Akiyoshi, Y. Komatsumaru, M. Donoshita, S. Dekura, Y. Yoshid, H. Kitagawa, Y. Kitagawa, L. F. Lindoy, S. Hayami, *Angew. Chem. Int. Ed.* **2021**, *60*, 12717–12722.

[27] S. Hayami, Y. Shigeyoshi, M. Akita, K. Inoue, K. Kato, K. Osaka, M. Takata, R. Kawajiri, T. Mitani, Y. Maeda, *Angew. Chem. Int. Ed.* **2005**, *44*, 4899-4903.

[28] J. A. Kitchen, N. G. White, C. Gandolfi, M. Albrecht, G. N. L. Jameson, J. L. Tallon, S. Brooker, *Chem. Commun.* **2010**, *46*, 6464-6466.

[29] a) S. Hayami, K. Kato, Y. Komatsu, A. Fuyuhiro, M. Ohba, *Dalton Trans.* **2011**, *40*, 2167-2169; b) S. Hayami, D. Urakami, Y. Kojima, H. Yoshizaki, Y. Yamamoto, K. Kato, A. Fuyuhiro, S. Kawata, K. Inoue, *Inorg. Chem.* **2010**, *49*, 1428-1432; c) Y. Komatsu, K. Kato, Y. Yamamoto, H. Kamihata, Y. H. Lee, A. Fuyuhiro, S. Kawata, S. Hayami, *Eur. J. Inorg. Chem.* **2012**, *2012*, 2769-2775; d) S. Hayami, Y. Komatsu, T. Shimizu, H. Kamihata, Y. H. Lee, *Coord. Chem. Rev.* **2011**, *255*, 1981-1990; e) S. Hayami, R. Moriyama, Y. Shigeyoshi, R. Kawajiri, T. Mitani, M. Akita, K. Inoue, Y. Maeda, *Inorg. Chem.* **2005**, *44*, 7295-7297; f) S. Hayami, K. Murata, D. Urakami, Y. Kojima, M. Akita, K. Inoue, *Chem. Commun.* **2008**, 6510-6512.

[30] O. A. Oyetade, V. O. Nyamori, B. S. Martincigh, S. B. Jonnalagadda, *RSC Adv.* **2016**, *6*, 2731-2745.

[31] a) E. C. Constable, in *Adv. Inorg. Chem. Radiochem., Vol. 30* (Ed.: H. J. Emeléus), Academic Press, **1986**, pp. 69-121; b) A. T. Baker, H. A. Goodwin, *Aust. J. Chem.* **1985**, *38*, 207-214; c) P. Laine, A. Gourdon, J. P. Launay, *Inorg. Chem.* **1995**, *34*, 5156-5165; d) Y. Nakayama, Y. Baba, H. Yasuda, K. Kawakita, N. Ueyama, *Macromolecules* **2003**, *36*, 7953-7958; e) S. K. Hain, F. W. Heinemann, K. Gieb, P. Müller, G. Hörner, A. Grohmann, *Eur. J. Inorg. Chem.* **2010**, *2010*, 221-232; f) L. J. Kershaw Cook, F. Tuna, M. A. Halcrow, *Dalton Trans.* **2013**, *42*, 2254-2265.

[32] R. J. Davidson, E. W. Ainscough, A. M. Brodie, G. B. Jameson, M. R. Waterland, H. R. Allcock, M. D. Hindenlang, B. Moubaraki, K. S. Murray, K. C. Gordon, R. Horvath, G. N. L. Jameson, *Inorg. Chem.* **2012**, *51*, 8307-8316.

[33] I. F. Mansoor, D. I. Wozniak, Y. Wu, M. C. Lipke, *Chem. Comm.* **2020**, *56*, 13864-13867.

[34] J. Chambers, B. Eaves, D. Parker, R. Claxton, P. S. Ray, S. J. Slattery, *Inorg. Chim. Acta* **2006**, *359*, 2400-2406.

[35] H. Ferreira, M. M. Conradie, J. Conradie, *Inorg. Chim. Acta* **2019**, *486*, 26-35.

[36] B. de Bruin, E. Bill, E. Bothe, T. Weyhermüller, K. Wieghardt, *Inorg. Chem.* **2000**, *39*, 2936-2947.

[37] J. Klein, A. Stuckmann, S. Sobottka, L. Suntrup, M. van der Meer, P. Hommes, H.-U. Reissig, B. Sarkar, *Chem. Eur. J.* **2017**, *23*, 12314-12325.

[38] J. England, E. Bill, T. Weyhermüller, F. Neese, M. Atanasov, K. Wieghardt, *Inorg. Chem.* **2015**, *54*, 12002-12018.

[39] S. Kremer, W. Henke, D. Reinen, *Inorg. Chem.* **1982**, *21*, 3013-3022.

[40] P. Nielsen, H. Toftlund, A. D. Bond, J. F. Boas, J. R. Pilbrow, G. R. Hanson, C. Noble, M. J. Riley, S. M. Neville, B. Moubaraki, K. S. Murray, *Inorg. Chem.* **2009**, *48*, 7033-7047.

[41] B. Odom, D. Hanneke, B. D'Urso, G. Gabrielse, *Phys. Rev. Lett.* **2006**, *97*, 030801.

European Journal of Inorganic Chemistry 10.1002/ejic.202300091

[42] a) J. A. Real, A. B. Gaspar, M. C. Muñoz, *Dalton Trans.* **2005**, 2062-2079; b) O. Sato, J. Tao, Y.-Z. Zhang, *Angew. Chem. Int. Ed.* **2007**, *46*, 2152-2187; c) M. A. Halcrow, *Chem. Soc. Rev.* **2011**, *40*, 4119-4142.

[43] G. R. Fulmer, A. J. M. Miller, N. H. Sherden, H. E. Gottlieb, A. Nudelman, B. M. Stoltz, J. E. Bercaw, K. I. Goldberg, *Organometallics* **2010**, *29*, 2176-2179.

[44] M. Krejčik, M. Daněk, F. Hartl, *J. Electroanal. Chem.* **1991**, *317*, 179-187.

[45] L. J. B. O. V. Dolomanov, R. J. Gildea, J. A. K. Howard, H. Puschmann, *J. Appl. Crytsallogr.* **2009**, *42*, 339-341.

[46] a) G. M. Sheldrick, *SHELXS-97, Program for Crystal Structure Solution and Refinement,* **1997**, University of Göttingen, Germany; b) G. Sheldrick, *Acta Crystallogr., Sect. A* **2008**, *64*, 112-122; c) G. M. Sheldrick, *SADABS Ver. 2008/1, SADABS. Program for Empirical Absorption Correction* **2012**, University of Göttingen, Germany; d) G. M. Sheldrick, *SHELXL Version 2014/7, Program for Chrystal Structure Solution and Refinement* **2014**, University of Göttingen, Germany; e) G. Sheldrick, *Acta Crystallogr. Sect. C* **2015**, *71*, 3-8; f) A. Spek, *J. Appl. Crystallogr.* **2003**, *36*, 7-13; g) SAINT+, *Data Integration Engine, Version 8.27b©*, Bruker AXS, Madison, Wisconsin, USA, 1997-2012; h) S. W. Kwok, J. R. Fotsing, R. J. Fraser, V. O. Rodionov, V. V. Fokin, *Org. Lett.* **2010**, *12*, 4217-4219.

[47] G. A. Bain, J. F. Berry, *J. Chem. Educ.* **2008**, *85*, 532.

[48] S. G. Balasubramani, G. P. Chen, S. Coriani, M. Diedenhofen, M. S. Frank, Y. J. Franzke, F. Furche, R. Grotjahn, M. E. Harding, C. Hättig, A. Hellweg, B. Helmich-Paris, C. Holzer, U. Huniar, M. Kaupp, A. M. Khah, S. K. Khani, T. Müller, F. Mack, B. D. Nguyen, S. M. Parker, E. Perlt, D. Rappoport, K. Reiter, S. Roy, M. Rückert, G. Schmitz, M. Sierka, E. Tapavicza, D. P. Tew, C. v. Wüllen, V. K. Voora, F. Weigend, A. Wodyński, J. M. Yu, *J. Chem. Phys.* **2020**, *152*, 184107.

[49] J. Tao, J. P. Perdew, V. N. Staroverov, G. E. Scuseria, *Phys. Rev. Lett.* **2003**, *91*, 146401.

[50] F. Weigend, R. Ahlrichs, *Phys. Chem. Chem. Phys.* **2005**, *7*, 3297-3305.

[51] S. Grimme, J. Antony, S. Ehrlich, H. Krieg, *J. Chem. Phys.* **2010**, *132*, 154104.

[52] S. Grimme, S. Ehrlich, L. Goerigk, *J. Comput. Chem.* **2011**, *32*, 1456-1465.

[53] A. Klamt, G. Schüürmann, *J. Chem. Soc., Perkin Trans. 2* **1993**, 799-805.

[54] M. Sierka, A. Hogekamp, R. Ahlrichs, *J. Chem. Phys.* **2003**, *118*, 9136-9148.

[55] F. Weigend, *Phys. Chem. Chem. Phys.* **2006**, *8*, 1057-1065.

[56] S. Grimme, *J. Chem. Phys.* **2006**, *124*, 034108.

[57] M. Reimann, M. Kaupp, *J. Chem. Theory Comput.* **2022**, *18*, 7442-7456.

[58] E. C. Constable, B. Kariuki, A. Mahmood, *Polyhedron* **2003**, *22*, 687-698.

[59] C. Adamo, V. Barone, *J. Chem. Phys.* **1999**, *110*, 6158-6170.

[60] J.-D. Chai, M. Head-Gordon, *Phys. Chem. Chem. Phys.* **2008**, *10*, 6615-6620.

[61] M. Haasler, T. M. Maier, R. Grotjahn, S. Gückel, A. V. Arbuznikov, M. Kaupp, *J. Chem. Theory Comput.* **2020**, *16*, 5645-5657.

[62] S. Grimme, *J. Chem. Phys.* **2006**, *124*, 034108.

[63] M. Reimann, M. Kaupp, *J. Chem. Theory Comput.* **2022**, *18*, 7442-7456.

[64] a) S. Aroua, T. K. Todorova, P. Hommes, L.-M. Chamoreau, H.-U. Reissig, V. Mougel, M. Fontecave, *Inorg. Chem.* **2017**, *56*, 5930-5940; b) S. Aroua, T. K. Todorova, V. Mougel, P. Hommes, H.-U. Reissig, M. Fontecave, *ChemCatChem* **2017**, *9*, 2099-2105.

European Journal of Inorganic Chemistry 10.1002/ejic.202300091

TOC:

Fluorinated terpyridine ligands form stable Fe(II) and Co(II) complexes that are redox-rich and display multiple oxidation and reduction steps. Additionally, the Co(II) complexes show spin crossover close to room temperature.

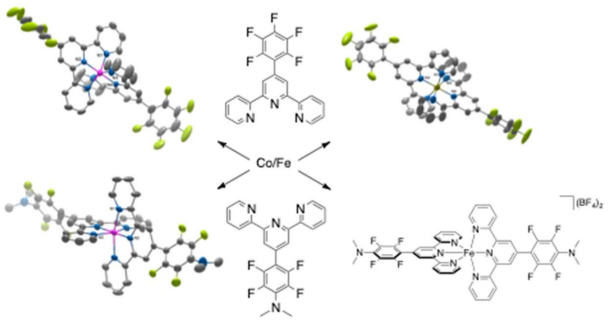

Twitter: @SarkarAg

Supporting Information

Electrochemistry and Spin-Crossover Behavior of Fluorinated Terpyridine-Based Co(II) and Fe(II) Complexes

Maite Nößler,[a] René Jäger,[a] David Hunger,[c] Marc Reimann,[d] Tobias Bens,[b] Nicolás I. Neuman,[b, e] Arijit Singha Hazari,[b] Martin Kaupp,[d] Joris van Slageren[b] and Biprajit Sarkar[a ,b]**

Content

S I

1. SQUID Magnetometry

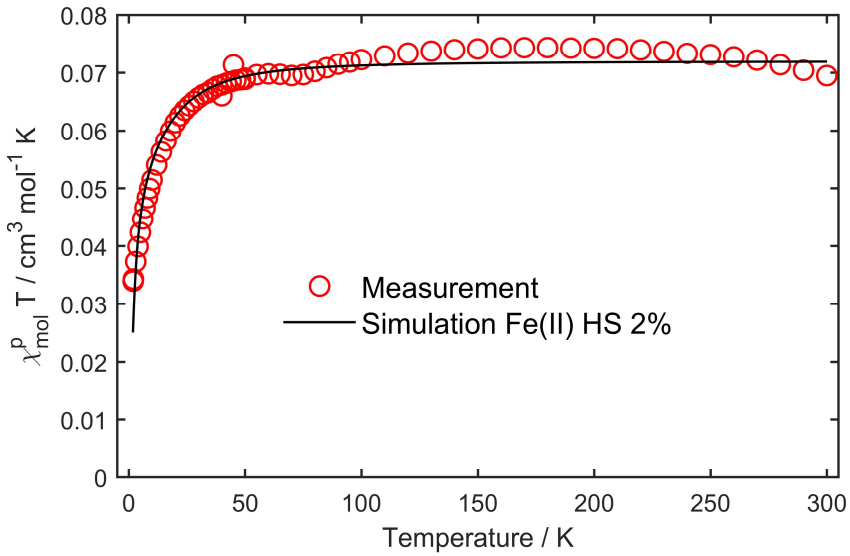

Figure S 1: $\chi_M T$ vs. T product for **3** in an applied magnetic field of 100 Oe. The simulations is based on the following spin Hamiltonian parameters: S = 2; g = 2.19, D = 13 cm^{-1} , E = 0.3D on the basis of usual parameters found in literature for Fe^{II} HS.[13] Parameters were adapted to fit the curvature of the measured curve and a 2 % fraction of Fe^{II} HS was assumed.

2. Cyclic Voltammetry

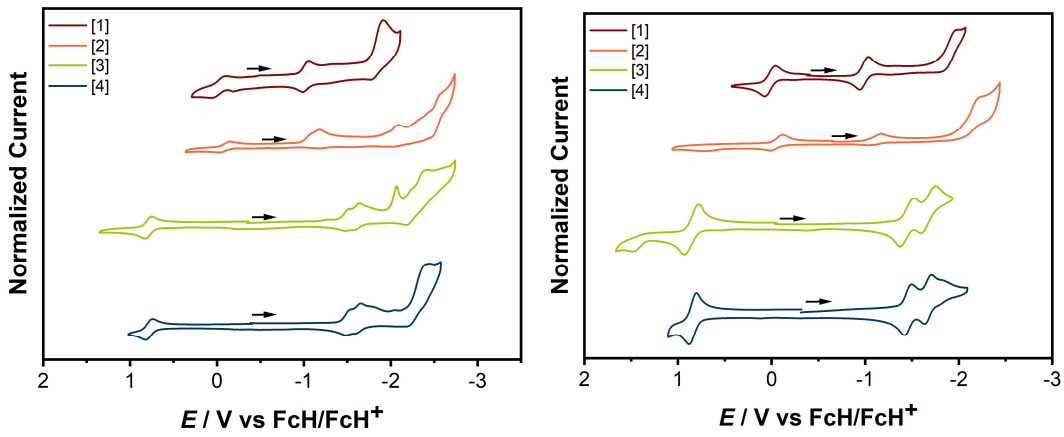

Figure S 2: cyclic voltammograms of complexes **1**-**4** left: in acetonitrile./NBu_4PF_6 measured with a glassy carbon working electrode (FcH = ferrocene; FcH^+ = ferrocenium), right: in CH_2Cl_2/NBu_4PF_6 measured with a glassy carbon working electrode (FcH = ferrocene; FcH^+ = ferrocenium).

Table S 1: Redox potentials vs. FcH/FcH^+ measured in different solvents at 100 mVs^{-1} with 0.1 M Bu_4NPF_6 at room temperature.[a]

	$E_{1/2}^{Ox2}$	$E_{1/2}^{Ox1}$	$E_{1/2}^{Red1}$	$E_{1/2}^{Red2}$	$E_{1/2}^{Red3}$	$E_{1/2}^{Red4}$
1 (MeCN)	-	-0.02	-1.02	-1.89	-	-
2 (MeCN)	-	-0.09	-1.14	-2.09[b]	-2.45[b]	
3 (MeCN)	-	0.79	-1.50	-1.62	-2.10[b]	-2.31
4 (MeCN)	-	0.78	-1.52	-1.62	-2.45[b]	-
1 (DCM)	-	-0.06	-0.99	-1.99[b]	-	-
2 (DCM)	0.72	-0.05	-1.10	-2.24[b]	-	-
3 (DCM)	1.51[b]	0.85	-1.45	-1.66[b]	-	-
4 (DCM)	-	0.84	-1.46	-1.68	-	-

[a] All measured with a glassy carbon electrode. [b] Forward peak potential at 0.1 V.

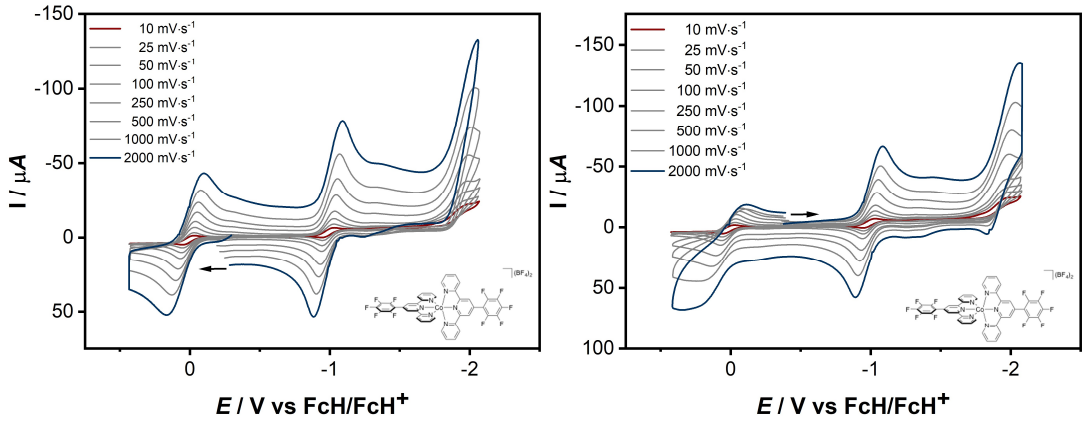

S 2

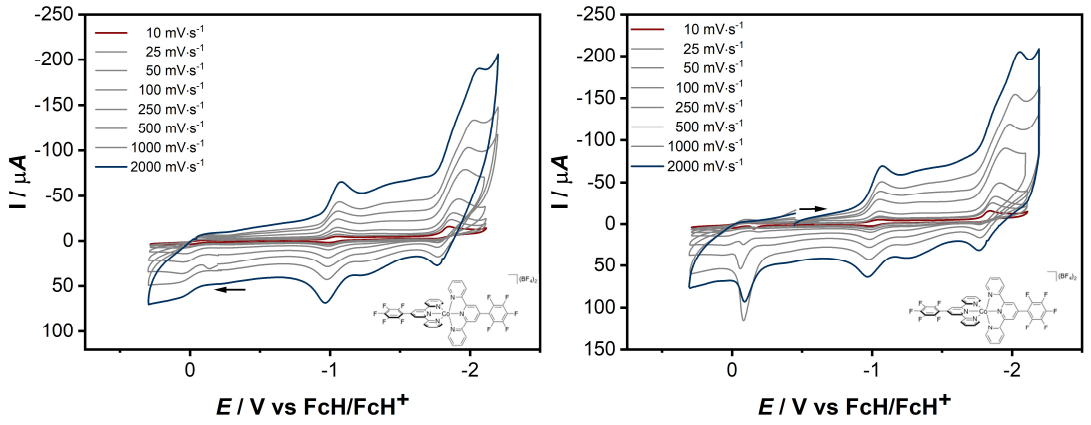

Figure S 3: Cyclic voltammogram of complex **1** measured in: top: a CH_2Cl_2 solution with 0.1 M NBu_4PF_6 with different scan rates, bottom: a MeCN solution with 0.1 M NBu_4PF_6 with different scan rates.

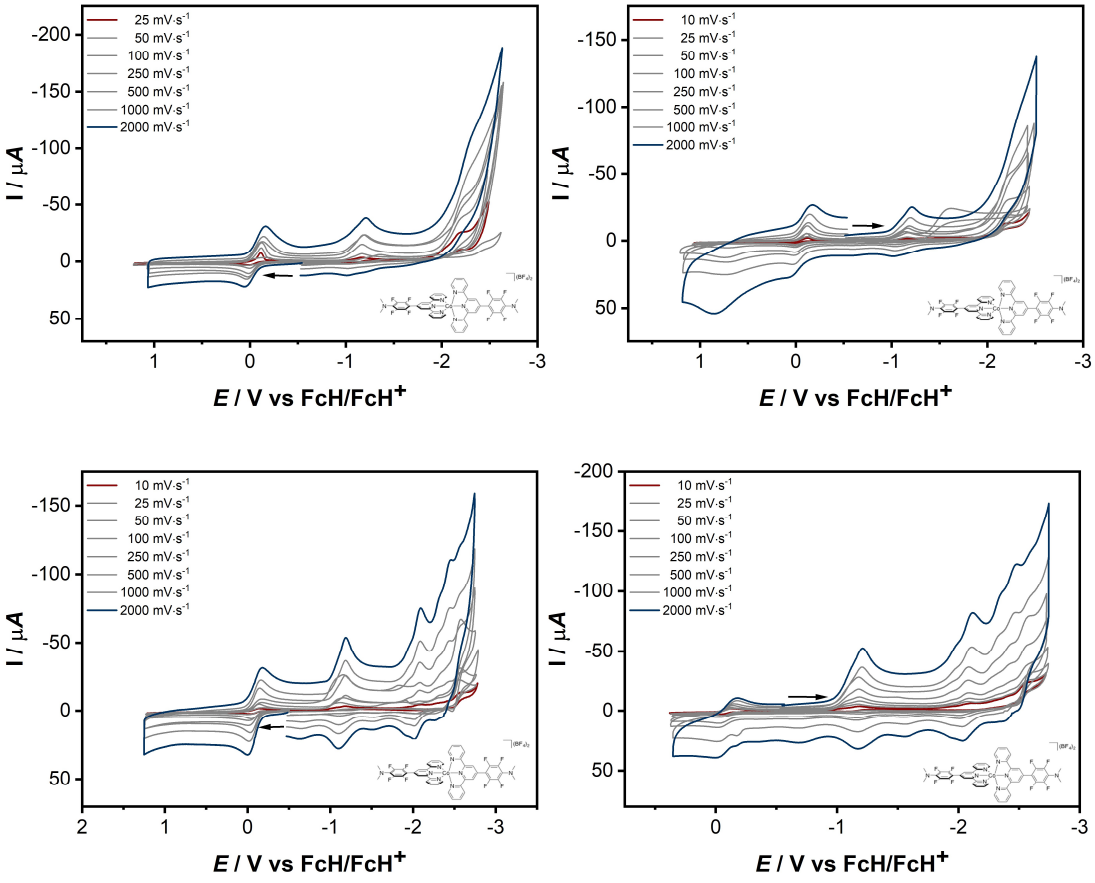

Figure S 4: Cyclic voltammogram of complex **2** measured in: top: a CH_2Cl_2 solution with 0.1 M NBu_4PF_6 with different scan rates, bottom: a MeCN solution with 0.1 M NBu_4PF_6 with different scan rates.

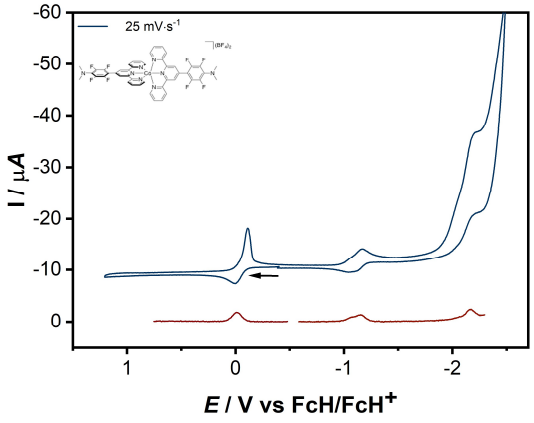

Figure S 5: CV and DPV of complex **2** (DCM).

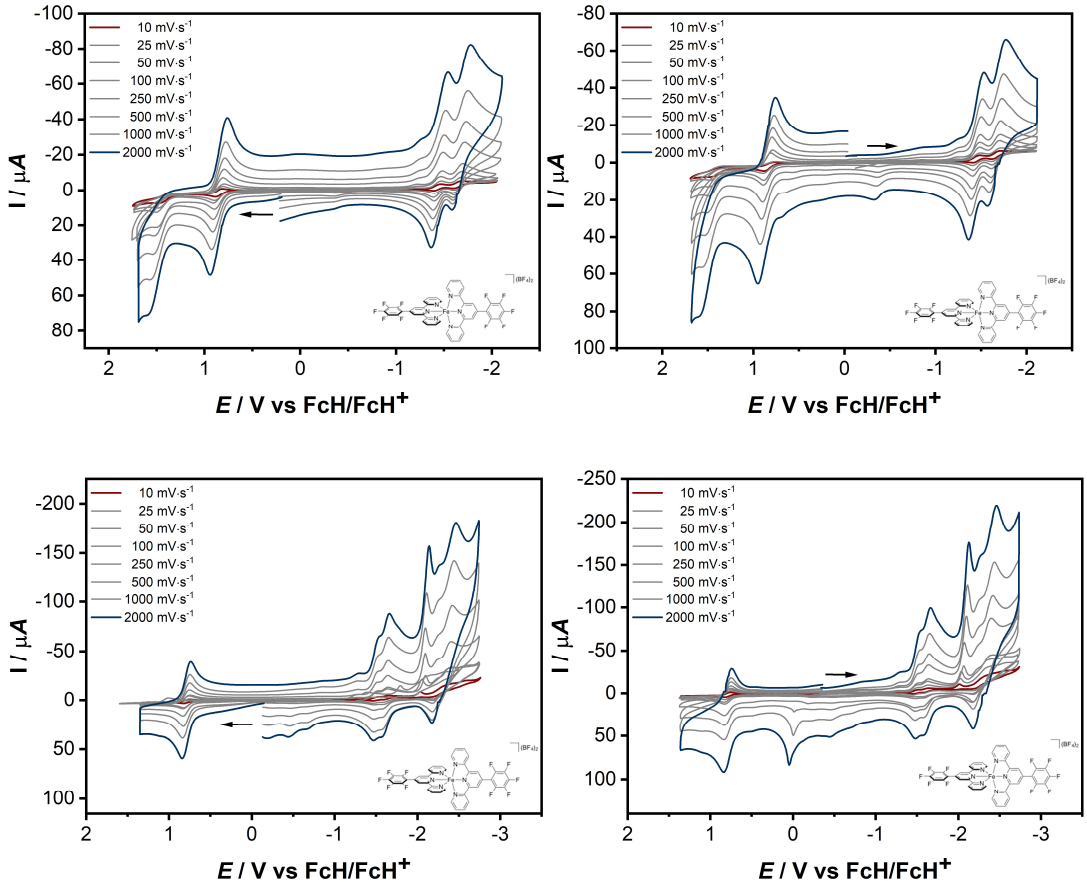

Figure S 6: Cyclic voltammogram of complex **3** measured in: top: a CH_2Cl_2 solution with 0.1 M NBu_4PF_6 with different scan rates, bottom: a MeCN solution with 0.1 M NBu_4PF_6 with different scan rates.

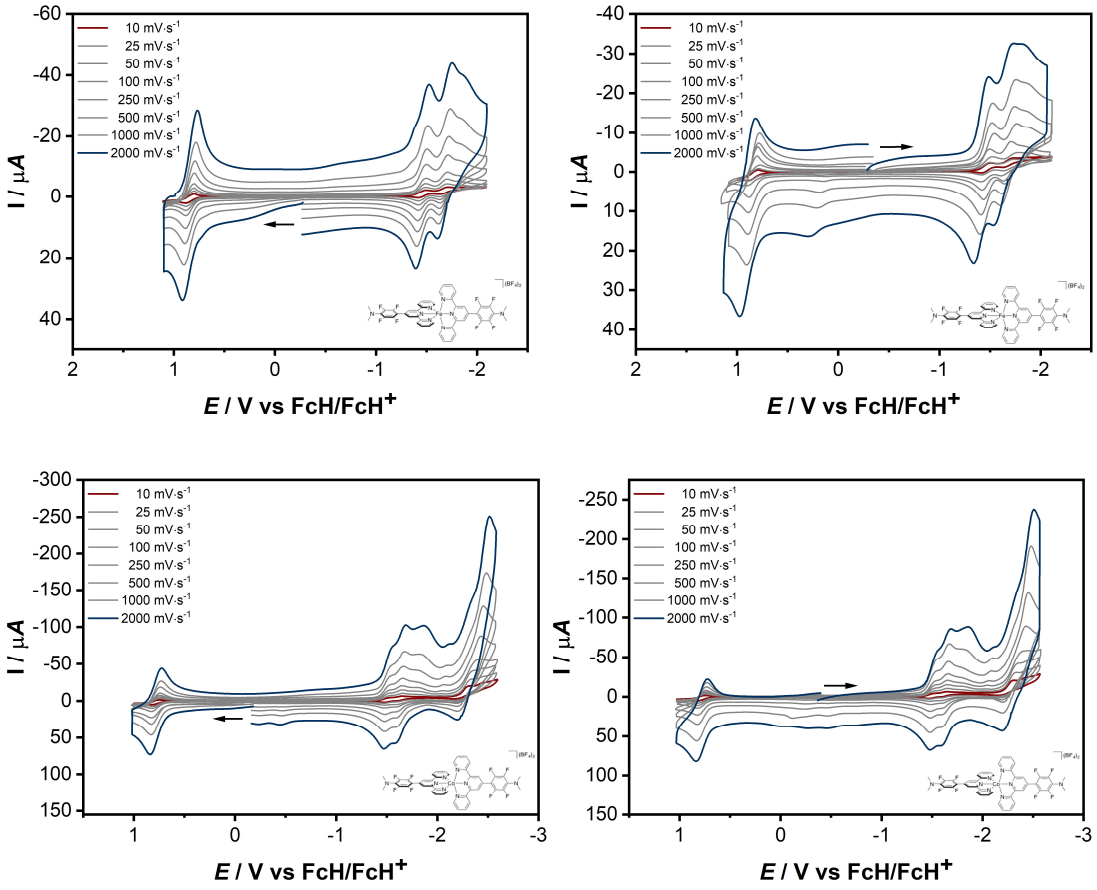

Figure S 7: Cyclic voltammogram of complex **4** measured in: top: a CH_2Cl_2 solution with 0.1 M NBu_4PF_6 with different scan rates, bottom: a MeCN solution with 0.1 M NBu_4PF_6 with different scan rates.

3. UV/Vis/NIR Spectroelectrochemistry

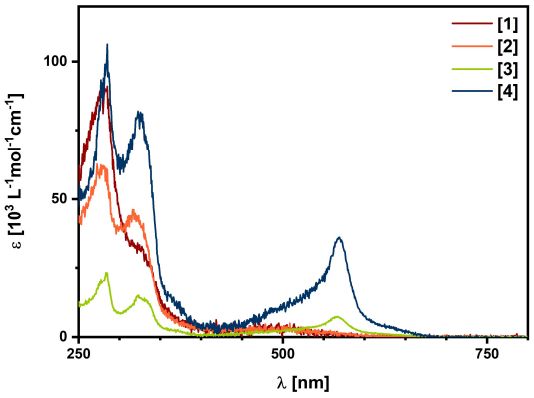

Figure S 8: UV/Vis Spectra of complexes **1**-**4**.

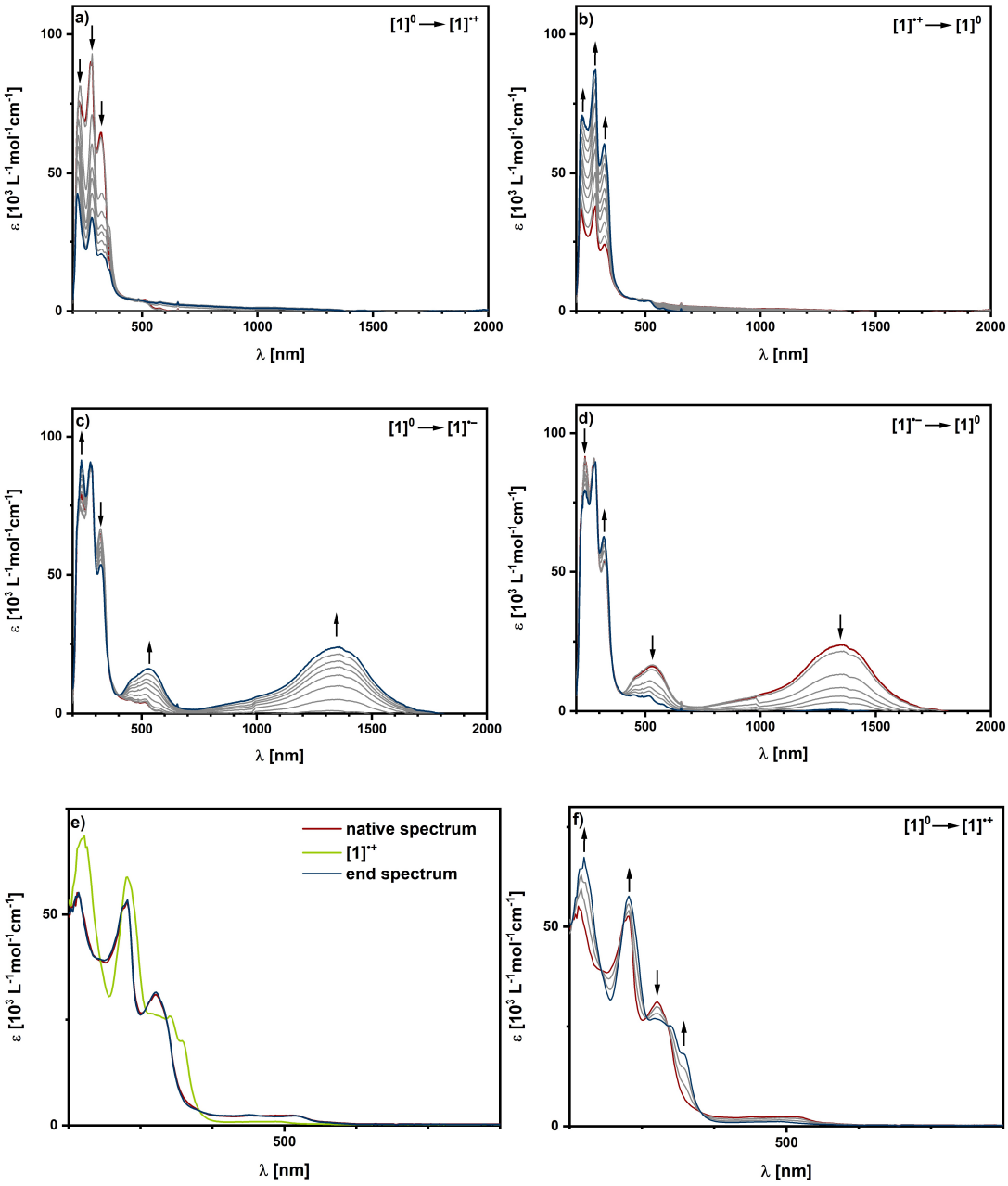
a)
[1]0 → [1]•+
b)
[1]•+ → [1]0
c)
[1]0 → [1]•−
d)
[1]•− → [1]0
e)
native spectrum
[1]•+
end spectrum
f)
[1]0 → [1]•+
ε [10³ L⁻¹mol⁻¹cm⁻¹]
λ [nm]

S 6

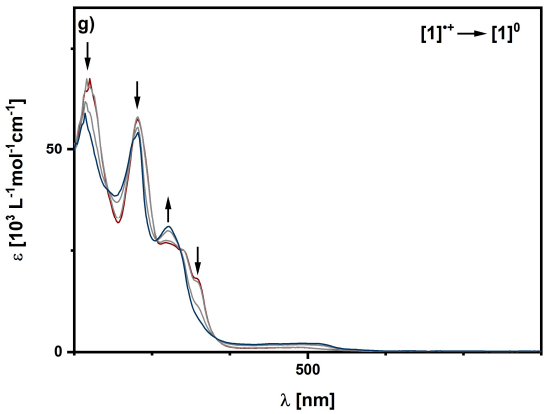

Figure S 9: UV/Vis SEC spectra of complex **1** a)-d) in CH_2Cl_2/NBu_4PF_6 measured with a gold working electrode, e) in $MeCN/NBu_4PF_6$ measured with a gold working electrode.

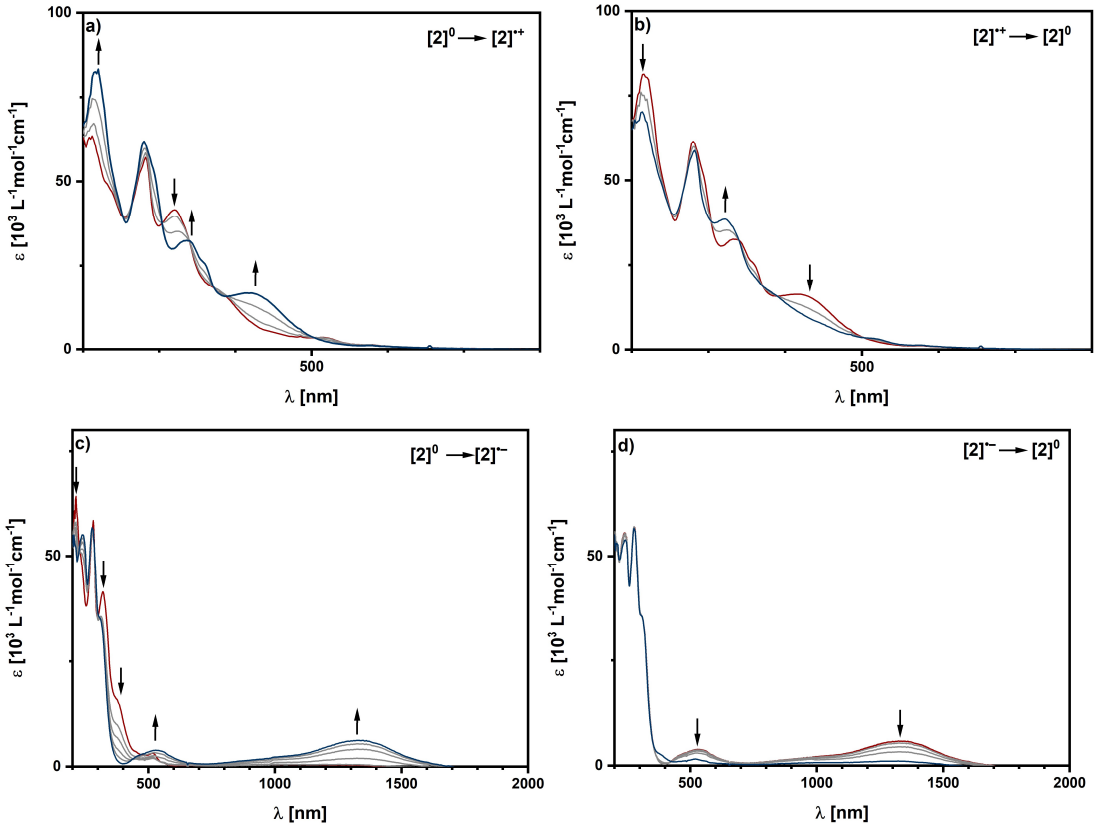

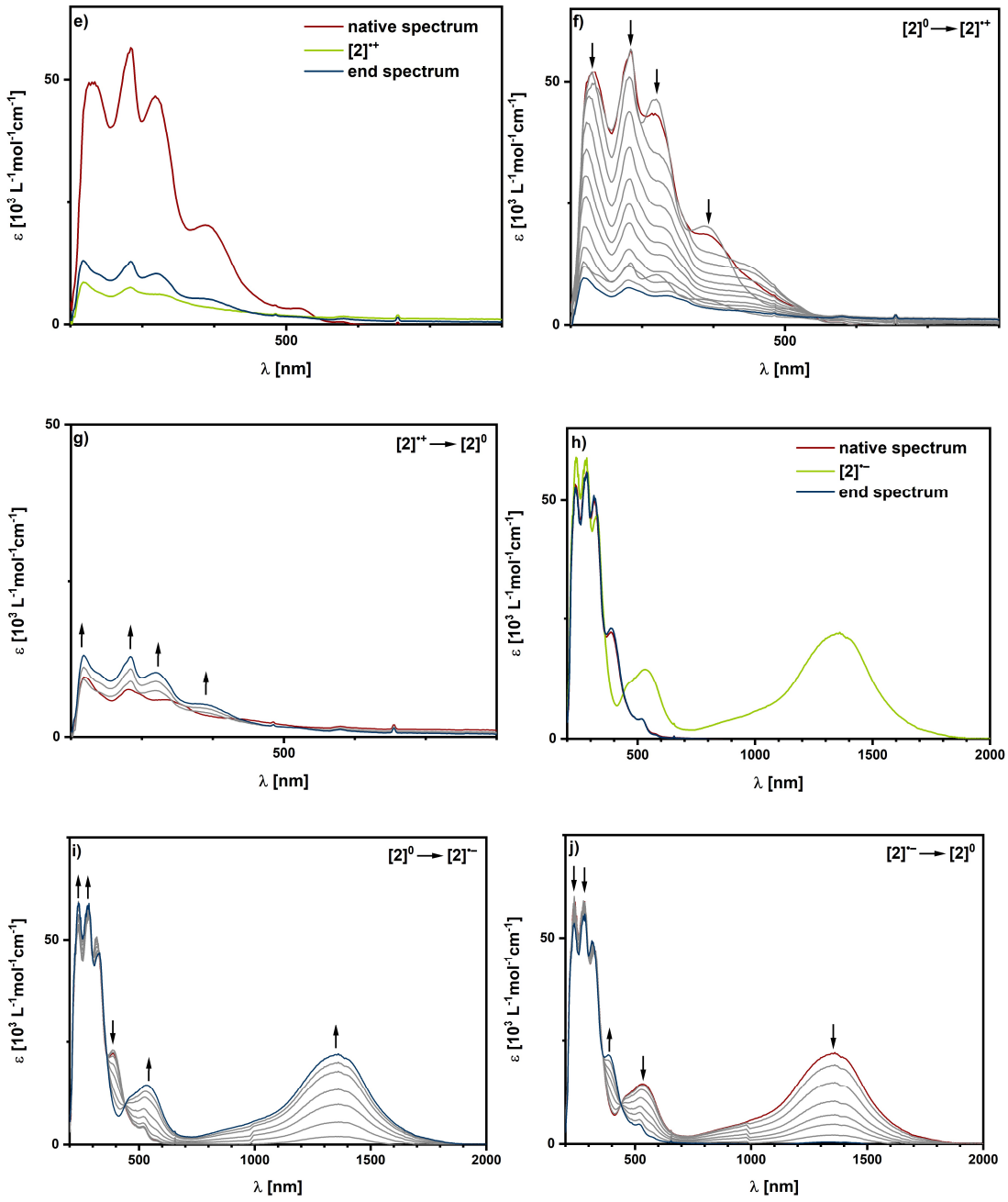
e)
native spectrum
[2]•+
end spectrum
f)
[2]0 → [2]•+
g)
[2]•+ → [2]0
h)
native spectrum
[2]•−
end spectrum
i)
[2]0 → [2]•−
j)
[2]•− → [2]0
ε [10³ L⁻¹mol⁻¹cm⁻¹]
λ [nm]

S 8

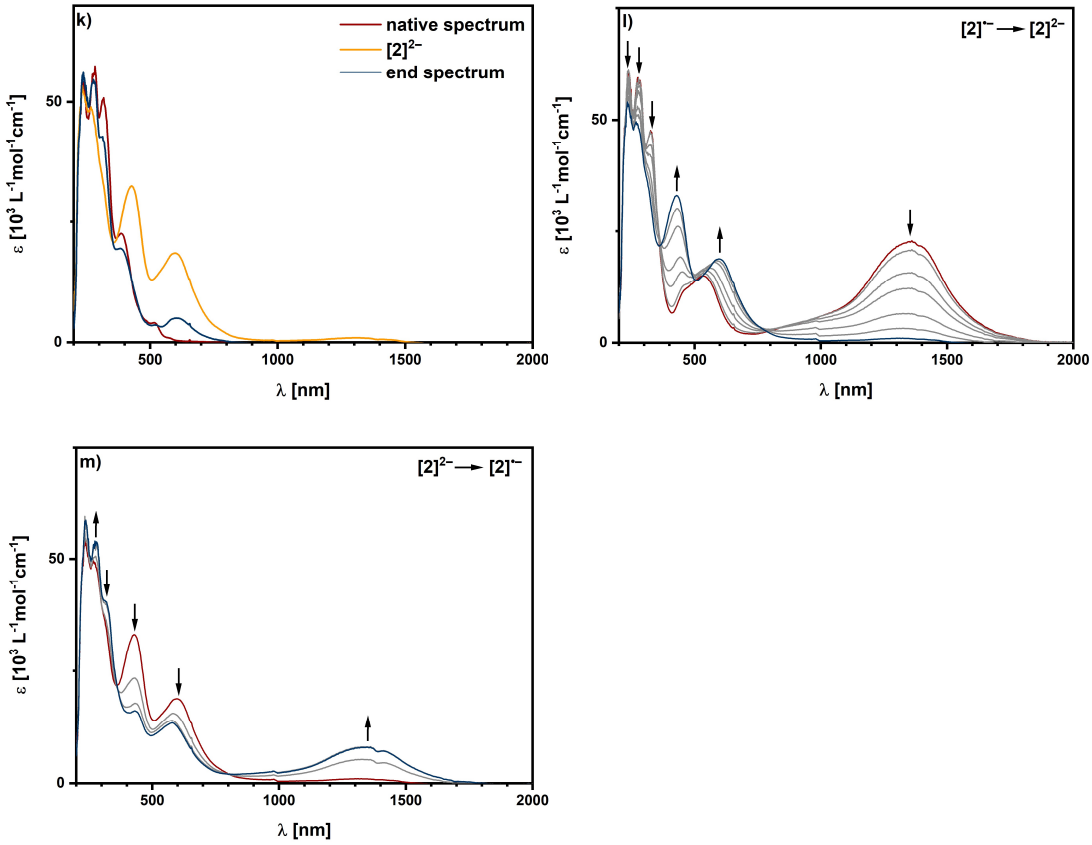

Figure S 10: UV/Vis SEC spectra of complex **2** a)-d) in MeCN/NBu_4PF_6 measured with a gold working electrode, e)-m) in CH_2Cl_2/NBu_4PF_6 measured with a gold working electrode.

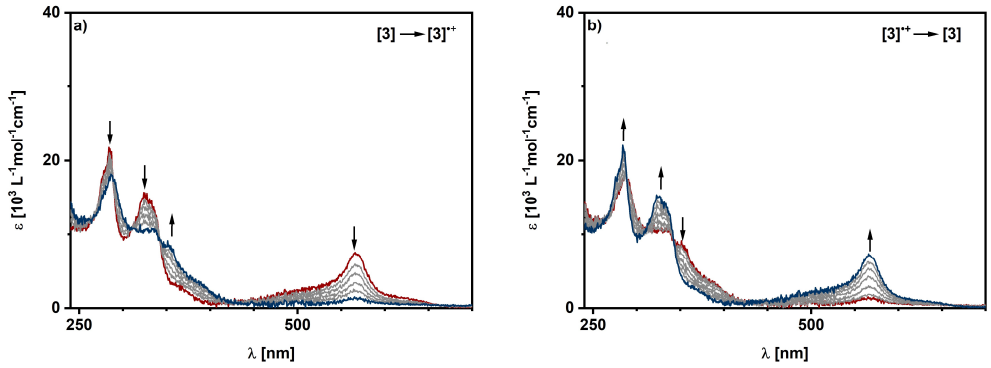

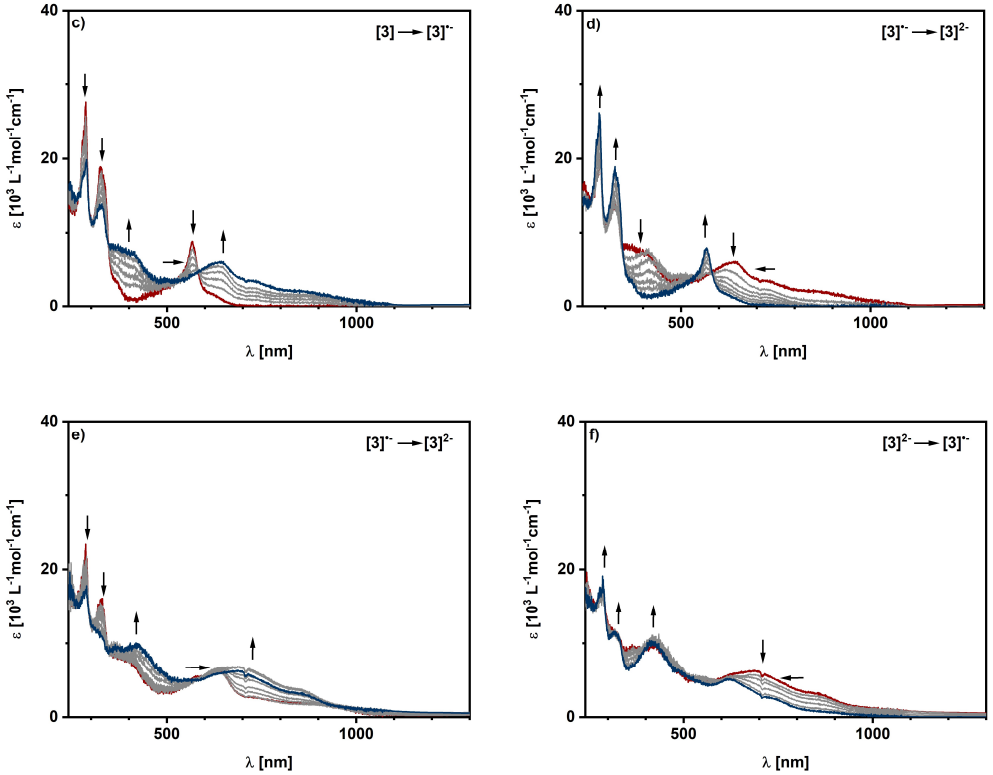

Figure S 11: UV/Vis SEC spectra of complex **3** (a) oxidation, b) rereduction of first oxidation, c) first reduction, d) reoxidation of first reduction, e) second reduction, f) reoxidation of second reduction in CH_2Cl_2/NBu_4PF_6 measured with a gold working electrode

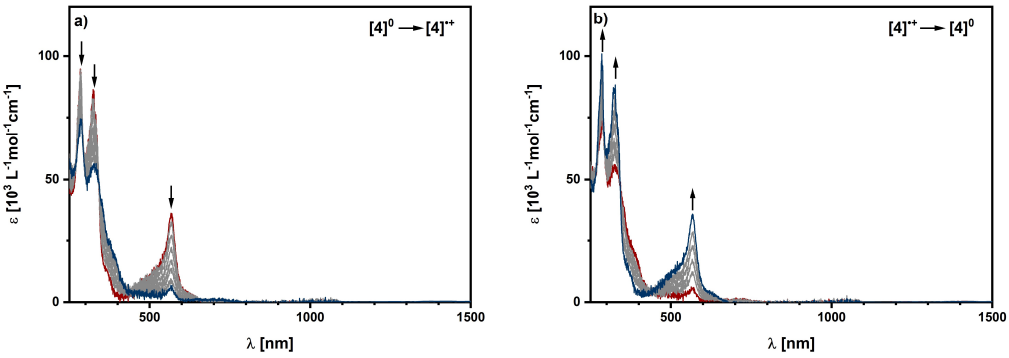

S 10

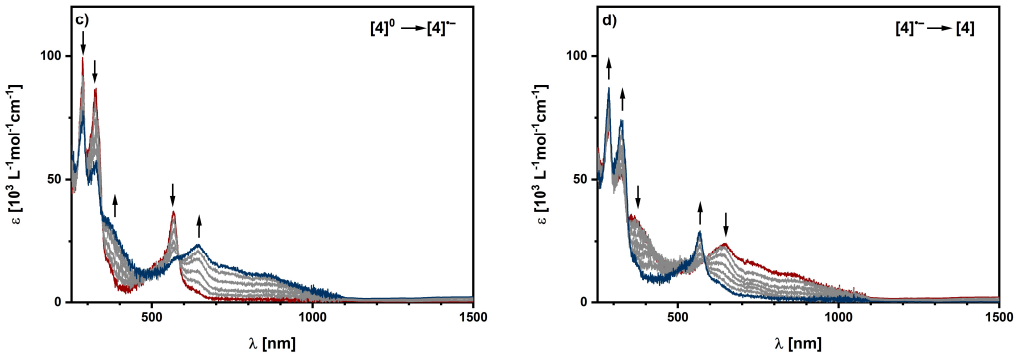

Figure S 12: UV/Vis SEC spectra of complex **4** (a) oxidation, b) rereduction of first oxidation, c) reduction, d) reoxidation of first reduction in CH_2Cl_2/NBu_4PF_6 measured with a silver working electrode;

4. EPR

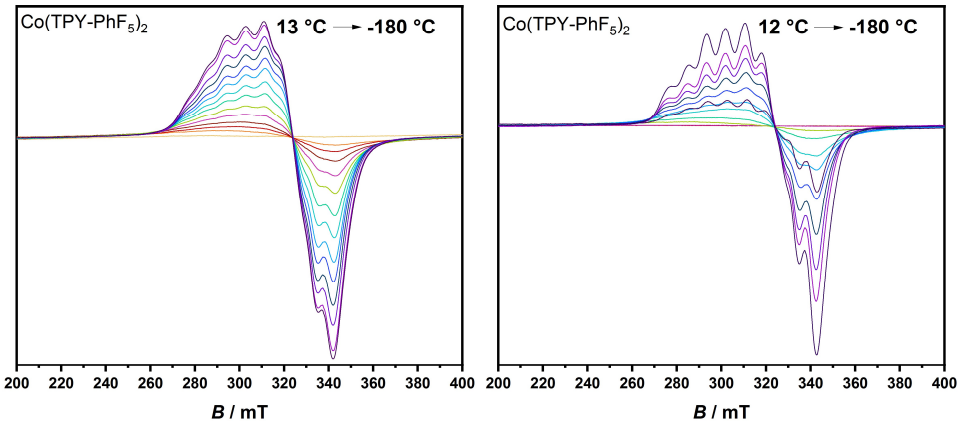

Figure S 13: EPR spectra of complex **1**, left: as powdered sample, right: in an acetonitrile solution.

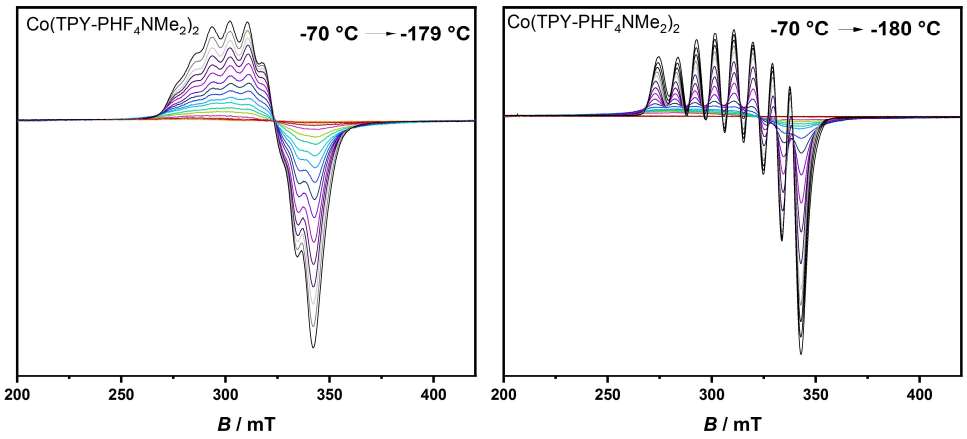

Figure S 14: EPR spectra of complex **2**, left: as powdered sample, right: in an acetonitrile solution.

5. X-Ray Crystallography

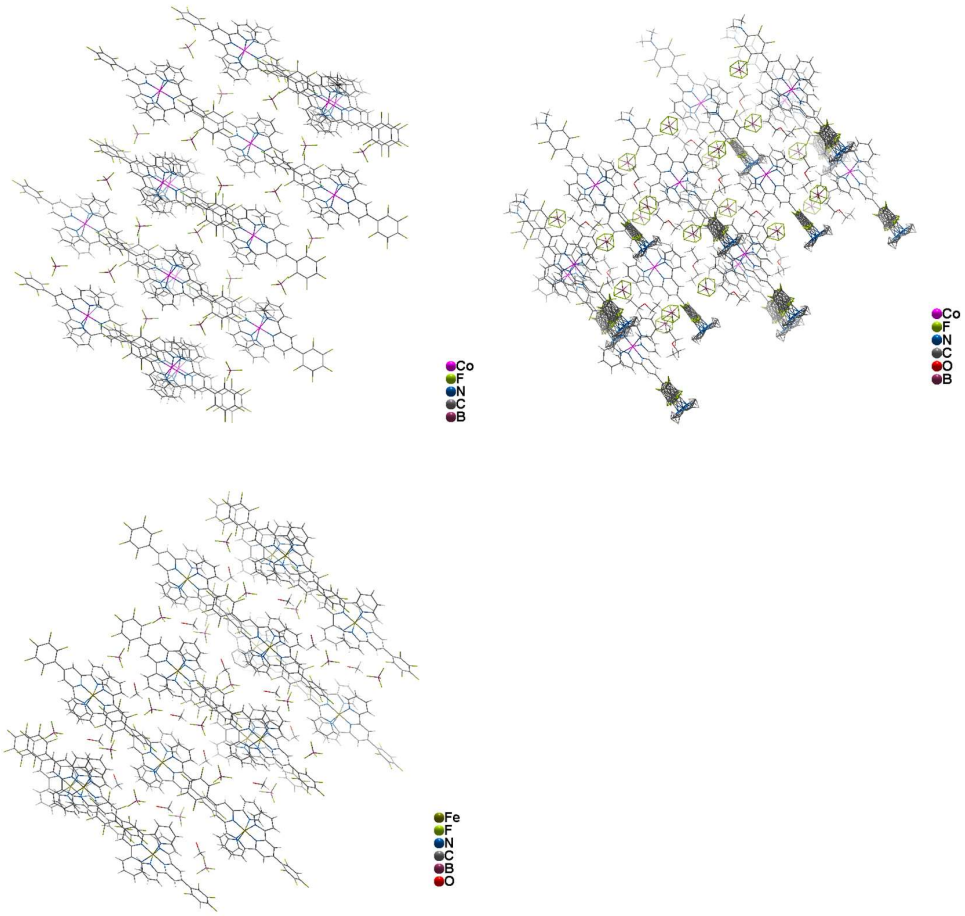

Figure S 15: Projection of the crystal structure of **1** (top left), **2** (top right) and **3** (bottom).

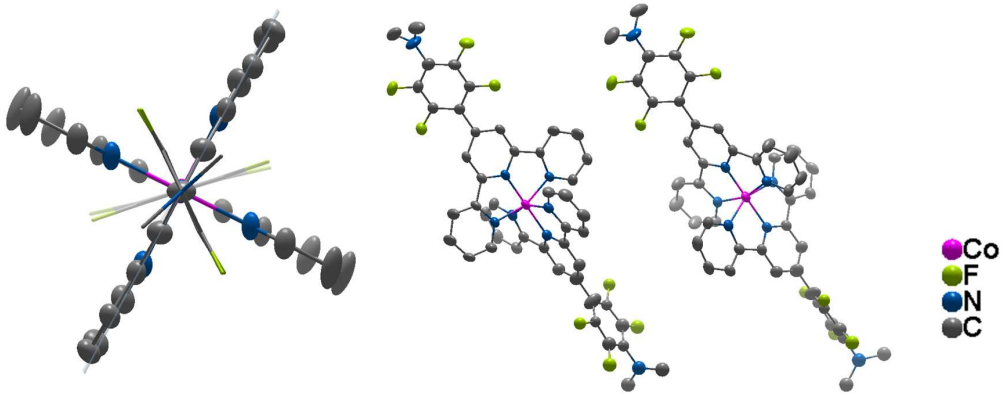

S 12

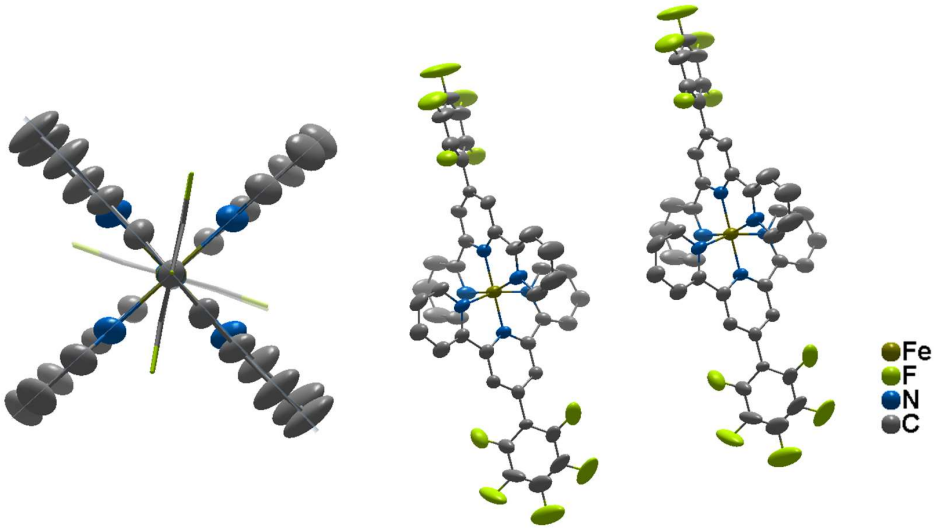

Figure S 16: Orthogonality and depiction of neighboring atoms of complex **2** (top) and **3** (bottom).

Table S 2: Crystallographic data of complexes **1**–**3**.

	Co(L1)$_2$(BF$_4$)$_2$ 1	**Co(L2)$_2$(BF$_4$)$_2$ 2**	**Fe(L1)$_2$(BF$_4$)$_2$ 3**
Chemical formula	$C_{42}H_{20}CoF_{18}N_6B_2$	$C_{54}H_{48}B_2CoF_{16}N_8O_2$	$C_{42}H_{20}CoF_{18}N_6B_2$
M_r	1031.0980	1224.985	1028.1003
Crystal System	Orthorombic	Orthorombic	Orthorombic
Space group	Fdd2	Fdd2	Fdd2
a (Å)	37.126(1)	36.745(1)	37.021(1)
b (Å)	10.8865(5)	11.2824(5)	10.9571(4
c (Å)	24.5859(8)	25.773(1)	24.5865(7)
□□□(°)	90	90	90
β (°)	90	90	90
□ (°)	90	90	90
V (Å^3)	9937.2(7)	10684.8(8)	9973.5(6)
Z	16	8	16

Density (g cm^{-3})	1.379	1.523	1.411
F(000)	4104	5003.260	4239.176
Radiation Type	Mo$\mathbf{K_\alpha}$	Mo$\mathbf{K_\alpha}$	Mo$\mathbf{K_\alpha}$
μ (mm^{-1})	0.448	0.428	0.408
Crystal size	0.52 x 0.36 x 0.09	0.16 x 0.10 x 0.09	0.33 x 0.16 x 0.11
Meas. Refl.	14452	19153	16515
Indep. Refl.	4406	4846	4297
Obsvd. [$I > 2\sigma(I)$] refl.	3953	4331	3683
R_{int}	0.0298	0.0384	0.0337
R [$F^2 > 2\sigma(F^2)$], wR(F^2), S	0.0481,0.1324,0.935	0.0528, 0.1503, 0.1415	0.0642, 0. 1908, 1.0616
$\Delta\rho_{max}$, $\Delta\rho_{min}$ (e $Å^{-3}$)	0.424, -0.232	0.4713, -0.4193	0.617, -0.3756

6. Quantum Chemical Calculations

We refer the reader to the Computational Details given in the main text for all calculations. Due to the qualitatively very similar behavior of all species (see Figures 4 and 5 of the main text), computational investigations were restricted to complexes **1** and **3**. All results should be largely transferable to complexes **2** and **4**, which showed almost identical spectral properties for all oxidation states.

When treating **3** with any hybrid functional such as the global hybrid PBE0,[59] the range-separated hybrid ωB97X-D[60] and the local hybrid LH20t,[61] no satisfactory agreement between theory and experiment could be obtained for the spectra, as the position of the MLCT band at 567 nm was underestimated by more than 100 nm and only one of the π-π* bands was predicted to be above 250 nm. Some of us have recently observed a very good performance of the GGA functional B97-D[62] for the relative spin state energies of Fe(II) complexes.[63] As good agreement with the experimental spectrum of **3** was found at the B97-D/def2-TZVP level, it has been used for all spectra calculations.

At this level, also the ground state is correctly predicted to be low-spin. The resulting spectra for **3** are presented in Figure S17. The qualitative agreement between these spectra and the

experimental spectra shown in Figure 5 of the main text is reasonably good. In case of the formation of $[\mathbf{3}]^{+}$, the relative intensity changes of the two ligand-centered bands below 400 nm are also reproduced well. The position of the MLCT band suggests the formation of a sextet state. NPA charges (see Table S3) clearly show the formation of a Fe(III) species.

For $[\mathbf{3}]^{-}$, the spectrum of the doublet state shows most trends featured by the experimental spectrum. NPA d-orbital populations and spin populations (Table S3) as well as spin-density isosurface plots (Figure S19) suggest a ligand-based reduction. It should, however, be noted that the quartet state is heavily spin-contaminated, and the corresponding results are less reliable. The same is true for the (broken-symmetry) singlet state of $[\mathbf{3}]^{2-}$. The strong increase in absorption beyond 600 nm is, however, captured by both calculated spectra. NPA populations (Table S3) again suggest a ligand-based (second) reduction.

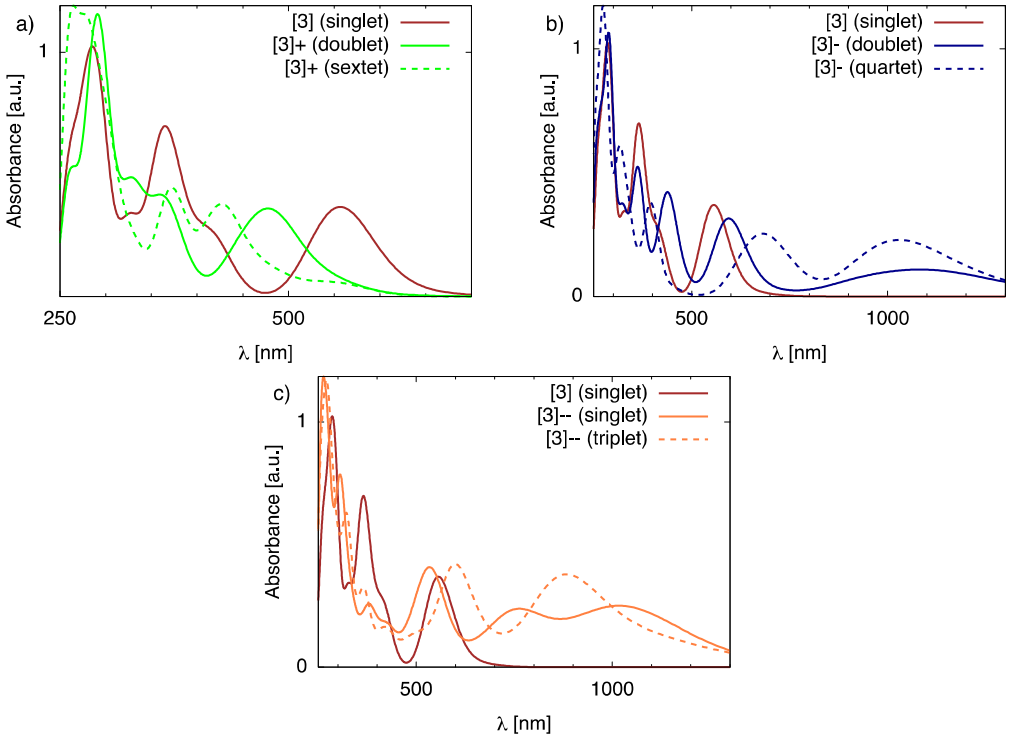

Figure S 17: Simulated spectra for all species obtained from **3** calculated at B97-D/def2-TZVP/COSMO level. Spectra were simulated using the panama script of the TURBOMOLE package with a full width at half maximum (FWHM) of 0.33 eV and using the mixed representation of the oscillator strengths.

For the Co complex **1**, the calculated spectrum (see Fig. S18) as well as the relative energies suggest a low-spin (doublet) ground state in agreement with the structures

obtained experimentally at 100 K. The quartet state lies about 43 kJ/mol higher in energy (B97-D/def2-TZVP), while its spectra look similar to those of the doublet ground state (not shown). Both doublet and quartet ground states have been found for related, non-fluorinated bis-terpy Co complexes.[64]

The oxidized species $[\mathbf{1}]^{+}$ is isoelectronic with the LS Fe(II) complex **3**. Both spin states investigated for $[\mathbf{1}]^{-}$ show the experimentally observed shift in intensity to larger wave lengths, while the singlet state is again strongly spin-contaminated.

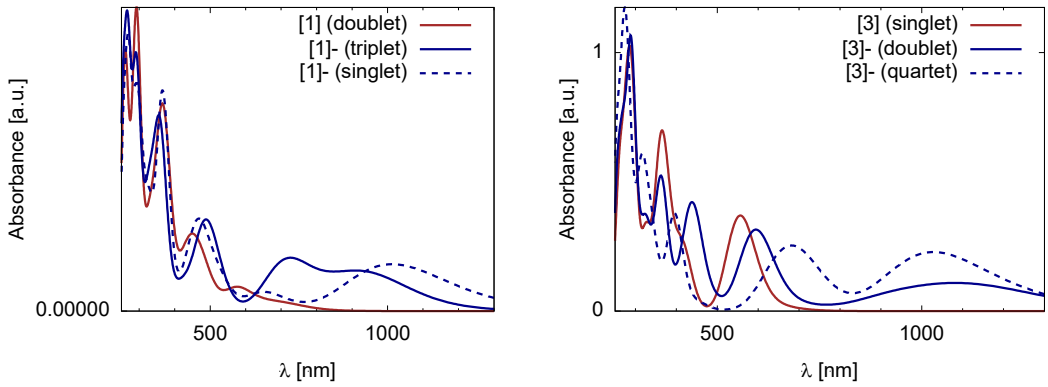

Figure S 18: Simulated spectra for all singly reduced species obtained from complexes **1** and **3** calculated at B97-D/def2-TZVP/COSMO level. Spectra were simulated using the panama script of the TURBOMOLE package with a full width at the half maximum (FWHM) of 0.33 eV and using the mixed representation of the oscillator strengths.

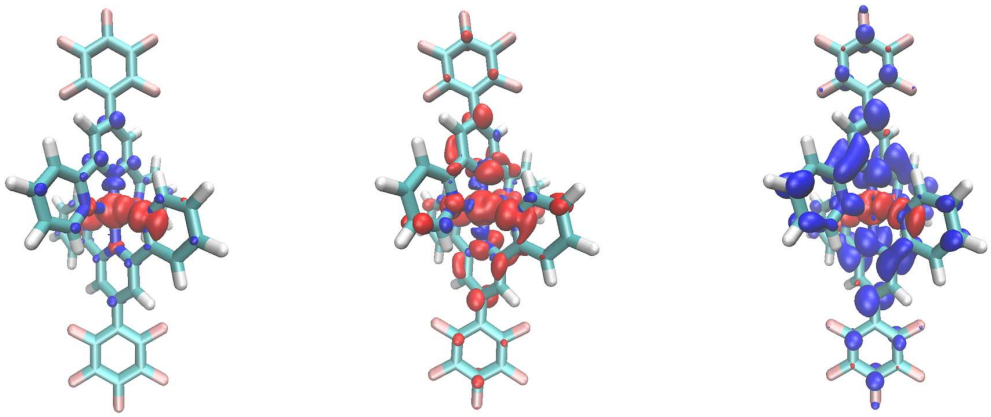

Figure S 19: Spin-density isosurface (+/- 0.001 a.u.) plots for (from left to right) the following states: **[1]** doublet, $\mathbf{[1]}^{-}$ triplet, and $\mathbf{[1]}^{-}$ broken-symmetry singlet (B97-D/def2-TZVP/COSMO).

However, for the two reduced species $[\mathbf{3}]^{2-}$ and $[\mathbf{1}]^{-}$, the energy differences between the different spin states (singlet and triplet in both cases) are below 10 kJ/mol (B97-D/def2-

TZVP), allowing for no clear assignment of the spin state that gives rise to the spectra. In the case of [**1**]$^-$, the metal d-orbital spin populations (Table S3) and spin-density plots (Figure S 19) are consistent with a predominantly ligand-based reduction. This agrees with the results for reduction of the isoelectronic [3]$^-$, while Co-based reductions seem to have been deduced for some other bis-terpy complexes.[64]

Table S 3: Calculated metal atom d-orbital population from natural population analysis (NPA) obtained from both total and spin densities at B97-D/def2-TZVP/COSMO level as well as the expectation value of the S^2 operator.

Complex (spin state)	n(d) (density)	n(d) (spin density)
[1]$^+$ (singlet, $\langle S^2\rangle = 0.00$)	7.98	0.00
[1] (quartet, $\langle S^2\rangle = 3.81$)	7.46	2.61
[1] (doublet, $\langle S^2\rangle = 0.78$)	7.89	0.96
[1]$^-$ (triplet, $\langle S^2\rangle = 2.06$)	7.85	1.36
[1]$^-$ (singlet, $\langle S^2\rangle = 1.03$)[a]	7.89	0.90
[3]$^+$ (sextet, $\langle S^2\rangle = 8.76$)	6.12	4.01
[3]$^+$ (doublet, $\langle S^2\rangle = 0.77$)	6.98	0.98
[3] (singlet, $\langle S^2\rangle = 0.00$)	7.25	0.00
[3]$^-$ (quartet, $\langle S^2\rangle = 4.58$)	6.44	3.49
[3]$^-$ (doublet, $\langle S^2\rangle = 0.75$)	7.24	0.15
[3]$^{2-}$ (triplet, $\langle S^2\rangle = 2.08$)	6.96	1.26
[3]$^{2-}$ (singlet, $\langle S^2\rangle = 0.96$)[a]	7.03	-0.03

[a]Broken-symmetry states.

As it could be argued that use of a GGA functional will result in an overly delocalized description, we have also performed calculations of the reduced Co species [**1**]$^-$ with the MN15 global hybrid functional (featuring 44% exact-exchange admixture). This functional was found to give relatively low errors compared to the amount of exact exchange used.[63] At this level, the spin density in [**1**]$^-$ is not distributed over both ligands (see Figure S 19), but concentrates only on one of the two ligands (Figure S 20).

While we are not able to unambiguously assign the character of the multi-valent system, it can be clearly seen that the quantum chemical description favors a predominantly ligand-centered reduction of [**1**] at both levels, with moderate delocalization over the metal center.

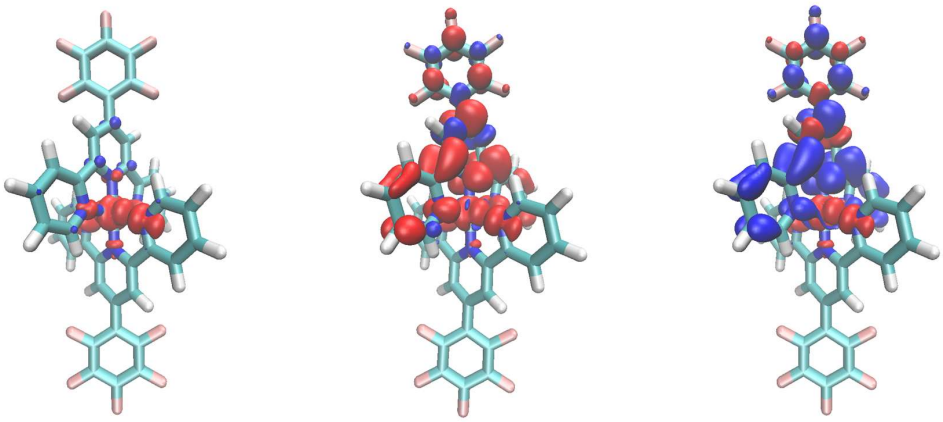

Figure S 20: Spin-density isosurface (+/- 0.001 a.u.) plots for (from left to right) the following states: **[1]** doublet, **[1]**$^{-}$ triplet, and **[1]**$^{-}$ broken-symmetry singlet (MN15/def2-TZVP/COSMO).

7. NMR Spectra

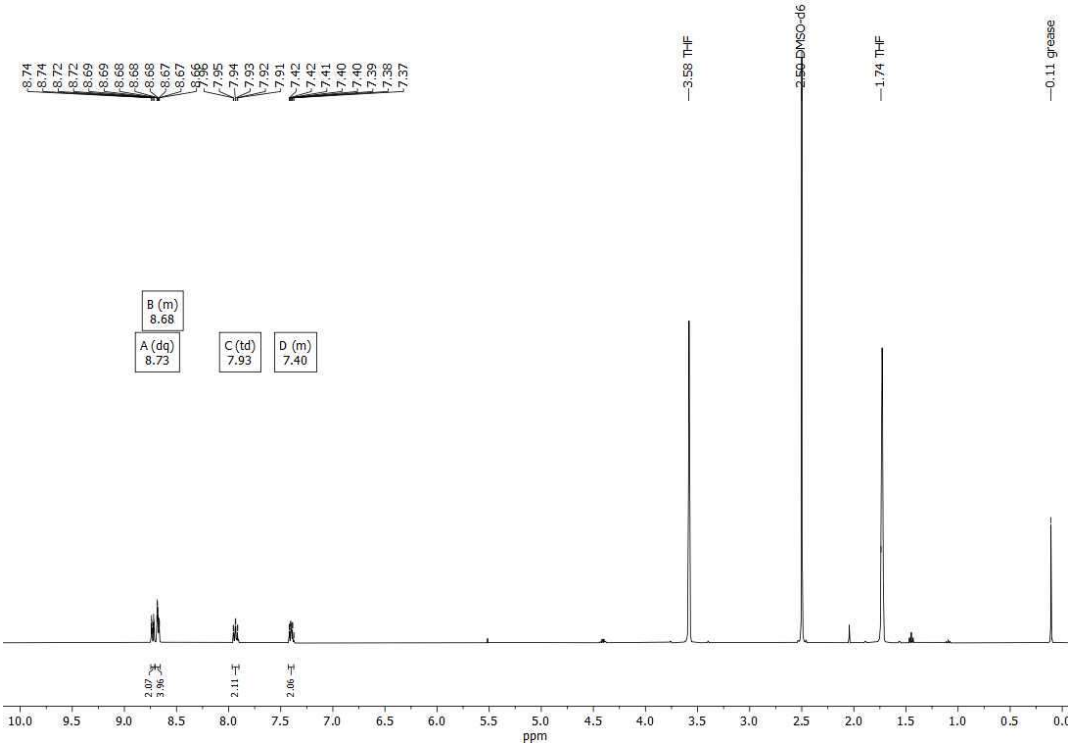

Figure S 21: ^{1}H NMR spectrum of **L1**.

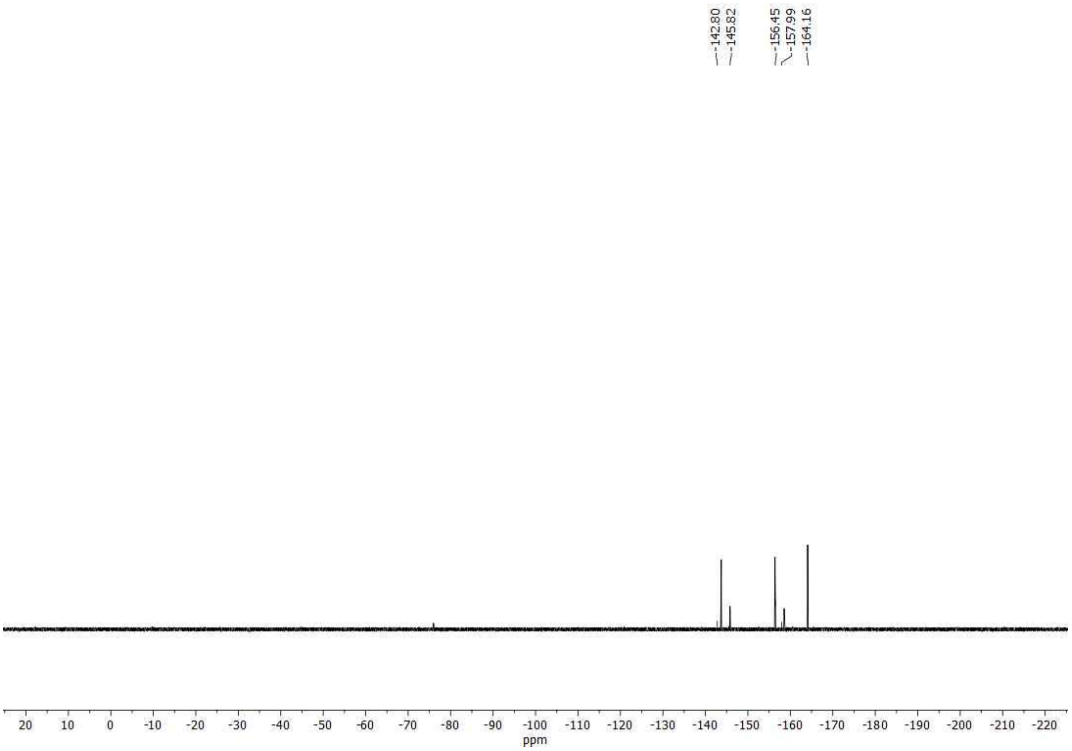

Figure S 22: ^{19}F NMR spectrum of **L1**.

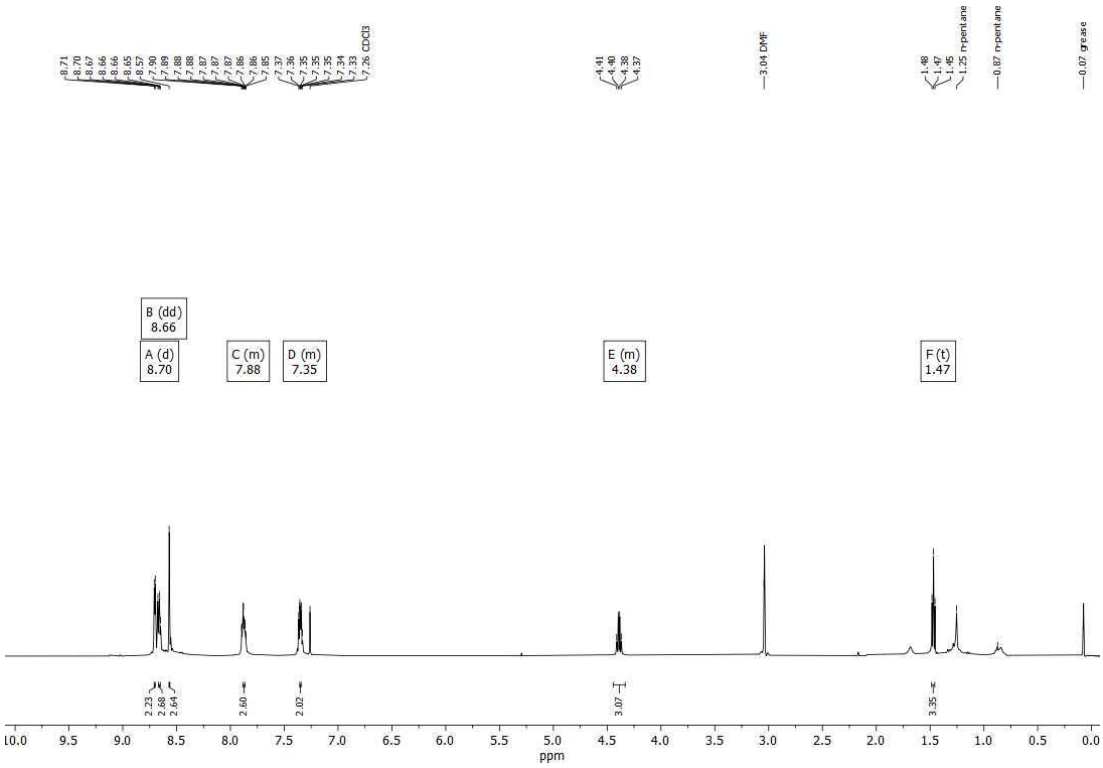

Figure S 23: ^{1}H NMR spectrum of **L2**.

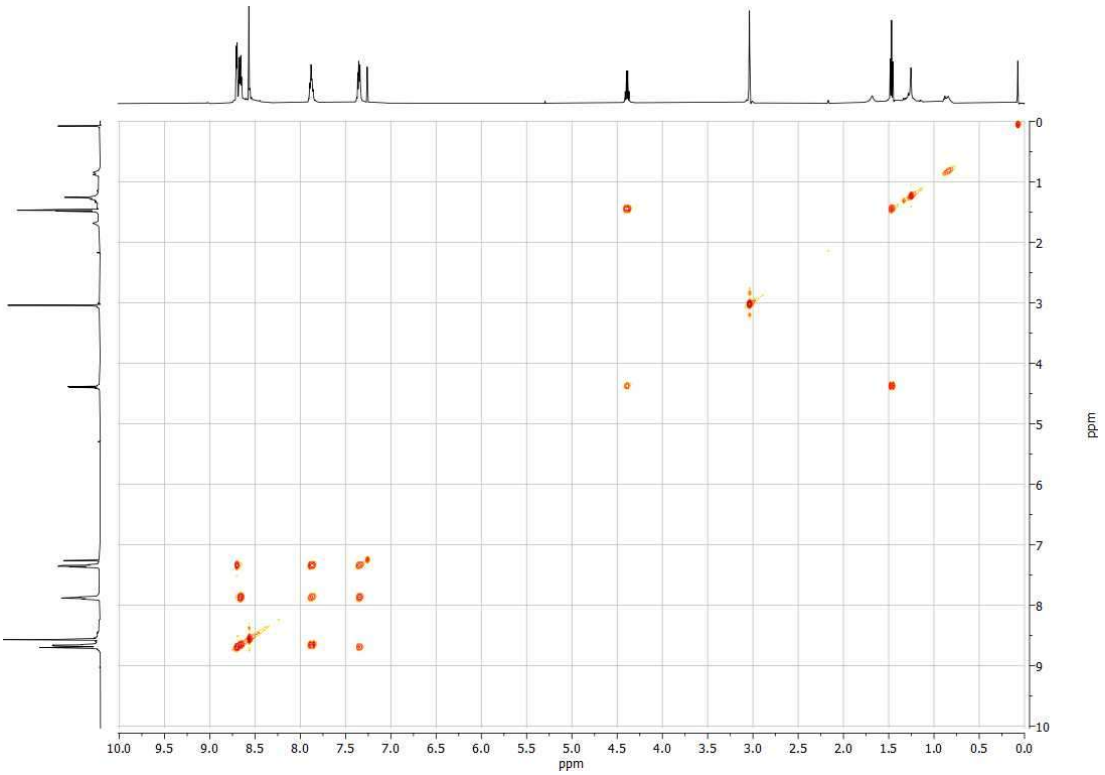

Figure S 24:[1]H [1]H COSY NMR spectrum of **L2**.

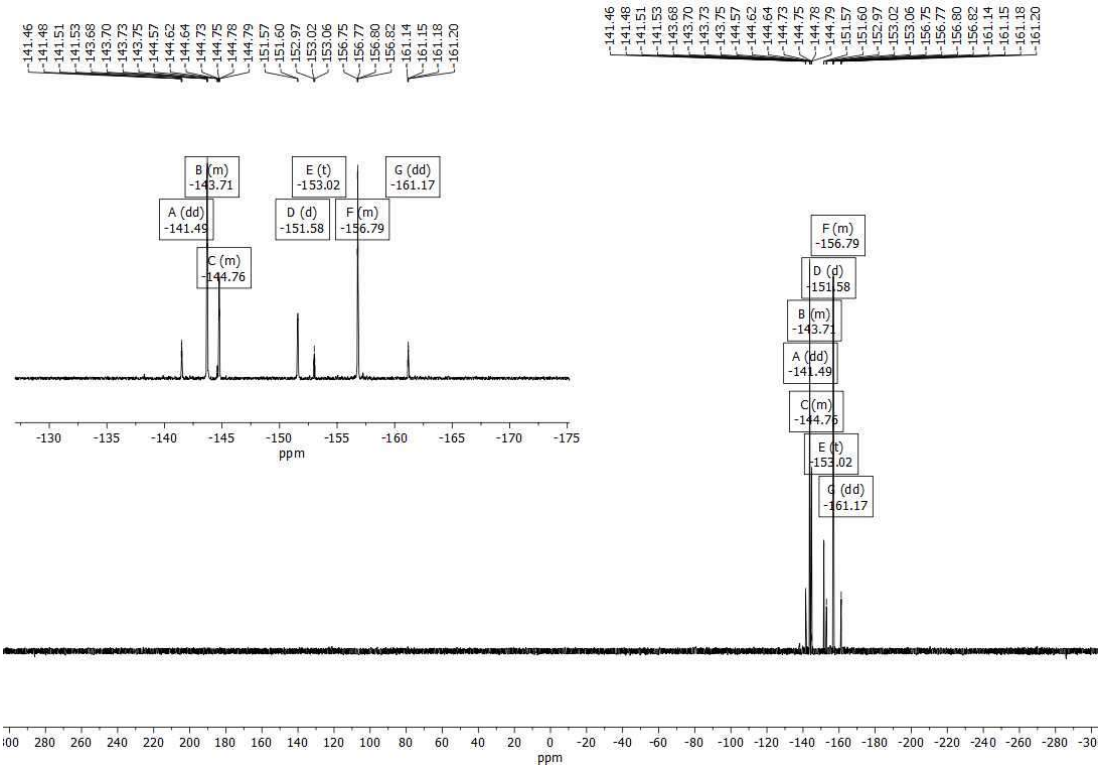

Figure S 25:[19]F NMR spectrum of **L2**.

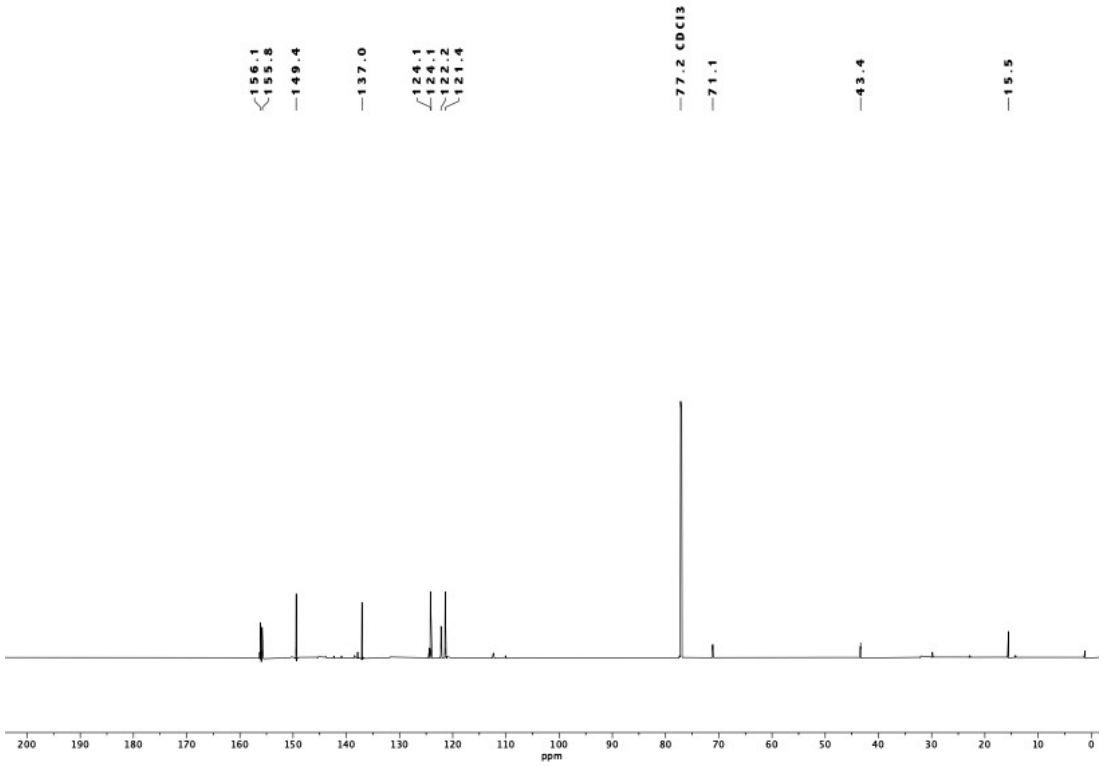

Figure S 26: ^{13}C NMR spectrum of **L2**.

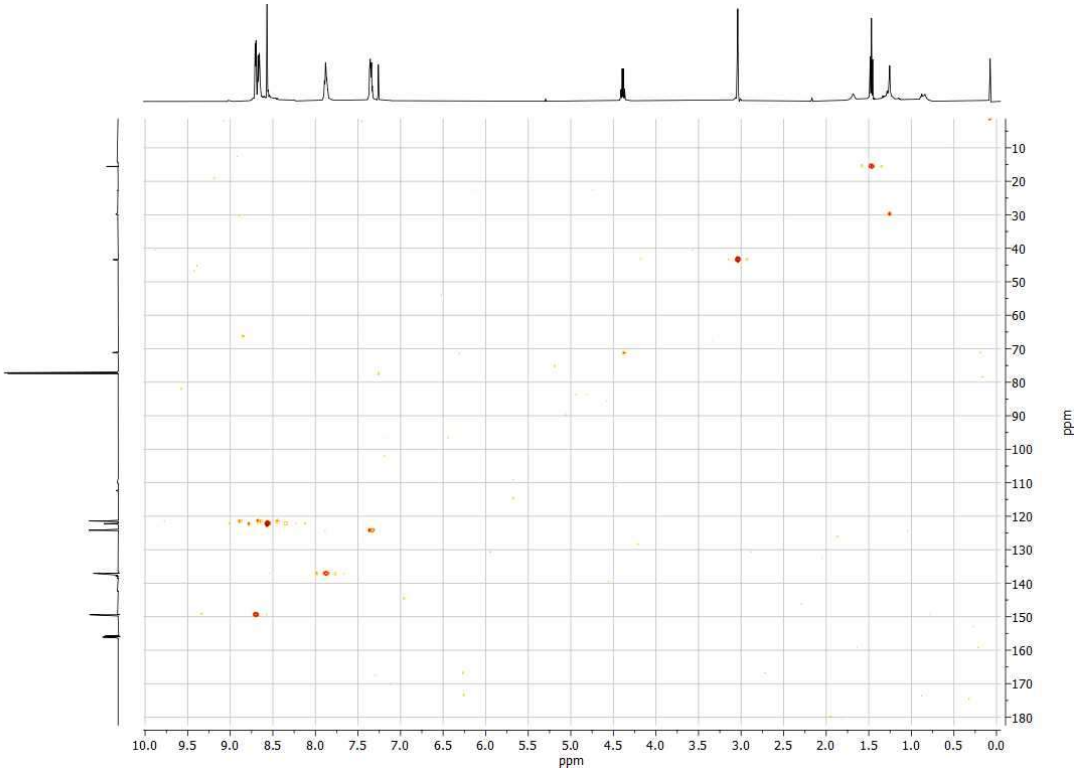

Figure S 27: ^{1}H ^{13}C HMBC NMR of **L2** in $CDCl_3$.

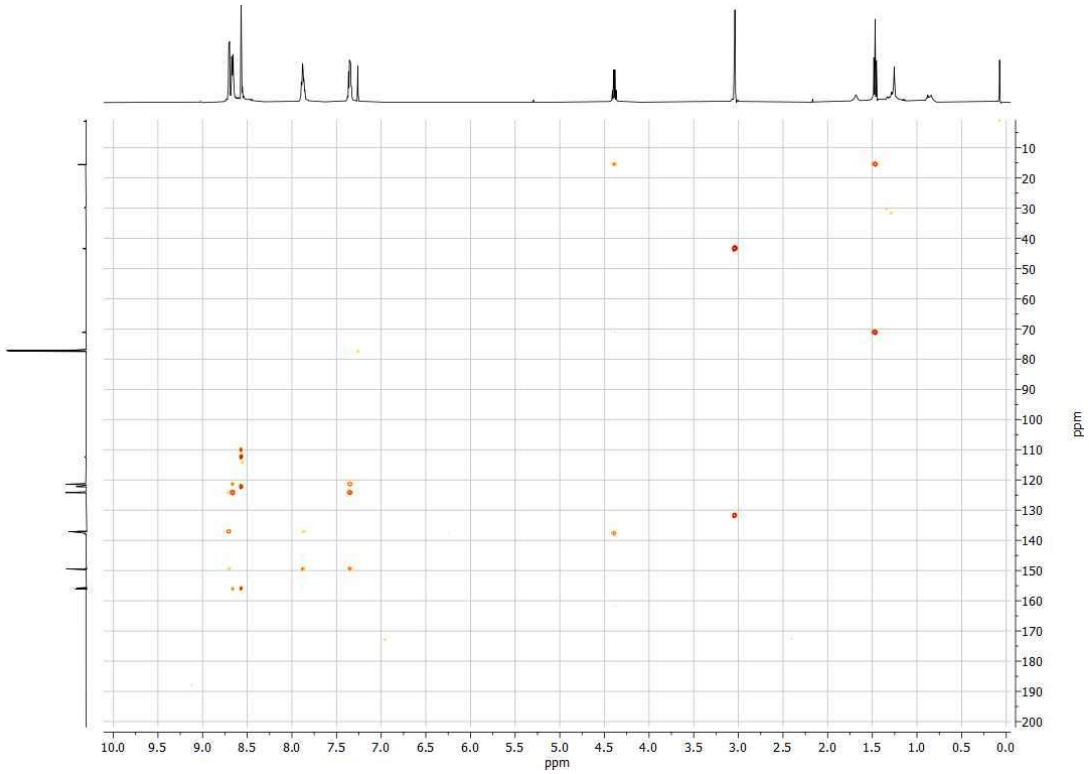

Figure S 28: ^{1}H ^{13}C HMQC NMR of **L2** in $CDCl_3$.

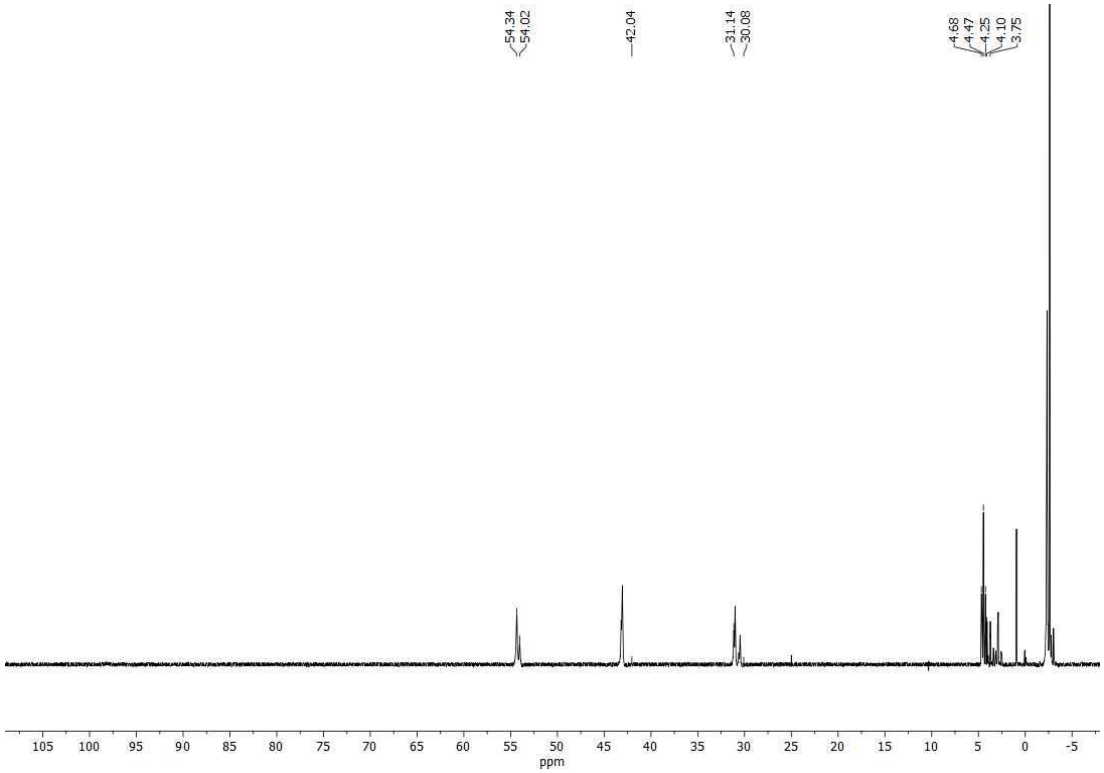

Figure S 29:^{1}H NMR spectrum of complex **1** in MeCN.

S 22

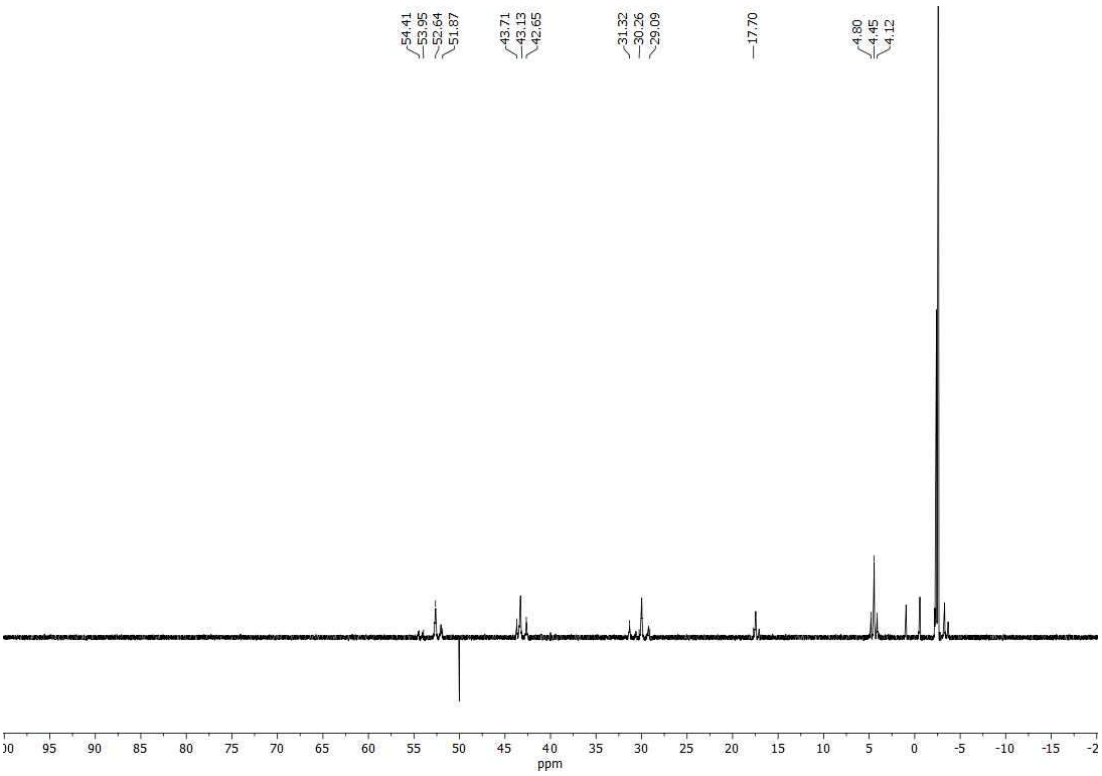

Figure S 30:[1]H NMR spectrum of complex **2** in MeCN.

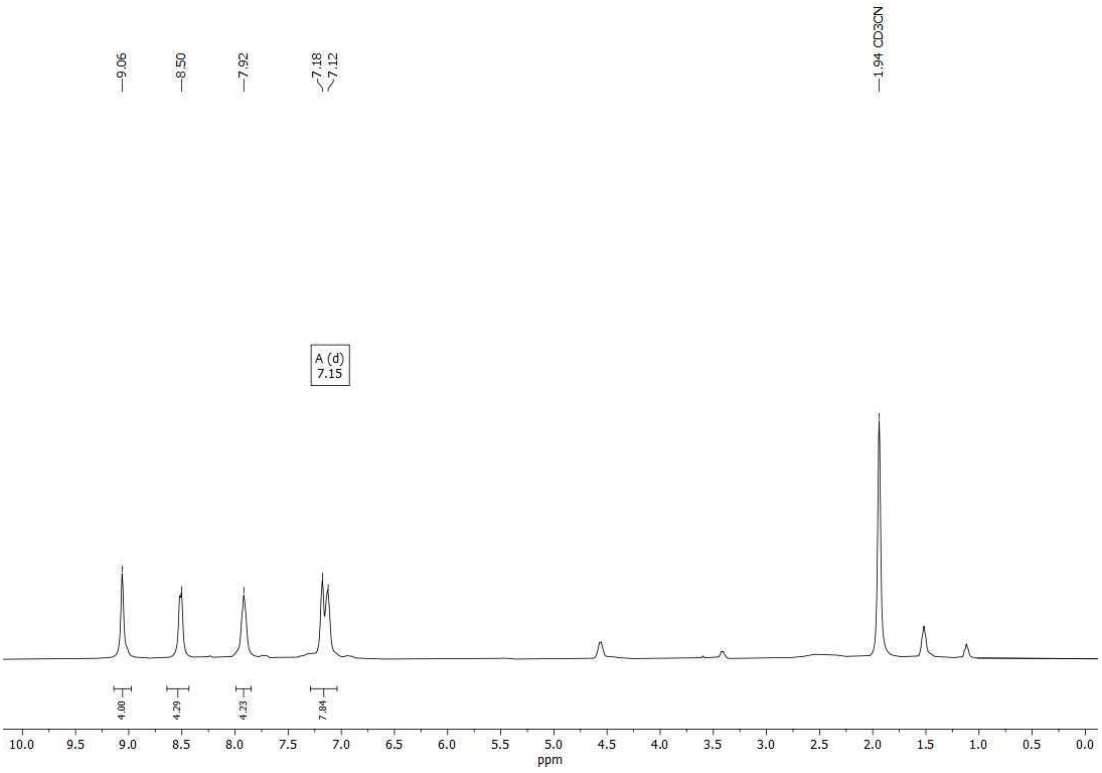

Figure S 31: [1]H NMR spectrum of complex **3** in MeCN.

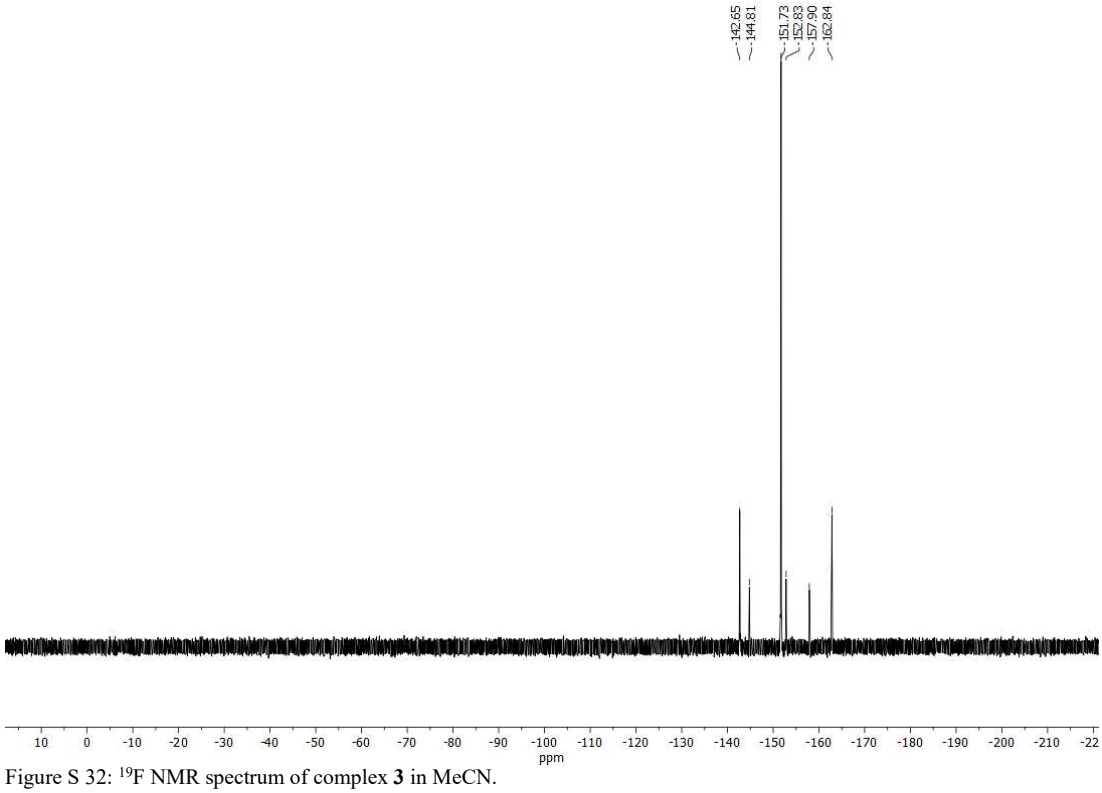

Figure S 32: ^{19}F NMR spectrum of complex **3** in MeCN.

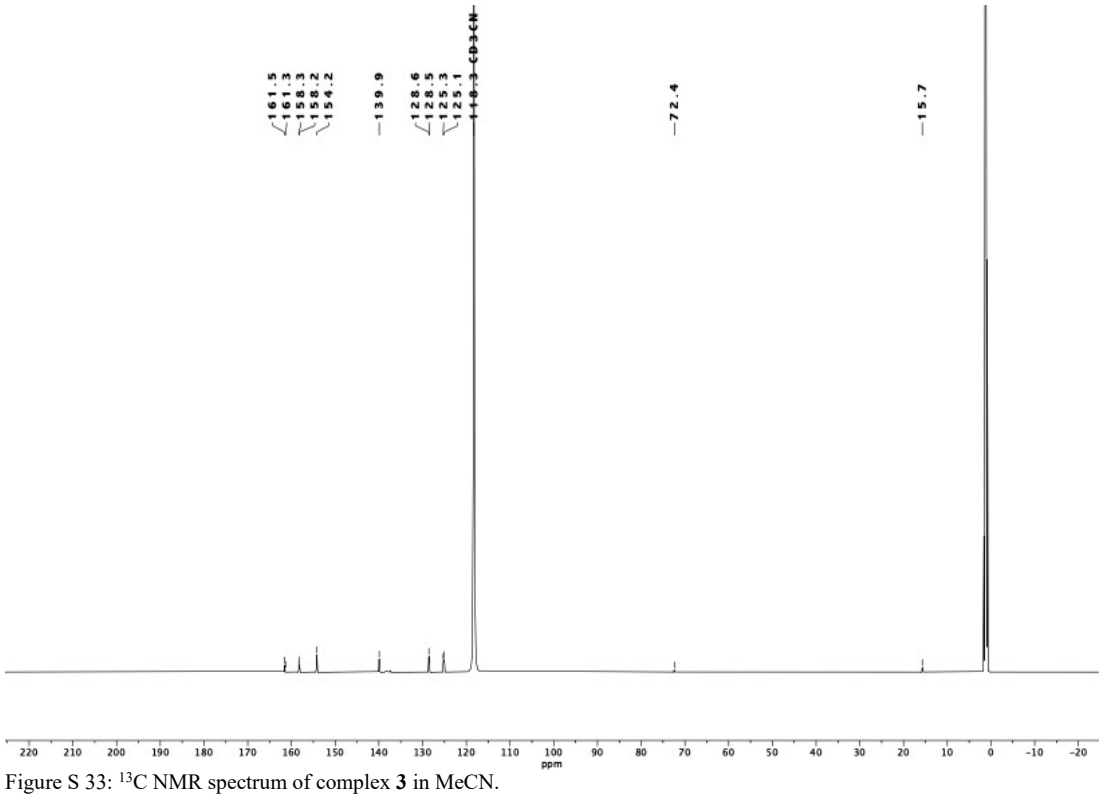

Figure S 33: ^{13}C NMR spectrum of complex **3** in MeCN.

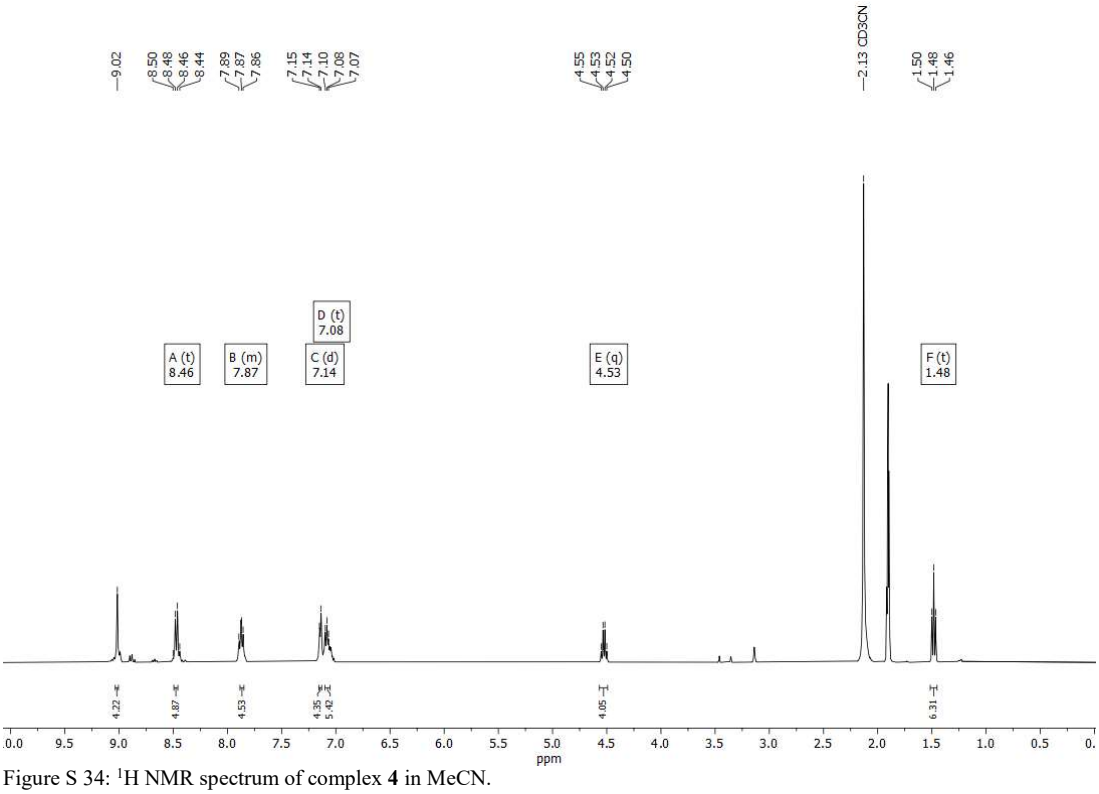

Figure S 34: ^{1}H NMR spectrum of complex **4** in MeCN.

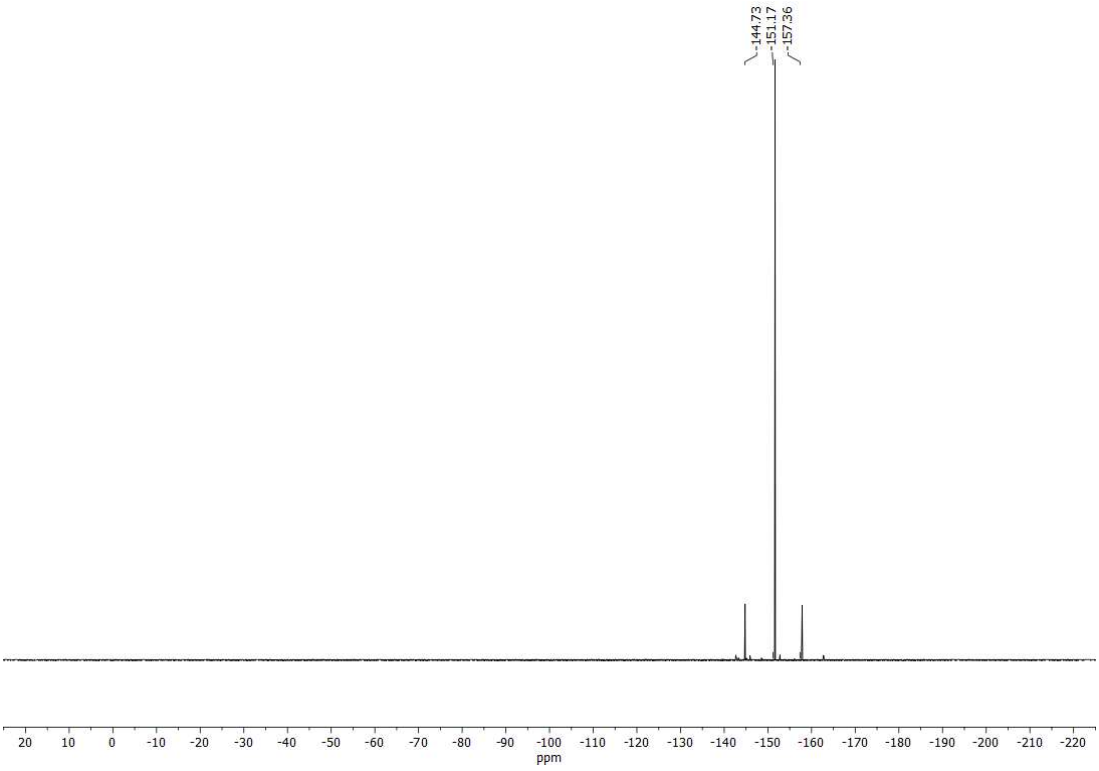

Figure S 35: ^{19}F NMR spectrum of complex **4** in MeCN.

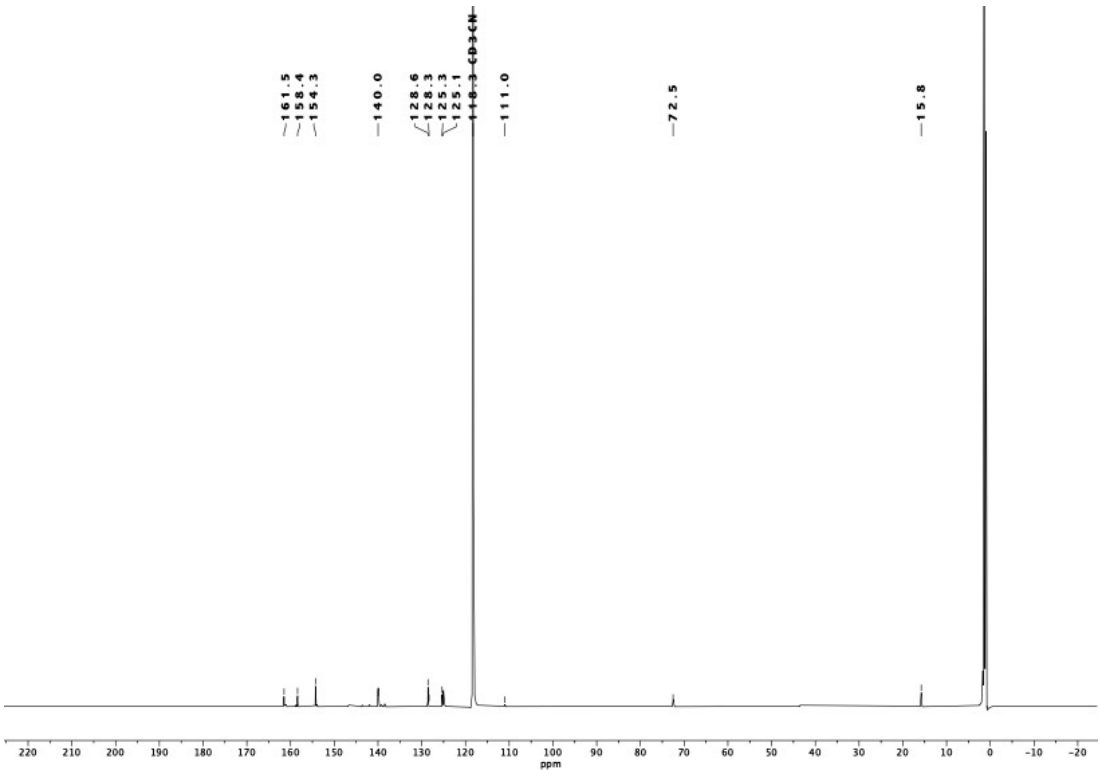

Figure S 36: ^{13}C NMR spectrum of complex **4** in MeCN.

8. References

[59] C. Adamo, V. Barone, *J. Chem. Phys.* **1999**, *110*, 6158-6170.
[60] J.-D. Chai, M. Head-Gordon, *Phys. Chem. Chem. Phys.* **2008**, *10*, 6615-6620.
[61] M. Haasler, T. M. Maier, R. Grotjahn, S. Gückel, A. V. Arbuznikov, M. Kaupp, *J. Chem. Theory Comput.* **2020**, *16*, 5645-5657.
[62] S. Grimme, *J. Chem. Phys.* **2006**, *124*, 034108.
[63] M. Reimann, M. Kaupp, *J. Chem. Theory Comput.* **2022**, *18*, 7442-7456.
[64] a) S. Aroua, T. K. Todorova, P. Hommes, L.-M. Chamoreau, H.-U. Reissig, V. Mougel, M. Fontecave, *Inorg. Chem.* **2017**, *56*, 5930-5940; b) S. Aroua, T. K. Todorova, V. Mougel, P. Hommes, H.-U. Reissig, M. Fontecave, *ChemCatChem* **2017**, *9*, 2099-2105.

3.2.2. Spin Crossover and Flourine-Specific Interactions in Metal Complexes of Terpyridines with Polyfluorocarbon Tails

Maite Nößler,[a] Nicolás I. Neuman,[b, c] Lisa Böser,[a] René Jäger,[a] Arijit Singha Hazari,[b] David Hunger,[d] Yixian Pan,[d] Clemens Lücke,[b] Tobias Bens,[b] Joris van Slageren[d], and Biprajit Sarkar[a,b],**

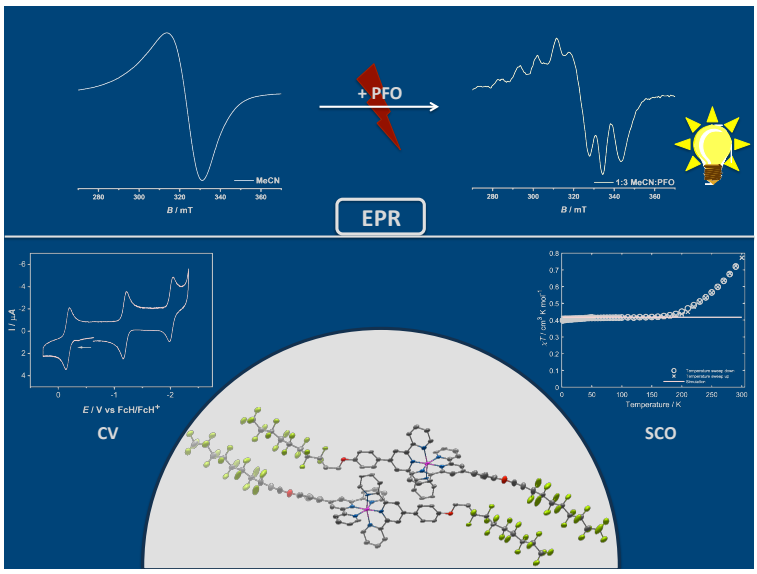

[a] Institut für Chemie und Biochemie,
Freie Universität Berlin, Fabeckstraße 34-36, D-14195, Berlin, Germany
[b] Institut für Anorganische Chemie,
Universität Stuttgart, Pfaffenwaldring 55, D-70569 Stuttgart, Germany.
[c] Instituto de Desarrollo Tecnológico para la Industria Química,
INTEC, UNL-CONICET Predio CCT Conicet "Dr. Alberto Cassano", Colectora RN 168, Km 0, Paraje El Pozo, (3000) Santa Fe, Argentina.
[d] Institut für Physikalische Chemie,
Universität Stuttgart, Pfaffenwaldring 55, 70569 Stuttgart, Germany.

Manuscript in preparation

Author contribution: The project was designed by Biprajit Sarkar and Maite Nößler. The ligands and complexes were synthesized and characterized by Maite Nößler. Lisa Böser and René Jäger worked in this project during a research internship. Cyclic voltammetric and UV/Vis/NIR-spectroelectrochemical measurements were performed by Lisa Böser, René Jäger, Clemens Lücke and Maite Nößler. The SQUID experiments were performed by David Hunger and Yixian Pan during her research internship. X-Ray diffraction analysis was carried out by Maite Nößler. DFT calculations were performed by Nicolás I. Neuman. EPR measurements were performed by Maite Nößler and Arijit Singha Hazari, subsequent simulation of the spectra was performed by Tobias Bens, Nicolás I. Neuman and Arijit Singha Hazari. The manuscript was written by Maite Nößler, David Hunger, Nicolás Neuman, and Biprajit Sarkar with inputs from Joris van Slageren.

Spin Crossover and Flourine-Specific Interactions in Metal Complexes of Terpyridines with Polyfluorocarbon Tails

Maite Nößler,[a] Nicolás I. Neuman,[b, c] Lisa Böser,[a] René Jäger,[a] Arijit Singha Hazari,[b] David Hunger,[d] Yixian Pan,[d] Clemens Lücke,[b] Tobias Bens,[b] Joris van Slageren[d,] and Biprajit Sarkar[a,b,*]*

Abstract

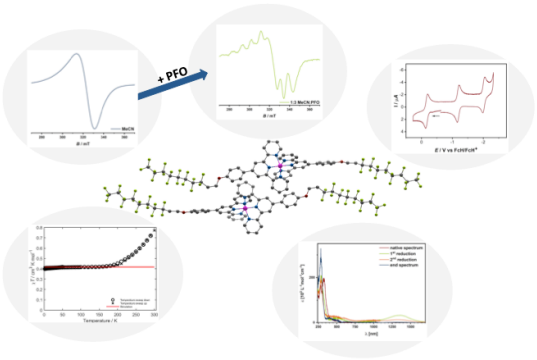

In coordination chemistry and material science, terpyridine ligands are of great interest, due to their ability to form stable complexes with a broad range of transition metal ions. The material properties of these frameworks can be modulated via judicious choices of functional groups on the ligand backbone. In this context, we report three terpyridine ligands containing different perfluoro carbon (PFC) tails on the backbone and the corresponding Fe^{II} and Co^{II} complexes. The Co^{II} complexes display spin crossover close to ambient temperature, and the nature of this spin transition is influenced by the length of the PFC tail on the ligand backbone. The electrochemical properties of the metal complexes were investigated with cyclic voltammetry revealing one oxidation and several reduction processes. Investigation of the fluorine specific interactions was performed by EPR measurements. Analysis of the EPR spectra of the complexes as microcrystalline powders and in solution reveals exchange narrowed spectra without resolved hyperfine splittings arising from the ^{59}Co nucleus, which suggests complex aggregation in solution mediated by interactions of the PFC tails. Interestingly, addition of perfluorooctanol in different ratios to the acetonitrile solution of the sample resulted in the disruption of the F ⋯ F interactions of the tails, revealed by the resolution of the hyperfine structure. To the best of our knowledge, this is the first investigation of fluorine specific interactions in metal complexes through EPR spectroscopy, as exemplified by exchange narrowing.

Introduction

In the last decades, 2,2’;6’,2’’-terpyridines became popular ligands in coordination chemistry due to their ability to form stable complexes with different transition-metal ions.[1] The synthesis of 2,2’;6’,2’’-terpyridine and its derivatives has been extensively studied for the past decades. However, there are limitations regarding the synthesis of new terpyridine ligands, especially those bearing electronically different substituents on the pyridine units.[2] The metal complexes bearing terpyridine ligands were investigated for various applications as photosensitizers,[3] gel systems,[4] ion sensors,[5] supramolecular polymers,[6] redox shuttles for dye sensitized solar cells (DSSC),[7] and catalysis for proton and CO_2 reduction[8] and water oxidation.[9] Moreover, metal-terpyridine complexes were reported to exhibit spin-crossover behavior. Spin-crossover (SCO), first described in the 1930s by Cambi *et al.*,[10] usually occurs in d^n (n = 4-7) transition metal

[a] Institut für Chemie und Biochemie, Freie Universität Berlin, Fabeckstraße 34-36, 14195, Berlin (Germany)
E-mail: biprajit.sarkar@iac.uni-stuttgart.de
[b] Institut für Anorganische Chemie, Universität Stuttgart, Pfaffenwaldring 55, 70569 Stuttgart (Germany)
[c] Instituto de Desarrollo Tecnológico para la Industria Química, INTEC, UNL-CONICET Predio CCT Conicet “Dr. Alberto Cassano”, Colectora RN 168, Km 0, Paraje El Pozo, (3000) Santa Fe, Argentina.
[d] Institut für Physikalische Chemie, Universität Stuttgart, Pfaffenwaldring 55, 70569 Stuttgart (Germany)

complexes providing bistability between the high-spin (HS) and low-spin (LS) states.[11] This phenomenon is most commonly observed in Co^{II} and Fe^{II} complexes.[12] Because of their potential use in information storage, sensors, electro-optical devices and spintronics, multifunctional molecular materials (materials that exhibit synergistic coexistence of two or more properties) are currently popular.[13] Among these, liquid crystals (LC) are considered as fascinating functional materials.[14] Metallomesogens, liquid crystals of transition metal complexes, which show multifunctonality (spin-crossover, mixed-valence etc.), have attracted significant attention due to the co-occurrence of physical properties (magnetic, optical and electrical properties).[14-15] A new class of functional materials was found as SCO metallomesogens, where LC properties and SCO are synchronized.[14-16] In addition, other multifunctional molecule-based materials are SCO compounds that are coupled with non-linear optical (NLO)[17] and/or luminescence properties.[18] One way to control SCO properties and the cooperativity in such molecules is the introduction of long alkyl chains.[19] Along this line, Hayami and co-workers reported a number of terpyridine Co-complexes containing long alkyl chains displaying interesting magnetic and LC properties.[11, 14, 19a, 20] The alkylated cobalt complexes published from the group of Hayami displayed not only "reverse spin transition" between the HS and LS state,[10] but also abrupt,[14] multi-phase[21] and gradual SCO[19a] properties. Additionally, a structural phase transition was shown to trigger a thermal hysteresis loop.[10] The flexibility of these complexes can directly influence cooperative interactions through structural changes, or indirectly, through random packing structure, and therefore play an important role in the aforementioned magnetic properties.[10, 19a] Although the use of perfluorinated alkyl chains is very interesting, only a handful of examples of metal complexes bearing fluorous tails exist in the literature.[4, 9] Usually, these systems were mostly investigated towards their gelation properties, as the perfluorinated compounds are typically lipophobic and hydrophobic at the same time and therefore show self-assembly behavior.[4, 22] The self-assembly can be controlled not only by H-bonds but also by halogen bonding and weak interactions, like fluorine-fluorine (F···F) interactions,[22] which can also be of great significance for hysteretic SCO behavior.[23] The area of research of fluorine chemistry is continuously developing, as there are various applications for metal complexes with perfluorocarbon (PFC) tails such as in catalysis, supramolecular chemistry, synthesis and separation technologies and novel technological developments.[9] Electron paramagnetic resonance (EPR) is a widely used technique to investigate radical species. One phenomenon observed in EPR is exchange narrowing, first suggested by Gorter and Van Vleck.[24] Exchange narrowing can be due to chemical interconversion between species with different magnetic parameters, for example caused by thermal motion of atoms in liquids and some solids, or due to electronic exchange interaction between the unpaired spins in different paramagnetic centers in an extended system.[24-25] Different mathematical methods were developed to model the narrowing of the resonance lines.[26] In diluted systems the line shape can be influenced by dipole-dipole interactions between paramagnetic centers,[26c, 27] as well as partially resolved fine and hyperfine splittings. Meanwhile, in magnetically undiluted systems the isotropic exchange interaction may be dominant, resulting in a single resonance for each magnetic field orientation, with a linewidth determined by the interplay of exchange narrowing and the broadening produced by all anisotropic magnetic interactions (anisotropic exchange, dipolar interaction and hyperfine splittings, for example).[28] The narrowing effect is mediated by an exchange frequency, related to the interelectronic exchange parameter *J*, coupling the magnetic centers from

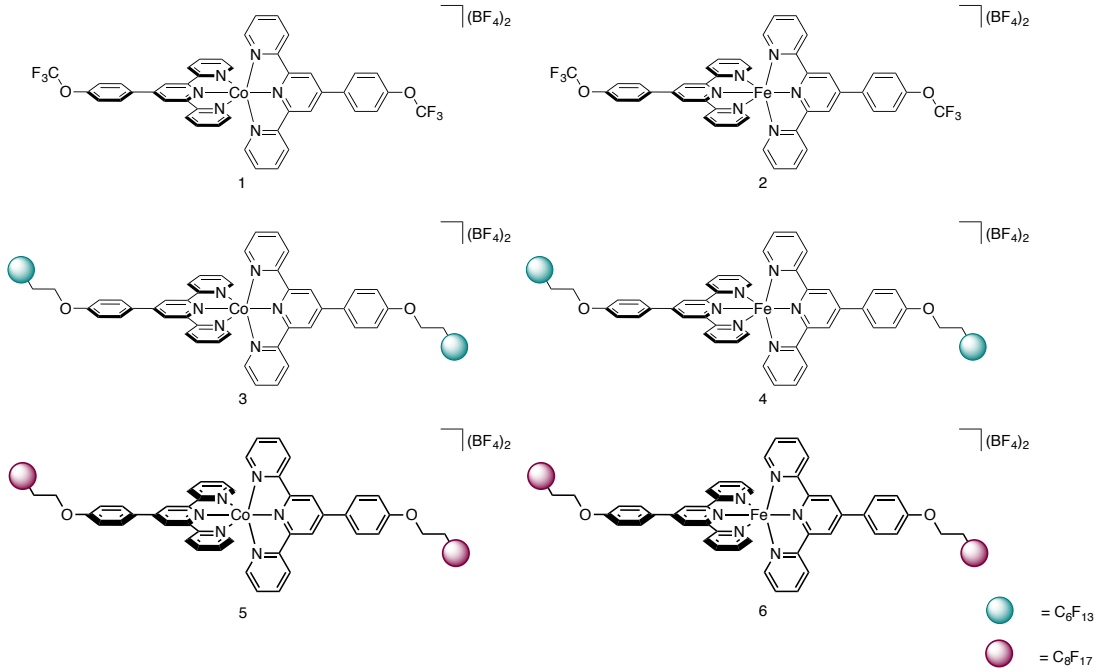

Figure 1: Terpyridine containing complexes with Co^{II} and Fe^{II} metal centers.

neighboring molecules. If the exchange frequency is much smaller than the fine and hyperfine splittings in each magnetic center, a well resolved spectrum may be observed. As the exchange interactions increase, the individual resonance lines broaden and merge into the "gravity center" of the spectra. Finally, if the exchange is larger than the separation between individual resonances, a single resonance is obtained, which becomes narrower with the increase of *J*.[29] To the best of our knowledge, exchange narrowing has not been investigated in the context of molecular aggregation mediated by fluorine specific interactions. As part of our recent interest in metal complexes of fluorinated terpyridine ligands,[30] we report here on several complexes of iron and cobalt centers containing terpyridine ligands with PFC tails (Figure 1). These complexes were investigated through SQUID magnetometry with a focus on SCO behavior. Furthermore, the exchange narrowing in the EPR spectra were investigated towards F···F interactions of the PFC tails. Regarding this also DFT calculations were performed.

Results and Discussion

Synthesis, Crystal Structures and Magnetic Properties

The ligands were synthesized by adapting previously published routes.[4, 31] The ligand **L1** was synthesized over a known synthetic route for terpyridine ligands (Scheme1).[31]

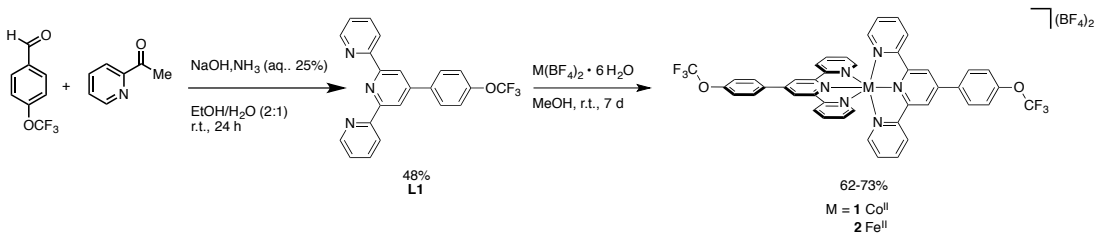

Scheme 1: Synthesis of ligand **L1** and complexes **1** and **2**.

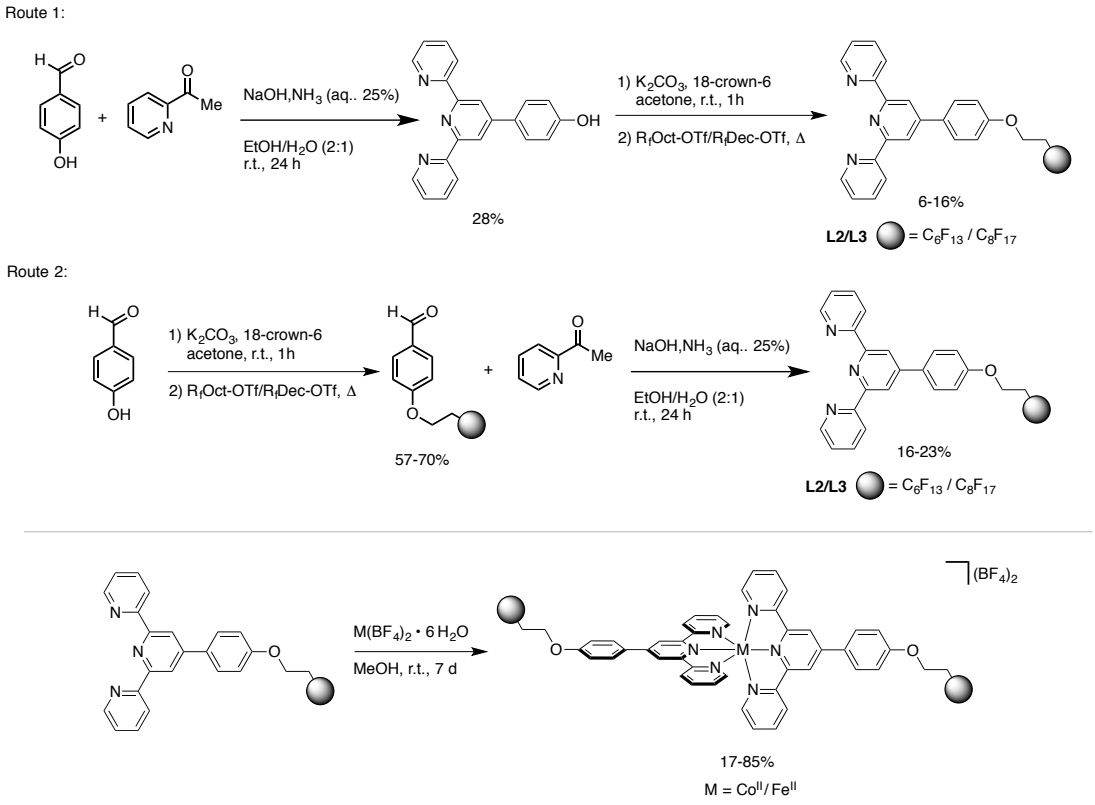

Scheme 2: Synthesis of ligands **L2** and **L3** and complexes **3**-**6**.

The ligands **L2** and **L3** were synthesized over two different routes by adding either 3,3,4,4,5,5,6,6,7,7,8,8,8-tridecafluorooctyl trifluoromethanesulfonate (R_fOct-OTf) or 3,3,4,4,5,5,6,6,7,7,8,8,9,9,10,10,10-heptadecafluorodecyl trifluoromethanesulfonate (R_fDec-OTf) to a basic solution of 2,2';6',2''-terpyridin-4'-ol (route 1, Scheme 2) or 4-hydroxyaldehyde (route 2, scheme 2) under basic conditions in acetone.[4] The aldehyde was further reacted to the corresponding terpyridine ligand. These ligands were then used to synthesize the respective iron or cobalt metal complexes. All complexes were purified by precipitating a solution of the complexes in acetonitrile with diethyl ether. The ligands as well as the complexes were characterized by NMR spectroscopy, mass spectrometry and elemental analysis.For complexes **1**, **2** and **5,** suitable single crystals for X-ray diffraction analysis were obtained. While, the data for other complexes were not of sufficient quality to obtain good solid-state structures, as the complexes crystallize in small plates leading to a broad range of difficulties during the refinement processes. In this regard, there is precedence that crystallizing compounds with long fluorous tails are comparatively complicated.[9] In spite of that, the data of complex **5** were of sufficient quality to prove the desired connectivity, intermolecular interactions and the discussion of the metal-ligand distances.

Complexes **1** and **2** crystallize in the triclinic $P\bar{1}$ space group and show the expected coordination motif. Three nitrogen atoms of each ligand coordinate in a distorted octahedral fashion to the metal center. The phenyl rings with the PFC tag on the backbone are twisted out of the plane of the terpyridine unit. Selected bond lengths are depicted in table 1.

The bond lengths between 1.874 (2) and 2.144 (2) Å, indicate a LS Co^{II} center in the complexes **1** and **5**.[32]

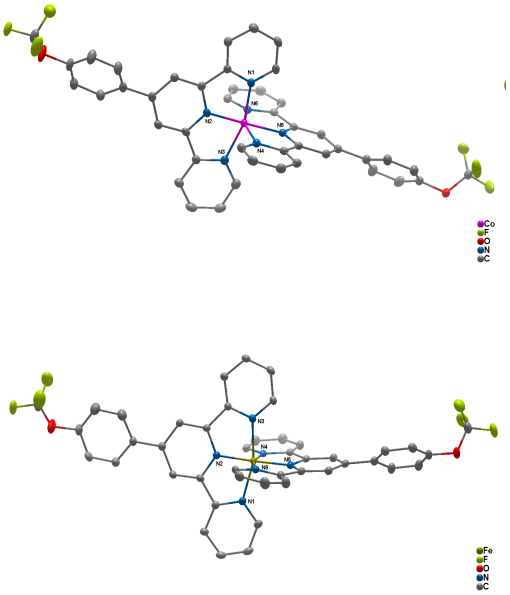

Figure 2: Perspective view of cobalt complex **1** (top) and iron complex **2** (bottom). Ellipsoids are at a probability level of 50%. H atoms, anions and solvent molecules are omitted for clarity.

Similarly, the bond lengths between 1.874 (2) and 1.975 (2) Å point towards a LS Fe^{II} center in complex **3**.[33] These measurements were carried out at 100 K. The angle between the planes of the tridentate ligands are nearly perpendicular to one another with values of 87.1° for complex **1**, 85.8° for complex **2** and 89.2° for complex **5**. The packing of the complexes is as observed for previous complexes.[30a, 34] Packing diagram reveals face-to-face orientation of the terpyridine units, while the BF_4^- anions and solvent molecules are found between the sheets (see figures S30 and S32). In complexes **1** and **2** the OCF_3 tails are aligned with the OCF_3 groups of the neighboring molecule (see figures S31 and S34).

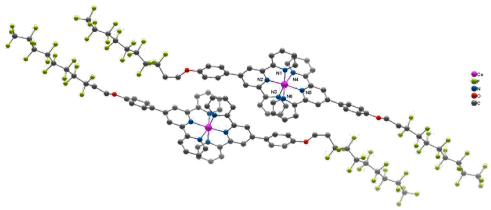

Figure 3: Perspective view of cobalt complex **5.** Ellipsoids are at a probability level of 50%. H atoms, anions and solvent molecules are omitted for clarity.

For the complexes described here different spin states can exist and in principle reversible switching between these spin states by external stimuli can be possible. SQUID magnetometry is an excellent method in this aspect to probe the temperature dependent SCO behavior of Fe^{II} and Co^{II} compounds. A change in the magnetic behavior can be observed if the energy difference from the LS state (S = 0 or S = $^1/_2$) to the HS state (S = 2 or S = $^3/_2$) is provided by thermal energy.[35] For this, complexes **1-6** were investigated by the means of SQUID magnetometry in the temperature [*T*] range of 1.8 to 300 K. The *T* dependence of the χT product is depicted in figure 4, where χ is the molar static magnetic susceptibility, which at low fields can be

Table 1: Selected bond lengths of complexes **1**, **2** and **5** in Å.

	M – N1	M – N2	M – N3	M – N4	M – N5	M – N6
1	2.000(2)	1.874(2)	2.013(2)	2.136(2)	1.921(2)	2.144(2)
2	1.973(2)	1.875(2)	1.975(2)	1.962(2)	1.874(2)	1.973(2)
5	1.980(9)	1.87(1)	1.99(1)	2.17(1)	1.93(1)	2.14(1)
$Co[TPYOC_{14}H_{29}]_2(BF_4)_2$[20a],[a]	2.137(4)/	1.910(3)	2.114(4)	1.977(4)	1.844(3)	1.976(4)
$Fe[N_3P_3(OPh)_5(OPhTPY)]_2(PF_6)_2$[33],[b]	1.886(3)	1.987(3)	1.995(3)	1.878(4)	1.976(3)	1.979(4)

[a]Complex with a LS Co^{II} center:. [b]Complex with a LS Fe^{II} center.

approximated as the ratio between the molar magnetization and the applied magnetic field.

For the cobalt complex **1** no SCO was observed, and the temperature dependence of the χT product hints towards the simultaneous existence of LS as well as HS Co^{II}. This is supported by the curvature at low temperatures, which indicates a significant ZFS. On the basis of the Curie Law, a χT of about 2 cm^3Kmol^{-1} at high temperatures for a g_{iso} = 2.3 is expected. The value of 0.9 cm^3Kmol^{-1} is significantly lower than this, which is indicative of a parallel existence of LS and HS state. Indeed, the obtained experimental data was found to be in good agreement with the simulated, when a composition of 18% HS state and 82% LS state is assumed. The spin Hamiltonian parameters for the LS species ($g_{x,y}$ = 2.08(2), g_z = 2.15(2)) are in good agreement with the values found by EPR. In the case of the HS species, values of $g_{x,y}$ = 2.0(1) and g_z = 2.5(1) as well as zero-field splitting parameters of D = -44(2) cm^{-1} and E = 0.25D were found. Additionally, the prominent decrease of $\chi_M T$ below 5 K is hinting towards a non-negligible intermolecular antiferromagnetic interaction. By means of magnetometry, this could be quantified to be 0.17 (3) cm^{-1}. A large contribution of the LS state is in agreement with the structural data described above.

For complex **3** a gradual thermal SCO behavior is observed from 210 K onwards with increasing temperature. Due to the absence of strong intermolecular interactions between the SCO units, this gradual SCO was expected. The $\chi_M T$ value for complex **3** increases from 0.35 cm^3Kmol^{-1} at 1.8 K to 0.42 cm^3Kmol^{-1} at 75 K and remains almost constant at 0.42 cm^3Kmol^{-1} up to 200K. From 200 K, the start of the SCO is observed with a gradual increase of the χ_MT value from 0.42 cm^3Kmol^{-1} at 200 K to 0.6 cm^3Kmol^{-1} at 300 K.

Complex **5** displays a similar SCO behavior as complex **3**. In contrast the $\chi_M T$ value remains almost constant at 0.42 cm^3Kmol^{-1} with growing temperature, until it starts increasing upon heating at 200 K. The curve is gradually increasing up to 300 K with a $\chi_M T$ value of 0.76 cm^3Kmol^{-1}.

Spin-Hamiltonian simulations of the temperature dependence of $\chi_M T$ of **3** and **5** based on the parameters obtained by powder EPR of the low spin species are displayed in figure 4. While for **5**, the measured $\chi_M T$ values between 5 and 100 K are in good accordance with the simulation, a strong deviation in the case of **3** is found. In the case of **3**, the measured curve also shows a bending to smaller $\chi_M T$ values below 5 K, hinting towards an interaction, which is not covered by the simulation.. An explanation for this is a residual of HS species at low temperatures, which is significantly higher in the case of **3** than it is for **5**. In the case of the three cobalt complexes investigated here, it is seen that the percentage of the HS form observed at ambient temperatures steadily increase with the size of the PFC tail on the terpyridine backbone.

In the case of Fe^{II} complexes no SCO and a minor $\chi_M T$ value was observed from 1.8 K up to 300 K. The LS state of Fe^{II} is S = 0 and hence it does not possess any magnetic moment. Nevertheless with 0.015 cm^3Kmol^{-1}, 0.0125 cm^3Kmol^{-1} and 0.06 cm^3Kmol^{-1}, a non-zero value of $\chi_M T$ is found at 300 K. This is even lower than the theoretical value for a S = ½ system with g = 2 (0.375 cm^3Kmol^{-1}). As in the case of all Fe^{II} compounds, this moment is attributed to a minor Fe^{II} HS amount in the sample (Figure S1), which we also observed in complexes that we investigated earlier.[30a]

Complexes **3**-**6** were investigated towards their liquid crystalline properties. However, none of the complexes show a phase transition under the POM in the temperature rate from room temperature to 350 °C, as the compounds stayed solid over the measured temperature range.

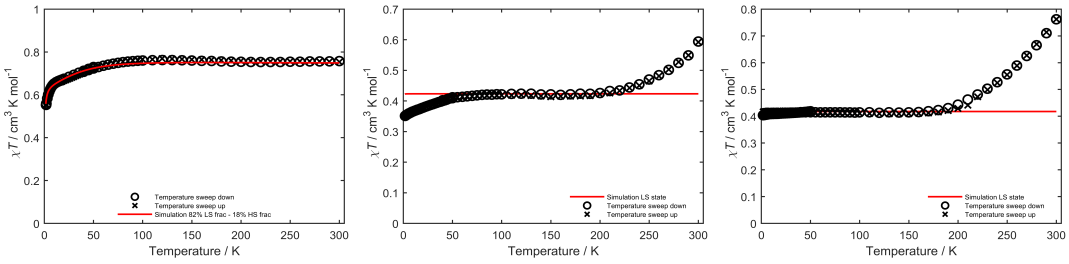

Figure 4: Temperature dependency of the $\chi_M T$ product for **1** (left), **3** (middle) and **5** (right) in an applied magnetic field of 1000 Oe as well as the corresponding LS spin Hamiltonian simulations.

Cyclic voltammetry

In order to investigate the electrochemical properties of the complexes cyclic voltammetric measurements of complexes **1-6** were performed (Figure 5). The measurements were performed in a 0.1 M NBu_4PF_6 dichloromethane or acetonitrile solution. For most of the complexes only one oxidation process could be observed. For the cobalt complexes the first oxidation is reversible and similar to the potential of –0.07 V of the $Co(TPY)_2^{2+}$[2a] complex (–0.11 for **1**; –0.16 V for **3** and –0.17 V for **5** in MeCN). The peak-to-peak separation for the first oxidation step is rather large for complex **1** with ΔE_p of 111 mV, while values of 79 mV for complex **3** and 75 mV for **5** were obtained. At ambient temperatures, these Co^{II} complexes are expected to exist in the HS state in solution (NMR spectroscopy indicates this). Oxidation of the complexes is expected to result in a LS Co^{III} center. The large structural change required for this transformation likely demands a large reorganization energy, which is reflected in the large peak-to-peak separation for the oxidation steps of these complexes.

Compared to the cobalt complexes, the iron complexes display a strongly anodically shifted first oxidation step (Figure 5 and Table 2). The difference in the oxidation potentials on changing the metal center is likely related to the removal of an electron from a largely stabilized formally t_{2g} orbital in LS Fe^{II} complexes. For the HS Co^{II} complexes an electron is removed from the destabilized e_g orbitals, which requires less energy.

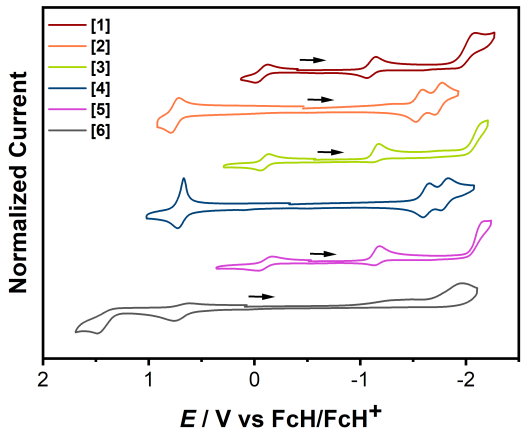

Figure 5: Cyclic voltammograms of complexes **1-6** in dichloromethane/NBu_4PF_6 measured with a glassy carbon working electrode (FcH = ferrocene; FcH^+ = ferrocenium)

In contrary to the first oxidation step, the potentials for the first reduction step are anodically shifted for the Co^{II} complexes (**1**, **3** and **5**) in comparison to the Fe^{II} complexes (**2**, **4** and **6**). As has been reported earlier for similar systems, the first reduction step in such iron complexes is tpy centered and that in the cobalt complexes is either cobalt centered or of a mixed metal-ligand nature.[30a, 36] We attribute the differences in the potentials of the first reduction step to the operation of a similar phenomenon for the complexes described here. The effect of the PFC tail on the redox potentials of the complexes is marginal. On changing the solvent from CH_2Cl_2 to CH_3CN (Figure S2), additional redox steps are observed. The observance of additional reduction peaks at large cathodic potentials can be attributed to the larger solvent

Table 2: Redox potentials vs. FcH/FcH$^+$ measured in acetonitrile at 100 mVs^{-1} with 0.1 M Bu_4NPF_6 at room temperature.[a]

	Solvent	E_{fp}^{Ox2}	$E_{1/2}^{Ox1}$	$E_{1/2}^{Red1}$	$E_{1/2}^{Red2}$	$E_{1/2}^{Red3}$	$E_{1/2}^{Red4}$	E_{fp}^{Red5}	E_{fp}^{Red6}
1	MeCN	-	–0.11	–1.13	–1.93	–2.26	–2.59	-	-
2	MeCN	-	0.72	–1.57	–1.68	–2.30	–2.48	–2.63[b]	–3.12[b]
		-							
3	MeCN	-	–0.16[b]	–1.18	–2.01	–2.39[b]	-	-	-
4	MeCN	-	0.69	–1.41	–1.63[b]	–1.70[b]	–2.04[b]	–2.45[b]	-
5	MeCN	-	–0.17	–1.19	–2.02	–2.35	-	-	-
6	MeCN	-	0.68	–1.71	–2.45	-	-	-	-

[a] All measured with a glassy carbon electrode. [b] Forward peak potential at 0.1 V.

potential window of acetonitrile in comparison to dichloromethane (see table 2 and table S1). Additionally, some irreversible reduction peaks are observed, which are likely related to the dissociation of one or more of the tpy arms and the coordination of acetonitrile to the metal center. Even though the effect of the PFC tails on the redox potentials of the metal complexes is minimal, they do have a strong effect on the forms of the cyclic voltammetric responses. This effect is most prominent for complexes **5** and **6** that contain the longest PFC tail on the tpy ligands (Figure 5). A likely explanation is perhaps the movement of the PFC tails during redox processes, which would demand a large reorganization energy.

We also tried to investigate the UV-vis-NIR signatures of these metal complexes in the different redox states, and these data are summarized in the supporting information. Unfortunately, the redox processes for most of the metal complexes were not reversible on the spectroelectrochemistry timescale. Hence no detailed discussion on the redox processes will be given here. Despite the irreversility of the redox steps in the cyclic voltammetry timescale, the data are quantitatively similar to what was recently reported by us for related Fe^{II} and Co^{II} complexes.[30a] This aspect would also support the assignment of the redox steps, which was done above indirectly from electrochemical data.

EPR Spectroscopy

For further investigations of the electronic structure, the EPR spectra of the cobalt complexes **1, 3** and **5** were measured. Spectra of all the complexes were recorded both in the powder form as well as in acetonitrile solution (see figures 6-8).

Complex **1** displays an anisotropic EPR signal in solution and in the solid state at 93 K, with partially resolved hyperfine splittings (see figure 6), which arises from interaction of the electron spin with the ^{59}Co nucleus (I = 7/2). The simulation of the EPR spectra obtained from powdered samples of **1**, **3** and **5** were performed with rhombic **g**- and **A**-matrices (values given in Tables 3 and 4). In agreement with the Co-N distances determined from X-ray diffraction, the g-values in the 2.00-2.20 range are consistent with a low-spin Co^{II} center. A metal centered spin is clearly indicated for **1** by the rhombic **g**-matrices, deviating from the free-electron value of 2, as well as the large hyperfine splitting. The unpaired electron would reside in the degenerate e_g orbitals in a perfectly octahedral geometry. This degeneracy is lifted by Jahn-Teller distortions, which might result in the unpaired electron being either on a $d_{x^2-y^2}$ or d_{z^2} orbital, or a mixture of the two, where the z-axis is that of the axial Jahn-Teller distortion.[37] It is indicated that the magnetic orbital is an admixture of the $d_{x^2-y^2}$ or d_{z^2} orbitals due to the rhombic nature of the g-values in complex **1**. For more than half-full d shells, if $g_z > g_x \sim g_y$, (usually called an axial spectrum even if there is a slight rhombicity) the unpaired electron is located in a $d_{x^2-y^2}$ orbital; on the other hand, if $g_z \sim 2.00 < g_x \sim g_y$ (usually called an inverted axial

spectrum), the magnetic orbital is the d_{z^2}.[38] The latter is the most common case in low-spin Co^{II} complexes and most $3d^7$ systems.[39] This is observed for **1**, indicating a mostly d_{z^2} magnetic orbital. The spectra of **3** and **5** recorded in the solid state and in solution have similar *g*-values while the *A*-values differ (see Tables 3 and 4). These differences are in accordance with small changes in the solution and solid-state structures, probably due to packing effects in the latter. The spectra in acetonitrile solution appear to be axial, suggesting a $d_{x^2-y^2}$ magnetic ground state, while in the powder samples the rhombicity is higher, which could be compatible with a d_{z^2} ground state with a certain degree of $d_{x^2-y^2}$ admixture. In all these cases the unresolved nature of the spectra limits the certainty with which the individual g-values can be obtained. DFT calculations performed on a truncated version of complex **5** suggest a d_{z^2} ground state. These calculations will be discussed in the following section and in the SI.

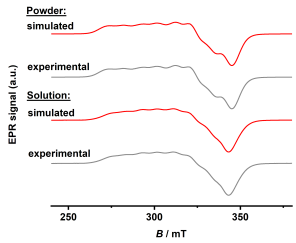

Figure 6: Experimental (grey) and simulated (red) EPR spectra of **1,** top: powdered sample at −180°C bottom: in acetonitrile at -180°C.

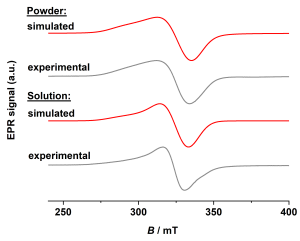

Figure 7: Experimental (grey) and simulated (red) EPR spectra of **3** top: powdered sample at −180 °C bottom: in acetonitrile at -180 °C.

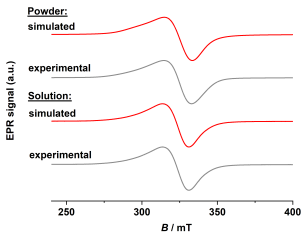

Figure 8: Experimental (grey) and simulated (red) EPR spectra of **5** left: powdered sample at −180°C right: in acetonitrile at -180°C.

Table 3: Simulation parameters of **1** and **3**. g-values, hyperfine A-values (MHz), anisotropic Gaussian broadening HS (MHz) and isotropic Gaussian and Lorentzian broadenings (mT).

	1		**3**	
	Acetonitrile	Powder	Acetonitrile	Powder
g_x	2.003	2.008	2.075	2.087
g_y	2.152	2.172	2.075	2.017
g_z	2.202	2.189	2.219	2.267
A_x / MHz	44	47	9	27
A_y / MHz	93	94	10	~0
A_z / MHz	283	287	194	132
HS_x / MHz	2.38	0.24	-	-
HS_y / MHz	90.57	121.3	-	-
HS_z / MHz	187.36	175.4	-	-
Line width for isotropic broadening / mT	[1.8 2.6]	[0 2.0]	[15.5 0.5]	[12.1 4.3]

Table 4: Simulation parameters of **5**. g-values, hyperfine A-values (MHz), anisotropic Gaussian broadening HS (MHz), axial A-strain and isotropic Gaussian and Lorentzian broadenings (mT).

	5		
	Acetonitrile/Perfluorooctanol 1:2	Acetonitrile	Powder
g_x	2.056	2.085	2.048
g_y	2.091	2.085	2.107
g_z	2.199	2.170	2.182
A_x / MHz	133	11.5	36
A_y / MHz	29	~0	18
A_z / MHz	293	158.3	136
HS_x / MHz	104	-	-
HS_y / MHz	32	-	-
HS_z / MHz	0	-	-
AS_z / MHz	40		
Line width for isotropic broadening / mT	[1.0 2.0]	[8.3 2.2]	8.4

For complexes **3** and **5** no hyperfine splittings could be observed, and the spectra resembled those of exchange-narrowed extended magnetic systems (See figures 7 and 8).[28b, 40] This phenomenon is suggestive of aggregation in solution, likely due to the F···F interactions of the PFC tails. To investigate this further, complexes **3** and **5** were measured in pentafluorobenzonitrile or acetonitrile:pentafluorobenzonitrile solution, respectively (See figure S24). For complex **5** additional measurements were performed in a mixture of 1:1 acetonitrile:1,2-difluorobenzene and in pure acetonitrile (See figure S25). As can be observed in the spectra, the diluted samples in acetonitrile, or in a mixture of acetonitrile and an aromatic fluorinated solvent, show a partially resolved hyperfine structure. This suggests that aggregation is partially avoided in these conditions, and further supports the association of the aggregation effect with the exchange-narrowed characteristics of the spectra. Finally, the measurements were performed with different ratios of an acetonitrile:perfluorooctanol (PFO) solution. Already with 1% of PFO a disruption of the complex aggregates is apparent and at a 3:1 (acetonitrile:perfluorooctanol) ratio hyperfine splitting is observed for both investigated complexes, which leads to the assumption that the fluorine specific interactions between the complexes are inhibited (See Figure 9).

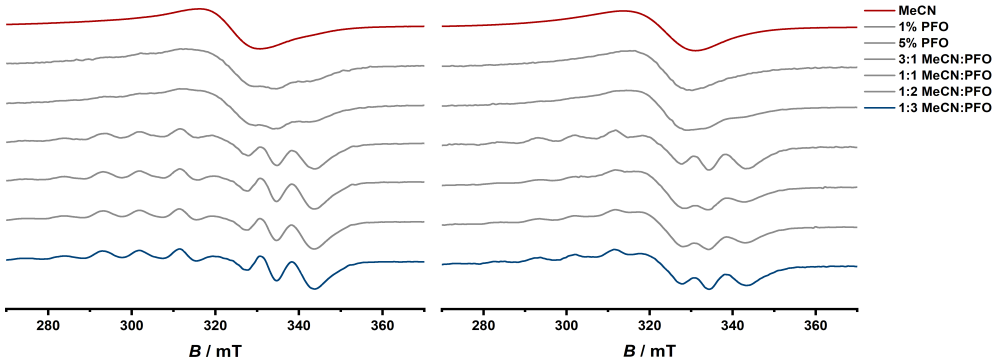

Figure 9: EPR measurements of **3**(left) and **5** (right) with different ratios of acetonitrile:perfluorooctanol

For higher ratios of PFO only marginal changes in the spectra can be observed. Comparing these results to complex **1** where no exchange narrowing was observed, the fluorine specific interactions of the PFC tails seem to have a huge impact on the aggregation of the molecules, thus leading to the observed exchange narrowing. To the best of our knowledge, this is the first time that aggregation-mediated exchange narrowing has been observed with reference to fluorine specific interactions of fluorinated alkyl chains.

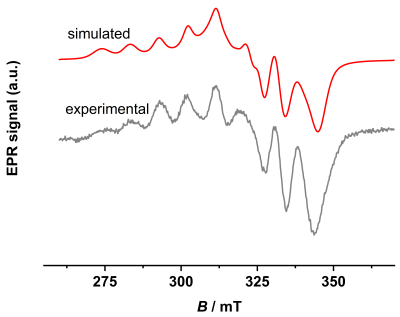

Figure 10: EPR measurement of **5** in a 1:2 acetonitrile:perfluorooctanol mixture, together with the corresponding simulation (see Table 4)

Density Functional Theory Calculations

DFT calculations, performed using the ORCA program (version 5.0)[41] were applied to a truncated form of complex **5** (see SI for further details). In order to calculate the exchange coupling between neighbouring molecules of complex **5**, two different truncated forms of the complex where designed based on the crystal structure of **5**. In one case, $\mathbf{5_{tr1}}$ (Figures S26 and S27), the fluorinated portion of the fluoroalkane chain was removed, leaving only the first $–CF_2$ group, which was capped with another F atom, following approximately the same bond distances and angles as the capping $–CF_3$ in the original complex. The monomer $\mathbf{5_{tr1}}$ was separately optimized (TPSSh/def2-SVP) in order to obtain the energies and orbitals around the SOMO-LUMO gap and determine the occupation of the 3*d* orbitals (Figure S26). For the dimer composed of two unoptimized $\mathbf{5_{tr1}}$ complexes, the BF_4^- counterions were maintained, and the molecular cluster had a net charge of zero. The following truncated form, $\mathbf{5_{tr2}}$ (Figure S28), was terminated with a $–OCH_3$ group, and in this calculation the counterions were removed, giving a system with +4 charge. For the calculation of exchange interactions between neighbours, the geometries were not optimized, as the purpose was to estimate the exchange coupling in the crystal, and the truncation of the long fluoroalkyl chains would have undoubtedly perturbed the packing considerably. As we believed the exchange coupling to be transmitted through weak π-π interactions, which are very sensitive to the distance and the eclipsed area between aromatic fragments, any small change in structure would have large effects in the exchange coupling, and we considered the unperturbed crystal structure to be the safest model. The calculation of $[\mathbf{5_{tr1}}]^{2+}$ revealed that the unpaired electron resides in a $3d_{z^2}$ orbital (Figure S26), as do the spin densities for the broken symmetry calculations (Figures S27 and S28), although with a certain degree of admixture with the $3d_{x^2-y^2}$ orbital. Calculated **g**-matrices using TPSSh (10 % HF exchange) or TPSS0 (25 % HF exchange) functionals (Figure S29 and Table S4) reveal highly rhombic **g**-matrices, although with smaller *g* deviations from the free electron *g*-value, which is a known limitation of DFT methods in the case of anisotropic transition metal complexes. The calculations predict that the smallest g-value is roughly in the direction of the $3d_{z^2}$ orbital, while the highest is roughly directed along the shortest Co-N distances, corresponding to the central pyridine composing the ligand. An in-depth analysis of the EPR properties of Co^{II} terpyridine complexes, containing long alkyl chains, was performed by Murray *et al.*[37a] The authors were able to simulate EPR spectra in solution quite similar to the one shown

in figures 9 and 10 with a very rhombic **g**-matrix and **A**-matrix, and concluded that the lowest g-value was associated with the direction of tetragonal elongation in the complex, and compatible with a $3d_{z^2}$ magnetic orbital aligned with the elongated axis, in agreement with our DFT results. While Murray *et al.* in general found resolved hyperfine splittings in solution, we observed for **3** and **5** exchange narrowed spectra, and needed to add fluorinated solvents to observe partially or totally resolved hyperfine splittings. In order to estimate the very small exchange couplings, presumably mediated by π-π interactions, that could lead to the exchange narrowing in solution, we had to perform calculations with a good theory level, tight convergence settings and accurate integration grids. Table S1 shows the results of Broken Symmetry calculations performed with Orca on the $\mathbf{[5_{tr1}(BF_4)_2]_2}$ and $\mathbf{[5_{tr2}]_2}^{4+}$ models, using the hybrid meta-GGA functional, TPSSh, with def2-TZVP basis sets on all atoms. Calculations were performed using TightSCF and DefGrid3 options in Orca. The calculated exchange coupling constants are both ferromagnetic, with values of 0.17 and 0.10 cm^{-1}, respectively, which amount to ~180 mT and ~107 mT. These values should be considered approximate, since they correspond to very small energy differences between the high-spin and broken symmetry states, on the order of 10^{-6}-10^{-7} Ha. Furthermore, even if the values are accurately calculated for the crystal, there are no guarantees that the same values are obtained for aggregated molecules in solution. However, the small values of the exchange constants are one order of magnitude larger than the hyperfine splitting of complex **5** in an MeCN:PFO mixture, and therefore appear to be enough to cause exchange narrowing of the EPR signals of the complex when this is aggregated in pure MeCN. The magnitude of the exchange coupling (~0.1-0.2 cm^{-1}) transmitted through π-π interactions between the terpyridine ligands, is much smaller than the values found for systems where the magnetic centers are connected through extended covalent pathways, and even small compared to exchange couplings transmitted through pathways involving H-bonds.[28b] These values are too small to be observed by standard magnetic measurements, and are usually only revealed by EPR spectroscopy, which is especially suitable to observe very small magnetic interactions. It has been shown before that π-π interactions are able to transmit very weak exchange interactions between magnetic metal centers ligated by polypyridyl[42] and phenanthrolyl ligands.[29b, 40b] As summary, we have observed the exchange narrowing effect in solution, which happens for the Co^{II} bis-terpyridine complexes with long fluoroalkyl chains and not for the $–OCF_3$ substituted one, nor the alkane substituted complexes reported by Murray *et al.*, and therefore is highly suggestive of aggregation induced by F ⋯ F interactions. The exchange narrowing phenomenon is caused by very small exchange interactions between neighboring Co^{II} centers communicated by non-covalent, π-π interactions.

Conclusion

We successfully synthesized the terpyridine ligands with different PFC tails and the corresponding bis-substituted Co^{II} and Fe^{II} complexes. The complexes were electrochemically investigated by cyclic voltammetry, EPR spectroscopy and DFT calculations. The cyclic voltammograms show marginal difference in the redox potentials on changing the substituents in the ligand backbone. However, the change in metal centers as well as use of different solvents leads to different redox potentials and additional processes. This is probably due to the reaction with the acetonitrile molecules during the measurement. For complexes **1**, **2** and **5** we were able to obtain solid-state structures, which showed the intermolecular interactions in the crystal packing. The bond distances of the complexes indicate a LS center at 100 K. Through SQUID magnetometric measurements the SCO behavior of the complexes were investigated. Complex **1** does not exhibit SCO

behavior, but the meaurements indicate, that the measured sample contains Co^{II} molecules in the HS as well as the LS state. The Co^{II} center in complexes **3** and **5** display an incomplete SCO, while the Fe^{II} complexes remain in the LS state over the measured temperature range. This is also supported by ^{1}H NMR spectroscopy that indicate a Fe^{II} LS center at room temperature. The magnetic properties of the cobalt complexes are influenced by the length of the PFC tails. To further investigate the determination of fluorine specific interactions with EPR spectroscopy, several EPR experiments were performed. An exchange narrowing was observed during the measurements of complexes **3** and **5** as powdered samples as well as in frozen acetonitrile solution. By adding different amounts of PFO, the aggregation of the complexes could be disrupted as confirmed from the hyperfine coupling. To the best of our knowledge, this is the first time that fluorine-specific interactions of the PFC tails and the influence thereof on exchange narrowing were investigated with EPR measurements.

Experimental Section

Compounds: Ligands **2** and **3** were synthesized following published procedures.[4] Commercially available chemicals were used without further purification. Dry solvents were available from MBRAUN MB-SPS- 800 solvent system. All solvents were degassed by standard techniques prior to use. Column chromatography was conducted using aluminum oxide (Aluminum Oxide basic, Macherey-Nagel, 50−200 μm). ^{1}H NMR, proton decoupled ^{13}C and ^{19}F NMR were recorded on JEOL ECS 400 spectrometer and JEOL ECZ 400R spectrometer at 20 °C. Chemical shifts are reported in ppm (relative to the TMS signal) with reference to the residual solvent peaks.[43] Multiplets are reported as follows: singlet (s), duplet (d), triplet (t), quartet (q), quintet (quint), septet (sept), and combinations thereof. Mass spectrometry was performed on an Agilent 6210 ESI-TOF. Elemental analysis was performed on a Perkin Elmer Analyser 240.

Electrochemistry

Cyclic voltammograms were recorded with a PAR VersaStat 4 potentiostat (Ametek) by working in anhydrous and degassed acetonitrile or dichloromethane with 0.1 M NBu_4PF_6 (dried, > 99.0%, electrochemical grade, Fluka) as supporting electrolyte. Concentrations of the complexes were about $1 \cdot 10^{-4}$ M. A three-electrode setup was used with a glassy carbon working electrode, a coiled platinum wire as counter electrode, and a coiled silver wire as a pseudoreference electrode. The ferrocene/ferrocenium or decamethylferrocene/decamethylferrocenium couples were used as internal reference.

UV/Vis spectra were recorded with an Avantes spectrometer consisting of a light source (AvaLight-DH-S-Bal), a UV/VIS detector (AcaSpec-ULS2048), and an NIR detector (AvaSpec-NIR256-TEC). Spectroelectrochemical measurements were carried out in an optically transparent thin-layer electrochemical (OTTLE) cell (CaF_2 windows) with a gold working electrode, a platinum mesh counter electrode, and a silver-foil pseudoreference electrode.[44] Anhydrous and degassed acetonitrile or dichloromethane with 0.1 M NBu_4PF_6 as supporting electrolyte was used as solvent.

Electron paramagnetic resonance

EPR spectra at X-band frequency (ca. 9.5 GHz) were obtained with a Magnettech MS-5000 benchtop EPR spectrometer equipped with a rectangular TE 102 cavity and TC HO4 temperature controller. The measurements were carried out in synthetic quarz glass tubes.

X-ray diffraction

X-ray data were collected on a Bruker Smart AXS or Bruker D8 Venture system at 100(2) K, respectively, using graphite-monochromated Moα radiation (λ_α = 0.71073 Å). Using the Smart software or using the APEX2 software, respectively, evaluated the strategy for the data collection. The data were collected by the standard omega scan or omega + phi scan techniques, and were scaled and reduced using

Saint + and SADABS software. Direct methods or intrinsic phasing using SHELXT-2014/7 solved the structures. Structures were refined by full matrix least-squares using SHELXL-2014/7, refining on F2. Non-hydrogen atoms were refined 40 anisotropically.[45]

SQUID Magnetometry

All susceptibility measurements were carried out on a Quantum Design MPMS3 SQUID magnetometer. The measurements at a constant magnetic field of 1000 Oe in a temperature range from 1.8 K to 50 K and at 10 000 Oe in a temperature range from 40 K to 300 K. The measured data in the intersection of the temperature ranges served to compensate for possible ferromagnetic impurities. Samples were pounded with little pressure and mixed with eicosane. The mixture was melted in a capsule with a hot air gun maximized to a temperature of 50°C (323.15 K) and the capsule was then fixed in a plastic tube. The temperature dependent measurements were limited to a temperature of 300 K due to the melting of the used eicosane matrix (melting point of eicosane: 311 K). Data were corrected for the diamagnetic contribution to the susceptibility by means of Pascal's constants.[46]

DFT Calculations

All calculations were performed using the ORCA program.[41] Geometry optimizations were carried out using the TPSSh functional[47] with def2-SVP basis sets[48] on all atoms, starting from the X-ray determined structures. The optimized structures were used for single point and frequency calculations with the TPSSh functional and def2-TZVP basis sets. A particular calculation of the g- and A-matrices was also performed using the TPSS0 functional[49] (with 25 % HFx) and a def2-QZVP basis set on the Co atom. The resolution-of-the-identity (RI) approximation[50] with matching basis sets (def2/J),[51] as well as the RIJCOSX approximation (combination of RI and chain-of-spheres algorithm for exchange integrals) were used to reduce the time of calculations. The optimized structures were confirmed to be minima by the absence of imaginary vibrational frequencies. Orbital and electron density isosurfaces were plot with Chemcraft. (Chemcraft - graphical software for visualization of quantum chemistry computations. https://www.chemcraftprog.com)

Synthesis

The synthesis of 3,3,4,4,5,5,6,6,7,7,8,8,8-tridecafluorooctyl trifluoromethanesulfonate and 3,3,4,4,5,5,6,6,7,7,8,8,9,9,10,10,10-heptadecafluorodecyl trifluoromethanesulfonate was synthesized according to literature known procedures.[52]

BenzaldehydeR_fOct

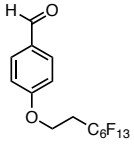

The synthesis was performed according to a literature known procedure.[4]

4-Hydroxy benzaldehyde (500 mg, 4.09 mmol, 1.0 equiv) was placed in a 100 mL round bottom flask and dissolved in acetone (60 mL). Then, K_2CO_3 (1.13 g, 8.18 mmol, 2.0 equiv) and 18-crown-6 (541 mg, 2.05 mmol, 0.5 equiv) were added and the suspension was stirred at rt for 30 min. Afterwards, the alkyl triflate (2.44 g, 4.91 mmol, 1.2 equiv) was added and the reaction mixture was refluxed for additional 48 h. The precipitate was filtered off, the solvent was removed and the crude product was purified via column chromatography (SiO_2, *n*-pentane → *n*-pentane/EtOAc 5:1), affording the product (1.10 g, 2.3 mmol, 57%) as a colorless solid.

^{1}H-NMR (401 MHz, $CDCl_3$): δ = 9.91 (s, 1H), 7.86 (d, *J* = 8.8 Hz, 2H), 7.02 (d, *J* = 8.7 Hz, 2H), 4.36 (t, *J* = 6.7 Hz, 2H), 2.68 (tt, *J* = 18.2, 6.7 Hz, 2H) ppm.

^{19}F-NMR (377 MHz, $CDCl_3$): δ = –80.6 (tt, *J* = 10.0, 2.4 Hz), –113.1–(–133.3) (m), –121.5–(–122.0) (m), –122.7–(–122.8) (m), –123.4–(–123.4) (m), –126.0–(–126.1) (m) ppm.

^{13}C-NMR (151 MHz, $CDCl_3$): δ = 190.9, 163.1, 132.2, 130.7, 114.9, 60.5, 31.3 (t, *J* = 21.7 Hz) ppm. The

signals of the fluorinated carbon atoms are missing due to poor signal-to-noise ratio.

HRMS (ESI): calcd. for $[C_{15}H_9F_{13}O_2Na]^+$ $[M - Na]^+$: *m/z* 491.0287; found 491.0361.

Anal. calcd, for $C_{15}H_9F_{13}O_2 \cdot 0.1\ C_5H_{12}$: C, 39.16; H, 2.16; N, 0. Found: C, 39.02; H, 1.98; N, 0.03.

BenzaldehydeR$_f$Dec

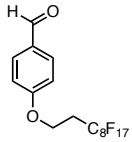

The synthesis was performed according to a literature known procedure.[4]

4-Hydroxy benzaldehyde (122 mg, 1.00 mmol, 1.0 equiv) was placed in a 50 mL round bottom flask and dissolved in acetone (15 mL). Then, K_2CO_3 (276 mg, 2.00 mmol, 2.0 equiv) and 18-crown-6 (132 mg, 500 µmol, 0.5 equiv) were added and the suspension was stirred at rt for 30 min. Afterwards, the alkyl triflate (894 mg, 1.50 mmol, 1.5 equiv) was added and the reaction mixture was refluxed for additional 48 h. The precipitate was filtered off, the solvent was removed and the crude product was purified via column chromatography (SiO_2, *n*-pentane → *n*-pentane/EtOAc 5:1), affording the product (399 mg, 0.7 mmol, 70%) as a colorless solid.

^{1}H-NMR (401 MHz, $CDCl_3$): δ = 9.91 (s, 1H), 7.86 (d, *J* = 8.6 Hz, 2H), 7.02 (d, *J* = 8.6 Hz, 2H), 4.36 (t, *J* = 6.7 Hz, 2H), 2.68 (tt, *J* = 18.1, 6.6 Hz, 2H) ppm.

^{19}F-NMR (377 MHz, $CDCl_3$): δ = –80.6 (t, *J* = 9.9 Hz), –113.2 (p, *J* = 17.7 Hz), –121.3–(–121.6) (m,), –121.6–(–121.9) (m), –122.5–(–122.9) (m), –123.2–(–123.4) (m), –125.8–(–126.1) (m) ppm.

^{13}C-NMR (151 MHz, $CDCl_3$): δ = 190.9, 163.1, 132.2, 130.7, 114.9, 60.5, 31.4 ppm. The signals of the fluorinated carbon atoms are missing due to poor signal-to-noise ratio.

HRMS (ESI): calcd. for $[C_{15}H_9F_{13}O_2Na]^+$ $[M - Na]^+$: *m/z* 591.0223; found 591.0231.

Anal. calcd. for $C_{17}H_9F_{17}O_2 \cdot 0.1\ C_5H_{12} \cdot 0.25\ CH_2Cl_2$: C, 35.73; H, 1.81; N, 0. Found: C, 36.11; H, 2.19; N, 0.03.

TPYPhOCF$_3$ L1

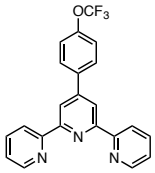

The synthesis was performed according to a literature known procedure.[31]

4-Trifluoromethoxy benzaldehyde (0.90 mL, 6.3 mmol, 1.0 equiv) was placed in a 50 mL round bottom flask and dissolved in EtOH/H_2O (2:1, 15 mL). 2-Acetylpyridine (1.4 mL, 12.6 mmol, 2.0 equiv), NH_3 (aq. solution, 25 wt.-%, 20 mL) and NaOH (957 mg, 23.9 mmol, 3.8 equiv) were added and the solution was stirred at rt for 48 h. The formed viscous residue was filtered off, dissolved in a minimal amount of EtOH, and the crude product was precipitated by slowly adding water to the solution. The solid was filtered off and washed with a mixture of EtOH/H_2O (1:1, 5x20 mL) to afford the product (1.20 g, 3.0 mmol 48%) as a pale yellow solid.

^{1}H-NMR (600 MHz, $CDCl_3$): δ = 8.73 (d, *J* = 4.4 Hz, 2H), 8.71 (s, 2H), 8.67 (d, *J* = 7.9 Hz, 2H), 7.92 (d, *J* = 8.6 Hz, 2H), 7.88 (td, *J* = 7.7, 1.7 Hz, 2H), 7.38–7.33 (m, 4H) ppm.

^{19}F-NMR (565 MHz, $CDCl_3$): δ = –57.6 ppm.

^{13}C-NMR (151 MHz, $CDCl_3$): δ = 156.3, 156.2, 150.0, 149.3, 149.1, 137.4, 137.1, 129.0, 124.1, 121.5, 121.4, 119.8, 118.9 ppm.

HRMS (ESI): calcd. for $[C_{22}H_{15}F_3N3O]^+$: *m/z* 394.1162; found 394.1148.

Anal. calcd. for $C_{22}H_{14}F_3N_3O$: C, 67.17; H, 3.59; N, 10.68. Found: C, 67.29; H, 3.63; N, 10.79.

TPYPhOH

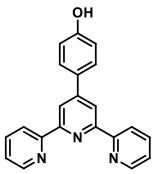

The synthesis was performed according to a literature known procedure.[31]

4-hydroxybenzaldehyde (1.2 g, 10 mmol) was dissolved in 15 mL EtOH/H_2O (2:1) and 2-acetylpyridine (2.4 g, 20 mmol) was added, followed by NaOH (1.5 g, 26 mmol) and 30 mL of ammonia solution (25%). The mixture was stirred at room temperature overnight, the white precipitate was filtered and washed with water (5 x 10 mL) and ethanol (3 x 5 mL) yielding a white solid (920.5 mg, 2.8 mmol, 28%).

^{1}H-NMR (DMSO, 401 MHz, 21 °C): δ = 8.74 (d, J = 5.0 Hz, 2H), 8.62 (d, J = 7.9 Hz, 2H), 8.55 (s, 2H), 7.99 (td, J = 7.8, 2.2 Hz, 2H), 7.66 – 7.27 (m, 4H), 6.39 (d, J = 8.7 Hz, 2H) ppm.

TPYPhRfOct L2

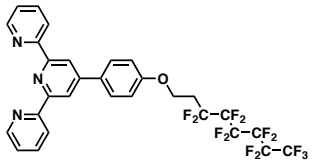

Route 1:

The synthesis was performed according to a literature known procedure.[4]

TPYPhOH (650.7 mg, 2.0 mmol), K_2CO_3 (420.0 mg, 3.0 mmol) and 18-crown-6 (264.0 mg, 1.0 mmol) were dissolved in acetone (45 mL) and stirred at room temperature for one hour. Afterwards R_fOct-OTf (1.5 g, 4 mmol) was added and the mixture was stirred at 60 °C overnight. After cooling to room temperature the white precipitate was filtered and the solvent was removed under reduced pressure. The crude product was purified by column chromatography (basic Al_2O_3, DCM) yielding in a yellow solid (86.6 mg, 0.1 mmol, 6%).

Route 2:

2-Acetylpyridine (0.50 mL, 4.44 mmol, 2.0 equiv) and TPYPhR_fOct (1.04 g, 2.22 mmol, 1.0 equiv) were placed in a 50 mL round bottom flask and dissolved in EtOH/H_2O (2:1, 12 mL). Then, NH_3 (aq. solution, 25 wt.-%, 6 mL) and NaOH (340 mg, 8.50 mol, 3.8 equiv) were added and the solution was stirred for 48 h at 60 °C. The formed precipitate was filtered off and washed with water (3x15 mL) and EtOH (3x15 mL), affording the product (350 mg, 1.0 mmol, 23%) as a colorless solid.

^{1}H-NMR ($CDCl_3$, 400 MHz, 20 °C): δ = 8.80 – 8.72 (m, 2H), 8.71 (s, 2H), 8.67 (dt, J = 8.0, 1.0 Hz, 2H), 7.35 (ddd, J = 7.4, 4.8, 1.2 Hz, 4H), 7.07 – 7.01 (m, 2H), 4.36 (t, J = 6.9 Hz, 2H), 2.68 (ddd, J = 24.8, 18.2, 6.7 Hz, 2H) ppm.

^{13}C-NMR ($CDCl_3$, 101 MHz, 0 °C) δ = 159.1, 157.3, 150.6, 149.3, 137.8, 128.8, 123.9, 122.0, 119.6, 115.7 ppm.

^{19}F-NMR (CDCl3, 376 MHz, 0°C): δ = –80.6, –113.11 (q, J = 17.3, 15.5 Hz), –121.7, –122.7, –123.4, –125.99 (dq, J = 13.8, 6.9 Hz) ppm.

HRMS (ESI): calcd. For $[C_{29}H_{18}F_{13}N_3ONa]^+$: m/z 694.1134; found 694.1106.

Anal. Calcd for $C_{29}H_{18}F_{13}N_3O \cdot 0.1$ C5H12: C, 52.21; H, 2.85; N, 6.19. Found: C, 52.04; H, 3.15; N, 6.26.

TPYPhRfDec L3

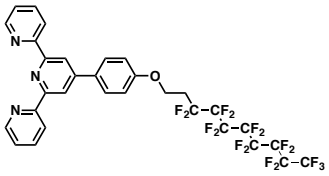

Route 1:

The synthesis was performed according to a literature known procedure.[4]

TPYPhOH (325.4 mg, 1.0 mmol), K_2CO_3 (210.0 mg, 1.5 mmol) and 18-crown-6 (132.0 mg, 0.5 mmol) were dissolved in acetone and stirred at room temperature for one hour. Afterwards R_fDec-OTf (1.2 g, 2 mmol) was added and the mixture was stirred at 60 °C overnight. After cooling to room temperature the white precipitate was filtered and the solvent was removed under reduced pressure. The crude product was purified by column chromatography (basic Al_2O_3, DCM) yielding in a yellow solid (127.5 mg, 0.16 mmol, 16%).

Route 2:

2-Acetylpyridine (0.40 mL, 3.56 mmol, 2.0 equiv) and TPYPhR_fDec (1.01 g, 1.78 mmol, 1.0 equiv) were

placed in a 50 mL round bottom flask and dissolved in EtOH/H_2O (2:1, 12 mL). Then, NH_3 (aq. solution, 25%, 6 mL) and NaOH (270 mg, 6.75 mol, 3.8 equiv) were added and the solution was stirred for 24 h at 60 °C. The formed precipitate was filtered off and washed with water (3x15 mL) and EtOH (3x15 mL), affording the product (187 mg, 0.57 mmol, 16%) as a pale yellow solid.

^{1}H-NMR ($CDCl_3$, 400 MHz, 20 °C): 8.73 (d, *J* = 4.8 Hz, 0H), 8.70 (s, 2H), 8.67 (d, *J* = 7.9 Hz, 2H), 7.93 – 7.84 (m, 4H), 7.36 (dd, *J* = 6.9, 5.4 Hz, 2H), 7.03 (d, *J* = 8.7 Hz, 2H), 4.35 (t, *J* = 6.8 Hz, 2H), 2.68 (ddd, *J* = 25.1, 18.2, 6.7 Hz, 2H) ppm.

^{13}C-NMR ($CDCl_3$, 101 MHz, 20 °C): 159.1, 156.4, 156.0, 149.3, 137.1, 128.9, 124.0, 121.6, 118.5, 115.9 ppm.

^{19}F-NMR ($CDCl_3$, 377 MHz, 21 °C): -80.84 (s), -113.35 – -113.73 (m), -121.87 (d, *J* = 83.8 Hz), -122.89 (d, *J* = 82.7 Hz), -123.64 (d, *J* = 84.2 Hz), -126.19 ppm.

HRMS (ESI): calcd. For $[C_{31}H_{19}F_{17}N_3O]^+$; *m/z* 772.1251; found 772.1212.

Anal. Calcd for $C_{31}H_{18}F_{17}N_3O \cdot 1.3\ H_2O$: C, 46.84; H, 2.61; N, 5.29. Found: C, 46.54; H, 2.28; N, 5.45.

$[Co(TpyPhOCF_3)_2](BF_4)_2$ 1

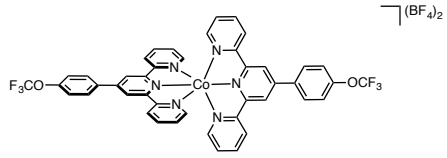

$Co(BF_4)_2 \cdot 6\ H_2O$ (17.0 mg, 0.05 mmol) was dissolved in 10 mL methanol and $TPYPhOCF_3$ (39.3 mg, 0.10 mmol) was added. The mixture was stirred for four days. The solvent was evaporated and the product was purified by crystallization in MeCN/Et_2O yielding in dark orange crystals (32.0 mg, 0.03 mmol, 62%).

HRMS (ESI): calcd. for $[C_{44}H_{28}CoF_6N_6O_2]^{2+}$ [M – $(BF_4)_2]^{2+}$: *m/z* 422.5749; found 422.5780.

Anal. calcd. for $C_{44}H_{28}B_2CoF_{14}N_6O_2 \cdot 0.5\ C_2H_3N \cdot 0.25\ C_4H_{10}O$: C, 52.21; H, 3.05; N, 8.60. Found: C, 52.11; H, 3.12; N, 8.67.

$[Fe(TpyPhOCF_3)_2](BF_4)_2$ 2

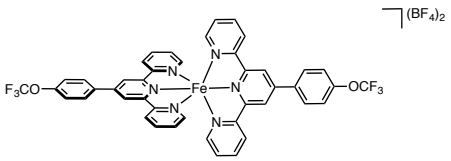

$Fe(BF_4)_2 \cdot 6\ H_2O$ (16.8 mg, 0.05 mmol) was dissolved in 10 mL methanol and $TPYPhOCF_3$ (39.3 mg, 0.10 mmol) was added. The mixture was stirred for four days. The solvent was evaporated and the product was purified by crystallization in MeCN/Et_2O yielding in dark violet crystals. (36.0 mg, 0.03 mmol, 73%).

^{1}H-NMR (600 MHz, CD_3CN) δ = 9.19 (s, 4H), 8.62 (d, *J* = 7.9 Hz, 4H), 8.42 (d, *J* = 8.6 Hz, 4H), 7.92 (t, *J* = 7.3 Hz, 4H), 7.74 (d, *J* = 8.2 Hz, 4H), 7.20 (d, *J* = 5.4 Hz, 4H), 7.10 (t, *J* = 6.4 Hz, 4H) ppm.

^{19}F-NMR (377 MHz, CD_3CN): δ = –58.3, –151.5, –151.5 ppm.

^{13}C-NMR (151 MHz, CD_3CN): δ = 161.4, 159.0, 154.1, 151.7, 150.0, 139.8, 136.9, 131.0, 128.4, 125.0, 123.1, 122.8, 122.5, 120.8 ppm. One more signal than expected is observed. This might be due to poor signal-to-noise ratio, so that no full resolution of the quartet expected for C–F coupling is possible.

HRMS (ESI): calcd. for $[C_{44}H_{28}F_6FeN_6O_2]^{2+}$ [M – $(BF_4)_2]^{2+}$: *m/z* 421.0758; found 421.0826.

Anal. calcd. for $C_{44}H_{28}F_6FeN_6O_2$: C, 52.01; H, 2.78; N, 8.27. Found: C, 52.06; H, 2.99; N, 8.40.

$[Co(TpyPhOR_fOct)_2](BF_4)_2$ 3

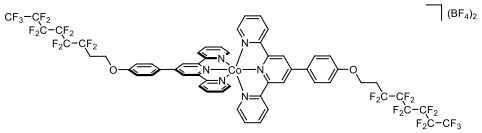

$Co(BF_4)_2 \cdot 6\ H_2O$ (20.57 mg, 0.06 mmol) was dissolved in 10 mL methanol and 4'-(4-((3,3,4,4,5,5,6,6,6-nonafluorohexyl)oxy)phenyl)-2,2':6',2"-terpyridine (81.10 mg, 0.12 mmol) was added. The mixture was stirred for one week, the solvent was evaporated and the crude product was dissolved in acetonitrile and precipitated in EtOH, yielding in a red solid (16.4 mg, 0.01 mmol, 17%).

HRMS (ESI): calcd. For $[C_{58}H_{36}CoF_{26}N_6O_2]^{2+}$ [M – $(BF_4)_2]^{2+}$: *m/z* 700.5903; found 700.5934.

$C_{58}H_{36}B_2CoF_{34}N_6O_2 \cdot 1.2\ C_2H_3N \cdot 1.75\ H_2O \cdot 0.4\ CH_2Cl_2$: C, 43.21; H, 2.62; N, 5.97. Found: C, 43.09; H, 2.49; N, 6.08.

$[Fe(TpyPhOR_fOct)_2](BF_4)_2$ 4

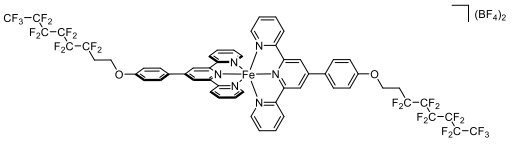

$Fe(BF_4)_2 \cdot 6\ H_2O$ (17.12 mg, 0.05 mmol) was dissolved in 10 mL methanol and 4'-(4-((3,3,4,4,5,5,6,6,6-nonafluorohexyl)oxy)phenyl)-2,2':6',2"-terpyridine (68,10 mg, 0.01 mmol) was added. The mixture was stirred for four days, the solvent was evaporated and the crude product was dissolved in acetonitrile and precipitated in EtOH, yielding in a red solid (30.90 mg, 0.02 mmol, 39%).

^{1}H-NMR (500 MHz, CD_3CN) δ = 9.15 (s, 4H), 8.61 (s, 4H), 8.32 (s, 3H), 7.91 (s, 4H), 7.37 (s, 3H), 7.19 (s, 5H), 7.09 (s, 5H), 4.54 (s, 4H), 2.84 (m, 4H) ppm.

^{19}F-NMR (471 MHz, CD_3CN): δ = –81.4, –113.4, –122.1, –123.2, –123.9, –126.4, –151.4 ppm.

^{13}C-NMR (151 MHz, CD_3CN): δ = 161.4, 161.1, 159.0, 153.9, 150.7, 139.5, 130.3, 130.3, 128.1, 124.6, 121.8, 116.6, 61.5, 31.6 (t, *J* = 21.3 Hz) ppm

HRMS (ESI): calcd. For $[C_{58}H_{36}F_{26}FeN_6O_2]^{2+}$ [M – $(BF_4)_2]^{2+}$: *m/z* 699.0912; found 699.0909.

Anal. Calcd for $C_{58}H_{36}B_2F_{34}FeN_6O_2 \cdot 2.3\ C_2H_3N \cdot 1\ C_4H_{10}O$: C, 45.95; H, 3.06; N, 6.68. Found: C, 46.33; H, 2.67; N, 6.29.

$[Co(TpyPhOR_fDec)_2](BF_4)_2$ 5

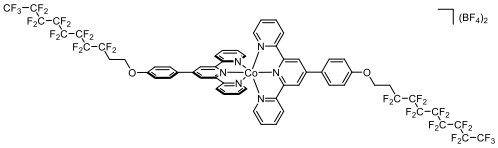

$Co(BF_4)_2 \cdot 6\ H_2O$ (12.20 mg, 0.04 mmol) was dissolved in 10 mL methanol and 4'-(4-((3,3,4,4,5,5,6,6,7,7,8,8,8-tridecafluorooctyl)oxy)phenyl)-2,2':6',2"-terpyridine (74.60 mg, 0.07 mmol) was added. The mixture was stirred for two days, the solvent was evaporated and the crude product was dissolved in acetonitrile and precipitated in EtOH, yielding in a red solid (35.20 mg, 0.02 mmol, 55%). Crystals suitable for X-Ray diffraction were grown by slow evaporation of an acetonitrile solution of the complex.

HRMS (ESI): calcd. For $[C_{62}H_{36}CoF_{34}N_6O]^{2+}$ [M – $(BF_4)_2]^{2+}$: *m/z* 800.5839; found 800.5877.

Anal. Calcd for $C_{62}H_{36}B_2F_{42}CoN_6O_2$: C, 41.94; H, 2.04; N, 4.73. Found: C, 41.95; H, 2.12; N, 4.84.

$[Fe(TpyPhOR_fDec)_2](BF_4)_2$ 6

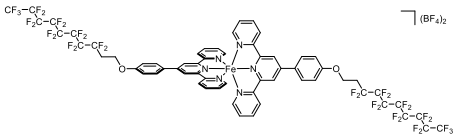

$Fe(BF_4)_2 \cdot 6\ H_2O$ (18.37 mg, 0.05 mmol) was dissolved in 10 mL Methanol and 4'-(4-((3,3,4,4,5,5,6,6,7,7,8,8,8-tridecafluorooctyl)oxy)phenyl)-2,2':6',2"-terpyridine (84.00 mg, 0.11 mmol) was added. The mixture was stirred for one week, the solvent was evaporated and the crude product was dissolved in acetonitrile and precipitated in EtOH, yielding in a purple solid (50.60 mg, 0.03 mmol, 57%).

^{1}H-NMR (401 MHz, CD_3CN) δ = 9.14 (s, 3H), 8.60 (d, *J* = 8.4 Hz, 4H), 8.31 (d, *J* = 8.4 Hz, 3H), 7.94 – 7.86 (m, 5H), 7.36 (d, *J* = 8.7 Hz, 3H), 7.18 (d, *J* = 6.1 Hz, 5H), 7.07 (t, *J* = 5.8 Hz, 5H), 4.54 (t, *J* = 6.0 Hz, 2H), 3.75(t, *J* = 6.1 Hz, 2H), 2.97 – 2.70 (m, 4H) ppm.

^{19}F-NMR (377 MHz, CD_3CN): δ = –81.4, –113.5 (d, *J* = 68.8 Hz), –122.1 (d, J = 85.0 Hz), –123.1, –123.9 (d, J = 77.8 Hz), –126.5, –151.4 ppm.

^{13}C-NMR (151 MHz, CD_3CN): δ = 161.4, 161.1, 159.0, 154.0, 150.7, 139.6, 130.4, 130.3, 128.1, 124.6, 121.8, 116.6, 63.4, 61.5, 31.6 (t, *J* = 21.7 Hz) ppm

HRMS (ESI): calcd. For $[C_{62}H_{36}FeF_{34}N_6O]^{2+}$ [M – $(BF_4)_2]^{2+}$: *m/z* 799.0848; found 799.0855.

Anal. Calcd for $C_{62}H_{36}B_2F_{42}FeN_6O_2 \cdot 2\ H_2O \cdot 1.4\ C_2H_3N$: C, 41.71; H, 2.39; N, 5.55. Found: C, 41.74; H, 2.44; N, 5.51.

Acknowledgments

Dr. Günther Thiele is kindly acknowledged for the help by structural solution of the crystals. We thank Johanna Schlögl for the help with some EPR

measurements. We thank Prof. Dr. Sabine Laschat and Eugen Wuckert for the POM measurements of the complexes. We would like to acknowledge the assistance of the Core Facility BioSupraMol supported by the DFG. Funded by the Deutsche Forschungsgemeinschaft [DFG, German Research Foundation – Project-ID 387284271 – SFB 1349]. NIN is a member of CONICET.

Conflicts of interest

There are no conflicts to declare.

References

[1] a) U. S. Schubert, H. Hofmeier, G. R. Newkome, *Modern Terpyridine Chemistry*, Wiley-VCH, Weinheim, **2006**; b) H. Hofmeier, U. S. Schubert, *Chem. Soc. Rev.* **2004**, *33*, 373-399.

[2] a) S. Aroua, T. K. Todorova, P. Hommes, L.-M. Chamoreau, H.-U. Reissig, V. Mougel, M. Fontecave, *Inorg. Chem.* **2017**, *56*, 5930-5940; b) P. Hommes, C. Fischer, C. Lindner, H. Zipse, H.-U. Reissig, *Angew. Chem. Int. Ed.* **2014**, *53*, 7647-7651; c) J. R. Colombe, S. Bernhardt, C. Stathakis, S. L. Buchwald, P. Knochel, *Org. Lett.* **2013**, *15*, 5754-5757.

[3] a) S. G. Shepard, S. M. Fatur, A. K. Rappé, N. H. Damrauer, *J. Am. Chem. Soc.* **2016**, *138*, 2949-2952; b) D. G. Brown, N. Sanguantrakun, B. Schulze, U. S. Schubert, C. P. Berlinguette, *J. Am. Chem. Soc.* **2012**, *134*, 12354-12357.

[4] R. Tatikonda, S. Bhowmik, K. Rissanen, M. Haukka, M. Cametti, *Dalton Trans.* **2016**, *45*, 12756-12762.

[5] A. Fermi, G. Bergamini, M. Roy, M. Gingras, P. Ceroni, *J. Am. Chem. Soc.* **2014**, *136*, 6395-6400.

[6] a) Z. Zheng, L. Opilik, F. Schiffmann, W. Liu, G. Bergamini, P. Ceroni, L.-T. Lee, A. Schütz, J. Sakamoto, R. Zenobi, J. VandeVondele, A. D. Schlüter, *J. Am. Chem. Soc.* **2014**, *136*, 6103-6110; b) G. Gröger, W. Meyer-Zaika, C. Böttcher, F. Gröhn, C. Ruthard, C. Schmuck, *J. Am. Chem. Soc.* **2011**, *133*, 8961-8971; c) U. S. Schubert, C. Eschbaumer, *Angew. Chem. Int. Ed.* **2002**, *41*, 2892-2926; d) F. Chen, Y.-K. Tian, Y. Chen, *Chem. Asian J.* **2018**, *13*, 3169-3172.

[7] a) J.-H. Yum, E. Baranoff, F. Kessler, T. Moehl, S. Ahmad, T. Bessho, A. Marchioro, E. Ghadiri, J.-E. Moser, C. Yi, M. K. Nazeeruddin, M. Grätzel, *Nat. Commun.* **2012**, *3*, 631; b) S. A. Sapp, C. M. Elliott, C. Contado, S. Caramori, C. A. Bignozzi, *J. Am. Chem. Soc.* **2002**, *124*, 11215-11222.

[8] a) N. Elgrishi, S. Griveau, M. B. Chambers, F. Bedioui, M. Fontecave, *Chem. Commun.* **2015**, *51*, 2995-2998; b) N. Elgrishi, M. B. Chambers, M. Fontecave, *Chem. Sci.* **2015**, *6*, 2522-2531; c) N. Elgrishi, M. B. Chambers, V. Artero, M. Fontecave, *Phys. Chem. Chem. Phys.* **2014**, *16*, 13635-13644.

[9] R. Tatikonda, M. Cametti, E. Kalenius, A. Famulari, K. Rissanen, M. Haukka, *Eur. J. Inorg. Chem.* **2019**, *2019*, 4463-4470.

[10] K. Kuroiwa, T. Arie, S. Sakurai, S. Hayami, T. J. Deming, *J. Mater. Chem. C* **2015**, *3*, 7779-7783.

[11] S. Hayami, R. Moriyama, Y. Shigeyoshi, R. Kawajiri, T. Mitani, M. Akita, K. Inoue, Y. Maeda, *Inorg. Chem.* **2005**, *44*, 7295-7297.

[12] a) M. A. Halcrow, *Chemical Society Reviews* **2011**, *40*, 4119-4142; b) M. A. Halcrow, *Spin-crossover materials. Properties and application*, Wiley, Chichester, **2013**; c) P. Gütlich, A. Hauser, H. Spiering, *Angew. Chem. Int. Ed.* **1994**, *33*, 2024-2054; d) P. Guionneau, M. Marchivie, G. Bravic, J.-F. Létard, D. Chasseau, *J. Mate. Chem.* **2002**, *12*, 2546-2551; e) A. B. Gaspar, M. C. Muñoz, V. Niel, J. A. Real, *Inorg. Chem.* **2001**, *40*, 9-10; f) J. Zarembowitch, O. Kahn, *Inorg. Chem.* **1984**, *23*, 589-593; g) F.

Fürmeyer, D. Münzberg, L. M. Carrella, E. Rentschler, *Molecules* **2020**, *25*; h) N. M. J. Nik Ibrahim, S. M. Said, A. Mainal, M. F. Mohd Sabri, N. Abdullah, M. M. I. Megat Hasnan, H. Che Hassan, M. F. Mohd Salleh, W. A. Wan Mohd Mahiyiddin, *Mater. Res. Bull.* **2020**, *126*, 110828; i) M. Griffin, S. Shakespeare, H. J. Shepherd, C. J. Harding, J.-F. Létard, C. Desplanches, A. E. Goeta, J. A. K. Howard, A. K. Powell, V. Mereacre, Y. Garcia, A. D. Naik, H. Müller-Bunz, G. G. Morgan, *Angew. Chem. Int. Ed.* **2011**, *50*, 896-900; j) W. Phonsri, B. A. I. Lewis, G. N. L. Jameson, K. S. Murray, *Chem. Commun.* **2019**, *55*, 14031-14034; k) C. Cook, F. Habib, T. Aharen, R. Clérac, A. Hu, M. Murugesu, *Inorg. Chem.* **2013**, *52*, 1825-1831.

[13] a) P. Silva, S. M. F. Vilela, J. P. C. Tomé, F. A. Almeida Paz, *Chem. Soc. Rev.* **2015**, *44*, 6774-6803; b) C.-L. Ho, Z.-Q. Yu, W.-Y. Wong, *Chem. Soc. Rev.* **2016**, *45*, 5264-5295; c) M. Castellano, R. Ruiz-García, J. Cano, J. Ferrando-Soria, E. Pardo, F. R. Fortea-Pérez, S.-E. Stiriba, W. P. Barros, H. O. Stumpf, L. Cañadillas-Delgado, J. Pasán, C. Ruiz-Pérez, G. de Munno, D. Armentano, Y. Journaux, F. Lloret, M. Julve, *Coord. Chem. Rev.* **2015**, *303*, 110-138; d) M. K. Singh, Y. Yang, C. G. Takoudis, *Coord. Chem. Rev.* **2009**, *253*, 2920-2934; e) E. Chelebaeva, J. Larionova, Y. Guari, R. A. S. Ferreira, L. D. Carlos, F. A. A. Paz, A. Trifonov, C. Guérin, *Inorg. Chem.* **2009**, *48*, 5983-5995; f) J. Long, J. Rouquette, J. M. Thibaud, R. A. Ferreira, L. D. Carlos, B. Donnadieu, V. Vieru, L. F. Chibotaru, L. Konczewicz, J. Haines, Y. Guari, J. Larionova, *Angew. Chem. Int. Ed.* **2015**, *54*, 2236–2240.

[14] S. Hayami, R. Moriyama, A. Shuto, Y. Maeda, K. Ohta, K. Inoue, *Inorg. Chem.* **2007**, *46*, 7692-7694.

[15] R. Akiyoshi, Y. Hirota, D. Kosumi, M. Tsutsumi, M. Nakamura, L. F. Lindoy, S. Hayami, *Chem. Sci.* **2019**, *10*, 5843-5848.

[16] a) M. Seredyuk, A. B.Gaspar, V. Ksenofontov, Y. Galyametdinov, J. Kusz, P. Gütlich, *Adv. Funct. Mater.* **2008**, *18*, 1089–2101; b) M. Seredyuk, A. B. Gaspar, V. Ksenofontov, Y. Galyametdinov, J. Kusz, P. Gütlich, *J. Am. Chem. Soc.* **2008**, *130*, 1431-1439; c) A. B. Gaspar, M. Seredyuk, P. Gütlich, *Coord. Chem. Rev.* **2009**, *253*, 2399-2413.

[17] a) A. B. Gaspar, V. Ksenofontov, M. Seredyuk, P. Gütlich, *Coord. Chem. Rev.* **2005**, *249*, 2661-2676; b) S. Bonhommeau, P. G. Lacroix, D. Talaga, A. Bousseksou, M. Seredyuk, I. O. Fritsky, V. Rodriguez, *J. Phys. Chem. C* **2012**, *116*, 11251-11255; c) W. Liu, X. Bao, L.-L. Mao, J. Tucek, R. Zboril, J.-L. Liu, F.-S. Guo, Z.-P. Ni, M.-L. Tong, *Chem. Commun.* **2014**, *50*, 4059-4061.

[18] a) I. Suleimanov, O. Kraieva, J. Sánchez Costa, I. O. Fritsky, G. Molnár, L. Salmon, A. Bousseksou, *J. Mater. Chem. C* **2015**, *3*, 5026-5032; b) A. Santoro, L. J. Kershaw Cook, R. Kulmaczewski, S. A. Barrett, O. Cespedes, M. A. Halcrow, *Inorg. Chem.* **2015**, *54*, 682-693; c) C. F. Wang, R. F. Li, X. Y. Chen, R. J. Wei, L. S. Zheng, J. Tao, *Angew. Chem. Int. Ed.* **2015**, *54*; d) M. Estrader, J. S. Uber, L. A. Barrios, J. Garcia, P. Lloyd-Williams, O. Roubeau, S. J. Teat, G. Aromi, *Angew. Chem. Int. Ed.* **2017**, *56*, 15622–15627; e) J.-Y. Ge, Z. Chen, L. Zhang, X. Liang, J. Su, M. Kurmoo, J.-L. Zuo, *Angew. Chem. Int. Ed.* **2019**, *58*; f) B. Benaicha, K. Van Do, A. Yangui, N. Pittala, A. Lusson, M. Sy, G. Bouchez, H. Fourati, C.

J. Gómez-García, S. Triki, K. Boukheddaden, *Chem. Sci.* **2019**, *10*, 6791-6798.

[19] a) S. Hayami, Y. Shigeyoshi, M. Akita, K. Inoue, K. Kato, K. Osaka, M. Takata, R. Kawajiri, T. Mitani, Y. Maeda, *Angew. Chem. Int. Ed.* **2005**, *44*, 4899-4903; b) J. A. Kitchen, N. G. White, C. Gandolfi, M. Albrecht, G. N. L. Jameson, J. L. Tallon, S. Brooker, *Chem. Commun.* **2010**, *46*, 6464-6466.

[20] a) S. Hayami, K. Murata, D. Urakami, Y. Kojima, M. Akita, K. Inoue, *Chem. Commun.* **2008**, 6510-6512; b) S. Hayami, D. Urakami, Y. Kojima, H. Yoshizaki, Y. Yamamoto, K. Kato, A. Fuyuhiro, S. Kawata, K. Inoue, *Inorg. Chem.* **2010**, *49*, 1428-1432; c) S. Hayami, Y. Komatsu, T. Shimizu, H. Kamihata, Y. H. Lee, *Coord. Chem. Rev.* **2011**, *255*, 1981-1990; d) Y. Komatsu, K. Kato, Y. Yamamoto, H. Kamihata, Y. H. Lee, A. Fuyuhiro, S. Kawata, S. Hayami, *Eur. J. Inorg. Chem.* **2012**, *2012*, 2769-2775; e) S. Hayami, M. Nakaya, H. Ohmagari, A. S. Alao, M. Nakamura, R. Ohtani, R. Yamaguchi, T. Kuroda-Sowa, J. K. Clegg, *Dalton Trans.* **2015**, *44*, 9345-9348.

[21] S. Hayami, K. Kato, Y. Komatsu, A. Fuyuhiro, M. Ohba, *Dalton Trans.* **2011**, *40*, 2167-2169.

[22] L. Arnedo-Sánchez, Nonappa, S. Bhowmik, S. Hietala, R. Puttreddy, M. Lahtinen, L. De Cola, K. Rissanen, *Dalton Trans.* **2017**, *46*, 7309-7316.

[23] D. Shao, L. Shi, L. Yin, B.-L. Wang, Z.-X. Wang, Y.-Q. Zhang, X.-Y. Wang, *Chem. Sci.* **2018**, *9*, 7986-7991.

[24] C. J. Gorter, J. H. van Vleck, *Phys. Rev.* **1947**, *72*, 1128-1129.

[25] N. Bloembergen, E. M. Purcell, R. V. Pound, *Phys. Rev.* **1948**, *73*, 679-712.

[26] a) J. H. Van Vleck, *Phys. Rev.* **1948**, *74*, 1168-1183; b) P. W. Anderson, P. R. Weiss, *Rev. Mod. Phys.* **1953**, *25*, 269-276; c) P. W. Anderson, *Phys. Rev.* **1951**, 342.

[27] a) V. A. Atsarkin, G. A. Vasneva, V. V. Demidov, F. S. Dzheparov, B. M. Odintsov, R. B. Clarkson, *JETP Lett.* **2000**, *72*, 369-372; b) L. Tagirov, *IEEE Trans. Magn.* **1987**, *23*, 2230-2232.

[28] a) P. Sati, A. Stepanov, V. Pashchenko, *Low Temp. Phys.* **2007**, *33*, 927-930; b) A. L. Pérez, A. Kemmerer, M. A. Rey, S. D. Dalosto, C. A. Ramos, M. C. G. Passeggi, A. C. Rizzi, C. D. Brondino, *Eur. J. Inorg. Chem.* **2018**, *2018*, 4604-4613.

[29] a) A. C. Rizzi, N. I. Neuman, P. J. González, C. D. Brondino, *Eur. J. Inorg. Chem.* **2016**, *2016*, 192-207; b) N. I. Neuman, E. Burna, R. Baggio, M. C. G. Passeggi, A. C. Rizzi, C. D. Brondino, *Inorg. Chem. Front.* **2015**, *2*, 837-845.

[30] a) M. Nößler, R. Jäger, D. Hunger, M. Reimann, T. Bens, N. I. Neuman, A. S. Hazari, M. Kaupp, J. van Slageren, B. Sarkar, *Eur. J. Inorg. Chem.* **2023**, *n/a*, e202300091; b) F. Stein, M. Nößler, A. S. Hazari, L. Böser, R. Walter, H. Liu, E. Klemm, B. Sarkar, *Chem. Eur. J.* **2023**, *n/a*, e202300405.

[31] O. A. Oyetade, V. O. Nyamori, B. S. Martincigh, S. B. Jonnalagadda, *RSC Adv.* **2016**, *6*, 2731-2745.

[32] P. Gütlich, H. A. Goodwin, *Spin Crossover in Transition Metal Compounds I, II, and III*, Springer, Berlin, Germany, **2004**.

[33] R. J. Davidson, E. W. Ainscough, A. M. Brodie, G. B. Jameson, M. R. Waterland, H. R. Allcock, M. D. Hindenlang, B. Moubaraki, K. S. Murray, K. C. Gordon, R. Horvath, G. N. L. Jameson, *Inorg. Chem.* **2012**, *51*, 8307-8316.

[34] A. Ondo, T. Ishida, in *Crystals, Vol. 8*, **2018**.

[35] a) J. A. Real, A. B. Gaspar, M. C. Muñoz, *Dalton Trans.* **2005**, 2062-2079; b) O. Sato, J. Tao, Y.-Z. Zhang, *Angew. Chem. Int. Ed.* **2007**, *46*, 2152-2187; c) M. A. Halcrow, *Chem. Soc. Rev.* **2011**, *40*, 4119-4142.

[36] a) J. England, E. Bill, T. Weyhermüller, F. Neese, M. Atanasov, K. Wieghardt, *Inorg. Chem.* **2015**, *54*, 12002-12018; b) J. England, C. C. Scarborough, T. Weyhermüller, S. Sproules, K. Wieghardt, *Eur. J. Inorg. Chem.* **2012**, *2012*, 4605-4621.

[37] a) P. Nielsen, H. Toftlund, A. D. Bond, J. F. Boas, J. R. Pilbrow, G. R. Hanson, C. Noble, M. J. Riley, S. M. Neville, B. Moubaraki, K. S. Murray, *Inorg. Chem.* **2009**, *48*, 7033-7047; b) S. Kremer, W. Henke, D. Reinen, *Inorg. Chem.* **1982**, *21*, 3013-3022.

[38] S. Ye, *MRL* **2022**.

[39] B. R. McGarvey, *Can. J. Chem.* **1975**, *53*, 2498-2511.

[40] a) R. Calvo, C. A. Steren, O. E. Piro, T. Rojo, F. J. Zuniga, E. E. Castellano, *Inorg. Chem.* **1993**, *32*, 6016-6022; b) N. I. Neuman, V. G. Franco, F. M. Ferroni, R. Baggio, M. C. G. Passeggi, A. C. Rizzi, C. D. Brondino, *J. Phys. Chem. A* **2012**, *116*, 12314-12320; c) A. L. Pérez, N. I. Neuman, R. Baggio, C. A. Ramos, S. D. Dalosto, A. C. Rizzi, C. D. Brondino, *Polyhedron* **2017**, *123*, 404-410.

[41] a) F. Neese, *WIREs Comput. Mol. Sci.* **2012**, *2*, 73-78; b) F. Neese, *WIREs Comput. Mol. Sci.* **2018**, *8*, e1327; c) F. Neese, *WIREs Comput. Mol. Sci.* **2022**, *n/a*, e1606.

[42] D. Venegas-Yazigi, K. A. Brown, A. Vega, R. Calvo, C. Aliaga, R. C. Santana, R. Cardoso-Gil, R. Kniep, W. Schnelle, E. Spodine, *Inorg. Chem.* **2011**, *50*, 11461-11471.

[43] G. R. Fulmer, A. J. M. Miller, N. H. Sherden, H. E. Gottlieb, A. Nudelman, B. M. Stoltz, J. E. Bercaw, K. I. Goldberg, *Organometallics* **2010**, *29*, 2176-2179.

[44] M. Krejčik, M. Daněk, F. Hartl, *J. Electroanal. Chem.* **1991**, *317*, 179-187.

[45] a) G. M. Sheldrick, *SHELXS-97, Program for Crystal Structure Solution and Refinement,* **1997**, University of Göttingen, Germany; b) G. Sheldrick, *Acta Crystallogr., Sect. A* **2008**, *64*, 112-122; c) G. M. Sheldrick, *SADABS Ver. 2008/1, SADABS. Program for Empirical Absorption Correction* **2012**, University of Göttingen, Germany; d) G. M. Sheldrick, *SHELXL Version 2014/7, Program for Chrystal Structure Solution and Refinement* **2014**, University of Göttingen, Germany; e) G. Sheldrick, *Acta Crystallogr. Sect. C* **2015**, *71*, 3-8; f) A. Spek, *J. Appl. Crystallogr.* **2003**, *36*, 7-13; g) SAINT+, *Data Integration Engine, Version 8.27b©*, Bruker AXS, Madison, Wisconsin, USA, 1997-2012.

[46] G. A. Bain, J. F. Berry, *J. Chem. Educ.* **2008**, *85*, 532.

[47] a) V. N. Staroverov, G. E. Scuseria, J. Tao, J. P. Perdew, *J. Chem. Phys.* **2003**, *119*, 12129-12137; b) J. Tao, J. P. Perdew, V. N. Staroverov, G. E. Scuseria, *Phys. Rev. Lett.* **2003**, *91*, 146401.

[48] F. Weigend, R. Ahlrichs, *Phys. Chem. Chem. Phys.* **2005**, *7*, 3297-3305.

[49] M. M. Quintal, A. Karton, M. A. Iron, A. D. Boese, J. M. L. Martin, *J. Phys. Chem. A* **2006**, *110*, 709-716.

[50] a) S. K. T. Petrenko, F. Neese, *J. Chem. Phys.* **2011**, *134*, 54116; b) F. Neese, G. Olbrich, *Chem. Phys. Lett.* **2002**, *362*, 170-178; c) R. Izsák, F. Neese, *J. Chem. Phys.* **2011**, *135*, 144105; d) J. L. Whitten, *J. Chem. Phys.* **1973**, *58*, 4496-4501; e) O. Vahtras, J. Almlöf, M. W. Feyereisen, *Chem. Phys. Lett.* **1993**, *213*, 514-518; f) F. Neese, F.

Wennmohs, A. Hansen, U. Becker, *Chem. Phys.* **2009**, *356*, 98-109.

[51] a) K. Eichkorn, O. Treutler, H. Öhm, M. Häser, R. Ahlrichs, *Chem. Phys. Lett.* **1995**, *240*, 283-290; b) K. Eichkorn, F. Weigend, O. Treutler, R. Ahlrichs, *Theor. Chem. Acc.* **1997**, *97*, 119-124; c) F. Weigend, *Phys. Chem. Chem. Phys.* **2006**, *8*, 1057-1065.

[52] a) D. Prescher, T. Thiele, R. Ruhmann, *J. Fluor. Chem.* **1996**, *79*, 145-148; b) J. Rábai, D. Szabó, E. K. Borbás, I. Kövesi, I. Kövesdi, A. Csámpai, Á. Gömöry, V. E. Pashinnik, Y. G. Shermolovich, *J. Fluor. Chem.* **2002**, *114*, 199-207.

Toc: 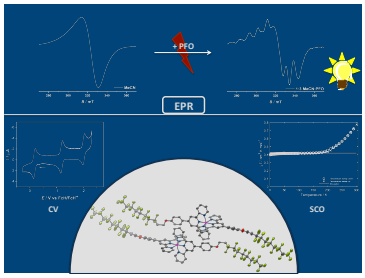

Supporting Information

Spin Crossover and Flourine-Specific Interactions in Metal Complexes of Terpyridines with Polyfluorocarbon Tails

Maite Nößler,[a] Nicolás I. Neuman,[b, c] Lisa Böser,[a] René Jäger,[a] Arijit Singha Hazari,[b] David Hunger,[d] Yixian Pan,[d] Clemens Lücke,[b] Tobias Bens,[b] Joris van Slageren[d], and Biprajit Sarkar[a,b],**

S I

Content

1. SQUID Magnetometry

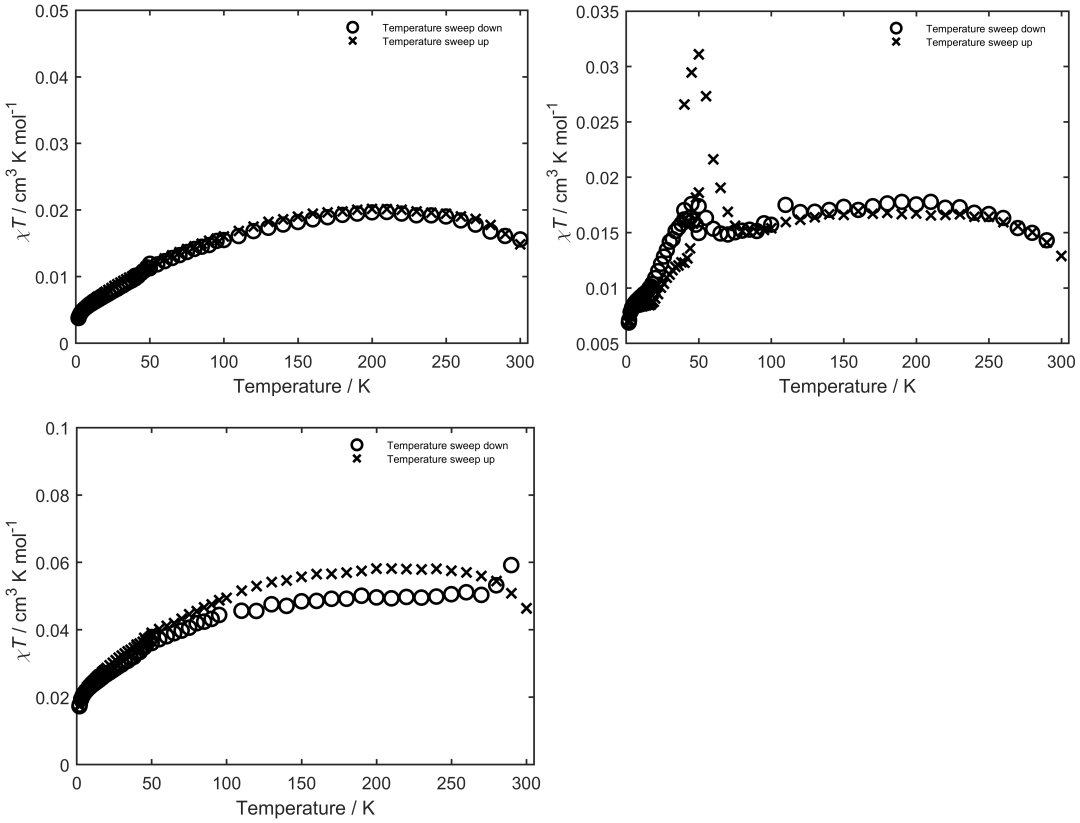

Figure S 1: Temperature dependency of the $\chi_M T$ product for **2** (top left), **4** (top right) and **6** (bottom) in an applied magnetic field of 1000 Oe as well as the corresponding LS spin Hamiltonian simulations.

2. Cyclic Voltamograms

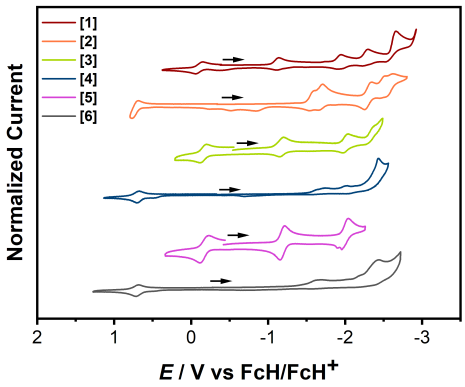

Figure S 2: Cyclic voltammograms of complexes **1-6** in acetonitrile/NBu_4PF_6 measured with a glassy carbon working electrode (FcH = ferrocene; FcH^+ = ferrocenium)

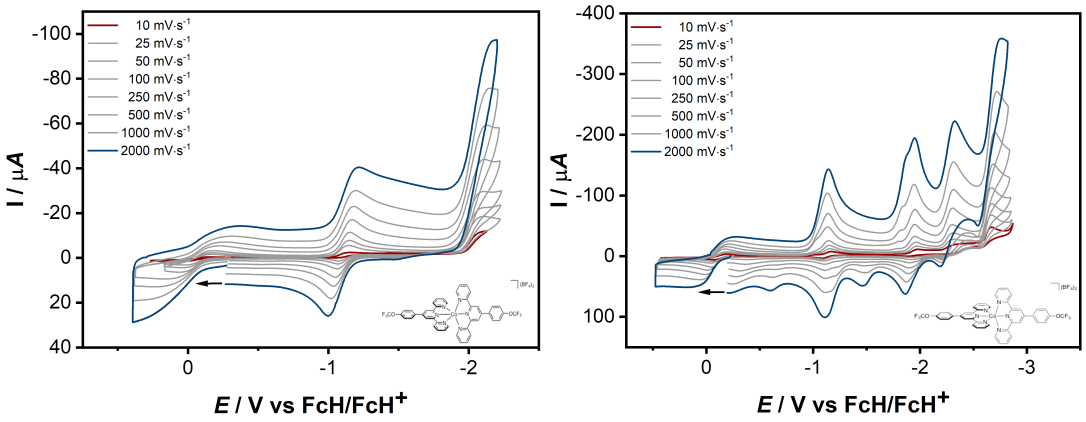

Figure S 3: Complex **1** in DCM at different scan rates (left) at MeCN at different scan rates (right).

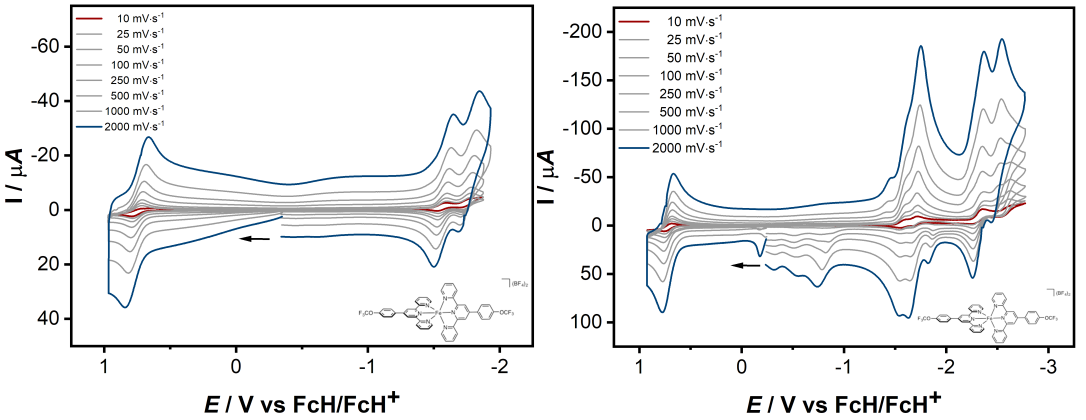

Figure S 4: Complex **2** in DCM at different scan rates (left) in MeCN at different scan rates (right).

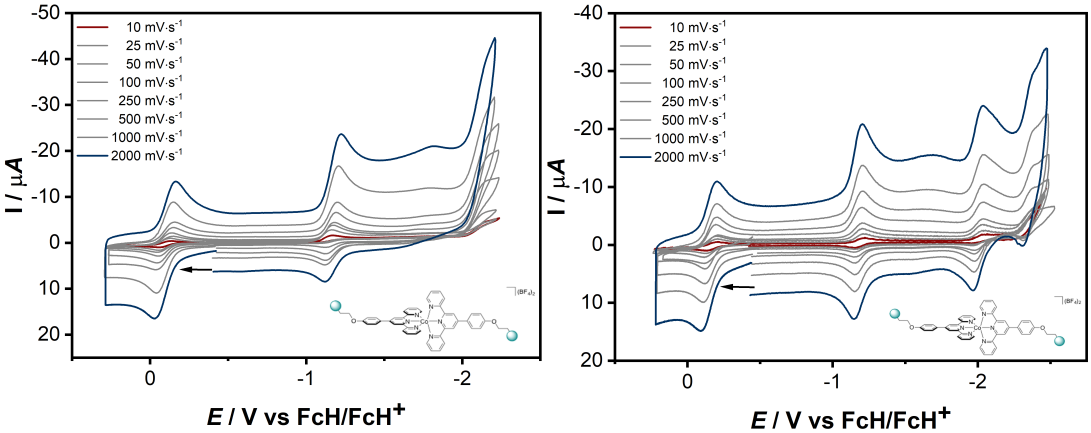

Figure S 5: Complex **3** in DCM at different scan rates (left) and in MeCN at different scan rates (right).

S 2

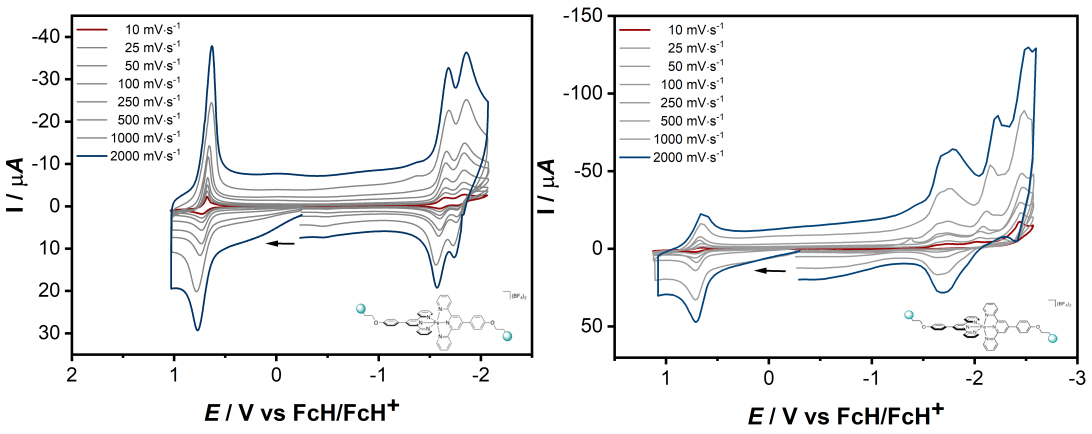

Figure S 6: Complex **4** in DCM at different scan rates (left) and in MeCN at different scan rates (right).

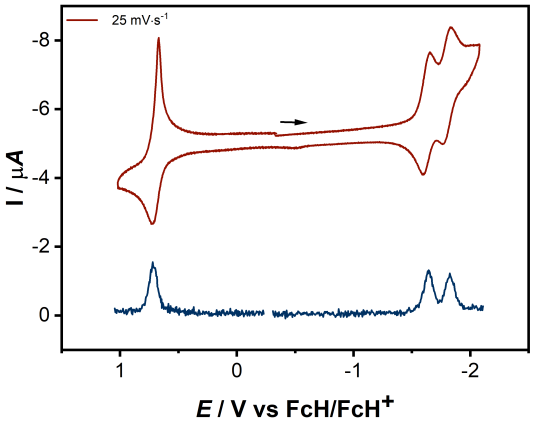

Figure S 7: CV and DPV of complex **4** in CH_2Cl_2/NBu_4PF_6 measured with a glassy carbon working electrode (FcH = ferrocene; FcH^+ = ferrocenium).

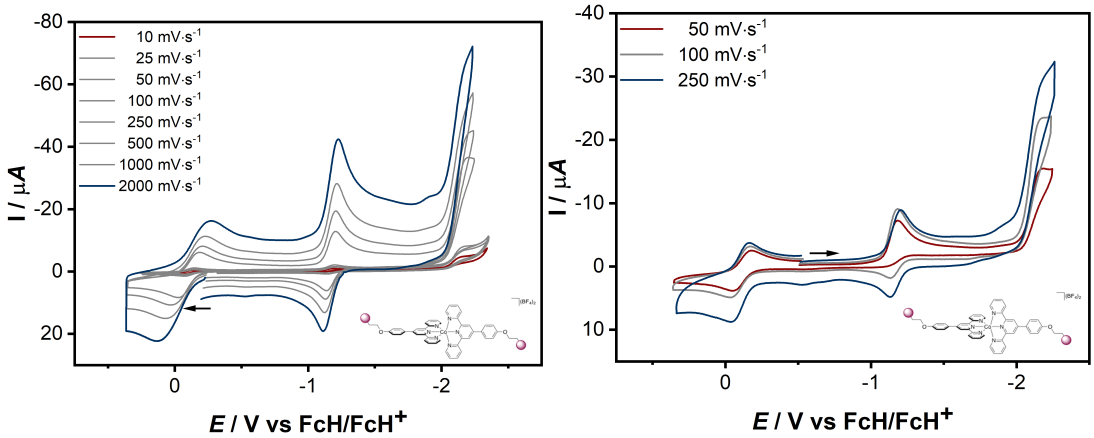

Figure S 8: Complex **5** in DCM at different scan rates.

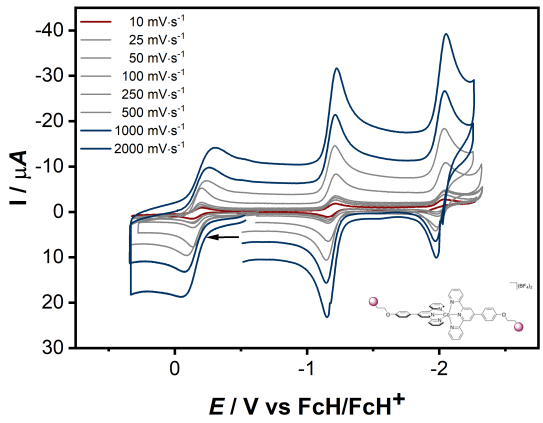

Figure S 9 Complex **5** in MeCN at different scan rates.

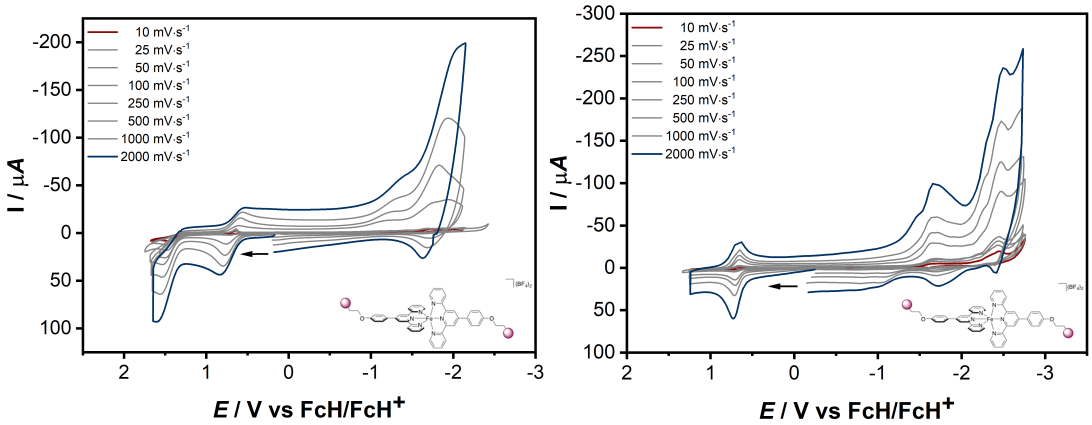

Figure S 10: Complex **6** in DCM at different scan rates (left) and in MeCN at different scan rates (right).

Table S 1: Redox potentials vs. FcH/FcH^+ measured in dichloromethane at 100 mVs^{-1} with 0.1 M Bu_4NPF_6 at room temperature.[a]

	Solvent	E_{fp}^{Ox2}	$E_{1/2}^{Ox1}$	$E_{1/2}^{Red1}$	$E_{1/2}^{Red2}$
1	DCM	-	–0.07	–1.11	–2.09[b]
2	DCM	-	0.75	–1.57	–1.74
3	DCM	-	–0.10	–1.15	–2.17[b]
4	DCM	-	0.71	–1.63	–1.80[b]
5	DCM	-	–0.11	–1.17	–2.18[b
6	DCM	1.49[b]	0.68	–1.59[b]	–1.96[b]

[a] All measured with a glassy carbon electrode. [b] Forward peak potential at 0.1 V.

3. UV/Vis/NIR Spectroelectrochemistry

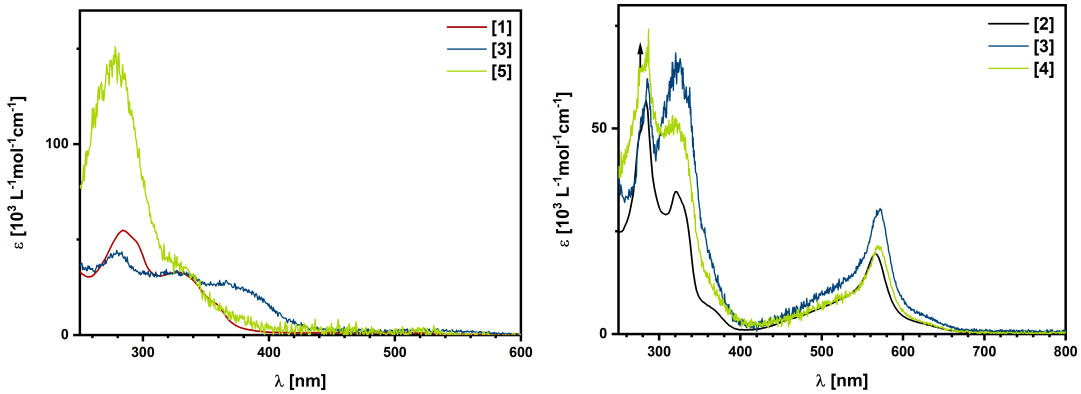

Figure S 11: UVVis of the cobalt complexes (left) and iron complexes (right). (**1**, **2**, **3**, **5** and **6** in MeCN and **4** in DCM)

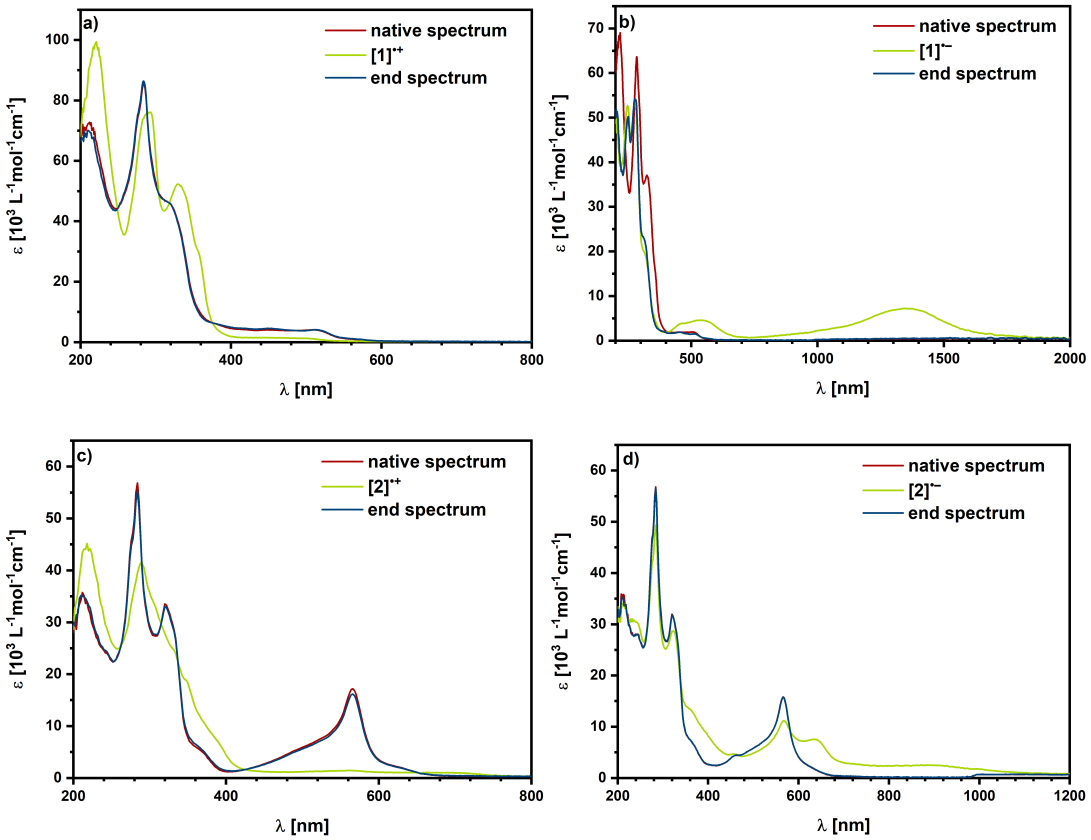

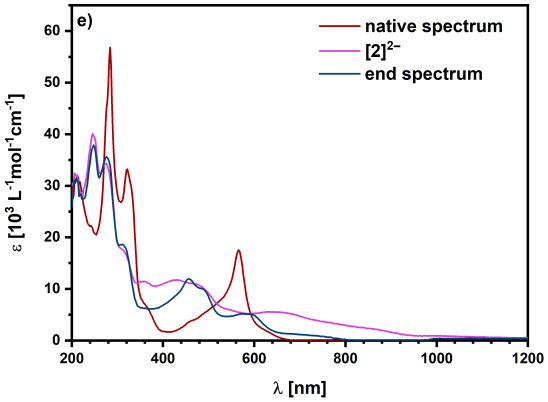

Figure S 12: UV/Vis/NIR SEC spectra of complex **1** in MeCN /NBu_4PF_6 measured with a gold working electrode (a-b) and complex **2** in MeCN/NBu_4PF_6 measured with a platinum working electrode (c-e).

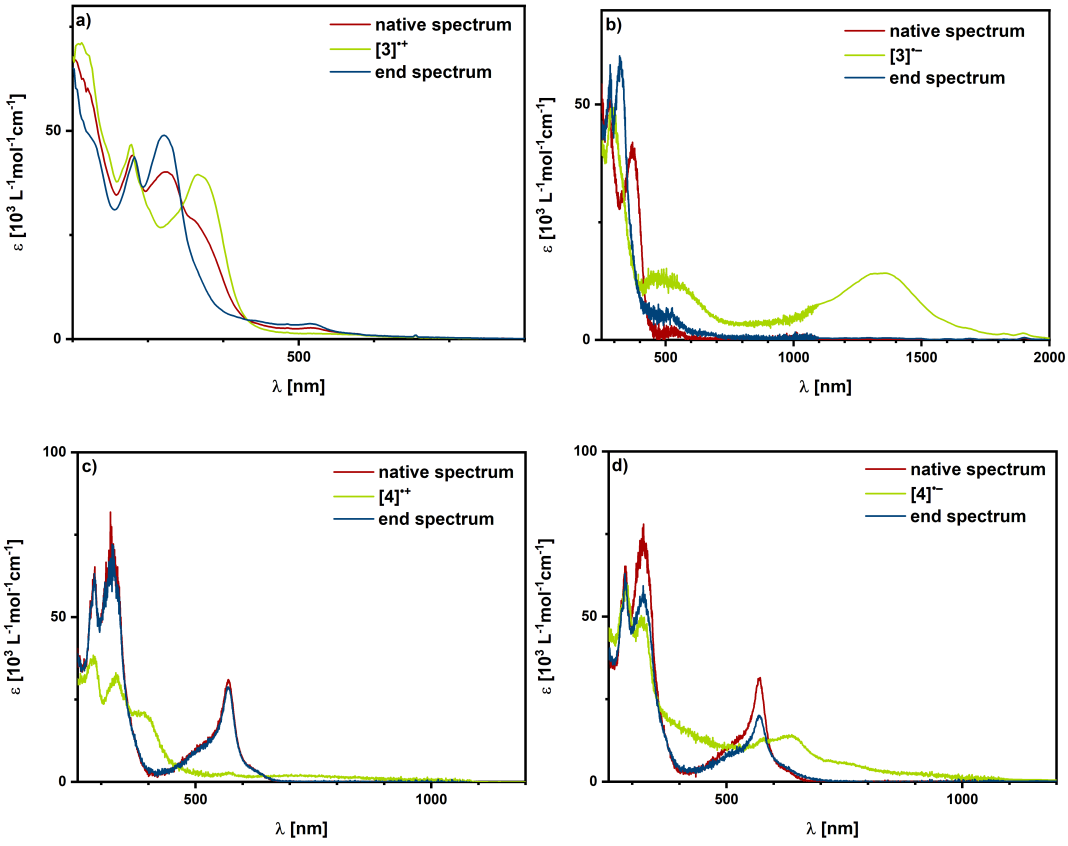

S 6

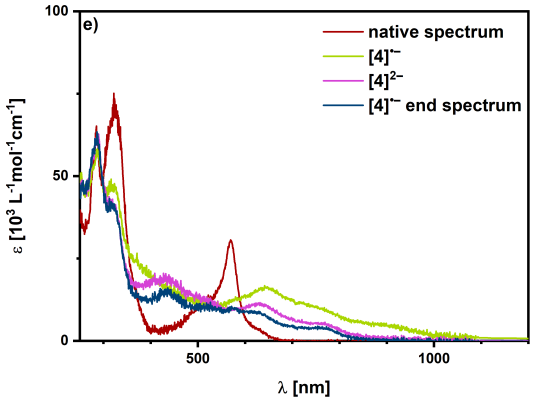

Figure S 13: UV/Vis/NIR SEC spectra of complex **3** in acetonitrile/NBu_4PF_6 measured with a gold working electrode (a-b) and complex **4** in dichloromethane /NBu_4PF_6 measured with a silver working electrode (c-e).

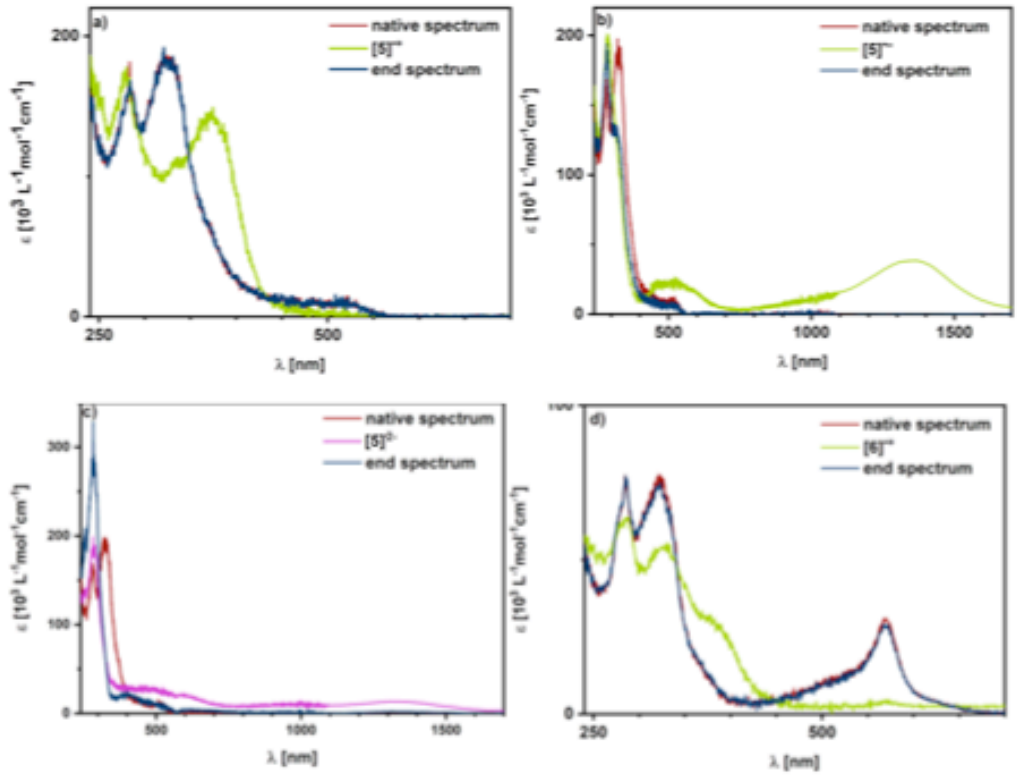

Figure S 14: UV/Vis/NIR SEC spectra of complexes **5** in acetonitrile/NBu_4PF_6 measured with a gold working electrode (a-c) complex **6** in acetonitrile/NBu_4PF_6 measured with a gold working electrode (d).

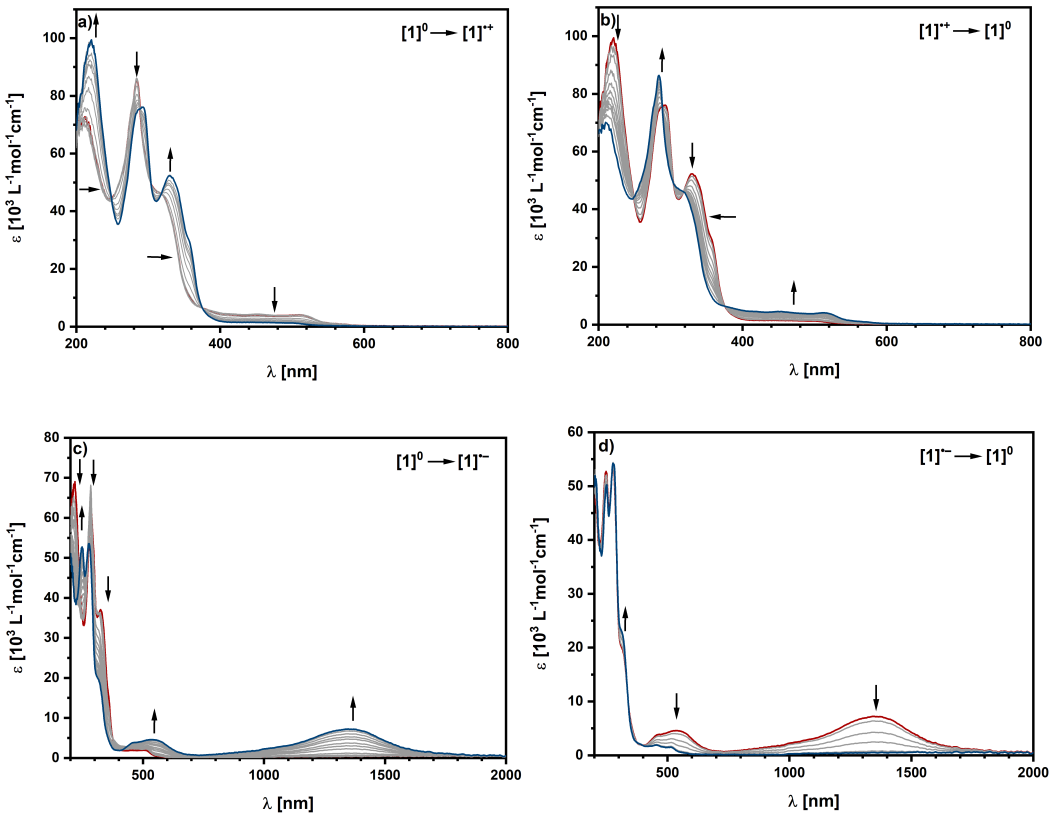

Figure S 15: UV/Vis/NIR SEC spectra of complex **1** in MeCN/NBu_4PF_6 measured with a gold working electrode.

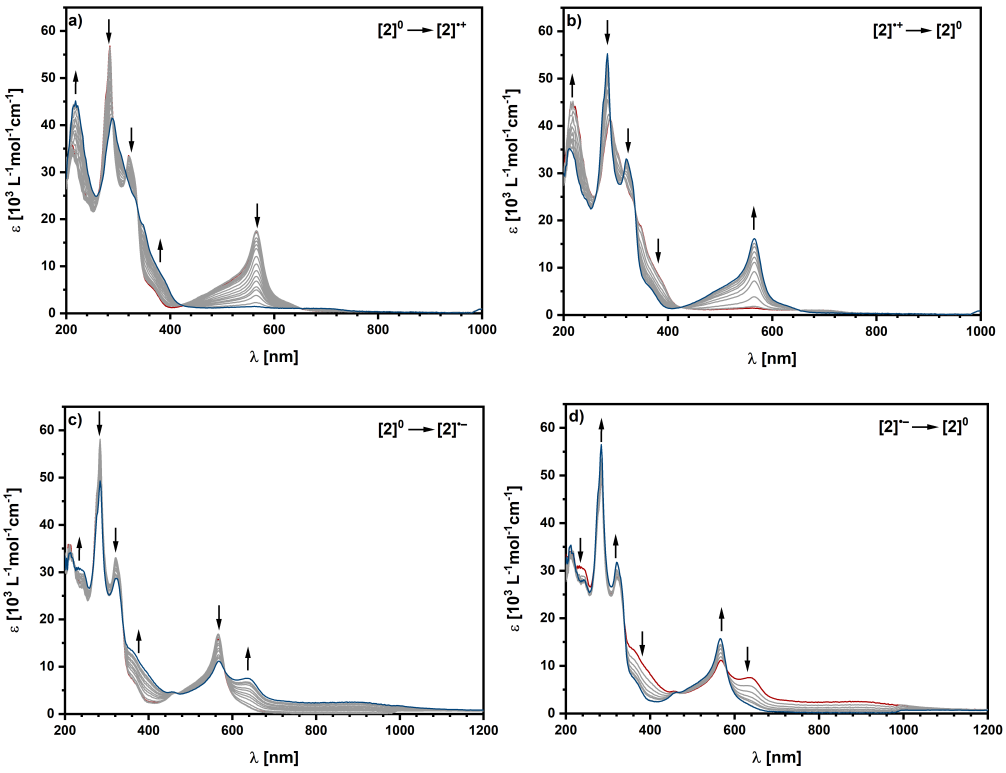

S 8

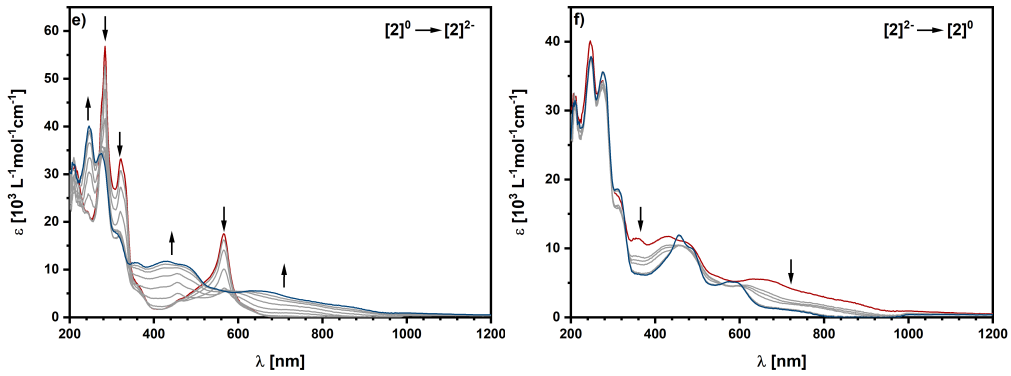

Figure S 16: UV/Vis/NIR SEC spectra of complex **2** in MeCN/NBu_4PF_6 measured with a gold working electrode.

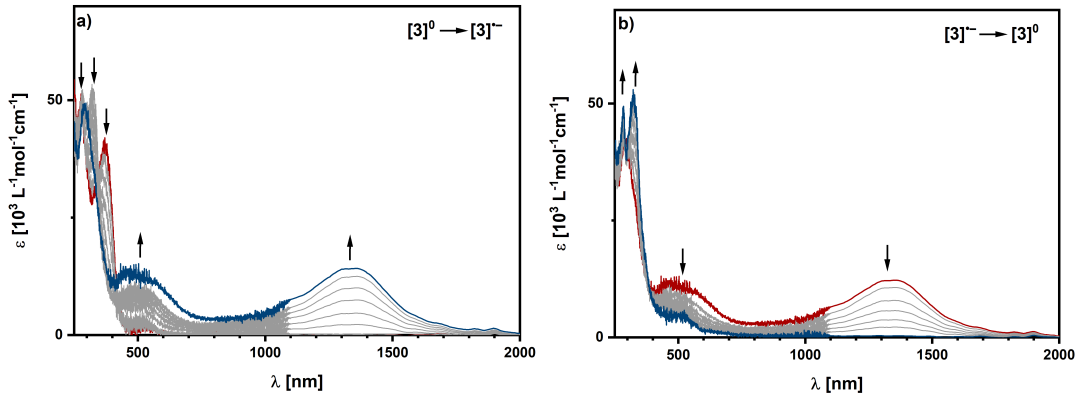

Figure S 17: UV/Vis/NIR SEC spectra of complex **3** in MeCN /NBu_4PF_6 measured with a gold working electrode.

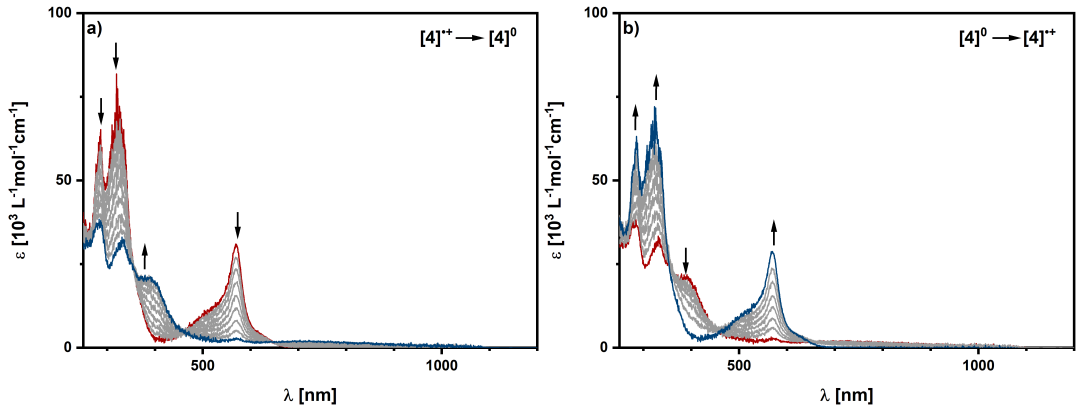

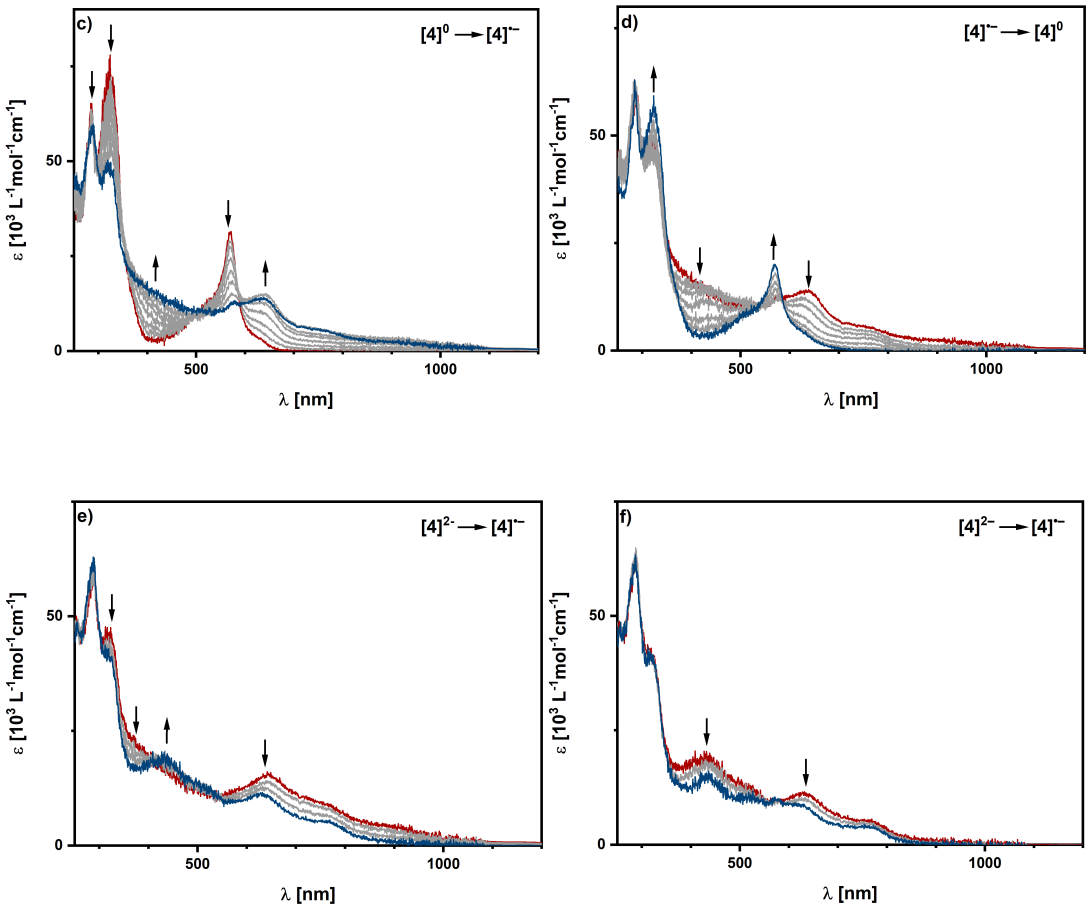

Figure S 18: UV/Vis/NIR SEC spectra of complex **4** in DCM/NBu_4PF_6 measured with a silver working electrode.

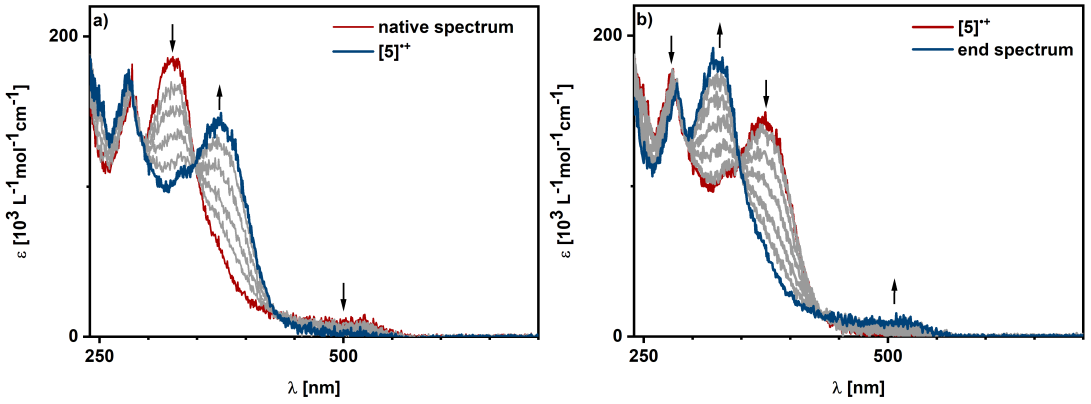

S 10

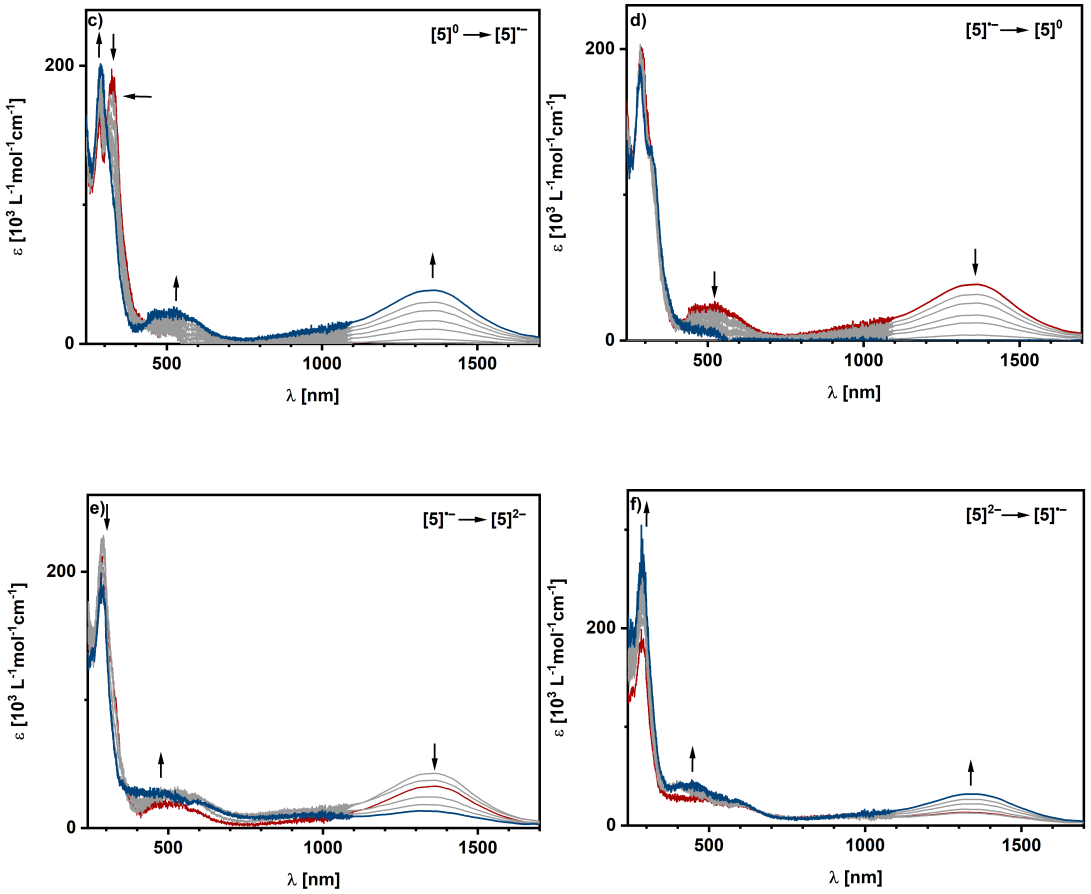

Figure S 19: UV/Vis/NIR SEC spectra of complex **5** in MeCN /NBu_4PF_6 measured with a gold working electrode.

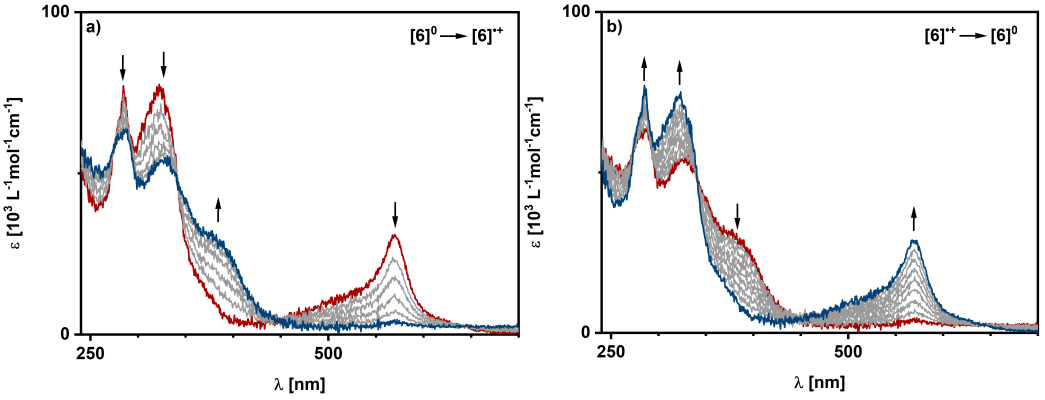

Figure S 20: UV/Vis/NIR SEC spectra of complex **6** in MeCN /NBu_4PF_6 measured with a gold working electrode

Table S 2: Data of the UV/Vis/NIR spectra during electrochemistry.for reversible redox steps.

	λ / nm (ε / $10^3 M^{-1} cm-1$)
[1]^0 native	212 (72.8), 276 sh, 284 (85.4), 319 sh, 511 sh
[1]$^{\bullet+}$ oxidation	221 (99.4), 292 (76.0), 330, 52.3), 357 sh
[1]^0 end	210 (70.2), 276 sh, 284 (86.4), 318 sh, 514 sh
[2]^0 native	212 (35.7), 276 sh, 284 (56.8), 320 (33.5), 364 sh, 502 sh, 566 (17.2), 626 sh
[2]$^{\bullet+}$ oxidation	218 (45.2), 288 (41.4), 332 sh, 348 sh, 390 sh
[2]$^{\bullet-}$ reduction	214 (34.1), 238 sh, 276 sh, 284 (49.3), 322 (28.6), 360 sh, 458 (4.6), 568 (11.2), 638 (7.5), 904 sh
[2]^0 end	212 (35.2), 276 sh, 284 (55.3), 320 (33.0), 364 sh, 502 sh, 566 (16.2), 632 sh
[4]^0 native	286 (65.2), 320 (81.8), 506 sh, 569 (31.0)
[4]$^{\bullet+}$ oxidation	283 (38.4), 331 (33.1), 388 sh,
[4]$^{\bullet-}$ reduction	289 (59.7), 319 (50.3), 577 (13.2), 638 (14.2), 754 sh
[4]^0 end	286 (63.2), 323 (72.1), 503 sh, 569 (28.7)
[5]^0 native	283 (181.4), 325 (186.5), 517 sh
[5]$^{\bullet+}$ oxidation	280 (177.7), 375 (149.0),
[5] end	283 (168.2), 325 (182.8), 516 sh
[6]^0 native	285 (77.2), 322 (77.6), 570 (31.0)
[6]$^{\bullet+}$ oxidation	287 (63.7), 328 (54.8), 377 sh
[6]^0 end	285 (77.1), 323 (75.1), 568 (28.7)

4. EPR Spectroscopy

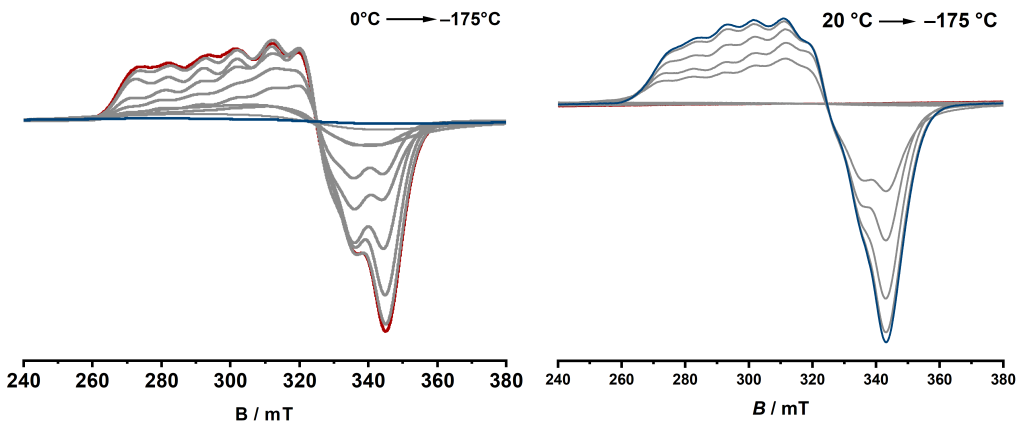

Figure S 21: EPR spectra of complex **1**. Left: powdered sample, right: dissolved sample in acetonitrile.

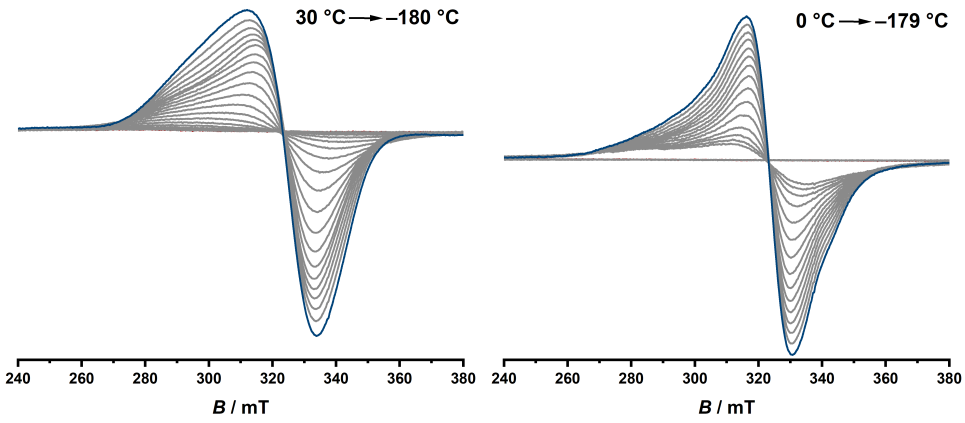

Figure S 22: EPR spectra of complex **3**. Left: powdered sample, right: dissolved sample in acetonitrile.

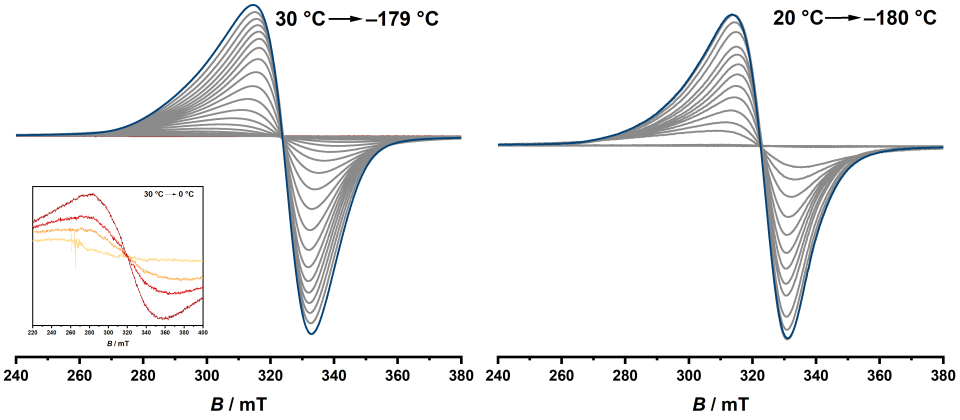

Figure S 23: EPR spectra of complex **5**. Left: powdered sample, right: dissolved sample in acetonitrile.

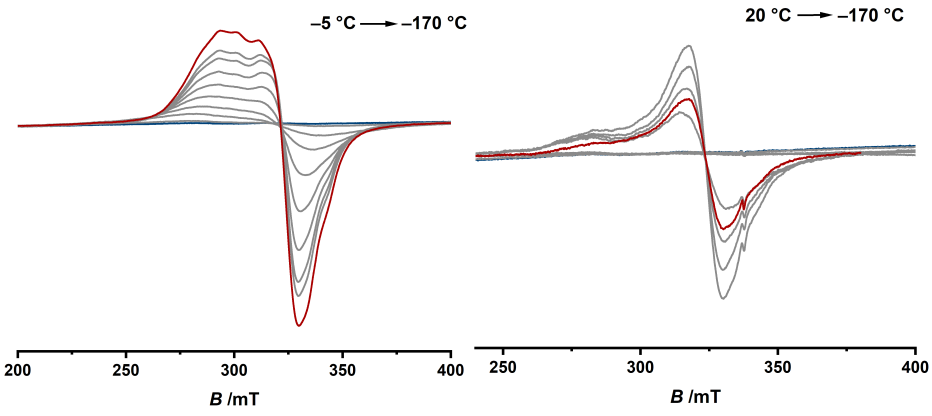

Figure S 24: Dilution control experiments of **3**: left: Diluted sample in pentafluorobenzonitrile, of **5** right: Diluted sample in acetonitrile:pentafluorobenzonitrile (1:1).

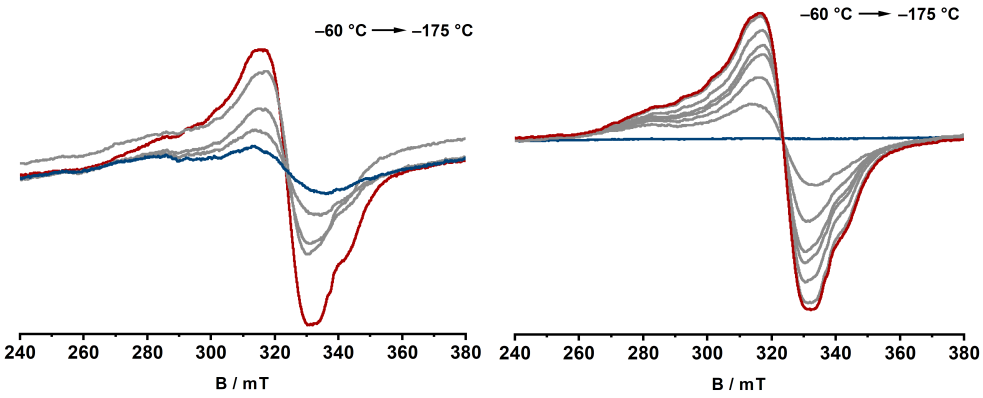

Figure S 25: Dilution control experiments of **5**: left: Diluted sample in acetonitrile, right: Sample in acetonitrile:1,2difluorobenzene (1:1).

5. DFT Calculations

Table S 3: Energies and exchange couplings derived from broken symmetry calculations on dimers of truncated forms of complex **5** with and without BF_4^- counterions.

	$[\mathbf{5}_{tr1}(BF_4)_2]_2$	$[\mathbf{5}_{tr2}]_2^{4+}$
Theory Level	TPSSh/def2-TZVP	TPSSh/def2-TZVP
E (High Spin)	–10323.556118 Ha	–7117.953009 Ha
E (Broken Symmetry)	–10323.556117 Ha	–7117.953009 Ha
E (HS) – E (BS)	–0.169 cm^{-1}	–0.102 cm^{-1}
J[a]	0.17 cm^{-1}	0.10 cm^{-1}
	(Ferromagnetic)	(Ferromagnetic)
J	~180 mT	~107 mT

[a] $H_{HDVV} = -2J\, S_A \cdot S_B$ convention, calculated as $-(E_{HS} - E_{BS})/(\langle S^2\rangle_{HS} - \langle S^2\rangle_{BS})$.[1, 2]

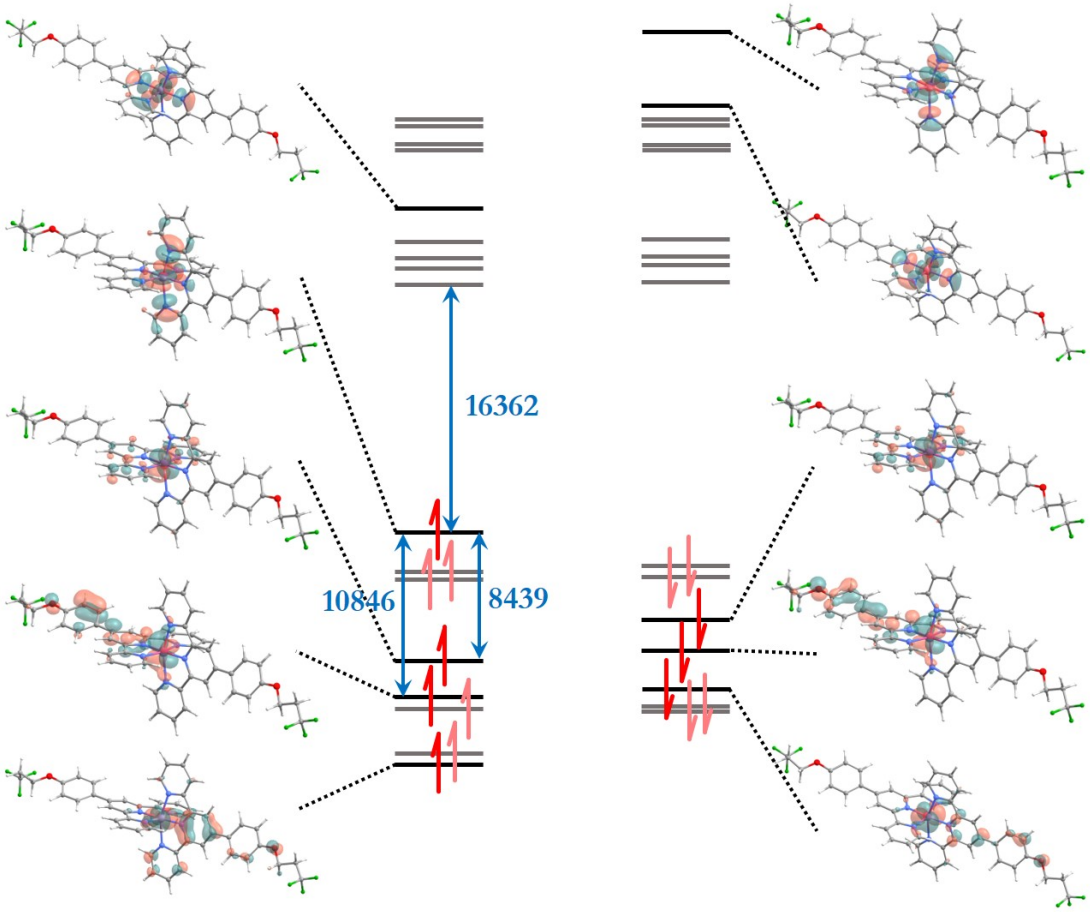

Figure S 26: Energy and orbital diagram for the orbitals with considerable metal 3*d* character (black lines and red arrows), as well as the occupied and empty ligand orbitals (grey lines with pink arrows) near the SOMO-LUMO gap of $[\mathbf{5}_{\mathbf{tr1}}]^{2+}$. Upward and downward arrows represent α and β spin, respectively. Orbital isosurfaces were plot using an isovalue of 0.03. The SOMO-LUMO gap as well as the $3d(z^2)$-$3d(xz,yz)$ energy separations for the α orbitals are indicated in cm^{-1}.

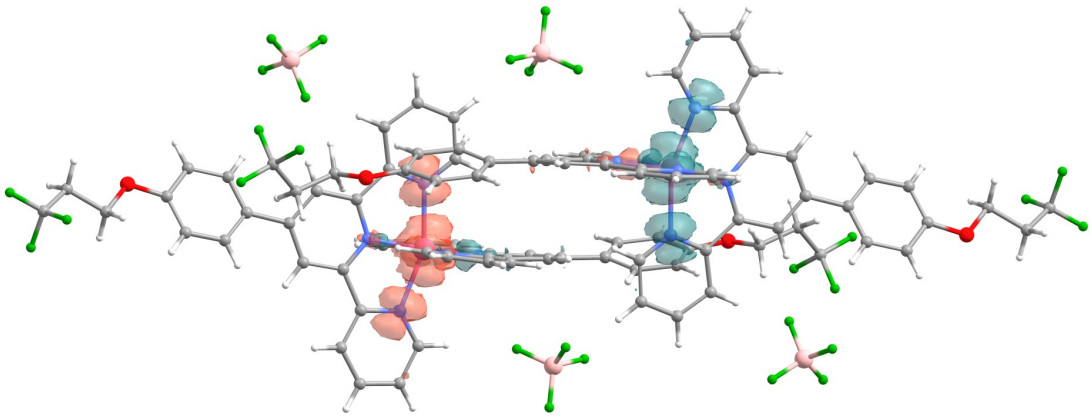

Figure S 27: Spin density for a dimer of complex $\mathbf{5}_{\mathbf{tr1}}$, with BF_4^- counterions and net charge of zero. Isovalue = 0.001.

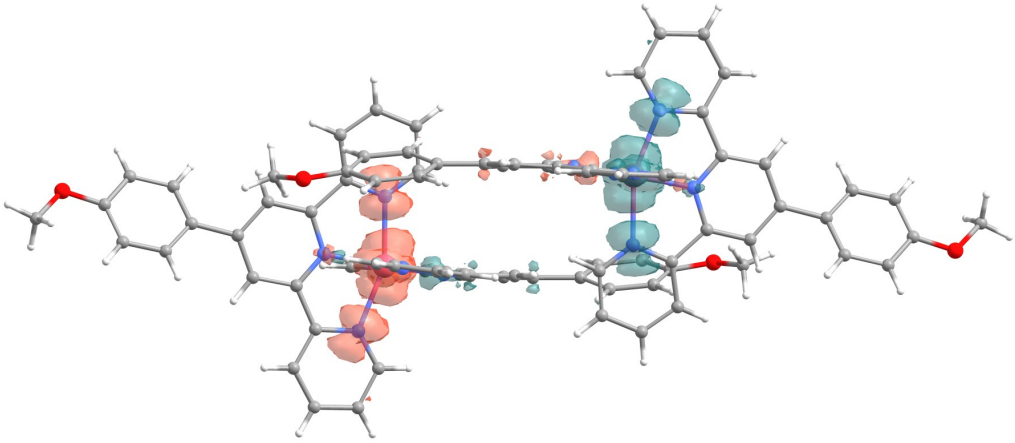

Figure S 28: Spin density for a dimer of complex $\mathbf{5}_{tr2}$, with no counterions and net charge of +4. Isovalue = 0.001.

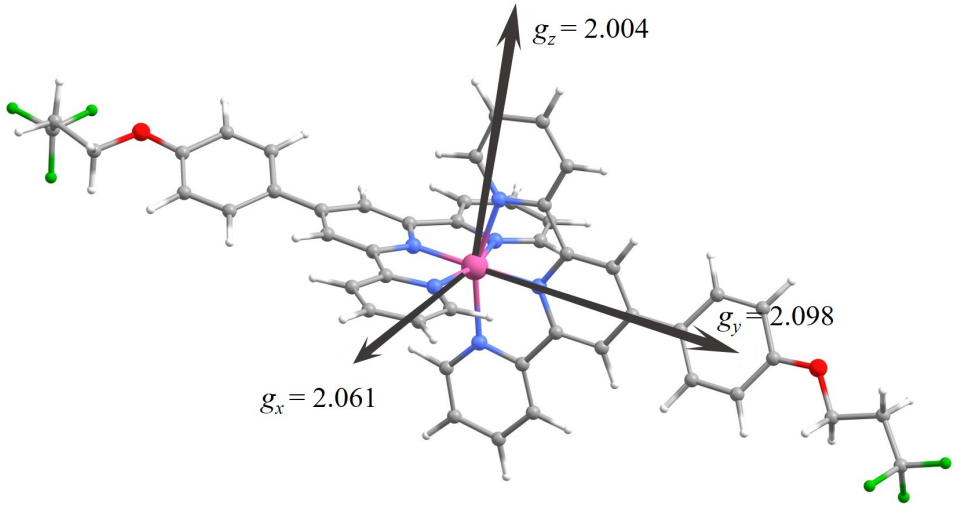

Figure S 29: Orientation of the **g**-matrix of $[\mathbf{5}_{tr1}]^{2+}$ calculated with the TPSSh functional and def2-TZVP basis set on all atoms. The lower *g*-value points near the direction of the longest Co-N bonds, along which the $3d_{z^2}$ orbital is situated. The orientation of the molecule is similar to that from Figure S22.

Table S 4: Components of the **g**- and **A**-matrices of the truncated monomer $[\mathbf{5}_{tr1}]^{2+}$ without counterions, calculated at two slightly different theory levels.

	$[\mathbf{5}_{tr1}]^{2+}$		$[\mathbf{5}_{tr1}]^{2+}$	
Theory Level	TPSSh/def2-TZVP		TPSS0/def2-TZVP/def2-QZVP(Co)	
	Eigenvalues	Eigenvectors	Eigenvalues	Eigenvectors
g_x	2.061	[0.8920; 0.3111;-0.3280]	2.075	[0.8939; 0.3092;-0.3244]
g_y	2.098	[-0.3640;0.9216;-0.1346]	2.121	[-0.3632;0.9238;-0.1204]
g_z	2.004	[0.2604; 0.2394; 0.9353]	2.003	[0.2611; 0.2250; 0.9387]

A_x	162	[0.8929; 0.3100;-0.3266]	-165	[-0.8942; -0.3083;0.3245]
A_y	~0	[-0.3677;0.9206;-0.1313]	-342	[-0.3634;0.9233;-0.1243]
A_z	567	[0.2600; 0.2374; 0.9360]	250	[-0.2613;-0.2290;-0.9377]

[a] $H_{HDVV} = -2J\, S_A \cdot S_B$ convention, calculated as $-(E_{HS} - E_{BS})/(\langle S^2\rangle_{HS} - \langle S^2\rangle_{BS})$.[1, 2]

Coordinates from DFT Optimizations

$[5_{tr1}]^{2+}$

Co	6.376490000000	9.755647000000	21.203027000000
F	7.279305000000	15.862749000000	10.201632000000
F	9.328577000000	15.238331000000	9.854163000000
N	7.065889000000	8.099104000000	20.320681000000
N	4.312214000000	9.036932000000	21.077878000000
N	6.587887000000	10.423296000000	19.470905000000
N	5.779776000000	11.633924000000	21.528499000000
O	6.953718000000	13.366253000000	11.564846000000
N	8.316286000000	10.147425000000	22.134712000000
N	6.106191000000	9.041378000000	22.986703000000
O	4.800474000000	5.761009000000	30.679997000000
C	7.317134000000	8.249031000000	18.987042000000
C	3.469014000000	9.084314000000	20.039580000000
H	3.852257000000	9.539622000000	19.122289000000
C	4.699655000000	7.951460000000	24.592857000000
H	3.743623000000	7.483397000000	24.820768000000
C	3.898928000000	8.485086000000	22.241409000000
C	6.333584000000	12.212583000000	17.907602000000
H	6.075201000000	13.254028000000	17.719177000000
C	7.134522000000	10.059569000000	17.173063000000
H	7.456755000000	9.373014000000	16.390741000000
C	8.036859000000	5.953748000000	18.813907000000
H	8.415310000000	5.116039000000	18.225236000000
C	7.026062000000	9.604079000000	18.484913000000
C	7.295437000000	6.906383000000	20.892924000000
H	7.082315000000	6.831654000000	21.960529000000
F	7.060238000000	4.902233000000	34.133213000000
C	6.856100000000	11.892668000000	15.465549000000
C	7.746554000000	11.332129000000	14.524962000000
H	8.429827000000	10.534116000000	14.824485000000
C	9.392655000000	10.739495000000	21.603734000000
H	9.307901000000	11.057134000000	20.560857000000
C	7.822854000000	11.800255000000	13.216258000000
H	8.541338000000	11.353413000000	12.529395000000
C	5.796600000000	12.418992000000	20.411518000000
C	7.802660000000	7.191300000000	18.211545000000
H	7.996747000000	7.334972000000	17.148217000000
C	7.779202000000	5.809297000000	20.179247000000
H	7.948581000000	4.861407000000	20.692031000000
C	5.716930000000	7.973677000000	25.574480000000
C	4.914997000000	8.484867000000	23.323036000000
F	6.862489000000	3.027456000000	33.054916000000
C	6.780657000000	11.391507000000	16.842253000000
C	6.029095000000	12.957823000000	15.028061000000
H	5.302121000000	13.405558000000	15.709138000000
C	8.356290000000	9.730238000000	23.420778000000
C	2.166128000000	8.585189000000	20.100013000000

H	1.513628000000	8.644936000000	19.227540000000
C	6.244953000000	11.705740000000	19.201961000000
C	10.570362000000	10.952144000000	22.323647000000
H	11.423791000000	11.439800000000	21.849909000000
C	2.605438000000	7.962294000000	22.383185000000
H	2.279825000000	7.519837000000	23.324588000000
C	7.108189000000	9.085825000000	23.901561000000
C	5.387750000000	12.172731000000	22.694156000000
H	5.391049000000	11.508600000000	23.560027000000
C	5.416956000000	13.764108000000	20.458392000000
H	5.442299000000	14.373403000000	19.554445000000
C	7.850629000000	12.882448000000	10.557532000000
H	7.644214000000	11.816705000000	10.361767000000
H	8.891342000000	12.988176000000	10.906263000000
C	6.979967000000	12.851408000000	12.799652000000
C	9.500929000000	9.908169000000	24.211184000000
H	9.523492000000	9.573142000000	25.248186000000
C	5.509250000000	7.410670000000	26.913379000000
C	6.080086000000	13.423850000000	13.726301000000
H	5.430174000000	14.230639000000	13.384723000000
C	6.940661000000	8.565298000000	25.184707000000
H	7.755800000000	8.639623000000	25.902731000000
C	1.729214000000	8.013952000000	21.297721000000
H	0.717994000000	7.612519000000	21.387916000000
F	8.033969000000	15.719013000000	8.173971000000
C	6.402242000000	6.397308000000	28.958242000000
H	7.265140000000	6.040876000000	29.520291000000
C	8.065249000000	15.141920000000	9.383663000000
C	5.839222000000	5.234523000000	31.513858000000
H	6.398715000000	4.456546000000	30.968694000000
H	6.535867000000	6.040482000000	31.798248000000
C	10.621082000000	10.527558000000	23.653667000000
H	11.521693000000	10.676456000000	24.252577000000
C	5.010637000000	14.316973000000	21.674401000000
H	4.712254000000	15.365447000000	21.731292000000
C	6.591498000000	6.957628000000	27.698100000000
H	7.610045000000	7.002704000000	27.306199000000
C	4.208602000000	7.289322000000	27.463913000000
H	3.341156000000	7.657574000000	26.912281000000
C	5.098785000000	6.285738000000	29.484296000000
C	7.629083000000	13.689010000000	9.289921000000
H	6.569798000000	13.667062000000	8.995613000000
H	8.213578000000	13.229871000000	8.479059000000
F	5.557402000000	3.453990000000	34.739084000000
C	4.995428000000	13.506583000000	22.812290000000
H	4.685598000000	13.896089000000	23.783096000000
C	4.003796000000	6.748638000000	28.721119000000
H	3.003682000000	6.671475000000	29.149949000000
C	6.164435000000	4.000205000000	33.680388000000
C	5.162973000000	4.641866000000	32.740656000000
H	4.440262000000	3.870568000000	32.437970000000
H	4.620550000000	5.419869000000	33.296760000000

$[5_{tr1}(BF_4)_2]_2$

Co	5.916458294786	6.831897363971	12.864703214608
F	5.156841287518	1.744007342820	24.583106905851

S 18

F	3.957266315432	2.970115262171	25.908130224116
N	5.169309232682	8.459832852287	13.705596026372
N	7.929278684085	7.513583496133	13.150935188592
N	5.647780188505	6.144666512594	14.585519893668
N	6.533046629307	4.961030359248	12.544917169620
O	5.834479213725	3.603022364698	22.631523966160
N	4.038378074982	6.460763662980	11.839608035885
N	6.262514285947	7.644700389004	11.144569703377
O	8.091516490970	11.239537969191	3.708009543367
C	4.901832358757	8.329224498752	15.030618286284
C	8.642613849155	7.472526750092	14.249985004572
H	8.311545745217	6.977788356457	14.989531906317
C	7.751774642744	8.847569489465	9.699713667897
H	8.604425772981	9.239603575082	9.549064842766
C	8.375536504053	8.216083757030	12.096395000203
C	5.950734692735	4.400901532954	16.167330176252
H	6.191716720157	3.500602224863	16.352217298571
C	5.147425636727	6.551067760522	16.869215533186
H	4.878901521026	7.156751339473	17.550558229313
C	4.126177576604	10.589822609705	15.136756954647
H	3.744924419080	11.310818673809	15.626364974853
C	5.185079243879	6.985350299345	15.547617050075
C	4.977764531393	9.661099604038	13.113273114604
H	5.212982231042	9.773319577347	12.199109891766
F	5.941669357283	12.695134715293	0.431403285411
C	5.473696219725	4.767396466180	18.629064326132
C	4.723399611344	5.450606628819	19.618551696947
H	4.152990458633	6.165576422411	19.361764732629
C	2.966965070008	5.827526353851	12.284705899323
H	2.986192196173	5.453018618720	13.157783271372
C	4.807855241930	5.097416269987	20.946998792014
H	4.318500168449	5.580793228086	21.600950744556
C	6.555874277475	4.189172423857	13.688477142367
C	4.365766280329	9.378833813535	15.770166246383
H	4.167811125846	9.267768504983	16.691176493646
C	4.435736212901	10.748854660815	13.828854107919
H	4.289031345806	11.582025718162	13.397450822507
C	6.776185583196	8.879220639082	8.689683636276
C	7.471762618144	8.242255805411	10.928868589848
F	6.260750538176	14.310097952527	1.797511396112
C	5.497864273864	5.239951220360	17.218446587840
C	6.219859424614	3.671359256279	19.015957454775
H	6.675548770691	3.159649089914	18.358582254610
C	4.054853479452	7.059948416137	10.607028807956
C	9.867287698161	8.126739587017	14.376666862919
H	10.384691811725	8.064245870620	15.170995251835
C	6.041993426034	4.881506131446	14.883393237953
C	1.821135985217	5.689868301005	11.528039055219
H	1.079491954034	5.185672451576	11.843031812686
C	9.605195731922	8.935168432910	12.127210049767
H	9.922321602880	9.429861846479	11.380815065243
C	5.333642581473	7.669076409802	10.209863819732
C	6.934810697002	4.415654465479	11.411629056452
H	6.895033501549	4.934456136158	10.617299609182
C	7.056349481666	2.887345061123	13.678205282787
H	7.100665430384	2.382488269310	14.482805002106

S 19

C	5.312488191767	4.450954292228	23.682639848571
H	5.577628218960	5.391980668934	23.528566717461
H	4.324880458540	4.400596197681	23.706605757001
C	5.617720274876	4.019098560269	21.327043837878
C	2.891685372920	7.022609669447	9.826394997067
H	2.861607467264	7.477858740053	8.990980757362
C	7.131795340411	9.491764471890	7.378355425214
C	6.315373272172	3.305470231003	20.354675351068
H	6.857195740714	2.567139378576	20.604615820138
C	5.558853539343	8.282648434004	8.970437567379
H	4.869908153679	8.287778807433	8.316485614837
C	10.293109751127	8.866273788508	13.298160236923
H	11.106342997263	9.350835574468	13.373483855723
F	5.868283056391	2.164177782767	26.616853080284
C	6.376196375995	10.673839023174	5.389110411536
H	5.668357245833	11.059663742952	4.885807284125
C	5.245399629316	2.699046333080	25.545204062258
C	7.057226328368	11.907339019516	2.947918393285
H	6.589917308257	12.579936003249	3.506003007866
H	6.393498355328	11.256168951773	2.608959198210
C	1.794418355092	6.323868683727	10.271492860505
H	1.014673032804	6.269234307832	9.730527659107
C	7.485267750716	2.346580947079	12.486711905648
H	7.823832708740	1.459894194541	12.462744938863
C	6.118945323229	10.078427832980	6.604570755459
H	5.226753539770	10.066158858462	6.933257561776
C	8.394610697993	9.551358826140	6.902443570567
H	9.102489516449	9.186185777682	7.422865581982
C	7.664256663418	10.703411564557	4.906350474109
C	5.897044369052	3.943215071939	24.976848117273
H	6.864653435684	3.752417039749	24.833046845744
H	5.842326383151	4.664319617379	25.651342201444
F	7.465085988794	14.144008264447	0.026864212223
C	7.421733671847	3.095612292658	11.332881131674
H	7.699470763453	2.729858207580	10.500889610415
C	8.689796880207	10.140505616060	5.663016259859
H	9.579951860436	10.152241709089	5.337752171988
C	6.896488738984	13.436746995841	1.016878114401
C	7.796331367110	12.577010182240	1.797511396112
H	8.540911802847	13.120621269883	2.157013251993
H	8.181379783863	11.881982962453	1.205187955166
Co	6.626381324954	10.047245534406	21.373607731549
F	7.385998332222	15.135135026379	9.655203511130
F	8.585573833485	13.909027107028	8.330180722041
N	7.373529328704	8.419309516913	20.532714390608
N	4.613561464832	9.365558873067	21.087375757565
N	6.895058372880	10.734476914960	19.652790523312
N	6.009792461255	11.918112009952	21.693393776538
O	6.708359347660	13.276120004502	11.606786979997
N	8.504460486404	10.418378706219	22.398702910272
N	6.280325333793	9.234441451018	23.093740713604
O	4.451323128770	5.639605458363	30.530301402790
C	7.641006731806	8.549918399625	19.207692659874
C	3.900226299762	9.406615619108	19.988325412408
H	4.231293345345	9.901354012743	19.248778510663
C	4.791064447819	8.031573408912	24.538596749083

S 20

H	3.938413317582	7.639539323294	24.689246103392
C	4.167303115687	8.663059670524	22.141915945954
C	6.592105456182	12.478241894600	18.070980240728
H	6.351122370405	13.378541202691	17.886093118409
C	7.395414512190	10.328074608678	17.369095412972
H	7.663938627891	9.722390500549	16.687752187667
C	8.416662572313	6.289320288672	19.101553462333
H	8.797915729837	5.568323166214	18.611945442127
C	7.357760375861	9.893792599032	18.690693366905
C	7.565075617524	7.218042765162	21.125037831554
H	7.329857388698	7.105822791852	22.039200525214
F	6.601170262457	4.184008183084	33.806907660746
C	7.069142341661	12.111745903019	15.609246090848
C	7.819440537573	11.428536798735	14.619759249210
H	8.389849690284	10.713565946788	14.876546213528
C	9.575874549732	11.051616015349	21.953604517657
H	9.556647952744	11.426123750480	21.080527674786
C	7.734984377810	11.781726099212	13.291312154144
H	8.224339451291	11.298348611936	12.637360201602
C	5.986965342265	12.689971003697	20.549833803790
C	8.177073868588	7.500308555664	18.468144170597
H	8.375027435539	7.611373335039	17.547134452512
C	8.107103406839	6.130287708384	20.409456309062
H	8.253807744756	5.297116651038	20.840859594473
C	5.766653507366	7.999922788472	25.548626780704
C	5.071076472418	8.636886563789	23.309441827132
F	6.282089610742	2.569044416673	32.440799550045
C	7.044974287522	11.639191678017	17.019864358317
C	6.322980724304	13.207783112921	15.222352962205
H	5.867290319872	13.719493808463	15.879728162370
C	8.487986669465	9.819195011417	23.631281609024
C	2.675551392402	8.752403840537	19.861643554061
H	2.158148337192	8.814896498580	19.067315694322
C	6.500846722883	11.997635708577	19.354917708204
C	10.721703634523	11.189274068195	22.710271890939
H	11.463347665706	11.693469917624	22.395278604294
C	2.937644416995	7.943974465467	22.111100896391
H	2.620516958506	7.449281581075	22.857495880915
C	7.209197567445	9.210066488575	24.028446597248
C	5.608029451915	12.463488962075	22.826681889705
H	5.647805589013	11.944685703865	23.621010807798
C	5.486490667251	13.991797837253	20.560105663371
H	5.442174189356	14.496655158244	19.755505414875
C	7.230351427973	12.428188076972	10.555670568409
H	6.965211400780	11.487161700265	10.709743699519
H	8.217958632023	12.478546700695	10.531704659979
C	6.925118286509	12.860043808931	12.911267108279
C	9.651153717643	9.856532699752	24.411915949090
H	9.681232681653	9.401284687501	25.247330188795
C	5.411043220975	7.387378426487	26.859954991766
C	6.227466347568	13.573673196551	13.883635065912
H	5.685644408203	14.312002990623	13.633695126019
C	6.983985551220	8.596493406018	25.267872849602
H	7.672930407706	8.591363561766	25.921824802143
C	2.249730397790	8.012868580691	20.940150709235
H	1.436497151654	7.528306794732	20.864826561257

S 21

F	6.670772946018	14.718214263919	7.614948985711
C	6.166642714568	6.205303346025	28.849200005445
H	6.874482373907	5.819478626248	29.352503132855
C	7.297440519602	14.180096036120	8.693106883900
C	5.485612233018	4.971804408038	31.290392552873
H	5.952922311483	4.299207424305	30.732307409114
H	6.149341264412	5.622973417427	31.629351218770
C	10.748420735471	10.555274743827	23.966818085652
H	11.528166057759	10.609908590545	24.507782757874
C	5.057572398201	14.532561951297	21.751598511333
H	4.719006381823	15.419248174658	21.775565478117
C	6.423894296511	6.800715594574	27.633740190698
H	7.316085550793	6.812983510737	27.305052855204
C	4.148229450924	7.327783543059	27.335866846413
H	3.440350103291	7.692956591517	26.815444834998
C	4.878583485499	6.175731333820	29.331960472049
C	6.645795250688	12.935926768083	9.261462828884
H	5.678186184056	13.126725858628	9.405263571236
H	6.700512707412	12.214822751820	8.586968744713
F	5.077753630946	2.735134633930	34.211446733935
C	5.121105418716	13.783531134896	22.905429814484
H	4.843369385465	14.149284161619	23.737420806565
C	3.853043268710	6.738636753139	28.575294157122
H	2.962887230127	6.726900660111	28.900558244992
C	5.646351409933	3.442395373359	33.221432302580
C	4.746508252630	4.302133245314	32.440799550045
H	4.001928346070	3.758522157671	32.081297694165
H	4.361460365054	4.997160465101	33.033122461814
F	2.220855312021	4.441766187654	17.567677113318
F	2.052806080588	6.668201673765	17.122579249880
F	0.502934290868	5.233329625443	16.297436340578
F	2.612661322244	5.237729205091	15.448325935314
B	1.857375101583	5.362369497612	16.588461072906
F	10.321984836896	12.437376710723	16.670633303662
F	10.490033009975	10.210940695434	17.115731167100
F	12.039905858050	11.645812743756	17.940874605580
F	9.930178826673	11.641412634931	18.789984481667
B	10.685465047335	11.516772871588	17.649849344074
F	10.296524531915	11.121399677529	9.792156699880
F	11.723722980949	10.009421532179	8.432895613604
F	12.107750085612	12.172271080051	8.953318683373
F	12.341431054530	10.562222841106	10.524856577200
B	11.668040834101	10.969171787487	9.436078620800
F	2.246314029471	5.757742691670	24.446153717100
F	0.819116109613	6.869721366198	25.805414803377
F	0.435089004951	4.706871289149	25.284991733607
F	0.201409094387	6.316920586448	23.713453839781
B	0.874799314817	5.909970581713	24.802231796180

$[5_{tr2}]_2^{4+}$

Co	5.916458000000	6.831897000000	12.864702000000
N	5.169309000000	8.459832000000	13.705595000000
N	7.929278000000	7.513583000000	13.150934000000
N	5.647780000000	6.144666000000	14.585519000000
N	6.533046000000	4.961030000000	12.544916000000
O	5.834479000000	3.603022000000	22.631522000000

S 22

N	4.038378000000	6.460763000000	11.839607000000
N	6.262514000000	7.644700000000	11.144569000000
O	8.091516000000	11.239537000000	3.708009000000
C	4.901832000000	8.329224000000	15.030617000000
C	8.642613000000	7.472526000000	14.249984000000
H	8.311545000000	6.977788000000	14.989531000000
C	7.751774000000	8.847569000000	9.699713000000
H	8.604425000000	9.239603000000	9.549064000000
C	8.375536000000	8.216083000000	12.096394000000
C	5.950734000000	4.400901000000	16.167329000000
H	6.191716000000	3.500602000000	16.352216000000
C	5.147425000000	6.551067000000	16.869214000000
H	4.878901000000	7.156751000000	17.550557000000
C	4.126177000000	10.589822000000	15.136756000000
H	3.744924000000	11.310818000000	15.626364000000
C	5.185079000000	6.985350000000	15.547616000000
C	4.977764000000	9.661099000000	13.113272000000
H	5.212982000000	9.773319000000	12.199109000000
C	5.473696000000	4.767396000000	18.629063000000
C	4.723399000000	5.450606000000	19.618550000000
H	4.152990000000	6.165576000000	19.361763000000
C	2.966965000000	5.827526000000	12.284705000000
H	2.986192000000	5.453018000000	13.157782000000
C	4.807855000000	5.097416000000	20.946997000000
H	4.318500000000	5.580793000000	21.600949000000
C	6.555874000000	4.189172000000	13.688476000000
C	4.365766000000	9.378833000000	15.770165000000
H	4.167811000000	9.267768000000	16.691175000000
C	4.435736000000	10.748854000000	13.828853000000
H	4.289031000000	11.582025000000	13.397450000000
C	6.776185000000	8.879220000000	8.689683000000
C	7.471762000000	8.242255000000	10.928868000000
C	5.497864000000	5.239951000000	17.218445000000
C	6.219859000000	3.671359000000	19.015956000000
H	6.675548000000	3.159649000000	18.358581000000
C	4.054853000000	7.059948000000	10.607028000000
C	9.867287000000	8.126739000000	14.376666000000
H	10.384691000000	8.064245000000	15.170994000000
C	6.041993000000	4.881506000000	14.883392000000
C	1.821136000000	5.689868000000	11.528038000000
H	1.079492000000	5.185672000000	11.843031000000
C	9.605195000000	8.935168000000	12.127209000000
H	9.922321000000	9.429861000000	11.380814000000
C	5.333642000000	7.669076000000	10.209863000000
C	6.934810000000	4.415654000000	11.411628000000
H	6.895033000000	4.934456000000	10.617299000000
C	7.056349000000	2.887345000000	13.678204000000
H	7.100665000000	2.382488000000	14.482804000000
C	5.312488000000	4.450954000000	23.682638000000
H	5.577628000000	5.391980000000	23.528565000000
H	4.324880000000	4.400596000000	23.706604000000
C	5.617720000000	4.019098000000	21.327042000000
C	2.891685000000	7.022609000000	9.826394000000
H	2.861607000000	7.477858000000	8.990980000000
C	7.131795000000	9.491764000000	7.378355000000
C	6.315373000000	3.305470000000	20.354674000000

S 23

H	6.857195000000	2.567139000000	20.604614000000
C	5.558853000000	8.282648000000	8.970437000000
H	4.869908000000	8.287778000000	8.316485000000
C	10.293109000000	8.866273000000	13.298159000000
H	11.106342000000	9.350835000000	13.373483000000
C	6.376196000000	10.673838000000	5.389110000000
H	5.668357000000	11.059663000000	4.885807000000
C	7.057226000000	11.907338000000	2.947918000000
H	6.589917000000	12.579935000000	3.506003000000
H	6.393498000000	11.256168000000	2.608959000000
C	1.794418000000	6.323868000000	10.271492000000
H	1.014673000000	6.269234000000	9.730527000000
C	7.485267000000	2.346581000000	12.486711000000
H	7.823832000000	1.459894000000	12.462744000000
C	6.118945000000	10.078427000000	6.604570000000
H	5.226753000000	10.066158000000	6.933257000000
C	8.394610000000	9.551358000000	6.902443000000
H	9.102489000000	9.186185000000	7.422865000000
C	7.664256000000	10.703411000000	4.906350000000
H	5.666507998058	4.160018261603	24.559078093274
C	7.421733000000	3.095612000000	11.332880000000
H	7.699470000000	2.729858000000	10.500889000000
C	8.689796000000	10.140505000000	5.663016000000
H	9.579951000000	10.152241000000	5.337752000000
H	7.455403111614	12.373824740498	2.172053251009
Co	6.626381000000	10.047245000000	21.373606000000
N	7.373529000000	8.419309000000	20.532713000000
N	4.613561000000	9.365558000000	21.087374000000
N	6.895058000000	10.734476000000	19.652789000000
N	6.009792000000	11.918111000000	21.693392000000
O	6.708359000000	13.276119000000	11.606786000000
N	8.504460000000	10.418378000000	22.398701000000
N	6.280325000000	9.234441000000	23.093739000000
O	4.451323000000	5.639605000000	30.530299000000
C	7.641006000000	8.549918000000	19.207691000000
C	3.900226000000	9.406615000000	19.988324000000
H	4.231293000000	9.901353000000	19.248777000000
C	4.791064000000	8.031573000000	24.538595000000
H	3.938413000000	7.639539000000	24.689244000000
C	4.167303000000	8.663059000000	22.141914000000
C	6.592105000000	12.478241000000	18.070979000000
H	6.351122000000	13.378540000000	17.886092000000
C	7.395414000000	10.328074000000	17.369094000000
H	7.663938000000	9.722390000000	16.687751000000
C	8.416662000000	6.289320000000	19.101552000000
H	8.797915000000	5.568323000000	18.611944000000
C	7.357760000000	9.893792000000	18.690692000000
C	7.565075000000	7.218042000000	21.125036000000
H	7.329857000000	7.105822000000	22.039199000000
C	7.069142000000	12.111745000000	15.609245000000
C	7.819440000000	11.428536000000	14.619758000000
H	8.389849000000	10.713565000000	14.876545000000
C	9.575874000000	11.051615000000	21.953603000000
H	9.556647000000	11.426123000000	21.080526000000
C	7.734984000000	11.781725000000	13.291311000000
H	8.224339000000	11.298348000000	12.637359000000

S 24

C	5.986965000000	12.689970000000	20.549832000000
C	8.177073000000	7.500308000000	18.468143000000
H	8.375027000000	7.611373000000	17.547133000000
C	8.107103000000	6.130287000000	20.409455000000
H	8.253807000000	5.297116000000	20.840858000000
C	5.766653000000	7.999922000000	25.548625000000
C	5.071076000000	8.636886000000	23.309440000000
C	7.044974000000	11.639191000000	17.019863000000
C	6.322980000000	13.207782000000	15.222352000000
H	5.867290000000	13.719493000000	15.879727000000
C	8.487986000000	9.819194000000	23.631280000000
C	2.675551000000	8.752403000000	19.861642000000
H	2.158148000000	8.814896000000	19.067314000000
C	6.500846000000	11.997635000000	19.354916000000
C	10.721703000000	11.189273000000	22.710270000000
H	11.463347000000	11.693469000000	22.395277000000
C	2.937644000000	7.943974000000	22.111099000000
H	2.620517000000	7.449281000000	22.857494000000
C	7.209197000000	9.210066000000	24.028445000000
C	5.608029000000	12.463488000000	22.826680000000
H	5.647805000000	11.944685000000	23.621009000000
C	5.486490000000	13.991797000000	20.560104000000
H	5.442174000000	14.496654000000	19.755504000000
C	7.230351000000	12.428187000000	10.555670000000
H	6.965211000000	11.487161000000	10.709743000000
H	8.217958000000	12.478546000000	10.531704000000
C	6.925118000000	12.860043000000	12.911266000000
C	9.651153000000	9.856532000000	24.411914000000
H	9.681232000000	9.401284000000	25.247328000000
C	5.411043000000	7.387378000000	26.859953000000
C	6.227466000000	13.573672000000	13.883634000000
H	5.685644000000	14.312002000000	13.633694000000
C	6.983985000000	8.596493000000	25.267871000000
H	7.672930000000	8.591363000000	25.921823000000
C	2.249730000000	8.012868000000	20.940149000000
H	1.436497000000	7.528306000000	20.864825000000
C	6.166642000000	6.205303000000	28.849198000000
H	6.874482000000	5.819478000000	29.352501000000
C	5.485612000000	4.971804000000	31.290390000000
H	5.952922000000	4.299207000000	30.732305000000
H	6.149341000000	5.622973000000	31.629349000000
C	10.748420000000	10.555274000000	23.966816000000
H	11.528165000000	10.609908000000	24.507781000000
C	5.057572000000	14.532561000000	21.751597000000
H	4.719006000000	15.419247000000	21.775564000000
C	6.423894000000	6.800715000000	27.633738000000
H	7.316085000000	6.812983000000	27.305051000000
C	4.148229000000	7.327783000000	27.335865000000
H	3.440350000000	7.692956000000	26.815443000000
C	4.878583000000	6.175731000000	29.331958000000
H	6.876331207254	12.719122503089	9.679229745683
C	5.121105000000	13.783530000000	22.905428000000
H	4.843369000000	14.149283000000	23.737419000000
C	3.853043000000	6.738636000000	28.575292000000
H	2.962887000000	6.726900000000	28.900556000000
H	5.087434469696	4.505317466377	32.066254658500

S 25

6. X-Ray Crystallography

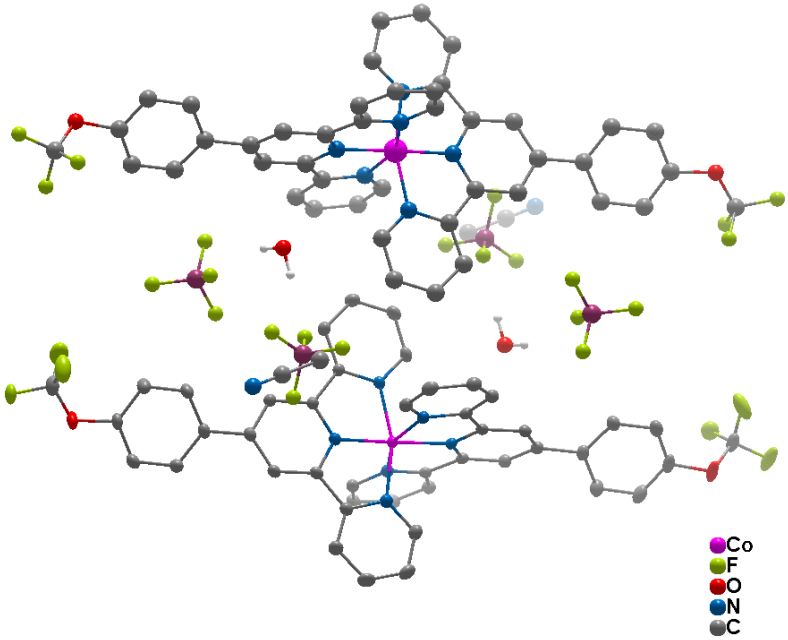

Figure S 30: Perspective view of cobalt complex **1.** Ellipsoids are at a probability level of 50%.

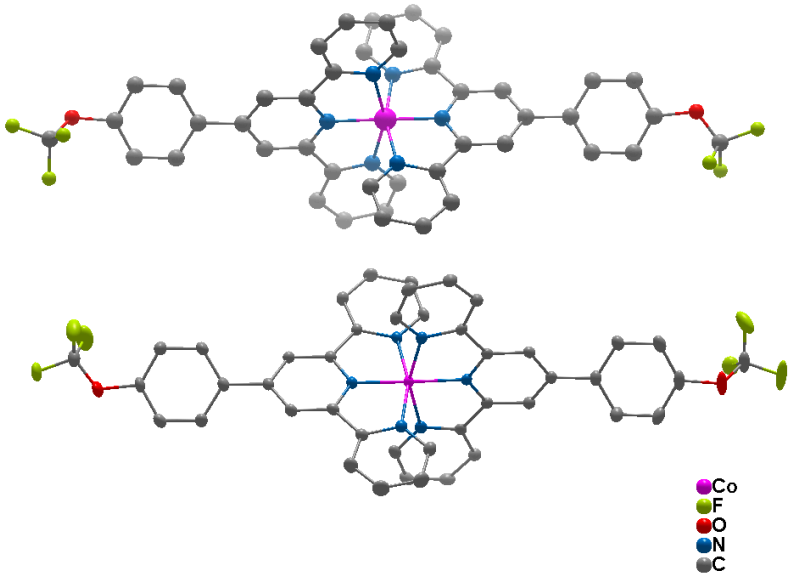

Figure S 31: Perspective view of cobalt complex **1.** Ellipsoids are at a probability level of 50%. H atoms, anions and solvent molecules are omitted for clarity.

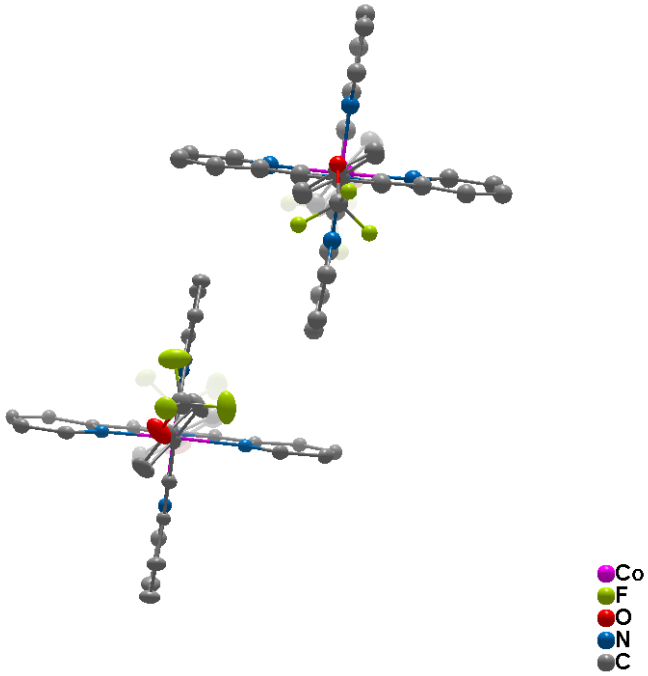

Figure S 32: Perspective view of cobalt complex **1.** Ellipsoids are at a probability level of 50%. H atoms, anions and solvent molecules are omitted for clarity.

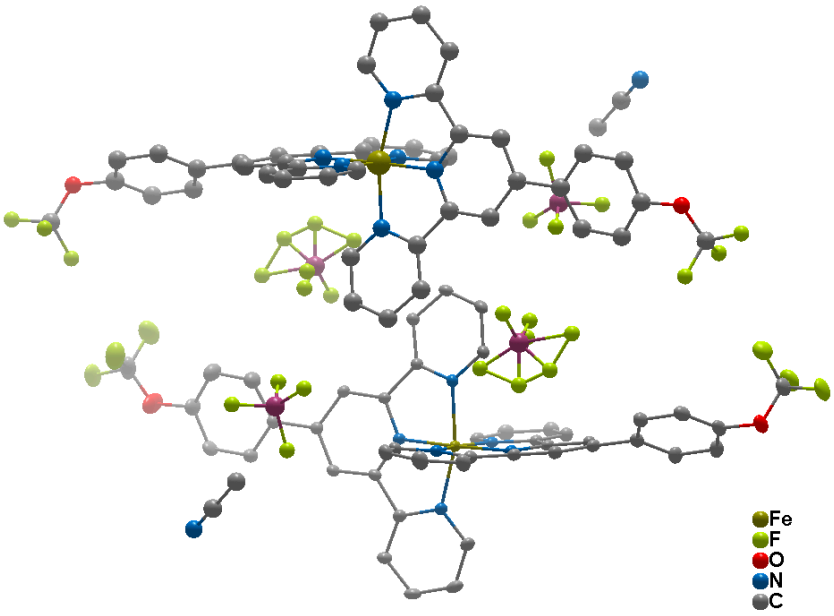

Figure S 33: Perspective view of iron complex **2.** Ellipsoids are at a probability level of 50%.

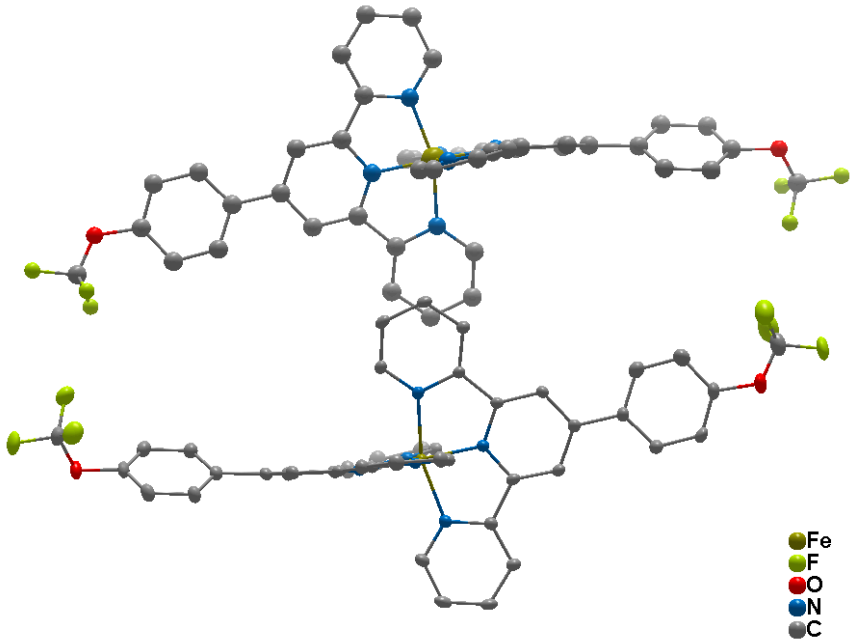

Figure S 34: Perspective view of iron complex **2.** Ellipsoids are at a probability level of 50%. H atoms, anions and solvent molecules are omitted for clarity.

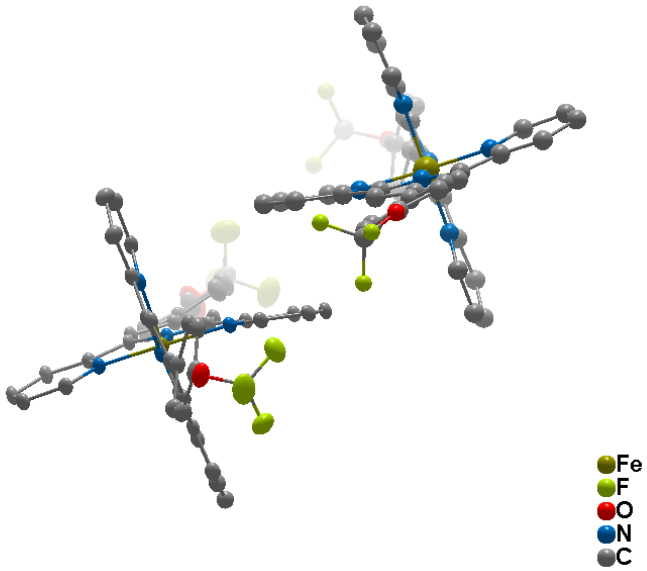

Figure S 35: Perspective view of iron complex **2.** Ellipsoids are at a probability level of 50%. H atoms, anions and solvent molecules are omitted for clarity.

Table S 5: Crystal Parameters for Complexes **1**,**2** and **5**.

	1	**2**	**5**
Chemical formula	$C_{46}H_{33}B_2CoF_{14}N_7O_3$	$C_{46}H_{31}B_2F_{14}FeN_7O_2$	$C_{31}H_{18}BCo_{0.5}F_{21}N_3O$
M_r	1078.34	1057.25	887.765
Crystal system	Triclinic	Triclinic	Triclinic
Space group	*P*-1	*P*-1	*P*-1
a (Å)	11.656(1)	11.7510(5)	8.8478(11)
b (Å)	13.4809(14)	13.4138(6)	11.5495(14)
c (Å)	15.300(1)	14.7100(6)	34.726(4)
α(°)	101.055(4)	89.523(2)	80.562(4)
β (°)	97.212(4)	84.030(2)	89.154(4)
γ (°)	100.905(4)	70.980(2)	74.006(4)
V (Å^3)	2284.2(4)	2179.39(16)	3363.3(7)
Z	2	2	4
Densitiy (g cm^{-3})	1.568	1.611	1.753
F(000)	1090	1068	1764.813
Radiation Type	MoK_α	MoK_α	MoK_α
μ (mm^{-1})	0.484	0.457	0.422
Crystal size	0.28 x 0.18 x 0.09	0.33 x 0.17 x .0.05	0.39x0.28x0.05
Meas. Refl.	64290	66631	34808
Indep. Refl.	8444	8640	12111
Obsvd. [$I > 2\sigma(I)$] refl.	7614	7991	8944
R_{int}	0.0398	0.0348	0.0618
R [$F^2 > 2\sigma(F^2)$], wR(F^2), S	0.0459, 0.1094, 1.076	0.0488, 0.1347 1.047	0.1528, 0.3802, 1.0873
$\Delta\rho_{max}$, $\Delta\rho_{min}$ (e Å^{-3})	1.233, -0.517	1.491, -0.555	1.2127, -1.4234

7. NMR Spectra

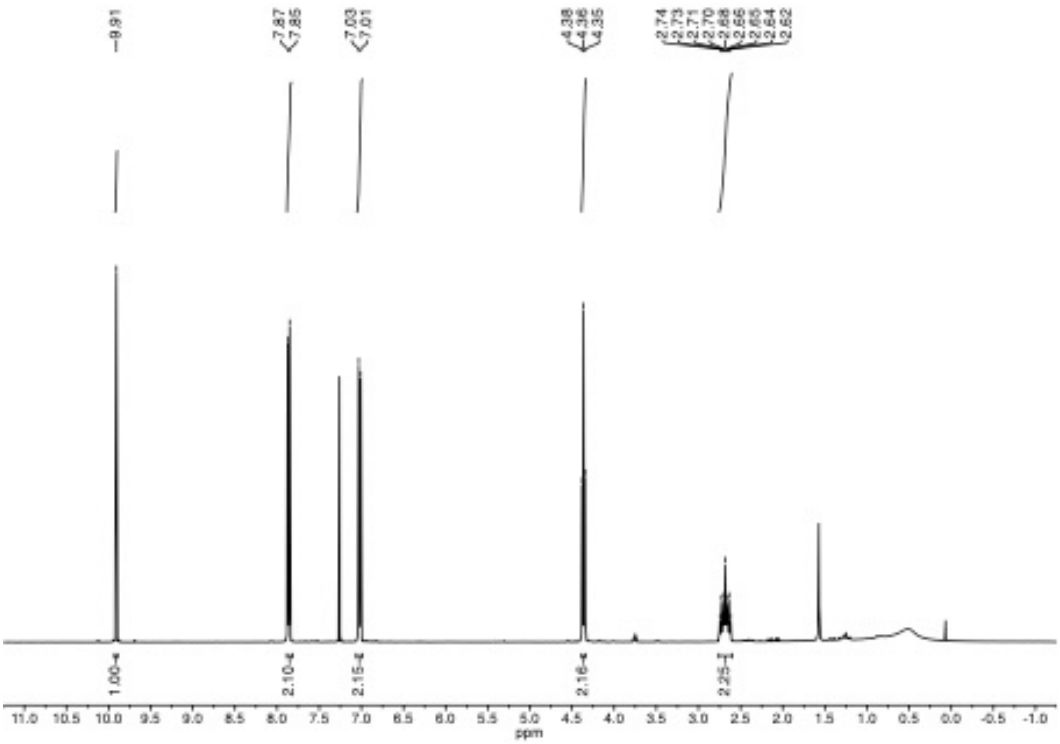

Figure S 36: ^{1}H NMR Spectrum of BenzaldehydeR$_f$Oct.

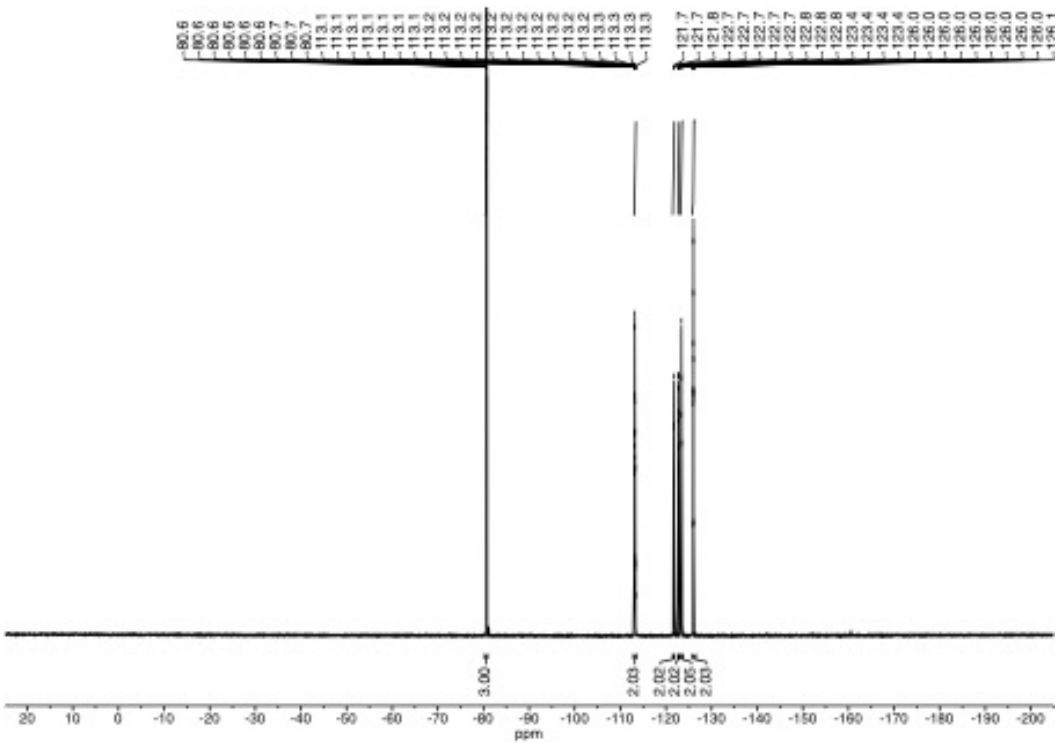

Figure S 37: ^{19}F NMR spectrum of BenzaldehydeR$_f$Oct.

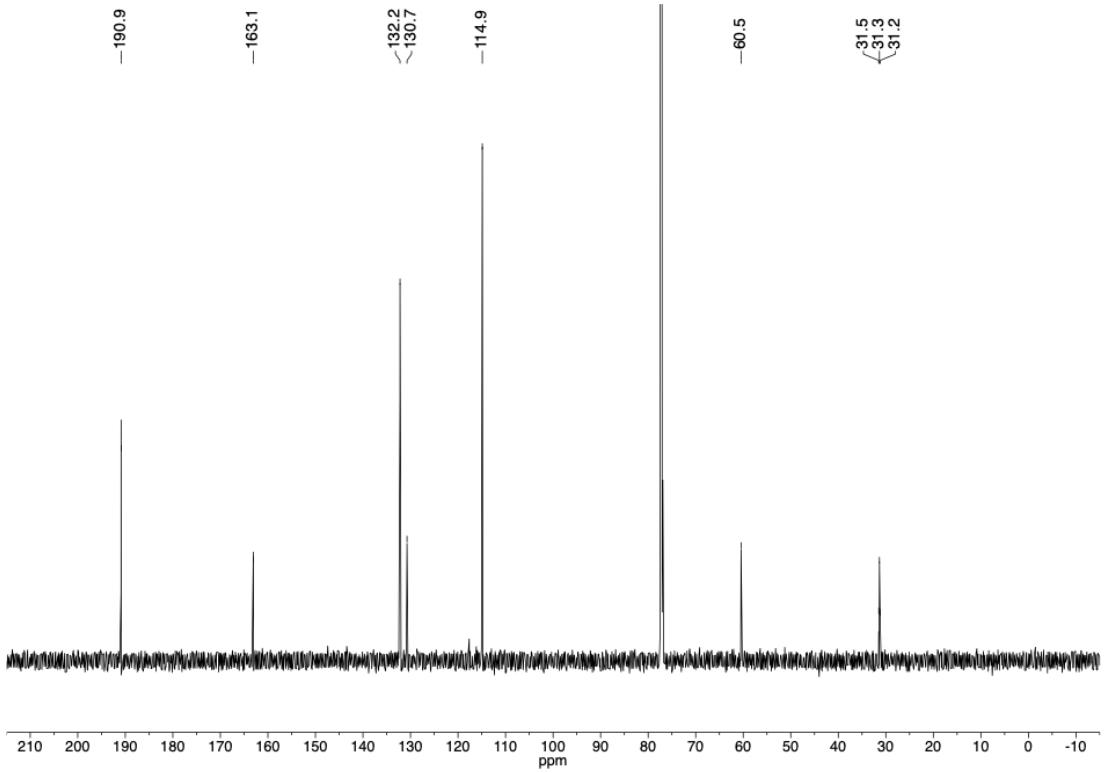

Figure S 38: ^{13}C NMR spectrum of BenzaldehydeR_fOct.

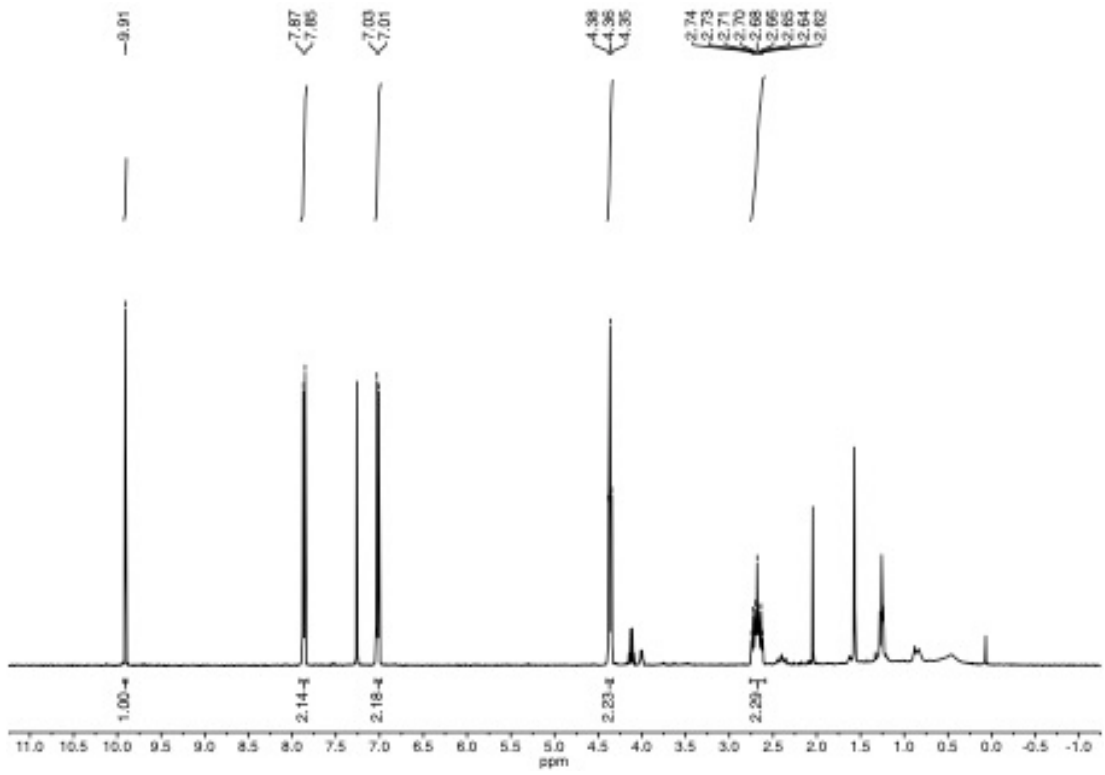

Figure S 39: ^{1}H NMR spectrum of BenzaldehydeR_fDec.

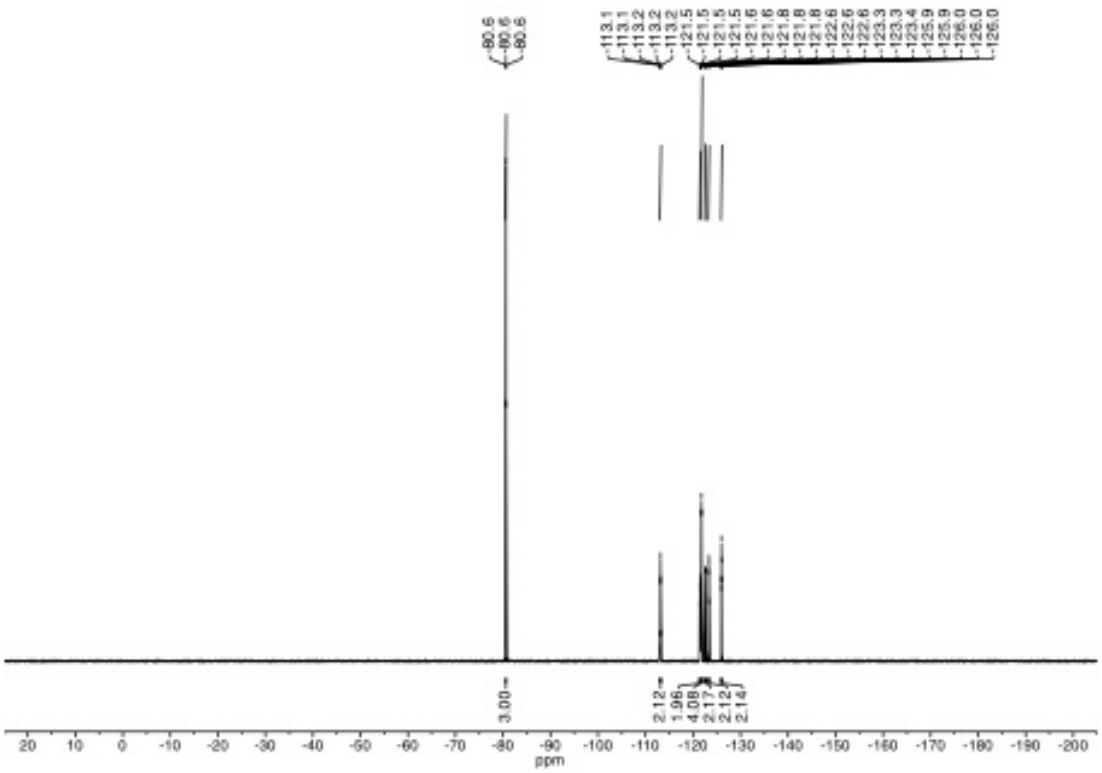

Figure S 40: ^{19}F NMR spectrum of BenzaldehydeR_fDec.

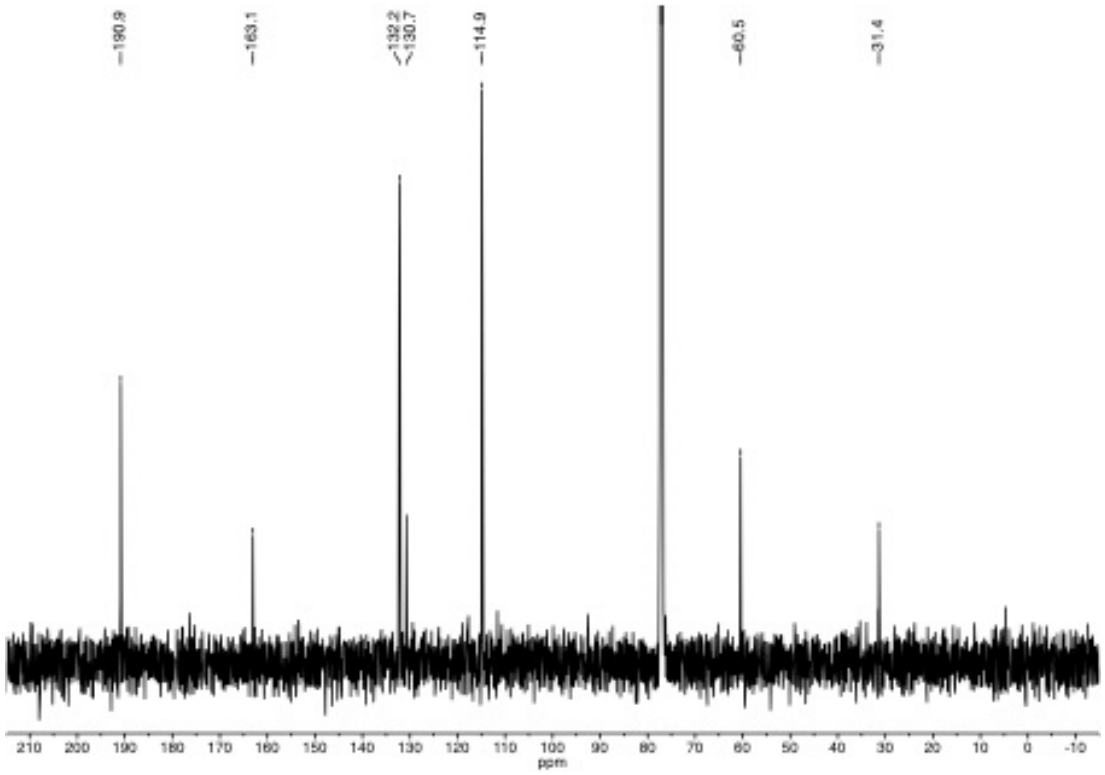

Figure S 41: ^{13}C NMR spectrum of BenzaldehydeR_fDec.

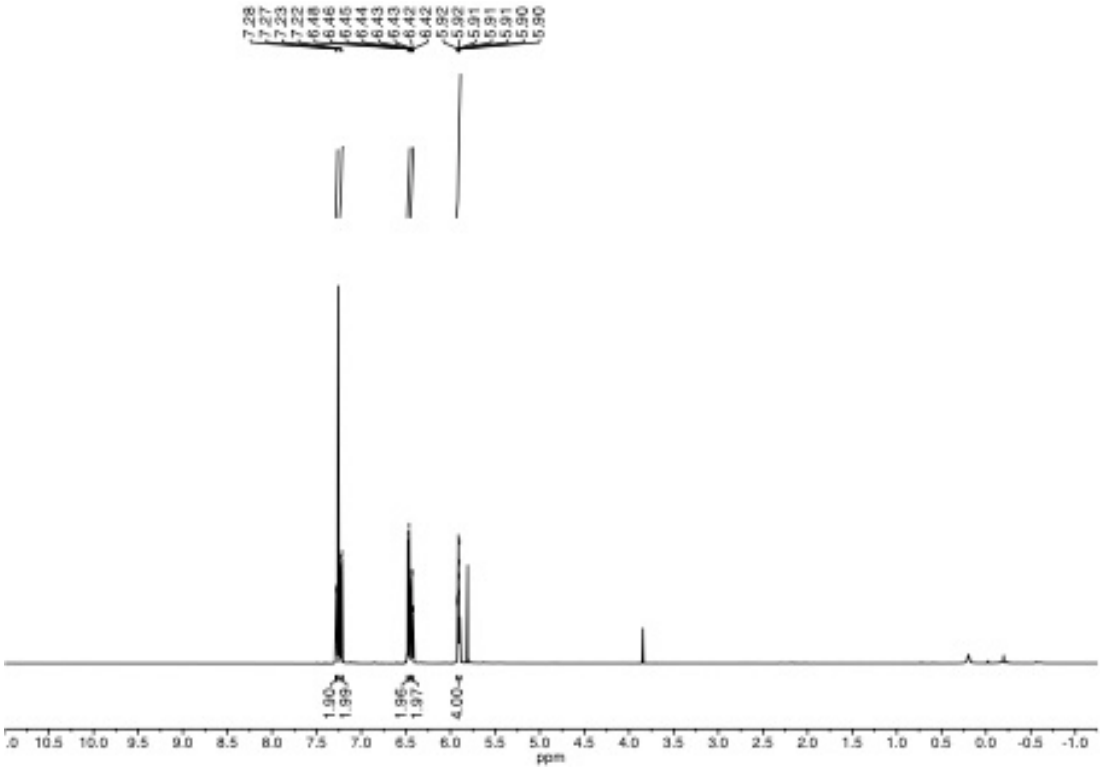

Figure S 42: ^{1}H NMR spectrum of TPYPhOCF$_3$.

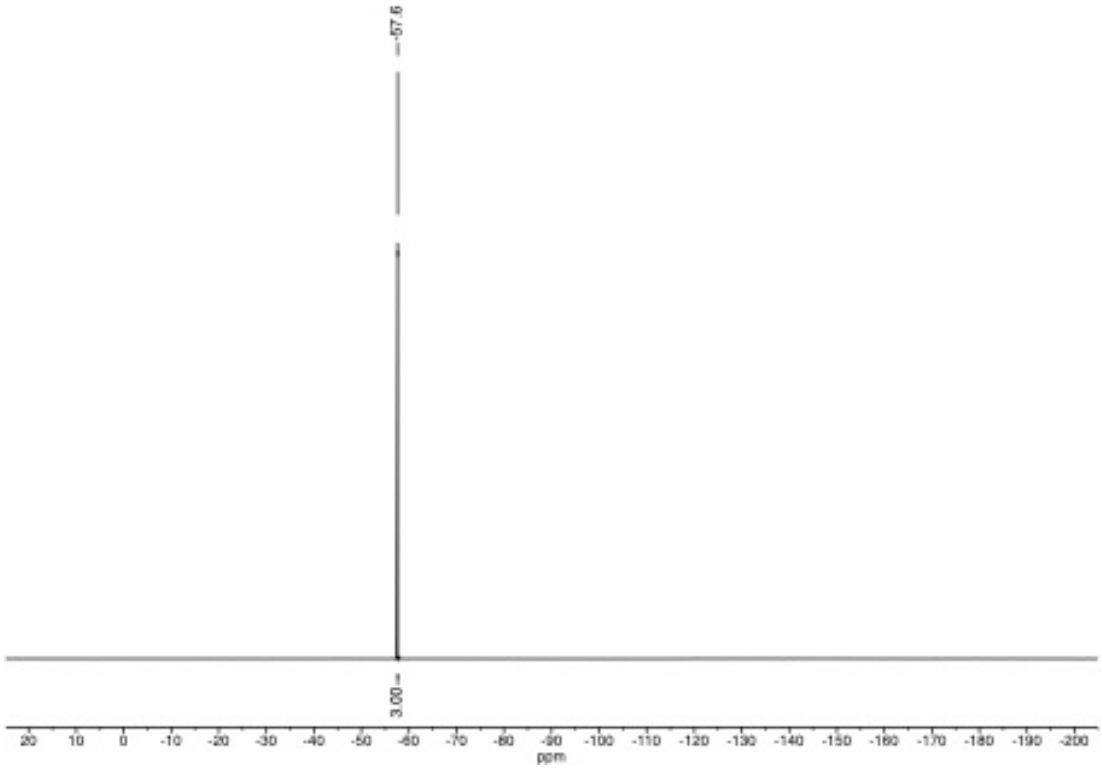

Figure S 43: ^{19}F NMR spectrum of TPYPhOCF$_3$.

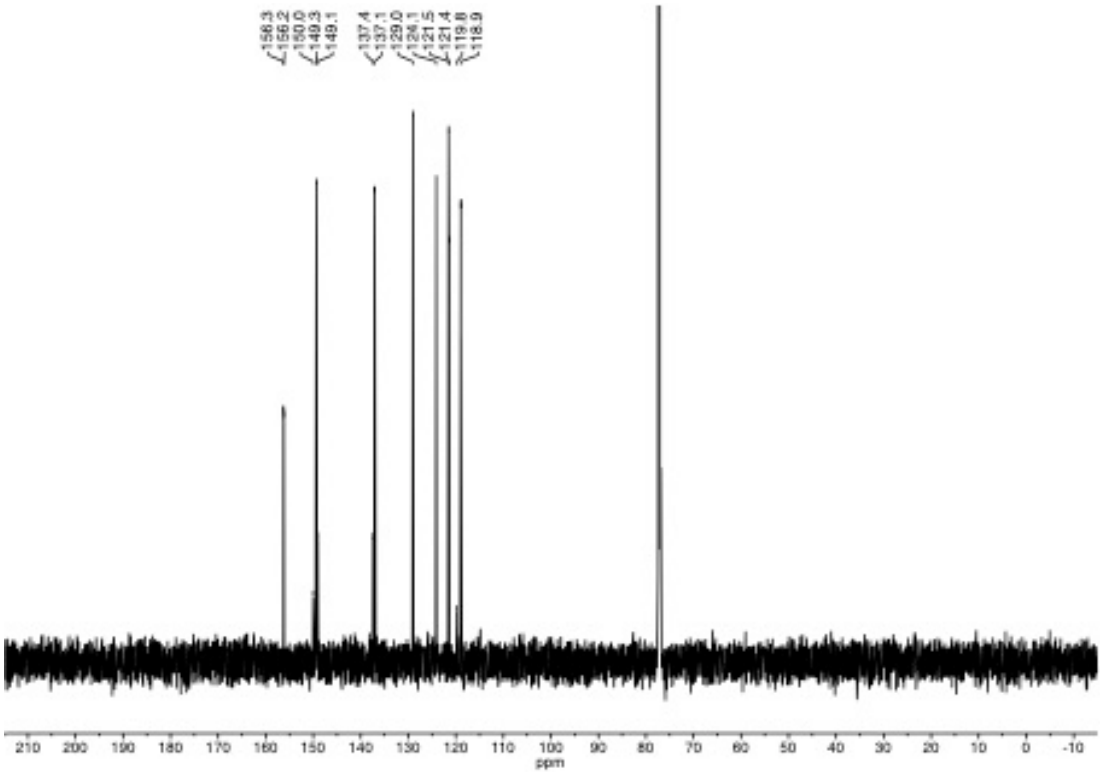

Figure S 44: ^{13}C NMR spectrum of TPYPhOCF$_3$.

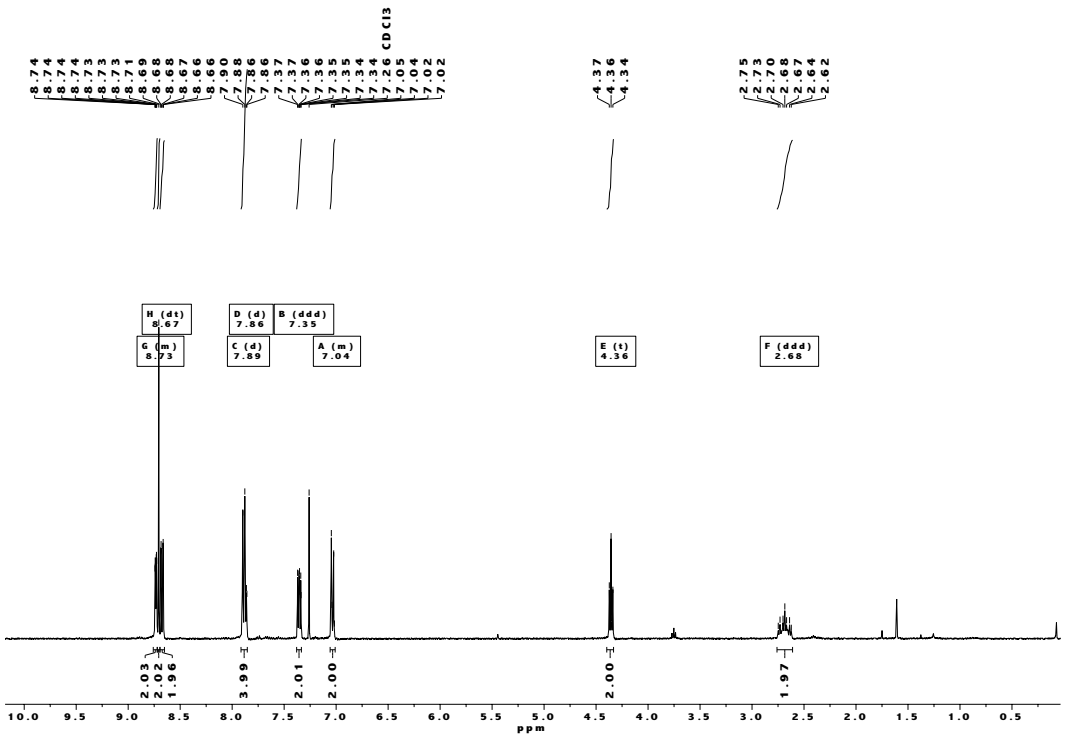

Figure S 45: ^{1}H NMR spectrum of TPY-Ph-RfOct.

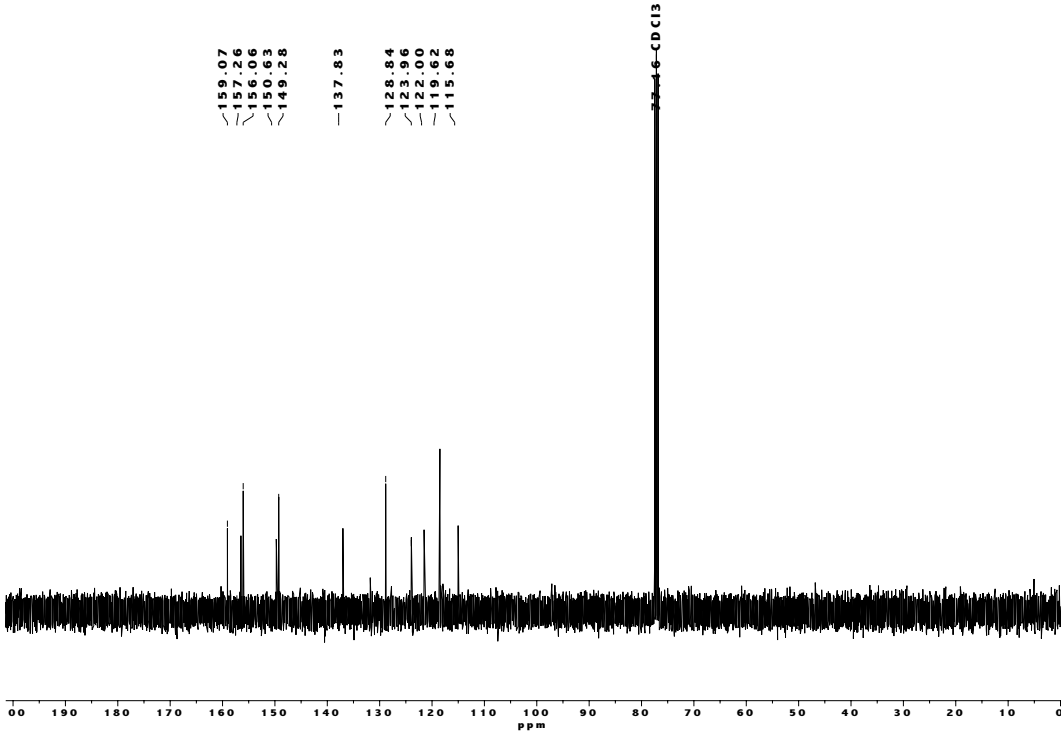

Figure S 46: ^{13}C NMR spectrum of TPY-Ph-RfOct.

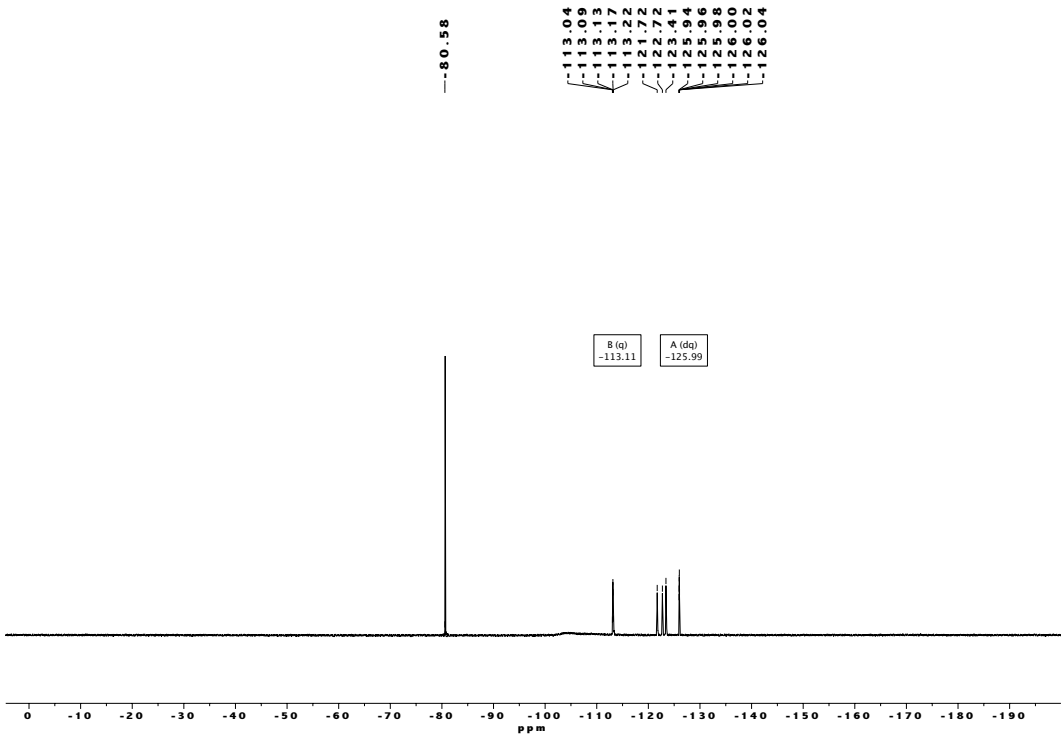

Figure S 47: ^{19}F NMR spectrum of TPYPhRfOct.

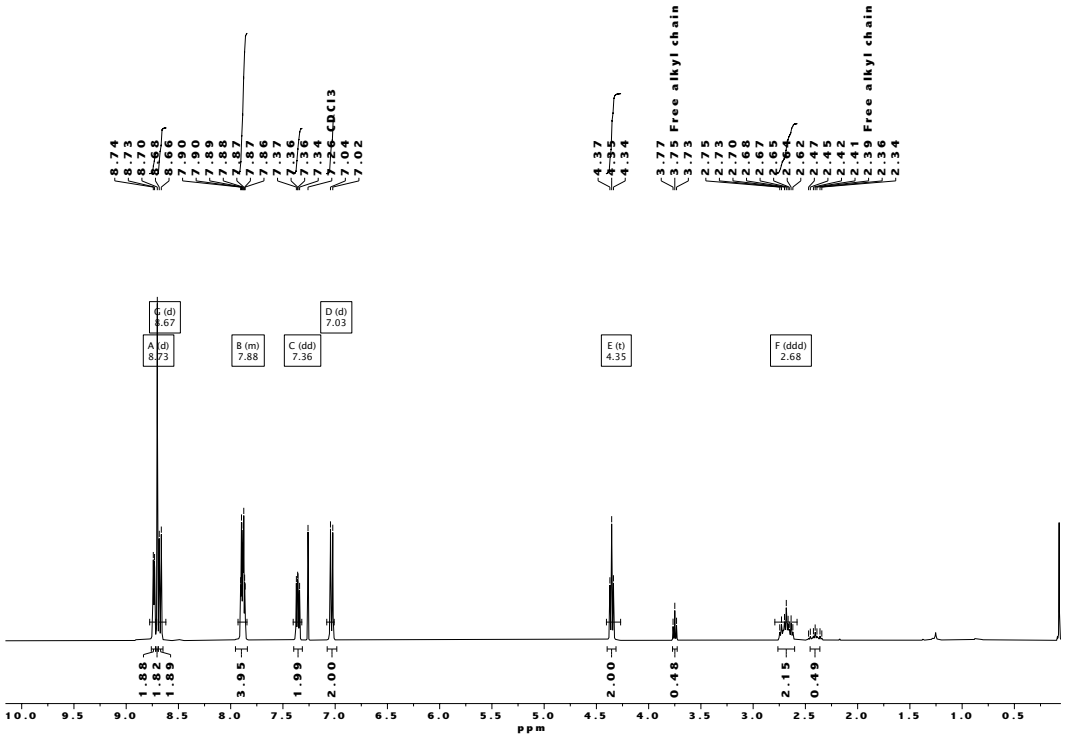

Figure S 48: ^{1}H NMR spectrum of TPYPhRfDec.

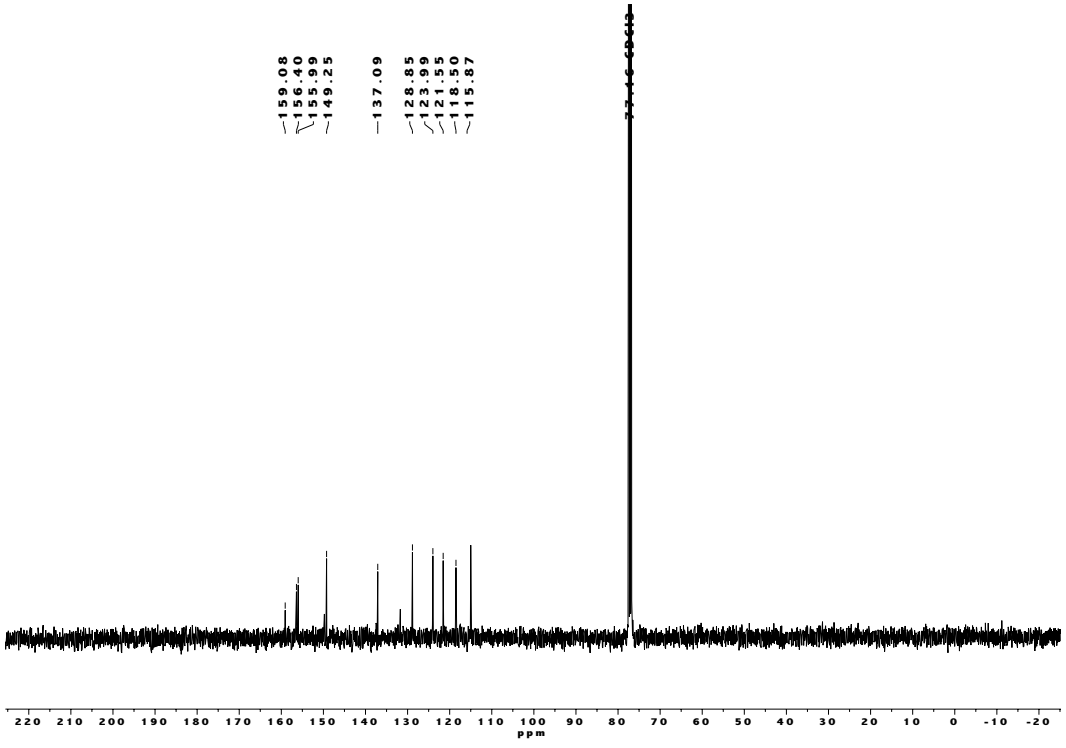

Figure S 49: ^{13}C NMR spectrum of TPYPhRfDec.

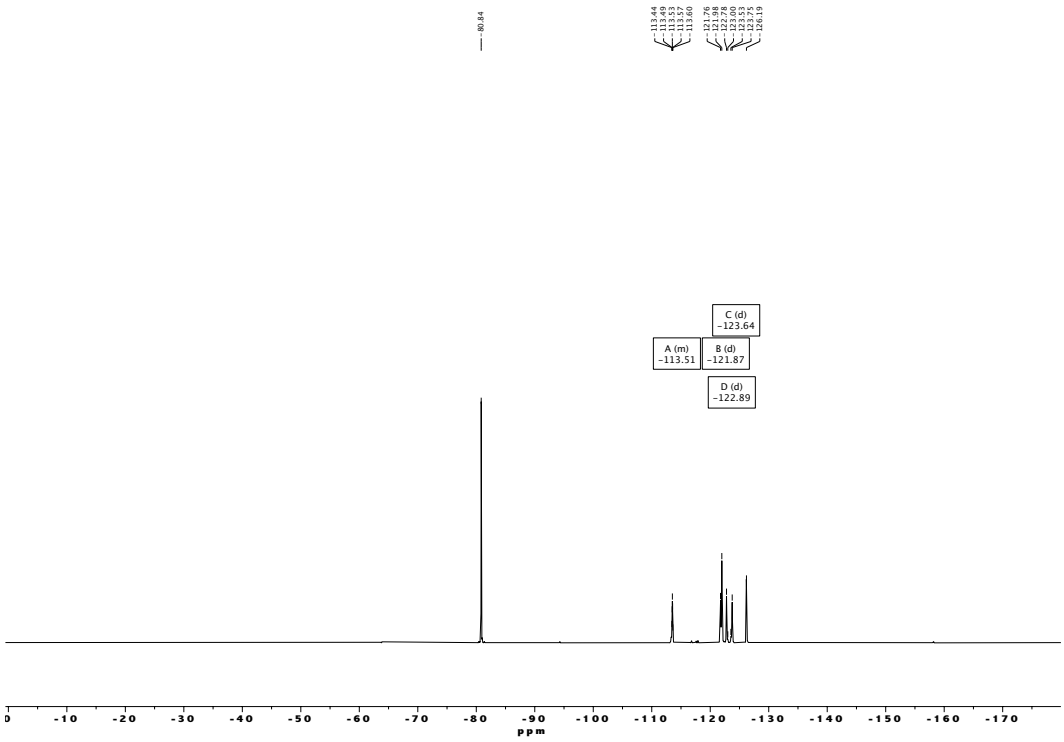

Figure S 50: ^{19}F NMR spectrum of TPYPhRfDec.

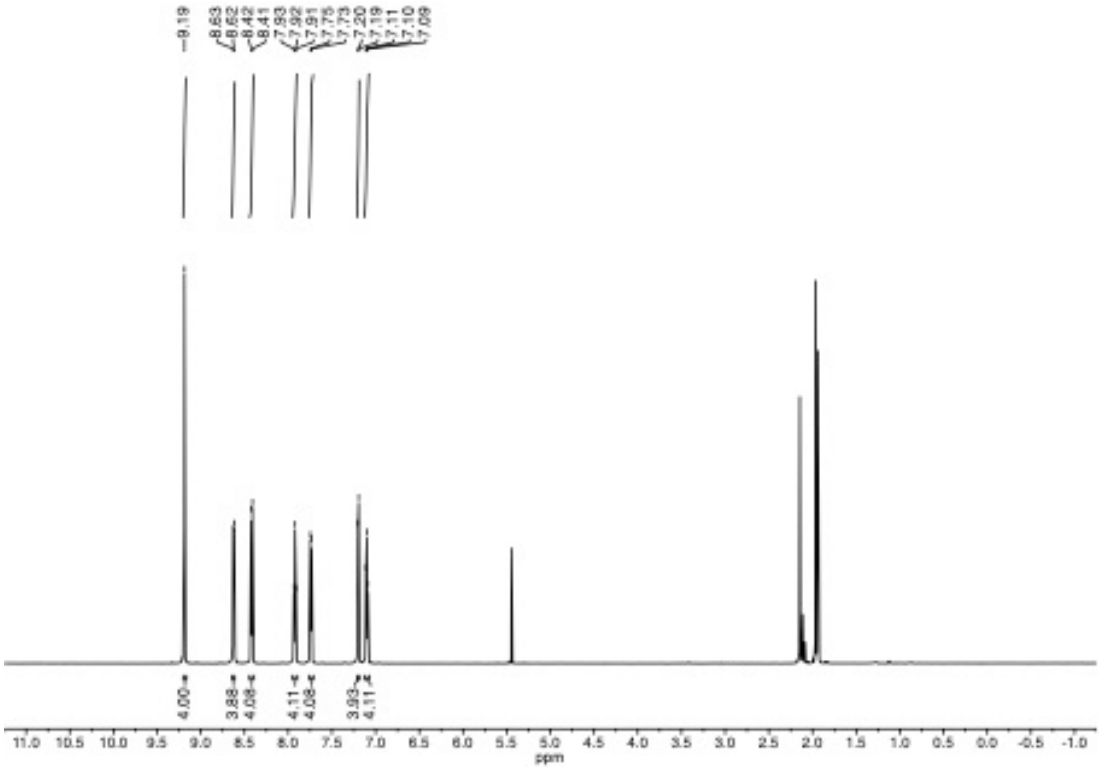

Figure S 51: ^{1}H NMR spectrum of **2**.

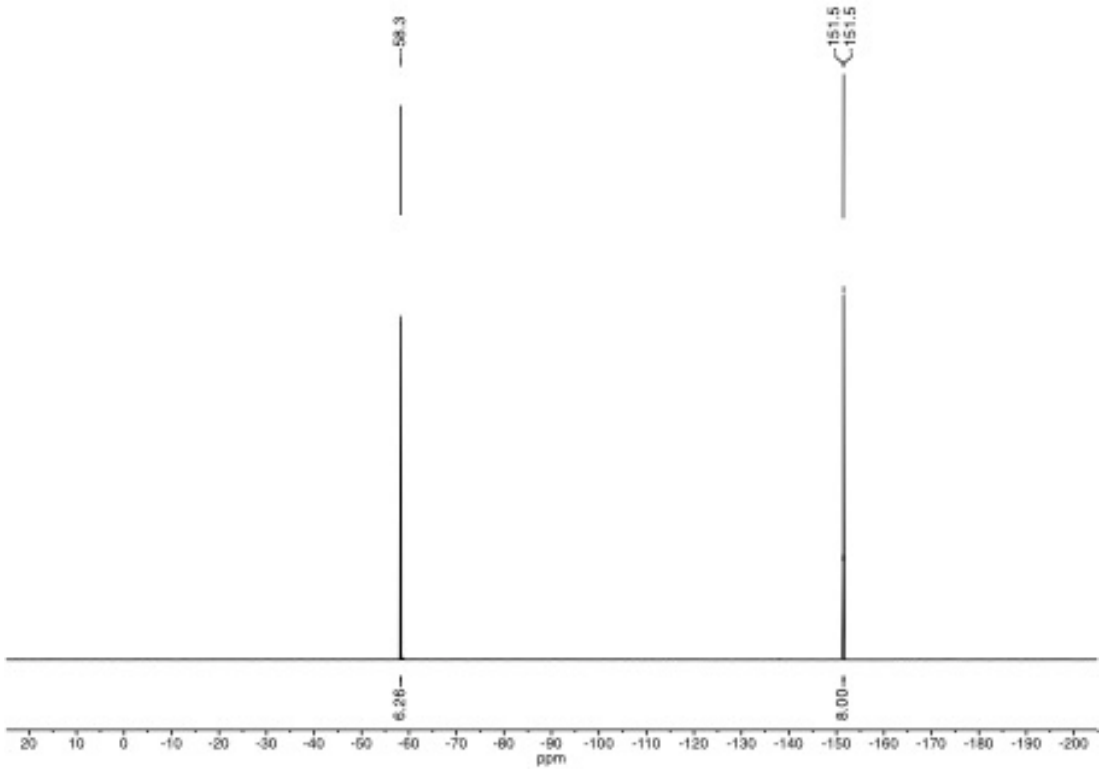

Figure S 52: ^{19}F NMR spectrum of **2**.

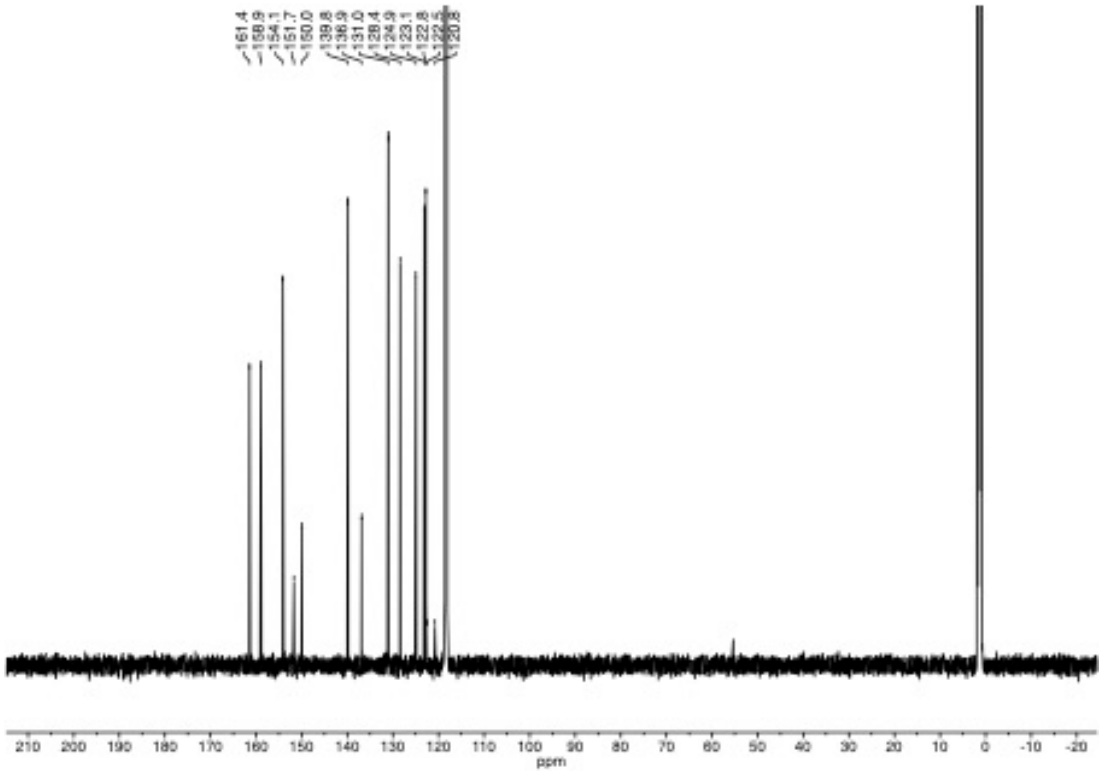

Figure S 53: ^{13}C NMR spectrum of **2**.

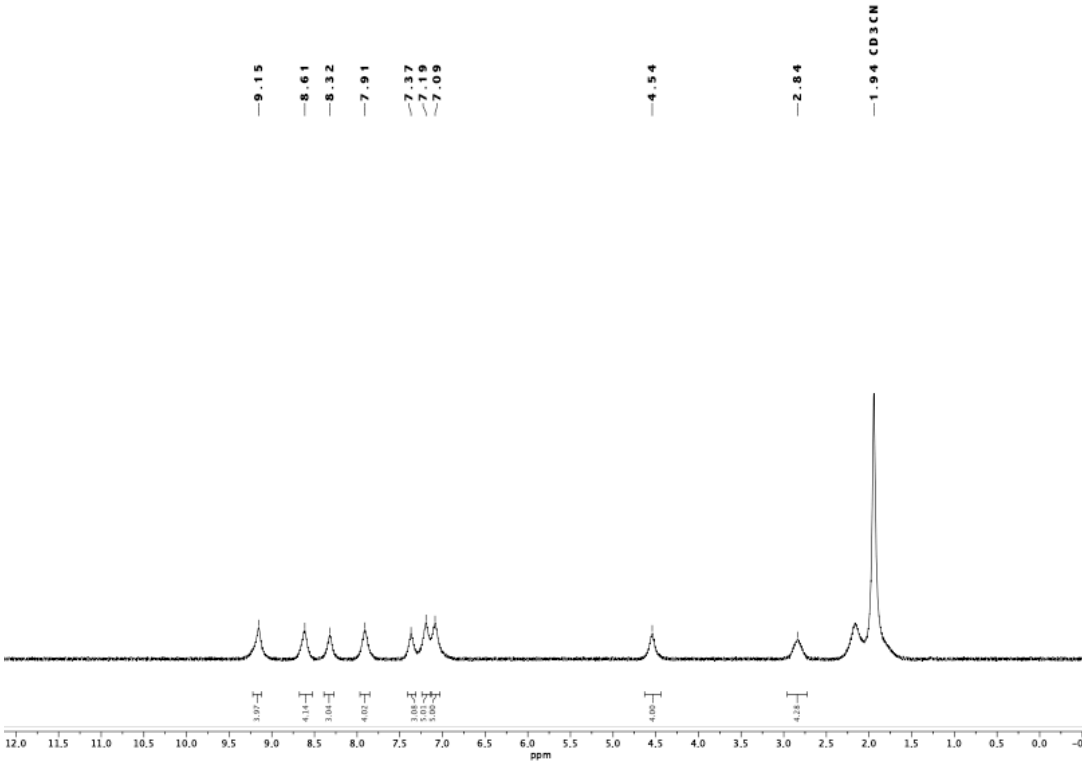

Figure S 54: ^{1}H NMR spectrum of **4**.

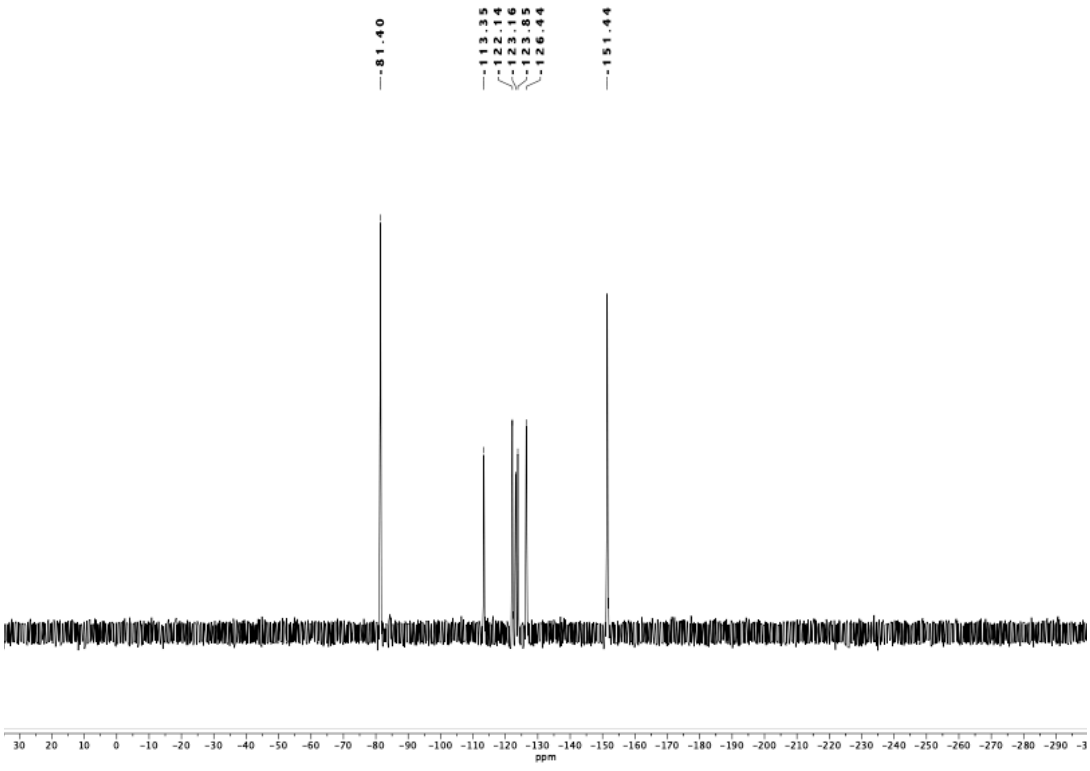

Figure S 55: ^{19}F NMR spectrum of **4**.

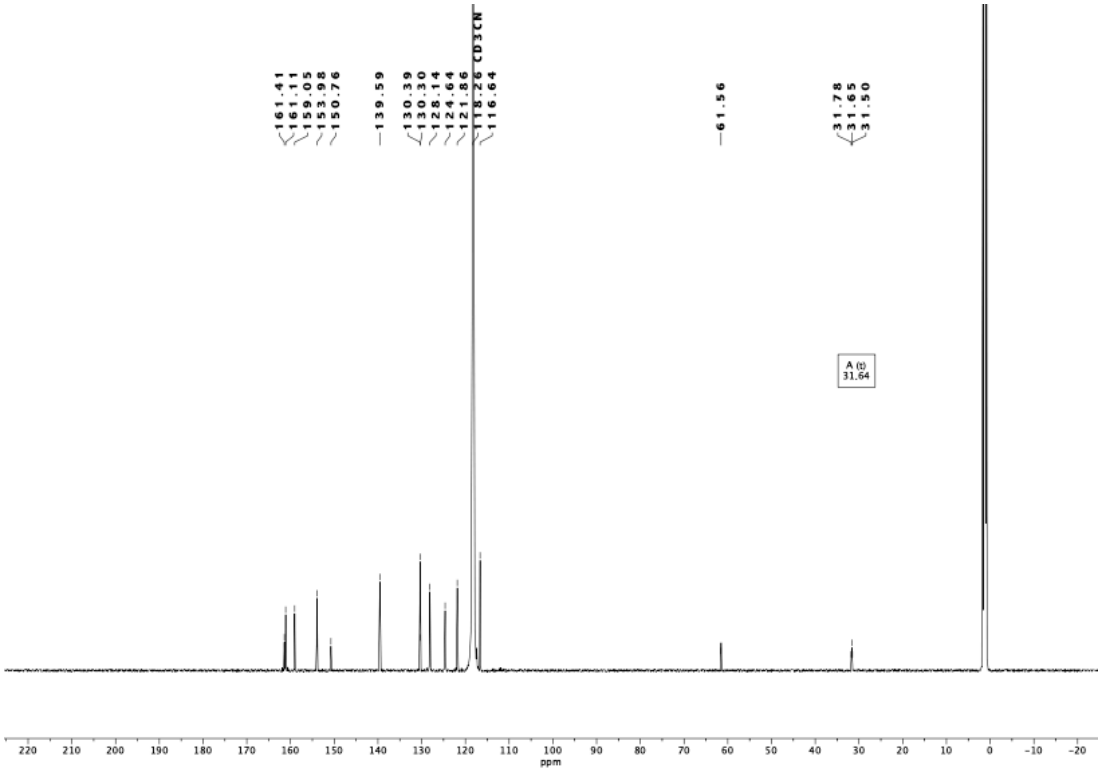

Figure S 56: ^{13}C NMR spectrum of **4**.

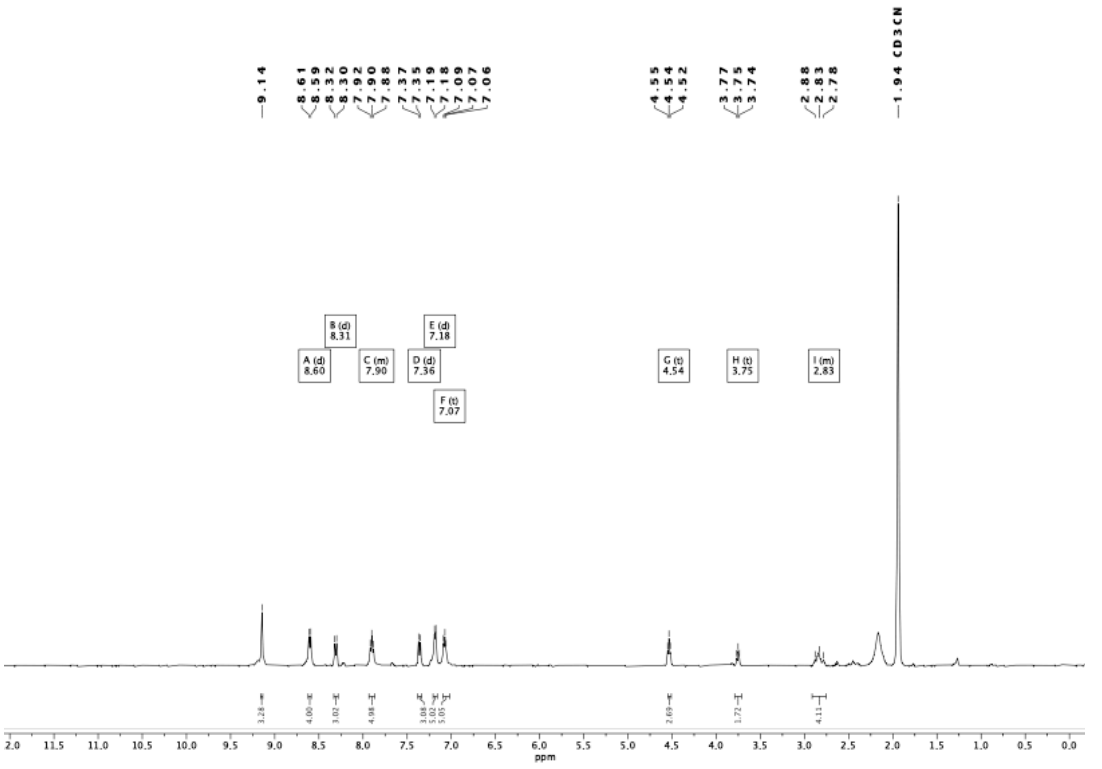

Figure S 57: ^{1}H NMR spectrum of **6**.

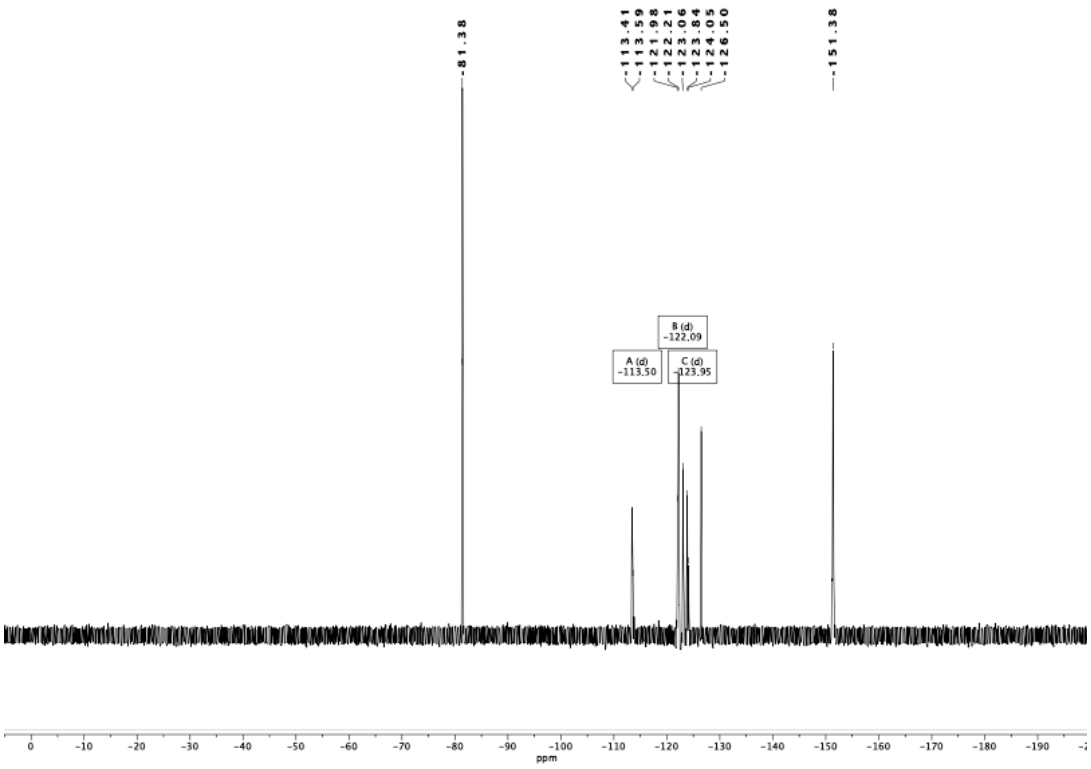

Figure S 58: ^{19}F NMR spectrum of **6**.

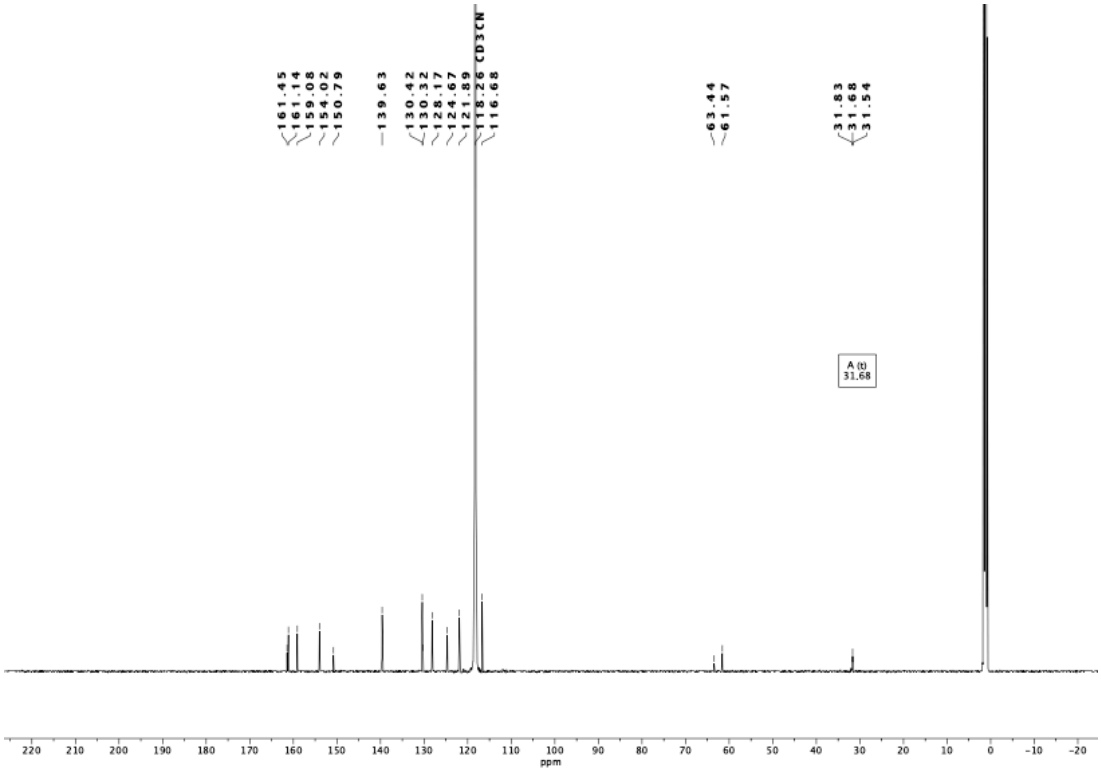

Figure S 59: ^{13}C NMR spectrum of **6**.

8. Polarized Optical Microscopy

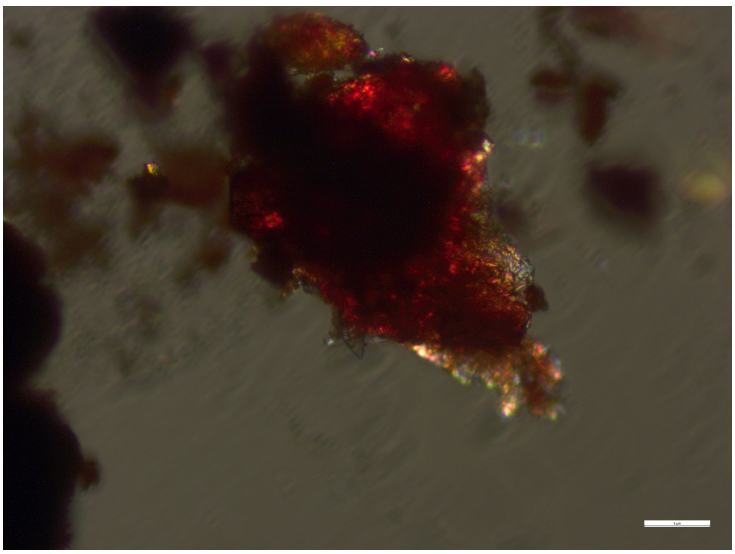

Figure S 60: Picture of complex **3** under POM at room temperature.

9. References

[1] K. Yamaguchi, Y. Takahara, T. Fueno, *Applied Quantum Chemistry*, Springer Dordrecht, D. Reidel Publishing Company, Dordrecht, Holland 1986, **1986**.

[2] T. Soda, Y. Kitagawa, T. Onishi, Y. Takano, Y. Shigeta, H. Nagao, Y. Yoshioka, K. Yamaguchi, *Chem. Phys. Lett.* **2000**, *319*, 223-230.

3.2.3. Ruthenium Complexes of Polyfluorocarbon Substituted Terpyridine and Mesoionic Carbene Ligands: An Interplay in CO_2 Reduction

Felix Stein,[a, b],# Maite Nößler,[a],# Arijit Singha Hazari,[b], Lisa Böser,[a, c] Robert Walter,[b] Hang Liu,[c] Elias Klemm,[c] Biprajit Sarkar[a, b]**

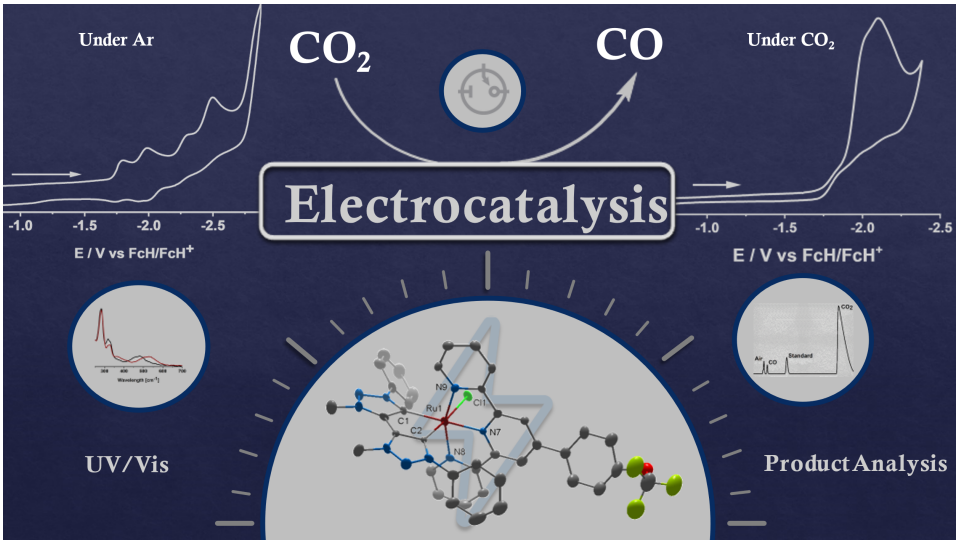

[a] Institut für Chemie und Biochemie, Anorganische Chemie
Freie Universität Berlin, Fabeckstraße 34-36, 14195, Berlin (Germany)
[b] Lehrstuhl für Anorganische Koordinationschemie
Universität Stuttgart, Pfaffenwaldring 55, 70569 Stuttgart (Germany)
[c] Institut für Technische Chemie
Universität Stuttgart, Pfaffenwaldring 55, 70569 Stuttgart (Germany)
#Equal contribution

This article was published and is reprinted with the permission from WILEY-VCH:

Felix Stein,[a, b],# Maite Nößler,[a],# Arijit Singha Hazari,[b],* Lisa Böser,[a, c] Robert Walter,[b] Hang Liu,[c] Elias Klemm,[c] Biprajit Sarkar[a, b]*, *Chem. Eur. J.* **2023**, e202300405.

DOI: https://doi.org/10.1002/chem.202300405

Author contribution: The project was designed by, Felix Stein, Maite Nößler and Biprajit Sarkar. The terpyridine ligands were synthesized and characterized by Maite Nößler. The mesoionic carbene ligands and ruthenium complexes were synthesized and characterized by Felix Stein. The X-ray diffraction analysis was carried out by Maite Nößler, Robert Walter and Arijit Singha Hazari. The CV, UV/Vis, UV/Vis-SEC, IR-SEC experiments were performed by Felix Stein. The bulk electrolysis was performed by Felix Stein and Arijit Singha Hazari. Theoretical calculations and efficiency calculations were performed by Arijit Singha Hazari. SEM/EDX measurements were done by Hang Liu. The paper was written by Felix Stein, Arijit Singha Hazari, Maite Nößler and Biprajit Sarkar.

Chemistry
A European
Journal

Chemistry Europe
European Chemical Societies Publishing

Accepted Article

Title: Ruthenium Complexes of Polyfluorocarbon Substituted Terpyridine and Mesoionic Carbene Ligands: An Interplay in CO2 Reduction

Authors: Felix Stein, Maite Nößler, Arijit Singha Hazari, Lisa Böser, Robert Walter, Hang Liu, Elias Klemm, and Biprajit Sarkar

To be cited as: *Chem. Eur. J.* **2023**, e202300405

Link to VoR: https://doi.org/10.1002/chem.202300405

WILEY VCH

Chemistry - A European Journal 10.1002/chem.202300405

Ruthenium Complexes of Polyfluorocarbon Substituted Terpyridine and Mesoionic Carbene Ligands: An Interplay in CO_2 Reduction

Felix Stein,[a, b],# Maite Nößler,[a],# Arijit Singha Hazari,[b], Lisa Böser,[a, c] Robert Walter,[b] Hang Liu,[c] Elias Klemm,[c] Biprajit Sarkar[a, b],**

[a] F. Stein, M. Nößler, L. Böser, Prof. Dr. B. Sarkar
Institut für Chemie und Biochemie, Anorganische Chemie
Freie Universität Berlin, Fabeckstraße 34-36, 14195, Berlin (Germany)
E-mail: biprajit.sarkar@iac.uni-stuttgart.de
[b] F. Stein, Dr. A. Singha Hazari, R. Walter, Prof. Dr. B. Sarkar
Lehrstuhl für Anorganische Koordinationschemie
Universität Stuttgart, Pfaffenwaldring 55, 70569 Stuttgart (Germany)
[c] Dr. Hang Liu, Prof. Dr.-Ing. E. Klemm
Institut für Technische Chemie
Universität Stuttgart, Pfaffenwaldring 55, 70569 Stuttgart (Germany)
#Equal contribution

Chemistry - A European Journal 10.1002/chem.202300405

Abstract

In recent years terpyridines (tpy) and mesoionic carbenes (MIC) have been widely used in metal complexes. With the right combination with a metal center, both of these ligands are individually known to generate excellent catalysts for CO_2 reduction. In this study, we combine the potentials of PFC (PFC = polyfluorocarbon) substituted tpy and MIC ligands within the same platform to obtain a new class of complexes, which we investigated with respect to their structural, electrochemical and UV/Vis/NIR spectroelectrochemical properties. We further show that the resulting metal complexes are potent electrocatalysts for CO_2 reduction in which CO is exclusively formed with a faradaic efficiency of 92%. A preliminary mechanistic study, including the isolation and characterization of a key intermediate is also reported.

Chemistry - A European Journal 10.1002/chem.202300405

Abstract

In recent years terpyridines (tpy) and mesoionic carbenes (MIC) have been widely used in metal complexes. With the right combination with a metal center, both of these ligands are individually known to generate excellent catalysts for CO_2 reduction. In this study, we combine the potentials of PFC (PFC = polyfluorocarbon) substituted tpy and MIC ligands within the same platform to obtain a new class of complexes, which we investigated with respect to their structural, electrochemical and UV/Vis/NIR spectroelectrochemical properties. We further show that the resulting metal complexes are potent electrocatalysts for CO_2 reduction in which CO is exclusively formed with a faradaic efficiency of 92%. A preliminary mechanistic study, including the isolation and characterization of a key intermediate is also reported.

Chemistry - A European Journal 10.1002/chem.202300405

Introduction

The increasing demand for energy and the threat of climate change show the need to further develop energy sources. One of the current focus is the study of molecular electrocatalysts for downstream reactions to new energy technologies.[1] In this regard, proton or oxygen reduction, water oxidation, or CO_2 reduction are a research focus because they involve the release or storage of energy.[2,3] One of the most important atmospheric gases contributing to the greenhouse effect is CO_2, and because it is the major source of carbon, its electrochemical reduction into fuels has attracted considerable interest.[4]

The selective electrochemical CO_2 reduction is still a subject of research despite extensive investigations in the last decades due to the high overpotential of the cathodic process.[2,5] One of the most prominent approaches to maximizing the catalytic activity of molecular electrocatalysts is to tune the electronic properties of the ligands.[6] For example, placement of a strong electron donating ligand increases the CO_2 activation rate, by making the metal center more nucleophilic.[7] However, this leads to an undesirable increase in the overpotential, since a stronger electron donating ligand typically leads to a more negative reduction potential.[8] The development of a catalyst, in which the kinetics of the chemical steps and the reduction potentials are controlled by two different ligands is one approach to solving this problem.[9] In this context, Miller and co-workers investigated ruthenium(II) complexes bearing a terpyridine and a bidentate pyridyl-NHC ligand, and showed an impact of the *trans* effect on the electrocatalysis.[8,9] More recently, the same group has reported on iron(II) and ruthenium(II) complexes with terpyridine and chelating bi-NHC ligands as electrocatalysts for CO_2 reduction.[10]

One way to control the reduction potential is to introduce highly tunable tridentate N-containing terpyridine (tpy) ligands, which is frequently used in coordination chemistry. Ruthenium(II) complexes of terpyridines have been intensively studied, as they exhibit well-defined electrochemical and photochemical properties and are also used in various catalytic processes[11,12] such as proton and CO_2 reduction,[13] or water oxidation.[14] However, the synthesis of structurally diverse terpyridine ligands, e.g., those with electronically different substituents, still remains a challenge.[15]

Currently, mesoionic carbene (MIC) ligands are of great interest in organometallic chemistry, due to their strong donor properties and unusual bonding situation.[16,17] They can be synthesized by the copper(I)-catalyzed azide-alkyne cycloaddition reaction, which is facile and modular.[18] A large number of complexes have already been reported with

Chemistry - A European Journal 10.1002/chem.202300405

these ligands, especially with the late transition metals.[19,20,21] For the generation of metal complexes with intriguing electrochemical and photochemical properties, MICs are a preferred class of ligands.[16,20,21] Moreover, the corresponding metal complexes can be used in homogeneous catalysis.[22] Furthermore, MICs have recently shown great potential as powerful ligands for generating metal complexes for electrocatalysis with relevance to energy related research.[23]

In this work, we present different ruthenium(II) complexes bearing a MIC ligand and tpy ligands with an incorporated perfluorocarbon chain (PFC) at the tail (Figure 1). The MIC ligands which are more strongly donating than the NHCs are used for controlling kinetics of electrocatalytic CO_2 reduction,[16,17,19,20,21,24] and the PFC tail in the tpy ligand for controlling the overpotential. The influence of the PFC tail on the overpotential for electrochemical CO_2 reduction is investigated. As the different chain-length of the PFC tail is expected to have an influence on the tpy based reduction process, we were interested in deciphering how these substitution patterns would influence the tuning of the overpotential in electrochemical CO_2 reduction with such complexes. Additionally, the chloride ligand is labile and provides a readily available vacant site for CO_2 binding. These complexes were studied electrochemically by cyclic voltammetry and UV/Vis/NIR-spectroelectrochemistry. In addition, metal complexes of these frameworks are investigated as electrocatalysts for CO_2 reduction together with a first mechanistic study. To the best of our knowledge, this is the first time that a MIC ligand is combined with a tpy ligand bearing a PFC tail.

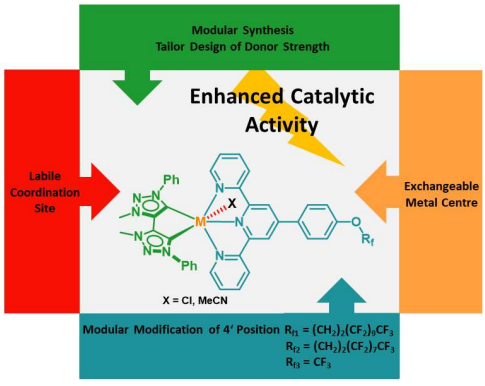

Figure 1: Synthetic access for the development of a molecular catalyst for the electrocatalytic CO_2 reduction.

Chemistry - A European Journal 10.1002/chem.202300405

Results and Discussion

Synthesis and Structural Characterization

The synthesis of the terpyridine ligands (tpy, **L1**–**L3**) with different per fluorinated alkyl chains as well as the ruthenium complex with cymene (**Ru$_1$**) and a bis MIC-ligand were recently developed by us. [25] To obtain the mixed ruthenium complexes with substituted terpyridine and MIC ligands (**Ru$_2$**–**Ru$_4$**), **Ru$_1$** was reacted with the respective terpyridines (**L$_1$** – **L$_3$**) in DMSO at 120 °C (Scheme 1). After chromatographic work up, we were able to isolate the complexes in moderate to good yields.[26] The corresponding acetonitrile complex **Ru$_5$** was synthesized by reacting **Ru$_4$** with $AgPF_6$ in acetonitrile in 95% yield (Scheme 2). The facile synthesis of **Ru$_5$** under ambient conditions already points to a somewhat labile Ru-Cl bond, as would be expected owing to the strong donor properties of the MIC-C donor that is trans to the chlorido ligand in complex **Ru$_4$**. This fact is expected to be beneficial in the use of **Ru$_4$** as an electrocatalyst (see below). Starting from **Ru$_5$**, the exchange of the acetonitrile with an CO was performed in ethanol under an atmosphere of CO gas at 70 °C. The formation of the desired complexes **Ru$_6$** was indicated by a color change from brownish to intense yellow. An intense peak at 1994 cm^{-1} in the IR-spectrum for the Ru-CO stretching frequency and the characteristic peak in the ^{13}C NMR spectrum at 194.8 ppm for the carbon atom of the CO confirms the generation of the desired complex. The aforementioned values fit well with data for related compounds reported in the literature (Figure S14 and S37).[27] All the complexes were characterized by NMR spectroscopy, mass spectrometry and elemental analysis (see supporting information).

The ^1H NMR spectra of all complexes show well defined signals in the expected region. The two resonances corresponding to the two methyl groups of the MIC ligands are in the typical range between 4.8 ppm and 4.5 ppm. All the signals in the aromatic region assigned to the tpy are shifted high field, compared to the free ligand, confirming the coordination to the ruthenium center. ^{13}C NMR spectra show typical resonances between 191 ppm and 183 ppm for metal bound carbene carbons. The specific signals for all the complexes in the ^{19}F NMR are a further proof for the formation of the desired complex (Figures S1 – S17, see supporting information).

Chemistry - A European Journal 10.1002/chem.202300405

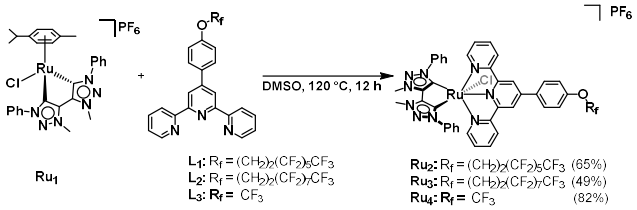

Scheme 1: Synthesis of the ruthenium complexes **Ru$_2$ – Ru$_4$**.

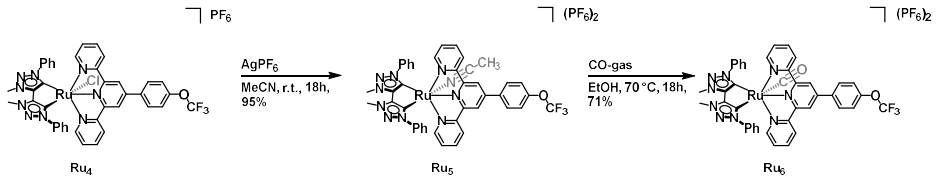

Scheme 2: Synthesis of the ruthenium complexes **Ru$_5$** and **Ru$_6$**.

The molecular structures of **Ru$_4$** and **Ru$_5$** in the crystal were investigated from single crystal X-ray diffraction studies (XRD). Unfortunately, it was not possible to grow suitable single crystals for the other two complexes with longer chain length, which is probably due to the precipitation problem. This phenomena has already been described previously in the literature.[9]

Complex **Ru$_4$** crystallizes in a triclinic P $\bar{1}$ space group. The ruthenium center is coordinated in a pseudo-octahedral fashion through three nitrogen atoms of the tpy ligand, two carbon atoms of the MIC ligand and the chloride. The Ru–N7 bond lengths to the central ring of the tridentate ligand is shorter than the bond lengths Ru–N8 and Ru–N9 to the terminal rings (Figure 2 and Table 1). This could be due to the rigidity of the ligands that prevent the three donor atoms of the same tpy ligand from approaching the ruthenium center equally closely.[7p] The rings of the MIC ligand are slightly out of plane and the two phenyl rings are also rotated out of plane. The connectivity and geometry of the nitrile complex **Ru$_5$** obtained by replacing the chloride with an acetonitrile was further approved with the solid structure. The Ru-C1 bond length is similar with **Ru$_4$**. As expected, the Ru-C2 bond length (Figure 2) is elongated by ca. 0.07 Å, due to changing donor ability from chloride to acetonitrile. This trend can also be seen in the elongation of the ruthenium nitrogen bond of the terpyridine.

Chemistry - A European Journal 10.1002/chem.202300405

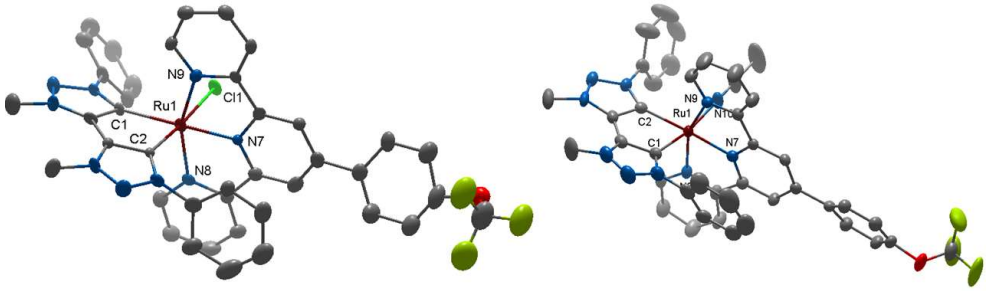

Figure 2: Perspective view of complex **Ru4** and **Ru5**. Ellipsoids are at a probability level of 50%. H atoms, anions and disordered atoms are omitted for clarity.

Table 1: Selected bond lengths in [Å] from measurements at 100 K.

Bond	**Ru4**	**Ru5**
Ru–N7	1.972(8)	1.995(2)
Ru–N8	2.055(8)	2.073(2)
Ru–N9	2.066(8)	2.084(2)
Ru–C1	2.077(9)	2.069(3)
Ru–C2	2.013(9)	2.084(2)
Ru–Cl1	2.472(2)	-
Ru-N (MeCN)	-	2.088(2)

Electrochemistry:

The electrochemical properties of the complexes were evaluated via cyclic voltammetric analysis in acetonitrile solution with 0.1 M tetrabutylammonium hexafluorophosphate (NBu_4PF_6) as the supporting electrolyte, at 100 mV/s scan rate. Table 2 summarizes electrochemical potentials of all the complexes. Investigation of cyclic voltammograms of all the complexes revealed a reversible $1e^-$ oxidation and reduction ($\Delta E_p \sim 71$ mV) for **Ru4**, in contrary to the irreversible redox processes in the case of **Ru2** containing octyl PFC tail, as illustrated in the Figure 3. Irreversibility of the redox process could be ascribed to the adsorption of the reduced species on the electrode bearing resemblance to the previously reported ruthenium terpyridine and electron donating ligands.[11] Interestingly, **Ru3**, the higher analogue of **Ru2** exhibited two and one reversible $1e^-$ oxidation and reduction processes respectively along with two quasireversible reduction waves (Figure 3). Based on the Mulliken spin population and literature reports on the similary type of complexes,

Chemistry - A European Journal 10.1002/chem.202300405

first reduction process can be assigned to terpyridine based, while second and third reduction processes are most likely focused on the MIC and terpyridine center, respectively. On the other hand, greater contribution of the metal center to the overall spin population on oxidation in **Ru2** and **Ru3** indicate metal-centered oxidation process Ru^{II}/Ru^{III}).

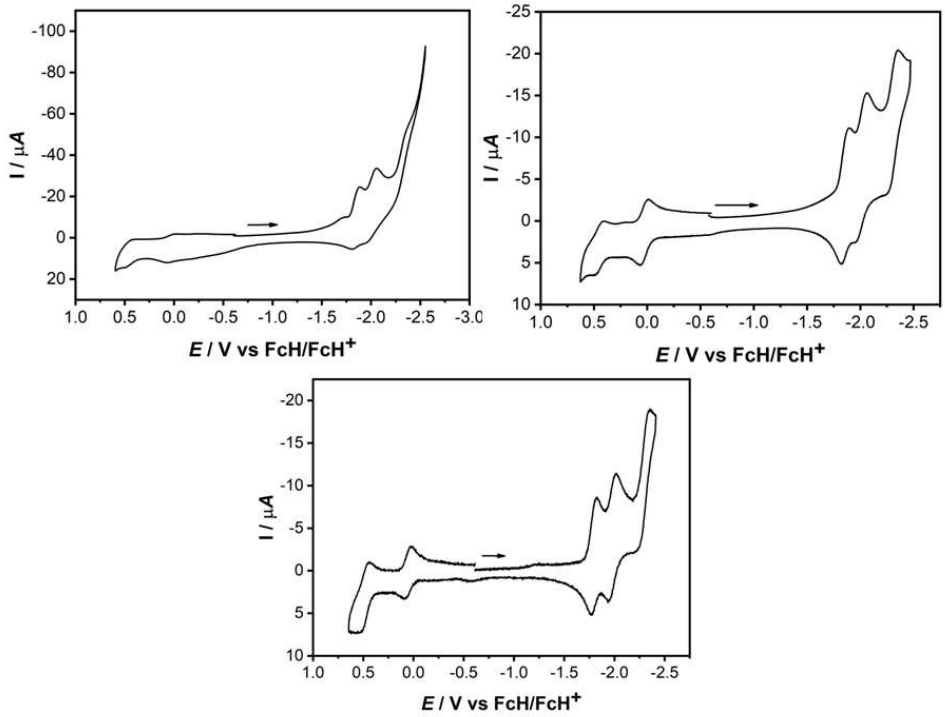

Figure 3: Cyclic voltammograms of **Ru2** (top left), **Ru3** (top right), and **Ru4** (bottom) in acetonitrile with 0.1 M NBu_4PF_6 as a supporting electrolyte. Scan rate: 100 mV/s, glassy carbon working electrode, electrochemical potentials were referenced against Fc/FcH+ redox couple.

Table 2: Redox potentials of the complexes referenced against Fc/FcH^+ redox couple measured in acetonitrile at room temperature.[a]

	$E_{1/2}^{Ox2}$ [V]	$E_{1/2}^{Ox1}$ [V]	$E_{1/2}^{Red1}$ [V]	$E_{1/2}^{Red2}$ [V]	$E_{1/2}^{Red3}$ [V]
Ru2[b]	0.450	0.07	−1.84	−2.00	−2.37
Ru3	0.453	0.14	−1.85	−2.00	−2.30
Ru4	0.482	0.06	−1.79	−1.96	−2.29

[a] All measured with a glassy carbon electrode. [b] Irreversible, forward peak potential.

Chemistry - A European Journal 10.1002/chem.202300405

Comparison of the redox potentials revealed no significant influence of the increasing chain length of the PFC tail at the peripheral position of the terpyridine ring. Scan dependent sweep of the potentials exhibited linear dependence of the peak current on the square root of the scan rate indicating a diffusion-controlled process, as illustrated in Figure 4 for **Ru$_4$**.

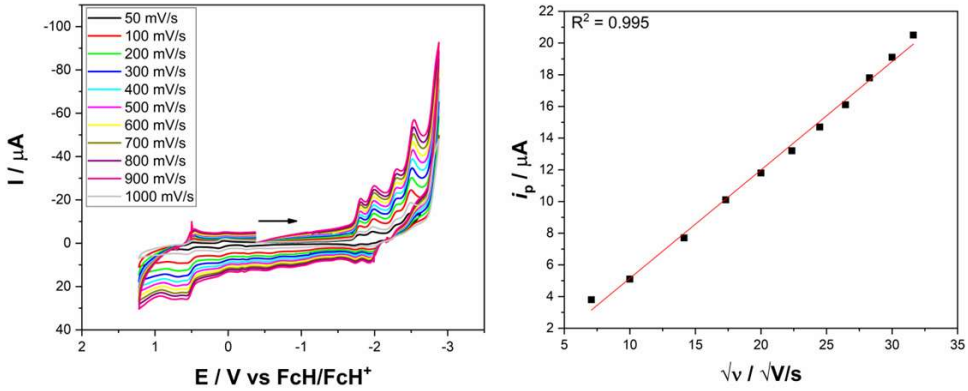

Figure 4: Cyclic voltammograms of **Ru$_4$** in acetonitrile containing 0.1M ^{n}Bu$_4$PF$_6$ at different scan rates (left). Diagram on the right depicts variation of peak current (i_p) against the square root of the scan rate for the first reduction waves (Conditions: GC working electrode, platinum wire as a counter electrode, and Fc/FcH$^+$ couple as an internal reference).

Cyclic voltammograms of the corresponding acetonitrile solvated complex **Ru$_5$** was also investigated in acetonitrile solution with 0.1 M tetrabutylammonium hexafluorophosphate (NBu$_4$PF$_6$) as the supporting electrolyte, at 100 mV/s scan rate (Figure S21). The complex displayed one reversible and multiple quasi-reversible redox processes with an irreversible process near to 0 V. This irreversible wave could be due to the adsorption of the complex at the surface of the working electrode. To address the problem, cyclic voltammetry was measured under an identical experimental condition replacing NBu$_4$PF$_6$ with tetrabutylammonium chloride (NBu$_4$Cl) as the supporting electrolyte to form an equilibrium between the chloride containing complex **Ru$_4$** and the complex **Ru$_5$** (Figure S21). The voltammograms displayed multiple redox processes without any irreversible process indicating an equilibrium between chloride and acetonitrile ligand in the presence of higher concentrations of chloride ion, and indicating the presence of a labile coordination site in **Ru$_5$** as the possible reason for the adsorption peak close of 0 V for **Ru$_5$**.

Chemistry - A European Journal 10.1002/chem.202300405

UV/Vis/NIR spectroelectrochemistry (UV/Vis-SEC)

The UV/Vis spectra of the complexes were recorded in acetonitrile. For **Ru4,** an immediate color change of the solution from intense purple to brownish/orange was observed. This could be followed from the UV/Vis spectra (Figure 5) by a red shift of the absorption band at 478 nm to 545 nm. If the solvent is removed and the remaining solid is dissolved in DCM or THF, the color of the solution turns intense purple again. The band in the visible region can be assigned to metal to ligand charge transfer (MLCT), which was further confirmed by DFT calculations (Figure S41). The absorption band at 326 nm is due to the MLCT from the ruthenium to the terminal pyridine rings of the tpy. The intense absorption in the UV region at 283 nm is a mixture of a ligand to ligand charge transfer (LLCT) and an inter-ligand charge transfer (ILCT) between the tpy -and MIC unit. Following this observations, the purple solution can be assigned to the Ru complex with a chloride ligand (**Ru$_4$**), while the orange solution is the Ru complex with an attached acetonitrile (**Ru$_5$**) which is formed due to a light induced exchange. Further proof for this transformation was obtained from ^{1}H NMR spectroscopy (Figure S17) and mass spectrometry. UV/Vis-SEC measurements of the two oxidation -and the three reduction processes of **Ru$_4$** were performed in an optically transparent thin layer electrochemical (OTTLE) cell in acetonitrile. In the first oxidation, which is entirely metal based (Ru(II) → Ru(III)), a small red shift and loss of intensity of the band at 545 nm were observed. After reoxidation, the spectra are in complete agreement with the initial spectra, indicating a fully reversible process. During the second oxidation, the MLCT band disappears completely and again, the process is reversible. DFT calculations corroborate the hypothesis that the oxidation is metal based (Figure S41). The first reduction leads to a red shift of the band at 326 nm by 30 nm. After reoxidation, the observed spectrum is comparable to the initial spectrum. From the spin density plots, it is clear that the reduction is manly based on the substituted tpy ligand (Figure S41). In the second reduction, the absorption is broadened in the visible region with a maximum at 410 nm.

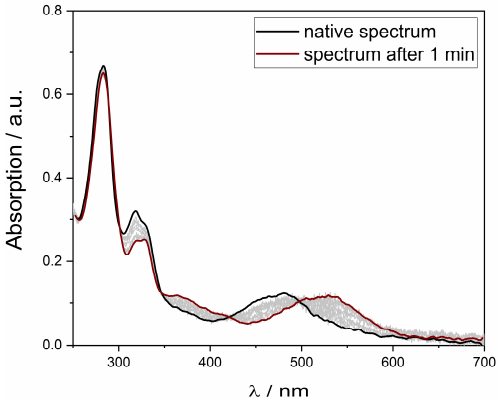

Figure 5: Changing of the UV/Vis spectrum of **Ru$_4$** after dissolving in MeCN at room temperature.

Chemistry - A European Journal 10.1002/chem.202300405

Comparing the initial and final spectra indicates, that this process is not fully reversible, as indicated by a loss of intensity in the UV region. The spin density plot shows, that the reduction occurs at the terpyridine ligand (Figure S41). The third reduction at -2.29 V is also fully reversible, with only minor changes in the visible region and a blue shift of 20 nm of the band at 283 nm. Analysis of the spin density plot of the reduced species also indicate predominant contribution of the terpyridine centre towards reduction (Figure S41).

Electrocatalytic CO_2 reduction:

The catalytic activity of the complexes (**Ru2**, **Ru3**, and **Ru4**) was studied in acetonitrile solution containing 0.1M NBu_4PF_6 under a CO_2 atmosphere. When the CVs of complexes **Ru2**, **Ru3**, and **Ru4** were measured in CO_2-saturated acetonitrile solution, a significant increase in current beyond the potential –2.1 V versus Fc/Fc^+ was observed, indicating a catalytic process (Figure 6(a)). A closer look at the voltammograms showed that the potential of the first reduction process under a CO_2 atmosphere remained relatively unaffected, with no noticeable change in the peak current as compared to measurements under Ar (Figure 6(a)). However, the cathodic waves become increasingly irreversible after the first reduction along with significant enhancement in catalytic current. This is indicative of a chemical reaction following the electron transfer process. Since the first reduction step is assigned to a reduction at the terpyridine backbone (see electrochemistry and UV/Vis-SEC section) the binding of CO_2 to the Ru(II) centre can be attributed to the chemical reaction, which is largely responsible for the enhancement of the cathodic current following an EC mechanism. Comparison of the onset potentials for the catalytic process in the case of **Ru2** and **Ru3** (–1.80 and –1.81 V, respectively) revealed insignificant changes (Figure 6(c)). Conversely, under identical experimental conditions for the corresponding **Ru4**, the onset potential (–1.59 V) showed an anodic shift of ~200 mV with a half-wave potential of –1.76 V versus Fc/FcH^+. The possible reasons for the decrease in the onset potential in **Ru4** compared to the long-chain analogues (**Ru2**, and **Ru3**) could be due to the better solubility of **Ru4** compared to **Ru3**, leading to better interactions with CO_2 in solution, as reported previously.[28] Considering the thermodynamic potential for CO_2 reduction in acetonitrile reported in the literature (–1.28 V versus Fc/FcH^+), an overpotential of 480 mV was calculated for **Ru4**, which is significantly lower than for the other two complexes (529 and 530 mV for **Ru2** and **Ru3**, respectively).[29] Thus, the overpotential for CO_2 reduction can be significantly influenced by changing the substituents on the typ ligand. Due to the lower overpotential observed

Chemistry - A European Journal 10.1002/chem.202300405

for catalytic reduction, further discussions will be limited to the catalytic properties of the complex **Ru4**.

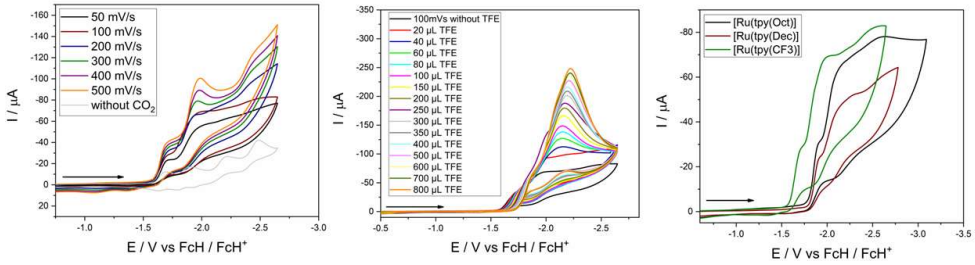

(a) **(b)** **(c)**

Figure 6. Cyclic voltammograms of **Ru4:** (a) under Ar (grey trace) and CO_2 atmosphere at different scan rates, (b) upon addition of increasing concentration of TFE in the CO_2 saturated solution. (c) Comparison of onset potentials of the complexes under investigation.

The use of 2,2,2-trifluoroethanol (TFE) as a proton source resulted in further enhancement of the irreversible cathodic current (Figure 6(b)), that followed a linear relationship with increasing concentrations of TFE, indicating a first-order rate dependence (Figure 7(b)). In addition, the linear increase in the value of $(i_{cat}/i_p)^2$ with TFE also indicates first-order reaction kinetics (Figure 7(c)).

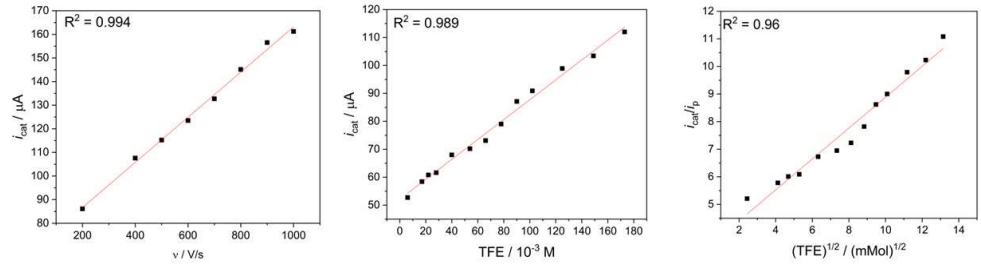

(a) **(b)** **(c)**

Figure 7. Plot of catalytic currents (i_{cat}) of 0.5 mM **Ru4** versus (a) scan rates and (b) the concentration of TFE. Diagram (c) depicts the variation of (i_{cat}/i_p) with the square root of the concentration of TFE.

However, the deviation of the cathodic wave from the ideal *S*-shaped diagram as predicted by Savéant and co-workers[30] under limiting scan rates (ν > 300 mV/s) and concentrations of TFE precluded extraction of the kinetic parameters. Therefore, the maximum turnover frequency (TOF_{max}) was determined from the slope of i_{cat}/i_p vs. $\nu^{-1/2}$ as 14.07 s^{-1} (Figure S45).[31] On the other hand, the overall catalytic rate constant calculated for the catalytic process was 3.17 s^{-1} (Figure S24, see supporting information).

Chemistry - A European Journal 10.1002/chem.202300405

Although a direct comparison of molecular catalysts for CO_2 reduction is not recommended, given the role of various competitive factors,[32] the catalyst studied here (**Ru4**) can be considered a reasonably active catalyst based on the elucidated kinetic parameters.

The products formed during the catalytic process were evaluated by controlled potential electrolysis at –1.74 V versus. Fc/FcH+ in anhydrous acetonitrile in the presence of 10% TFE, followed by gas chromatographic analysis of the gaseous reaction mixture (Figure S30). Electrolysis of the 0.05 mM acetonitrile solution of catalyst **Ru4** for 1.5 hours resulted in the consumption of 1.91 C of charge along with selective production of 8.99 µmol of CO with a faradaic efficiency of 92% (see supporting information). Further analysis of the reaction mixture revealed an almost negligible amount of H_2 production during the electrolysis process indicating selectivity of the catalyst towards CO (Figure S30). The formation of HCOOH could also be ruled out, as no characteristic peak corresponding to formate appeared in the ^{1}H NMR spectra of the solution after electrolysis (Figure S16).

Various control experiments were performed to rule out adverse effects of any side-phenomena in the catalytic process. UV/Vis spectra of the catalyst solution recorded before and after electrolysis show no change in the position of the absorption maxima, demonstrating the integrity of the core molecular structure of the catalysts (Figure S39). To exclude any effects of catalyst decomposition during electrolysis, rinse test was performed. The absence of any catalytic current beyond the background rules out any role of physically adsorbed species in catalysis (Figure S23). Furthermore, the SEM/EDX analysis of the working electrode after electrolysis showed the absence of ruthenium nanoparticles, ruling out any possible involvement of the nanoparticles in catalysis (Figure S31).[33] Since the presence of a proton source (TFE) can in some cases negatively affect the catalytic process by decomposition of the catalysts, an acid stability test was performed by monitoring the UV/Vis spectra of the 1:1 acetonitrile/TFE solution of the catalyst for 72 hours (Figure S35). Identical electronic spectra during the experiment illustrated the stability of the catalysts in the presence of a proton source.

The plausible mechanism of the catalytic reaction was investigated by spectroelectrochemical, FTIR, and NMR studies of the intermediates of the catalyst **Ru4** under investigation. Since the irreversible cathodic wave occurs after the first reduction process, it can be assumed that one electron reduced species is involved in the catalytic reduction. The spectroelectrochemical analysis described above clearly indicates the

Chemistry - A European Journal 10.1002/chem.202300405

participation of terpyridine in the first reduction step. Since the exchange of chloride ion with acetonitrile takes place instantaneously, $[Ru(tpy)(MIC)CH_3CN]^{2+}$ (**Ru5**) can be assigned as a key species involved in the catalytic process. Electrochemical measurements were also performed with the corresponding $[Ru(tpy)(MIC)CH_3CN]^{2+}$ (**Ru5**) in CH_3CN with both NBu_4PF_6 and NBu_4Cl as a supporting electrolyte under CO_2 atmosphere. The response of the catalysts **Ru5** in NBu_4Cl was found to agree well with the observation noted with **Ru4** in NBu_4PF_6 indicating the significance of a prequilibrium (**Ru4** ⇄ **Ru5**) between chloride and acetonitrile solvated complex in the catalytic activity (Figure S28).[34] A precatalytic wave before the irreversible cathodic wave at -1.59 V could probably be assigned to the exchange between chloride and acetonitrile ligand, which results in a shift of the onset potential (Figure S28). Moreover, it was observed that the electrochemical response of **Ru5** under CO_2 atmosphere was more pronounced in the presence of NBu_4Cl than NBu_4PF_6, suggesting that a higher concentration of chloride ions facilitates the catalytic process (Figure S28(a)). Importantly in the spectroelectrochemical analysis, the UV/Vis/NIR spectra of the acetonitrile solutions of **Ru4** under Ar and CO_2 environments at open circuit potential (-0.23 V) revealed no difference in the position of absorption bands at 545 nm, which rules out any side reaction or decomposition under CO_2 atmosphere. Now, based on the spectroelectrochemical analysis of **Ru4** in acetonitrile under Ar (Figure S34, see **UV/Vis-SEC** section), the one electron reduced form of the acetonitrile complex can be formulated as $[Ru(tpy^{\bullet-})(MIC)CH_3CN]^{+}$. Upon electrolysis of the CO_2 saturated solution **Ru4** at –1.75 V, a blue shift of the absorption band to 445 nm was observed. Analysis of this solution by IR spectroscopy showed the formation of new bands at 1620 and 1670 cm^{-1}, which could be assigned to the carbonyl stretching frequencies of HCO_3^- (Figure S40).[35] However, the formation of HCOOH, and HCHO, was not detected in either the IR or the NMR spectra of the solution. Notably, electrolysis of the CO_2 saturated solution of **Ru4** containing 150 µL of TFE did not show peaks corresponding to HCO^{3-} in the IR spectroscopy. However, controlled potential electrolysis of the CO_2 saturated acetonitrile solution of **Ru4** containing 0.1 M *N*Bu_4PF_6 and TFE at -1.75 V over a period of 30 min resulted in the appearance of a band at 2008 cm^{-1}, which is characteristic of Ru-CO stretching vibrations (Figure S38). Based on these observations, we can say that in the absence of TFE, $[Ru(tpy)(MIC)CO_2^{\bullet-}]$ forms Ru-CO via disproportionation reaction with CO_2. While, in the presence of proton source, i.e. TFE, the ruthenium carboxylate intermediate $[Ru(tpy)(MIC)CO_2^{\bullet-}]$, forms the Ru-CO species through the ruthenium-hydroxycarbonyl

Chemistry - A European Journal 10.1002/chem.202300405

([Ru(tpy)(MIC)COOH]$^{+}$) intermediate (Figure S40). In accordance with all the observations, the plausible mechanistic pathway for the **Ru4** catalysed CO_2 reduction can be described as follows (Scheme 3).[36] The Ru-CO_2 adduct [Ru(tpy)(MIC)CO2$^{\bullet-}$]$^{+}$ formed from the binding of CO_2 (Steps **c**), undergoes reduction (Steps **d**) followed by a formation of ruthenium-hydroxycarbonyl ([Ru(tpy)(MIC)COOH]$^{+}$) intermediate in the presence of TFE (Steps **e**). The hydroxycarbonyl intermediate upon subsequent protonation and dehydration (Steps **f**) leads to the formation of metal-carbonyl ([Ru(tpy)(MIC)CO]$^{2+}$) intermediate, which is followed by a reduction and ligand exchange to complete the cycle.

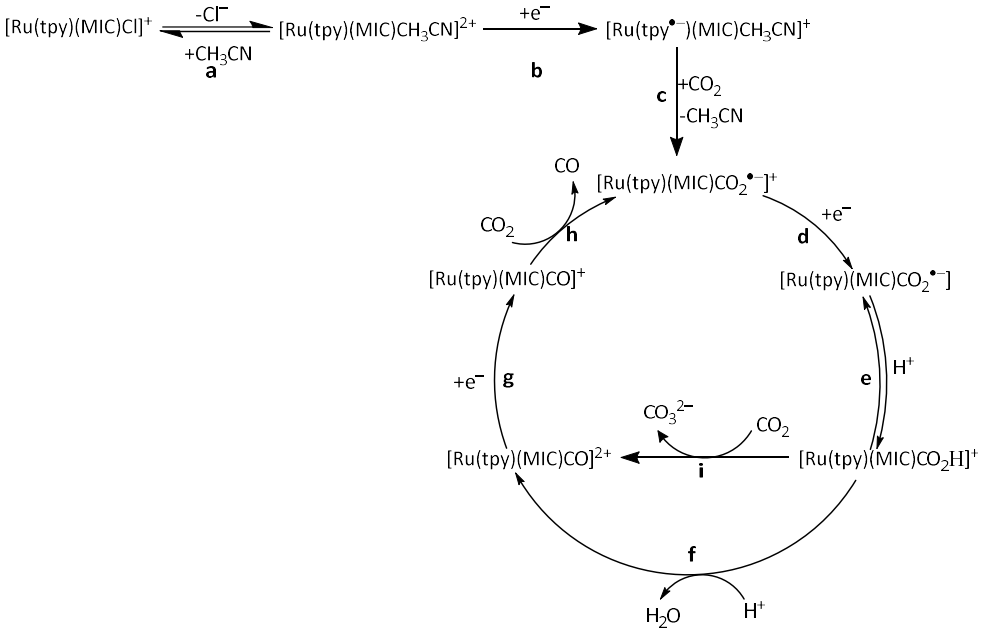

Scheme 3: Possible reaction mechanism for the electrocatalytic CO_2 reduction.

Chemistry - A European Journal 10.1002/chem.202300405

Conclusion

In summary, we have reported here the synthesis and characterization of five Ru(II) complexes (**Ru2**-**Ru6**) bound with terpyridines with different PFC tails, a bis-MIC ligand and different monodentate ligands. A detailed study of the optical properties showed, that in acetonitrile the chloride ligand is immediately exchanged by a solvent molecule. A combination of DFT calculations and UV/Vis-SEC measurements showed that both oxidations are reversible and metal-based, whereas the first two reductions occur at the tpy ligand. The catalytic activity for the electrochemical CO_2 reduction in the presence of TFE as a proton source was investigated for all complexes. Based on the lower onset potential of **Ru4** by 200 mV compared to the other two complexes, **Ru4** was used for a detailed investigation of electrochemical CO_2 reduction. With that complex, a faradaic efficiency of 92% and a turnover frequency (TOF_{max}) of 14.07 s^{-1} were achieved. Based on control experiments, the formation of hydrogen and HCOOH could be excluded. The stability of the catalyst was also demonstrated by UV/Vis experiments and SEM/EDX analysis. A combination of UV/Vis and IR spectroscopy shows that in the presence of a proton an ECE mechanism is followed. We have demonstrated here that tpy centered reductions can be used to open up electrocatalytic CO_2 reduction pathways at the bound metal centre, and the overpotential for CO_2 reduction can be controlled via remote substitution at the tpy ligands. Additionally, we have shown that the strongly donating MIC ligands are helpful in generating favourable kinetic parameters in electrocatalytic CO_2 reduction. Considering the steric and electronic tuning that are synthetically possible for both terpyridine and MIC ligands, we believe that the results presented here will be useful for orthogonal tuning of thermodynamic and kinetic parameters for electrocatalytic CO_2 reduction by combining these two ligand classes within the same catalyst platform.

Chemistry - A European Journal 10.1002/chem.202300405

Experimental Section

General experimental considerations and instrumentation:

Unless otherwise noted, all reactions were carried out using standard Schlenk-line techniques under an inert atmosphere of argon (Linde, HiQ Argon 5.0, purity≥99.999%) or in a MBraun Unilab SP GloveBox. Commercially available chemicals were used without further purification. THF and diethyl ether were dried and distilled from sodium/benzophenone. Other solvents were available from MBRAUN MB-SPS-800 solvent system. For the synthesis part, all solvents were degassed by standard techniques prior to use. For NMR, $CDCl_3$ was passed through a small plug basic alumina. ^1H NMR and $^{13}C\{^1H\}$ spectra were recorded on JEOL ECS/ECZ 400/400R spectrometer and JEOL ECZ 400R spectrometer at room temperature. Kinetic NMR spectra were recorded in Fourier transform mode with a Bruker AVANCE 500 spectrometer at 298 K. Chemical shifts are reported in ppm (relative to the TMS signal) with reference to the residual solvent peaks.[37] Multiplets are reported as follows: singlet (s), doublet (d), triplet (t), quartet (q), quintet (quint), and combinations thereof. Mass spectrometry was performed on an Agilent 6210 ESI-TOF. UV/Vis/NIR spectra were recorded with an on a J&M TIDAS spectrometer instrument.

X-ray data were collected on a Bruker D8Venture system at 100(2) K, using graphite-monochromated $Mo_{K\alpha}$ radiation (λ_α= 0.71073 Å). The strategy for the data collection was evaluated by using the APEX3 software. The data were collected by ω+φscan techniques and were scaled and reduced using Saint+ and SADABS software. The structures were solved by intrinsic phasing methods using SHELXT-2014/7. The structure was refined by full matrix least-squares usingSHELXL-2014/7, refining on F2. Non-hydrogen atoms were refined anisotropically.[38] The contribution of disordered solvent molecules to the diffraction pattern was subtracted from the observed data by the "SQUEEZE" method as implemented in PLATON.[39] Deposition Numbers CSD2203803 (for **Ru_4**) and CSD2203804 (for **Ru_5**) contain the supplementary crystallographic data for this paper. These data are provided free of charge by the joint Cambridge Crystallographic Data Centre and Fachinformationszentrum Karlsruhe.

Electrochemistry:

Cyclic voltammograms were recorded with a PalmSens4 potentiostat or with a Metrohm Autolab PGSTAT101 by working in anhydrous and degassed acetonitrile (MeCN) with

Chemistry - A European Journal 10.1002/chem.202300405

0.1 M $^{N}Bu_4PF_6$ (dried, >99.0%, electrochemical grade, Fluka) as the supporting electrolyte. A three-electrode setup was used with a glassy carbon working electrode, a coiled platinum wire as counter electrode, and a coiled silver wire as a pseudoreference electrode. The ferrocene/ ferrocenium couple was used as an internal reference.[40]

Bulk electrolysis measurements were performed in a two-compartment cell divided by microporous membrane (Celgard® 2325). A 0.05 mM MeCN solution of **Ru$_4$** containing 0.1 M $^{N}Bu_4PF_6$ and 0.1 M of TFE was sparged with argon before measurements. The measurements were performed with a Glassy (Vitreous) Carbon rod electrode - GCR 6/60 mmas a working electrode, coiled platinum wire as a counter electrode and a coiled silver wire as a pseudoreference electrode. Samples of the headspace (500 µL) were taken using a gastight syringe (Hamillton). The headspace composition was analyzed using a gas chromatograph equipped with a shincarbon column and a TCD detector using helium as a carrier gas for CO and Ar for the detection of H_2.

Density Functional Theory:

All calculations were performed with the ORCA program package, versions 4.0.1.2 and 4.2.8.[41] The geometries of all species were optimized using the PBE0 functional,[42] the def2-SVP basis sets on all atoms except for Ru, for which the def2-TZVP basis set was used.[43] Solvation was taken into account using the using the SMD method together with the CPCM model[44] using MeCN as solvent, and dispersion corrections were included using the D3 dispersion correction model.[45] The resolution-of-the identity (RI) approximation,[46] with matching basis sets,[47] as well as the RIJCOSX approximation (combination of RI and chain-of-spheres algorithm for exchange integrals) were used to reduce the time of calculations. Numerical frequencies calculations were used in order to check that the optimized structures were local minima and to obtain Gibbs free enthalpies. To obtain more reliable energetics single-point calculations were performed using the optimized geometries, the PBE0 functional and def2-TZVP basis sets on all atoms. Low-lying excitation energies were calculated with time-dependent DFT (TD-DFT). For all calculations spin densities were calculated according to the Löwdin population analysis.[48] Broken-symmetry calculations[48,49] were carried out using optimized geometry to evaluate the exchange coupling constants. Plots of spin-densities and optimized geometries were performed using Chemcraft.[50]

Synthesis

[Ru(tpy-O-(CH$_2$)$_2$-(CF$_2$)$_5$-CF$_3$)(bicarbene)(Cl)] (Ru$_2$)

Chemistry - A European Journal 10.1002/chem.202300405

Ru1 (36.6 mg, 0.05 mmol 1 eq.) and tpy-O-$(CH_2)_2$-$(CF_2)_5CF_3$ **(L_1)** (33.5 mg, 0.05 mmol, 1.0 eq.) were dissolved in DMSO (1.5 mL) and the solution was purged with argon for 5 min. The mixture was stirred at 120 °C for 16 h. The DMSO was evaporated under high vacuum and **Ru2** was purified via column chromatography (neutral Alox, DCM:MeOH = 100:1) to give the product as a deep purple solid (41.2 mg, 0.032 mmol, 65%).

^{1}H NMR (400 MHz, CD_3CN): δ = 8.29 (m, 2H, CH_{arom}), 8.17 (m, 2H, CH_{arom}), 8.08 (s, 2H, CH_{arom}), 7.95 (m, 2H, CH_{arom}), 7.91 (m, 4H, CH_{arom}), 7.58 (m, 3H, CH_{arom}), 7.31 (m, 2H, CH_{arom}), 7.24 (m, 3H, CH_{arom}), 7.06 (m, 2H, CH_{arom}), 6.36 (m, 2H, CH_{arom}), 4.73 (s, 3H, N-CH_3), 4.48 (s, 3H, N-CH_3), 4.44 (t, *J* = 6.26Hz 2H, CH_2), 2.79 (t, *J* = 6.76 Hz 2H, CH_2) ppm. ^{13}C NMR (176 MHz, $(CD_3)_2CO$): δ = 160.2, 160.4, 157.0, 144.6, 142.4, 141.5, 140.3, 138.7, 135.8, 130.8, 130.2, 130.0, 129.8, 129.0, 127.6, 127.1, 126.5, 126.1, 124.1, 119.1, 116.2, 115.7, 61.1, 40.3, 40.2, 31.6 ppm. ^{19}F NMR (376 MHz, $(CD_3)_2CO$): δ = -68.59, -70.47, -78.18, -110.19, -118.85, -119.92, -120.58, -123.26 ppm .HRMS(ESI): m/z calc. 1124.1411 (M^+), found 1124.1262 (M^+).

[Ru(tpy-O-$(CH_2)_2$-$(CF_2)_7$-CF_3)(bicarbene)(Cl)] (Ru_3)

Ru1 (36.6 mg, 0.05 mmol 1 eq.) and tpy-O-$(CH_2)_2$-$(CF_2)_5CF_3$ **(L_2)** (38.6 mg, 0.05 mmol, 1.0 eq.) were dissolved in DMSO (1.5 mL) and the solution was purged with argon for 5 min. The mixture was stirred at 120 °C for 16 h. The DMSO was evaporated under high vacuum and **Ru3** was purified via column chromatography (neutral Alox, DCM:MeOH = 100:1) to give the product as a deep purple solid (33.5 mg, 0.025 mmol, 49%).

^{1}H NMR (400 MHz, CD_2Cl_2): δ = 8.26 (m, 2H, CH_{arom}), 8.16 (m, 2H, CH_{arom}), 8.05 (s, 2H, CH_{arom}), 7.93 (m, 2H, CH_{arom}), 7.90 (m, 4H, CH_{arom}), 7.60 (m, 3H, CH_{arom}), 7.31 (m, 2H, CH_{arom}), 7.22 (m, 3H, CH_{arom}), 7.06 (m, 2H, CH_{arom}), 6.37 (m, 2H, CH_{arom}), 4.69 (s, 3H, N-CH_3), 4.47 (s, 3H, N-CH_3), 4.45 (t, *J* = 6.99 Hz 2H, CH_2), 2.79 (t, *J* = 6.81 Hz 2H, CH_2) ppm.^{13}C NMR (176 MHz, $(CD_3)_2CO$): δ = 189.9, 183.1, 160.2, 160.0, 159.3, 157.1, 156.9, 156.3, 148.1, 144.6, 142.4, 141.5, 140.4, 138.7, 135.7, 130.8, 130.1, 130.1, 129.9, 129.8, 129.0, 128.4, 127.6, 127.1, 126.2, 126.1, 124.33 120.1, 119.1, 116.2, 115.6, 61.1, 40.3, 40.2, 31.6 ppm. ^{19}F NMR (376 MHz, $(CD_3)_2CO$): δ = -68.35, -70.23, -78.32, -110.13, -118.75, -119.02, -119.88, -120.59, -123.34 ppm. HRMS(ESI): m/z calc. 1224.1347 (M^+), found 1224.1297 (M^+).

[Ru(tpy-OCF_3)(bicarbene)(Cl)] (Ru_4)

Chemistry - A European Journal 10.1002/chem.202300405

Ru$_1$ (65.15 mg, 0.11 mmol 1 eq.) and tpy-O-CF_3 **(L_3)** (36.87 mg, 0.169 mm0l, 1.6 eq.) were dissolved in DMSO (2 mL) and the solution was purged with argon for 5 min. The mixture was stirred at 120 °C for 16 h. The DMSO was evaporated under high vacuum and **Ru$_4$** was purified via column chromatography (neutral Alox, DCM:MeOH = 100:1) to give the product as a deep purple solid (89.3 mg, 0.09 mmol, 82%).

^{1}H NMR (400 MHz, CD_2Cl_2): δ = 8.03 (m, 6H, CH_{arom}), 7.81 (s, 2H, CH_{arom}), 7.71 (m, 4H, CH_{arom}), 7.47 (m, 2H, CH_{arom}), 7.37 (m, 2H, CH_{arom}), 7.20 (m, 3H, CH_{arom}), 6.97 (m, 2H, CH_{arom}), 6.30 (m, 2H, CH_{arom}), 4.81 (s, 3H, N-CH_3), 4.50 (s, 3H, N-CH_3). ppm.^{13}C NMR (176 MHz, $(CD_3)_2CO$): δ = 191.1, 186.1, 159.8, 157.6, 156.1, 150.4, 146.5, 143.6, 142.4, 141.4, 140.2, 138.8, 137.5, 135.9, 130.3, 130.4, 130.1, 129.9, 129.0, 127.6, 127.3, 126.2, 124.0, 123.9, 122.2, 119.6, 40.4, 40.3. ppm. ^{19}F NMR (376 MHz (CD_3CN): δ = -58.45, -72.06, -73.94 ppm. Anal. Calcd. for Ru C_{40} H_{30} N_9 O P F_9 Cl: C, 48.47; H, 3.03; N, 12.72. Found: C, 48.11; H, 3.274; N, 12.55. HRMS(ESI): m/z calc. 846.1257 (M^+), Found 846.1319 (M^+).

[Ru(tpy-OCF_3)(bicarbene)(MeCN)] (Ru$_5$)

Ru$_4$ (20.0 mg, 0.02 mmol, 1 eq.) and $AgPF_6$ (5.6 mg, 0.022 mmol, 1.1 eq.) were suspended in MeCN (5 mL) and stirred overnight under exclusion of light. The orange solution with white precipitate was filtered over celite. After evaporation of the solvent, the crude mixture was recrystallized in MeCN and Et_2O. **Ru$_5$** was obtained as an orange solid (22 mg, 0.0195 mmol, 95%).

^{1}H NMR (250 MHz, CD_3CN): δ = 8.25 (m, 2H, CH_{arom}), 8.17 (s, 2H, CH_{arom}), 8.06 (m, 2H, CH_{arom}), 7.98 (m, 2H, CH_{arom}), 7.91 (m, 3H, CH_{arom}), 7.59 (m, 5H, CH_{arom}), 7.33 (m, 2H, CH_{arom}), 7.23 (m, 1H, CH_{arom}), 7.07 (m, 2H, CH_{arom}), 6.36 (m, 2H, CH_{arom}), 4.71 (s, 3H, N-CH_3), 4.46 (s, 3H, N-CH_3) ppm.^{13}C NMR (176 MHz, $(CD_3)_2CO$): δ = 189.7, 182.9, 161.6, 159.6, 153.4, 149.4, 144.9, 143.4, 143.1, 141.0, 140.4, 139.6, 133.9, 133.2, 132.9, 132.8, 132.6, 131.0, 130.1, 128.7, 127.1, 127.0, 125.1, 124.7, 124.7, 123.3, 123.2, 123.3, 120.3, 42.9, 42.7, 31.8, 5.2, 3.5 ppm. ^{19}F NMR (376 MHz, $(CD_3)_2CO$): δ = -55.16, -68.4, -70.28 ppm. HRMS(ESI): m/z calc. 426.0917 (M^{2+}), found 426.0912 (M^{2+}).

[Ru(tpy-OCF_3)(bicarbene)(CO)] (Ru$_6$)

Ru$_5$ (25.0 mg, 0.02 mmol, 1 eq.) was suspended in Ethanol (10 mL) and CO gas was bubbled through the solution at 0 °C for 10 minutes. The suspension was stirred overnight under exclusion of light at 70 °C. The yellow solution with yellow precipitate was filtered

Chemistry - A European Journal 10.1002/chem.202300405

over celite and washed with cold ethanol. **Ru_6** was obtained as a yellow solid (16 mg, 0.014 mmol, 71%).

^{1}H NMR (500 MHz, CD_3CN): δ = 8.34 (m, 2H, CH_{arom}), 8.22 (s, 2H, CH_{arom}), 8.10 (m, 2H, CH_{arom}), 8.05 (m, 2H, CH_{arom}), 7.98 (m, 2H, CH_{arom}), 7.87 (m, 2H, CH_{arom}), 7.63 (m, 5H, CH_{arom}), 7.43 (m, 2H, CH_{arom}), 7.23 (m, 1H, CH_{arom}), 7.10 (m, 2H, CH_{arom}) 6.43 (m, 2H, CH_{arom}), 4.73 (s, 3H, N-CH_3), 4.52 (s, 3H, N-CH_3) ppm.^{13}C NMR (176 MHz, $(CD_3)_2CO$): δ = 194.8, 184.2, 178.1, 158.1, 157.4, 155.6, 150.5, 141.7, 140.5, 138.9, 137.0, 135.6, 132.3, 131.3, 131.0, 130.8, 130.6, 129.0, 128.0, 126.08, 124.7, 122.8, 122.2, 41.1, 40.9 ppm. HRMS(ESI): m/z calc. 984.1160 (M^+), found 984.1162 (M^+).

Chemistry - A European Journal 10.1002/chem.202300405

Acknowledgments

Dr. Anja Wiesner is kindly acknowledged for the help by structural solution of the crystal of complex **Ru4 and Ru5**. We would like to acknowledge the assistance of the Core Facility BioSupraMol supported by the DFG. Funded by the Deutsche Forschungsgemeinschaft [DFG, German Research Foundation – Project-IDs 358283783 – SFB 1333/2 2022 and 387284271 – SFB 1349]. Arijit Singha Hazari kindly acknowledges funding from the European Union's Horizon 2020 research and innovation programme under the Marie Skłodowska-Curie grant agreement No. 894082. The authors acknowledge support by the state of Baden-Württemberg through bwHPC and the German Research Foundation (DFG) through grant no INST 40/575-1 FUGG (JUSTUS 2 cluster).

Keywords: CO_2 reduction; mesoionic carbenes; ruthenium; spectroelectrochemistry; terpyridine

Chemistry - A European Journal 10.1002/chem.202300405

References

[1] a) K. J. Lee, N. Elgrishi, B. Kandemir, J. L. Dempsey, *Nat. Rev. Chem.*, **2017**, *1*, 6879–6893; b) J. L. Dempsey, A. J. Esswein, D. R. Manke, J. Rosenthal, J. D. Soper, D. G. Nocera, *Inorg. Chem.*, **2005**, *44*, 6879–6892.

[2] E. E. Benson, C. P. Kubiak, A. J. Sathrum and J. M. Smieja, *Chem. Soc. Rev.*, **2009**, *38*, 89–99.

[3] a) M. D. Kärkäs, O. Verho, E. V. Johnston, B. Åkermark, *Chem. Rev.*, **2014**, *114*, 11863–12001; b) N. S. Lewis, D. G. Nocera, *P. Natl. A. Sci. USA*, **2006**, *103*, 15729–15735; c) J. R. McKone, S. C. Marinescu, B. S. Brunschwig, J. R. Winkler, H. B. Gray, *Chem. Sci.*, **2014**, *5*, 865–878.

[4] J.-M. Savéant, *Chem. Rev.*, **2008**, *108*, 2348–2378.

[5] J. Qiao, Y. Liu, F. Hong, J. Zhang, *Chem. Soc. Rev.*, **2014**, *43*, 631–675.

[6] a) M. L. Clark, P. L. Cheung, M. Lessio, E. A. Carter, C. P. Kubiak, *ACS Catal.*, **2018**, *8*, 2021–2029; b) M. L. Pegis, C. F. Wise, B. Koronkiewicz, J. M. Mayer, *J. Am. Chem. Soc.*, **2017**, *139*, 11000–11003; c) I. Azcarate, C. Costentin, M. Robert, J.-M. Savéant, *J. Phys. Chem. C*, **2016**, *120*, 28951–28960.

[7] R. Francke, B. Schille. M. Roemelt, *Chem. Rev.*, **2018**, *118*, 4631–4701.

[8] S. Gonell, E. A. Assaf, K. D. Duffee, C. K. Schauer, A. J. M. Miller, *J. Am. Chem. Soc.*, **2020**, *142*, 8980–8999.

[9] S. Gonell, M. D. Massey, I. P. Moseley, C. K. Schauer, J. T. Muckerman, A. J. M. Miller, *J. Am. Chem. Soc.*, **2019**, *141*, 6658–6671.

[10] a)S. Gonell, E. A. Assaf, J. Lloret-Fillol, A. J. Miller, *ACS Catal*. **2021**, *11*, 24, 15212–15222; b) E. A. Assaf, S. Gonell, C.-H. Chen, A. J. Miller, *ACS Catal*. **2022**, *12*, 20, 12596–12606.

[11] a) E. Baranoff, J.-P. Collin, L. Flamigni, J.-P. Sauvage, *Chem. Soc. Rev.,* **2004**, *33*, 147–155. c) H. Hofmeier, U. S. Schubert, *Chem. Soc. Rev.*, **2004**, *33*, 373–399; d) H.-J. Nie, C.-J. Yao, M.-J. Sun, Y.-W. Zhong, J. Yao, *Organometallics*, **2014**, *33*, 6223–6231; e) J. P. Sauvage, J. P. Collin, J. C. Chambron, S. Guillerez, C. Coudret, V. Balzani, F. Barigelletti, L. de Cola, L. Flamigni, *Chem. Rev.*, **1994**, *94*, 993–1019; f) U. Schubert, G. R. Newkome, H. Hofmeier, *Modern terpyridine chemistry*, Wiley-VCH, Weinheim, **2006**; g) M.-J. Sun, J.-Y. Shao, C.-J. Yao, Y.-W. Zhong, J. Yao, *Inorg. Chem.*, **2015**, *54*, 8136–8147.

[12] J. Klein, A. Stuckmann, S. Sobottka, L. Suntrup, M. van der Meer, P. Hommes, H.-U. Reissig, B. Sarkar, *Chem. Eur. J.*, **2017**, *23*, 12314–12325.

[13] a) N. Elgrishi, M. B. Chambers, V. Artero, M. Fontecave, *Phys. Chem. Chem. Phys.* **2014**, *16*, 13635–13644; b) N. Elgrishi, M. B. Chambers, M. Fontecave, *Chem. Sci.*, **2015**, *6*, 2522–2531; c) N. Elgrishi, S. Griveau, M. B. Chambers, F. Bedioui, M. Fontecave, *Chem. Commun.*, **2015**, *51*, 2995–2998.

[14] R. Tatikonda, M. Cametti, E. Kalenius, A. Famulari, K. Rissanen, M. Haukka, *Eur. J. Inorg. Chem.*, **2019**, *2019*, 4463–4470.

[15] a) P. Hommes, C. Fischer, C. Lindner, H. Zipse, H.-U. Reissig, *Angew. Chem. Int. Ed.*, **2014**, *53*, 7647–7651; b) S. Aroua, T. K. Todorova, P. Hommes, L.-M. Chamoreau, H.-U. Reissig, V. Mougel, M. Fontecave, *Inorg. Chem.*, **2017**, *56*, 5930–5940.

[16] R. H. Crabtree, *Coord. Chem. Rev.*, **2013**, *257*, 755–766.

[17] O. Schuster, L. Yang, H. G. Raubenheimer, M. Albrecht, *Chem. Rev.*, **2009**, *109*, 3445–3478.

[18] a) R. Huisgen, G. Szeimies, L. Möbius, *Chem. Ber.*, **1967**, *100*, 2494–2507; b) C. W. Tornøe, C. Christensen, M. Meldal, *J. Org. Chem.*, **2002**, *67*, 3057–3064; c) V. V. Rostovtsev, L. G. Green, V. V. Fokin, K. B. Sharpless, *Angew. Chem. Int. Ed.*, **2002**, *41*,

Chemistry - A European Journal 10.1002/chem.202300405

2596–2599; d) H. C. Kolb, M. G. Finn, K. B. Sharpless, *Angew. Chem. Int. Ed.*, **2001**, *40*, 2004–2021.

[19] a) D. Schweinfurth, N. Deibel, F. Weisser, B. Sarkar, *Nachr. Chem.*, **2011**, *59*, 937–941; b) D. Schweinfurth, L. Hettmanczyk, L. Suntrup, B. Sarkar, *Z. Anorg. Allg. Chem.*, **2017**, *643*, 554–584.

[20] B. Schulze, U. S. Schubert, *Chem. Soc. Rev.*, **2014**, *43*, 2522–2571.

[21] K. F. Donnelly, A. Petronilho, M. Albrecht, *Chem. Commun.*, **2013**, *49*, 1145–1159.

[22] a) S. Hohloch, C. Y. Su, B. Sarkar, *Eur. J. Inorg. Chem.*, **2011**, *2011*, 3067–3075; b) M. Gazvoda, M. Virant, A. Pevec, D. Urankar, A. Bolje, M. Kočevar, J. Košmrlj, *Chem. Commun.*, **2016**, *52*, 1571–1574; c) R. Maity, S. Hohloch, C.-Y. Su, M. van der Meer, B. Sarkar, *Chem. Eur. J.*, **2014**, *20*, 9952–9961; d) A. Petronilho, M. Rahman, J. A. Woods, H. Al-Sayyed, H. Müller-Bunz, J. M. Don MacElroy, S. Bernhard, M. Albrecht, *Dalton Trans.,* **2012**, *41*, 13074–13080.

[23] a) S. Friães, S. Realista, C. S. B. Gomes, P. N. Martinho, B. Royo, *Molecules*, **2021**, *26*–39; b) L. Suntrup, F. Stein, J. Klein, A. Wilting, F. G. L. Parlane, C. M. Brown, J. Fiedler, C. P. Berlinguette, I. Siewert, B. Sarkar, *Inorg. Chem*, **2020**, *59*, 4215–4227; c) T. Scherpf, C. R. Carr, L. J. Donnelly, Z. S. Dubrawski, B. S. Gelfand, W. E. Piers, *Inorg. Chem.*, **2022**, *61*, 13644–13656; d) M. van der Meer, E. Glais, I. Siewert, B. Sarkar, *Angew. Chem. Int. Ed.,* **2015**, *54*, 13792–13795.

[24] G. Meng, L. Kakalis, S. P. Nolan, M. Szostak, *Tetrahedron Lett.*, **2019**, *60*, 378-381.

[25] L. Suntrup, S. Hohloch, B. Sarkar, *Chem. Eur. J.,* **2016**, *22*, 18009–18018.

[26] Z. Chen, C. Chen, D. R. Weinberg, P. Kang, J. J. Concepcion, D. P. Harrison, M. S. Brookhart, T. J. Meyer, *Chem. Commun.*, **2011**, *47*, 12607–12609.

[27] S. Gonell, M. D. Massey, I. P. Moseley, C. K. Schauer, J. T. Muckerman, A. J. M. Miller, *J. Am. Chem. Soc.*, **2019**, *141*, 6658–6671.

[28] F. Cheng, J. Zhu, A. Adronov, *Chem. Mater.*, **2011**, *23*, 3188–3194.

[29] C. Costentin, S. Drouet, M. Robert, J.-M. Savéant, *Science*, 2012, *338*, 90–94.

[30] J.-M. Saveant, *ChemElectroChem*, **2016**, *3*, 1967–1977.

[31] M. E. Ahmed, A. Rana, R. Saha, S. Dey, A. Dey, *Inorg. Chem.*, **2020**, *59*, 5292–5302.

[32] E. S. Rountree, B. D. McCarthy, T. T. Eisenhart, J. L. Dempsey, *Inorg. Chem.*, **2014**, *53*, 9983–10002.

[33] K. J. Lee, B. D. McCarthy, J. L. Dempsey, *Chem. Soc. Rev.*, **2019**, *48*, 2927–2945.

[34] H. Shirley, M. T. Figgins, C. M. Boudreaux, N. P. Liyanage, R. W. Lamb, C. E. Webster, E. T. Papish, J. H. Delcamp, *ChemCatChem*, **2020**, *12,* 4879–4885.

[35] E. Oberem, A. F. Roesel, A. Rosas-Hernández, T. Kull, S. Fischer, A. Spannenberg, H. Junge, M. Beller, R. Ludwig, M. Roemelt, R. Francke, *Organometallics*, **2019**, 38, 1236–1247.

[36] a) B. A. Johnson, S. Maji, H. Agarwala, T. A. White, E. Mijangos, S. Ott, *Angew. Chem. Int. Ed.*, **2016**, *55*, 1825–1829; b) B. Giri, A. Mahata, T. Kella, D. Shee, F. de Angelis, S. Maji, *J. Catal.*, **2022**, *405*, 15–23.

[37] G. R. Fulmer, A. J. M. Miller, N. H. Sherden, H. E. Gottlieb, A. Nudelman, B. M. Stoltz, J. E. Bercaw, K. I. Goldberg, *Organometallics*, **2010**, *29*, 2176–2179.

[38] (a) *APEX3*, Bruker AXS Inc., Madison, Wisconsin, USA, **2015**, (b) G. M. Sheldrick, *SADABS Ver. **2008**/1, Program for Empirical Absorption Correction*, University of Göttingen, Germany, **2008**, (c) *SAINT+, Data Integration Engine, Version 8.27b* ©, Bruker AXS Inc., Madison, Wisconsin, USA, **1997–2012**, (d) G. M. Sheldrick, *SHELXL Version **2014**/7, Program for Chrystal Structure Solution and Refinement*, University of Göttingen, Germany, **2014**, (e) C. B. Hübschle, G. M. Sheldrick, B. Dittrich, *J. Appl. Cryst*., **2011**, *44*, 1281–1284, (f) G. M. Sheldrick, *Acta Cryst*., **2008**, *A64*, 112–122, (g) G. M. Sheldrick, *Acta Cryst.*, **2015**, *C71*, 3.17 (h) A. L. Spek, *Acta Cryst*., **2015**, *C71*, 9–

Chemistry - A European Journal 10.1002/chem.202300405

18. (i) A. L. Spek, *ActaCryst.*, **2009**, *D65*, 148–155. (j) A. L. Spek, *J. Appl. Cryst*., **2003**, *36*, 7–13.

[39] A. L. Spek, *PLATON*, A multipurpose Crystallographic Tool, Utrecht, the Netherlands, **1998**.

[40] L. Fabbrizzi, *ChemTexts*, **2020**, *6*, 1039–1059.

[41] F. Neese, *WIREs Comput Mol Sci*, **2018**, *8,* 33–9.

[42] C. Adamo, V. Barone, *J. Chem. Phys.*, **1999**, *110*, 6158–6170.

[43] F. Weigend, R. Ahlrichs, *Phys. Chem. Chem. Phys*, **2005**, *7,* 3297–3305.

[44] V. Barone, M. Cossi, *J. Phys. Chem. A*, **1998**, *102*, 1995–2001.

[45] a) S. Grimme, *J. Comput. Chem.* **2006**, *27*, 1787–1799; b) S. Grimme, *J. Comput. Chem.* **2004**, *25*, 1463–1473; c) S. Grimme, J. Antony, S. Ehrlich, H. Krieg, *J. Chem. Phys.* **2010**, *132*, 154104–154122; d) S. Grimme, S. Ehrlich, L. Goerigk, *J. Comput. Chem.* **2011**, *32*, 1456–1465.

[46] a) P. Seth, P. L. Ríos, R. J. Needs, *J. Chem. Phys.* **2011**, *134*, 84105–84114; b) F. Neese, G. Olbrich, *Chem. Phys. Lett.* **2002**, *362*, 170–178; c) R. Izsák, F. Neese, *J. Chem. Phys.* **2011**, *135*, 144105–144117; d) J. L. Whitten, *J. Chem. Phys.* **1973**, *58*, 4496–4502; e) O. Vahtras, J. Almlöf, M. W. Feyereisen, *Chem. Phys. Lett.* **1993**, *213*, 514–518; f) F. Neese, F. Wennmohs, A. Hansen, *J. Chem. Phys* **2009**, *130*, 114108–114126; g) F. Neese, *J. Comput. Chem.* **2003**, *24*, 1740–1747.

[47] a) K. Eichkorn, O. Treutler, H. Öhm, M. Häser, R. Ahlrichs, *Chem. Phys. Lett.***1995**, *240*, 283–290; b) K. Eichkorn, F. Weigend, O. Treutler, R. Ahlrichs, *Theor. Chem. Acc.* **1997**, *97*, 119–124; c) F. Weigend, *Phys. Chem. Chem. Phys.* **2006**, *8*, 1057–1065.

[48] P.-O. Löwdin, *J. Chem. Phys* **1950**, *18*, 365–377.

[49] a) D. Doehnert, J. Koutecky, *J. Am. Chem. Soc.* **1980**, *102*, 1789–1796; b) J. Gräfenstein, E. Kraka, M. Filatov, D. Cremer, *Int. J. Mol. Sci.* **2002**, *3*, 360–394; c) F. Neese, *J. Phys. Chem. Solids* **2004**, *65*, 781–785; d) K. Yamaguchi, *Chem. Phys. Lett.* **1975**, *33*, 330–335.

[50] Chemcraft - graphical software for visualization of quantum chemistry computations (Chemcraft,).

Chemistry - A European Journal 10.1002/chem.202300405

TOC

Ruthenium(II) complexes of PFC substituted terpyridines and MIC ligands are presented as molecular electrocatalysts for CO_2 reduction. The MIC ligand is used to tune the kinetics of CO_2 electrocatalysis and the terpyridine ligands are used for controlling the overpotential.

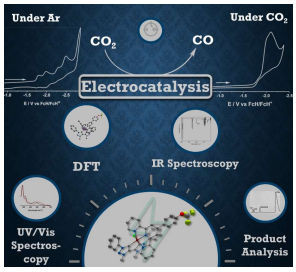

Twitter Handle: SarkarAg

Supporting Information

Ruthenium Complexes of Polyfluorocarbon Substituted Terpyridine and Mesoionic Carbene Ligands: An Interplay in CO_2 Reduction

Felix Stein,[a, b],# Maite Nößler,[a],# Arijit Singha Hazari,[b], Lisa Böser,[a, c] Robert Walter,[b] Hang Liu,[c] Elias Klemm,[c] Biprajit Sarkar[a, b],**

Content

General Information

General experimental considerations and instrumentation:

Unless otherwise noted, all reactions were carried out using standard Schlenk-line techniques under an inert atmosphere of argon (Linde, HiQ Argon 5.0, purity≥99.999%) or in a MBraun Unilab SP GloveBox. Commercially available chemicals were used without further purification. THF and diethyl ether were dried and distilled from sodium/benzophenone. Other solvents were available from MBRAUN MB-SPS-800 solvent system. For the synthesis part, all solvents were degassed by standard techniques prior to use. For NMR, $CDCl_3$ was passed through a small plug basic alumina.^{1}H NMR and $^{13}C\{^{1}H\}$ spectra were recorded on JEOL ECS/ECZ 400/400R spectrometer and JEOL ECZ 400R spectrometer at room temperature. Kinetic NMR spectra were recorded in Fourier transform mode with a Bruker AVANCE 500 spectrometer at 298 K. Chemical shifts are reported in ppm (relative to the TMS signal) with reference to the residual solvent peaks. [1] Multiplets are reported as follows: singlet (s), doublet (d),triplet (t) quartet (q), quintet (quint), and combinations thereof. Mass spectrometry was performed on an Agilent 6210 ESI-TOF. UV/Vis/NIR spectra were recorded with an on a J&M TIDAS spectrometer instrument.

X-ray data were collected on a Bruker D8Venture system at 100(2) K, using graphite-monochromated $Mo_{K\alpha}$ radiation (λ_{α}= 0.71073 Å). The strategy for the data collection was evaluated by using the APEX3 software. The data were collected by ω+ϕscan techniques and were scaled and reduced using Saint+ and SADABS software. The structures were solved by intrinsic phasing methods using SHELXT-2014/7. The structure was refined by full matrix least-squares usingSHELXL-2014/7, refining on F2. Non-hydrogen atoms were refined anisotropically.[2] The contribution of disordered solvent molecules to the diffraction pattern was subtracted from the observed data by the "SQUEEZE" method as implemented in PLATON.[3]

Electrochemistry:

Cyclic voltammograms were recorded with a PalmSens4 potentiostat or with a Metrohm Autolab PGSTAT101 by working in anhydrous and degassed acetonitrile (MeCN) with 0.1 M $^{N}Bu_4PF_6$ (dried, >99.0%, electrochemical grade, Fluka) as the supporting electrolyte. A three-electrode setup was used with a glassy carbon working electrode, a coiled platinum wire as counter electrode, and a coiled silver wire as a pseudoreference electrode. The ferrocene/ ferrocenium couple was used as an internal reference.[4]

Bulk electrolysis measurements were performed in a two-compartment cell divided by microporous membrane (Celgard® 2325). A 0.05 mM MeCN solution of **Ru_4** containing 0.1 M $^{N}Bu_4PF_6$ and 0.1 M of TFE was sparged with argon before measurements. The measurements were performed with a Glassy (Vitreous) Carbon rod electrode - GCR 6/60 mmas a working electrode, coiled platinum wire as a counter electrode and a coiled silver wire as a pseudoreference electrode. Samples of the headspace (500 µL) were taken using a gastight syringe (Hamillton). The headspace composition was analyzed using a gas chromatograph equipped with a shincarbon column and a TCD detector using helium as a carrier gas for CO and Ar for the detection of H_2.

Density Functional Theory:

All calculations were performed with the ORCA program package, versions 4.0.1.2 and 4.2.8.[5] The geometries of all species were optimized using the PBE0 functional,[6] the def2-SVP basis sets on all atoms except for Ru, for which the def2-TZVP basis set was used.[7] Solvation was taken into account using the using the SMD method together with the CPCM model[8] using MeCN as solvent, and dispersion corrections were included using the D3 dispersion correction model.[9] The resolution-of-the identity (RI) approximation,[10] with matching basis sets,[11] as well as the RIJCOSX approximation (combination of RI and chain-of-spheres algorithm for exchange integrals) were used to reduce the time of calculations. Numerical frequencies calculations were used in order to check that the optimized structures were local minima and to obtain Gibbs free enthalpies. To obtain more reliable energetics single-point calculations were performed using the optimized geometries, the PBE0 functional and def2-TZVP basis sets on all atoms. Low-lying excitation energies were calculated with time-dependent DFT (TD-DFT). For all calculations spin densities were calculated according to the Löwdin population analysis.[12] Broken-symmetry calculations[12,13] were carried out using optimized geometry to evaluate the exchange coupling constants. Plots of spin-densities and optimized geometries were performed using Chemcraft.[14]

Ru_1 was synthesised according to the literature.[15]

L_1, **L_2** and **L_3** were synthesized based on a literature known procedures.[16]

Synthesis

[Ru(tpy-O-$(CH_2)_2$-$(CF_2)_5$-CF_3)(bicarbene)(Cl)] (Ru_2)

Ru_1 (36.6 mg, 0.05 mmol 1 eq.) and tpy-O-$(CH_2)_2$-$(CF_2)_5CF_3$ **(L_1)** (33.5 mg, 0.05 mmol, 1.0 eq.) were dissolved in DMSO (1.5 mL) and the solution was purged with argon for 5 min. The mixture was stirred at 120 °C for 16 h. The DMSO was evaporated under high vacuum and **Ru_2** was purified via column chromatography (neutral Alox, DCM:MeOH = 100:1) to give the product as a deep purple solid (41.2 mg, 0.032 mmol, 65%).

^{1}H NMR (400 MHz, CD_3CN): δ = 8.29 (m, 2H, CH_{arom}), 8.17 (m, 2H, CH_{arom}), 8.08 (s, 2H, CH_{arom}), 7.95 (m, 2H, CH_{arom}), 7.91 (m, 4H, CH_{arom}), 7.58 (m, 3H, CH_{arom}), 7.31 (m, 2H, CH_{arom}), 7.24 (m, 3H, CH_{arom}), 7.06 (m, 2H, CH_{arom}), 6.36 (m, 2H, CH_{arom}), 4.73 (s, 3H, N-CH_3), 4.48 (s, 3H, N-CH_3), 4.44 (t, *J* = 6.26Hz 2H, CH_2), 2.79 (t, *J* = 6.76 Hz 2H, CH_2) ppm. ^{13}C NMR (176 MHz, $(CD_3)_2CO$): δ = 160.2, 160.4, 157.0, 144.6, 142.4, 141.5, 140.3, 138.7, 135.8, 130.8, 130.2, 130.0, 129.8, 129.0, 127.6, 127.1, 126.5, 126.1, 124.1, 119.1, 116.2, 115.7, 61.1, 40.3, 40.2, 31.6 ppm. ^{19}F NMR (376 MHz, $(CD_3)_2CO$): δ = -68.59, -70.47, -78.18, -110.19, -118.85, -119.92, -120.58, -123.26 ppm .HRMS(ESI): m/z calc. 1124.1411 (M^+), found 1124.1262 (M^+).

[Ru(tpy-O-$(CH_2)_2$-$(CF_2)_7$-CF_3)(bicarbene)(Cl)] (Ru_3)

Ru_1 (36.6 mg, 0.05 mmol 1 eq.) and tpy-O-$(CH_2)_2$-$(CF_2)_5CF_3$ **(L_2)** (38.6 mg, 0.05 mmol, 1.0 eq.) were dissolved in DMSO (1.5 mL) and the solution was purged with argon for 5 min. The mixture was stirred at 120 °C for 16 h. The DMSO was evaporated under high vacuum and **Ru_3** was purified via column chromatography (neutral Alox, DCM:MeOH = 100:1) to give the product as a deep purple solid (33.5 mg, 0.025 mmol, 49%).

^{1}H NMR (400 MHz, CD_2Cl_2): δ = 8.26 (m, 2H, CH_{arom}), 8.16 (m, 2H, CH_{arom}), 8.05 (s, 2H, CH_{arom}), 7.93 (m, 2H, CH_{arom}), 7.90 (m, 4H, CH_{arom}), 7.60 (m, 3H, CH_{arom}), 7.31 (m, 2H, CH_{arom}), 7.22 (m, 3H, CH_{arom}), 7.06 (m, 2H, CH_{arom}), 6.37 (m, 2H, CH_{arom}), 4.69 (s, 3H, N-CH_3), 4.47 (s, 3H, N-CH_3), 4.45 (t, *J* = 6.99 Hz 2H, CH_2), 2.79 (t, *J* = 6.81 Hz 2H, CH_2) ppm.^{13}C NMR (176 MHz, $(CD_3)_2CO$): δ = 189.9, 183.1, 160.2, 160.0, 159.3, 157.1, 156.9, 156.3, 148.1, 144.6, 142.4, 141.5, 140.4, 138.7, 135.7, 130.8, 130.1, 130.1, 129.9, 129.8, 129.0, 128.4, 127.6, 127.1, 126.2, 126.1,

124.33 120.1, 119.1, 116.2, 115.6, 61.1, 40.3, 40.2, 31.6 ppm. ^{19}F NMR (376 MHz, $(CD_3)_2CO$): δ = -68.35, -70.23, -78.32, -110.13, -118.75, -119.02, -119.88, -120.59, -123.34 ppm. HRMS(ESI): m/z calc. 1224.1347 (M^+), found 1224.1297 (M^+).

[Ru(tpy-OCF$_3$)(bicarbene)(Cl)] (Ru$_4$)

Ru$_1$ (65.15 mg, 0.11 mmol 1 eq.) and tpy-O-CF$_3$ **(L$_3$)** (36.87 mg, 0.169 mm0l, 1.6 eq.) were dissolved in DMSO (2 mL) and the solution was purged with argon for 5 min. The mixture was stirred at 120 °C for 16 h. The DMSO was evaporated under high vacuum and **Ru$_4$** was purified via column chromatography (neutral Alox, DCM:MeOH = 100:1) to give the product as a deep purple solid (89.3 mg, 0.09 mmol, 82%).

^{1}H NMR (400 MHz, CD_2Cl_2): δ = 8.03 (m, 6H, CH_{arom}), 7.81 (s, 2H, CH_{arom}), 7.71 (m, 4H, CH_{arom}), 7.47 (m, 2H, CH_{arom}), 7.37 (m, 2H, CH_{arom}), 7.20 (m, 3H, CH_{arom}), 6.97 (m, 2H, CH_{arom}), 6.30 (m, 2H, CH_{arom}), 4.81 (s, 3H, N-CH_3), 4.50 (s, 3H, N-CH_3). ppm.^{13}C NMR (176 MHz, $(CD_3)_2CO$): δ = 191.1, 186.1, 159.8, 157.6, 156.1, 150.4, 146.5, 143.6, 142.4, 141.4, 140.2, 138.8, 137.5, 135.9, 130.3, 130.4, 130.1, 129.9, 129.0, 127.6, 127.3, 126.2, 124.0, 123.9, 122.2, 119.6, 40.4, 40.3. ppm. ^{19}F NMR (376 MHz (CD_3CN): δ = -58.45, -72.06, -73.94 ppm. Anal. Calcd. for Ru C_{40} H_{30} N_9 O P F_9 Cl: C, 48.47; H, 3.03; N, 12.72. Found: C, 48.11; H, 3.274; N, 12.55. HRMS(ESI): m/z calc. 846.1257 (M^+), Found 846.1319 (M^+).

[Ru(tpy-OCF$_3$)(bicarbene)(MeCN)] (Ru$_5$)

Ru$_4$ (20.0 mg, 0.02 mmol, 1 eq.) and $AgPF_6$ (5.6 mg, 0.022 mmol, 1.1 eq.) were suspended in MeCN (5 mL) and stirred overnight under exclusion of light. The orange solution with white precipitate was filtered over celite. After evaporation of the solvent, the crude mixture was recrystallized in MeCN and Et_2O. **Ru$_5$** was obtained as an orange solid (22 mg, 0.0195 mmol, 95%).

^{1}H NMR (250 MHz, CD_3CN): δ = 8.25 (m, 2H, CH_{arom}), 8.17 (s, 2H, CH_{arom}), 8.06 (m, 2H, CH_{arom}), 7.98 (m, 2H, CH_{arom}), 7.91 (m, 3H, CH_{arom}), 7.59 (m, 5H, CH_{arom}), 7.33 (m, 2H, CH_{arom}), 7.23 (m, 1H, CH_{arom}), 7.07 (m, 2H, CH_{arom}), 6.36 (m, 2H, CH_{arom}), 4.71 (s, 3H, N-CH_3), 4.46 (s, 3H, N-CH_3)

ppm.^{13}C NMR (176 MHz, $(CD_3)_2CO$): δ = 189.7, 182.9, 161.6, 159.6, 153.4, 149.4, 144.9, 143.4, 143.1, 141.0, 140.4, 139.6, 133.9, 133.2, 132.9, 132.8, 132.6, 131.0, 130.1, 128.7, 127.1, 127.0, 125.1, 124.7, 124.7, 123.3, 123.2, 123.3, 120.3, 42.9, 42.7, 31.8, 5.2, 3.5 ppm. ^{19}F NMR (376 MHz, $(CD_3)_2CO$): δ = -55.16, -68.4, -70.28 ppm. HRMS(ESI): m/z calc. 426.0917 (M^{2+}), found 426.0912 (M^{2+}).

[Ru(tpy-OCF_3)(bicarbene)(CO)] (Ru_6)

Ru_5 (25.0 mg, 0.02 mmol, 1 eq.) was suspended in Ethanol (10 mL) and CO gas was bubbled through the solution at 0 °C for 10 minutes. The suspension was stirred overnight under exclusion of light at 70 °C. The yellow solution with yellow precipitate was filtered over celite and washed with cold ethanol. **Ru_6** was obtained as a yellow solid (16 mg, 0.014 mmol, 71%).

^{1}H NMR (500 MHz, CD_3CN): δ = 8.34 (m, 2H, CH_{arom}), 8.22 (s, 2H, CH_{arom}), 8.10 (m, 2H, CH_{arom}), 8.05 (m, 2H, CH_{arom}), 7.98 (m, 2H, CH_{arom}), 7.87 (m, 2H, CH_{arom}), 7.63 (m, 5H, CH_{arom}), 7.43 (m, 2H, CH_{arom}), 7.23 (m, 1H, CH_{arom}), 7.10 (m, 2H, CH_{arom}) 6.43 (m, 2H, CH_{arom}), 4.73 (s, 3H, N-CH_3), 4.52 (s, 3H, N-CH_3) ppm.^{13}C NMR (176 MHz, $(CD_3)_2CO$): δ = 194.8, 184.2, 178.1, 158.1, 157.4, 155.6, 150.5, 141.7, 140.5, 138.9, 137.0, 135.6, 132.3, 131.3, 131.0, 130.8, 130.6, 129.0, 128.0, 126.08, 124.7, 122.8, 122.2, 41.1, 40.9 ppm. HRMS(ESI): m/z calc. 984.1160 (M^+), found 984.1162 (M^+).

NMR Spectra

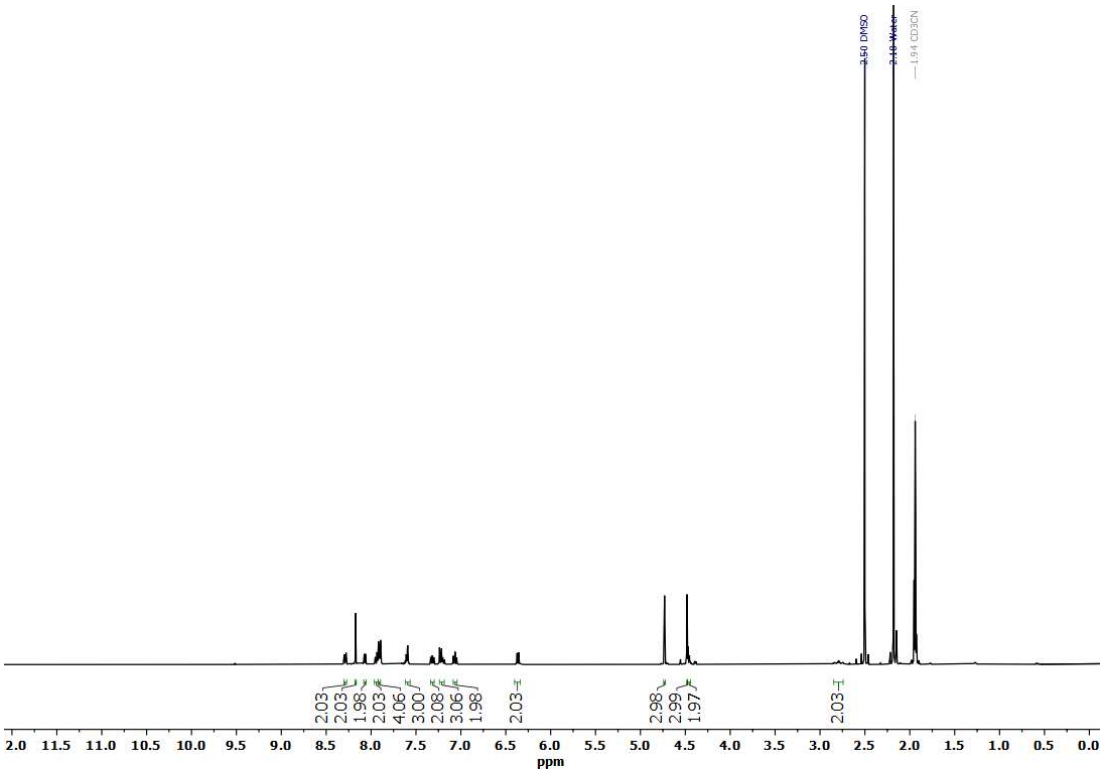

Figure S1: ^{1}H-NMR-Spectrum of compound **Ru$_2$**.

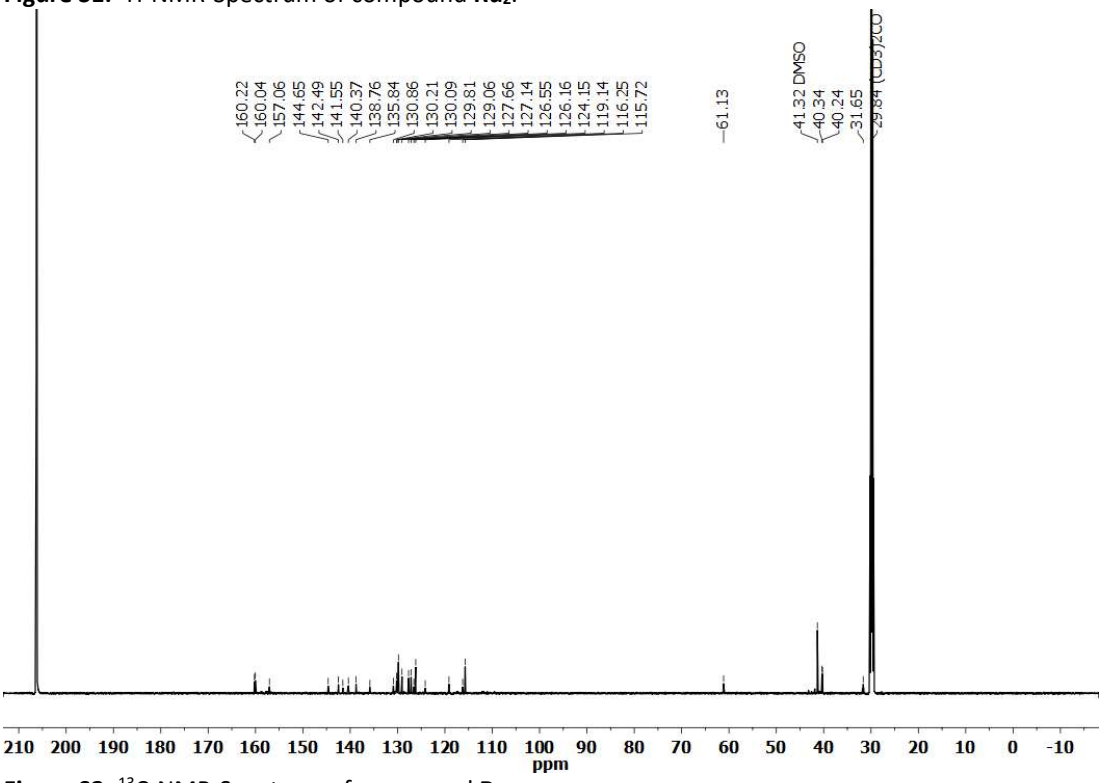

Figure S2: ^{13}C-NMR-Spectrum of compound **Ru$_2$**.

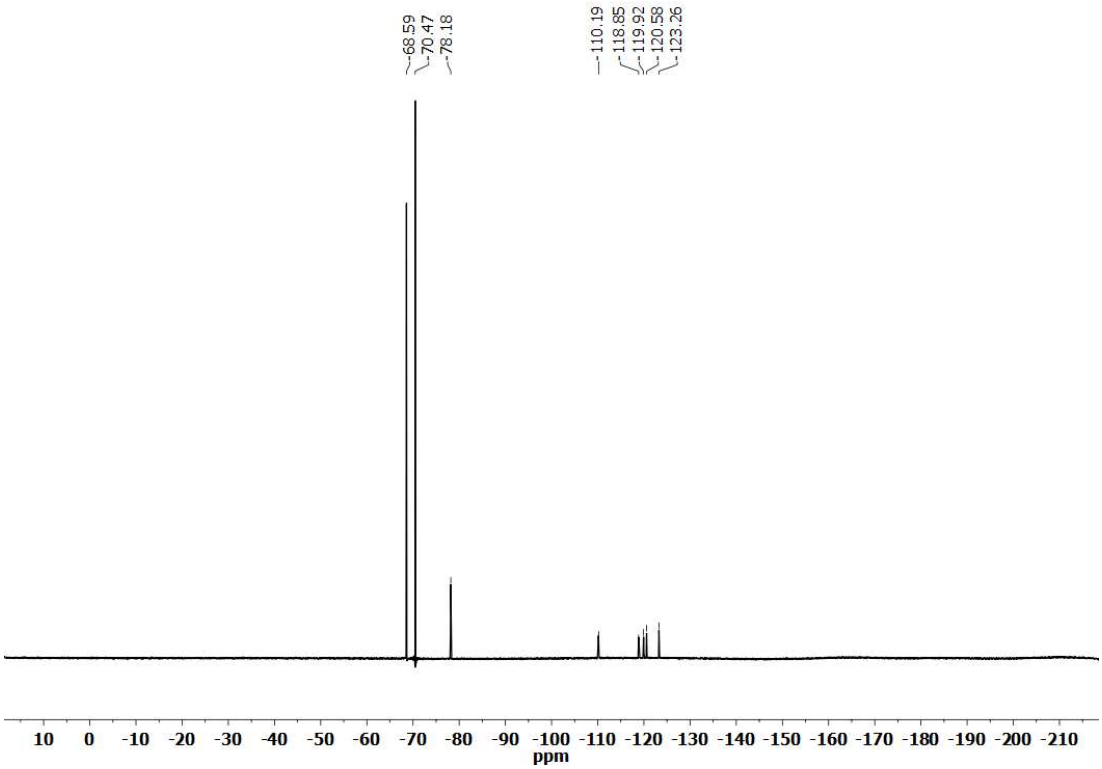

Figure S3: ^{19}F-NMR-Spectrum of compound **Ru$_2$**.

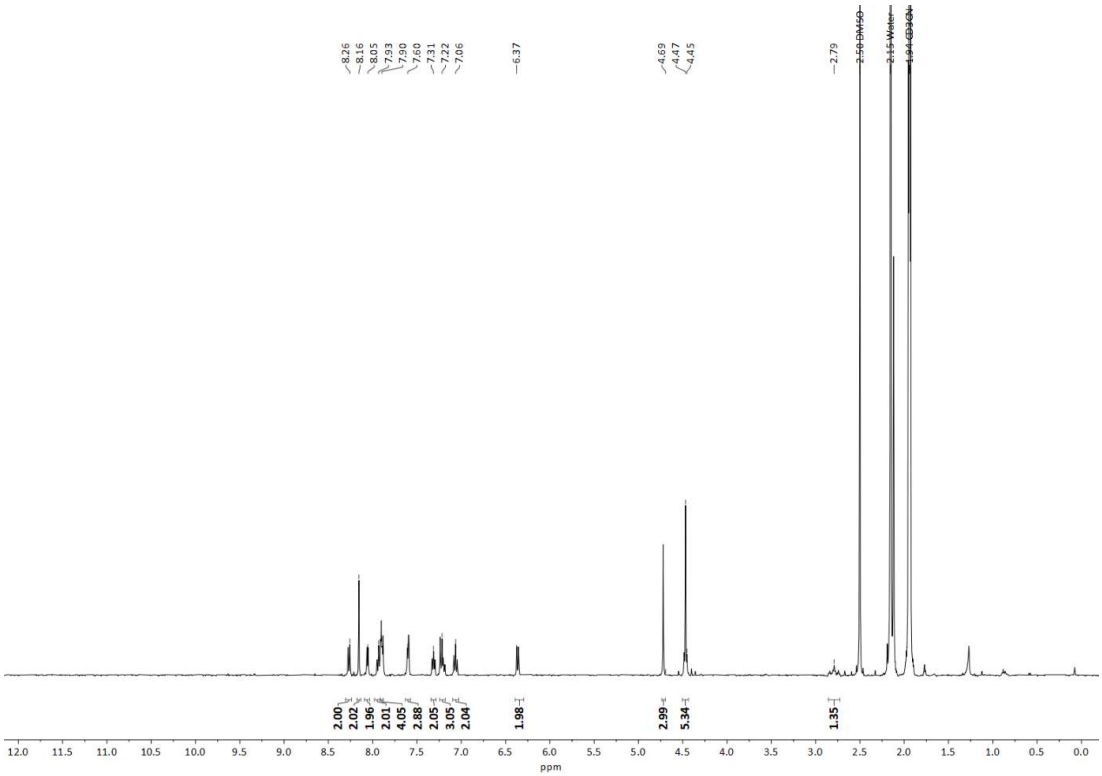

Figure S4: [1]H-NMR-Spectrum of compound **Ru_3**.

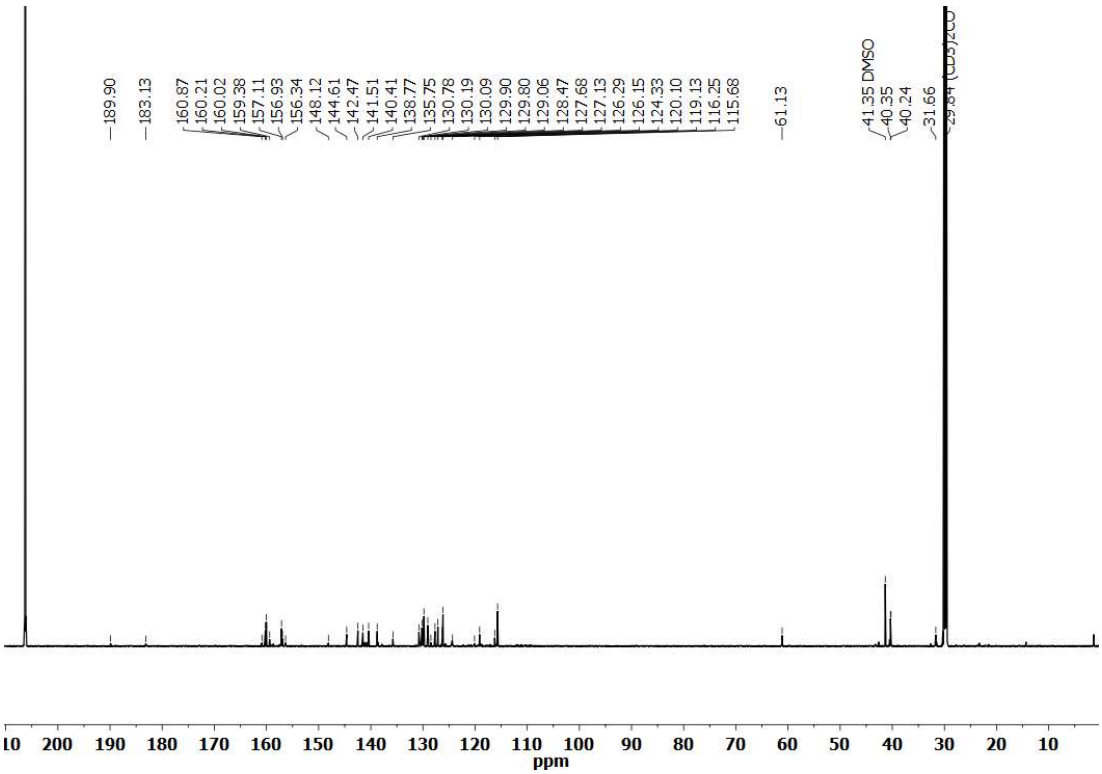

Figure S5: [13]C-NMR-Spectrum of compound **Ru_3**.

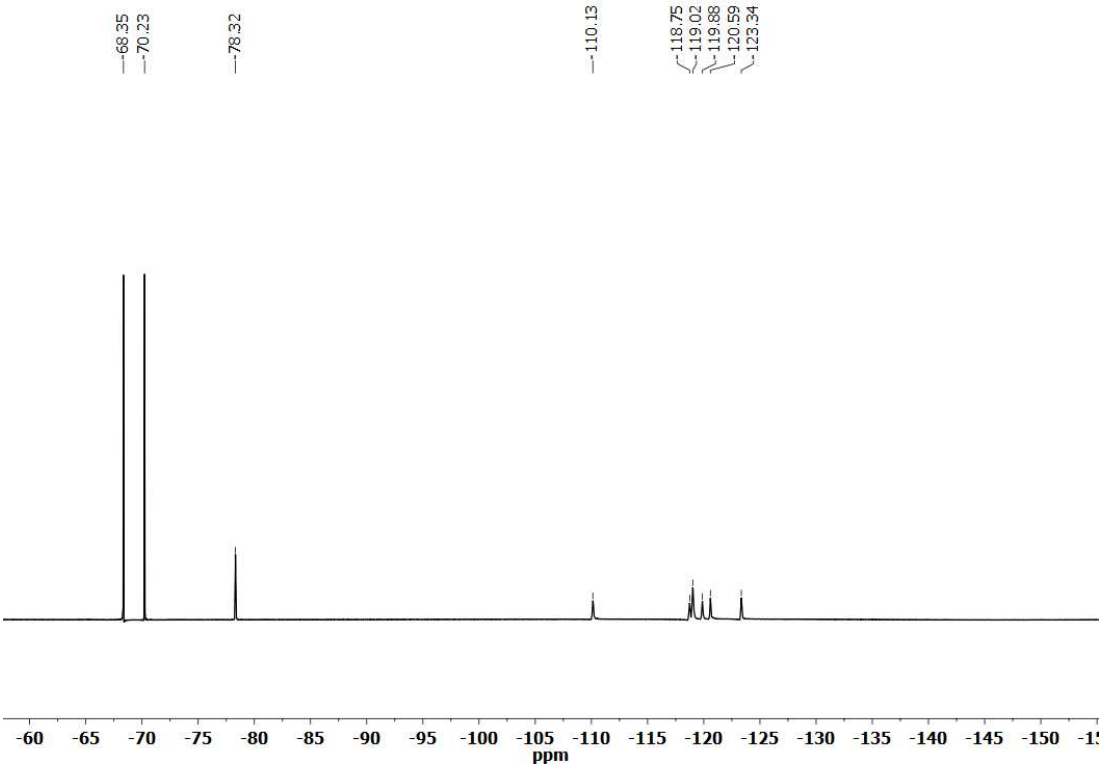

Figure S6: ^{19}F-NMR-Spectrum of compound **Ru$_3$**.

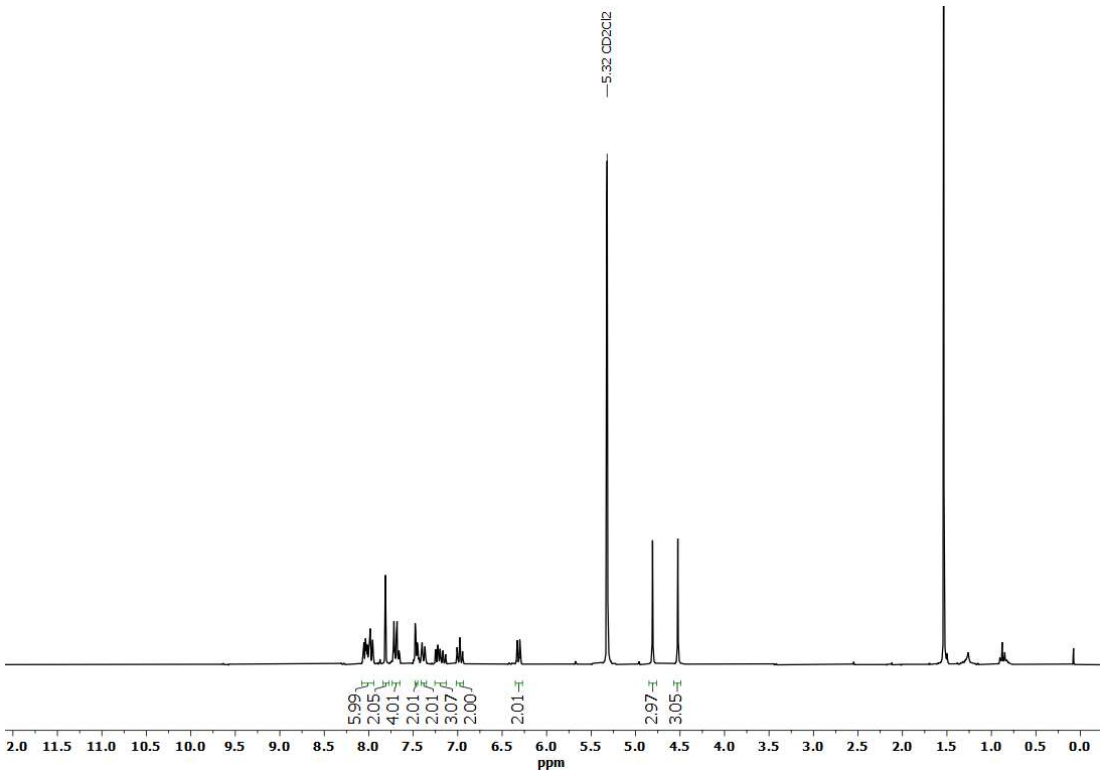

Figure S7: ^{1}H-NMR-Spectrum of compound **Ru$_4$**.

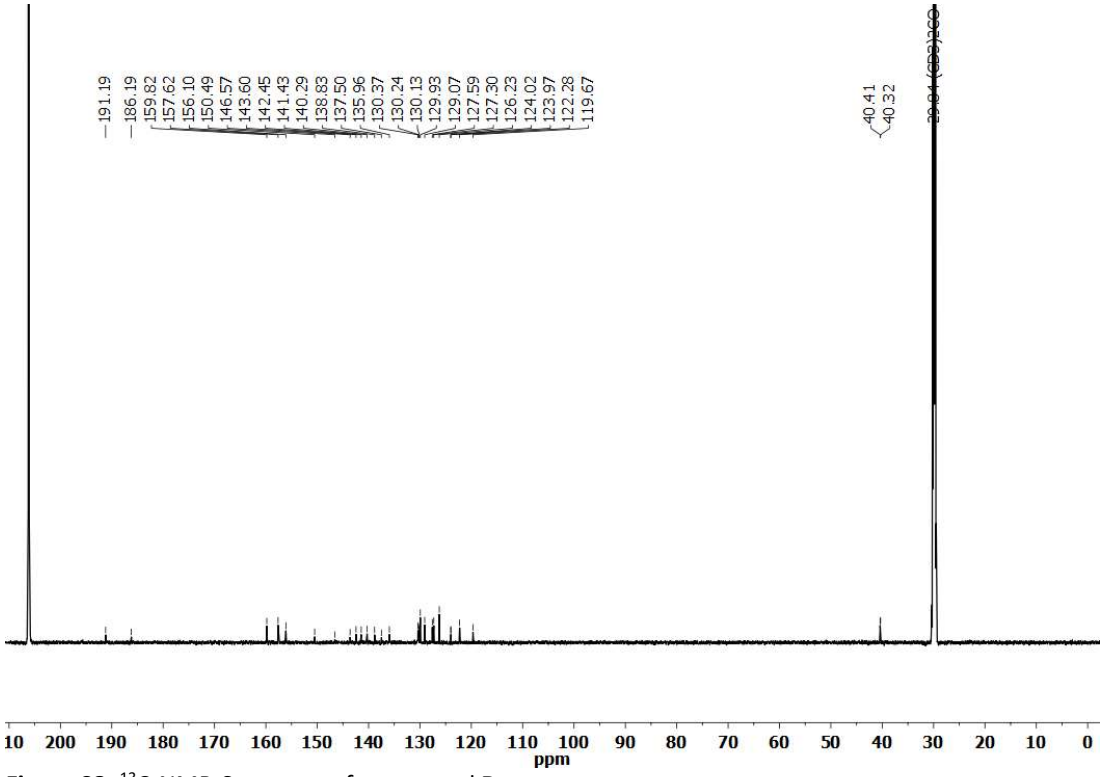

Figure S8: ^{13}C-NMR-Spectrum of compound **Ru$_4$**.

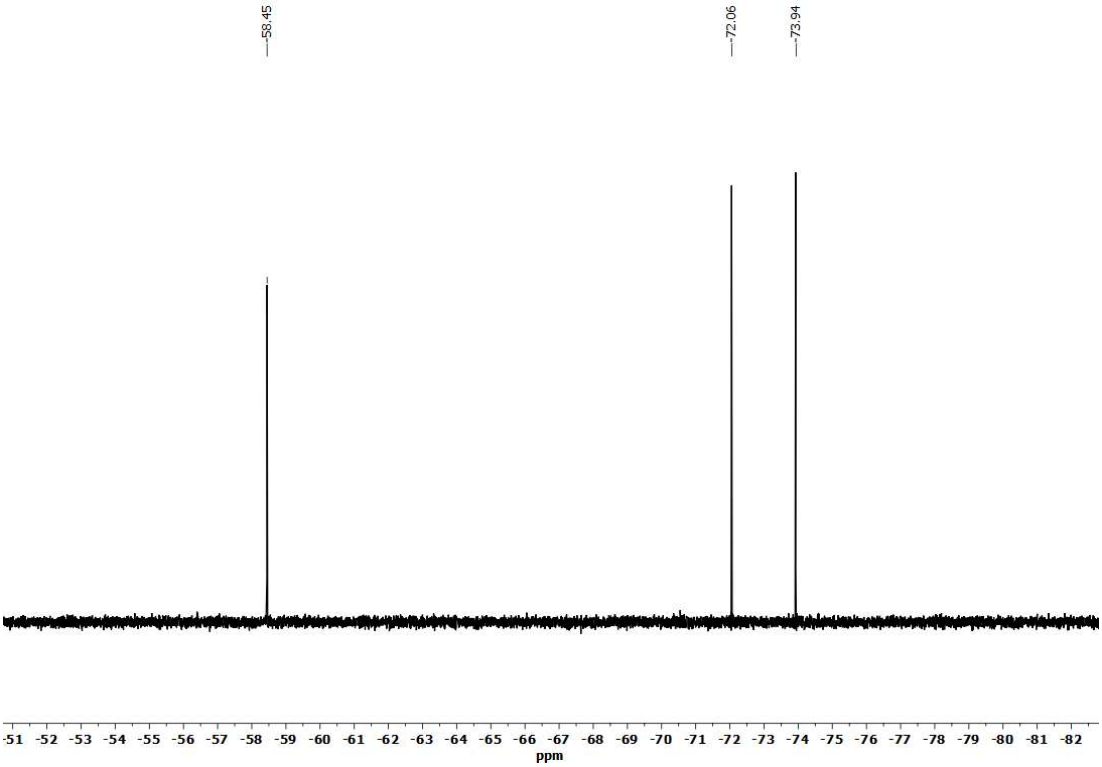

Figure S9: ^{19}F-NMR-Spectrum of compound **Ru$_4$**.

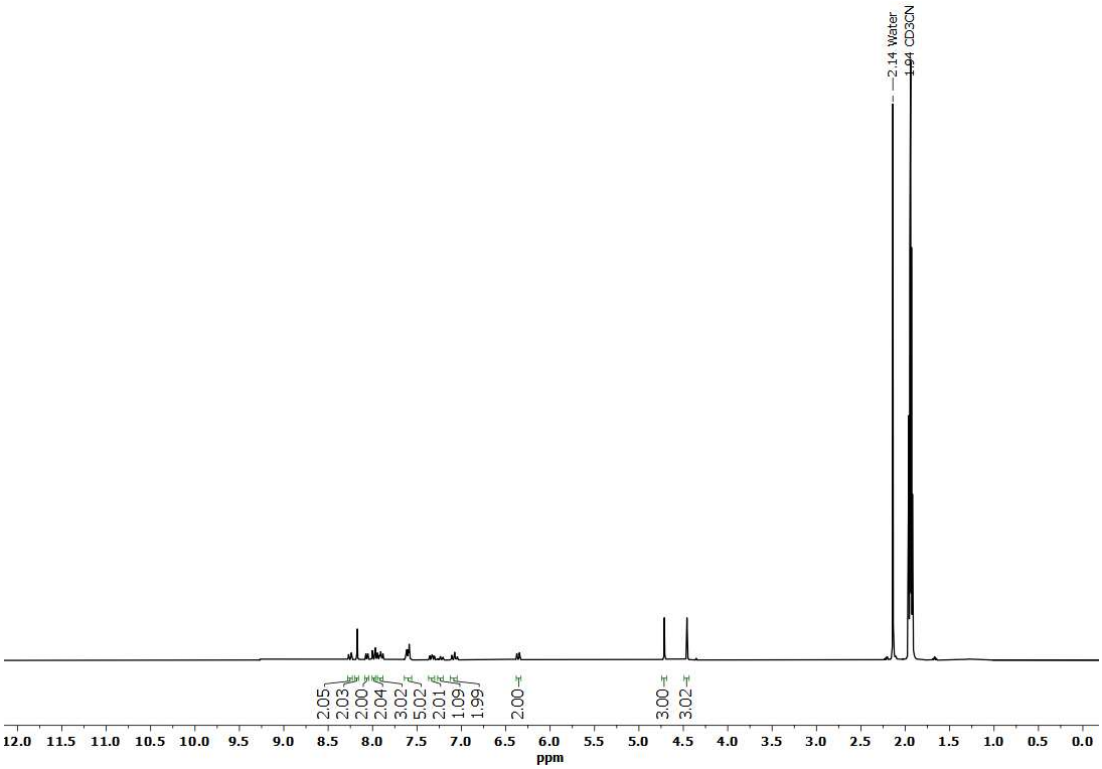

Figure S10: ^{1}H-NMR-Spectrum of compound **Ru$_5$**.

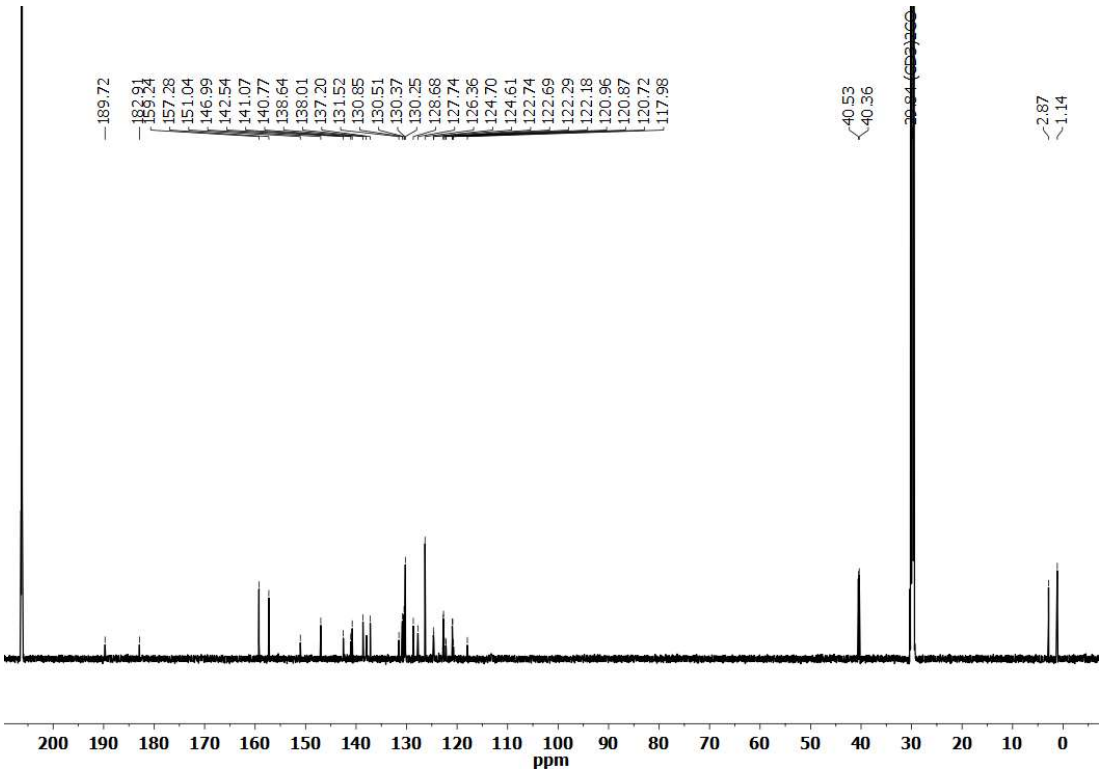

Figure S11: ^{13}C-NMR-Spectrum of compound **Ru$_5$**.

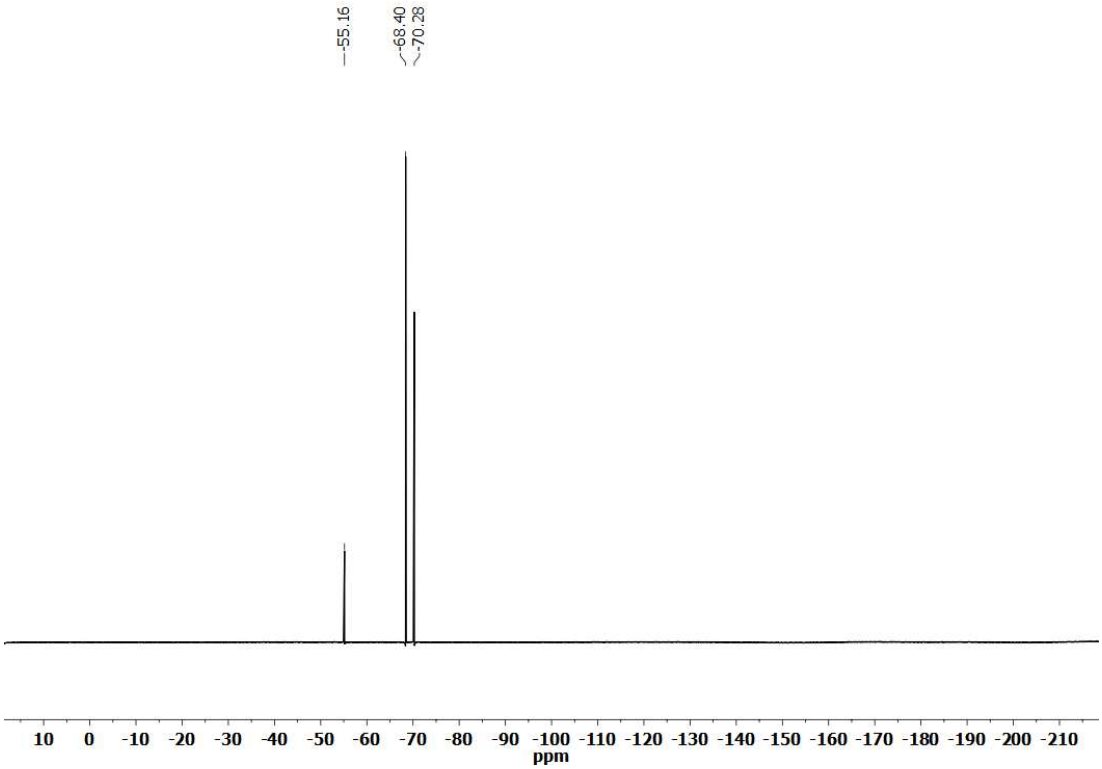

Figure S12: ^{19}F-NMR-Spectrum of compound **Ru$_5$**.

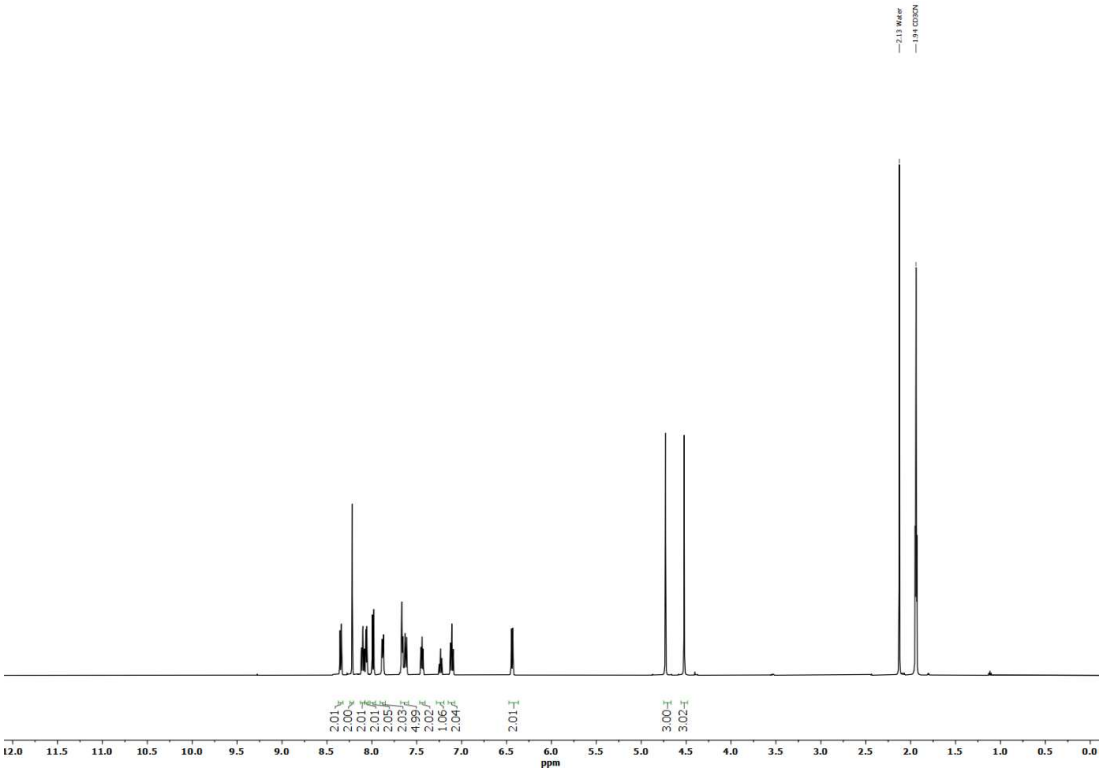

Figure S13: ^{1}H-NMR-Spectrum of compound **Ru$_6$**.

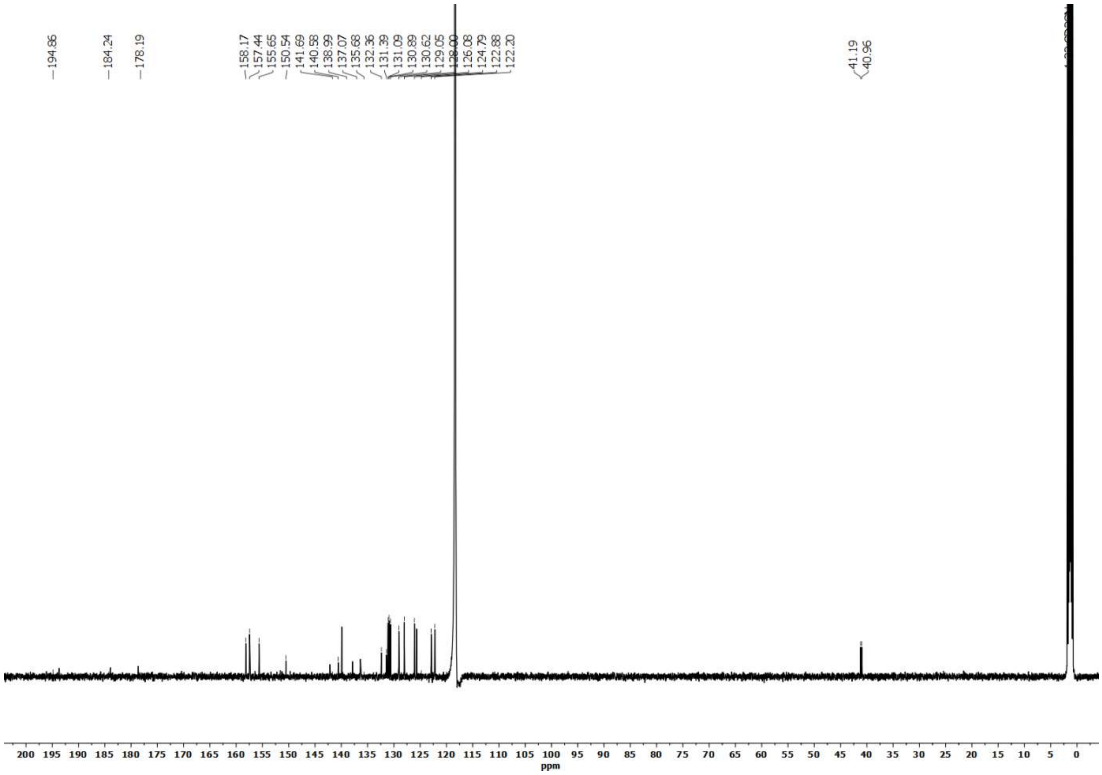

Figure S14: ^{13}C-NMR-Spectrum of compound **Ru_6**.

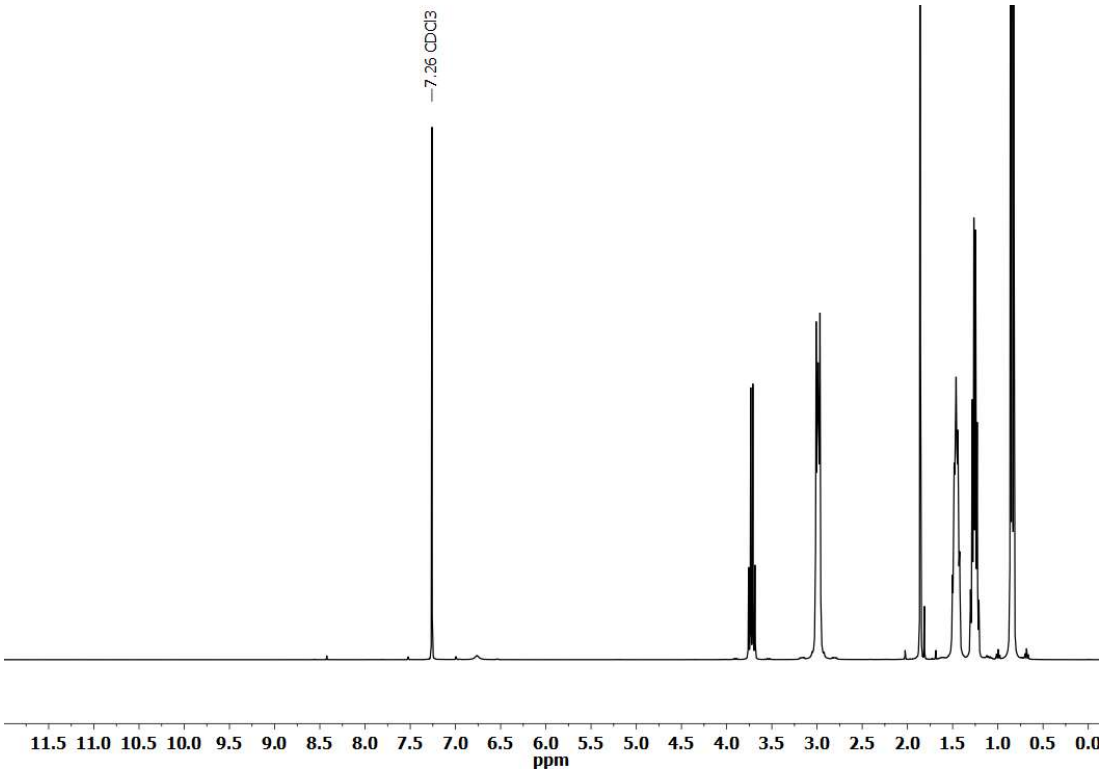

Figure S15: ^{1}H-NMR-Spectrum of the solution after the bulk electrolysis containing **Ru_4** and supporting electrolyte**.**

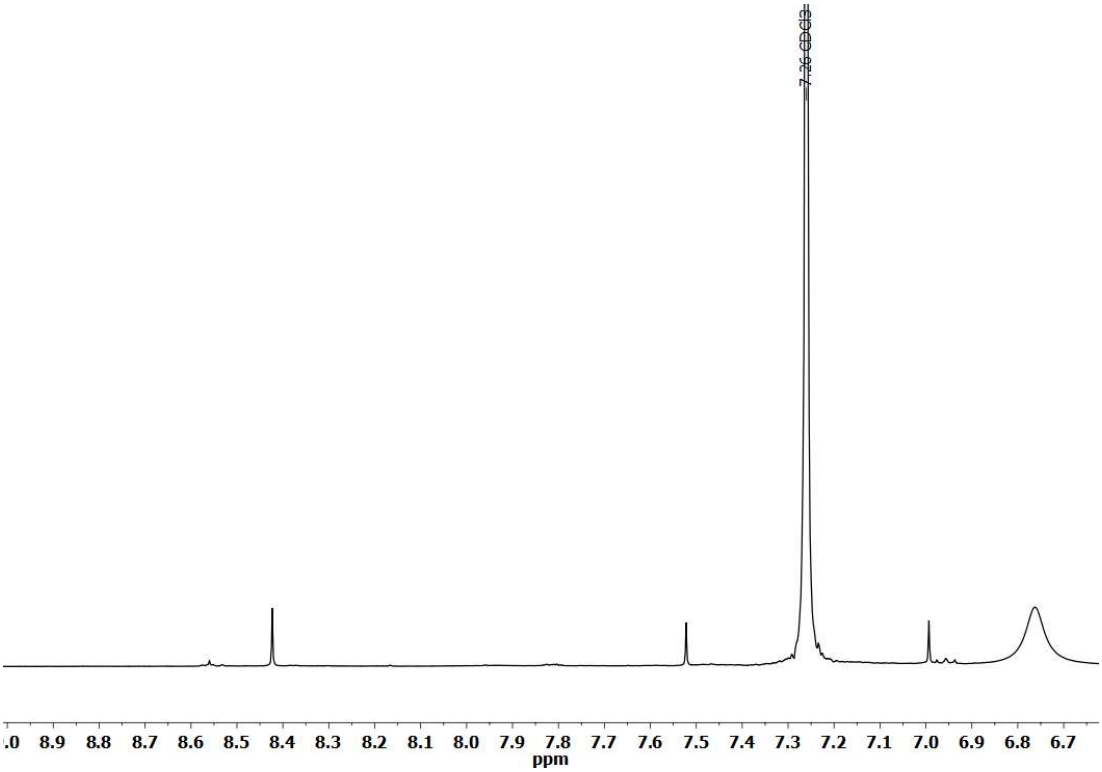

Figure S16: Zoom of the ^{1}H-NMR-Spectrum between 9 ppm and 6.7 ppm of the solution after the bulk electrolysis**.**

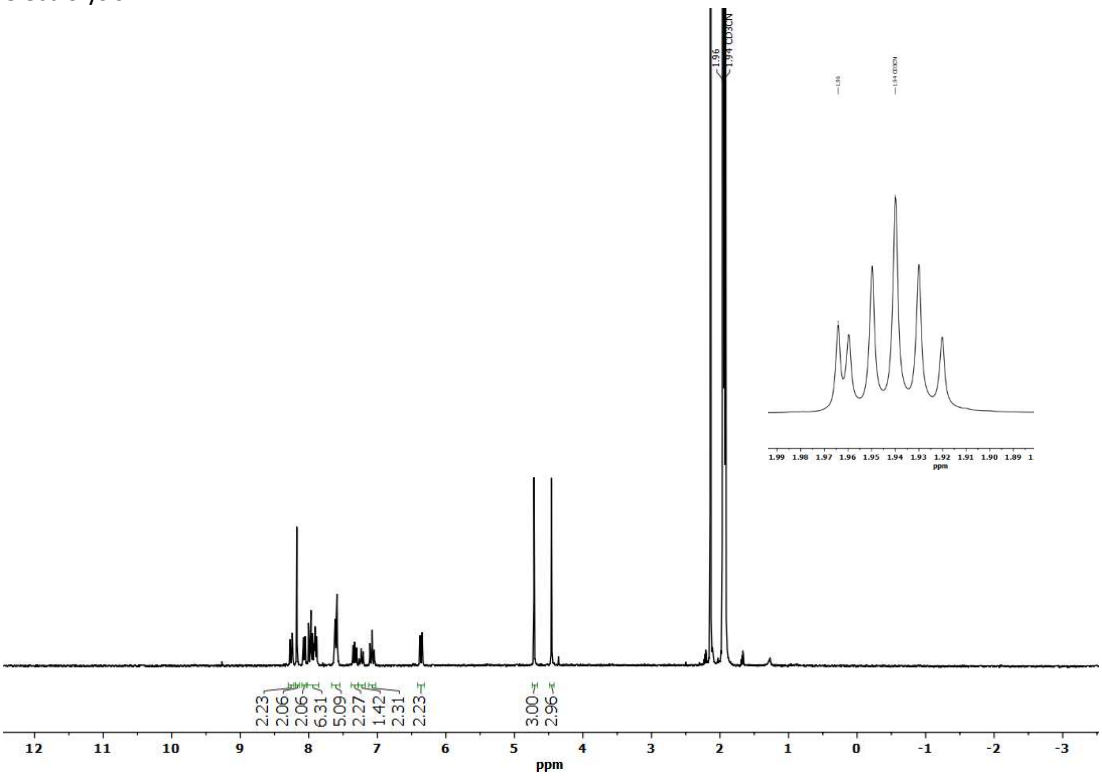

Figure S17: ^{1}H-NMR-Spectrum of the compound **Ru_4** in acetonitrile. Top right: Zoom in the region around 2 ppm with the peak of the bound MeCN at 1.96 ppm.

Cyclic voltammetry

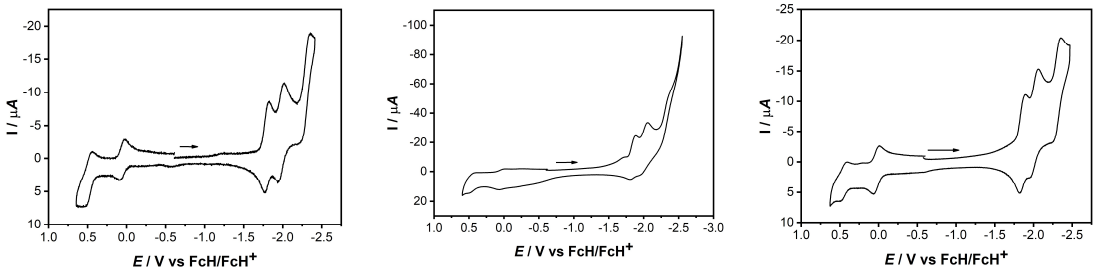

Figure S18: Cyclic voltammograms in MeCN with 0.1 M ^{t}BuNH$_4$PF$_6$ as supporting electrolyte, in a 3-electrode setup (WE: GC, CE: Pt, RE: Ag) at 100 mV/s of **Ru$_4$** (left), **Ru$_3$** (middle) and **Ru$_2$** (right).

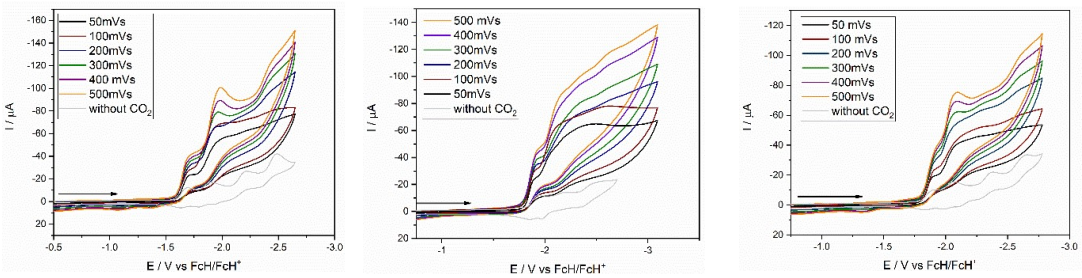

Figure S19: Cyclic voltammograms of a saturated CO_2 solution in MeCN with 0.1 M ^{t}BuNH$_4$PF$_6$ as supporting electrolyte, in a 3-electrode setup (WE: GC, CE: Pt, RE: Ag) at different scan rates of **Ru$_4$** (left), **Ru$_3$** (middle) and **Ru$_2$** (right).

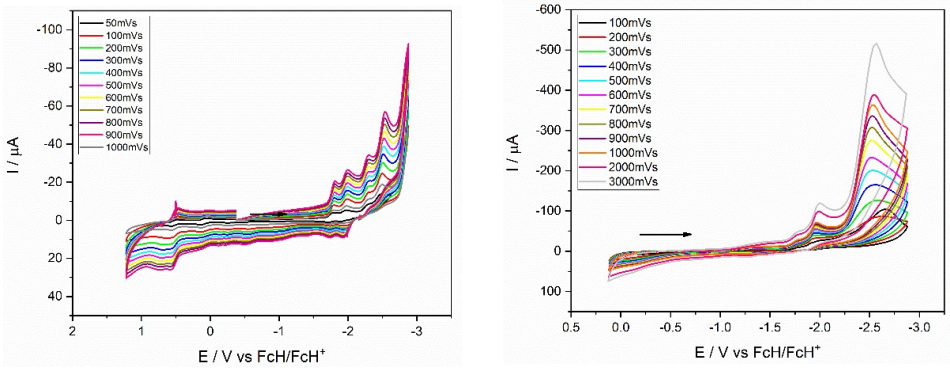

Figure S20: Cyclic voltammograms in MeCN with 0.1 M ^{t}BuNH$_4$PF$_6$ as supporting electrolyte, in a 3-electrode setup (WE: GC, CE: Pt, RE: Ag) at different scan rates. Left: **Ru$_4$** without CO_2. Right: **Ru$_4$** with a saturated CO_2-solution.

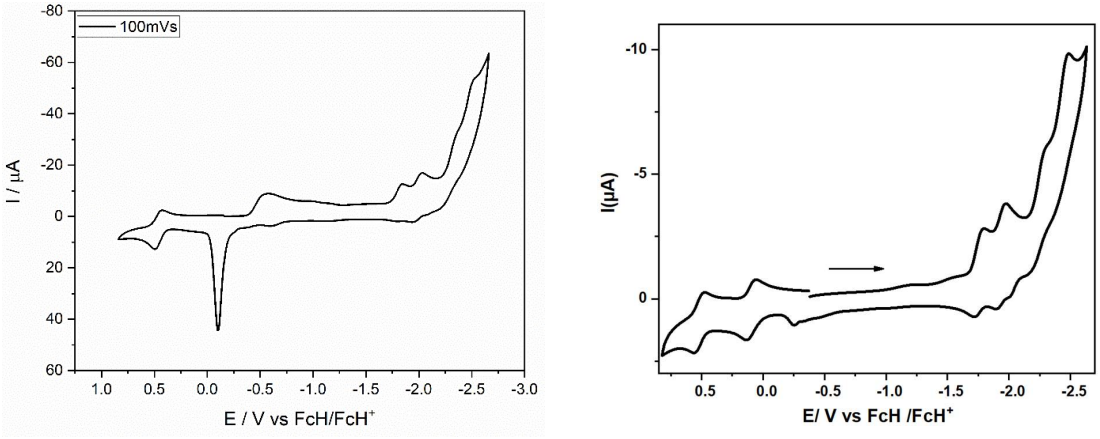

Figure S21: Cyclic voltammograms of **Ru_5** in acetonitrile with 0.1 M NBu_4PF_6 (left) and NBu_4Cl (right) as a supporting electrolyte. Scan rate: 100 mV/s, glassy carbon working electrode, electrochemical potentials were referenced against Fc/FcH+ redox couple.

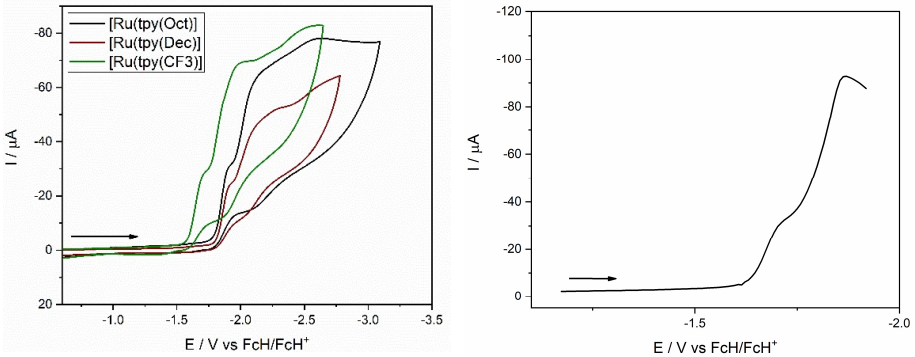

Figure S22: Cyclic voltammograms of a saturated CO_2 solution in MeCN with 0.1 M $^tBuNH_4PF_6$ as supporting electrolyte, in a 3-electrode setup (WE: GC, CE: Pt, RE: Ag) Left: different onset potentials of **Ru_2**, **Ru_3** and **Ru_4**. Right: S-Shaped curve of **Ru_4**.

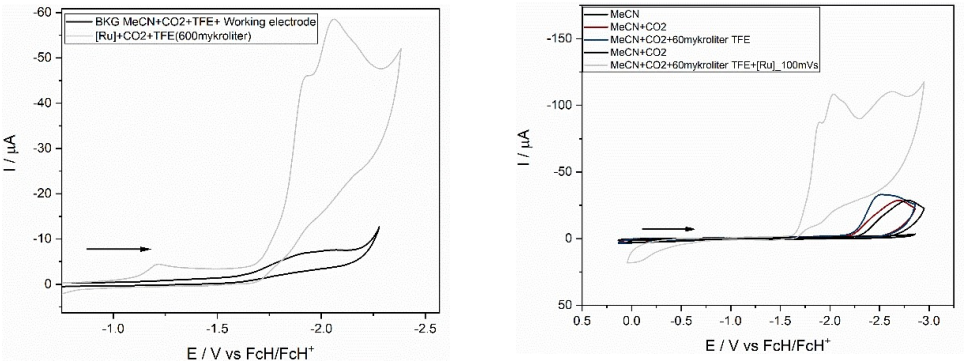

Figure S23: Cyclic voltammograms in MeCN with 0.1 M ^{t}BuNH$_4$PF$_6$ as supporting electrolyte, in a 3-electrode setup (WE: GC, CE: Pt, RE: Ag) at different scan rates. **Left**: Rinse test: Cyclic voltammogram of **Ru$_4$** (grey) in the presence of 600 µL TFE at 100 mV/s. Glassy carbon electrode is then taken out from the solution and washed thoroughly with acetone before reusing it for recording cyclic sweep voltammogram (black line) with a fresh acetonitrile solution containing 0.1 M ^{t}Bu$_4$PF$_6$ and 600 µL TFE at 100 mV/s. **Right**: **Ru$_4$**: Comparison of solution with catalyst (grey) and without catalyst (blue and red).

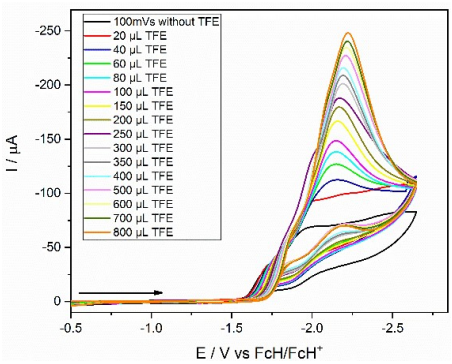

Figure S24: Cyclic voltammograms of a saturated CO_2 solution in MeCN with 0.1 M ^{t}BuNH$_4$PF$_6$ as supporting electrolyte, in a 3-electrode setup (WE: GC, CE: Pt, RE: Ag) at different TFE concentrations of **Ru$_4$**.

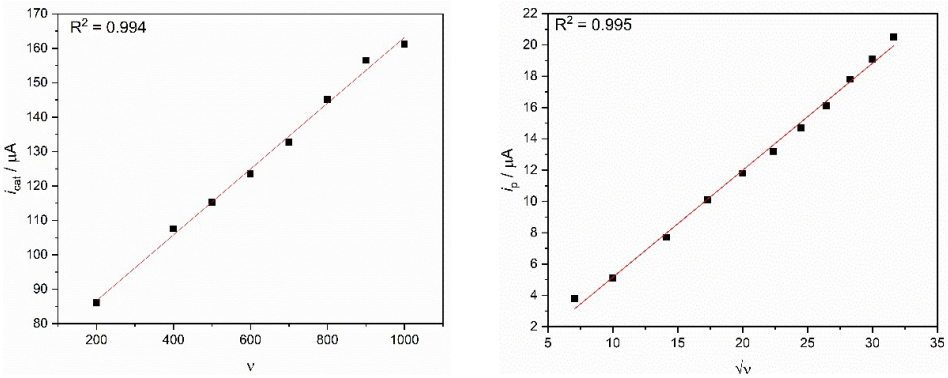

Figure S25: Left: Plot of i_{cat} vs the scan rate of **Ru_4** with 150 microliter of TFE. Right: Plot of i_p vs the square root of the scan rate of **Ru_4.**

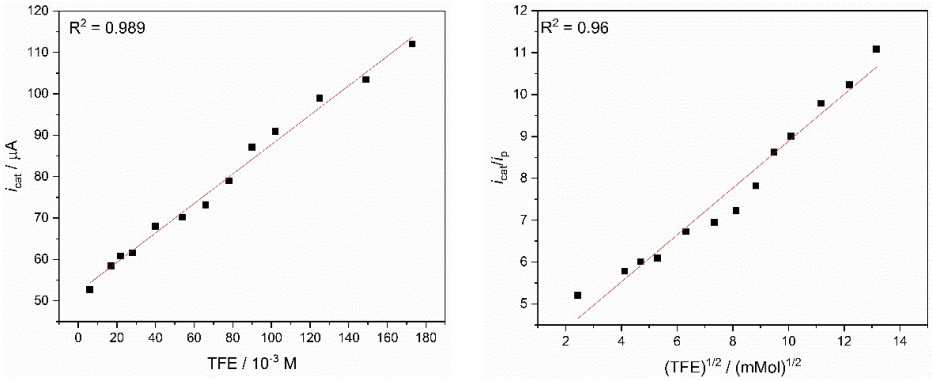

Figure S26: Left: Plot of i_{cat} vs the TFE concentration of **Ru_4**. Right: Plot of i_p/I_p vs the square root of the TFE concentration of **Ru_4.**

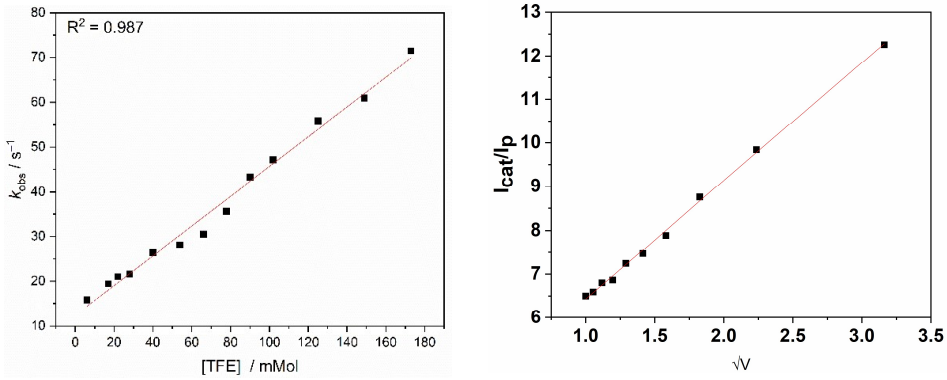

Figure S27: Left: Plot of K_{obs} vs the TFE concentration of **Ru_4**; Right: Plot of Icat/Ip vs the square root of the scan rate of **Ru_4**.

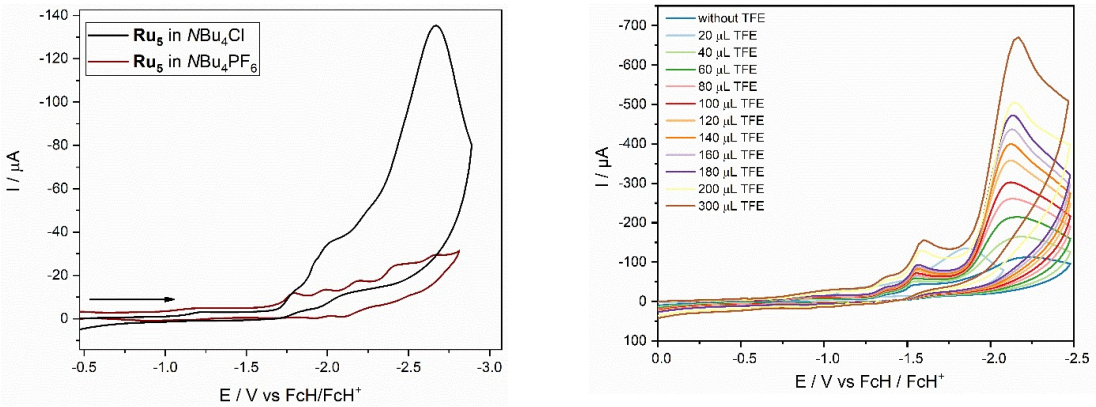

Figure S28: Cyclic voltammograms of a saturated CO_2 solution in MeCN with 0.1 M $^{t}BuNH_4Cl$ as supporting electrolyte, in a 3-electrode setup (WE: GC, CE: Pt, RE: Ag) at different TFE concentrations of **Ru_5**.

Bulk electrolysis

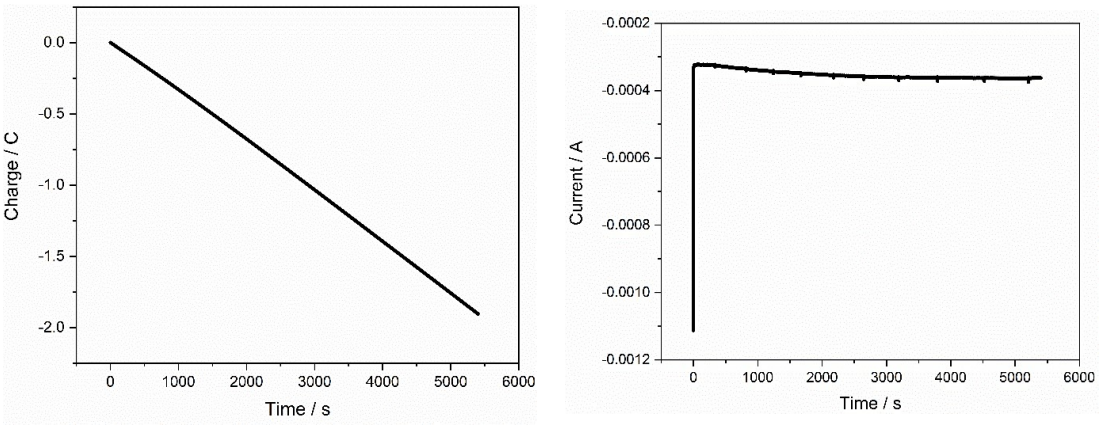

Figure S29. Plot of charge versus time (left) and current versus time (right) during the electrolysis of CO_2 saturated 0.05 mM acetonitrile solution of **Ru_4**containing 10% of TFE.

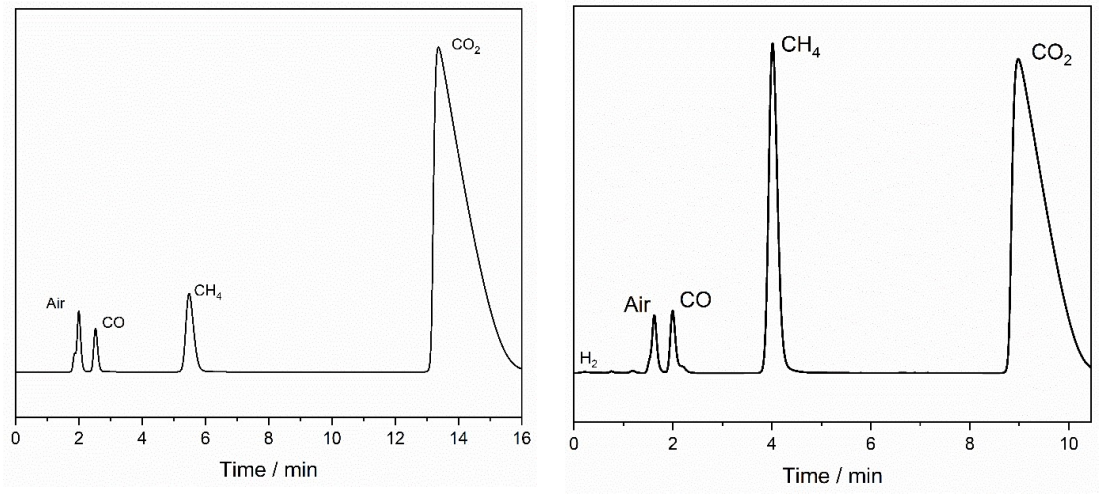

Figure S30. Gas chromatogram of the gaseous analyte obtained after the electrolysis of CO_2 saturated 0.05 mM acetonitrile solution of **Ru_4** containing 10% of TFE. The headspace gas was analysed after 1.5 hours of the electrolysis. The diagram in the left represents detection of CO in the reaction mixture, and the diagram on the right depicts absence of H_2 under the identical experimental conditions.

SEM/EDX

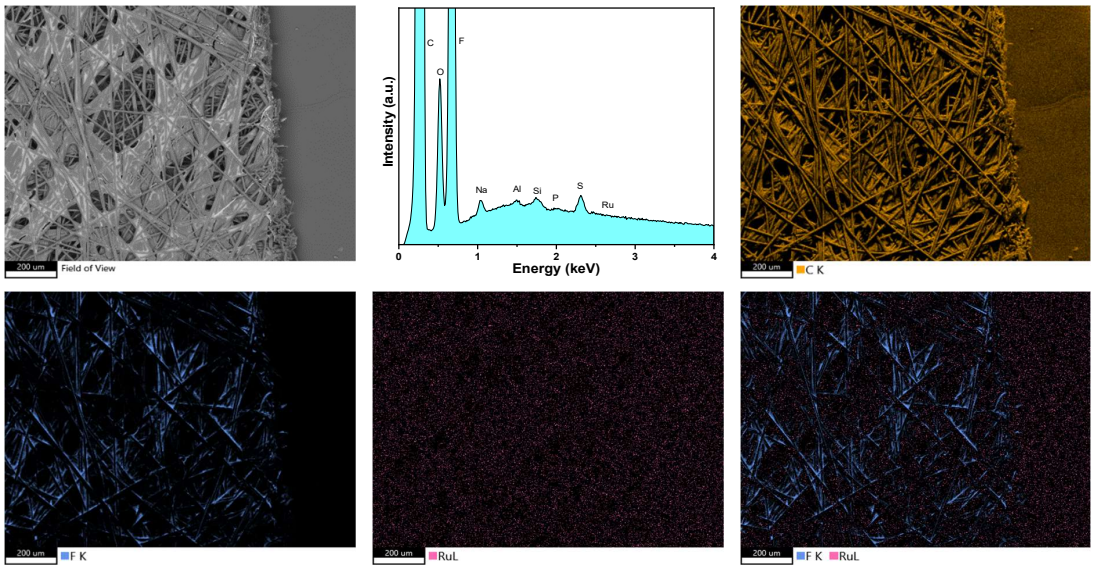

Figure 31. SEM/EDX of the surface of the working electrode after bulk electrolysis. Reaction condition: constant potential of -1.75 V *vs.* Fc/FcH^+ for 1.5 hours.

UV/Vis-SEC

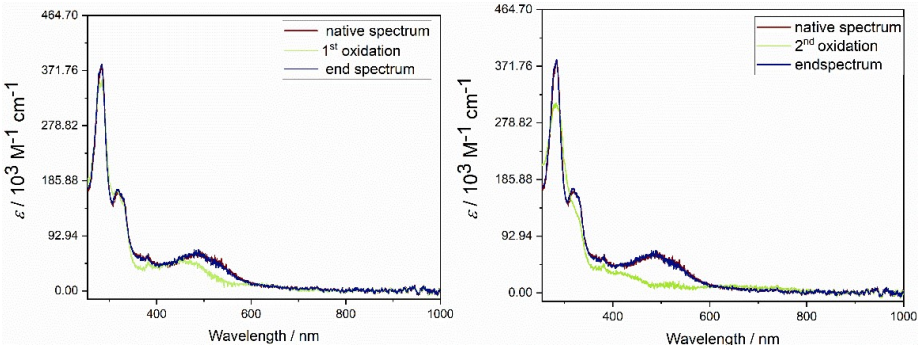

Figure S32: UV/Vis-SEC measurement of the oxidation of **Ru_4** in MeCN with 0.1 mmol $NBuNH_4PF_6$ as supporting electrolyte, in a 3 electrode Ottle-cell (WE: Pt, CE: Pt, RE: Ag). Scan rate: 50 mV/s.

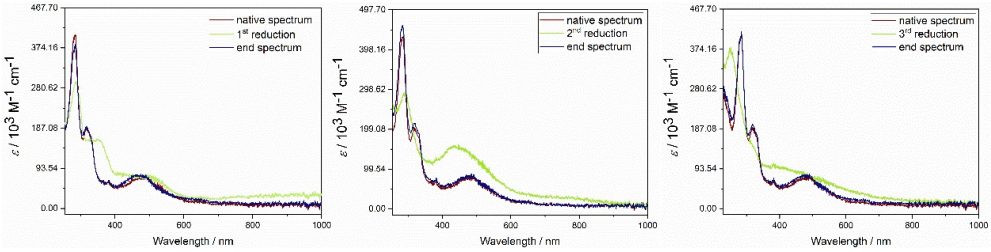

Figure S33: UV/Vis-SEC measurement of the reduction of **Ru_4** in MeCN with 0.1 mmol $NBuNH_4PF_6$ as supporting electrolyte, in a 3 electrode Ottle-cell (WE: Pt, CE: Pt, RE: Ag). Scan rate: 50 mV/s.

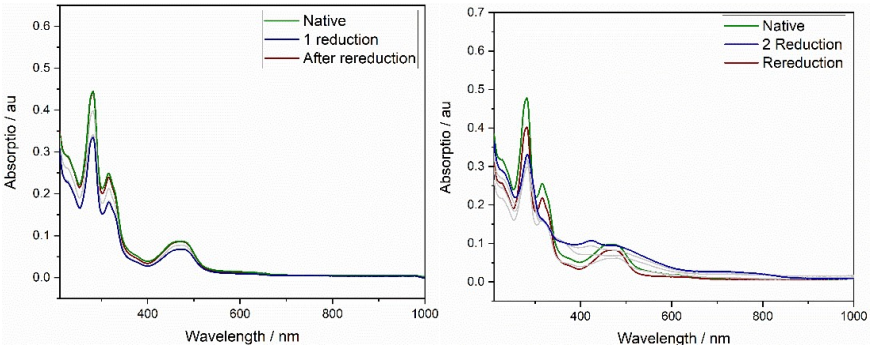

Figure S34: UV/Vis-SEC measurement of the 1st and 2nd reduction of **Ru_5** in MeCN with 0.1 mmol $^tBuNH_4PF_6$ as supporting electrolyte, in a 3 electrode Ottle-cell (WE: Pt, CE: Pt, RE: Ag). Scan rate: 50 mV/s.

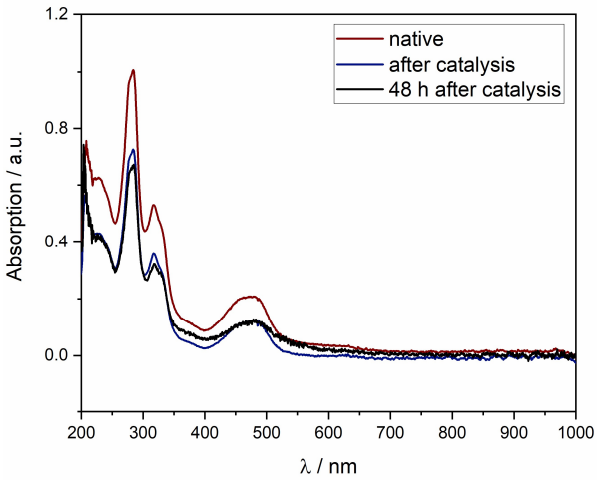

Figure S35. UV/Vis-NIR absorption spectrum of **Ru_4** in acetonitrile before (blue) and after (red) electrolysis. No change in the position of absorption maxima indicate stability of the catalyst during the electrolysis process.

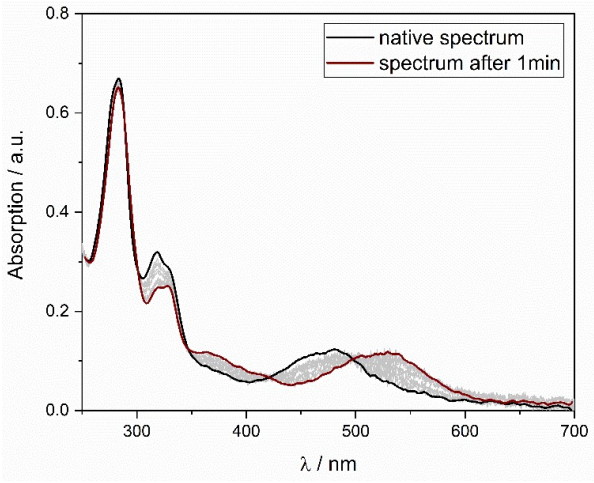

Figure S36: Change of the UV/Vis spectrum of **Ru_4** in MeCN. Black spectrum: directly after dissolving in MeCN. Red spectrum: After 120 minutes in the MeCN solution (colour change from deep purple to dark orange). Grey spectra: Change during the time.

IR-spectra

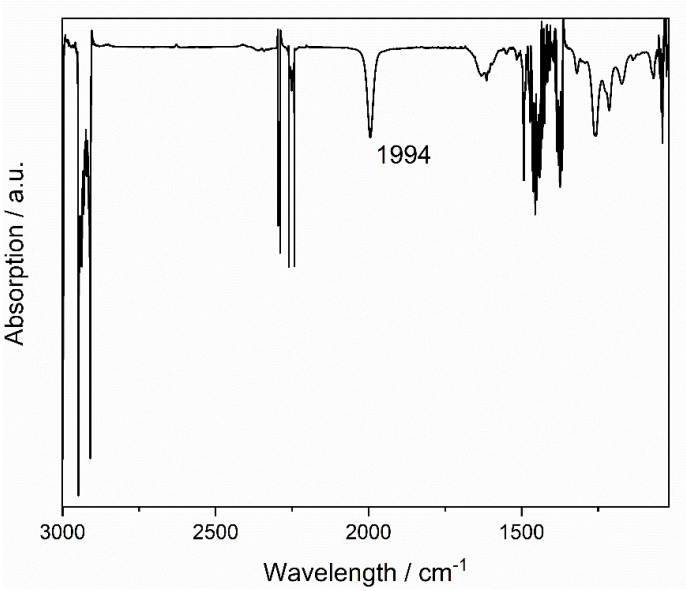

Figure S37: IR-spectrum of **Ru_6** at ambient conditions in acetonitrile.

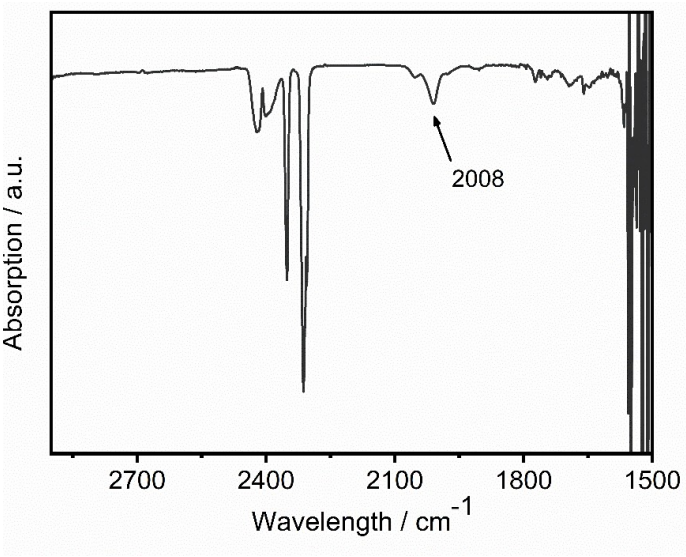

Figure S38: IR-spectrum of the $[Ru\text{-}CO]^{2+}$ intermediate generated via an IR-SEC experiments with **Ru_4**. Controlled potential electrolysis of the CO_2 saturated acetonitrile solution of **Ru4** containing 0.1 M $N Bu_4PF_6$ and TFE at -1.75 V over a period of 30 minutes.

Control experiments

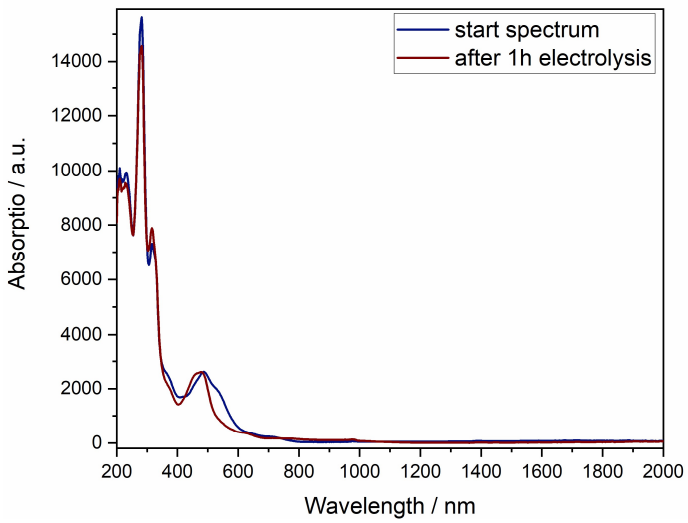

Figure S39: UV/Vis spectra of 0.05 mM acetonitrile solution of **Ru_4** in presence of 0.1 mmol $NBuNH_4PF_6$ as supporting electrolyte. Blue: Under CO_2 atmosphere before electrolysis; Red: Under CO_2 after 1 h electrolysis at –1.5 V.

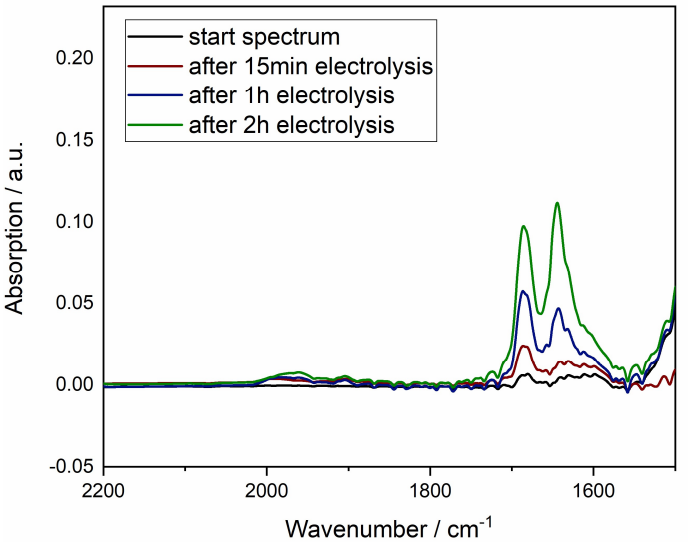

Figure S40: IR-spectrum after bulk electrolysis at -1.75 V of 0.05 mMol **Ru_4** in CO_2 saturated condition in anhydrous CH_3CN. Catalysis was performed for 2 h using Glassy carbon rod as working electrode, Ag-wire as reference electrode and platinum wire as counter electrode. The appearance of weak bicarbonate peak is due to the low concentration as compared to TBAP.

DFT

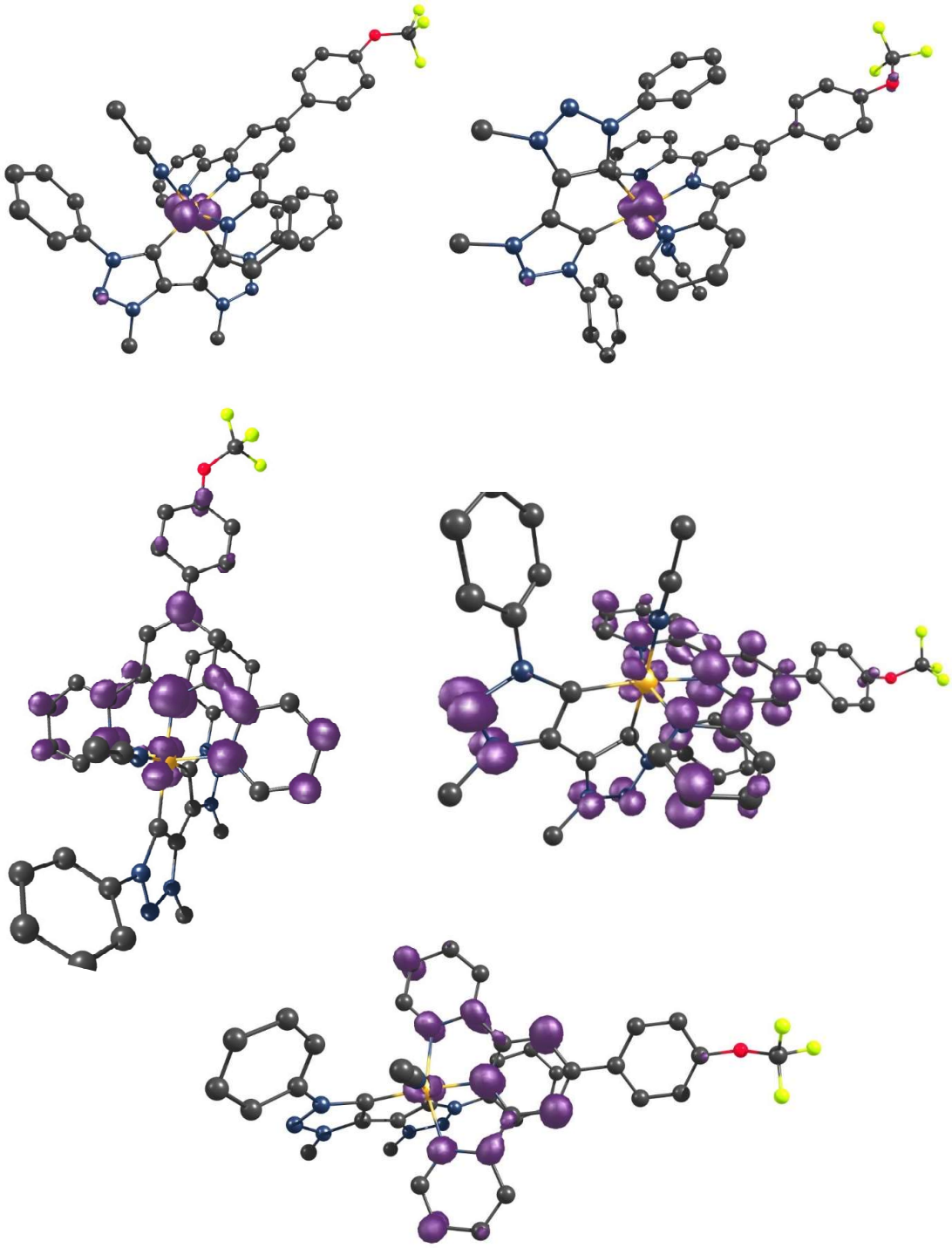

Figure S41: Spin density plots of the oxidised and reduced species of **Ru_4**: Top left: first oxidation; Top right: second oxidation; Middle left: first reduction; Middle right: second reduction; Bottom: third reduction.

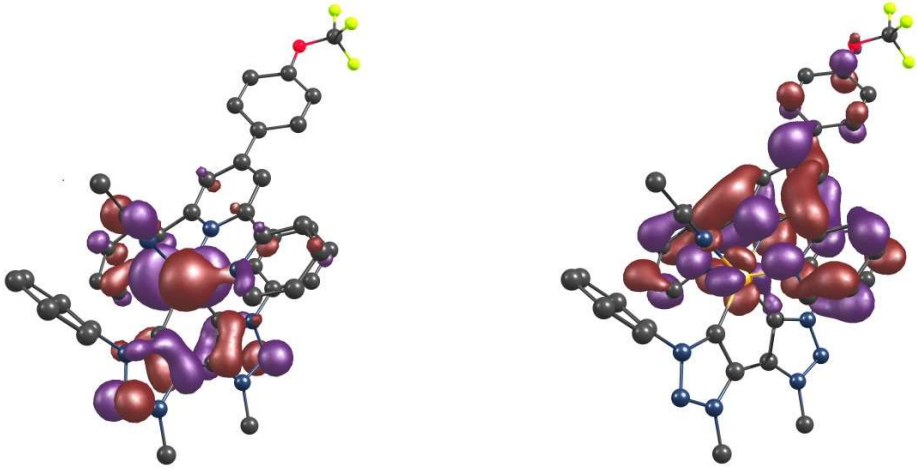

Figure S42: Left HOMO of **Ru$_4$**; Right: LUMO of **Ru$_4$**.

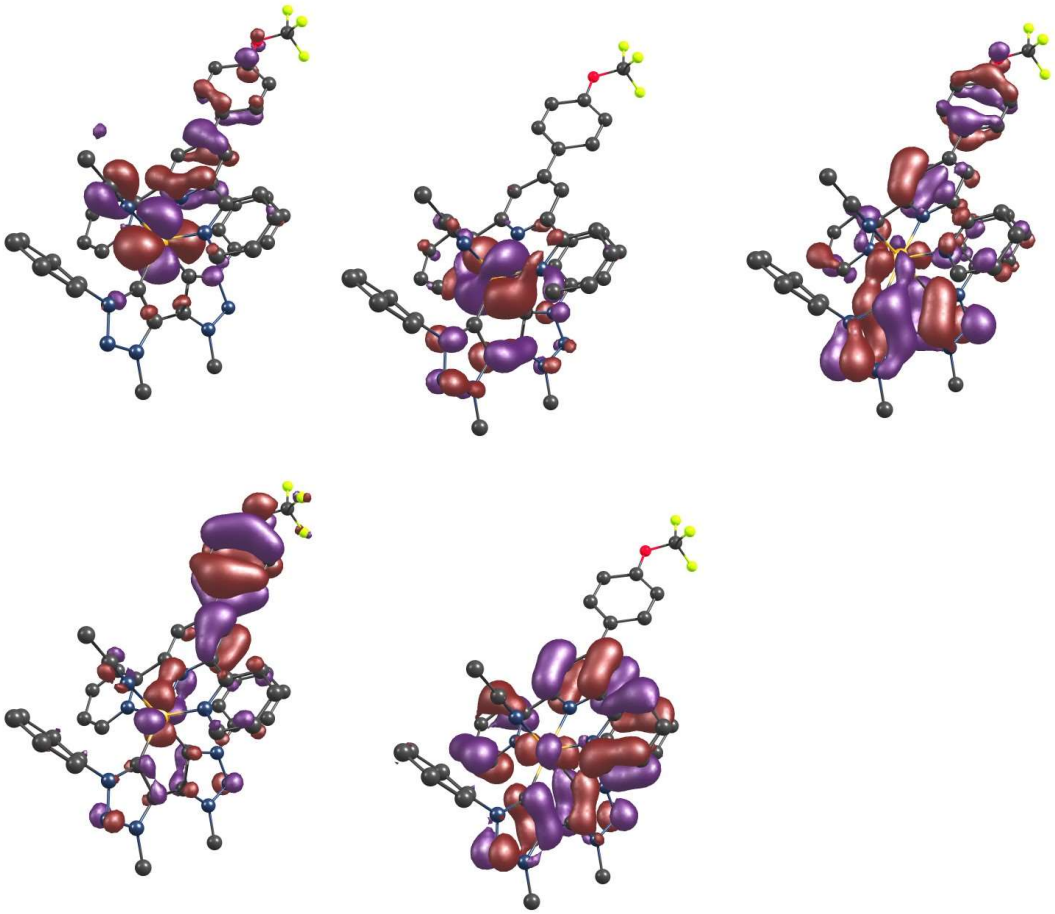

Figure S43: TD-DFT calculations of **Ru$_4$**: Top left HOMO-1 ;Top middle: HOMO-2; Top right: HOMO-3; Bottom left: HOMO-4; Bottom middle: HOMO-5.

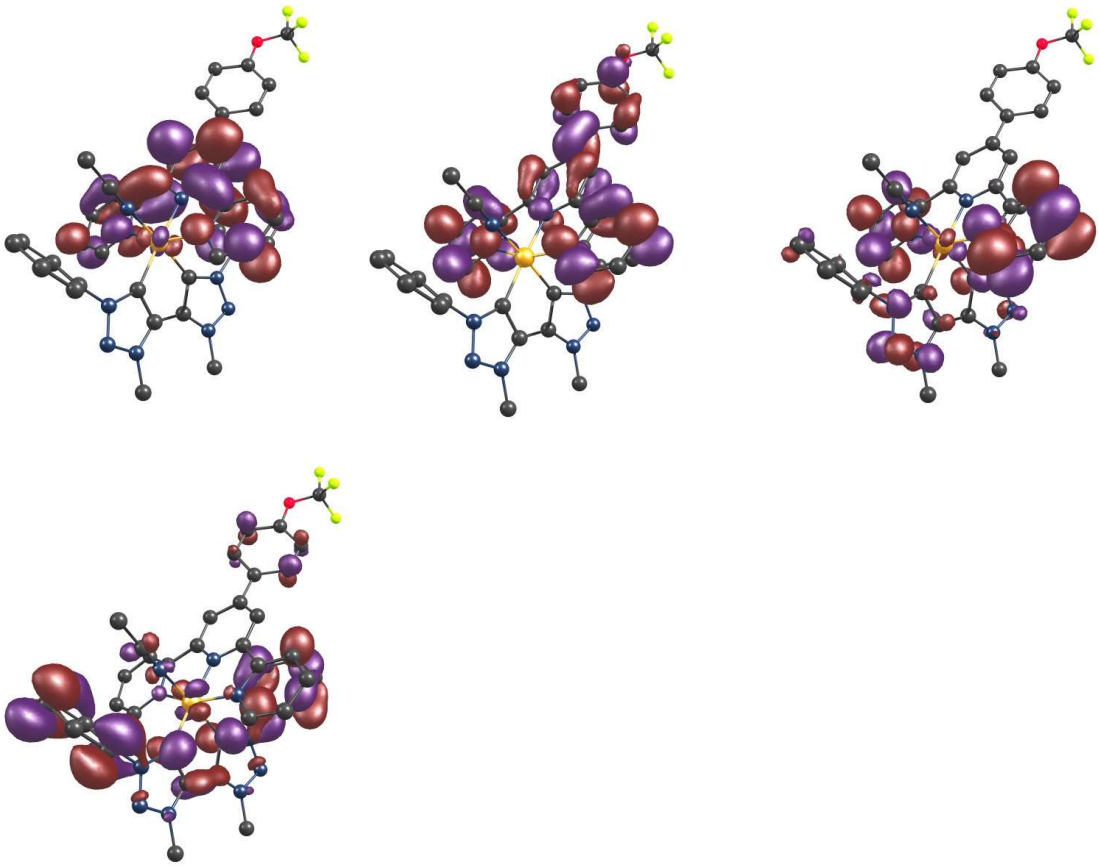

Figure S44: TD-DFT calculations of **Ru_4**: Top left LUMO+1 ;Top middle: LUMO+3; Top right: LUMO+4; Bottom left: LUMO+7.

Table S1: UV/Vis-NIR Data of *trans*-**Ru_4** in the native, oxidized, and reduced state, together with corresponding TD-DFT Data.

State	Main contribution excitation (%)	$\lambda_{exp}(\lambda_{DFT})$ (nm)	ε / 10^4 $M^{-1}cm^{-1}$ (f)
2	HOMO → LUMO (99)	545 (589)	9.83(0.011)
18	HOMO-3 → LUMO (25) HOMO-2 → LUMO+3 (18) HOMO-1 → LUMO+4 (16) HOMO → LUMO+7 (13)	326(322)	18.14(0.027)
29	HOMO-5 → LUMO (26) HOMO-4 → LUMO+1 (33)	283(293)	37.35(0.125)

Table S2: Cartesian coordinates of the computed structures:

Ru_4^{2+} (native, *S* = 0)							
N	4.699919000	0.240759000	-8.450490000	N	2.316396000	5.065522000	-5.138866000
N	4.909624000	1.340625000	-7.708765000	O	12.507667000	6.626430000	-2.595346000
C	3.788415000	2.112458000	-7.496517000	C	1.845455000	5.820754000	-4.378985000
C	2.796664000	1.369637000	-8.189851000	C	1.237317000	6.744888000	-3.445343000
N	3.404134000	0.272102000	-8.730894000	F	14.412297000	6.604343000	-1.556201000
C	1.472154000	1.901772000	-8.026971000	C	13.353313000	5.850497000	-1.863192000
C	1.429178000	3.042576000	-7.174999000	F	12.788876000	5.410045000	-0.718470000
N	0.077259000	3.330224000	-7.191404000	F	13.783055000	4.766162000	-2.546737000
N	-0.670972000	2.492094000	-7.934295000	H	6.103851000	-0.193703000	-5.889806000
N	0.198794000	1.628425000	-8.435605000	H	8.395044000	0.182817000	-4.919082000
C	-0.602370000	4.405738000	-6.525548000	H	9.762931000	2.145671000	-5.674026000
C	6.226511000	1.552878000	-7.174239000	H	8.849566000	3.725948000	-7.391771000
C	6.721345000	0.656183000	-6.213927000	H	6.565115000	3.332782000	-8.369170000
C	7.998874000	0.874637000	-5.676994000	H	0.435479000	5.933241000	-7.668604000
C	8.762757000	1.975628000	-6.099574000	H	-0.755317000	7.817692000	-6.513793000
C	8.252662000	2.862880000	-7.062456000	H	-2.448960000	7.321286000	-4.730498000
C	6.978319000	2.653799000	-7.609665000	H	-2.956622000	4.944843000	-4.109718000
C	-0.308652000	5.729664000	-6.886525000	H	-1.759411000	3.062226000	-5.273018000
C	-0.977484000	6.776637000	-6.236211000	H	2.057748000	-1.329574000	-8.939446000
C	-1.928420000	6.496419000	-5.239547000	H	3.650510000	-1.508886000	-9.770414000
C	-2.214081000	5.165616000	-4.890758000	H	2.404319000	-0.396742000	-10.458056000
C	-1.551059000	4.109480000	-5.534942000	H	-1.371742000	0.731694000	-9.458182000
C	2.834951000	-0.807832000	-9.527048000	H	-0.133448000	-0.415689000	-8.817067000
C	-0.293019000	0.564612000	-9.302443000	H	0.235209000	0.605542000	-10.271985000
Ru	3.193139000	3.673387000	-6.345312000	H	2.975291000	6.747341000	-10.580811000
C	3.556551000	6.492473000	-9.683802000	H	5.142772000	7.954092000	-10.017959000
C	4.753398000	7.155223000	-9.371030000	H	6.399650000	7.260559000	-7.954842000
C	5.452254000	6.772309000	-8.220540000	H	2.166276000	4.936109000	-9.045580000
C	4.943843000	5.751213000	-7.402213000	H	7.398960000	6.496658000	-6.170543000
N	3.751781000	5.120187000	-7.706868000	H	7.049990000	3.478135000	-3.055588000
C	3.093862000	5.485037000	-8.831962000	H	5.795230000	1.805857000	-2.401224000
C	5.630788000	5.245580000	-6.200839000	H	4.155320000	0.028950000	-1.712179000
C	6.853617000	5.682197000	-5.676493000	H	1.982057000	-0.189399000	-3.012932000
C	7.407879000	5.034007000	-4.548329000	H	1.563586000	1.370827000	-4.938589000
C	6.674344000	3.976862000	-3.958198000	H	9.232323000	3.440712000	-3.270091000
C	5.448944000	3.586088000	-4.509321000	H	11.444932000	4.059152000	-2.403743000
N	4.972337000	4.209395000	-5.618325000	H	10.841966000	8.144256000	-3.760928000
N	3.364446000	2.392820000	-4.721288000	H	8.590345000	7.522436000	-4.632240000
C	4.547033000	2.526794000	-4.021188000	H	0.326078000	6.290919000	-3.007527000
C	4.844527000	1.685715000	-2.938075000	H	0.952695000	7.679461000	-3.968061000
C	3.930818000	0.695657000	-2.556908000	H	1.947994000	6.987955000	-2.630555000
C	2.731106000	0.571204000	-3.273299000				
C	2.487103000	1.435583000	-4.345997000				
C	9.561152000	4.484830000	-3.372647000				
C	10.827234000	4.828881000	-2.882381000				
C	11.273980000	6.152309000	-3.032451000				
C	10.470360000	7.114148000	-3.666568000				
C	9.214131000	6.751475000	-4.157093000				
C	8.731089000	5.428782000	-4.018006000				

Ru_4^+ (1e⁻ reduced, *S* = 1/2)							
N	4.707771000	0.269431000	-8.448945000	N	2.355655000	5.094667000	-5.117580000
N	4.911772000	1.393881000	-7.739658000	O	12.631421000	6.411509000	-2.690280000
C	3.775523000	2.140775000	-7.498361000	C	1.915061000	5.859863000	-4.346153000
C	2.780720000	1.350983000	-8.144870000	C	1.317922000	6.796819000	-3.414643000
N	3.400713000	0.258078000	-8.682392000	F	14.266988000	6.643381000	-1.279495000
C	1.451113000	1.860904000	-7.961877000	C	13.194463000	5.896550000	-1.570545000
C	1.413929000	3.038731000	-7.149814000	F	12.355941000	5.907829000	-0.512392000
N	0.049724000	3.296359000	-7.142634000	F	13.614955000	4.615518000	-1.733052000
N	-0.704035000	2.410347000	-7.827089000	H	6.246291000	-0.099962000	-5.991515000
N	0.171344000	1.543244000	-8.316080000	H	8.585494000	0.330220000	-5.162323000
C	-0.635047000	4.382557000	-6.509117000	H	9.850609000	2.334491000	-5.984217000
C	6.246948000	1.648620000	-7.276010000	H	8.790880000	3.894869000	-7.636170000
C	6.824078000	0.763585000	-6.351230000	H	6.463574000	3.443944000	-8.473954000
C	8.126258000	1.012595000	-5.893255000	H	0.594412000	5.886338000	-7.476837000
C	8.834100000	2.134942000	-6.355156000	H	-0.612685000	7.796914000	-6.383032000
C	8.241888000	3.010489000	-7.280685000	H	-2.513790000	7.341267000	-4.809633000
C	6.943523000	2.769070000	-7.751279000	H	-3.208145000	4.976325000	-4.337915000
C	-0.238987000	5.700873000	-6.786125000	H	-1.988516000	3.069327000	-5.435226000
C	-0.918401000	6.761509000	-6.170344000	H	2.120754000	-1.409225000	-8.804856000
C	-1.984890000	6.505095000	-5.291282000	H	3.679820000	-1.524482000	-9.709514000
C	-2.375140000	5.181318000	-5.026992000	H	2.346921000	-0.484349000	-10.347777000
C	-1.700829000	4.111443000	-5.635232000	H	-1.426639000	0.549835000	-9.195004000
C	2.844243000	-0.859020000	-9.434552000	H	-0.085051000	-0.523343000	-8.634869000
C	-0.331847000	0.437891000	-9.122219000	H	0.117249000	0.478839000	-10.131747000
Ru	3.171854000	3.690055000	-6.356003000	H	2.958007000	6.813478000	-10.563083000
C	3.543540000	6.546609000	-9.672032000	H	5.154025000	7.998171000	-10.006904000
C	4.760747000	7.199298000	-9.361621000	H	6.418153000	7.272197000	-7.963003000
C	5.460683000	6.799387000	-8.224184000	H	2.144979000	5.005031000	-9.031901000
C	4.955627000	5.774150000	-7.395772000	H	7.417403000	6.483956000	-6.182930000
N	3.738427000	5.156714000	-7.699068000	H	7.078522000	3.410337000	-3.105933000
C	3.081534000	5.542847000	-8.823726000	H	5.787261000	1.768713000	-2.421862000
C	5.641685000	5.250749000	-6.217252000	H	4.133020000	0.013251000	-1.727817000
C	6.870518000	5.664896000	-5.696877000	H	1.940057000	-0.175633000	-3.027950000
C	7.440272000	4.985032000	-4.584380000	H	1.531930000	1.398085000	-4.935225000
C	6.694758000	3.924834000	-3.997015000	H	9.212378000	3.360337000	-3.266131000
C	5.454921000	3.557759000	-4.525026000	H	11.457776000	3.926741000	-2.420180000
N	4.977697000	4.201794000	-5.638008000	H	11.005110000	7.980693000	-3.900697000
N	3.342199000	2.408451000	-4.732168000	H	8.734636000	7.419280000	-4.758921000
C	4.548673000	2.524972000	-4.034459000	H	0.301455000	6.453721000	-3.134550000
C	4.830777000	1.662444000	-2.953202000	H	1.233290000	7.797223000	-3.884847000
C	3.913176000	0.685928000	-2.569551000	H	1.936404000	6.883122000	-2.498831000
C	2.697233000	0.577334000	-3.288128000				
C	2.461660000	1.449160000	-4.349115000				
C	9.578675000	4.389156000	-3.394818000				
C	10.856906000	4.700314000	-2.915963000				
C	11.355863000	5.999789000	-3.102971000				
C	10.594260000	6.968656000	-3.773472000				
C	9.324528000	6.638912000	-4.256305000				
C	8.776662000	5.342189000	-4.074164000				

Ru_4 ($2e^-$ reduced, $S = 1$)

N	4.740393000	0.345018000	-8.493662000	N	2.376184000	5.097891000	-5.068691000
N	4.922715000	1.505726000	-7.823206000	O	12.782704000	5.774868000	-2.608420000
C	3.768605000	2.172949000	-7.485662000	C	1.938545000	5.842191000	-4.272424000
C	2.765125000	1.311850000	-8.018359000	C	1.338693000	6.760248000	-3.322542000
N	3.403392000	0.239341000	-8.593473000	F	14.250525000	6.429478000	-1.141170000
C	1.435520000	1.791002000	-7.800814000	C	12.938949000	6.257407000	-1.353364000
C	1.388933000	3.036780000	-7.095173000	F	12.315236000	7.446067000	-1.169070000
N	0.020216000	3.258023000	-7.045609000	F	12.459792000	5.416219000	-0.404526000
N	-0.749867000	2.286085000	-7.610949000	H	6.616168000	0.328062000	-6.132470000
N	0.148583000	1.393351000	-8.060577000	H	8.982938000	1.064853000	-5.667201000
C	-0.663793000	4.379018000	-6.494497000	H	9.919574000	3.068304000	-6.850242000
C	6.272082000	1.915668000	-7.569153000	H	8.508737000	4.327173000	-8.498185000
C	7.052538000	1.193357000	-6.652262000	H	6.151400000	3.573459000	-8.964384000
C	8.368046000	1.611657000	-6.398044000	H	0.759450000	5.805912000	-7.293748000
C	8.892146000	2.735862000	-7.062973000	H	-0.460606000	7.791514000	-6.363754000
C	8.102857000	3.442739000	-7.984337000	H	-2.574338000	7.463350000	-5.045773000
C	6.785612000	3.033275000	-8.247976000	H	-3.459407000	5.142456000	-4.671464000
C	-0.164361000	5.675499000	-6.715394000	H	-2.228392000	3.163564000	-5.607283000
C	-0.852467000	6.777720000	-6.190222000	H	2.199645000	-1.491256000	-8.567292000
C	-2.037059000	6.594151000	-5.454140000	H	3.693246000	-1.561366000	-9.578734000
C	-2.533753000	5.295331000	-5.247040000	H	2.264183000	-0.616043000	-10.148351000
C	-1.852597000	4.184144000	-5.765181000	H	-1.443137000	0.241232000	-8.722113000
C	2.850609000	-0.923689000	-9.260633000	H	-0.008542000	-0.706454000	-8.171237000
C	-0.340449000	0.197304000	-8.719205000	H	0.030004000	0.152013000	-9.762058000
Ru	3.168094000	3.708222000	-6.327323000	H	3.144662000	6.926152000	-10.488884000
C	3.706424000	6.612540000	-9.597976000	H	5.403265000	7.976112000	-9.890347000
C	4.959379000	7.189638000	-9.261663000	H	6.602425000	7.156544000	-7.847948000
C	5.624399000	6.737797000	-8.125798000	H	2.217629000	5.142859000	-8.982207000
C	5.060756000	5.719443000	-7.313038000	H	7.567456000	6.265290000	-6.098455000
N	3.804691000	5.180487000	-7.643537000	H	7.051271000	3.157287000	-3.071652000
C	3.183576000	5.622608000	-8.762576000	H	5.675739000	1.572251000	-2.430699000
C	5.706867000	5.145794000	-6.149435000	H	3.930029000	-0.095428000	-1.757279000
C	6.967822000	5.483057000	-5.615509000	H	1.719438000	-0.145605000	-3.049107000
C	7.493681000	4.745848000	-4.518651000	H	1.403249000	1.472513000	-4.944086000
C	6.699225000	3.709551000	-3.952559000	H	9.140382000	3.042224000	-3.127483000
C	5.428877000	3.422382000	-4.494094000	H	11.431946000	3.509031000	-2.265376000
N	4.986646000	4.126911000	-5.582292000	H	11.257544000	7.509205000	-3.915812000
N	3.260192000	2.379053000	-4.728798000	H	8.950847000	7.075819000	-4.752989000
C	4.480315000	2.426607000	-4.034739000	H	0.241640000	6.804016000	-3.482923000
C	4.713265000	1.527640000	-2.960371000	H	1.755794000	7.779337000	-3.452989000
C	3.744267000	0.600182000	-2.589482000	H	1.536648000	6.429786000	-2.282861000
C	2.517558000	0.565807000	-3.303181000				
C	2.333688000	1.466255000	-4.356136000				
C	9.579776000	4.037672000	-3.286497000				
C	10.871025000	4.284218000	-2.807062000				
C	11.460663000	5.535099000	-3.040955000				
C	10.776633000	6.534670000	-3.747954000				
C	9.485792000	6.275535000	-4.221378000				
C	8.847188000	5.023263000	-4.004836000				

Ru_4^- (3e⁻ reduced, *S* = 1/2)							
N	4.691205000	0.242447000	-8.463190000	N	2.430762000	5.049068000	-5.047675000
N	4.897843000	1.447576000	-7.852639000	O	12.740840000	5.884536000	-2.492244000
C	3.759556000	2.146896000	-7.526032000	C	2.024378000	5.776320000	-4.216498000
C	2.727572000	1.279279000	-7.985486000	C	1.440553000	6.674189000	-3.236536000
N	3.330502000	0.155241000	-8.514199000	F	14.166858000	6.593683000	-1.009190000
C	1.410023000	1.773217000	-7.752145000	C	12.861638000	6.402991000	-1.249397000
C	1.378087000	3.040275000	-7.094262000	F	12.224140000	7.591324000	-1.112031000
N	0.010361000	3.283979000	-7.029463000	F	12.367388000	5.585043000	-0.287244000
N	-0.792118000	2.290688000	-7.547455000	H	6.763892000	0.061130000	-6.544254000
N	0.112160000	1.360623000	-7.977185000	H	9.158238000	0.769361000	-6.206934000
C	-0.645540000	4.432411000	-6.530617000	H	9.955484000	2.963193000	-7.136858000
C	6.250159000	1.851306000	-7.656386000	H	8.366939000	4.431516000	-8.410736000
C	7.134089000	1.012682000	-6.952643000	H	5.987088000	3.700466000	-8.760533000
C	8.466408000	1.415564000	-6.768783000	H	0.945280000	5.778910000	-7.123387000
C	8.912753000	2.645810000	-7.291108000	H	-0.235488000	7.826612000	-6.291457000
C	8.024189000	3.468705000	-8.002613000	H	-2.512558000	7.629490000	-5.233725000
C	6.690956000	3.073095000	-8.198059000	H	-3.591447000	5.366116000	-5.038949000
C	-0.044842000	5.703515000	-6.656607000	H	-2.398553000	3.325978000	-5.879892000
C	-0.713229000	6.840054000	-6.186211000	H	2.090540000	-1.545496000	-8.339988000
C	-1.989594000	6.731993000	-5.596961000	H	3.556498000	-1.711182000	-9.377724000
C	-2.592728000	5.465318000	-5.492368000	H	2.127784000	-0.786117000	-9.975631000
C	-1.934376000	4.318525000	-5.957983000	H	-1.486846000	0.184796000	-8.556399000
C	2.738053000	-1.031553000	-9.081378000	H	-0.053566000	-0.747803000	-7.984476000
C	-0.383198000	0.141276000	-8.563878000	H	-0.033912000	0.027964000	-9.612204000
Ru	3.186599000	3.700805000	-6.346813000	H	3.132348000	7.022949000	-10.442756000
C	3.695990000	6.692123000	-9.559320000	H	5.378554000	8.086760000	-9.802383000
C	4.942654000	7.275965000	-9.198433000	H	6.577804000	7.233466000	-7.778136000
C	5.608858000	6.804486000	-8.072912000	H	2.225318000	5.186367000	-8.982579000
C	5.059455000	5.750944000	-7.284673000	H	7.565556000	6.304978000	-6.064307000
N	3.806149000	5.203432000	-7.642805000	H	7.072562000	3.148155000	-3.074767000
C	3.186681000	5.670274000	-8.749094000	H	5.728913000	1.508928000	-2.493498000
C	5.711206000	5.157696000	-6.143646000	H	4.006215000	-0.189459000	-1.847669000
C	6.973241000	5.510901000	-5.592191000	H	1.791701000	-0.251087000	-3.142430000
C	7.501490000	4.760321000	-4.504598000	H	1.457030000	1.400481000	-5.011506000
C	6.726451000	3.697269000	-3.959906000	H	9.131205000	3.106962000	-3.030895000
C	5.455660000	3.393546000	-4.522309000	H	11.395775000	3.616216000	-2.121951000
N	5.011574000	4.110260000	-5.602594000	H	11.232991000	7.568904000	-3.886370000
N	3.294842000	2.329630000	-4.775649000	H	8.950592000	7.093897000	-4.766726000
C	4.523627000	2.384067000	-4.083453000	H	0.411400000	6.950380000	-3.548869000
C	4.765221000	1.463969000	-3.021821000	H	2.042221000	7.601292000	-3.144511000
C	3.809510000	0.518346000	-2.667737000	H	1.391463000	6.190148000	-2.239842000
C	2.579556000	0.476415000	-3.382945000				
C	2.385843000	1.397268000	-4.419697000				
C	9.566535000	4.101651000	-3.204699000				
C	10.843489000	4.371773000	-2.699378000				
C	11.429937000	5.621215000	-2.951621000				
C	10.755357000	6.595358000	-3.703058000				
C	9.478643000	6.312403000	-4.201505000				
C	8.840903000	5.060514000	-3.968313000				

Ru$_4$ $^{3+}$ (1e$^-$ oxidised, *S* = 1/2)							
N	4.658119000	0.276408000	-8.533206000	N	2.346379000	5.053466000	-5.096192000
N	4.866988000	1.335867000	-7.743295000	O	12.444802000	6.736935000	-2.574662000
C	3.742317000	2.092021000	-7.516895000	C	1.915908000	5.815812000	-4.322170000
C	2.755112000	1.382934000	-8.245465000	C	1.367456000	6.755030000	-3.374739000
N	3.370693000	0.312062000	-8.831123000	F	14.348652000	6.753679000	-1.533372000
C	1.438946000	1.917134000	-8.068704000	C	13.297716000	5.983592000	-1.821774000
C	1.405295000	3.033191000	-7.186406000	F	12.733732000	5.568257000	-0.668613000
N	0.061371000	3.347802000	-7.186725000	F	13.733320000	4.888120000	-2.480613000
N	-0.686520000	2.543298000	-7.944645000	H	5.941894000	-0.175571000	-5.833262000
N	0.159883000	1.672588000	-8.475797000	H	8.196328000	0.176681000	-4.772433000
C	-0.583765000	4.426975000	-6.486173000	H	9.650311000	2.074292000	-5.532044000
C	6.173379000	1.524737000	-7.167428000	H	8.864439000	3.612418000	-7.347939000
C	6.595511000	0.647347000	-6.156497000	H	6.615028000	3.247117000	-8.415467000
C	7.853576000	0.851701000	-5.570159000	H	0.383820000	5.944373000	-7.708165000
C	8.665499000	1.916285000	-5.996222000	H	-0.707376000	7.836218000	-6.469845000
C	8.226769000	2.780975000	-7.013821000	H	-2.274948000	7.349776000	-4.572744000
C	6.972325000	2.588239000	-7.611038000	H	-2.758665000	4.978724000	-3.917152000
C	-0.301915000	5.745817000	-6.872417000	H	-1.658318000	3.085148000	-5.156962000
C	-0.916963000	6.796902000	-6.177410000	H	2.028268000	-1.276046000	-9.127389000
C	-1.797806000	6.521305000	-5.116951000	H	3.628671000	-1.415901000	-9.954427000
C	-2.070293000	5.193103000	-4.747658000	H	2.389185000	-0.267214000	-10.597066000
C	-1.462779000	4.130762000	-5.434385000	H	-1.431335000	0.815809000	-9.500894000
C	2.809424000	-0.728980000	-9.685442000	H	-0.191927000	-0.355647000	-8.901985000
C	-0.352356000	0.635094000	-9.364921000	H	0.166150000	0.702236000	-10.338017000
Ru	3.160090000	3.632925000	-6.349126000	H	3.013354000	6.554284000	-10.668869000
C	3.585919000	6.334036000	-9.757763000	H	5.130123000	7.835418000	-10.089079000
C	4.754113000	7.037749000	-9.432899000	H	6.374263000	7.227613000	-7.992242000
C	5.448542000	6.703076000	-8.263500000	H	2.240498000	4.737099000	-9.125335000
C	4.958131000	5.684150000	-7.436383000	H	7.389428000	6.472229000	-6.204124000
N	3.797517000	5.014576000	-7.759079000	H	7.042123000	3.499949000	-3.040805000
C	3.142261000	5.322381000	-8.901176000	H	5.778068000	1.840009000	-2.350177000
C	5.628373000	5.215217000	-6.211835000	H	4.181535000	0.003294000	-1.724862000
C	6.843504000	5.671012000	-5.690326000	H	2.078616000	-0.315377000	-3.114393000
C	7.392563000	5.051203000	-4.541957000	H	1.677903000	1.208753000	-5.068009000
C	6.665374000	3.993165000	-3.945469000	H	9.192911000	3.516403000	-3.159401000
C	5.447921000	3.585607000	-4.501455000	H	11.387752000	4.177434000	-2.287585000
N	4.971846000	4.194016000	-5.612956000	H	10.802019000	8.198936000	-3.834483000
N	3.422395000	2.316734000	-4.760376000	H	8.569419000	7.534641000	-4.718824000
C	4.570363000	2.505003000	-4.023145000	H	0.452694000	6.327893000	-2.917616000
C	4.856590000	1.681340000	-2.925908000	H	1.103462000	7.695960000	-3.897288000
C	3.965644000	0.657584000	-2.581311000	H	2.111360000	6.970533000	-2.582312000
C	2.804596000	0.475584000	-3.346390000				
C	2.569362000	1.320238000	-4.435459000				
C	9.521481000	4.555268000	-3.305613000				
C	10.777643000	4.923573000	-2.811025000				
C	11.224318000	6.241235000	-3.011990000				
C	10.430239000	7.173301000	-3.702047000				
C	9.185211000	6.786624000	-4.199051000				
C	8.703510000	5.469436000	-4.007621000				

Ru$_4$ $^{3+}$ (1e$^-$ oxidised, S = 1/2)							
N	4.735724000	0.416006000	-8.630529000	N	2.328459000	5.141793000	-5.178550000
N	4.911764000	1.375948000	-7.716853000	O	12.476070000	6.642124000	-2.694705000
C	3.778112000	2.104069000	-7.465999000	C	1.909293000	6.054411000	-4.581137000
C	2.822966000	1.496621000	-8.316226000	C	1.388700000	7.174826000	-3.842856000
N	3.467632000	0.495778000	-8.991827000	F	14.366278000	6.720413000	-1.620532000
C	1.505141000	2.031968000	-8.156307000	C	13.294434000	5.960206000	-1.795323000
C	1.418497000	3.026278000	-7.140656000	F	12.675101000	5.775805000	-0.622430000
N	0.084113000	3.361863000	-7.182203000	F	13.662568000	4.767666000	-2.282201000
N	-0.609818000	2.692620000	-8.104185000	H	5.684937000	-0.116312000	-5.662560000
N	0.259439000	1.890904000	-8.698869000	H	7.878220000	0.080817000	-4.437074000
C	-0.620409000	4.306753000	-6.356432000	H	9.554600000	1.803959000	-5.155054000
C	6.186564000	1.479373000	-7.049764000	H	9.066025000	3.303500000	-7.102219000
C	6.442105000	0.620342000	-5.968152000	H	6.878794000	3.089525000	-8.335065000
C	7.664003000	0.739590000	-5.291264000	H	-1.098809000	5.595912000	-8.038503000
C	8.601833000	1.705001000	-5.696500000	H	-2.348500000	7.236747000	-6.592333000
C	8.329354000	2.549329000	-6.788509000	H	-2.540434000	6.832561000	-4.125623000
C	7.114114000	2.439402000	-7.479924000	H	-1.497685000	4.796717000	-3.097675000
C	-1.198838000	5.435228000	-6.955495000	H	-0.253766000	3.157974000	-4.547233000
C	-1.891251000	6.343840000	-6.141274000	H	2.129292000	-1.023742000	-9.547343000
C	-1.997117000	6.115297000	-4.758675000	H	3.786236000	-1.108843000	-10.271977000
C	-1.410312000	4.976417000	-4.179304000	H	2.605845000	0.126837000	-10.873940000
C	-0.714285000	4.058448000	-4.978537000	H	-1.265731000	1.267657000	-9.962847000
C	2.955732000	-0.439659000	-9.991855000	H	-0.111043000	-0.034021000	-9.464093000
C	-0.206973000	1.021481000	-9.777857000	H	0.394153000	1.218159000	-10.683965000
Ru	3.176651000	3.619984000	-6.273615000	H	2.917554000	6.563461000	-10.591486000
C	3.524502000	6.317151000	-9.709293000	H	5.116746000	7.745828000	-10.120004000
C	4.736270000	6.967161000	-9.443320000	H	6.421342000	7.103193000	-8.073499000
C	5.466594000	6.610677000	-8.301563000	H	2.128428000	4.797184000	-8.997732000
C	4.969438000	5.616287000	-7.449946000	H	7.433438000	6.358986000	-6.282435000
N	3.772570000	4.992020000	-7.722615000	H	7.067670000	3.451937000	-3.036437000
C	3.073933000	5.328815000	-8.827218000	H	5.768446000	1.851660000	-2.264695000
C	5.659445000	5.139628000	-6.238386000	H	4.115666000	0.098436000	-1.558971000
C	6.885533000	5.577001000	-5.744234000	H	1.983163000	-0.190088000	-2.907141000
C	7.440192000	4.968231000	-4.583373000	H	1.604859000	1.285139000	-4.906464000
C	6.695946000	3.930671000	-3.949879000	H	9.080638000	3.566444000	-2.872919000
C	5.461948000	3.545012000	-4.469491000	H	11.266693000	4.231315000	-2.023895000
N	4.983409000	4.146934000	-5.593331000	H	11.018375000	7.971697000	-4.264652000
N	3.392243000	2.336532000	-4.655254000	H	8.793298000	7.309009000	-5.134710000
C	4.557965000	2.507591000	-3.941831000	H	0.893748000	6.810948000	-2.919782000
C	4.833242000	1.711728000	-2.823046000	H	0.646658000	7.714028000	-4.466023000
C	3.910101000	0.732237000	-2.433616000	H	2.217117000	7.861253000	-3.574048000
C	2.732939000	0.566866000	-3.175673000				
C	2.509169000	1.382773000	-4.289977000				
C	9.477921000	4.544618000	-3.175554000				
C	10.726538000	4.910705000	-2.694438000				
C	11.273240000	6.156535000	-3.096407000				
C	10.567157000	7.010111000	-3.982992000				
C	9.329679000	6.623128000	-4.465709000				
C	8.743746000	5.380561000	-4.071885000				

Efficiency calculations

Faradaic Yield Calculation:

Faradaic efficiency for the electrochemical CO_2 reduction was calculated following the equation:

$$FE = \frac{n_{CO}.2.F}{\int Idt}$$

where, n_{CO} is amount of CO produced (in mol), F is Faraday's constant, $\int Idt$ is the charge consumed during the electrolysis.

Calculation of diffusion coefficient:

The peak current, i_p could be related to the scan rate, ν following the Randles-Sevcik equation:

$$i_p = 0.4463nFAC\sqrt{\frac{nF\nu D}{RT}}$$

where, *F* is Farady's constant (*F* = 96500 C/mol), A is the active surface area of the electrode (A = 7.85 x 10^{-3} cm^2), R is the universal gas constant (R = 8.314 J K^{-1} mol^{-1}), T is the temperature (300 K), n_p is the number of electrons transferred, C is the concentration of the catalyst (mM), D is the diffusion coefficient, ν is scan rate in V. Diffusion coefficient is then calculated from the slope of i_p versus $\nu^{1/2}$ plot. The value of D was calculated as 4.09 x 10^{-6} cm^2s^{-1}.

Calculation of TOF_{max}:

The TOF values were calculated from the equation below:

$$I_{cat}/I_p = 4.484 \times (RT/F)^{1/2}(TOF_{max})^{1/2}\ \nu^{-1/2}$$

where, I_p is the peak current, I_{cat} is the catalytic current, *F* is Farady's constant (*F* = 96500 C/mol), R is the universal gas constant (R = 8.314 J K^{-1} mol^{-1}), T is the temperature (300 K). From the slope of I_{cat}/I_p versus $\nu^{-1/2}$ plot. Therefore, TOF_{max} was calculated as 14.07 s^{-1}.

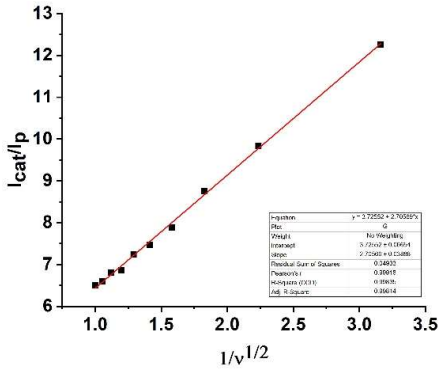

Figure S45: Plot of i_{cat}/i_p vs. $\nu^{-1/2}$ of **Ru_4**.

Calculation of TOF from controlled potential electrolysis experiments:

Considering a stable current during the electrolysis process, following formula can be used to extract TOF form the CPE data:

$$TOF = k_{cat} = \frac{i^2}{F^2A^2DC^2}$$

where *i* is the stable current (0.35 mA), *F* is Farady's constant (*F* = 96500 C/mol), A is the surface area of the working electrode (GC-rod), D is diffusion coefficient determine, C is the concentration of the catalyst.

Crystallographic Details

	RU$_4$	**RU$_5$**
Chemical formula	C_{80} H_{59} Cl_2 F_{18} N_{18} O_2 P_2 Ru_2	C_{42} H_{33} F_{15} N_{10} O P_2 Ru
M_r	1981.43	1141.79
Crystal system	Triclinic	Triclinic
Space group	P -1	P -1
a (Å)	10.5995(10)	13.8121(16)
b (Å)	18.3736(17)	13.8533(15)
c (Å)	24.656(2)	16.460(2)
α(°)	73.447(5)	67.652(6)
β (°)	88.444(4)	85.674(7)
γ (°)	86.225(5)	81.135(7)
V (Å^3)	4592.7(7)	2877.7(6)
Z	2	2
Densitiy (g cm^{-3})	1.433	1.318
F(000)	1990	1144
Radiation Type	MoK_α	CuK_α
μ (mm^{-1})	0.512	3.514
Crystal size	0.592 x 0.246 x 0.07	0.153 x 0.141 x 0.113
Meas. Refl.	56748	33096
Indep. Refl.	16767	9593
Obsvd. [$I > 2\sigma(I)$] refl.	11858	8574
R_{int}	0.0752	0.0441
[$F^2>2\sigma(F^2)$], w$R(F^2)$, S	0.1100, 0.2871, 1.020	0.0385, 0.0896, 1.061
$\Delta\rho_{max}$, $\Delta\rho_{min}$ (e Å^{-3})	4.093, -2.673	0.834, -0.468

Deposition Numbers CSD2203803 (for **Ru$_4$**) and CSD2203804 (for **Ru$_5$**) contain the supplementary crystallographic data for this paper. These data are provided free of charge by the joint Cambridge Crystallographic Data Centre and Fachinformationszentrum Karlsruhe.

References

[1] G. R. Fulmer, A. J. M. Miller, N. H. Sherden, H. E. Gottlieb, A. Nudelman, B. M. Stoltz, J. E. Bercaw, K. I. Goldberg, *Organometallics*, **2010**, *29*, 2176–2179.

[2] (a) *APEX3*, Bruker AXS Inc., Madison, Wisconsin, USA, **2015**, (b) G. M. Sheldrick, *SADABS Ver. **2008**/1, Program for Empirical Absorption Correction*, University of Göttingen, Germany, **2008**, (c) *SAINT+, Data Integration Engine, Version 8.27b ©*, Bruker AXS Inc., Madison, Wisconsin, USA, **1997–2012**, (d) G. M. Sheldrick, *SHELXL Version **2014**/7, Program for Chrystal Structure Solution and Refinement*, University of Göttingen, Germany, **2014**, (e) C. B. Hübschle, G. M. Sheldrick, B. Dittrich, *J. Appl. Cryst*., **2011**, *44*, 1281–1284, (f) G. M. Sheldrick, *Acta Cryst*., **2008**, *A64*, 112–122, (g) G. M. Sheldrick, *Acta Cryst.*, **2015**, *C71*, 3.17 (h) A. L. Spek, *Acta Cryst*., **2015**, *C71*, 9–18. (i) A. L. Spek, *ActaCryst.*, **2009**, *D65*, 148–155. (j) A. L. Spek, *J. Appl. Cryst*., **2003**, *36*, 7–13.

[3] A. L. Spek, *PLATON*, A multipurpose Crystallographic Tool, Utrecht, the Netherlands, **1998**.

[4] L. Fabbrizzi, *ChemTexts*, **2020**, *6*, 1039–1059.

[5] F. Neese, *WIREs Comput Mol Sci*, **2018**, *8,* 33–9.

[6] C. Adamo, V. Barone, *J. Chem. Phys.*, **1999**, *110*, 6158–6170.

[7] F. Weigend, R. Ahlrichs, *Phys. Chem. Chem. Phys*, **2005**, *7,* 3297–3305.

[8] V. Barone, M. Cossi, *J. Phys. Chem. A*, **1998**, *102*, 1995–2001.

[9] a) S. Grimme, *J. Comput. Chem.* **2006**, *27*, 1787–1799; b) S. Grimme, *J. Comput. Chem.* **2004**, *25*, 1463–1473; c) S. Grimme, J. Antony, S. Ehrlich, H. Krieg, *J. Chem. Phys.* **2010**, *132*, 154104–154122; d) S. Grimme, S. Ehrlich, L. Goerigk, *J. Comput. Chem.* **2011**, *32*, 1456–1465.

[10] a) P. Seth, P. L. Ríos, R. J. Needs, *J. Chem. Phys.* **2011**, *134*, 84105–84114; b) F. Neese, G. Olbrich, *Chem. Phys. Lett.* **2002**, *362*, 170–178; c) R. Izsák, F. Neese, *J. Chem. Phys.* **2011**, *135*, 144105–144117; d) J. L. Whitten, *J. Chem. Phys.* **1973**, *58*, 4496–4502; e) O. Vahtras, J. Almlöf, M. W. Feyereisen, *Chem. Phys. Lett.* **1993**, *213*, 514–518; f) F. Neese, F. Wennmohs, A. Hansen, *J. Chem. Phys* **2009**, *130*, 114108–114126; g) F. Neese, *J. Comput. Chem.* **2003**, *24*, 1740–1747.

[11] a) K. Eichkorn, O. Treutler, H. Öhm, M. Häser, R. Ahlrichs, *Chem. Phys. Lett.***1995**, *240*, 283–290; b) K. Eichkorn, F. Weigend, O. Treutler, R. Ahlrichs, *Theor. Chem. Acc.* **1997**, *97*, 119–124; c) F. Weigend, *Phys. Chem. Chem. Phys.* **2006**, *8*, 1057–1065.

[12] P. O. Löwdin, *J. Chem. Phys* **1950**, *18*, 365–377.

[13] a) D. Doehnert, J. Koutecky, *J. Am. Chem. Soc.* **1980**, *102*, 1789–1796; b) J. Gräfenstein, E. Kraka, M. Filatov, D. Cremer, *Int. J. Mol. Sci.* **2002**, *3*, 360–394; c) F. Neese, *J. Phys. Chem. Solids* **2004**, *65*, 781–785; d) K. Yamaguchi, *Chem. Phys. Lett.* **1975**, *33*, 330–335.

[14] Chemcraft - graphical software for visualization of quantum chemistry computations (Chemcraft,).

[15] L. Suntrup, S. Hohloch, B. Sarkar, *Chem. Eur. J.*, **2016**, *22*, 18009–18018.

[16] R. Tatikonda, S. Bhowmik, K. Rissanen, M. Haukka, M. Cametti, *Dalton Trans*. **2016**, *45*, 12756–12762

3.3. Azobenzene-based Platinum Complexes

3.3.1. Dinuclear Quinonoid-Bridged Pt(II) Complexes with (Perfluorinated-) Alkyl Chain Containing Azobenzene Ligands: A Combined Synthetic, Electrochemical and Spectroelectrochemical Investigation

*Maite Nößler,[a] Lisa Böser,[a] René Jäger,[a] Clemens Lücke,[b] Arijit Singha Hazari,[b] Eugen Wuckert,[c] Julia Beerhues,[a,b] Sabine Laschat[c] and Biprajit Sarkar[a,b]**

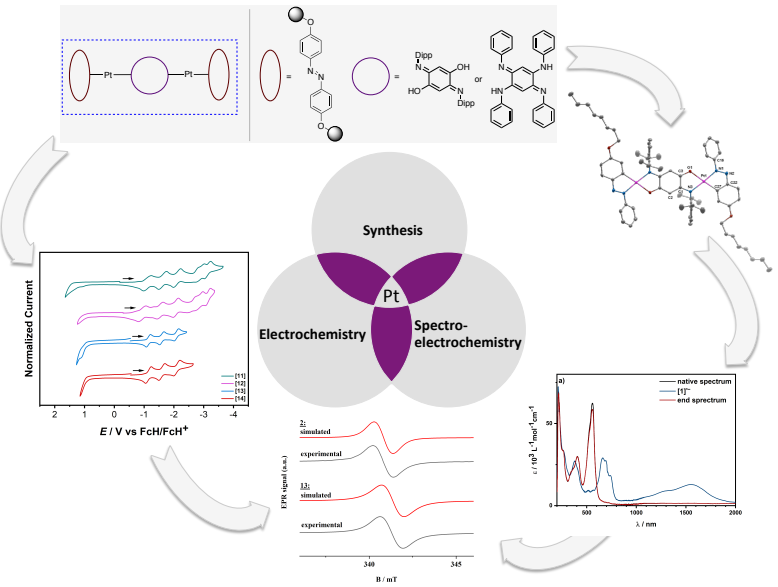

[a]Institut für Chemie und Biochemie,
Freie Universität Berlin, Fabeckstraße 34-36, D-14195, Berlin, Germany
[b] Institut für Anorganische Chemie,
Universität Stuttgart, Pfaffenwaldring 55, D-70569 Stuttgart, Germany
[c] Institut für Organische Chemie,
Universität Stuttgart, Pfaffenwaldring 55, 70569 Stuttgart, Germany

Manuscript in preparation

Author contribution: The project was designed by Biprajit Sarkar and Maite Nößler. The ligands and complexes were synthesized and characterized by Maite Nößler. Lisa Böser and René Jäger worked in this project during a research internship. Cyclic voltammetric and UV/Vis/NIR-spectroelectrochemical measurements were performed by Lisa Böser, René Jäger, Clemens Lücke and Maite Nößler. X-Ray diffraction analysis was carried out by Maite Nößler and Julia Beerhues. EPR measurements were performed by Maite Nößler and Arijit Singha Hazari, subsequent simulation was performed by Arijit Singha Hazari. The manuscript was written by Maite Nößler and Biprajit Sarkar.

Dinuclear Quinonoid-Bridged Pt(II) Complexes with (Perfluorinated-) Alkyl Chain Containing Azobenzene Ligands: A Combined Synthetic, Electrochemical and Spectroelectrochemical Investigation

*Maite Nößler,[a] Lisa Böser,[a] René Jäger,[a] Clemens Lücke,[b] Arijit Singha Hazari,[b] Eugen Wuckert,[c] Julia Beerhues,[a,b] Sabine Laschat[c] and Biprajit Sarkar[a,b]**

Abstract

Different complexes of the form $[(az_x)Pt(\mu\text{-}L)Pt(az_x)]$ were generated by reaction of the ligands 2,5-bis[2,6-(diisopropyl)aniline]-1,4-benzo-quinone (L_1) and azophenine (L_2) with $[(az_x)Pt(\mu\text{-}Cl)Pt(az_x)]$. Structural characterization of **1** revealed that the metal center and the ligand donor atoms are almost coplanar, while the diisopropylphenyl rings are twisted out of plane. The influence of alkylation of the azobenzene stoppers was investigated towards the liquid crystalline properties. All complexes were investigated electrochemically, which revealed several reversible and irreversible redox processes in their cyclic voltammograms. The bridging ligand shows a huge impact on the redox potentials, whereas only a marginal influence of the alkyl chains could be observed.

Introduction

Donor-acceptor metal complexes were synthesized with metals in the d^8 electronic configuration because of their intriguing redox and photochemical properties.[1] Unique photochemical and photophysical properties of such metal complexes are usually due to intense ligand-to-ligand charge transfers (LLCTs).[1g, 2] In this regard the use of strong π-acceptor and strong σ- and/or π-donor ligands can be used to obtain compounds with strong LLCT transition.[3]

[a] Institut für Chemie und Biochemie, Freie Universität Berlin, Fabeckstraße 34-36, 14195, Berlin (Germany) E-mail: biprajit.sarkar@iac.uni-stuttgart.de

[b] Institut für Anorganische Chemie, Universität Stuttgart, Pfaffenwaldring 55, 70569 Stuttgart (Germany)

[c] Institut für Organische Chemie, Universität Stuttgart, Pfaffenwaldring 55, 70569 Stuttgart (Germany)

Examples of ligands that have been employed in this regard are shown in figure 1. Well established donor ligands are catecholate/amidophenolate/diamidobenzene ligands, while 2,2´-bipyridine (bpy), phenylazopyridine (pap), azobenzene or similar systems can be used as acceptor ligands.[1g-i, 4] Furthermore azobenzene is widely used in coordination chemistry as it exhibits unique photochromic behavior and photoactivity.[5]

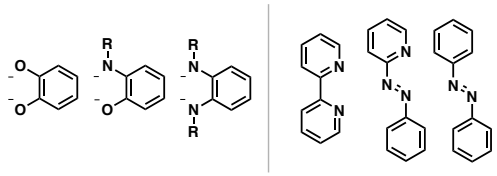

Figure 1:Typical donor (left) and acceptor (right) ligands.

Quinones are typical examples of noninnocent ligands.[6] The fascinating redox properties and electronic structures of these ligands have led to their intensive use in coordination chemistry.[1h, 7] A further example of a quinonoid ligand is 2,5-dihydroxy-1,4-benzoquinone (L_Q, figure 2) which has been widely used as a bridging ligand in molecular metal complexes and in coordination polymers.[7e] In order to improve the tuning of steric and electronic properties of L_Q we[8] and others[9] have developed several synthetic routes for potentially bridging quinone ligands where the [O] donors are (partially) substituted with isoelectronic [NR] groups. This led to the development of e.g. 2,5-bis-[2,6-(diisopropyl)aniline]-1,4-benzoquinone) (L_{Q1}, figure 2).[10] Furthermore, the all-nitrogen-donating-ligand azophenine (L_{Q2}, figure 2) has been known for decades but was only sporadically used in coordination chemistry.[9f, 11] Some of the azophenine containing

transition metal complexes exhibit interesting magnetic properties[8d, 11d, 12] and catalytical activity.[13]

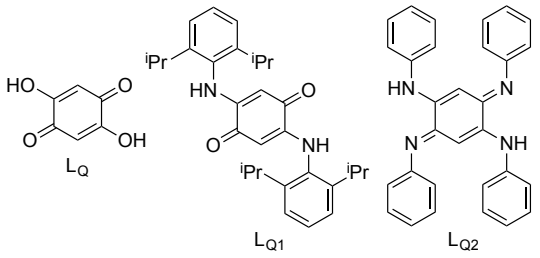

Figure 2: Ligand L_Q and Related Ligands with isolectronic [NR] groups.

Due to their photophysical and mesomorphic properties and their possible use as antitumor agents, square planar platinum complexes are of great interest.[14] In this regard, donor acceptor complexes have been reported that exhibit exceptional photophysical and electrochemical properties.[15] Additionally, catechol containing platinum(II) complexes have been proposed as promising candidates for inorganic dye-sensitized solar cells (DSSC's).[1g]

Another interesting class of compounds is metallomesogens, liquid crystals of transition metal complexes, which have attracted attention due to the co-occurrence of photophysical properties (optical, magnetic and electrical properties).[16] If photochromic and liquid crystalline properties in the same molecule are combined new materials for several applications (nonlinear optics or optical data storage) can be provided.[17] Therefore, entities, such as azobenzene, that can react to luminous stimuli should be integrated.[17b] Even though azobenzene-containing compounds have widely been used in systems to obtain photoresponsive materials, there are rather few examples of azobenzene-containing metallomesogens.[17b, 18]

Although the use of perfluorocarbon (PFC) tails is very interesting, rather few examples with azobenzene can be found. Some studies have been performed on the effect of perfluorinated alkyl or alkoxy chains and fluorinating aromatic mesogenic cores on the LC properties of, for example, benzoate with a biphenyl moiety or pyrimidine-based molecules[19] where the focus was on mesomorphic temperature ranges, ferroelectricity or low melt viscosities.[20] The strong interactions in the perfluoroalkyl tails result in the favored formation of the smetic A LC phase, the improvement of the thermal stability of the mesophase and a broader mesophase temperature range.[20-21] Also studies on azobenzene containing compounds bearing a PFC tail have been performed,[21-22] where e.g. the length of the fluorinated tail plays a role on the phase transitions.[23]

The focus of this work is on the influence of terminal alkoxy- and perfluoroalkoxy tails on the azobenzene unit on the properties of the resulting platinum(II) complexes. We present several complexes bearing different amounts of (perfluorinated)alkoxy substituents. The electrochemistry of these complexes will be discussed and they will be probed for liquid crystalline behavior. Furthermore, we present a simple synthesis for nitrophenol and azobenzene compounds with a perfluorinated alkyl chain.

Results and Discussion

Synthesis and Structural Characterization

The azobenzene ligands and the precursor $[(\eta^3\text{-}C_4H_7)Pt(\mu\text{-}Cl)]_2$ were synthesized according to literature known procedures.[24]

4,4'-dihydroxyazobenzene **L1** or 4-hydroxyazobenzene was reacted with either 1-bromooctane or 1-bromohexadecane in acetone to generate the ligands **L2-L5** (Scheme 1). For the synthesis of **P1-P4** one of the ligands **L2-L5** was added to a solution of $[(\eta^3\text{-}C_4H_7)Pt(\mu\text{-}Cl)]_2$ in $CHCl_3$ which led to the isolation of the platinum containing precursors after work up (Scheme 1). The ligands and **P1-P3** were characterized by NMR spectroscopy, mass spectrometry and elemental analysis. Due to low solubility of **P4** only elemental analysis could be used for characterization.

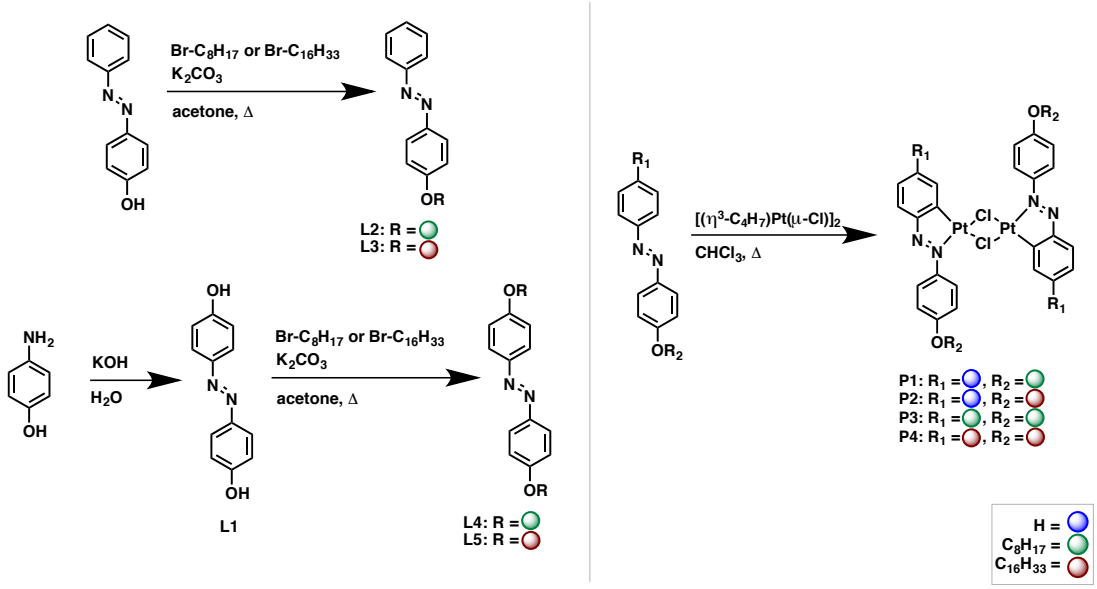

Scheme 1: Synthetic route for the azobenzene ligands **L1**-**L5** (left) and the precursors **P1**-**P4** (right).

The combination of quinone and azobenzene ligands in square planar palladium(II) and platinum(II) metal centers give access to completely delocalized, redox active and electro chromic systems.[25] Thus, the synthesis of such platinum complexes were targeted here by using the aforementioned platinum precursors.[26]

The platinum(II) precursors **P1**-**P4** and the ligands H_2Q_{Dipp} or H_2Q_{Az} were dissolved in MeCN and treated with Et_3N. After reaction for 1-2 days the precipitated solids were filtrated and after the work up (see experimental section) the desired complexes were obtained as purple (**1**-**4**) or blue (**7**-**10**) solids.

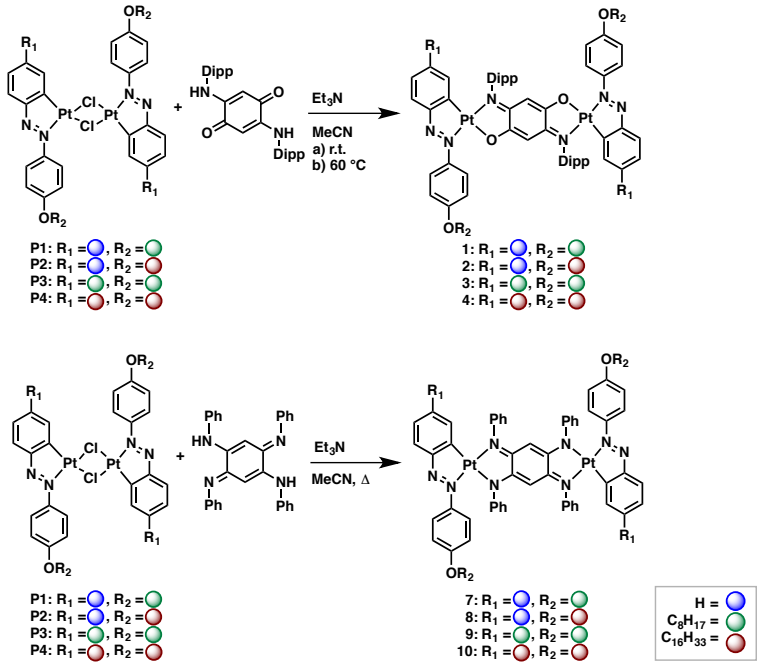

Scheme 2: Synthesis of the platinum(II) complexes: top reaction conditions for a) complexes **1**-**3**, b) complex **4**, bottom: reaction conditions for complexes **7**-**10**.

Furthermore, two additional complexes, **5** and **6**, (see figure 3) containing three to four long alkyl chains were synthesized in order to investigate the influence of the additional chains on the properties of these complexes. The synthesis of these complexes was similar to that described for complexes **1-3**.

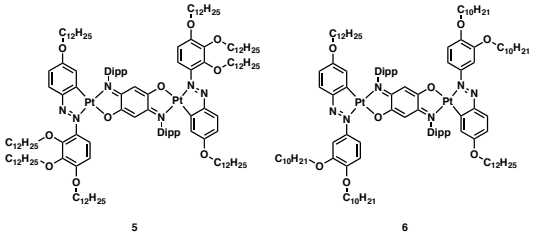

Figure 3: Complexes **5** and **6** with three and more alkyl chains on the azobenzene ligands.

In order to get insight of the influence of fluorine on the alkyl chains, several complexes with azobenzene ligands, which contain perfluoro carbon tails (PFC), were synthesized. The azobenzene ligands **L8** and **L9** were synthesized by first implementing a fluorinated alcohol with a triflate group to increase the reactivity (Scheme 3). Afterwards it could be added on the hydroxyl group of the azobenzene. Attempts were made to synthesize the symmetric azobenzene ligands, but it was not possible to isolate the desired compounds. Neither the direct reaction of the alkyltriflate with 4,4' dihydroxyazobenzene nor the synthesis of the amine followed by the azobenzene formation led to the desired ligands. Precursors **P7-P10** and complexes **11-17** were prepared as the other platinum complexes described above.

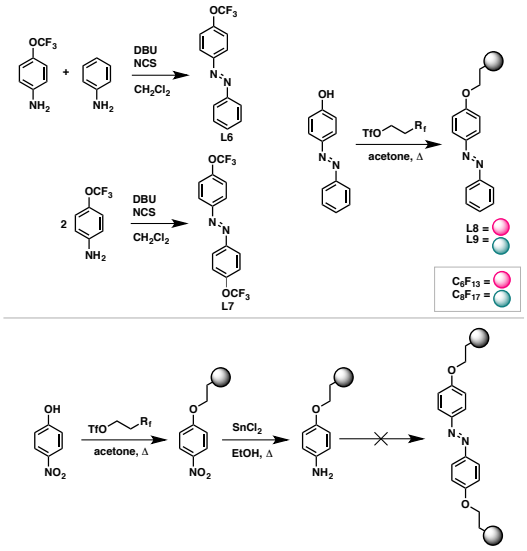

Scheme 3: Synthetic route for the azobenzene ligands **L6-L9**.

It was possible to obtain suitable single crystals for X-ray diffraction analysis of **1**. The obtained crystals of **3** were not of sufficient quality to obtain a structure in the solid state, but the obtained picture proves the desired connectivity of the atoms, but no significant conclusions of the bond lengths can be made (See Supporting Information).

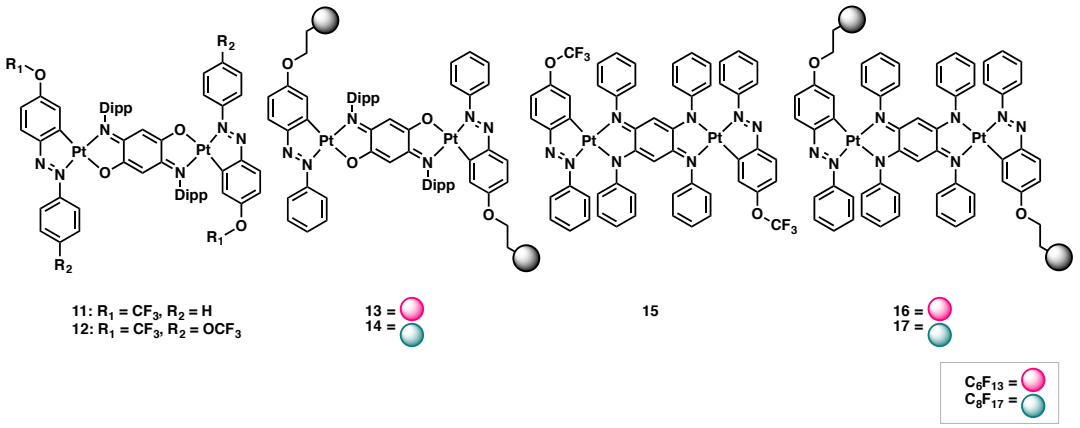

Figure 4: Complexes **11-17**.

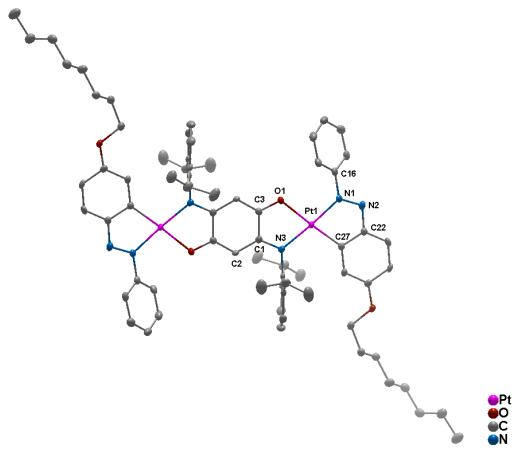

Figure 5: Perspective view of complexes **1**. Ellipsoids are at a probability level of 50%. H atoms are omitted for clarity.

1 crystallized in the triclinic $P\bar{1}$ space group. The metal center in **1** shows a distorted square planar environment (Figure 5), which is caused by the chelating nature of $L_{Q1\text{-}2H}$ and $\mathbf{L1}_{\text{-}H}$.[26] The distortion is already obvious from the O1-Pt-N3 angle of 78.5(1)°, which is comparable to known platinum complexes.[26] Regarding the azo-bond N1-N2, which is of 1.29 Å, we observe a slight elongation compared to normal N=N azo double bonds. This elongation takes place due to π back-bonding from filled dπ orbitals of Pt(II) to the empty π^* orbital of the **L1**.[27] Furthermore, the Pt-O1 bond is comparable to the literature known complex and is relatively long.[26] The bond lengths within $L_{Q1\text{-}2H}$ are also comparable to previously reported values.[8a, 8c, 8d] The C3-O1 bond is about 1.29 Å and therefore closer to a C–O single-bond lengths whereas the C1-N3 bond length of 1.32 Å is closer to a C=N double-bond length. Due to the shorter bond length of C2–C3 of 1.37 Å in comparison to C1–C2 of 1.41 Å the best localized description of the bridge $L_{Q1\text{-}2H}$ is, where the negative charge that is possibly better stabilized at the more electronegative O atom and thus, of a "dimino-dialkoxy" donor type. This is similar to observations in other dinuclear complexes with related ligands.[8a-d, 26, 28] As the C1–C3 bond with 1.49 Å fits to a single bond, the bridging ligands have single bonds that connect localized double bonds in the "lower" and "upper" part of the molecule.

The metal centers are at a distance of 8 Å from each other. The dihedral angle between the planes (Pt-N1-N2-C27-C22 and Pt-N3-C1-C3-O1) shows that the metal center and the O and N donor atoms are nearly coplanar at 4.4°, while the diisopropylphenyl rings of the bridging ligand are twisted with a dihedral angle of 83.7° and the uncoordinated phenyl ring of **L1** with an angle of 45.0°, respectively. All these values are similar to the previously published azobenzene-based complex with the identical bridging-ligand.[26]

Table 1: Selected bond lengths (Å) and Bond Angles (deg) of **1**.

	1
Pt-O1	2.102(2)
Pt-N3	2.026(3)
Pt-C27	1.988(3)
Pt-N1	1.998(3)
O1-C3	1.293(4)
N3-C1	1.320(4)
N1-N2	1.293(4)
C1-C2	1.419(4)
C1-C3	1.496(5)
C2-C3	1.370(4)
M-M	7.976(2)
O1-Pt-N3	78.5(1)
N3-Pt-C27	104.3(1)
N1-Pt-C27	78.6(1)
O1-Pt_N1	98.4(1)
N1-Pt-N3	175.3(1)
O1-Pt-C27	177.1(1)

Most of the ligands and complexes were investigated under a polarized optical microscope (POM) to examine the liquid crystalline properties. The ligands **L4** and **L14** (See figure S2) show a phase transition, but as the complexes were of greater interest it was not further investigated. For **P5** typical textures for columnar-hexagonal mesophases were found (Figure 6), while for **L14** we see a nematic phase.

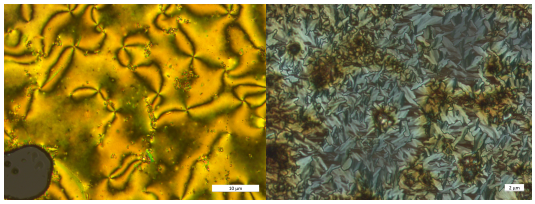

Figure 6: **L4** while cooling from 133°C with 5K/min at 114°C (left). **P5**: Cooling from 88°C with 5°C/min, at 60°C (right).

Since typical LC textures were found for **P5** the sample was probed with differential scanning calorimetry (DSC). But the DSC measurements does not align with the observed textures for **P5** as the typical course of the curve with a melting point and a clearing point could not be observed (See Supporting Information).

Cyclic Voltammetry

Due to the redox activity of the quinone as well as the azobenzene ligands all complexes were electrochemically characterized, as such compounds are likely to be redox-rich. In order to probe this fact, the complexes were investigated in CH_2Cl_2/0.1 M Bu_4PF_6 as well as in THF/0.1 M Bu_4PF_6. To get better insights in the oxidative side, CH_2Cl_2 was used whereas THF should provide a larger potential window on the reductive side. The cyclic voltammograms of **1**-**4** resemble each other. For all complexes in CH_2Cl_2 one quasi-reversible oxidation can be observed at around 0.8 V vs. the Fc/Fc^+ couple. In case of complexes **3** and **4** a second irreversible oxidation was observed. In THF only irreversible oxidations can be observed at around 1 V.

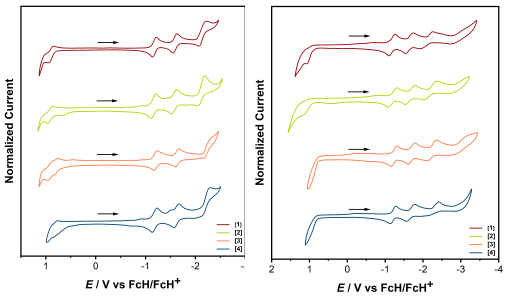

Figure 7: Cyclic voltammograms of complexes **1**-**4**, left: in a CH_2Cl_2 solution containing 0.1 M Bu_4NPF_6 as supporting electrolyte, right: in a THF solution containing 0.1 M Bu_4NPF_6 as supporting electrolyte.

Table 2: Electrochemical Data of the Complexes **1**-**4** from Cyclic Voltammetry in DCM.

Complex	E^{Ox2} [V]	E^{Ox1} [V]	E^{Red1} [V]	E^{Red2} [V]	E^{Red3} [V]
1	-	0.91[a]	–1.18[a]	–1.59[a]	–2.14[a]
2	-	0.92[a]	–1.16[a]	–1.58[a]	–2.13[b]
3	0.86[b]	0.82[a]	–1.20[a]	–1.63[a]	–2.23[b]
4	0.80[b]	0.74[a]	–1.18[a]	–1.62[a]	–2.29[b]

[a]Half-wave potentials from cyclic voltammetric measurements in different solvents for reversible processes at a scan rate of 100 mV/s. Ferrocene/ferrocenium was used as an internal standard. [b]E_{fp} for the irreversible processes.

Table 3: Electrochemical Data of the Complexes **1**-**6** from Cyclic Voltammetry in THF.

Complex	E^{Ox1} [V]	E^{Red1} [V]	E^{Red2} [V]	E^{Red3} [V]	E^{Red4} [V]
1	1.08[b]	–1.18[a]	–1.62[a]	–2.13[a]	-
2	1.17[b]	–1.20[a]	–1.66[a]	–2.20[a]	-
3	1.04[b]	–1.23[a]	–1.70[a]	–2.23[a]	–3.05[b]
4	1.03[b]	–1.21[a]	–1.67[a]	-2.13[a]	-
5		–1.21	–1.65	–2.19	-
6	1.02	–1.18	–1.65	–2.16	-

[a]Half-wave potentials from cyclic voltammetric measurements in different solvents for reversible processes at a scan rate of 100 mV/s. Ferrocene/ferrocenium was used as an internal standard. [b]E_{fp} for the irreversible processes.

In a CH_2Cl_2 solution these complexes display two reversible reduction steps at around -1.20 V and –1.60 V and a third irreversible reduction step at around –2.2 V (Table 2). The third reduction becomes quasi-reversible at higher scan rates (see Supporting Information). To further investigate the reduction side the measurements were repeated in THF. During these measurements the third reduction for **1-3** is quasi-reversible and for **3** even a fourth, irreversible reduction can be observed (Figure 7).

Complexes **5** and **6** were only investigated in THF. For both complexes three reductions were found. The first, second and third reductions of complex **5** are reversible (Figure 8). Furthermore, a fourth irreversible reduction is indicated, but was not fully detected, because of the limit of the potential window of THF. After reduction, two irreversible processes can be observed at 0.1 V and 0.5 V (See figure 8), which could indicate structural changes of the complex during oxidation.

Regarding the three reductions of complex **6** all are reversible and one irreversible oxidation can be observed. As observed for **5** an irreversible process appears at around 0.45 V, which again might appear due to structural changes upon oxidation.

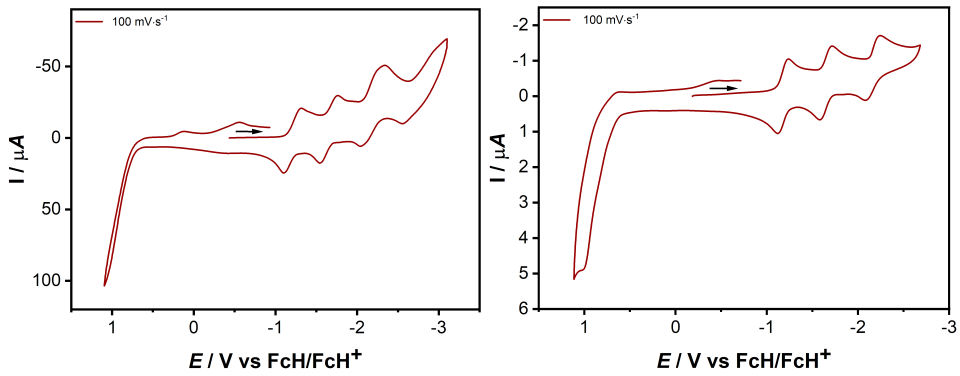

Figure 8: Cyclic voltammograms of complexes **5** (left) and **6** (right) in a THF solution containing 0.1 M Bu_4NPF_6 as supporting electrolyte.

To ascertain the impacts of a different bridging ligand, complexes **7-10** with the azophenine ligand were investigated electrochemically. As before, the complexes were measured in in CH_2Cl_2/0.1 M Bu_4PF_6 as well as in THF/0.1 M Bu_4PF_6 and as for **1-4** the obtained cyclic voltammograms resemble each other. The complexes with the fully deprotonated [N,N,N,N] azophenine bridging ligand show two irreversible oxidation processes at around 0.3 V and 0.6 V in CH_2Cl_2. These show a strong cathodic shift compared to the complexes **1-4**. This is due to the difference in electronegativity of the [N,N,N,N] coordination mode compared to the [O,N,O,N] coordination motif.[26] At the reduction side, two reversible reductions at around –1.3 V and –1.6 V can be observed as well as one irreversible reduction at around -2.3 V. After the first cycle an additional redox-process is seen at around –0.5 V. This additional process might be due to the rereduction of the irreversible first oxidation, as it does not appear if only the reduction processes are measured (see Supporting Information).

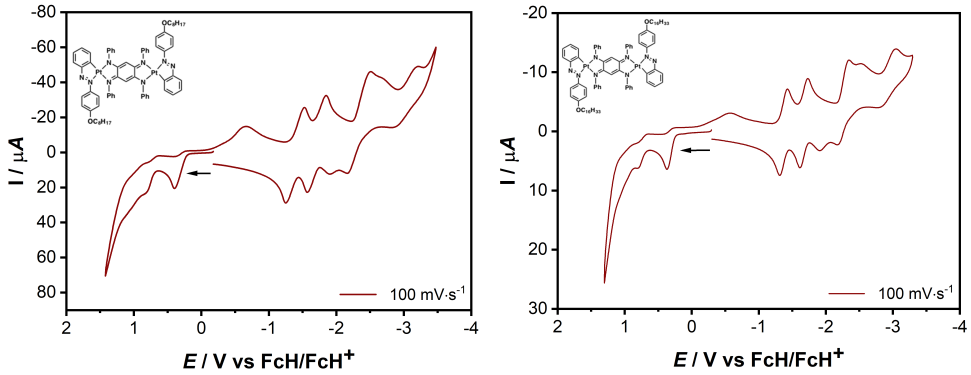

Figure 9: Cyclic voltammogram of complex **7** (left) and complex **8** (right) in a THF solution containing 0.1 M Bu_4NPF_6 as supporting electrolyte.

For **9** and **10** the cyclic voltammograms do not show additional reduction processes, however, the cyclic voltammograms of **7** and **8** in THF differ from the ones obtained in CH_2Cl_2. The third reduction appears at slightly different potentials and two additional reduction processes can be observed at around –2.5 V and –2.85 V (Table 5).

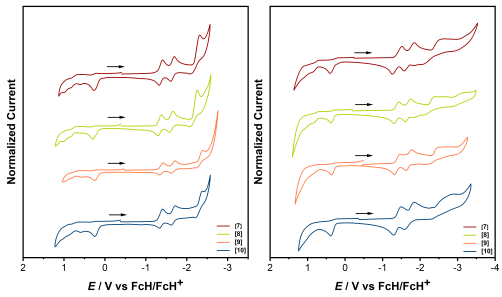

Figure 10: Cyclic voltammograms of complexes **7**-**10**, left: in a CH_2Cl_2 solution containing 0.1 M Bu_4NPF_6 as supporting electrolyte, right: in a THF solution containing 0.1 M Bu_4NPF_6 as supporting electrolyte.

The data obtained from the cyclic voltammetric measurements indicate, that the substitution of the azobenzene-ligand only has a negligible impact on the potentials of the redox-processes. Furthermore, the influence of the solvents on the potentials is only marginal. However, the redox-potentials are strongly dependent on the bridging ligand. The first reduction shifts to higher potentials for complexes **7**-**10**. Furthermore, the cyclic voltammograms show several additional redox-processes for **7**-**10**. In comparison to the literature-known complexes with the non-alkylated azobenzene moiety two observations can be made: i) for the presented complexes the azobenene ligands with the alkyl chains do not have a huge impact on the redox-potentials, ii) the third reduction becomes irreversible.[26]

Table 4: Electrochemical Data of the Complexes **7**-**10** from Cyclic Voltammetry in DCM.

Complex	E^{Ox2} [V]	E^{Ox1} [V]	E^{Red1} [V]	E^{Red2} [V]	E^{Red3} [V]
7	0.60[b]	0.26[b]	–1.37[a]	–1.66[a]	–2.28[b]
8	0.61[b]	0.28[b]	–1.34[a]	–1.63[a]	–2.18[b]
9	0.58[b]	0.25[b]	–1.37[a]	–1.67[a]	–2.40[b]
10	0.59[b]	0.27[b]	–1.37[a]	–1.67[a]	–2.30[b]

[a]Half-wave potentials from cyclic voltammetric measurements in different solvents for reversible processes at a scan rate of 100 mV/s. Ferrocene/ferrocenium was used as an internal standard. [b]E_{fp} for the irreversible processes.

Table 5: Electrochemical Data of the Complexes **7**-**10** from Cyclic Voltammetry in THF.

Complex	E^{Ox2} [V]	E^{Ox1} [V]	E^{Red1} [V]	E^{Red2} [V]	E^{Red3} [V]	E^{Red4} [V]	E^{Red5} [V]
7	0.81[b]	0.40[b]	–1.39[a]	–1.73[a]	–2.16[b]	–2.50[b]	–2.84[b]
8	0.74[b]	0.31[b]	–1.37[a]	–1.68[a]	–2.26[b]	–2.53[b]	–2.92[b]
9	-	0.30[b]	–1.40[a]	–1.71[a]	–2.40[b]	-	-
10	-	0.36[b]	–1.39[a]	–1.71[a]	–2-37[b]	-	-

[a]Half-wave potentials from cyclic voltammetric measurements in different solvents for reversible processes at a scan rate of 100 mV/s. Ferrocene/ferrocenium was used as an internal standard. [b]E_{fp} for the irreversible processes.

Furthermore, the PFC containing complexes were probed by cyclic voltammetry. In case of both trifluoromethoxy-substituted complexes **11** and **12**, one oxidation process was found for each when measured in CH_2Cl_2. The oxidation is irreversible for complex **11**, but quasi-reversible for complex **12**. Additionally, three reduction processes were observed for each complex. For both complexes, the first two reductions are fully reversible, whereas the third reduction is quasi-reversible. According to the half-wave potentials measured in CH_2Cl_2, it is indicated that complex **11** and **12** are slightly harder to oxidize than **13** and **14**, whereas reduction is more facile for these complexes (see table 6). This demonstrates the electron-withdrawing nature of the trifluoromethoxy-substituents and is thus in accordance with the expectation.

When measured in THF, the cyclic voltammograms of both complexes **11** and **12** again look very similar. However, in both cases no oxidation process can be observed anymore. On the reductive side, three additional processes occurred for each complex, whereby the first three reductions are fully reversible and all further reductions irreversible or only quasi-reversible.

The first three reduction processes of both complexes (except the first reduction of **12**) are shifted towards more cathodic potentials compared to the measurement in CH_2Cl_2, however this effect gets more significant for the second and third reduction.

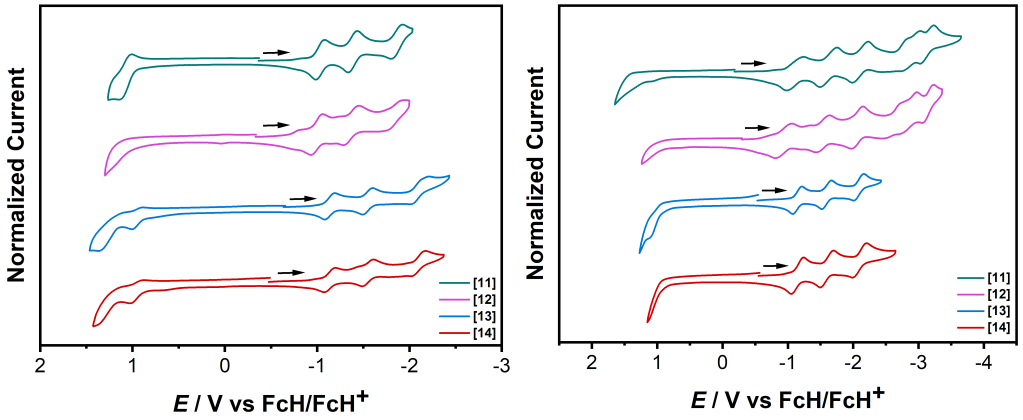

Figure 11: Cyclic voltammograms of complexes **11**-**14**, left: in a CH_2Cl_2 solution containing 0.1 M Bu_4NPF_6 as supporting electrolyte, right: in a THF solution containing 0.1 M Bu_4NPF_6 as supporting electrolyte.

Table 6: Electrochemical Data of the Complexes **11-14** from Cyclic Voltammetry in DCM.

Complex	E^{Ox2} [V]	E^{Ox1} [V]	E^{Red1} [V]	E^{Red2} [V]	E^{Red3} [V]
11		1.05	–1.03	–1.39	–1.87
12		1.15	–1.00	–1.34	–1.81
13	1.37[b]	0.95	–1.14	–1.54	–2.11
14		0.95	–1.14	–1.55	–2.18[b]

[a]Half-wave potentials from cyclic voltammetric measurements in different solvents for reversible processes at a scan rate of 100 mV/s. Ferrocene/ferrocenium was used as an internal standard. [b]E_{fp} for the irreversible processes.

Table 7: Electrochemical Data of the Complexes **11-14** from Cyclic Voltammetry in THF.

Complex	E^{Ox1} [V]	E^{Red1} [V]	E^{Red2} [V]	E^{Red3} [V]	E^{Red4} [V]	E^{Red5} [V]	E^{Red6} [V]
11		–1.12	–1.62	–2.11	–2.85	–2.88	–3.13
12		–0.94	–1.54	–2.07	–2.60	–2.84	–2.14
13	1.12[b]	–1.15	–1.59	–2.09			
14		–1.15	–1.60	–2.10	-	-	

[a]Half-wave potentials from cyclic voltammetric measurements in different solvents for reversible processes at a scan rate of 100 mV/s. Ferrocene/ferrocenium was used as an internal standard. [b]E_{fp} for the irreversible processes.

In the case of the PFC tail containing complexes with the azophenine bridge, all show similar redox processes for the measurements in CH_2Cl_2. Two reversible reductions and two irreversible oxidations can be observed. For **15** and **16** the third reduction seems reversible, while it appears to be quasi reversible for **17**. Additionally, complex **16** has one more irreversible oxidation process at 0.4 V. Measurements in THF also gave similar results for the three complexes. Two reversible reductions and one irreversible oxidation occur. At lower potentials no specific processes can be distinguished for **16** and **17**, but two more processes are indicated, whereas for **15** one reversible and two irreversible reductions were measured.

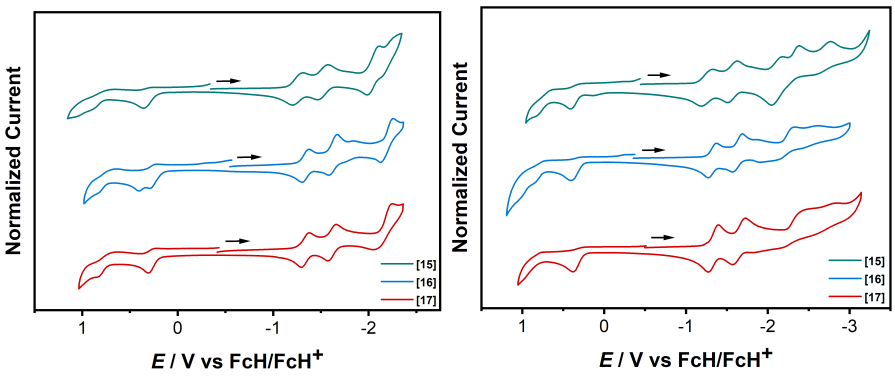

Figure 12: Cyclic voltammograms of complexes **15-17**, left: in a CH_2Cl_2 solution containing 0.1 M Bu_4NPF_6 as supporting electrolyte, right: in a THF solution containing 0.1 M Bu_4NPF_6 as supporting electrolyte.

Table 8: Electrochemical Data of the Complexes **15-17** from Cyclic Voltammetry in DCM.

Complex	E^{Ox2} [V]	E^{Ox1} [V]	E^{Red1} [V]	E^{Red2} [V]	E^{Red3} [V]
15		0.36	–1.26	–1.52	–2.05
16	0.40[b]	0.29[b]	–1.34	–1.63	–2.19
17		0.31	–1.34	–1.62	–2.15

[a]Half-wave potentials from cyclic voltammetric measurements in different solvents for reversible processes at a scan rate of 100 mV/s. Ferrocene/ferrocenium was used as an internal standard. [b]E_{fp} for the irreversible processes.

Table 9: Electrochemical Data of the Complexes **15-17** from Cyclic Voltammetry in THF.

Complex	E^{Ox1} [V]	E^{Ox1} [V]	E^{Red1} [V]	E^{Red2} [V]	E^{Red3} [V]	E^{Red4} [V]	E^{Red5} [V]
15	0.83[b]	0.41[b]	–1.26	–1.57	–2.12	–2.38[b]	–2.78[b]
16		0.41[b]	–1.32	–1.63	–2.31[b]	–2.63[b]	
17		0.38[b]	–1.33	–1.65	–2.46[b]	–2.85[b]	

[a]Half-wave potentials from cyclic voltammetric measurements in different solvents for reversible processes at a scan rate of 100 mV/s. Ferrocene/ferrocenium was used as an internal standard. [b]E_{fp} for the irreversible processes.

The data obtained from the measurements of **11-17** indicate, that for these complexes the PFC tail on the azobenzene does have a marginal influence. Over all, the redox processes of complexes bearing an -OCF3 group shift toward more cathodic potentials. In addition, more reduction processes could be observed for these complexes in the measurements in THF. As mentioned before, this can be explained with the electron-withdrawing nature of the trifluoromethoxy-substituents.

If now the complex with the same chain lengths is examined, in regard to the effect of fluorine, it points out that fluorine makes no real difference to the redox potentials. The potentials are similar for **1** and **13** and for **7** and **16**. This is not surprising, as the reductions take place either at the quinone bridge, which should not be effected by the PFC tails, or at the azo group that might show a little effect. In addition, the oxidation is metal centered. However, the introduction of trifluoromethoxy groups have an impact on the potentials, as has already been discussed before. To shed light on the redox states of these complexes a combination of UV/Vis/NIR and EPR spectroelectrochemistry were used.

UV/Vis/NIR Spectroelectrochemistry

UV/Vis/NIR spectroelectrochemistry was applied using an optically transparent electrochemical thin film cell (OTTLE) to investigate the interplay of optical and electrochemical properties and to verify the reversibility of the different processes.

For the complexes with the same bridging ligand the UV/Vis spectra look similar to each other. For complexes **1-6** and **11-14** bands around 400 nm and a band around 600 nm can be observed (See figure S45 and table S2). The extinction coefficient differs, depending on the alkyl chains on the azobenzene moiety. For example, the extinction coefficients for complexes **1** and **2** are higher than for complexes **3** and **4.** In comparison the extinction coefficient of complex **3** is slightly lower than for complex **4**. This might be due to the fact, that the C_{16}-chains at the azobenzene ligand are more flexible and therefore have a mildly less effect on the intensity than the C_8-chains, which are more rigid. Additionally, the electron density of the different chains may have an

impact. If the complexes bear more than 4 chains, the spectra are less defined and in case of **5** exhibit a band with a large extinction coefficient at 300 nm. Furthermore, complexes **7-10** and **15-17** exhibit similar spectra, but for the complexes with the non-fluorinated chains a larger extinction coefficient is observed. The effect of the fluorination seems more intense for the azophenin-bridged complexes (See Supporting information). Since the complexes show similar properties, the spectra are compared to the ones of literature-known complexes. Thus, the intense band at around 600 nm can be assigned to a MLCT-transition of the platinum(II) center to both ligands, as well as to a LLCT and $\pi \rightarrow \pi^*$ transition inside of the Q_{Dipp}^{2-} ligand.[26]

The spectra during SEC measurements show similar bands for complexes **1** and **3** (Figure 13). During the first reduction two bands arise, a narrow band around 700 nm and a broad one around 1500 nm while the band ~550 nm disappears. During the second reduction the broad bands in the NIR region increases in intensity whereas almost the entire band at ~700 nm disappears. Upon the third reduction, the spectra differ for both complexes. While the band in the NIR region decreases for **1**, it almost disappears for **3**. For both complexes two new bands arise at 1000 nm and 1200 nm. Furthermore, the bands at around 220 nm and around 400 nm only show small changes in intensity for all processes. The reduction processes seem reversible, as the native and end spectra are similar. The loss in intensity might be explained by slight decomposition of the complexes during the measurement. Even though the spectra show similar behavior, a difference can be observed regarding the extinction coefficient. For all processes complex **3** exhibits a smaller extinction coefficient, which indicates, that the amount of alkyl chains on the azobenzene moiety does have at least an impact in this regard. This effect is less pronounced for the longer alkyl chains, which could be due to the fact that they are more flexible. Furthermore, complexes **7-10** were also investigated with UV/Vis/NIR SEC, which were performed in CH_2Cl_2. All complexes exhibit similar spectra. During the first reduction the band at 600 nm increases and two bands at ~800 nm and 1200 nm appear. In case of **9** these two bands only exhibit a low

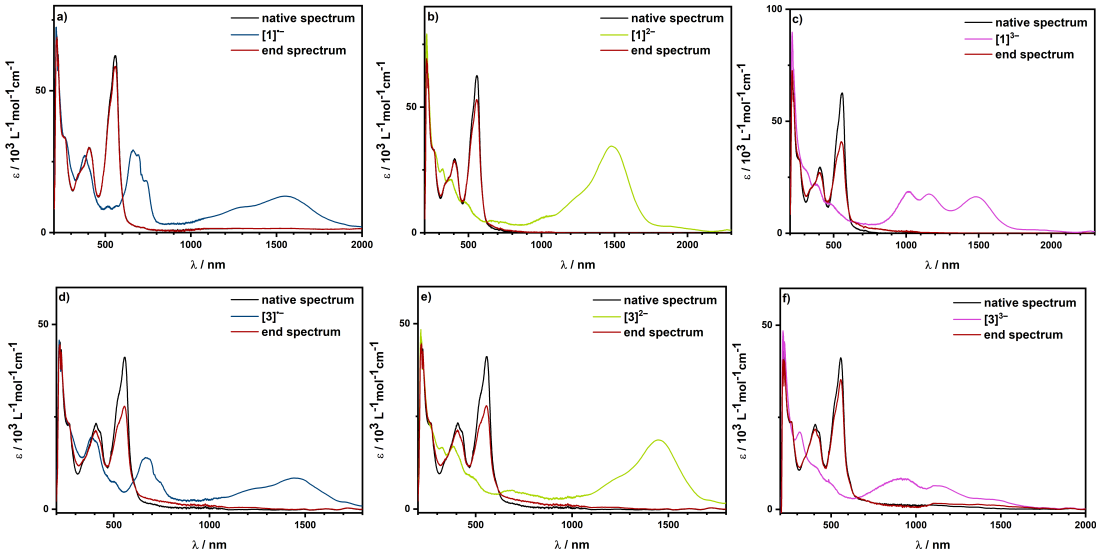

Figure 13: UV/Vis/NIR SEC spectra of complex **1** in THF/NBu_4PF_6 measured with a gold working electrode (a-c) and complex **3** in THF/NBu_4PF_6 measured with a gold working electrode (d-f).

extinction coefficient. During the second reduction the band at 800 nm decreases in intensity, while the other increases. For all processes, the reductions seem reversible, as the native and end spectra are similar. Only a difference in the extinction coefficient is obtained, which indicates, that the complexes decompose slightly during the measurements. In addition, the extinction coefficient is dependent on the substitution of the azobenzene. The highest value is obtained for **8** with one flexible C_{16}-chain. Thus the length of the chains and the use of asymmetric or symmetric azobenzene ligands seem to have an impact on the extinction coefficient.

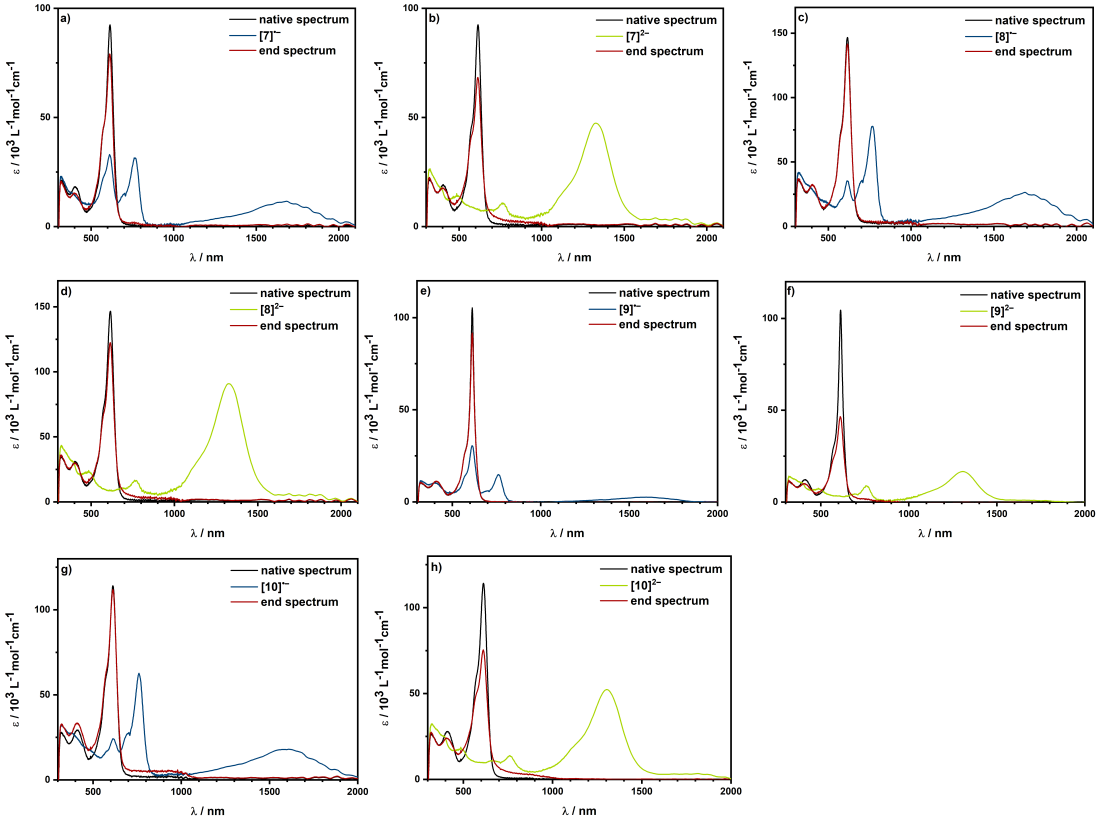

Figure 14: UV/Vis/NIR SEC spectra of complexes **7-10** in CH_2Cl_2/NBu_4PF_6 measured with a gold working.

Furthermore, the complexes containing fluorinated substituents were studied. For the first and second reduction the spectra of **13** and **14** are similar to the ones of **1** and **3**, but in case of the third reduction the spectra differ. Moreover, the spectra of the second and third reduction show a higher extinction coefficient than for the corresponding, non-fluorinated complexes (Figure 15). This indicates, that the fluorination of the alkyl chains does have a slight impact on the optical properties of the complexes. The same observation is made in case of the azophenine containing complexes (See SI figures S61 and S62). However, for the complexes with the dipp-containing bridging ligand, the introduction of OCF_3 groups on the azobenzene stoppers does have a larger impact on the spectra. During the first reduction two bands arise, that show a shift to a higher wavelength for the band in the NIR region of ~300 nm. During the second reduction, the band subsequently shifts back to wavelengths comparable to the complexes previously discussed. The spectrum obtained for the third reduction is comparable to the spectra of **13** and **14**. The discussed differences are also obtained for **12** (See SI figure S57). In the case of **15** the spectra are similar to the other ones discussed for the azobenzene containing

complexes. Here, the substituents on the azobenzene seem to have a less pronounced effect.

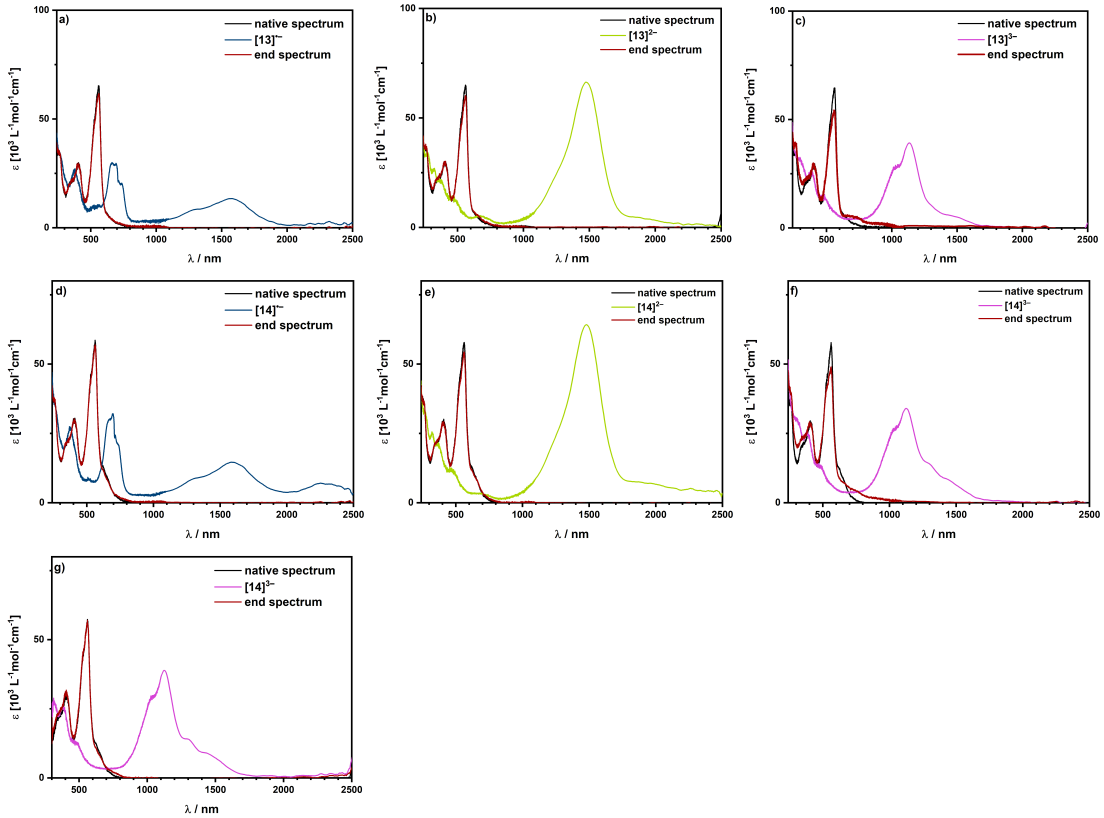

Figure 15: UV/Vis/NIR SEC spectra of complex **13** in THF/NBu_4PF_6 measured with a gold working electrode (a-c) and complex **14** in THF/NBu_4PF_6 measured with a gold working electrode (d-g).

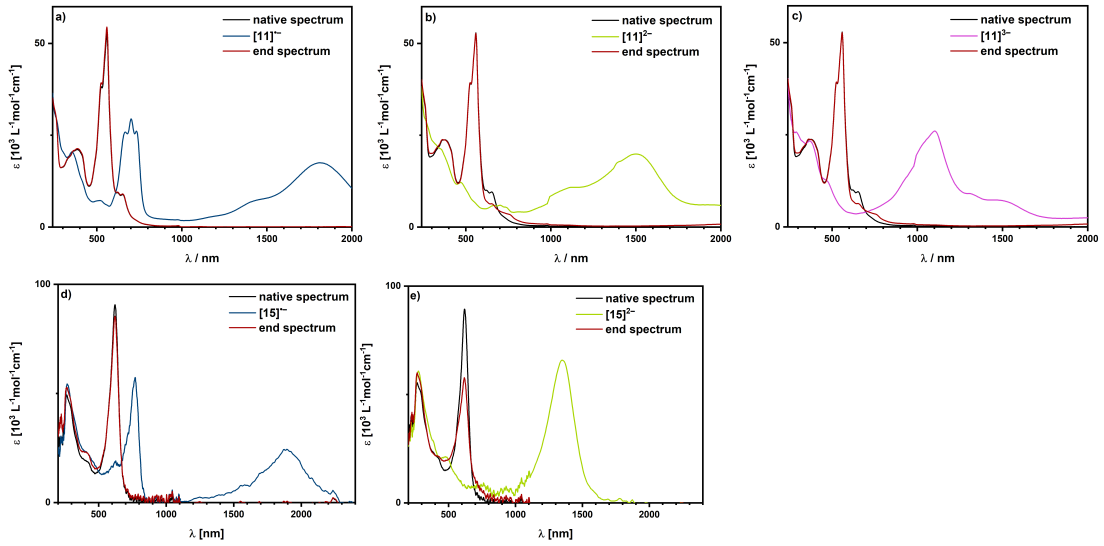

Figure 16: UV/Vis/NIR SEC spectra of complex **11** in THF/NBu_4PF_6 measured with a gold working electrode (a, b) and complex **15** in CH_2Cl_2/NBu_4PF_6 measured with a gold working electrode (c, d).

Comparing all the obtained UV/Vis/NIR spectra with the spectra of the unsubstituted azobenzene complexes, the absorption spectra of the reduction processes are similar in the case of both bridging ligands. The band in the NIR-region can be assigned to a mixture of LLCT- [Q_{Dipp}^{2-}→az_{-H}] and MLCT- [Pt(II)→Q_{Dipp}^{2-}] transitions.[26] For the second reduction the transitions for the band in the NIR-region might be of the same nature.[26] However, several differences can be assigned. For the presented complexes with the azophenine bridging ligand, no third reduction could be investigated during the SEC measurements. Furthermore, the extinction coefficient is higher than for the corresponding complexes with non-substituted azobenzene-stoppers, for example in case of **7** ε = 92.4 for the band at 615 nm, and ε = 18.5 for the band at 619 nm for the literature known complex[26] (See Supporting Information table S2 for further data). For these complexes higher oscillator strength and a more favorable orbital overlap are likely present, resulting in higher values. In contrast, there is a loss of the intensity of the extinction coefficient in all the presented complexes with the dipp-containing bridging ligand. Therefore, the substitution on the azobenzene ligand does have an impact on the electrochemical- and optical properties.

EPR Spectroscopy

One species was selected from each set of complexes **1-6, 7-10**, **11-14** and **15-16** to be studied representatively by EPR spectroscopy. EPR-SEC of the *in situ* generated one-electron-reduced species of $\mathbf{2}^{\bullet-}$, $\mathbf{9}^{\bullet-}$, $\mathbf{13}^{\bullet-}$ and $\mathbf{17}^{\bullet-}$ in THF solution with Bu_4NPF_6 (0.15 M) at 298 K displays a broad, isotropic signal with *g*-values of 1.983, 1.985, 1.980 and 1.981, respectively. A very small deviation of the g-tensors from the value of the free electron for all the complexes indicates predominantly ligand-centered reduction processes.[26] However, no hyperfine lines due to the nitrogen atoms could be detected, which could probably be related to the exchange narrowing effects.[26]

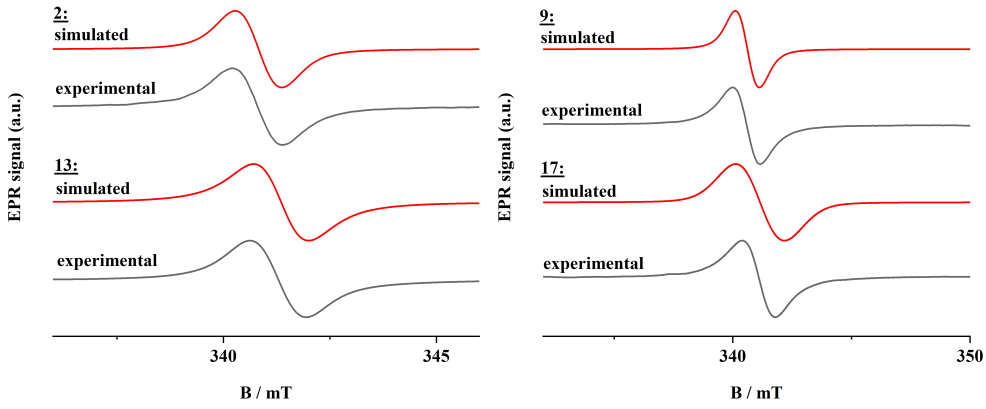

Figure 17: EPR Spectra during the first reduction of **2**, **9**, **13** and **17** in THF.

Table 10: Simulation parameters for $\mathbf{2}^{\bullet-}$, $\mathbf{9}^{\bullet-}$, $\mathbf{13}^{\bullet-}$ and $\mathbf{17}^{\bullet-}$ in a THF solution containing Bu_4NPF_6 as supporting electrolyte.

Parameters	$\mathbf{2}^{\bullet-}$	$\mathbf{9}^{\bullet-}$	$\mathbf{13}^{\bullet-}$	$\mathbf{17}^{\bullet-}$
S	½	½	½	½
g_x	1.983	1.985	1.980	1.981
A_x / MHz	1.90	1.95	1.98	1.53
Line width for isotropic broadening / mT	[0.78 0.52]	[0.73 0.47]	[0.63 0.97]	[1.84 0]

Conclusion

In summary, we were able to synthesize 17 azobenzene based platinum(II) complexes bridged over two different quinone ligands. In the first part long alkyl chains were introduced on the azobenzene moiety, in order to synthesize complexes suitable as liquid crystals. Only **L4**, **L14** and **P5** showed typical textures under POM, but none of the quinone- or azophenine-bridged complexes shows LC behavior. Further research can focus on the integration of long alkyl chains on the quinone bridge, which might lead to LC properties, which than might be used for redox active metallomesogens. In the second part, fluorinated alkyl chains were introduced on the azobenzene moieties and compared to the previous complexes.

The impact of the substitution on the azobenzene ligands was investigated regarding the electrochemical and optical properties. The addition of (fluorinated) alkyl chains onto the azobenzene leads to a change in the extinction coefficient in the UV/Vis-NIR spectra, but the redox potentials, as measured by cyclic voltammetry, are similar for all investigated complexes. Only for the complexes containing OCF_3 groups, the electron-withdrawing nature demonstrates an effect on the redox potentials. With regard to EPR spectra of the one-electron reduced compounds, the *g* values for the investigated complexes were similar.

We were able to establish a simple method for the introduction of fluorinated alkyl chains on alkoxy groups of different starting materials. This can help for the introduction of such chains on other ligand systems bearing OH groups. Furthermore, our results show, how to generate square-planar metal centers with are redox-rich and exhibit electrochromic behavior. Moreover, this study might help to design liquid crystalline material that exhibits redox-activity and electrochromic properties.

Experimental Section

General Remarks and Instrumentation. Unless otherwise noted, all reactions were performed using standard Schlenk-line techniques under an inert atmosphere of argon (Linde, Argon 4.8, purity ≥ 99.998). Commercially available chemicals were used without further purification. Diethyl ether and tetrahydrofuran were dried and distilled from sodium/benzophenone, methanol was distilled from magnesium methoxide. Other solvents were available from MBRAUN MB-SPS-800 solvent system and additionally degassed using standard techniques.

Column chromatography was performed using silica (Silica 60, Macherey-Nagel, 0.04-0.063 mm) or aluminum oxide (neutral, Acros Organics, XXX). ^{1}H NMR and proton decoupled ^{13}C NMR spectra were recorded on a JEOL ECS 400 spectrometer or a JEOL ECZ 401R spectrometer. Chemical shifts are reported in ppm (relative to the TMS signal) with reference to the residual solvent peaks.[29] Multiplets are reported as follows: singlet (s), duplet (d), triplet (t), quartet (q), pentet (p), heptet (h), multiplet (m) or combinations thereof. Mass spectrometry was performed on an Agilent 6210 ESI-TOF-spectrometer.

Electrochemistry

Cyclic voltammograms were recorded with a PAR VersaStat 4 potentiostat (Ametek) by working in anhydrous and degassed acetonitrile, dichloromethane or tetrahydrofuran with 0.1 M NBu_4PF_6 (dried, > 99.0%, electrochemical grade, Fluka) as supporting electrolyte. Concentrations of the complexes were about $1 \cdot 10^{-4}$ M. A three-electrode setup was used with a glassy carbon working electrode, a coiled platinum wire as counter electrode, and a coiled silver wire as a pseudoreference electrode. The ferrocene/ferrocenium or decamethylferrocene/decamethylferrocenium couples were used as internal reference.

UV/Vis spectra were recorded with an Avantes spectrometer consisting of a light source (AvaLight-DH-S-Bal), a UV/VIS detector (AcaSpec-ULS2048), and an NIR detector (AvaSpec-NIR256-TEC) or on a J&M Tidas UV- Vis-NIR spectrophotometer. Spectroelectrochemical measurements were carried out in an optically transparent thin-layer

electrochemical (OTTLE) cell (CaF_2 windows) with a gold working electrode, a platinum mesh counter electrode, and a silver-foil pseudoreference electrode.[30] Anhydrous and degassed tetrahydrofuran or dichloromethane with 0.1 M NBu_4PF_6 as supporting electrolyte was used as solvent.

Electron paramagnetic resonance

EPR spectra at X-band frequency (ca. 9.5 GHz) were obtained with a Magnettech MS-5000 benchtop EPR spectrometer equipped with a rectangular TE 102 cavity and TC HO4 temperature controller. The measurements were carried out in synthetic quarz glass tubes. For EPR spectroelectrochemistry a three-electrode setup was employed using two teflon-coated platinum wires (0.005"bare, 0.008" coated) as working and counter electrode and a Teflon-coated silver wire (0.005" bare, 0.007" coated) as pseudoreference electrode. Spectral simulations were performed with EasySpin 5.1.4[7] and MatLab R2012a.

X-ray diffraction

X-ray data were collected on a Bruker Smart AXS or Bruker D8 Venture system at 140(2) K or 100(2) K, respectively, using graphite-monochromated Moα radiation (λ_α = 0.71073 Å). Using the Smart software or using the APEX2 software, respectively, evaluated the strategy for the data collection. The data were collected by the standard omega scan or omega + phi scan techniques, and were scaled and reduced using Saint + and SADABS software. Direct methods or intrinsic phasing using SHELXT-2014/7 solved the structures. Structures were refined by full matrix least-squares using SHELXL-2014/7, refining on F2. Non-hydrogen atoms were refined 40 anisotropically.[31]

Synthesis

L1

The synthesis was done following a literature procedure.[24b, 24c]

To a mixture of *p*-nitrophenol (5.0 g, 36.0 mmol) and water (5 mL) KOH was added (21.3 g in 5 mL water, 0.4 mmol) and heated to 120 °C for 1 h. The temperature was increased to 200 °C and after destillation of water a brown/violet viscous liquid was obtained. The reaction was completed as no more gas formation was observed and the product was dissolved in water (500 mL). The dark red solution was acidified to pH 3 using concentrated HCl and afterwards extracted with Et_2O. Afterwards the organic layers were dried over Na_2SO_4 and the solvent was evaporated to dryness. The crude product was recrystallized in 50% v/v ethanol/water yielding a black solid (799.2 mg, 3.6 mmol, 10%).

^{1}H NMR (401 MHz, DMSO-d_6, 21 °C) δ = 10.08 (s, 1H, OH), 7.67 (d, ^3J = 8.8 Hz, 4H, azo-H), 6.87 (d, ^3J = 8.8 Hz, 1H, azo-H) ppm.

L2 and L3

The synthesis was done following a literature procedure.[24a]

General procedure: 4-hydroxyazobenzene (198.2 mg, 1.0 mmol) was dissolved in 50 mL acetone and K_2CO_3 (0.9 g, 6.2 mmol) was added. A solution of 1-bromooctane (1.1 mL, 6.2 mmol) or 1-bromohexadecane (1.9 mL, 6.2 mmol) in 50 mL acetone was added dropwise and heated to reflux for 7 h. In both cases the yellowish red solution was allowed to cool to room temperature and remaining K_2CO_3 was filtered off. The solvent was then evaporated and the crude product was purified by column chromatography (SiO_2, DCM:Hexan 9:1). The desired product was obtained as orange crystals for **L2** (155.0 mg, 0.5 mmol 50%) and as yellow crystals for **L3** (226.1 mg, 0.5 mmol 53%).

L2:

^{1}H NMR (401 MHz, $CDCl_3$, 23 °C) δ = 7.91 (d, ^3J = 9.1 Hz, 2H, H_d), 7.89–7.85 (m, 2H, H_c), 7.54–7.40 (m, 3H, $H_{a,b}$), 7.00 (d, ^3J = 9.1 Hz, 2H, H_e), 4.04 (t, ^3J = 6.6 Hz, 2H, H_f), 190–1.80 (m, 2H, H_g), 1.42 (dt, ^3J = 15.2, 6.8 Hz, 2H, H_i), 1.35–1.21 (m, 8H, H_h), 0.92–0.85 (m, 3H, H_j) ppm.

L3:

^{1}H NMR (401 MHz, $CDCl_3$, 22 °C) δ = 7.94–7.85 (m, 4H, $H_{c,d}$), 7.52–7.47 (m, 2H, H_b), 7.45–7.40 (m, 1H,

H_a), 7.03–6.98 (m, 2H, H_e), 4.04 (t, ^3J = 6.6 Hz, 2H, H_f), 1.87–1.75 (m, 2H, H_g), 1.52–1.44 (m, 2H H_h), 1.38–1.29 (m, 2H, H_i), 1.29 (s, 22H, H_j), 0.90–0.86 (m, 3H, H_k) ppm.

L4 and L5

The synthesis was done following a literature procedure.[24a]

4,4'-Diydroxyazobenzene (214.2 mg, 1.0 mmol) was dissolved in 50 mL acetone and K_2CO_3 (1.7 g, 12.4 mmol) was added followed by dropwise addition of either 1-bromooctan (2.2 mL, 12.4 mmol) or 1-bromohexadecane (4.1 mL, 12.4 mmol) in 50 mL acetone. Next, the solution was heated to reflux for 9 h and the yellow solution was allowed to cool to room temperature. For **L4** remaining K_2CO_3 was filtered off, the solvent was evaporated to dryness and the desired product crystallized out of the remaining oil. The product was filtered and washed with acetone several times. For **L5** the solid was filtered and remaining K_2CO_3 was dissolved in water. The remaining yellow product was washed with acetone. The pure products were obtained as yellow crystals with moderate yields for **L4** (186.3 mg, 0.4 mmol, 43%) and **L5** (290.9 mg, 0.4 mmol, 44%).

L4:

^{1}H NMR (401 MHz, $CDCl_3$, 21 °C) δ = 7.87–7.81 (m, 4H, H_a), 7.00–6.94 (m, 4H, H_b), 4.02 (t, ^3J = 6.6 Hz, 4H, H_c), 1.86–1.75 (m, 4H, H_d), 1.46 (dd, ^3J = 17.4, 6.2 Hz, 4H, H_e), 1.37–1.22 (m, 16H, H_f), 0.91–0.84 (m, 6H, H_g) ppm.

L5:

^{1}H NMR (401 MHz, $CDCl_3$, 21 °C) δ = 7.86 (d, ^3J = 9.0 Hz, 4H, H_b), 6.98 (d, ^3J = 9.1 Hz, 4H, H_a), 4.03 (t, ^3J = 6.6 Hz, 4H, H_c), 1.86–1.76 (m, 4H, H_d), 1.51–1.43 (m, 4H, H_e), 1.26 (s, 44H, H_f), 0.90–0.85 (m, 6H, H_g) ppm.

L6

This ligand was synthesized according to a reported procedure.[32]

To a solution of 4-Trifluormethoxyaniline (139.7 mg, 1.5 mmol) and Aniline (265.7 mg, 1.5 mmol) in dry DCM (20 mL) was added DBU (0.9 mL) and the mixture was stirred at room temperature for 5 minutes. When cooled down to -78 °C NCS (801.2 mg, 6 mmol) was added and the mixture was stirred for 1 hour. Subsequently, saturated $NaHCO_3$ (15 mL) was added and the organic layer was separated, washed with destilled water (50 mL) and 1 M HCl (50 ml) and dried over Na_2SO_4. The crude product was purified by column chromatography (SiO_2, DCM:*n*-pentane 1:1) the same day yielding the desired product as orange solid (81.5 mg, 0.3 mmol, 20%). The ^{1}H-NMR data correspond to literature.[33]

^{1}H-NMR ($CDCl_3$, 401 MHz, 22 °C): 8.01 – 7.95 (m, 2H), 7.95 – 7.90 (m, 2H), 7.58 – 7.45 (m, 3H), 7.41 – 7.32 (m, 4H) ppm.

L7

This ligand was synthesized according to a reported procedure.[32]

To a solution of 4-Trifluormethoxyaniline (531.4 mg, 3 mmol) in dry DCM (20 mL) was added DBU (0.9 mL) and the mixture stirred at room temperature for 5 minutes. When cooled down to -78 °C NCS (801.2 mg, 6 mmol) was added and the mixture was stirred for 1 hour. Subsequent saturated $NaHCO_3$ (15 mL) was added and the organic layer was separated, washed with destilled water (50 mL) and 1 M HCl (50 ml) and dried over Na_2SO_4. The crude product was purified by column chromatography (SiO_2, DCM:*n*-pentane 1:1) the same day yielding the desired product as orange solid (169.0 mg, 0.5 mmol, 17%).

^{1}H-NMR ($CDCl_3$, 401 MHz, 21 °C): 8.00 – 7.94 (m, 4H), 7.37 (dd, ^3J = 9.1, 1.0 Hz, 4H) ppm.

The ^{1}H-NMR data correspond to literature.[33]

L8

The ligand was synthesized according to a reported procedure.[34]

A mixture of 18-crown-6 (132.0 mg, 0.5 mmol), K_2CO_3 (210.0 mg, 1.5 mmol) and 4-hydroxyazobenzene (198.0 mg, 1.0 mmol) in acetone (30 mL) was stirred at room temperature for one hour. 3,3,4,4,5,5,6,6,7,7,8,8,8-tridecafluorooctyl

trifluoromethanesulfonate (728.2 mg, 2.0 mmol) was added and the mixture was stirred at 60 °C overnight. After cooling to room temperature the solvent was removed under reduced pressure and the product was purified through coloumn chromatography (SiO_2, DCM) yielding in an orange solid (221.2 mg, 0.4 mmol, 41%).

^{1}H NMR ($CDCl_3$, 400 MHz, 20°C): δ = 8.09 – 7.84 (m, 4H), 7.64 – 7.37 (m, 3H), 7.12 – 6.96 (m, 2H), 4.36 (t, J = 6.8 Hz, 2H), 2.85 – 2.54 (m, 2H) ppm.

^{13}C NMR ($CDCl_3$, 101 MHz, 22°C): δ = 160.5, 152.9, 147.6, 130.7, 129.2, 124.9, 122.8, 114.9, 60.4, 31.3 ppm.

^{19}F NMR ($CDCl_3$, 376 MHz, 20°C): δ = -80.8, -113.30 (t, J = 13.7 Hz), 121.9, 122.9, 123.6, -125.32 – -127.31 (m) ppm.

HRMS (ESI): calcd. For $[C_{20}H_{14}F_{13}N_2O]^+$: *m/z* 545.0893; found 545.0905.

Anal. Calcd for $C_{20}H_{13}F_{13}N_2O$: C, 44.13; H, 2.41; N, 5.15. Found: C, 44.27; H, 2.49; N, 5.17.

L9

The ligand was synthesized according to a reported procedure.[34]

A mixture of 18-crown-6 (132.0 mg, 0.5 mmol), K_2CO_3 (210.0 mg, 1.5 mmol) and 4-hydroxyazobenzene (198.0 mg, 1.0 mmol) in acetone (30 mL) was stirred at room temperature for one hour. 3,3,4,4,5,5,6,6,7,7,8,8,9,9,10,10,10-heptadecafluorodecyl trifluoromethanesulfonate (1.2 g, 2.0 mmol) was added and the mixture was stirred at 60 °C overnight. After cooling to room temperature the solvent was removed under reduced pressure and the product was purified through coloumn chromatography (SiO_2, DCM) yielding in an orange solid (368.0 mg, 0.6 mmol, 57%).

^{1}H NMR ($CDCl_3$, 400 MHz, 20°C): δ = 8.10 – 7.79 (m, 4H), 7.65 – 7.40 (m, 3H), 7.13 – 6.80 (m, 2H), 4.37 (t, J = 6.8 Hz, 2H), 2.69 (tt, J = 18.2, 6.9 Hz, 2H) ppm.

^{13}C NMR ($CDCl_3$, 101 MHz, 20°C): δ = 160.5, 152.8, 147.9, 130.7, 129.2, 124.5, 122.8, 114.9, 60.4, 31.4 ppm.

^{19}F NMR ($CDCl_3$, 377 MHz, 21°C): δ = -80.74 (t, J = 10.1 Hz), -111.95 – -115.26 (m), -121.6, -121.9, -122.7, -123.5, -126.1 ppm.

HRMS (ESI): calcd. For $[C_{22}H_{13}F_{17}N_2ONa]^+$: *m/z* 667.0649; found 667.0656.

Anal. Calcd for $C_{22}H_{13}F_{17}N_2O \cdot 0.45\ C_3H_6O \cdot 0.3\ CH_2Cl_2$: C, 40.82; H, 2.36; N, 4.03. Found: C, 40.81; H, 2.41; N, 4.02.

L10

This ligand was synthesized according to a reported procedure.[34] 4-Nitrophenol (392.0 mg, 2.2 mmol, 1.0 equiv) was placed in a 100 mL round bottom flask and dissolved in acetone (35 mL). Then, K_2CO_3 (600.0 mg, 4.3 mmol, 2.0 equiv) and 18-crown-6 (288.0 mg, 1.1 mmol, 0.5 equiv) were added and the solution was stirred at rt for 30 min. Afterwards, the alkyl triflate (1.3 g, 2.6 mmol, 1.2 equiv) was added and the reaction mixture was refluxed for additional 24 h. After cooling to rt, the precipitate was filtered off and the solution was concentrated under reduced pressure. The crude product was loaded on silica and purified via column chromatography (SiO_2, *n*-pentane/CH_2Cl_2 3:1 → CH_2Cl_2) to obtain the product (860.0 mg, 1.7 mmol, 82%) as a colorless solid.

^{1}H NMR (401 MHz, $CDCl_3$): δ = 8.23 (d, J = 9.2 Hz, 2H), 6.98 (d, J = 9.2 Hz, 2H), 4.37 (t, J = 6.7 Hz, 2H), 2.69 (tt, J = 18.1, 6.6 Hz, 2H) ppm.

^{19}F NMR (377 MHz, $CDCl_3$): δ = –80.6 (tt, J = 10.0, 2.3 Hz, 3F), –112.9–(–113.4) (m, 2F), –121.6–(–121.9) (m, 2F), –122.6–(–122.9) (m, 2F), –123.3–(–123.4) (m, 2F), –126.0–(–126.1) (m, 2F) ppm.

The spectroscopic data are consistent with those reported in the literature.[35]

L11

This ligand was synthesized according to a reported procedure.[36]

Under argon, the nitrobenzene (1.1 g, 2.3 mmol, 1.0 equiv) was placed in a dry 50 mL Schlenk flask and dissolved in anhydrous EtOH (20 mL). Tin chloride (2.3 g, 12.0 mmol, 5.3 equiv) was added and the mixture was stirred at 70 °C for 48 h. Afterwards, the solvent was removed under reduced pressure and the residue was dissolved in NaOH (aq. solution, 30 wt.-%, 30 mL) and CH_2Cl_2 (30 mL). The layers were separated and the aqueous layer was extracted with CH_2Cl_2 (3x100 mL). The combined organic layers were dried over Na_2SO_4 and concentrated under reduced pressure. Column chromatography (SiO_2, CH_2Cl_2/EtOAc 5:1 → EtOAc) gave the product (614 mg, 1.4 mmol, 59%) as a pale yellow oil that solidified in the fridge.

^{1}H NMR (401 MHz, $CDCl_3$): δ = 6.78–6.72 (m, 2H), 6.68–6.63 (m, 2H), 4.20 (t, *J* = 6.9 Hz, 2H), 3.48 (s, br, 2H), 2.58 (tt, *J* = 18.5, 6.8 Hz, 2H) ppm.

^{19}F NMR (377 MHz, $CDCl_3$): δ = –80.7 (tt, *J* = 10.0, 2.5 Hz, 3F), –113.1–(–113.3) (m, 2F), –121.5–(–121.9) (m, 2F), –122.6–(–122.8) (m, 2F), –123.4–(–123.8) (m, 2F), –125.9–(–126.1) (m, 2F) ppm.

The spectroscopic data are consistent with those reported in the literature.[35]

L12

This ligand was synthesized according to a reported procedure.[34]

4-Nitrophenol (750.0 mg, 5.4 mmol, 1.0 equiv) was placed in a 250 mL round bottom flask and dissolved in acetone (75 mL). Then, K_2CO_3 (1.1 g, 8.1 mmol, 2.0 equiv) and 18-crown-6 (710.0 mg, 12.7 mmol, 0.5 equiv) were added and the solution was stirred at rt for 30 min. Afterwards, the alkyl triflate (3.2 g, 5.4 mmol, 1.0 equiv) was added and the reaction mixture was refluxed for additional 24 h. After cooling to rt, the precipitate was filtered off and the solution was concentrated under reduced pressure. The crude product was loaded on silica and purified via column chromatography (SiO_2, *n*-pentane → *n*-pentane/CH_2Cl_2 3:1) to obtain the product (2.18 g, 3.7 mmol, 69%) as a colorless solid.

^{1}H NMR (401 MHz, $CDCl_3$): δ = 8.23 (d, *J* = 9.2 Hz, 2H), 6.98 (d, *J* = 9.2 Hz, 2H), 4.37 (t, *J* = 6.6 Hz, 2H), 2.69 (tt, *J* = 18.0, 6.5 Hz, 2H) ppm.

^{19}F NMR (377 MHz, $CDCl_3$): δ = –80.6 (t, *J* = 9.9 Hz, 3F), –113.1 (p, *J* = 17.4 Hz, 2F), –121.4–(–121.6) (m, 2F), –121.6–(–121.9) (m, 4F), –122.4–(–122.7) (m, 2F), –123.3–(–123.4) (m, 2F), –125.9–(–126.1) (m, 2F) ppm.

The spectroscopic data are consistent with those reported in the literature.[37]

L13

This ligand was synthesized according to a reported procedure.[36]

Under argon, the nitrobenzene (2.2 g, 3.7 mmol, 1.0 equiv) was placed in a dry 100 mL Schlenk flask and dissolved in anhydrous EtOH (30 mL). Tin chloride (3.7 g, 19.5 mmol, 5.3 equiv) was added and the mixture was stirred at 70 °C for 3 d. Afterwards, the solvent was removed under reduced pressure and the residue was dissolved in NaOH (aq. solution, 30 wt.-%, 50 mL) and CH_2Cl_2 (50 mL). The layers were separated and the aqueous layer was extracted with CH_2Cl_2 (3x100 mL). The combined organic layers were dried over Na_2SO_4 and concentrated under reduced pressure. Column chromatography (SiO_2, *n*-pentane/EtOAc 1:1) gave the product (476.0 mg, 1.3 mmol, 35%) as a pale yellow oil that solidified in the fridge.

^{1}H NMR (401 MHz, $CDCl_3$): δ = 6.75 (d, *J* = 8.7 Hz, 2H), 6.65 (d, *J* = 8.7 Hz, 2H), 4.20 (t, *J* = 6.9 Hz, 2H), 3.47 (s, br, 2H), 2.58 (tt, *J* = 18.4, 6.8 Hz, 2H) ppm.

^{19}F NMR (377 MHz, $CDCl_3$): δ = –80.6 (t, *J* = 9.9 Hz, 3F), –113.2 (p, *J* = 17.7 Hz, 2F), –121.2–(–121.7)

(m, 2F), −121.8–(−122.0) (m, 4F), −122.4–(−122.7) (m, 2F), −123.3–(−123.6) (m, 2F), −125.9–(−126.2) (m, 2F) ppm.

^{13}C NMR (151 MHz, $CDCl_3$): δ = 152.3, 151.3, 140.9, 140.0, 116.5, 116.2 (t, J = 63.4 Hz), 64.2, 61.1, 31.5 (t, J = 21.6 Hz), 29.9, 15.1 ppm. Three signals are missing probably due to signal overlap.

HRMS (ESI): calcd. for $[C_{16}H_{11}F_{17}NO]^+$: *m/z* 556.0564; found 556.0547.

EA calcd. for $C_{16}H_{10}F_{17}NO \cdot 0.15\ C_5H_{12}$: C, 35.54; H, 2.10; N, 2.47. Found: C, 35.51; H, 2.37; N, 2.59.

P1

The synthesis was done in accordance with a literature procedure.[18b]

To a refluxing solution of $[(\eta^3\text{-}C_4H_7)Pt(\mu\text{-}Cl)]_2$ (76.5 mg, 0.1 mmol) in $CHCl_3$ (7 mL) **L2** (77.6 mg, 0.3 mmol) was added and the resulting mixture was heated to reflux for 25 h. Then the solvent was removed under reduced pressure and the resulting red solid was dissolved in DCM and layered with *n*-pentane. After filtration an orange solid was obtained (85.4 mg, 0.6 mmol, 63%).

^{1}H NMR (400 MHz, $CDCl_3$) δ = 7.88–7.76 (m, 4H), 7.54–7.41 (m, 8H), 6.77–6.68 (m, 4H), 4.07–4.02 (m, 4H), 1.87–1.74 (m, 4H), 1.51–1.42 (m, 4H), 1.31 (s, 8H), 0.90 (s, 6H) ppm.

^{13}C-NMR (101 MHz, $CDCl_3$) δ = 128.7, 124.1, 111.8, 68.1, 32.0, 26.1, 25.8, 22.8, 14.3 ppm.

HRMS (ESI): calcd. for $[C_{40}H_{50}ClN_4O_2{}^{194}Pt_2]^+$ [M–Cl]$^+$: *m/z* 1041.2876; found 1041.2857.

EA calcd. for $C_{40}H_{50}Cl_2N_4O_2Pt_2 \cdot 0.25\ CHCl_3$: C 43.56; H 4.56; N 5.05; found C 43.57, H 4.62, N 4.98.

P2

The synthesis was done in accordance with a literature procedure.[18b]

L3 (105.7 mg, 0.3 mmol) was added to a refluxing solution of $[(\eta^3\text{-}C_4H_7)Pt(\mu\text{-}Cl)]_2$ (76.5 mg, 0.1 mmol) in $CHCl_3$ (7 mL) and the resulting mixture was heated to reflux for 24 h. The solvent was evaporated and the resulting solid was washed with Et_2O and acetone. The obtained orange solid was filtered and dried yielding the desired product (88.2 mg, 0.2 mmol, 54%).

^{1}H NMR (401 MHz, $CDCl_3$) δ = 7.72 (dd, ^3J = 7.8 Hz, ^4J = 1.7 Hz, 4H), 7.48 (dt, ^3J = 13.6 Hz, ^4J = 7.0 Hz, 8H), 6.75–6.68 (m, 4H), 4.08–4.00 (m, 4H), 1.90–1.75 (m, 12H), 1.57–1.42 (m, 12H), 1.26 (s, 22H), 0.88 (s, 6H) ppm.

^{13}C-NMR (101 MHz, $CDCl_3$) δ = 163.3, 151.5, 131.3, 130.1, 128.7, 128.4, 124.1, 116.1, 111.9, 68.8, 32.1, 29.9, 29.5, 29.3, 29.2, 26.1, 22.9, 14.3 ppm.

HRMS (ESI): calcd. for $[C_{56}H_{82}ClN_4O_2Pt_2^+]^+$ [M–Cl]$^+$: *m/z* 1266.5395; found 1266.5413.

EA calcd. for $C_{56}H_{82}Cl_2N_4O_2Pt_2 \cdot 0.25\ CHCl_3$: C 50.64; H 6.21; N 4.20; found C 50.78, H 6.4, N 3.98.

P3

The synthesis was done in accordance with a literature procedure.[18b]

L4 (109.7 mg, 0.3 mmol) was added to a refluxing solution of $[(\eta^3\text{-}C_4H_7)Pt(\mu\text{-}Cl)]_2$ (76.5 mg, 0.1 mmol) in $CHCl_3$ (7 mL) and the resulting mixture was heated to reflux for 18 h. The solvent was evaporated and the resulting red solid was washed with Et_2O (30 mL) and acetone. After filtration the resulting red solid was dried yielding the desired product (95.0 mg, 0.2 mmol, 57%).

^{1}H NMR (401 MHz, $CDCl_3$) δ = 7.76 (d, ^3J = 8.6 Hz, 2H), 7.71–7.67 (m, 4H), 6.96 (d, ^3J = 9.1 Hz, 4H), 6.69 (dd, ^3J = 8.6, 2.5 Hz, 4H), 4.03 (t, ^3J = 6.6 Hz, 8H), 1.89–1.73 (m, 16H), 1.30 (s, 32H), 0.91–0.87 (m, 12H) ppm.

^{13}C-NMR (101 MHz, $CDCl_3$) δ = 130.5, 125.4, 116.4, 114.4, 111.5, 100.2, 68.7, 32.0, 29.5, 29.4, 26.2, 26.1, 22.8, 14.3 ppm.

HRMS (ESI): calcd. for $[C_{56}H_{82}ClN_4O_4{}^{194}Pt_2]^+$ [M–Cl]$^+$: *m/z* 1297.5272; found 1297.5487.

EA calcd. for $C_{56}H_{82}Cl_2N_4O_4Pt_2 \cdot 1.55\ C_4H_{10}O$: C 51.48; H 6.77; N 3.86; found C 51.68; H 6.56; N 4.06.

P4

The synthesis was done in accordance with a literature procedure.[18b]

To a refluxing solution of $[(\eta^3\text{-}C_4H_7)Pt(\mu\text{-}Cl)]_2$ (76.5 mg, 0.1 mmol) in $CHCl_3$ (7 mL) **L5** (165.8 mg, 0.3 mmol) was added and the resulting mixture was heated to reflux for 18 h. The resulting orange solid was filtered and washed several times with $CHCl_3$, yielding the desired product (134.0 mg, 0.06 mmol, 60%).

Since the product is largely insoluble in all common solvents no NMR spectra could be obtained.

EA calcd. for $C_{88}H_{146}Cl_2N_4O_4Pt_2 \cdot 0.85\ CHCl_3$: C 56.56; H 7.85; N 2.97 found: C 56.58; H 7.89; N 2.92.

P5

The synthesis was done in accordance with a literature procedure.[18b]

To a refluxing solution of $[(\eta^3\text{-}C_4H_7)Pt(\mu\text{-}Cl)]_2$ (108.0 mg, 0.2 mmol) in $CHCl_3$ (15 mL) **L14** (330.0 mg, 0.4 mmol) was added and the resulting mixture was heated to reflux for overnight. The solvent was removed under reduced pressure and the resulting red solid was washed with Et_2O yielding in the desired product $[(azo_{4Dodec})Pt(\mu\text{-}Cl_2)Pt(azo_{4Dodec})]$ (277.0 mg, 0.1 mmol, 64%). Due to problematic workup, the ligand could not be separated from the desired product. However, this did not interfere with the subsequent complex synthesis.

^{1}H NMR (401 MHz, $CDCl_3$) δ = 7.69 (d, J = 8.7 Hz, 1H), 6.92 (d, J = 8.2 Hz, 1H), (6.49 (s, 2H), 4.32 (t, J = 6.6 Hz, 1H), 4.19 (dd, J = 14.4, 8.0 Hz, 1H), 4.04 (dt, J = 26.6, 6.6 Hz, 3H), 3.90 (t, J = 7.1 Hz, 2H), 1.81 (p, J = 6.6 Hz, 3H), 1.26 (s, 160H), 0.88 (t, J = 6.6 Hz, 14H) ppm.

^{13}C-NMR (101 MHz, $CDCl_3$) δ = 125.5, 113.9, 32.1, 29.9, 29.5, 25.6, 22.9, 23.6 ppm. (Only few signals are detected due to low concentration and poor signal-to-noise ratio.)

The mass of the product cannot be detected via mass spectrometry.

P6

The synthesis was done in accordance with a literature procedure.[18b]

To a refluxing solution of $[(\eta^3\text{-}C_4H_7)Pt(\mu\text{-}Cl)]_2$ (108.0 mg, 0.2 mmol) in $CHCl_3$ (15 mL) **L15** (244.0 mg, 0.4 mmol) was added and the resulting mixture was heated to reflux for overnight. The solvent was removed under reduced pressure and the resulting red solid was washed with *n*-pentane yielding in the desired product $[(azo_{2Dec})Pt(\mu\text{-}Cl_2)Pt(azo_{2Dec})]$ (307.0 mg, 0.02 mmol, 89%).

^{1}H NMR (401 MHz, $CDCl_3$) δ = 7.83 (d, J = 15.9 Hz, 3H), 7.57 (s, 2H), 7.45 (s, 1H), 7.39 (s, 2H), 6.97 (bs, 2H), 6.75 – 6.64 (m, 2H), 4.32 – 3.81 (m, 12H), 1.76 (bs, 12H), 1.27 (bs, 72H), 0.87 (s, 18H) ppm.

^{13}C-NMR (101 MHz, $CDCl_3$) δ = 32.1, 29.8, 29.5, 22.9, 14.3 ppm. (Only few signals are detected due to low concentration and poor signal-to-noise ratio.)

The mass of the product cannot be detected via mass spectrometry.

EA calcd. for $C_{88}H_{146}Cl_2N_4O_6Pt_2$: C 58.16; H 8.10; N 3.08 found: C 58.54; H 8.11; N 3.07.

P7

The synthesis was done in accordance with a literature procedure.[18b]

To a refluxing solution of $[(\eta^3\text{-}C_4H_7)Pt(\mu\text{-}Cl)]_2$ (264.0 mg, 0.4 mmol) in $CHCl_3$ (20 mL) **L6** (234.0 mg, 0.9 mmol) was added and the resulting mixture was heated to reflux for overnight. The solvent was removed under reduced pressure and the resulting red solid was washed with *n*-pentane yielding in the desired product $[(azo_{OCF3})Pt(\mu\text{-}Cl_2)Pt(azo_{OCF3})]$ (255.0 mg, 0.2 mmol, 56%).

Since the product is largely insoluble in all common solvents no NMR spectra could be obtained.

HRMS (ESI): calcd. for $C_{28}H_{19}ClF_6N_5O_2Pt_2$ $[C_{28}H_{19}F_6N_5O_2{}^{194}Pt_2Cl]^+$ $[M - Cl + CH_3CN]^+$: *m/z* 995,0406; found 995.0386.

EA calcd. for $C_{26}H_{16}F_6Cl_2N_4O_2Pt_2$: C 31.50; H 1.63; N 5.65 found: C 31.54; H 1.67; N 5.68.

P8

The synthesis was done in accordance with a literature procedure.[18b]

To a refluxing solution of $[(\eta^3\text{-}C_4H_7)Pt(\mu\text{-}Cl)]_2$ (131.0 mg, 0.2 mmol) in $CHCl_3$ (15 mL) **L7** (153.0 mg, 0.4 mmol) was added and the resulting mixture was heated to reflux for overnight. The solvent was removed under reduced pressure and the resulting red solid was washed with *n*-pentane yielding in the desired product $[(azo_{(OCF3)2})Pt(\mu\text{-}Cl_2)Pt(azo_{(OCF3)2})]$ (141.0 mg, 0.1 mmol, 53%).

Since the product is largely insoluble in all common solvents no NMR spectra could be obtained.

HRMS (ESI): calcd. for $[C_{28}H_{14}F_{12}N_4O_4{}^{194}Pt_2Cl]^+$ [M – Cl]$^+$: *m/z* 1121.9781; found 1121.9728.

EA calcd. for $C_{28}H_{14}F_{12}Cl_2N_4O_4Pt_2$: C 29.00; H 1.22; N 4.83 found: C 29.02; H 1.29; N 4.88.

P9

The synthesis was done in accordance with a literature procedure.[18b]

To a refluxing solution of $[(\eta^3\text{-}C_4H_7)Pt(\mu\text{-}Cl)]_2$ (51.3 mg, 0.1 mmol) in $CHCl_3$ (7 mL) **L8** (114.3 mg, 0.2 mmol) was added and the resulting mixture was heated to reflux for overnight. The solvent was removed under reduced pressure and the resulting red solid was washed with *n*-pentane yielding in the desired product $[(azo_{OctRf})Pt(\mu\text{-}Cl_2)Pt(azo_{OctRf})]$ (65.7 mg, 42%).

Since the product is largely insoluble in all common solvents no NMR spectra could be obtained.

HRMS (ESI): calcd. for $[C_{42}H_{27}ClF_{26}N_5O_2{}^{194}Pt_2]^+$ [M – Cl + CH_3CN]$^+$: *m/z* 1551,0712; found 1551.0684.

EA calcd. for $C_{40}H_{24}F_{26}Cl_2N_4O_2Pt_2 \cdot 0.45\ CHCl_3$: C 30.33; H 1.51; N 3.50 found: C 30.16; H 1.60; N 3.67.

P10

The synthesis was done in accordance with a literature procedure.[18b]

To a refluxing solution of $[(\eta^3\text{-}C_4H_7)Pt(\mu\text{-}Cl)]_2$ (51.3 mg, 0.1 mmol) in $CHCl_3$ (7 mL) **L9** (135.3 mg, 0.2 mmol) was added and the resulting mixture was heated to reflux for overnight. The solvent was removed under reduced pressure and the resulting red solid was washed with *n*-pentane yielding in the desired product $[(azo_{DecRf})Pt(\mu\text{-}Cl_2)Pt(azo_{DecRf})]$ (77.1 mg, 44%).

Since the product is largely insoluble in all common solvents no NMR spectra could be obtained.

HRMS (ESI): calcd. for $[C_{44}H_{24}F_{34}N_4O_2{}^{194}Pt_2Cl]^+$ [M – Cl]$^+$: *m/z* 1710.0314; found 1710.0252.

EA calcd. for $C_{44}H_{24}F_{34}Cl_2N_4O_2Pt_2$: C 30.24; H 1.38; N 3.21 found: C 30.29; H 1.44; N 3.23.

General procedure for complexes **1-6** and **11-12**

The synthesis was done in accordance with a literature-known procedure.[26]

The corresponding precursor and H_2Q_{Dipp} were dissolved in dry MeCN and dry Et_3N was added. The reaction mixture was stirred at room temperature for 1–3 days. The resulting solid was filtered and dissolved in Et_2O and was then evaporated under reduced pressure. Recrystallization in DCM/MeOH yielded in the desired product. For **11** and **12** the crude product was was purified by column chromatography (Al_2O_3, *n*-pentane:DCM 3:1) before recrystallization.

General procedure for complexes **7-10** and **13-17**

The synthesis was done in accordance with a literature-known procedure.[26]

The corresponding precursor and H_2Q_{Dipp} were dissolved in dry MeCN and dry Et_3N was added. The reaction mixture was stirred at 60°C. The solvent was evaporated and the crude product was purified by column chromatography (Al_2O_3, *n*-pentane:DCM 3:1). The product was recrystallized by slow diffusion of methanol in a solution of the product in DCM. For **15-17** the crude product was filtered and purified by column chromatography.

$[(az_{\text{-}Oct})Pt^{II}(\mu\text{-}Q_{Dipp}{}^{2-})Pt^{II}((az_{\text{-}Oct})]$ 1

P1 (54.0 mg, 0.05 mmol) and H_2Q_{Dipp} (18.0 mg, 0.05 mmol) in dry MeCN (10 mL) and dry Et_3N (0.50 mL)

for 24 h. The product was obtained as purple solid in a moderate yield (29.4 mg, 0.02 mmol, 40 %).

^{1}H NMR (401 MHz, $CDCl_3$) δ = 7.94–7.90 (m, 4H), 7.78 (d, ^3J = 8.6 Hz, 2H), 7.47–7.39 (m, 6H), 7.39–7.32 (m, 6H), 6.55 (dd, ^3J = 8.6 Hz, ^4J = 2.5 Hz, 2H), 5.09–4.99 (m, 2H), 4.99 (s, 2H), 3.33 (t, ^3J = 6.5 Hz, 4H), 3.26 (p, ^3J = 6.7 Hz, 4H), 1.63 (p, ^3J = 6.4 Hz, 4H), 1.40–1.33 (m, 20H), 1.19 (dd, ^3J = 6.8, 3.2 Hz, 12H), 1.08 (dd, ^3J = 6.7, 3.2 Hz, 12H), 0.98–0.91 (m, 6H) ppm.

^{13}C-NMR (101 MHz, $CDCl_3$) δ = 179.0, 173.4, 162.5, 159.0, 151.5, 131.1, 128.5, 128.4, 128.2, 124.4, 124.2, 115.3, 97.7, 68.4, 32.1, 29.5, 29.5, 28.0, 26.0, 24.2, 23.7, 22.9, 14.5 ppm.

HRMS (ESI): calcd. for $[C_{70}H_{86}KN_6O_4{}^{194}Pt_2]^+$ [M + K]$^+$: *m/z* 1502,5617; found 1502,5539.

EA calcd. for $C_{70}H_{86}N_6O_4Pt_2 \cdot 0.15\ CH_2Cl_2$: C 56.99; H 5.88; N 5.68 found: C 56.82; H 6.06; N 5.52.

[(az$_{\text{-Hexdec}}$)Pt$^{\text{II}}$(μ-Q$_{\text{Dipp}}{}^{2-}$)Pt$^{\text{II}}$((az$_{\text{-Hexdec}}$)] 2

P2 (59.5 mg, 0.05 mmol) and H_2Q_{Dipp} (18.0 mg, 0.05 mmol) in dry MeCN (10 mL) and dry Et_3N (0.50 mL) for 24 h. The product was obtained as purple solid in a moderate yield (56.7 mg, 0.04 mmol, 73%).

^{1}H NMR (401 MHz, $CDCl_3$) δ = 7.93–7.89 (m, 4H), 7.77 (d, ^3J = 8.6 Hz, 2H), 7.45–7.40 (m, 6H), 7.39–7.32 (m, 6H), 6.55 (dd, ^3J = 8.5, 2.4 Hz, 2H), 5.03 (d, ^3J = 2.5 Hz, 2H), 4.95 (s, 2H), 3.33 (t, ^3J = 6.4 Hz, 4H), 3.25 (p, ^3J = 6.8 Hz, 4H), 1.67–1.56 (m, 12H), 1.25 (s, 20H), 1.19 (d, ^3J = 6.9 Hz, 12H), 1.07 (d, ^3J = 6.8 Hz, 12H), 0.88 (t, ^3J = 6.8 Hz, 2H) ppm.

^{13}C-NMR (101 MHz, $CDCl_3$) δ = 178.9, 173.4, 162.6, 143.7, 143.2, 131.1, 129.9, 128.4, 128.2, 124.4, 124.2, 113.2, 97.7, 68.4, 32.1, 29.9, 29.8, 29.5, 29.2, 28.0, 26.0, 24.2, 23.7, 22.9, 14.3 ppm.

HRMS (ESI): calcd. for $[C_{86}H_{118}KN_6O_4{}^{194}Pt_2]^+$ [M + K]$^+$: *m/z* 1726,8121; found 1726,8042.

EA calcd. for $C_{86}H_{118}N_6O_4Pt_2 \cdot 2\ CH_3OH \cdot 1.3\ CH_2Cl_2$: C 57.52; H 6.95; N 4.51 found: C: 57.31 H: 7.19, N: 4.29.

[(az$_{\text{-2Oct}}$)Pt$^{\text{II}}$(μ-Q$_{\text{Dipp}}{}^{2-}$)Pt$^{\text{II}}$((az$_{\text{-2Oct}}$)] 3

P3 (66.7 mg, 0.05 mmol) and H_2Q_{Dipp} (18.0 mg, 0.05 mmol) in dry MeCN (10 mL) and dry Et_3N (0.5 mL) for 24 h. The product was obtained as purple solid in a moderate yield (36.4 mg, 0.02 mmol, 42%).

^{1}H NMR (401 MHz, $CDCl_3$) δ = 7.91 (d, ^3J = 9.1 Hz, 4H), 7.72 (d, ^3J = 8.5 Hz, 2H), 7.44–7.28 (m, 6H,), 6.93–6.87 (m, 4H), 6.68–6.37 (m, 2H), 5.00 (d, ^3J = 2.5 Hz, 2H), 4.97 (s, 2H), 4.02 (t, ^3J = 6.6 Hz, 4H), 3.32 (t, ^3J = 6.6 Hz, 4H), 3.26 (p, ^3J = 6.8 Hz, 4H), 1.81 (dt, ^3J = 14.6, 6.6 Hz, 4H), 1.62 (p, ^3J = 6.6 Hz, 4H), 1.40–1.29 (m, 40H), 1.19 (d, ^3J = 6.9 Hz, 12H), 1.07 (d, ^3J = 6.8 Hz, 12H), 0.93 (q, ^3J = 6.9 Hz, 12H) ppm.

^{13}C-NMR (101 MHz, $CDCl_3$) δ = 178.6, 171.0, 161.6, 160.5, 159.5, 158.2, 143.0, 125.4, 124.2, 113.9, 112.8, 98.3, 68.4, 31.9, 29.4, 29.2, 29.1, 27.8, 26.0, 24.1, 23.5, 22.7, 14.1 ppm.

HRMS (ESI): calcd. for $[C_{86}H_{118}N_6O_6{}^{194}Pt_2]^+$ [M]$^+$: *m/z* 1719,8382; found 1719,8255.

EA calcd. for $C_{86}H_{118}N_6O_6Pt_2$: C 59.98; H 6.91; N 4.88; found C 59.62; H 6.88; N 4.75.

[(az$_{\text{-2Hexdec}}$)Pt$^{\text{II}}$(μ-Q$_{\text{Dipp}}{}^{2-}$)Pt$^{\text{II}}$((az$_{\text{-2Hexdec}}$)] 4

P4 (44.6 mg, 0.03 mmol) and H_2Q_{Dipp} (9.0 mg, 0.03 mmol) in dry MeCN (10 mL) and dry Et_3N (1 mL) for 48 h. The product was obtained as purple solid in a moderate yield (31.2 mg, 0.03 mmol, 57%).

^{1}H NMR (401 MHz, $CDCl_3$) δ = 7.92–7.87 (m, 4H), 7.71 (d, ^3J = 8.5 Hz, 2H), 7.42–7.28 (m, 6H), 7.00–6.82 (m, 4H), 6.52 (dd, ^3J = 8.5 Hz, ^4J = 2.5 Hz, 2H), 4.99 (d, ^4J = 2.5 Hz, 2H), 4.96 (s, 2H), 4.01 (t, ^3J = 6.6 Hz, 4H), 3.31 (t, ^3J = 6.6 Hz, 4H), 3.24 (p, ^3J = 6.6 Hz, 4H), 1.86–1.74 (m, 4H), 1.66–1.56 (m, 4H), 1.52–1.39 (m, 4H), 1.26 (s, 80H), 1.18 (d, ^3J = 6.9 Hz, 12H), 1.05 (d, ^3J = 6.8 Hz, 12H), 0.92–0.79 (m, 12H) ppm.

^{13}C-NMR (101 MHz, $CDCl_3$) δ = 178.8, 173.3, 161.7, 160.7, 159.0, 143.2, 130.2, 128.2, 125.6, 124.4, 114.1, 110.2, 68.6, 68.3, 32.1, 29.9, 29.9, 29.8, 29.6, 29.5, 29.3, 28.0, 26.2, 24.2, 23.7, 22.9, 14.3 ppm.

HRMS (ESI): calcd. for $[C_{118}H_{182}N_6O_6Pt_2]^+$ [M]$^+$: *m/z* 2171,3446; found 2171.3535.

EA calcd. for $C_{118}H_{182}N_6O_6Pt_2 \cdot 2\ CH_4O \cdot 2\ CH_2Cl_2 \cdot 4\ H_2O$: C 58.66; H 8.22; N 3.39; found: C 58.66; H 8.21; N 3.17.

[(az$_{\text{-4Dodec}}$)Pt$^{\text{II}}$(μ-Q$_{\text{Dipp}}^{2-}$)Pt$^{\text{II}}$((az$_{\text{-4Dodec}}$)] 5

P5 (172.0 mg, 0.07 mmol) and H_2Q_{Dipp} (34.3 mg, 0.07 mmol) in dry MeCN (10 mL) and dry Et_3N (0.75 mL) for three days. The product was obtained as purple solid in a moderate yield (130.0 mg, 0.05 mmol, 65%).

^{1}H NMR (400 MHz, $CDCl_3$): δ = 7.90 (d, *J* = 8.9 Hz, 4H), 7.33 (q, *J* = 6.1 Hz, 6H), 6.87 (d, *J* = 8.9 Hz, 4H), 4.91 (s, 2H), 4.86 (s, 2H), 4.25 (t, *J* = 6.5 Hz, 4H), 4.01 (t, *J* = 6.6 Hz, 4H), 3.82 (t, *J* = 6.5 Hz, 4H), 3.30 – 3.16 (m, 8H), 1.81 (p, *J* = 6.6 Hz, 4H), 1.69 (dq, J = 21.8, 6.9 Hz, 13H), 1.43 (td, *J* = 13.1, 11.9, 7.4 Hz, 22H), 1.37 – 1.21 (m, 120H), 1.17 (d, *J* = 6.8 Hz, 11H), 1.05 (d, *J* = 6.7 Hz, 11H), 0.93 – 0.83 (m, 26H) ppm

^{13}C NMR (151 MHz, $CDCl_3$): δ = 157.3, 143.3, 133.4, 125.6, 113.9, 75.9, 32.1, 29.9, 29.8, 29.8, 29.7, 29.5, 26.2, 26.1, 24.2, 23.7, 22.9, 14.3, 1.2 ppm. Only few signals are detected due to poor signal-to-noise ratio.

EA calcd. for $C_{150}H_{246}N_6O_{10}Pt_2 \cdot 0.15\ CH_2Cl_2$: C, 66.88; H, 9.21; N, 3.12. Found: C, 66.61; H, 9.47; N 3.29.

The mass of the product cannot be detected via mass spectrometry.

[(az$_{\text{-2Dec}}$)Pt$^{\text{II}}$(μ-Q$_{\text{Dipp}}^{2-}$)Pt$^{\text{II}}$((az$_{\text{-2Dec}}$)] 6

P6 (136.0 mg, 0.07 mmol) and H_2Q_{Dipp} (34.3 mg, 0.07 mmol) in dry MeCN (10 mL) and dry Et_3N (0.75 mL) for three days. The product was obtained as purple solid in a moderate yield (130.0 mg, 0.06 mmol, 79%).

^{1}H NMR (400 MHz, $CDCl_3$): δ = 7.90 (d, *J* = 8.6 Hz, 1H), 7.86 (s, 1H), 7.73 (d, *J* = 8.5 Hz, 1H), 7.36 (dq, *J* = 13.4, 7.6, 7.2 Hz, 8H), 6.88 (dd, *J* = 13.0, 8.6 Hz, 2H), 6.54 (d, *J* = 8.7 Hz, 1H), 5.09 – 4.84 (m, 2H), 4.02 (dt, *J* = 12.0, 6.2 Hz, 6H), 3.90 (t, *J* = 6.6 Hz, 1H), 3.36 – 3.18 (m, 8H), 1.81 (td, *J* = 17.1, 15.9, 9.2 Hz, 5H), 1.62 (p, *J* = 7.7, 7.1 Hz, 6H), 1.54 – 1.23 (m, 95H), 1.18 (d, *J* = 6.6 Hz, 10H), 1.05 (d, *J* = 6.9 Hz, 12H), 0.89 (dt, *J* = 8.4, 5.2 Hz, 19H) ppm

^{13}C NMR (151 MHz, $CDCl_3$): δ = 161.3, 151.6, 150.8, 149.7, 148.3, 147.2, 147.1, 143.3, 143.2, 130.4, 128.5, 125.5, 124.4, 119.7, 115.9, 114.8, 114.1, 113.0, 112.6, 111.2, 104.4, 69.5, 69.4, 69.3, 69.2, 69.1, 68.9, 68.5, 68.3, 32.1, 30.0, 29.8, 29.7, 29.6, 29.5, 29.4, 29.3, 29.2, 27.9, 26.4, 26.2, 26.0, 24.4, 24.3, 24.2, 24.2, 23.6, 22.8, 14.3, 1.2 ppm. (Mixture of isomers)

EA calcd. for $C_{118}H_{182}N_6O_8Pt_2 \cdot 0.7\ CH_2Cl_2$: C, 62.44; H, 8.01; N, 3.81. Found: C, 62.09; H, 8.41; N, 4.09.

The mass of the product cannot be detected via mass spectrometry.

[(az$_{\text{-Oct}}$)Pt$^{\text{II}}$(μ-Q$_{\text{Az}}^{2-}$)Pt$^{\text{II}}$((az$_{\text{-Oct}}$)] 7

P1 (54.0 mg, 0.05 mmol) and H_2Q_{Az} (22.0 mg, 0.05 mmol) in dry MeCN (10 mL) and dry Et_3N (1 mL) were heated overnight. The product was obtained as blue solid in a moderate yield (29.7 mg, 0.02 mmol, 41%).

^{1}H NMR (401 MHz, $CDCl_3$) δ = 7.76 (d, ^3J = 8.5 Hz, 2H), 7.36–7.27 (m, 4H), 7.26–7.07 (m, 10H), 7.03–6.96 (m, 2H), 6.96–6.88 (m, 4H), 6.77–6.66 (m, 10H), 6.52 (dd, ^3J = 8.5, 2.5 Hz, 2H), 5.32 (d, ^3J = 2.5 Hz, 2H), 4.51 (s, 2H), 3.30 (t, ^3J = 6.7 Hz, 4H), 1.63–1.54 (m, 4H), 1.32 (s, 20H), 0.96–0.89 (m, 4H) ppm.

^{13}C-NMR (101 MHz, $CDCl_3$) δ = 169.6, 167.4 (2C, CN-quinone), 162.4, 159.1, 151.9, 150.5, 148.9, 147.3, 130.4, 129.0, 128.5, 128.2, 128.2, 127.5, 126.0, 125.6, 124.8, 122.6, 116.2, 113.1, 91.4, 68.3, 32.0, 29.5, 29.4, 29.2, 26.0, 22.8, 14.3 ppm.

HRMS (ESI): calcd. for $[C_{70}H_{73}N_8O_2Pt_2^+]^+$ $[M + H]^+$: *m/z* 1446.5125; found 1446.5026.

EA calcd. for $C_{70}H_{72}N_8O_2Pt_2 \cdot 0.25\ CH_2Cl_2$: C 57.45; H 4.98; N 7.63; found: C 57.37; H 5.05; N 7.63.

[(az$_{\text{-Hexdec}}$)Pt$^{\text{II}}$(μ-Q$_{\text{Az}}^{2-}$)Pt$^{\text{II}}$((az$_{\text{-Hexdec}}$)] 8

P2 (59.5 mg, 0.05 mmol) and H_2Q_{Az} (22.0 mg, 0.05 mmol) in dry MeCN (10 mL) and dry Et_3N (1 mL) were heated overnight. The product was obtained as blue solid in a moderate yield (62.2 mg, 0.04 mmol, 74%).

^{1}H NMR (401 MHz, $CDCl_3$) δ = 7.76 (d, ^3J = 8.5 Hz, 2H), 7.34–7.28 (m, 2H), 7.26–7.08 (m, 12H), 6.98 (q, ^3J = 7.4 Hz, 2H), 6.91 (td, ^3J = 7.4, 6.9, 5.8 Hz, 4H), 6.77–6.64 (m, 10H), 6.52 (dt, ^3J = 8.6, 2.3 Hz, 2H), 5.36–5.28 (m, 2H), 4.69–4.34 (m, 2H), 3.38–3.23 (m, 4H), 1.59 (q, ^3J = 6.4 Hz, 4H), 1.28 (s, 52H), 0.94–0.83 (m, 6H) ppm.

^{13}C-NMR (101 MHz, $CDCl_3$) δ = 171.1, 169.6, 167.4, 166.3, 162.4, 159.2, 151.9, 150.5, 149.0, 147.7, 147.3, 129.0, 128.5, 128.2, 128.1, 127.5, 125.6, 125.6, 122.6, 91.4, 68.3, 32.1, 29.9, 29.5, 29.2, 26.0, 22.9, 14.3 ppm.

HRMS (ESI): calcd. for $[C_{86}H_{105}N_8O_2Pt_2]^+$ $[M + H]^+$: *m/z* 1670.7629; found 1670.7601.

EA calcd. for $C_{86}H_{104}N_8O_2Pt_2$: C 61.78; H 6.27; N 6.70; found: C 61.72, H 6.32; N 6.62.

[(az$_{\text{-oct2}}$)Pt^{II}(μ-Q$_{Az}^{2-}$)Pt^{II}((az$_{\text{-Oct2}}$)] 9

P3 (66.7 mg, 0.05 mmol) and H_2Q_{Az} (22.0 mg, 0.05 mmol) in dry MeCN (10 mL) and dry Et_3N (1 mL) were heated overnight. The product was obtained as blue solid in a good yield (76.8 mg, 0.04 mmol, 90%).

^{1}H NMR (401 MHz, $CDCl_3$) δ = 7.73 (d, ^3J = 9.2 Hz, 2H), 7.35–7.28 (m, 4H), 7.26–7.07 (m, 10H), 6.83–6.77 (m, 2H), 6.77–6.62 (m, 8H), 6.51 (dt, ^3J = 8.5, 2.0 Hz, 2H), 6.41–6.33 (m, 4H), 5.30 (t, ^3J = 2.5 Hz, 2H), 4.81–4.36 (m, 2H,), 3.85 (q, ^3J = 6.7 Hz, 4H), 3.30 (q, ^3J = 6.8 Hz, 4H), 1.76 (h, ^3J = 6.8 Hz, 4H), 1.60 (dt, ^3J = 12.7, 6.4 Hz, 4H), 1.48 (dt, ^3J = 14.4, 7.7 Hz, 4H), 1.32 (s, 20H), 1.02–0.87 (m, 12H) ppm.

^{13}C-NMR (101 MHz, $CDCl_3$) δ = 169.6, 167.3, 162.1, 162.0, 159.1, 145.5, 145.4, 129.0, 128.0, 127.5, 126.0, 124.7, 123.8, 91.4, 68.2, 32.0, 31.1, 29.5, 29.4, 29.2, 26.1, 26.0, 22.9 ppm.

HRMS (ESI): calcd. for $[C_{86}H_{104}N_8O_4{}^{194}Pt_2]^+$ $[M]^+$: *m/z* 1700.7428; found 1700.7324.

EA calcd. for $C_{86}H_{104}N_8O_4Pt_2 \cdot 0.25\ CH_2Cl_2$: C 60.05; H 6.11; N 6.49; found: C 59.99, H 6.16; N 6.51.

[(az$_{\text{-Hexdec2}}$)Pt^{II}(μ-Q$_{Az}^{2-}$)Pt^{II}((az$_{\text{-Hexdec2}}$)] 10

P4 (89.2 mg, 0.05 mmol) and H_2Q_{Az} (22.0 mg, 0.05 mmol) in dry MeCN (10 mL) and dry Et_3N (1 mL) were heated overnight. The product was obtained as blue solid in a moderate yield (39.5 mg, 0.02 mmol 37%).

^{1}H NMR (401 MHz, $CDCl_3$) δ = 7.72 (dd, ^3J = 8.5 Hz, ^4J = 0.6 Hz, 2H), 7.33–7.28 (m, 2H), 7.25–7.07 (m, 12H), 6.80–6.75 (m, 2H), 6.74–6.65 (m, 8H), 6.51 (ddd, ^3J = 8.6, 2.5 Hz, ^4J = 1.6 Hz, 2H), 6.39–6.34 (m, 4H), 5.30 (t, ^3J = 2.6 Hz, 2H), 4.74–4.38 (m, 1H), 3.85 (q, ^3J = 6.7 Hz, 4H), 3.30 (q, ^3J = 6.8 Hz, 4H), 1.76 (h, ^3J = 7.0 Hz, 4H), 1.59 (q, ^3J = 6.2, 5.7 Hz, 4H), 1.49–1.42 (m, 4H), 1.40–1.34 (m, 4H), 1.28 (s, 88H), 0.92–0.85 (m, 12H) ppm.

^{13}C-NMR (101 MHz, $CDCl_3$) δ = 169.6, 162.0, 159.1, 145.5, 129.0, 128.0, 127.5, 127.3, 126.2, 126.0, 125.9, 123.8, 114.2, 100.2, 68.3, 32.1, 29.9, 29.8, 29.5,29.4, 29.3, 26.2, 26.0, 22.9, 14.3 ppm.

HRMS (ESI): calcd. for $[C_{118}H_{169}N_8O_4Pt_2]^+$ ($[M + H]^+$) *m/z* 2152.2569 found 2152.2431

EA calcd. for $C_{118}H_{168}N_8O_4Pt_2 \cdot 0.2\ CH_2Cl_2$: C 65.43; H 7.82; N 5.16 found: C 65.41; H 7.80; N 5.15.

[(azo$_{OCF3}$)Pt(μ-Q$_{Dipp}$)Pt(azo$_{OCF3}$)] 11

P7 (68.0 mg, 0.07 mmol) and H_2Q_{Dipp} (31.5 mg, 0.07 mmol) in dry MeCN (10 mL) and dry Et_3N (0.75 mL) for three days. The product was obtained as purple solid in a moderate yield (68.0 mg, 0.05 mmol, 72%).

^{1}H NMR (600 MHz, CDCl3): δ = 8.06 (t, ^3J = 8.1 Hz, 3H), 7.97–7.93 (m, 3H), 7.54–7.48 (m, 4H), 7.41–7.37 (m, 4H), 7.32 (d, ^3J = 7.9 Hz, 4H), 6.91 (d, ^3J = 6.6 Hz, 2H), 5.12 (s, 2H), 5.10 (s, 1H), 4.83 (s, 1H), 3.17 (sept, ^3J = 6.6 Hz, 4H), 1.22 (d, ^3J = 6.4 Hz, 12H), 1.03 (d, ^3J = 5.9 Hz, 12H) ppm. (Main isomer)

^{13}C NMR (151 MHz, CDCl3): δ = 178.9, 178.6, 178.5, 173.7, 173.4, 164.6, 163.4, 163.1, 151.6, 151.2, 151.0, 150.5, 150.2, 149.8, 142.8, 142.6, 142.2, 141.5, 132.0, 131.8, 131.3, 130.5, 130.1, 129.5, 128.7, 128.5, 126.3, 124.7, 124.4, 121.4, 120.8, 119.7, 119.2, 117.5, 117.4, 97.8, 53.6, 29.9, 28.1, 24.3, 23.4, 23.2, 14.3, 1.3 ppm. (Mixture of isomers)

^{19}F NMR (565 MHz, $CDCl_3$, 21 °C) δ = -56.9, -57.5 ppm. (Main isomer)

HRMS (ESI): calcd. for $[C_{56}H_{53}F_6N_6O_4{}^{195}Pt_2]^+$ [M – H]$^+$: *m/z* 1376.3301; found 1376.3969.

EA calcd. for $C_{56}H_{53}F_6N_6O_4Pt_2 \cdot 0.7\ C_5H_{12} \cdot 1.1\ CH_2Cl_2$: C, 47.84; H, 4.17; N, 5.50; found: C, 47.51; H, 4.56; N, 5.89.

[(azo$_{(OCF3)2}$)Pt(μ-Q$_{Dipp}$)Pt(azo$_{(OCF3)2}$)] 12

P8 (58.00 mg, 0.05 mmol) and H_2Q_{Dipp} (23.0 mg, 0.05 mmol) in dry MeCN (7 mL) and dry Et_3N (0.5 mL) for three days. The product was obtained as purple solid in a moderate yield (33.0 mg, 0.04 mmol, 57%).

^{1}H NMR (600 MHz, $CDCl_3$): δ = 8.04 (d, ^3J = 9.0 Hz, 4H), 7.94 (d, ^3J = 8.4 Hz, 2H), 7.53 (t, ^3J = 7.7Hz, 2H), 7.40 (d, ^3J = 7.7Hz, 4H), 7.32 (d, ^3J = 8.6Hz, 4H), 6.91 (d, ^3J=9.1Hz, 2H), 5.11 (s, 2H), 4.80 (s, 2H), 3.18–3.101 (m, 4H), 1.21 (d, ^3J = 6.9 Hz, 12H), 1.01 (d, ^3J = 6.8 Hz, 12H) ppm.

^{13}C NMR (151 MHz, CDCl3): δ = 126.2, 124.7, 120.8, 28.1, 24.3, 23.2, 1.2. Only few signals are detected due to poor signal-to-noise ratio.

^{19}F NMR (565 MHz, $CDCl_3$) δ = -57.0, -57.5 ppm.

HRMS (ESI): calcd. for $[C_{58}H_{51}F_{12}N_6O_6Pt_2]^+$ [M – H]$^+$: *m/z* 1544.2947; found 1544.3057.

EA calcd. for $C_{58}H_{51}F_{12}N_6O_6Pt_2 \cdot 2\ C_5H_{12} \cdot C_4H_{10}O$: C 49.67; H 5.16; N 4.57 found: C 49.64; H 4.94; N 4.19.

[(azo$_{OctRf}$)Pt(μ-Q$_{Dipp}$)Pt(azo$_{OctRf}$)] 13

P9 (47.00 mg, 0.03 mmol) and H_2Q_{Dipp} (13.80 mg, 0.03 mmol) were dissolved in dry MeCN (10 mL) and dry Et_3N (0.50 mL) were heated overnight. The product was obtained as purple solid in a moderate yield (44.2 mg, 76%).

^{1}H NMR (401 MHz, $CDCl_3$) δ = 7.91 (dd, ^3J = 7.9, 1.9 Hz, 4H), 7.80 (d, ^3J = 8.6 Hz, 2H), 7.48 – 7.31 (m, 12H), 6.57 (dd, ^3J = 8.5, 2.6 Hz, 2H), 5.01 (d, ^3J = 2.4 Hz, 2H), 4.96 (s, 2H), 3.64 (t, $^{3,4}J$ = 6.9 Hz, 4H), 3.25 (dt, $^{3,4}J$ = 13.9, 7.0 Hz, 4H), 2.64 – 2.39 (m, 4H), 1.20 (d, ^3J = 6.7 Hz, 14H), 1.06 (d, ^3J = 6.7 Hz, 10H) ppm.

^{13}C NMR (761 MHz, $CDCl_3$) δ = 178.9, 173.4, 160.9, 159.6, 151.9, 143.2, 141.9, 131.0, 130.2, 128.4, 126.2, 124.5, 124.1, 114.6, 114.2, 113.3, 97.6, 60.4, 31.2, 29.8, 27.9, 24.1, 23.5, 1.1 ppm.

^{19}F NMR (101 MHz, $CDCl_3$) δ = -80.5, -113.00 (td, $^{3,4}J$ = 13.9, 4.7 Hz), -121.8, -122.8, -123.6, -125.38, -126.75 (m) ppm.

HRMS (ESI): calcd. for $[C_{70}H_{60}F_{26}N_6NaO_4Pt_2]^+$ [M + Na]$^+$*m/z* 1955,3449; found 1955.3477.

EA calcd. for $C_{70}H_{60}F_{26}N_6O_4Pt_2$: C 44.49; H 3.13; N 4.35 found: C 43.94; H 3.42; N 4.08.

[(azo$_{DecRf}$)Pt(μ-Q$_{Dipp}$)Pt(azo$_{DecRf}$)] 14

P10 (52.40 mg, 0.03 mmol) and H_2Q_{Dipp} (13.80 mg, 0.03 mmol) in dry MeCN (10 mL) and dry Et_3N (0.50 mL) were heated overnight. The product was obtained as blue solid in a moderate yield (47.6 mg, 74%).

^{1}H NMR (401 MHz, $CDCl_3$,) δ = 7.91 (d, *J* = 7.1 Hz, 3H), 7.81 (d, *J* = 8.5 Hz, 2H), 7.44 (d, *J* = 7.6 Hz, 6H), 7.38 – 7.32 (m, 5H), 7.03 – 6.92 (m, 2H), 6.57 (d, *J* = 8.6 Hz, 2H), 5.08 (d, *J* = 4.2 Hz, 1H), 4.96 (s, 1 H), 4.37 (t, *J* = 6.8 Hz, 2H), 3.64 (t, *J* = 7.1 Hz, 3H), 3.24 (td, *J* = 13.3, 6.7 Hz, 4H). 2.58 – 2.42 (m, 4H), 1.21 (t, *J* = 6.1 Hz, 14H), 1.07 (d, *J* = 6.5 Hz, 10H) (Main Isomer) ppm.

^{19}F NMR (376.88 MHz, $CDCl_3$) δ = -78.82 – -82.23 (m), -110.39 – -114.80 (m), -121.73 (d, ^3J = 116.1 Hz), -122.67, -123.50, -126.09 ppm.

^{13}C-NMR (101 MHz, $CDCl_3$, 21 °C) δ = 146.2, 122.9, 118.7, 29.0, 27.7, 25.2, 23.8, 23.2, 23.0 ppm. Only few signals are detected due to poor signal-to-noise ratio.

HRMS (ESI): calcd. for $[C_{74}H_{60}F_{34}N_6NaO_4Pt_2]^+$ [M + Na]$^+$: *m/z* 2155,3321; found 2155,3207.

EA calcd. for $C_{74}H_{60}F_{34}N_6O_4Pt_2 \cdot 0.95\ C_5H_{12}$ C 42.95; H 3.27 N 3.82 found: C 42.69; H 3.36; N 3.55.

[(azo$_{OCF3}$)Pt(μ-Q$_{Az}$)Pt(azo$_{OCF3}$)] 15

P7 (49.50 mg, 0.05 mmol) and H_2Q_{Az} (22.00 mg, 0.05 mmol) in dry MeCN (10 mL) and dry Et_3N (1 mL) were heated overnight. The product was obtained as blue solid in a moderate yield (15.0 mg, 22%).

^{1}H NMR (401 MHz, $CDCl_3$,) δ = 7.96 – 7.84 (m, 2H), 7.43 – 7.31 (m, 4H), 7.29 (d, J = 6.0 Hz, 3H), 7.21 – 7.11 (m, 6H), 7.07 – 7.01 (m, 1H), 6.95 (td, J = 7.8, 3.8 Hz, 4H), 6.88 – 6.82 (m, 2H), 6.82 – 6.51 (m, 12H), 5.55 (dt, J = 8.6, 4.4 Hz, 1H), 5.32 (s, 1H), 4.73 – 4.48 (m, 2H) ppm.

^{19}F NMR (101 MHz, $CDCl_3$) δ = –57.03 (s), -57.49 (d, J = 8.5 Hz) ppm.

^{13}C-NMR: No signals are detected due to low concentration (due to low solubility) and poor signal-to-noise ratio.

HRMS (ESI): calcd. for $[C_{56}H_{38}F_6N_8NaO_2{}^{194}Pt_2]^+$ [M + Na]$^+$: *m/z* 1380,2189; found 1380,2130.

EA calcd. for $C_{56}H_{38}F_6N_8O_2Pt_2$: C 49.49; H 2.82 N 8.24 found: C 49.55; H 2.99; N 8.24.

[(azo$_{OctRf}$)Pt(μ-Q$_{Az}$)Pt(azo$_{OctRf}$)] 16

P9 (47.00 mg, 0.03 mmol) and H_2Q_{Az} (13.2 mg, 0.03 mmol) in dry MeCN (10 mL) and dry Et_3N (1 mL) were heated overnight. The product was obtained as blue solid in a moderate yield (25.1 mg, 44%).

^{1}H NMR (401 MHz, $CDCl_3$, 22 °C) δ = 7.79 (d, J = 8.7 Hz, 2H), 7.25 – 7.12 (m, 8H), 6.97 (dt, J = 31.4, 7.0 Hz, 6H), 6.84 – 6.63 (m, 14H), 6.53 (d, J = 8.6 Hz, 2H), 6.41 (d, J = 8.9 Hz, 2H), 4.69 – 4.46 (m, 2H), 4.19 (t, J = 6.6 Hz, 2H), 3.60 (q, J = 6.9 Hz, 4H), 2.55 – 2.33 (m, 4H) ppm.

^{19}F NMR (101 MHz, $CDCl_3$) δ = -80.59 – -80.77 (m), -113.09, -121.74, -122.76, -123.54, -125.95 ppm.

^{13}C-NMR: No signals are detected due to low concentration (low solubility) and poor signal-to-noise ratio.

HRMS (ESI): calcd. for $[C_{70}H_{47}F_{26}N_8O_2{}^{194}Pt_2]^+$ [M + H]$^+$: *m/z* 1915,2697; found 1915.2421.

EA calcd. for $C_{70}H_{46}F_{26}N_8O_2Pt_2 \cdot 0.55\ CH_2Cl_2$: C 43.19; H 2.42; N 5.71 found: C 43.43; H 2.33; N 5.45.

[(azo$_{DecRf}$)Pt(μ-Q$_{Az}$)Pt(azo$_{DecRf}$)] 17

P10 (36.0 mg, 0.02 mmol) and H_2Q_{Az} (9.1 mg, 0.02 mmol) were dissolved in dry MeCN (10 mL) and dry Et_3N (1 mL) was added. The reaction mixture was stirred at 60°C for two days. The crude product was filtered and purified by column chromatography (Al_2O_3, *n*-pentane:DCM 3:1). The product was recrystallized by slow diffusion of methanol in a solution of the product in DCM yielding the desired product in a moderate yield (18.3 mg, 43%).

^{1}H NMR (401 MHz, $CDCl_3$, 22 °C) δ = 7.79 (d, J = 8.6 Hz, 2H), 7.33 (t, J = 7.6 Hz, 4H), 7.17 (dt, J = 21.0, 7.4 Hz, 7H), 6.97 (dq, J = 31.1, 7.3 Hz, 2H), 6.80 – 6.61 (m, 4H), 6.53 (d, J = 8.4 Hz, 11H), 6.41 (d, J = 8.7 Hz, 2H), 5.30 (d, J = 9.6 Hz, 1H), 4.75 – 4.45 (m, 2H), 4.19 (t, J = 6.6 Hz, 1H), 3.60 (q, J = 6.8 Hz, 4H), 2.56 – 2.39 (m, 4H) ppm.

^{19}F NMR (101 MHz, $CDCl_3$) δ = -80.48 – -80.87 (m), -113.08, -121.54, -121.80, -122.61, -123.47, -126.11 ppm.

^{13}C-NMR (101 MHz, $CDCl_3$, 21 °C) δ = 156.0, 100.8, 89.4 ppm. Only few signals are detected due to low concentration (low solubility) and poor signal-to-noise ratio.

HRMS (ESI): calcd. for $[C_{74}H_{47}F_{34}N_8O_2Pt_2]^+$ [M + H]$^+$: *m/z* 2115,2569; found 2115,2263.

EA calcd. for $C_{74}H_{46}F_{34}N_8O_2Pt_2$: C 42.02; H 2.19 N 5.30 found: C 42.51; H 2.34; N 5.48.

Acknowledgements

Eugen Wuckert is thanked for providing **L14** and **L15**. We would like to acknowledge the assistance of the Core Facility BioSupraMol supported by the DFG. Funded by the Deutsche Forschungsgemeinschaft [DFG, German Research Foundation – Project-ID 387284271 – SFB 1349]. CCDC of bip_537_a: 2213469

References

[1] a) E. Baggaley, J. A. Weinstein, J. A. G. Williams, *Coord. Chem. Rev.* **2012**, *256*, 1762-1785; b) L. K. McKenzie, H. E. Bryant, J. A. Weinstein, *Coord. Chem. Rev.* **2019**, *379*, 2-29; c) J. Best, I. V. Sazanovich, H. Adams, R. D. Bennett, E. S. Davies, A. J. H. M. Meijer, M. Towrie, S. A. Tikhomirov, O. V. Bouganov, M. D. Ward, J. A. Weinstein, *Inorg. Chem.* **2010**, *49*, 10041-10056; d) K.

Tahara, Y. Ashihara, T. Higashino, Y. Ozawa, T. Kadoya, K. Sugimoto, A. Ueda, H. Mori, M. Abe, *Dalton Trans.* **2019**, *48*, 7367-7377; e) L. A. Cameron, J. W. Ziller, A. F. Heyduk, *Chem. Sci.* **2016**, *7*, 1807-1814; f) W. W. Kramer, L. A. Cameron, R. A. Zarkesh, J. W. Ziller, A. F. Heyduk, *Inorg. Chem.* **2014**, *53*, 8825-8837; g) P. A. Scattergood, P. Jesus, H. Adams, M. Delor, I. V. Sazanovich, H. D. Burrows, C. Serpa, J. A. Weinstein, *Dalton Trans.* **2015**, *44*, 11705-11716; h) N. Deibel, D. Schweinfurth, J. Fiedler, S. Zalis, B. Sarkar, *Dalton Trans.* **2011**, *40*, 9925-9934; i) N. Deibel, D. Schweinfurth, S. Hohloch, J. Fiedler, B. Sarkar, *Chem. Commun.* **2012**, *48*, 2388-2390.

[2] a) W. B. Connick, D. Geiger, R. Eisenberg, *Inorg. Chem.* **1999**, *38*, 3264-3265; b) S. D. Cummings, R. Eisenberg, *J. Am. Chem. Soc.* **1996**, *118*, 1949-1960; c) J. A. Weinstein, M. T. Tierney, E. S. Davies, K. Base, A. A. Robeiro, M. W. Grinstaff, *Inorg. Chem.* **2006**, *45*, 4544-4555.

[3] S. Sobottka, M. Nößler, A. L. Ostericher, G. Hermann, N. Z. Subat, J. Beerhues, M. B.-v. d. Meer, L. Suntrup, U. Albold, S. Hohloch, J. C. Tremblay, B. Sarkar, *Chem. Eur. J.* **2020**, *26*, 1314–1327.

[4] a) S. Reinhardt, K. Heinze, *Z. Anorg. Allg. Chem.* **2006**, *632*, 1465–1470; b) K. Heinze, S. Reinhardt, *Chem. Eur. J.* **2008**, *14*, 9482–9486.

[5] a) T. H. L. Nguyen, N. Gigant, D. Joseph, *ACS Catal.* **2018**, *8*, 1546-1579; b) K. Yadav, T. Halbritter, A. Heckel, T. G. Gopakumar, *J. Phys. Chem. C* **2018**, *122*, 15330-15337.

[6] a) F. I. o. R.-A. Ligands:, *Inorg. Chem.* **2011**, *50*, 9737-9914; b) *Eur. J. Inorg. Chem.* **2012**, 340–580.

[7] a) M. D. Ward, J. A. McCleverty, *J. Chem. Soc., Dalton Trans.* **2002**, 275-288; b) C. G. Pierpont, *Coord. Chem. Rev.* **2001**, *95*, 216−217; c) A. I. Poddel'sky, V. K. Cherkasov, G. A. Abakumov, *Coord. Chem. Rev.* **2009**, *253*, 291-324; d) P. Chaudhuri, C. N. Verani, E. Bill, E. Bothe, T. Weyhermüller, K. Wieghardt, *J. Am. Chem. Soc.* **2001**, *123*, 2213-2223; e) M. van der Meer, Y. Rechkemmer, F. D. Breitgoff, S. Dechert, R. Marx, M. Dorfel, P. Neugebauer, J. van Slageren, B. Sarkar, *Dalton Trans.* **2016**, *45*, 8394-8403.

[8] a) H. S. Das, F. Weisser, D. Schweinfurth, C.-Y. Su, L. Bogani, J. Fiedler, B. Sarkar, *Chem. Eur. J.* **2010**, *16*, 2977-2981; b) D. Schweinfurth, H. S. Das, F. Weisser, D. Bubrin, B. Sarkar, *Inorg. Chem.* **2011**, *50*, 1150-1159; c) F. Weisser, R. Huebner, D. Schweinfurth, B. Sarkar, *Chem. Eur. J.* **2011**, *17*, 5727-5736; d) D. Schweinfurth, M. M. Khusniyarov, D. Bubrin, S. Hohloch, C.-Y. Su, B. Sarkar, *Inorg. Chem.* **2013**, *52*, 10332-10339; e) A. Paretzki, R. Pattacini, R. Huebner, P. Braunstein, B. Sarkar, *Chem. Comm.* **2010**, *46*, 1497-1499.

[9] a) P. Braunstein, O. Siri, J.-p. Taquet, M.-M. Rohmer, M. Bénard, R. Welter, *J. Am. Chem. Soc.* **2003**, *125*, 12246-12256; b) Q.-Z. Yang, O. Siri, P. Braunstein, *Chem. Eur. J.* **2005**, *11*, 7237-7246; c) D. Kumbhakar, B. Sarkar, S. Maji, S. M. Mobin, J. Fiedler, F. A. Urbanos, R. Jiménez-Aparicio, W. Kaim, G. K. Lahiri, *J. Am. Chem. Soc.* **2008**, *130*, 17575-17583; d) S. Kar, B. Sarkar, S. Ghumaan, D. Janardanan, J. van Slageren, J. Fiedler, V. G. Puranik, R. B. Sunoj, W. Kaim, G. K. Lahiri, *Chem. Eur. J.* **2005**, *11*, 4901-4911; e) J. Mattsson, P. Govindaswamy, A. K. Renfrew, P. J. Dyson, P. Štěpnička, G. Süss-Fink, B. Therrien,

Organometallics **2009**, *28*, 4350-4357; f) Y. Su, Y. Zhao, J. Gao, Q. Dong, B. Wu, X.-J. Yang, *Inorg. Chem.* **2012**, *51*, 5889-5896; g) G. Nawn, R. McDonald, R. G. Hicks, *Inorg. Chem.* **2013**, *52*, 10912-10919.

[10] D. Zhang, G.-X. Jin, *Organometallics* **2003**, *22*, 2851-2854.

[11] a) O. Siri, J.-p. Taquet, J.-P. Collin, M.-M. Rohmer, M. Bénard, P. Braunstein, *Chem. Eur. J.* **2005**, *11*, 7247-7253; b) J. Rall, A. F. Stange, K. Hübler, W. Kaim, *Angew. Chem. Int. Ed.* **1998**, *37*, 2681-2682; c) O. Siri, P. Braunstein, M.-M. Rohmer, M. Bénard, R. Welter, *J. Am. Chem. Soc.* **2003**, *125*, 13793-13803; d) I.-R. Jeon, J. G. Park, D. J. Xiao, T. D. Harris, *J. Am. Chem. Soc.* **2013**, *135*, 16845-16848; e) S. Frantz, J. Rall, I. Hartenbach, T. Schleid, S. Záliš, W. Kaim, *Eur. J. Chem.* **2004**, *10*, 149-154.

[12] J. A. DeGayner, I.-R. Jeon, T. D. Harris, *Chem. Sci.* **2015**, *6*, 6639-6648.

[13] a) K. Ohno, A. Nagasawa, T. Fujihara, *Dalton Trans.* **2015**, *44*, 368-376; b) Y.-B. Huang, G.-R. Tang, G.-Y. Jin, G.-X. Jin, *Organometallics* **2008**, *27*, 259-269.

[14] a) J. Brooks, Y. Babayan, S. Lamansky, P. I. Djurovich, I. Tsyba, R. Bau, M. E. Thompson, *Inorg. Chem.* **2002**, *41*, 3055-3066; b) N. Godbert, T. Pugliese, I. Aiello, A. Bellusci, A. Crispini, M. Ghedini, *Eur. J. Inorg. Chem.* **2007**, *2007*, 5105-5111.

[15] B. Sarkar, R. Hubner, R. Pattacini, I. Hartenbach, *Dalton Trans.* **2009**, 4653-4655.

[16] a) S. Hayami, R. Moriyama, A. Shuto, Y. Maeda, K. Ohta, K. Inoue, *Inorg. Chem.* **2007**, *46*, 7692-7694; b) R. Akiyoshi, Y. Hirota, D. Kosumi, M. Tsutsumi, M. Nakamura, L. F. Lindoy, S. Hayami, *Chem. Sci.* **2019**, *10*, 5843-5848.

[17] a) N. G. Nagaveni, M. Gupta, A. Roy, V. Prasad, *J. Mater. Chem.* **2010**, *20*, 9089-9099; b) M. J. Baena, P. Espinet, C. L. Folcia, J. Ortega, J. Etxebarría, *Inorg. Chem.* **2010**, *49*, 8904-8913.

[18] a) I. Aiello, M. Ghedini, M. La Deda, D. Pucci, O. Francescangeli, *Eur. J. Inorg. Chem.* **1999**, *1999*, 1367-1372; b) M. Ghedini, D. Pucci, A. Crispini, G. Barberio, *Organometallics* **1999**, *18*, 2116-2124; c) M. Ghedini, D. Pucci, A. Crispini, I. Aiello, F. Barigelletti, A. Gessi, O. Francescangeli, *Appl. Organomet. Chem.* **1999**, *13*, 565-581; d) J. Arias, M. Bardají, P. Espinet, C. L. Folcia, J. Ortega, J. Etxebarría, *Inorg. Chem.* **2009**, *48*, 6205-6210.

[19] a) F. Guittard, E. Taffin de Givenchy, S. Geribaldi, A. Cambon, *J. Fluor. Chem.* **1999**, *100*, 85-96; b) R. Asep, Y. Aoki, T. Hirose, H. Nohira, *Liq. Cryst.* **2001**, *28*, 785-791; c) Y. Yang, H. Li, K. Wang, J. Wen, *Liq. Cryst.* **2001**, *28*, 375-379; d) K. Wang, Y. Yang, J. Wen, *Liq. Cryst.* **2001**, *28*, 1649-1653; e) H. Liu, H. Nohira, *Liq. Cryst.* **1997**, *22*, 217-222; f) J. Wen, H. Chen, Y. Shen, *Liq. Cryst.* **1999**, *26*, 1833-1834; g) M. L. Rahman, G. Hegde, M. Azazpour, M. M. Yusoff, S. Kumar, *J. Fluor. Chem.* **2013**, *156*, 230-235.

[20] a) K. N. Kim, E. D. Do, Y. W. Kwon, J. I. Jin, *Liq. Cryst.* **2005**, *32*, 229-237; b) W.-K. Lee, K.-N. Kim, M. F. Achard, J.-I. Jin, *J. Mater. Chem.* **2006**, *16*, 2289-2297.

[21] J.-W. Lee, Y. Park, J.-I. Jin, M. F. Achard, F. Hardouin, *J. Mater. Chem.* **2003**, *13*, 1367-1372.

[22] L. Hamryszak, H. Janeczek, E. Schab-Balcerzak, *J. Mol. Liq.* **2012**, *165*, 12-20.

[23] T. Thiele, D. Prescher, R. Ruhmann, D. Wolff, *J. Fluor. Chem.* **1997**, *85*, 155-161.

[24] a) T. Hashimoto, M. Yamazaki, H. Ishii, T. Yamada, T. Hayashita, *Chem. Lett.* **2014**, *43*, 228-230; b) R. Willstätter, M. Benz, *Ber. Dtsch. Chem. Ges.* **1906**, *39*, 3492-3503; c)

W.-h. Wei, T. Tomohiro, M. Kodaka, H. Okuno, *J. Org. Chem.* **2000**, *65*, 8979-8987; d) D. J. Mabbott, B. E. Mann, P. M. Maitlis, *J. Chem. Soc., Dalton Trans.* **1977**, 294-299.

[25] W. Kaim, B. Schwederski, *Coord. Chem. Rev.* **2010**, *254*, 1580-1588.

[26] N. Deibel, M. G. Sommer, S. Hohloch, J. Schwann, D. Schweinfurth, F. Ehret, B. Sarkar, *Organometallics* **2014**, *33*, 4756-4765.

[27] a) N. Deibel, S. Hohloch, M. G. Sommer, D. Schweinfurth, F. Ehret, P. Braunstein, B. Sarkar, *Organometallics* **2013**, *32*, 7366-7375; b) S. Roy, I. Hartenbach, B. Sarkar, *Eur. J. Inorg. Chem.* **2009**, 2553–2558.

[28] M. G. Sommer, D. Schweinfurth, F. Weisser, S. Hohloch, B. Sarkar, *Organometallics* **2013**, *32*, 2069-2078.

[29] G. R. Fulmer, A. J. M. Miller, N. H. Sherden, H. E. Gottlieb, A. Nudelman, B. M. Stoltz, J. E. Bercaw, K. I. Goldberg, *Organometallics* **2010**, *29*, 2176-2179.

[30] M. Krejčik, M. Daněk, F. Hartl, *J. Electroanal. Chem.* **1991**, *317*, 179-187.

[31] a) G. M. Sheldrick, *SHELXS-97, Program for Crystal Structure Solution and Refinement,* **1997**, University of Göttingen, Germany; b) G. Sheldrick, *Acta Crystallogr., Sect. A* **2008**, *64*, 112-122; c) G. M. Sheldrick, *SADABS Ver. 2008/1, SADABS. Program for Empirical Absorption Correction* **2012**, University of Göttingen, Germany; d) G. M. Sheldrick, *SHELXL Version 2014/7, Program for Chrystal Structure Solution and Refinement* **2014**, University of Göttingen, Germany; e) G. Sheldrick, *Acta Crystallogr. Sect. C* **2015**, *71*, 3-8; f) A. Spek, *J. Appl. Crystallogr.* **2003**, *36*, 7-13; g) SAINT+, *Data Integration Engine, Version 8.27b©*, Bruker AXS, Madison, Wisconsin, USA, 1997-2012.

[32] A. Antoine John, Q. Lin, *J. Org. Chem.* **2017**, *82*, 9873-9876.

[33] J. Wang, J. He, C. Zhi, B. Luo, X. Li, Y. Pan, X. Cao, H. Gu, *RSC Advances* **2014**, *4*, 16607-16611.

[34] R. Tatikonda, S. Bhowmik, K. Rissanen, M. Haukka, M. Cametti, *Dalton Trans.* **2016**, *45*, 12756-12762.

[35] A. V. Malkov, M. Figlus, S. Stončius, P. Kočovský, *J. Org. Chem.* **2007**, *72*, 1315-1325.

[36] L. H. Heitman, R. Narlawar, H. de Vries, M. N. Willemsen, D. Wolfram, J. Brussee, A. P. Ijzerman, *J. Med. Chem.* **2009**, *52*, 2036-2042.

[37] E. V. Filatova, O. V. Turova, A. G. Nigmatov, S. G. Zlotin, *Tetrahedron* **2018**, *74*, 157-164.

TOC

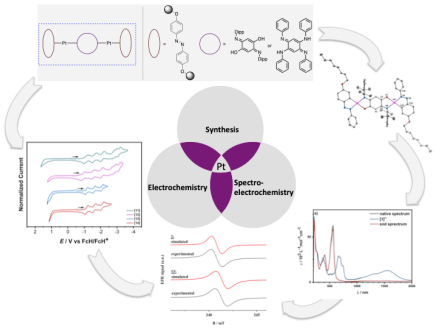

Supporting Information

Dinuclear Quinonoid-Bridged Pt(II) Complexes with (Perfluorinated-) Alkyl Chain Containing Azobenzene Ligands: A Combined Synthetic, Electrochemical and Spectroelectrochemical Investigation

*Maite Nößler,[a] Lisa Böser,[a] René Jäger,[a] Clemens Lücke,[b] Arijit Singha Hazari,[b] Eugen Wuckert,[c] Julia Beerhues,[a,b] Sabine Laschat[c] and Biprajit Sarkar[a,b]**

[a]Institut für Chemie und Biochemie, Freie Universität Berlin, Fabeckstraße 34-36, D-14195, Berlin, Germany

[b] Institut für Anorganische Chemie, Universität Stuttgart, Pfaffenwaldring 55, D-70569 Stuttgart, Germany

[c] Institut für Organische Chemie, Universität Stuttgart, Pfaffenwaldring 55, 70569 Stuttgart, Germany

Content

S II

1. X-Ray Crystallography

Table S 1: Crystallographic data of complexes **1**.

	1
Chemical formula	$C_{42}H_{20}CoF_{18}N_6B_2$
M_r	1031.0980
Crystal System	Orthorombic
Space group	Fdd2
a (Å)	37.126(1)
b (Å)	10.8865(5)
c (Å)	24.5859(8)
a (°)	90
β (°)	90
g (°)	90
V (Å^3)	9937.2(7)
Z	16
Density (g cm^{-3})	1.379
F(000)	4104
Radiation Type	Mo$\mathbf{K_\alpha}$
μ (mm^{-1})	0.448
Crystal size	0.52 x 0.36 x 0.09
Meas. Refl.	14452
Indep. Refl.	4406
Obsvd. [$I > 2\sigma(I)$] refl.	3953
R_{int}	0.0298
R [$F^2 > 2\sigma(F^2)$], wR(F^2), S	0.0481,0.1324,0.935
$\Delta\rho_{max}$, $\Delta\rho_{min}$ (e Å^{-3})	0.424, -0.232

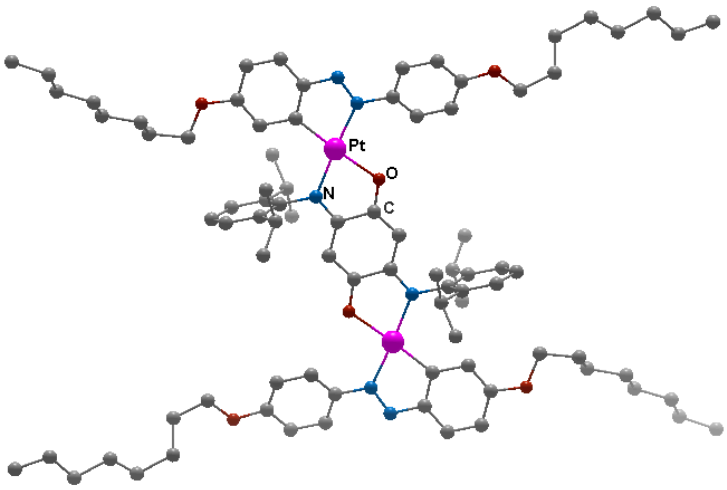

Figure S 1: Picture of **3** to prove desired connectivity of the ligands an metal centers. H-atoms have been omitted for clarity.

2. Polarized Optical Microscopy

L14:

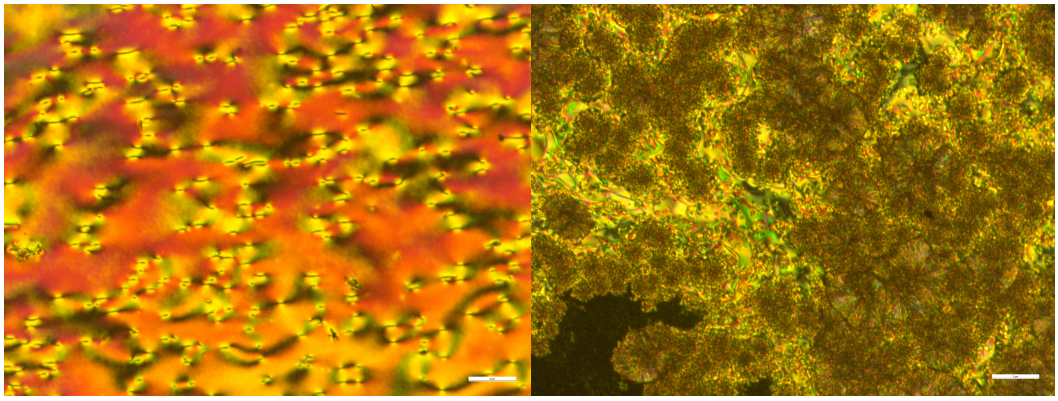

Figure S 2: Left: Cooling from Iso at 20°C, right: crystallization at 14°C.

P5:

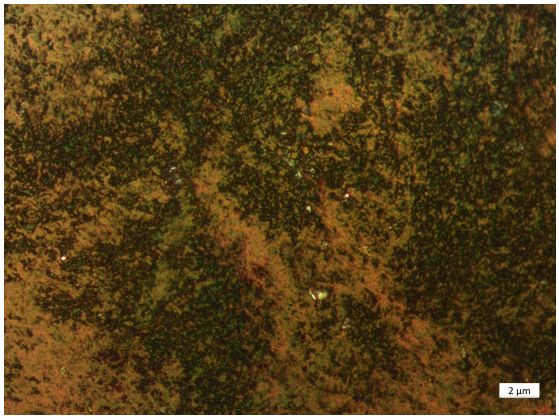

Figure S 3: Heating from rt with 30°C/min at 50°C fluid. Possible textures.

P6:

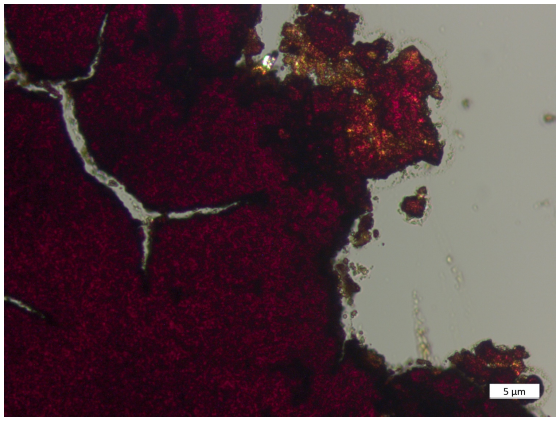

Figure S 4: Cooling from 87°C with 5°C/min. At 60°C.

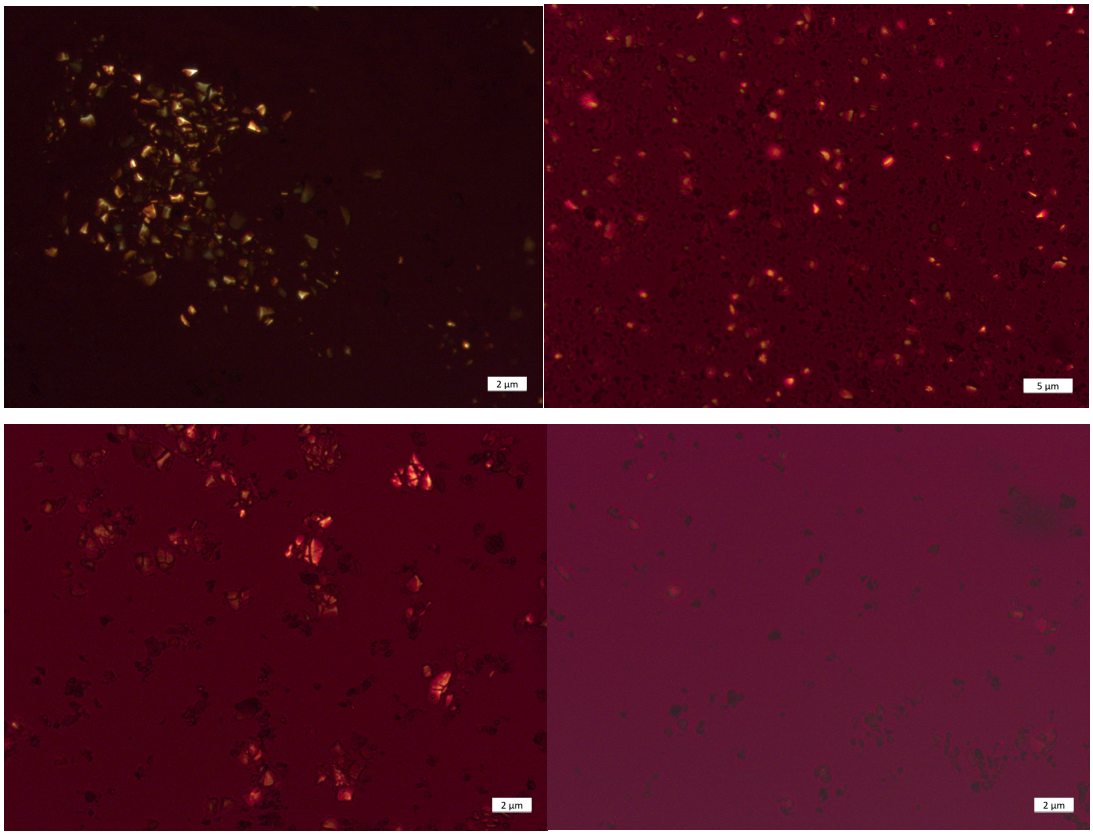

Figure S 5: Heating with 5°C/min at 80°C (top left), at 114°C (top right) and at 150°C (bottom left).

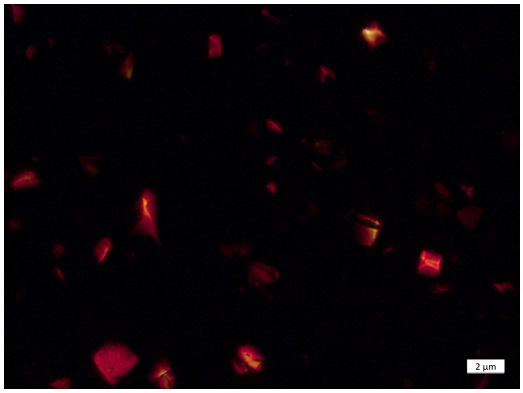

Figure S 6: Heating from 87°C to 94°C.

After cooling from 150°C with 10°C/min the sample solidifies at 25°C.

Complex 5:

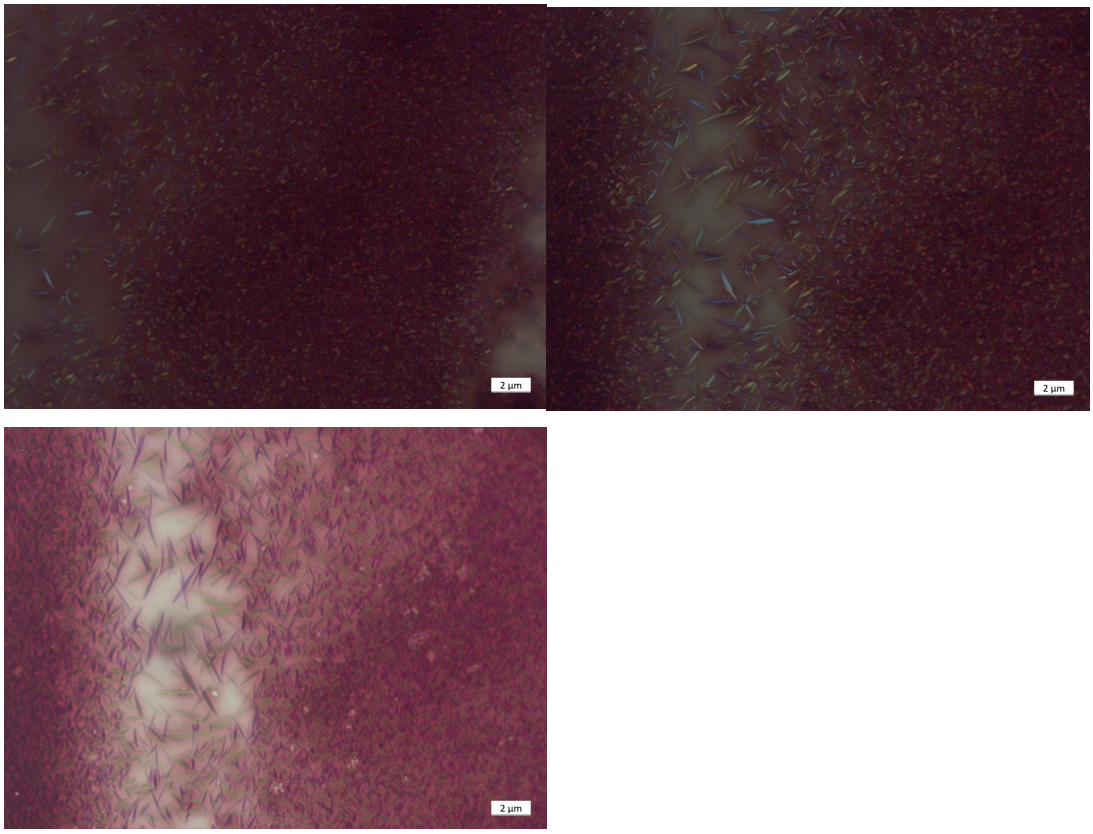

Figure S 7: Top: Cooling from 105°C with 10°C/min, at 92°C left and 87°C right with polifilter, bottom: at 72°C without polifilter.

S 4

Complex 6:

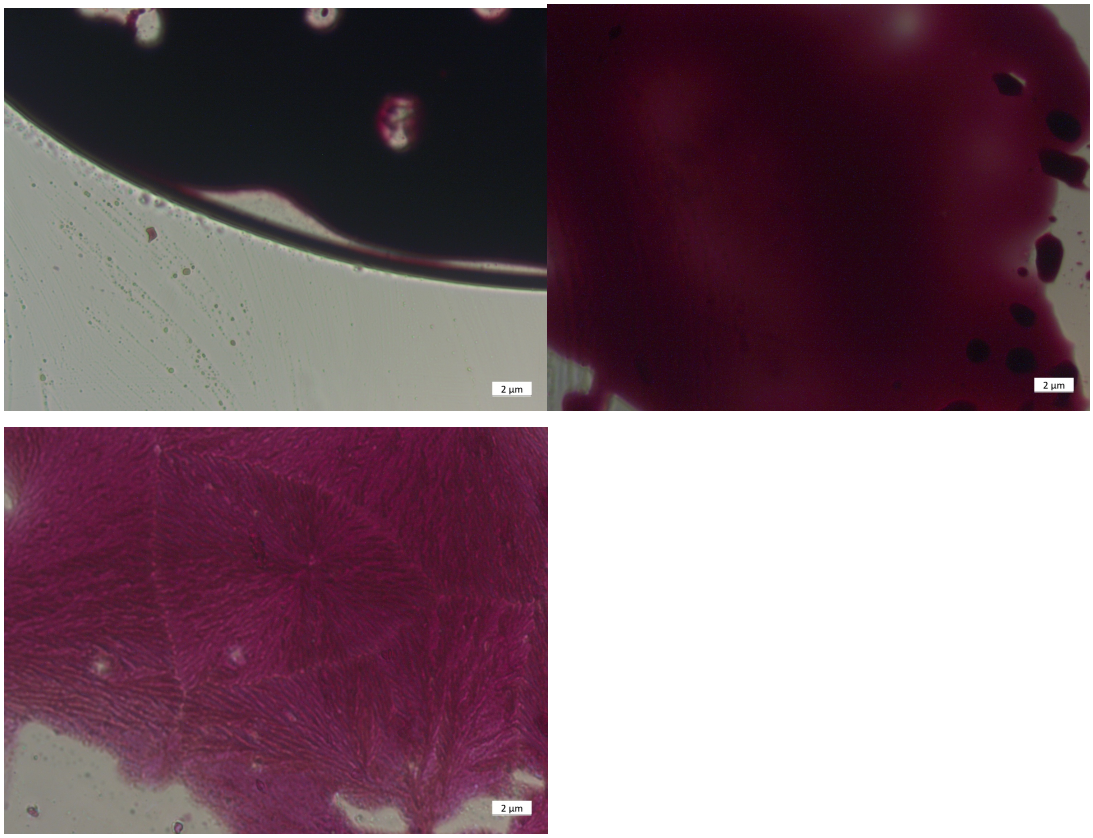

Figure S 8: Top: Heating from rt with 30°C/min at 80°C (left) and at 60°C (right). Bottom: Cooling from 80°C with 10 K/min at 44°C.

3. Differential Scanning Calorimetry

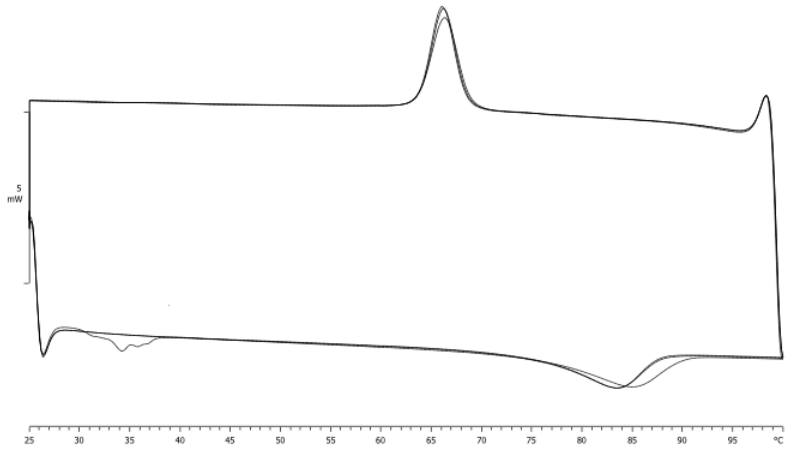

Figure S 9: DSC measurement of $(Azo_{3tetradec}Pt)_2\mu Cl_2$.

4. Cyclic Voltammetry

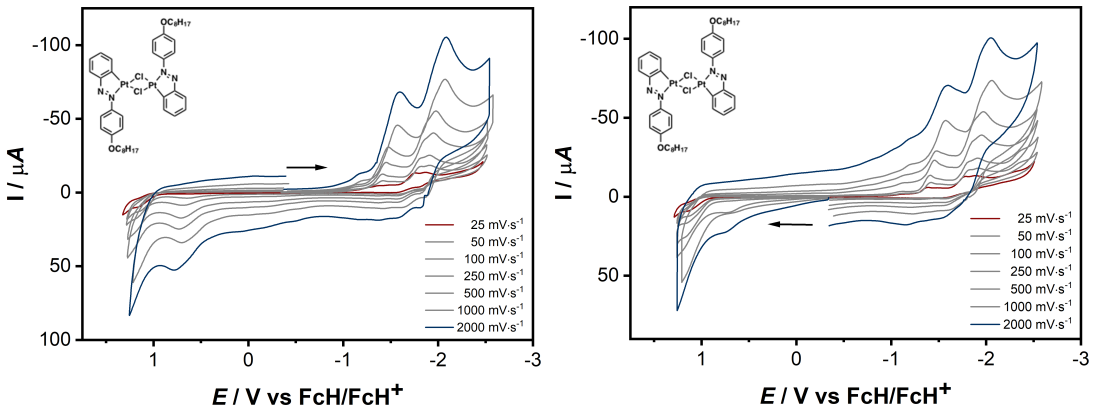

Figure S 10: Cyclic voltammogram of **P1** in a DCM solution containing 0.1 M Bu_4NPF_6 as supporting electrolyte. Left: scan direction: first reduction side than oxidation side, right: scan direction: first oxidation side than reduction side.

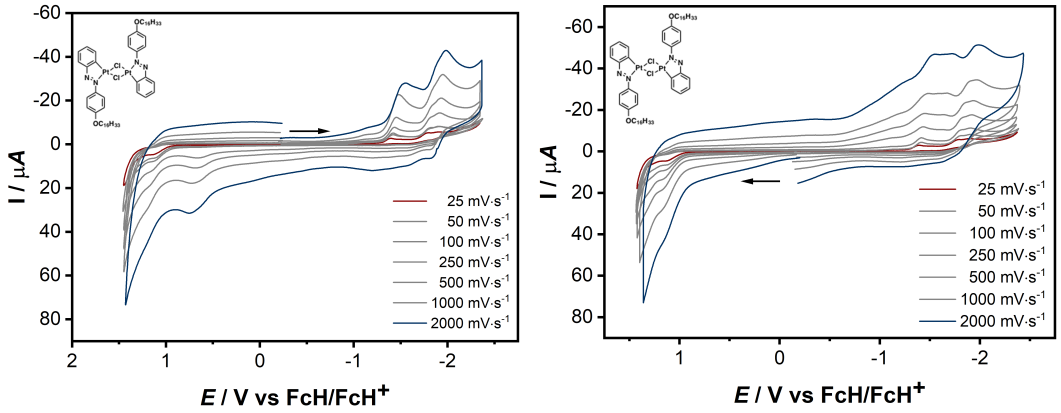

Figure S 11: Cyclic voltammogram of **P2** in a DCM solution containing 0.1 M Bu_4NPF_6 as supporting electrolyte. Left: scan direction: first reduction side than oxidation side, right: scan direction: first oxidation side than reduction side.

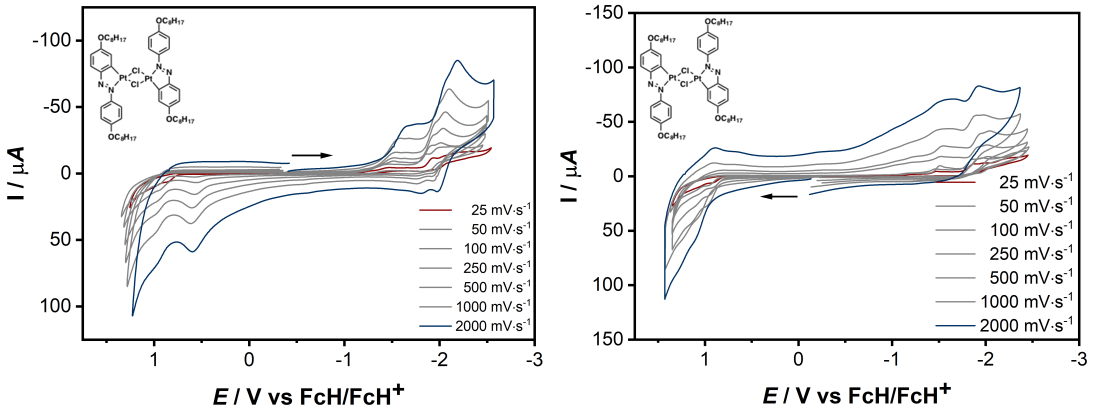

Figure S 12: Cyclic voltammogram of **P3** in a DCM solution containing 0.1 M Bu_4NPF_6 as supporting electrolyte. Left: scan direction: first reduction side than oxidation side, right: scan direction: first oxidation side than reduction side.

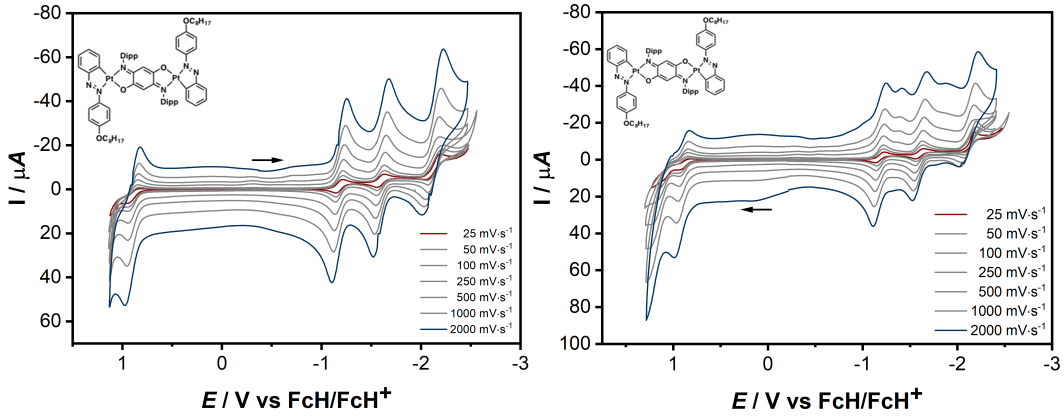

Figure S 13: Cyclic voltammogram of complex **1** in a DCM solution containing 0.1 M Bu_4NPF_6 as supporting electrolyte. Left: scan direction: first reduction side than oxidation side, right: scan direction: first oxidation side than reduction side.

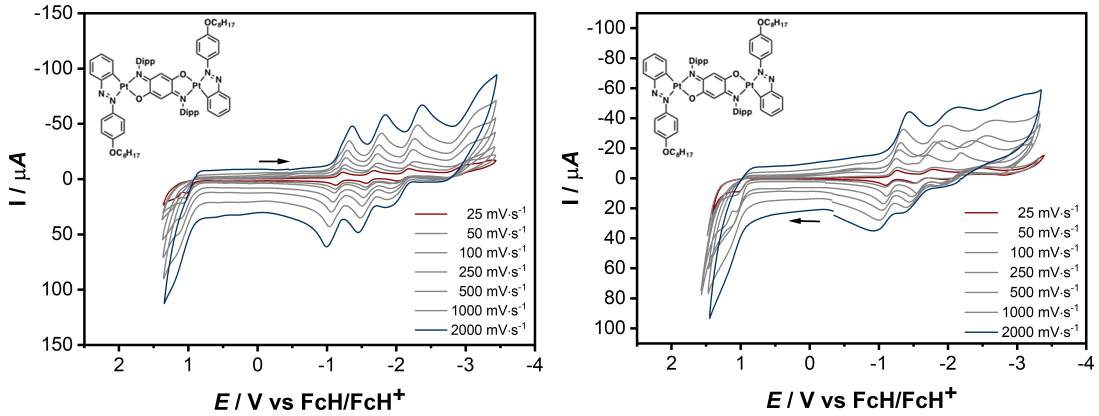

Figure S 14: Cyclic voltammogram of complex **1** in a THF solution containing 0.1 M Bu_4NPF_6 as supporting electrolyte. Left: scan direction: first reduction side than oxidation side, right: scan direction: first oxidation side than reduction side.

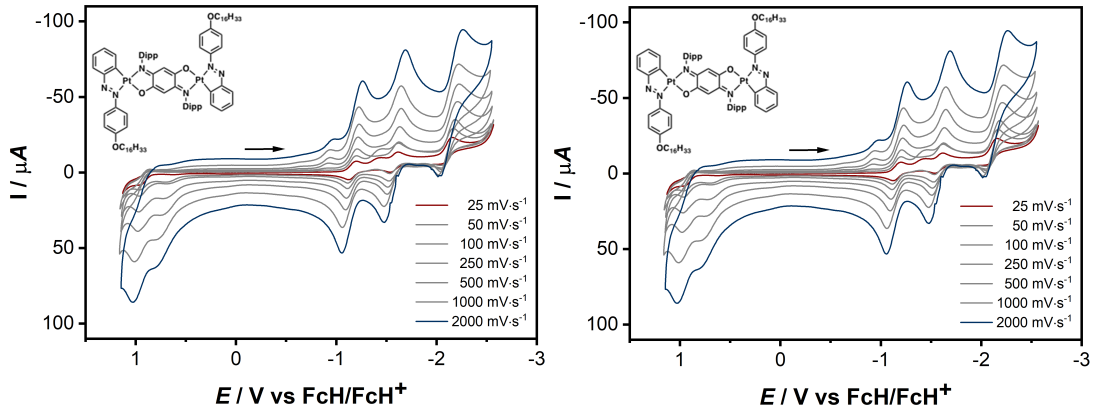

Figure S 15: Cyclic voltammogram of complex **2** in a DCM solution containing 0.1 M Bu_4NPF_6 as supporting electrolyte. Left: scan direction: first reduction side than oxidation side, right: scan direction: first oxidation side than reduction side.

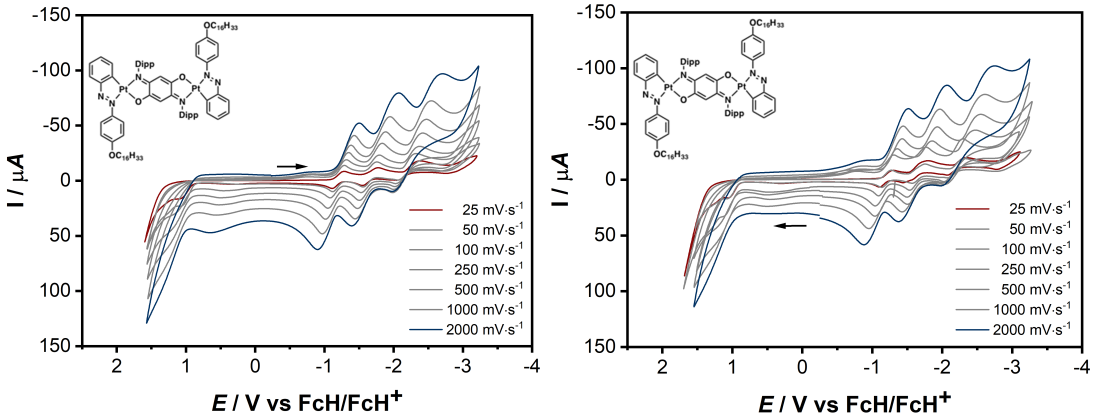

Figure S 16: Cyclic voltammogram of complex **2** in a THF solution containing 0.1 M Bu_4NPF_6 as supporting electrolyte. Left: scan direction: first reduction side than oxidation side, right: scan direction: first oxidation side than reduction side.

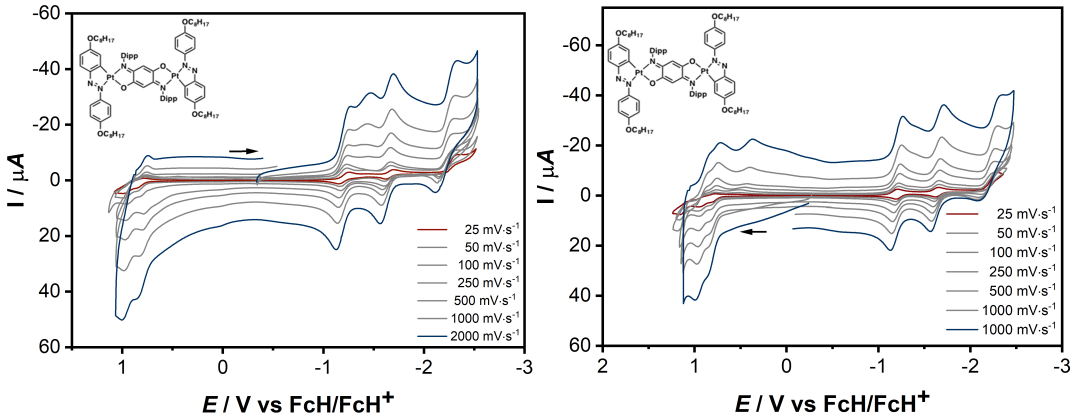

Figure S 17: Cyclic voltammogram of complex **3** in a DCM solution containing 0.1 M Bu_4NPF_6 as supporting electrolyte. Left: scan direction: first reduction side than oxidation side, right: scan direction: first oxidation side than reduction side.

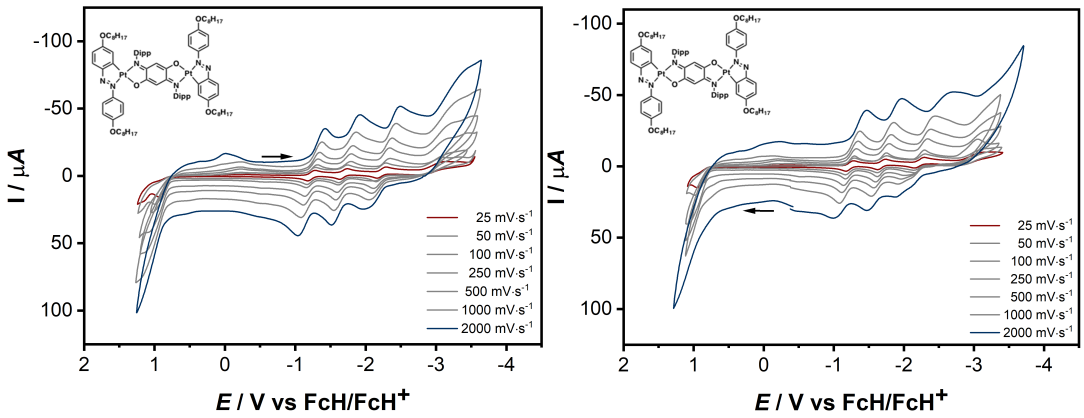

Figure S 18: Cyclic voltammogram of complex **3** in a THF solution containing 0.1 M Bu_4NPF_6 as supporting electrolyte. Left: scan direction: first reduction side than oxidation side, right: scan direction: first oxidation side than reduction side.

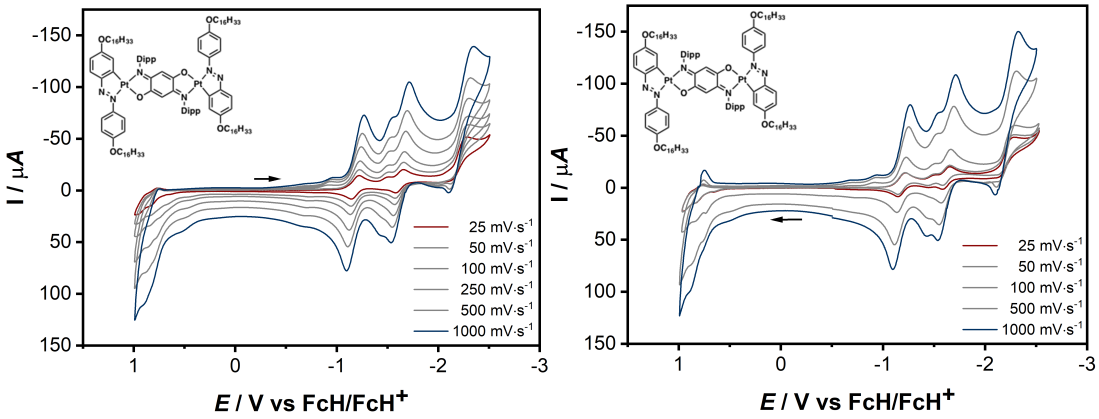

Figure S 19: Cyclic voltammogram of complex **4** in a DCM solution containing 0.1 M Bu_4NPF_6 as supporting electrolyte. Left: scan direction: first reduction side than oxidation side, right: scan direction: first oxidation side than reduction side.

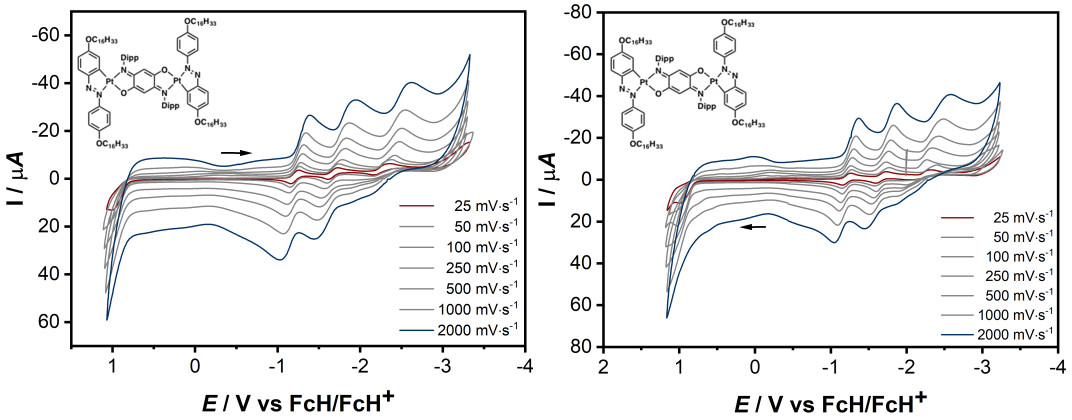

Figure S 20: Cyclic voltammogram of complex **4** in a THF solution containing 0.1 M Bu_4NPF_6 as supporting electrolyte. Left: scan direction: first reduction side than oxidation side; right: scan direction: first oxidation side than reduction side.

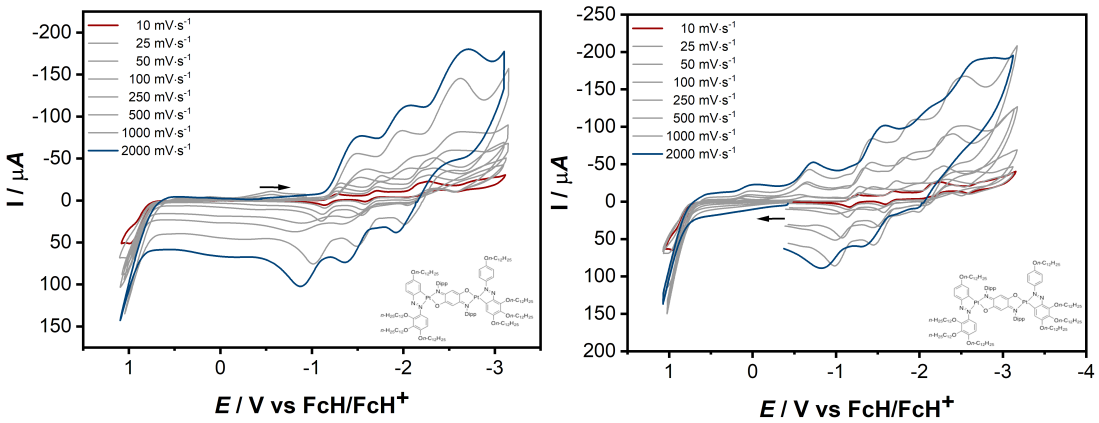

Figure S 21: Cyclic voltammogram of complex **5** in a THF solution containing 0.1 M Bu_4NPF_6 as supporting electrolyte. Left: scan direction: first reduction side than oxidation side; right: scan direction: first oxidation side than reduction side.

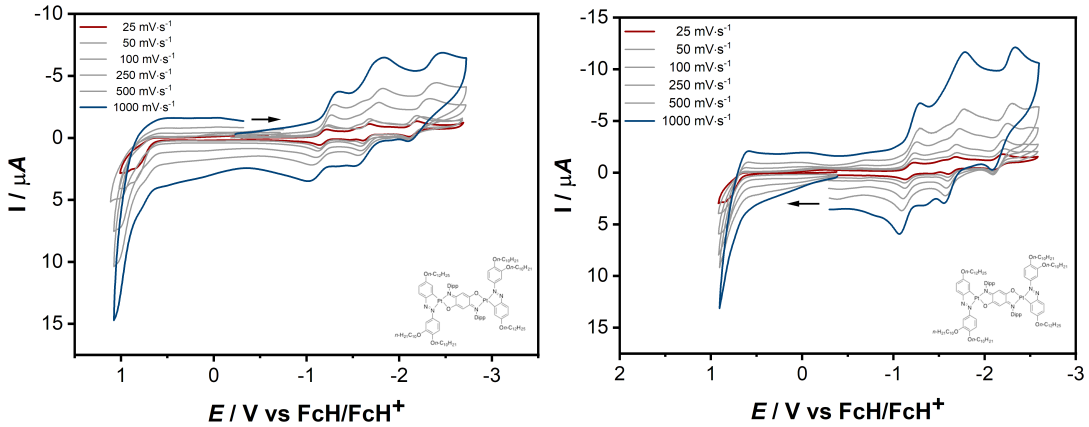

Figure S 22: Cyclic voltammogram of complex **6** in a THF solution containing 0.1 M Bu_4NPF_6 as supporting electrolyte. Left: scan direction: first reduction side than oxidation side; right: scan direction: first oxidation side than reduction side.

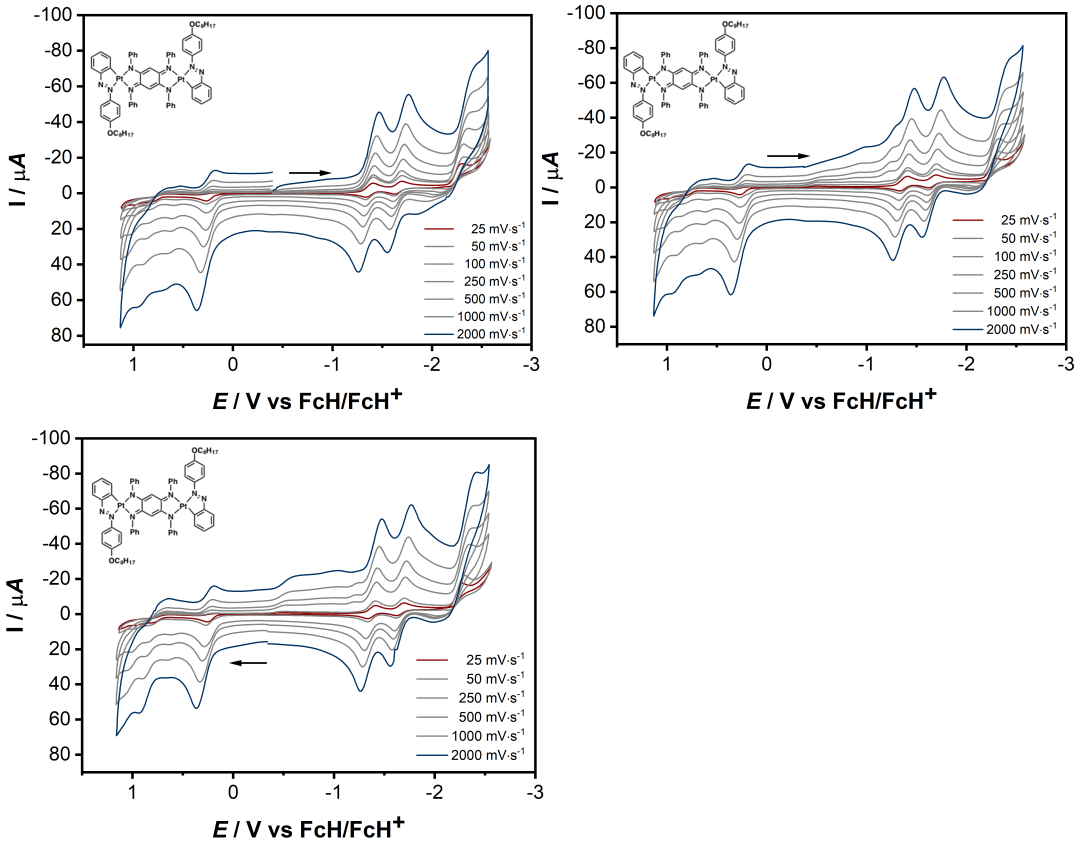

Figure S 23: Cyclic voltammogram of complex **7** in a DCM solution containing 0.1 M Bu_4NPF_6 as supporting electrolyte. Top: Left: scan direction: first reduction side than oxidation side (1st cycle), right: scan direction: first reduction side than oxidation side (2nd cycle); bottom: scan direction: first oxidation side than reduction side.

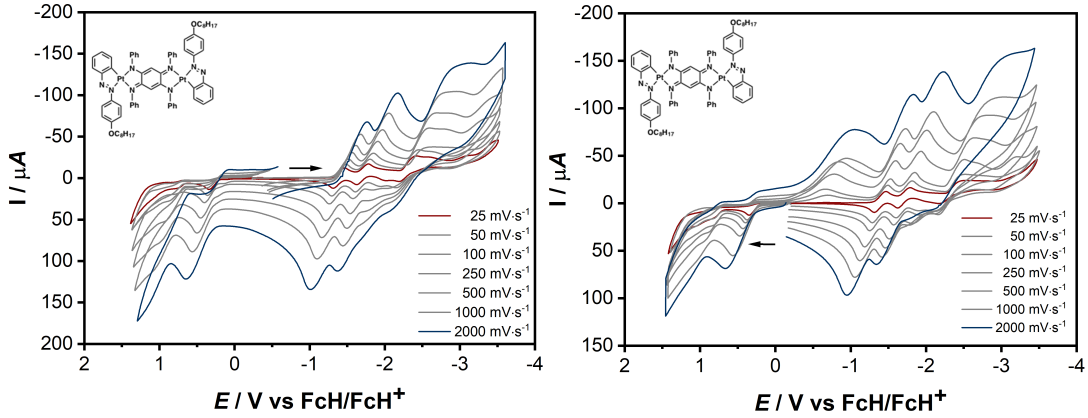

Figure S 24: Cyclic voltammogram of complex **7** in a THF solution containing 0.1 M Bu_4NPF_6 as supporting electrolyte. Left: scan direction: first reduction side than oxidation side; right: scan direction: first oxidation side than reduction side.

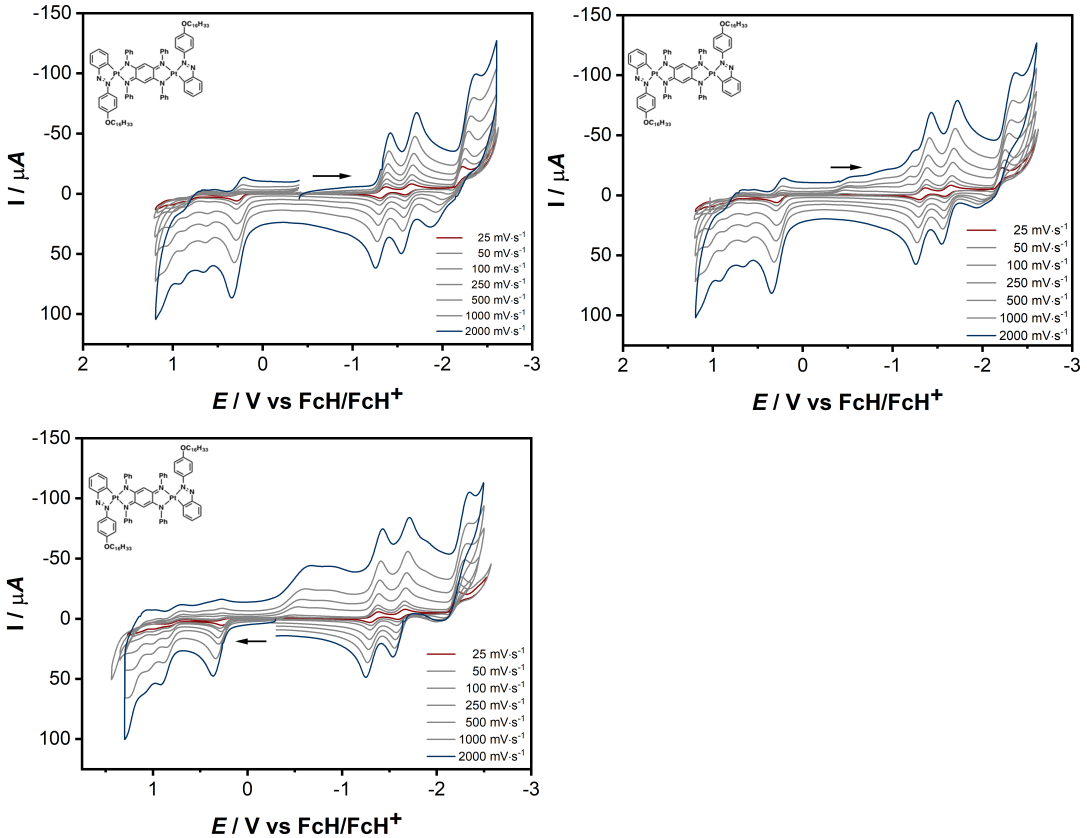

Figure S 25: Cyclic voltammogram of complex **8** in a DCM solution containing 0.1 M Bu_4NPF_6 as supporting electrolyte. Top: Left: scan direction: first reduction side than oxidation side (1st cycle), right: scan direction: first reduction side than oxidation side (2nd cycle); bottom: scan direction: first oxidation side than reduction side

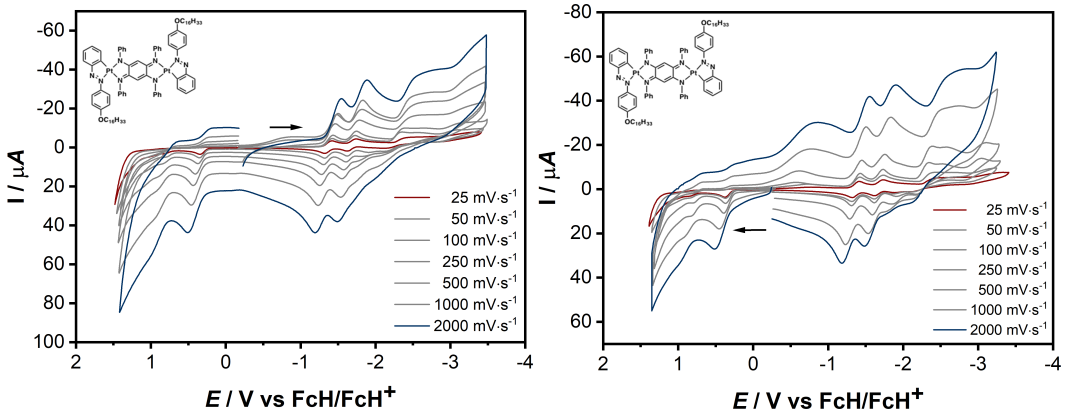

Figure S 26: Cyclic voltammogram of complex **8** in a THF solution containing 0.1 M Bu_4NPF_6 as supporting electrolyte. Left: scan direction: first reduction side than oxidation side; right: scan direction: first oxidation side than reduction side.

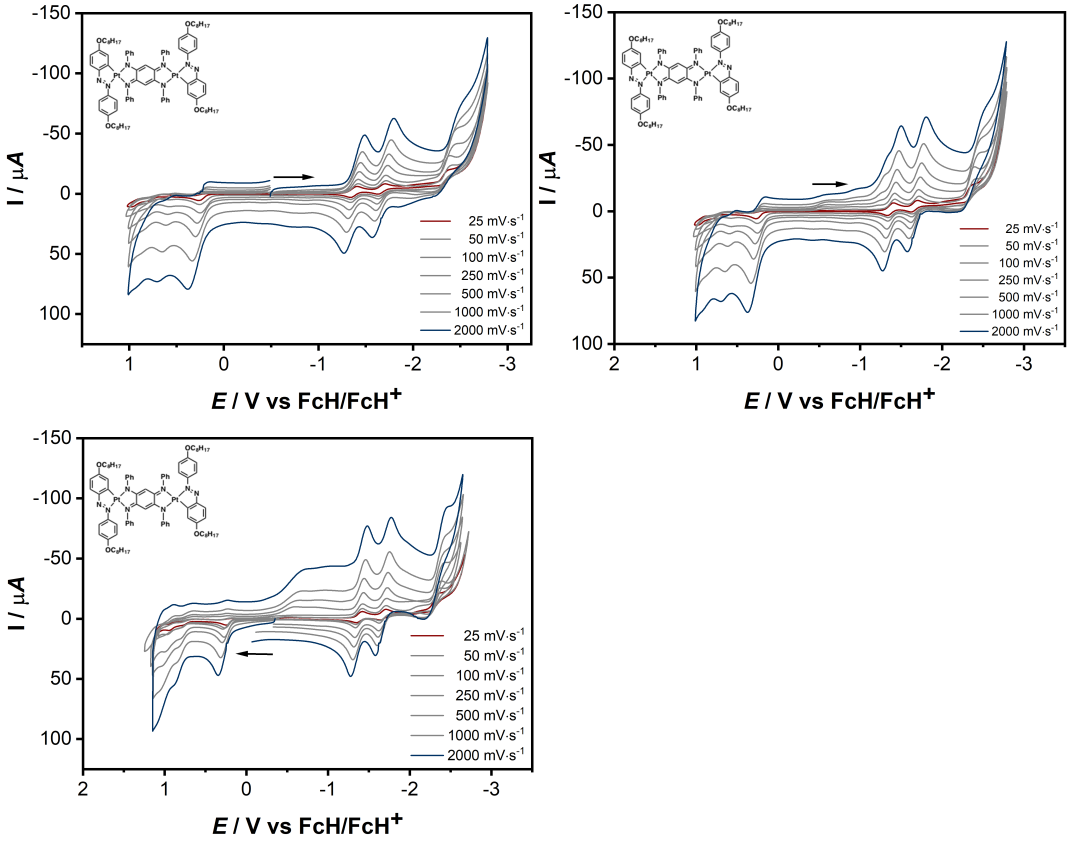

Figure S 27: Cyclic voltammogram of complex **9** in a DCM solution containing 0.1 M Bu_4NPF_6 as supporting electrolyte. Top: Left: scan direction: first reduction side than oxidation side (1st cycle), right: scan direction: first reduction side than oxidation side (2nd cycle); bottom: scan direction: first oxidation side than reduction side

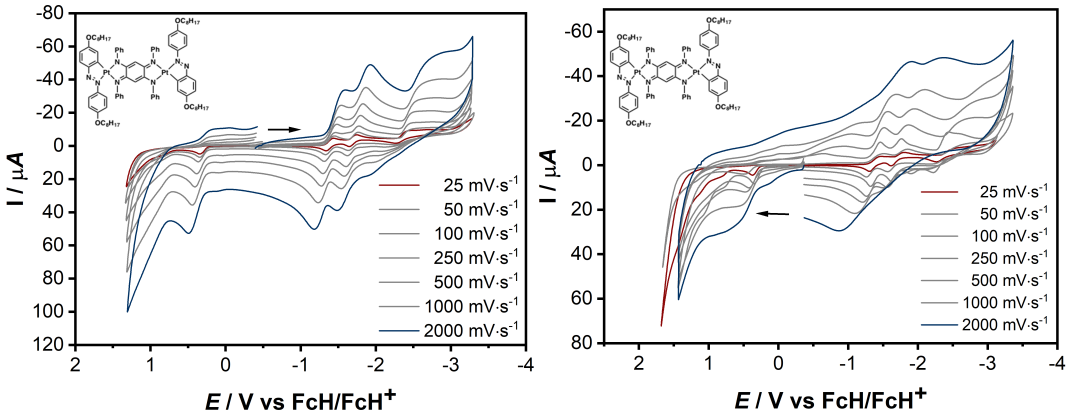

Figure S 28: Cyclic voltammogram of complex **9** in a THF solution containing 0.1 M Bu_4NPF_6 as supporting electrolyte. Left: scan direction: first reduction side than oxidation side; right: scan direction: first oxidation side than reduction side.

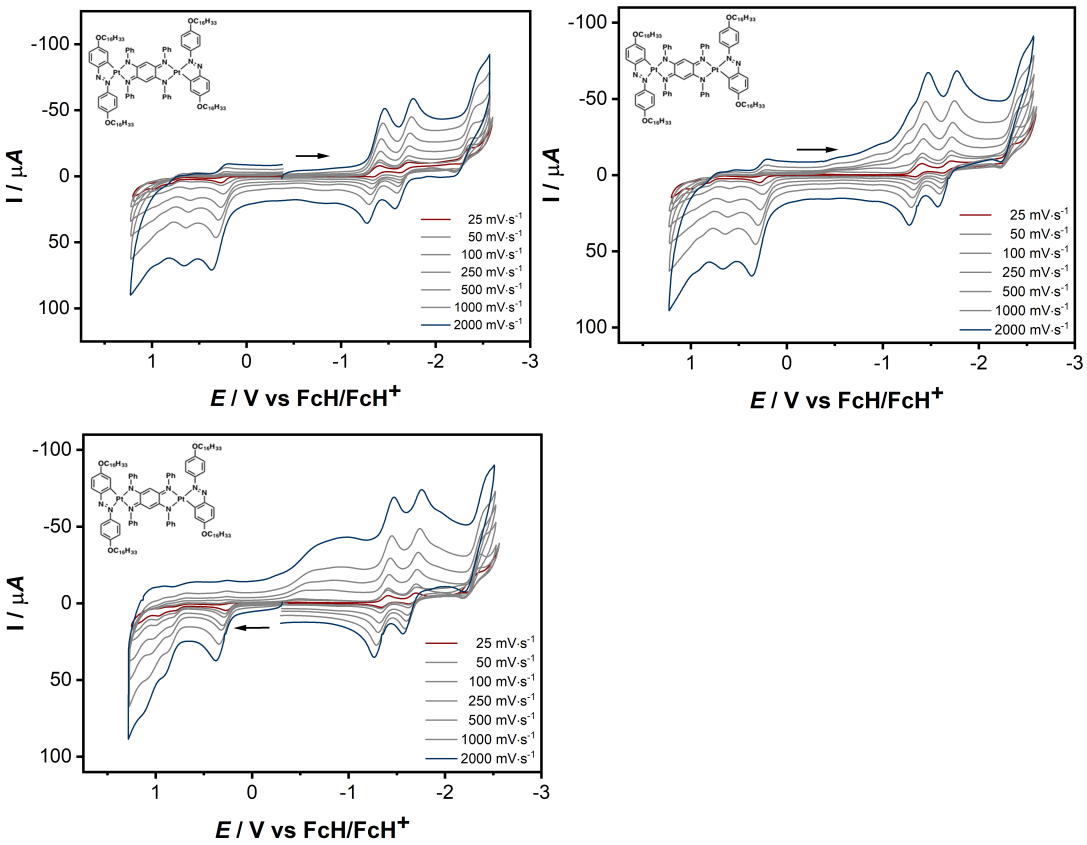

Figure S 29: Cyclic voltammogram of complex **10** in a DCM solution containing 0.1 M Bu_4NPF_6 as supporting electrolyte. Top: Left: scan direction: first reduction side than oxidation side (1st cycle), right: scan direction: first reduction side than oxidation side (2nd cycle); bottom: scan direction: first oxidation side than reduction side

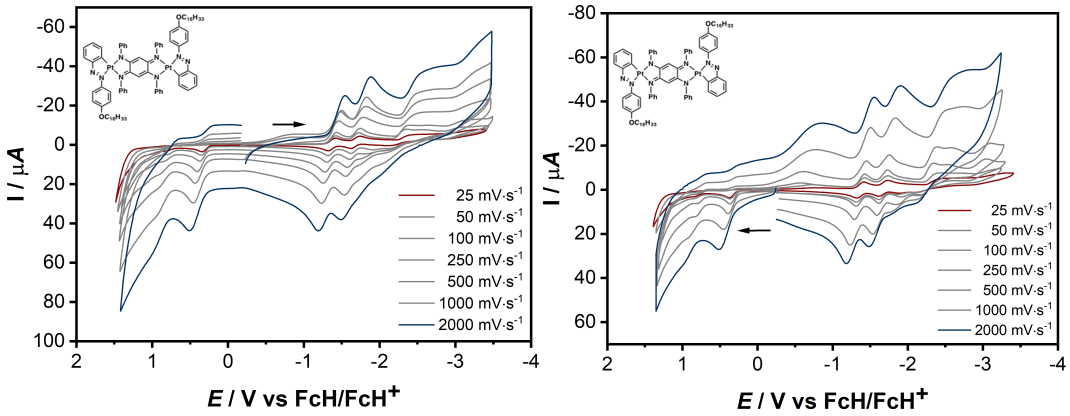

Figure S 30: Cyclic voltammogram of complex **10** in a THF solution containing 0.1 M Bu_4NPF_6 as supporting electrolyte. Left: scan direction: first reduction side than oxidation side; right: scan direction: first oxidation side than reduction side.

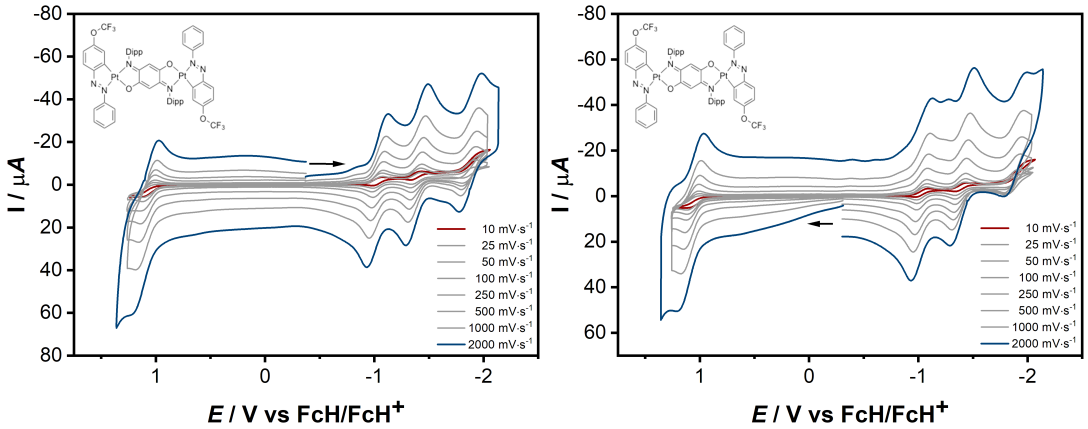

Figure S 31: Cyclic voltammogram of complex **11** in a DCM solution containing 0.1 M Bu_4NPF_6 as supporting electrolyte. Left: scan direction: first reduction side than oxidation side; right: scan direction: first oxidation side than reduction side.

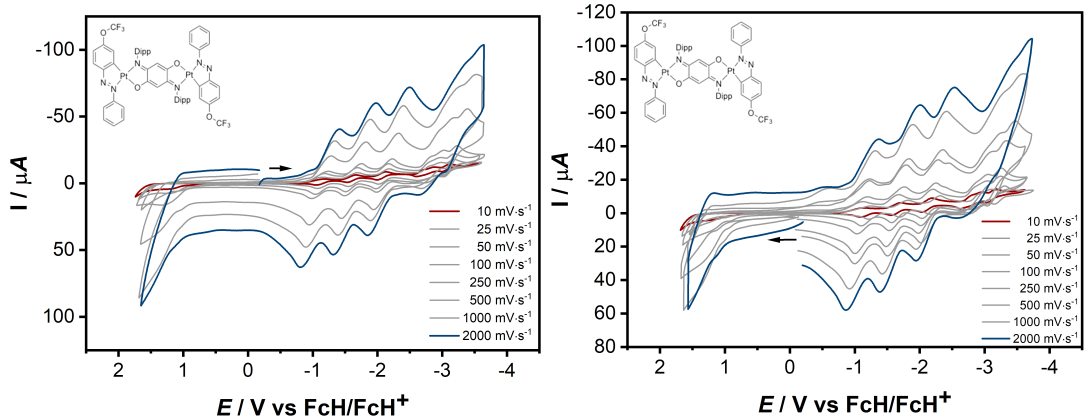

Figure S 32: Cyclic voltammogram of complex **11** in a THF solution containing 0.1 M Bu_4NPF_6 as supporting electrolyte. Left: scan direction: first reduction side than oxidation side; right: scan direction: first oxidation side than reduction side.

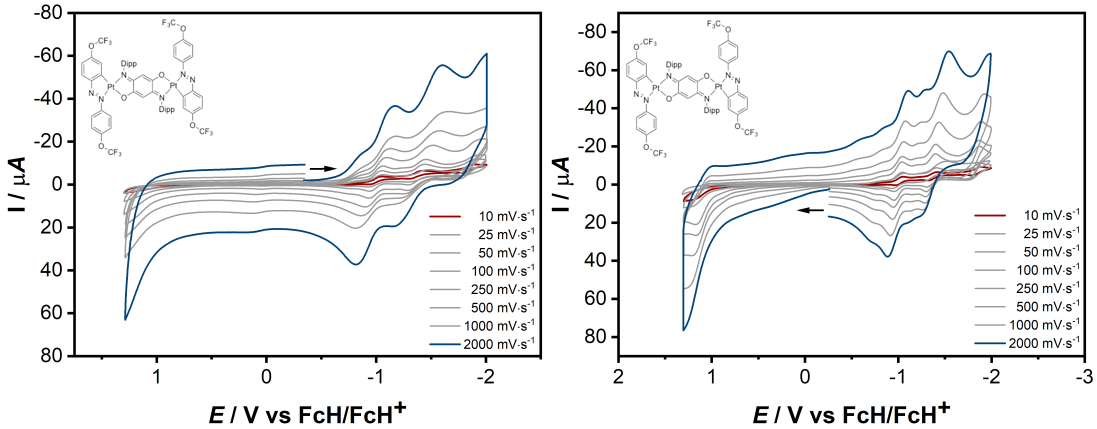

Figure S 33: Cyclic voltammogram of complex **12** in a DCM solution containing 0.1 M Bu_4NPF_6 as supporting electrolyte. Left: scan direction: first reduction side than oxidation side; right: scan direction: first oxidation side than reduction side.

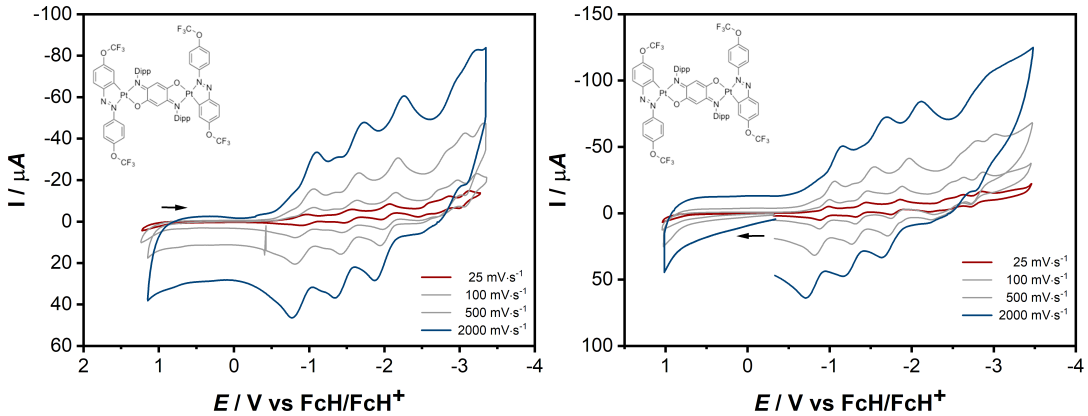

Figure S 34: Cyclic voltammogram of complex **12** in a THF solution containing 0.1 M Bu_4NPF_6 as supporting electrolyte. Left: scan direction: first reduction side than oxidation side; right: scan direction: first oxidation side than reduction side.

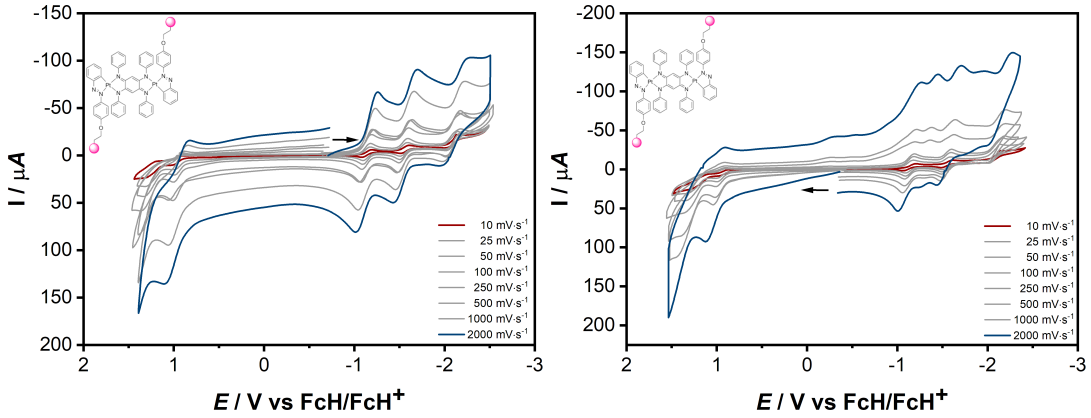

Figure S 35: Cyclic voltammogram of complex **13** in a DCM solution containing 0.1 M Bu_4NPF_6 as supporting electrolyte. Left: scan direction: first reduction side than oxidation side; right: scan direction: first oxidation side than reduction side.

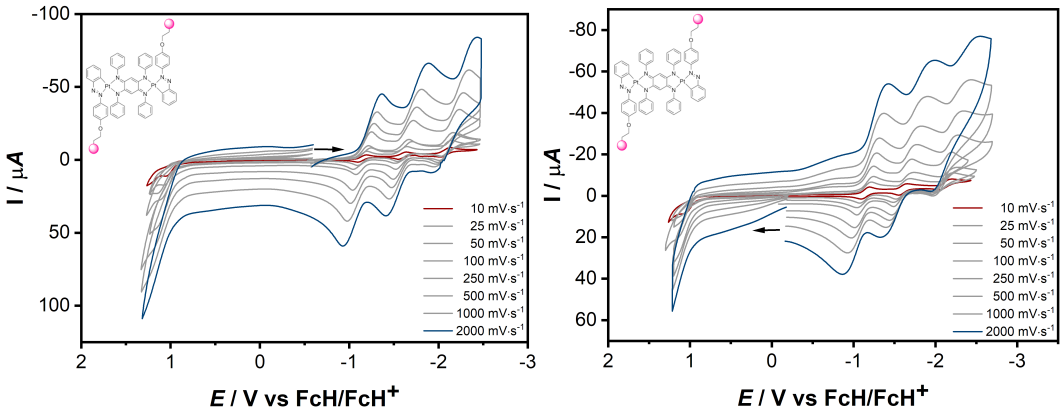

Figure S 36: Cyclic voltammogram of complex **13** in a THF solution containing 0.1 M Bu_4NPF_6 as supporting electrolyte. Left: scan direction: first reduction side than oxidation side; right: scan direction: first oxidation side than reduction side.

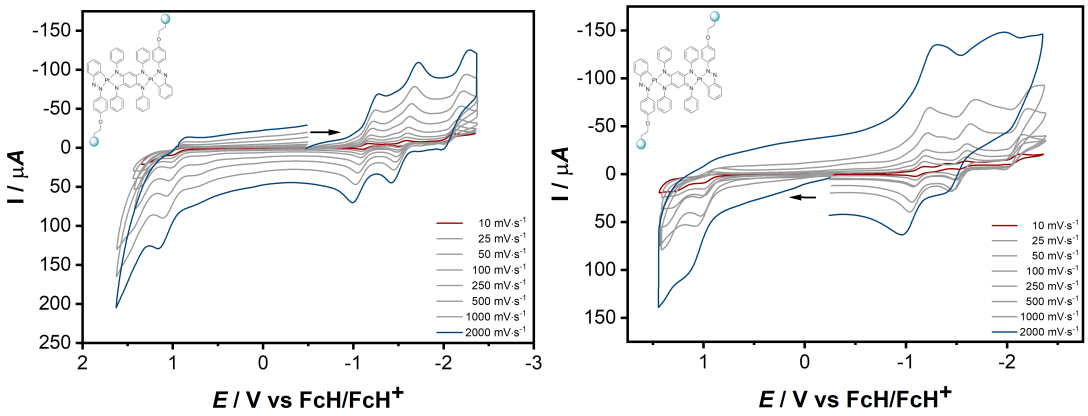

Figure S 37: Cyclic voltammogram of complex **14** in a DCM solution containing 0.1 M Bu_4NPF_6 as supporting electrolyte. Left: scan direction: first reduction side than oxidation side; right: scan direction: first oxidation side than reduction side.

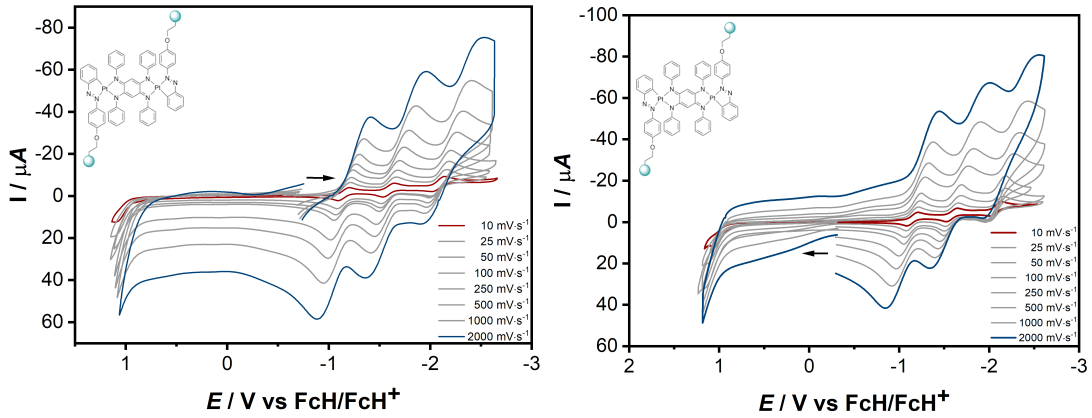

Figure S 38: Cyclic voltammogram of complex **14** in a THF solution containing 0.1 M Bu_4NPF_6 as supporting electrolyte. Left: scan direction: first reduction side than oxidation side; right: scan direction: first oxidation side than reduction side.

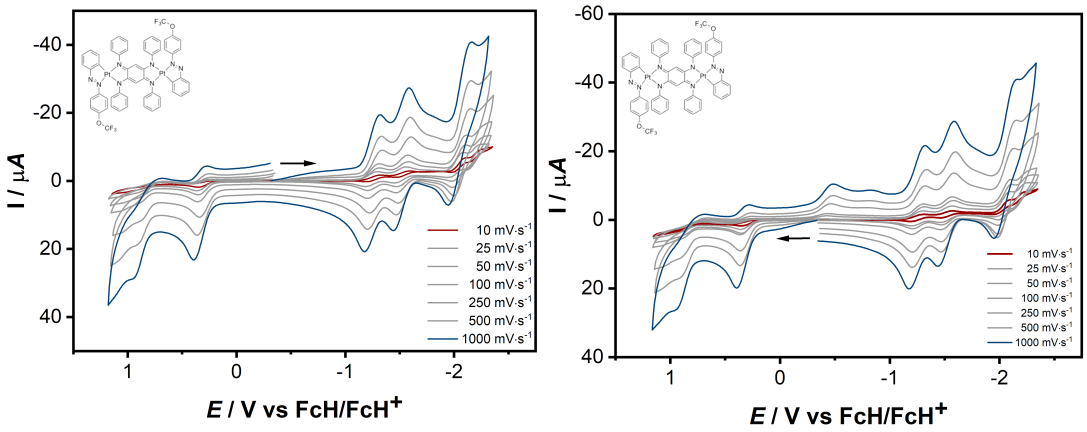

Figure S 39: Cyclic voltammogram of complex **15** in a DCM solution containing 0.1 M Bu_4NPF_6 as supporting electrolyte. Left: scan direction: first reduction side than oxidation side; right: scan direction: first oxidation side than reduction side.

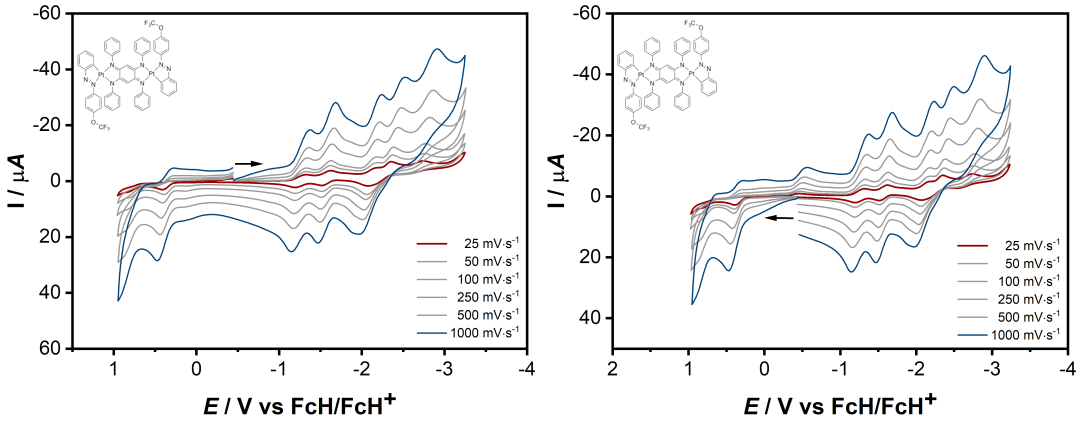

Figure S 40: Cyclic voltammogram of complex **15** in a THF solution containing 0.1 M Bu_4NPF_6 as supporting electrolyte. Left: scan direction: first reduction side than oxidation side; right: scan direction: first oxidation side than reduction side.

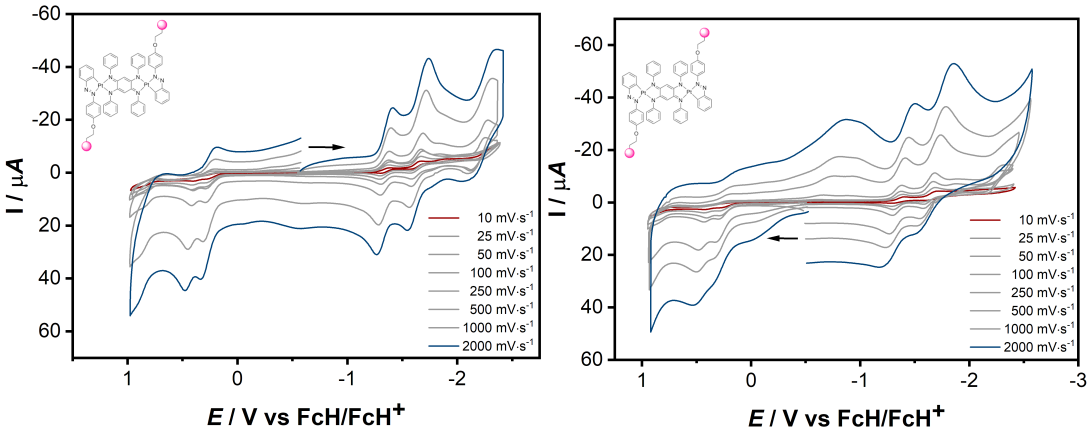

Figure S 41: Cyclic voltammogram of complex **16** in a DCM solution containing 0.1 M Bu_4NPF_6 as supporting electrolyte. Left: scan direction: first reduction side than oxidation side; right: scan direction: first oxidation side than reduction side.

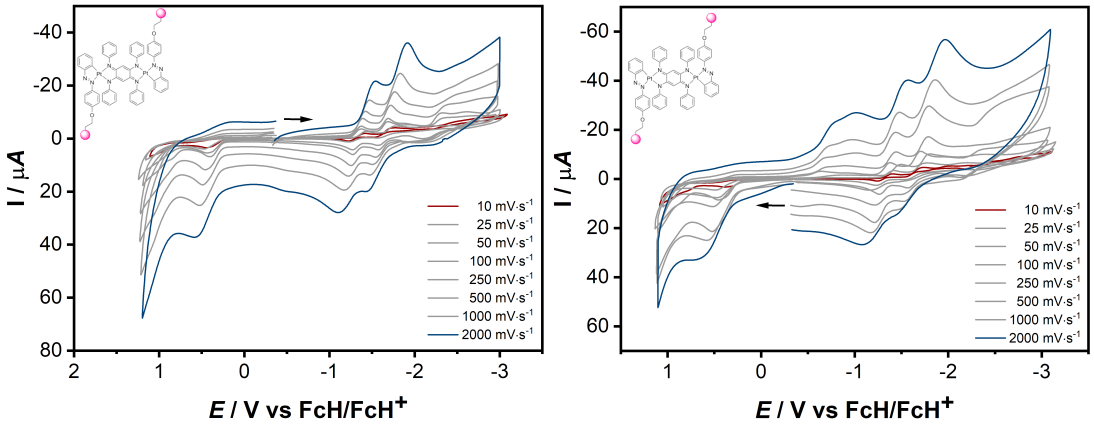

Figure S 42: Cyclic voltammogram of complex **16** in a THF solution containing 0.1 M Bu_4NPF_6 as supporting electrolyte. Left: scan direction: first reduction side than oxidation side; right: scan direction: first oxidation side than reduction side.

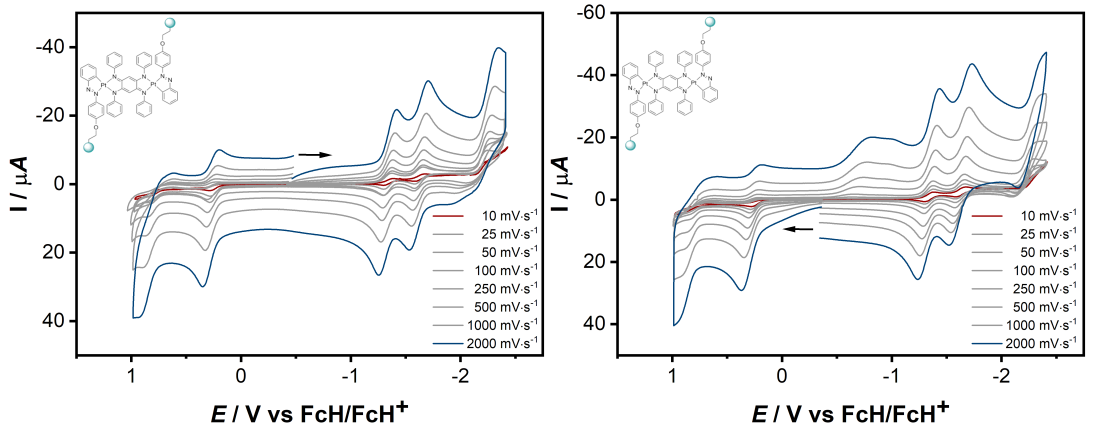

Figure S 43: Cyclic voltammogram of complex **17** in a DCM solution containing 0.1 M Bu_4NPF_6 as supporting electrolyte. Left: scan direction: first reduction side than oxidation side; right: scan direction: first oxidation side than reduction side.

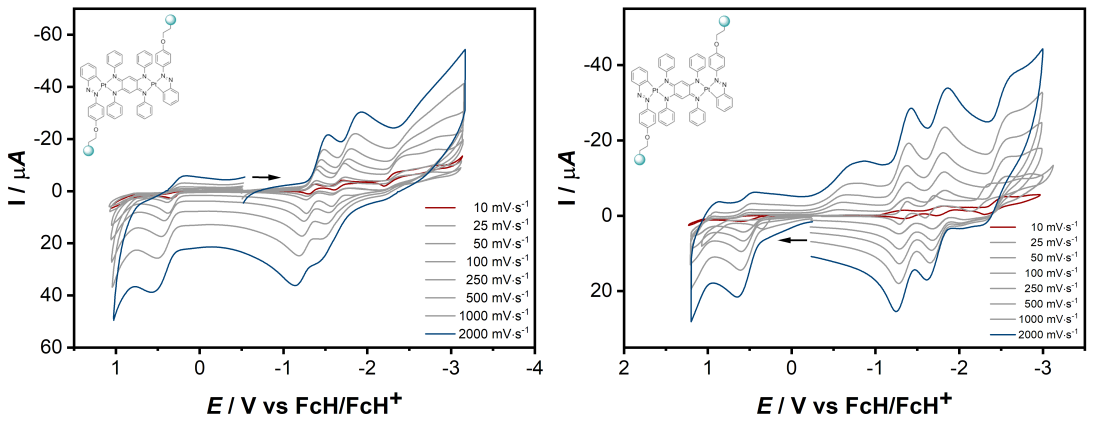

Figure S 44: Cyclic voltammogram of complex **17** in a THF solution containing 0.1 M Bu_4NPF_6 as supporting electrolyte. Left: scan direction: first reduction side than oxidation side; right: scan direction: first oxidation side than reduction side.

5. UV/Vis/NIR Spectroelectrochemistry

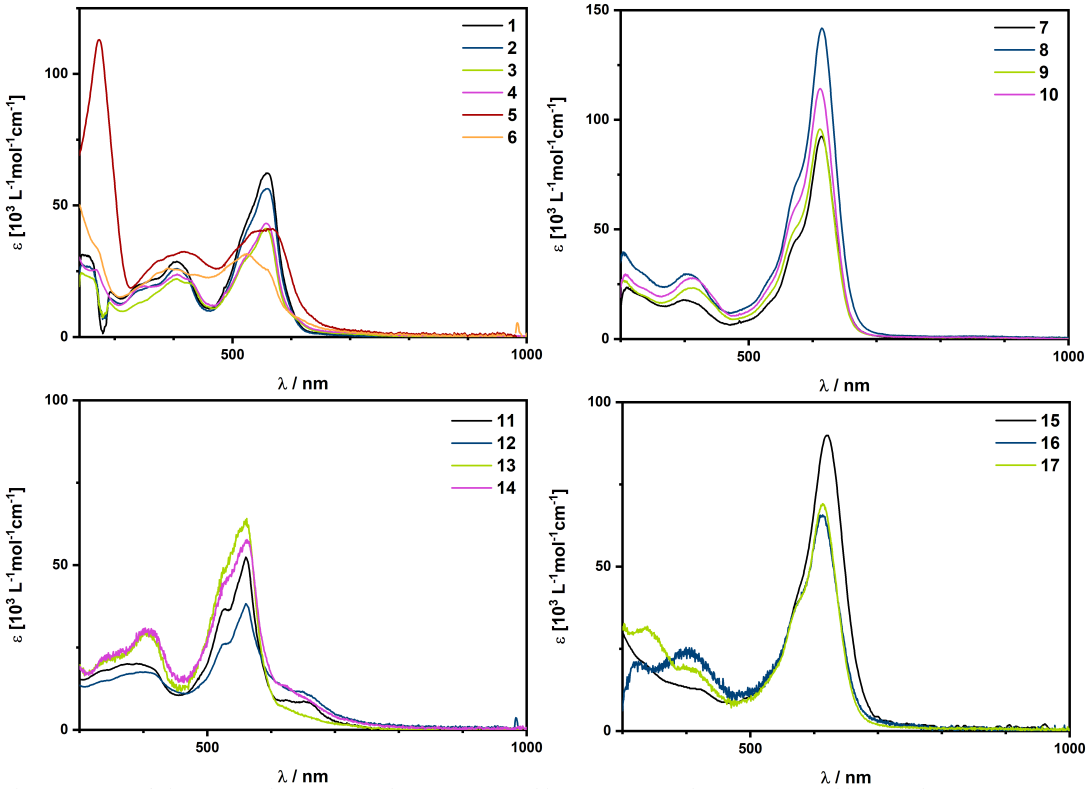

Figure S 45: UV/Vis spectra of **1-17**, **1-6** and **11-14** measured in THF, **7-10** and **15-17** measured in CH_2Cl_2.

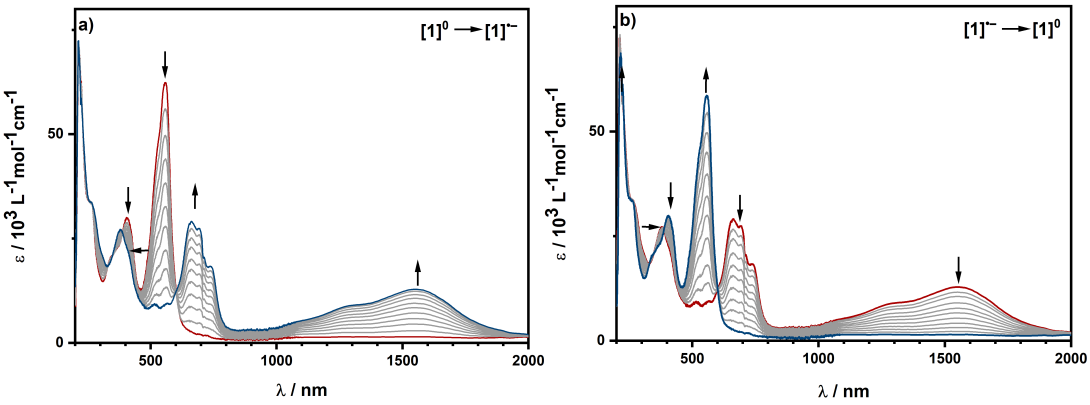

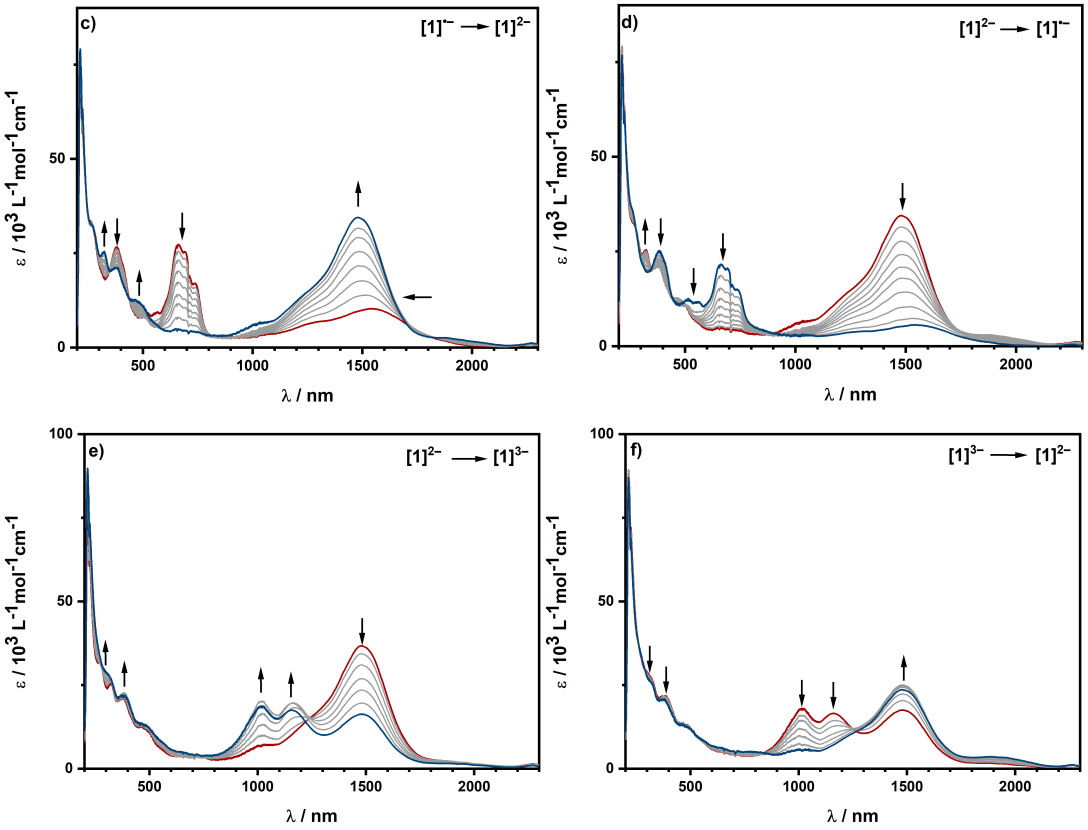

Figure S 46: UV/Vis/NIR SEC spectra of complex **1** in THF/NBu_4PF_6 measured with a gold working electrode.

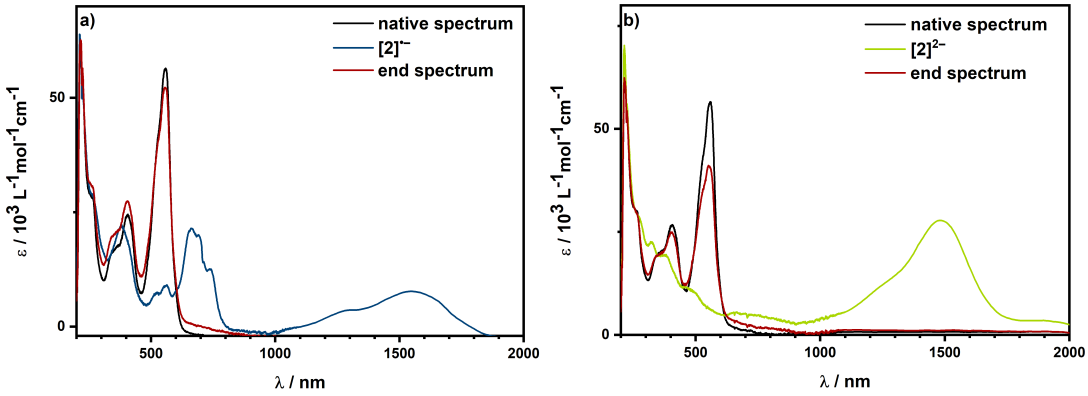

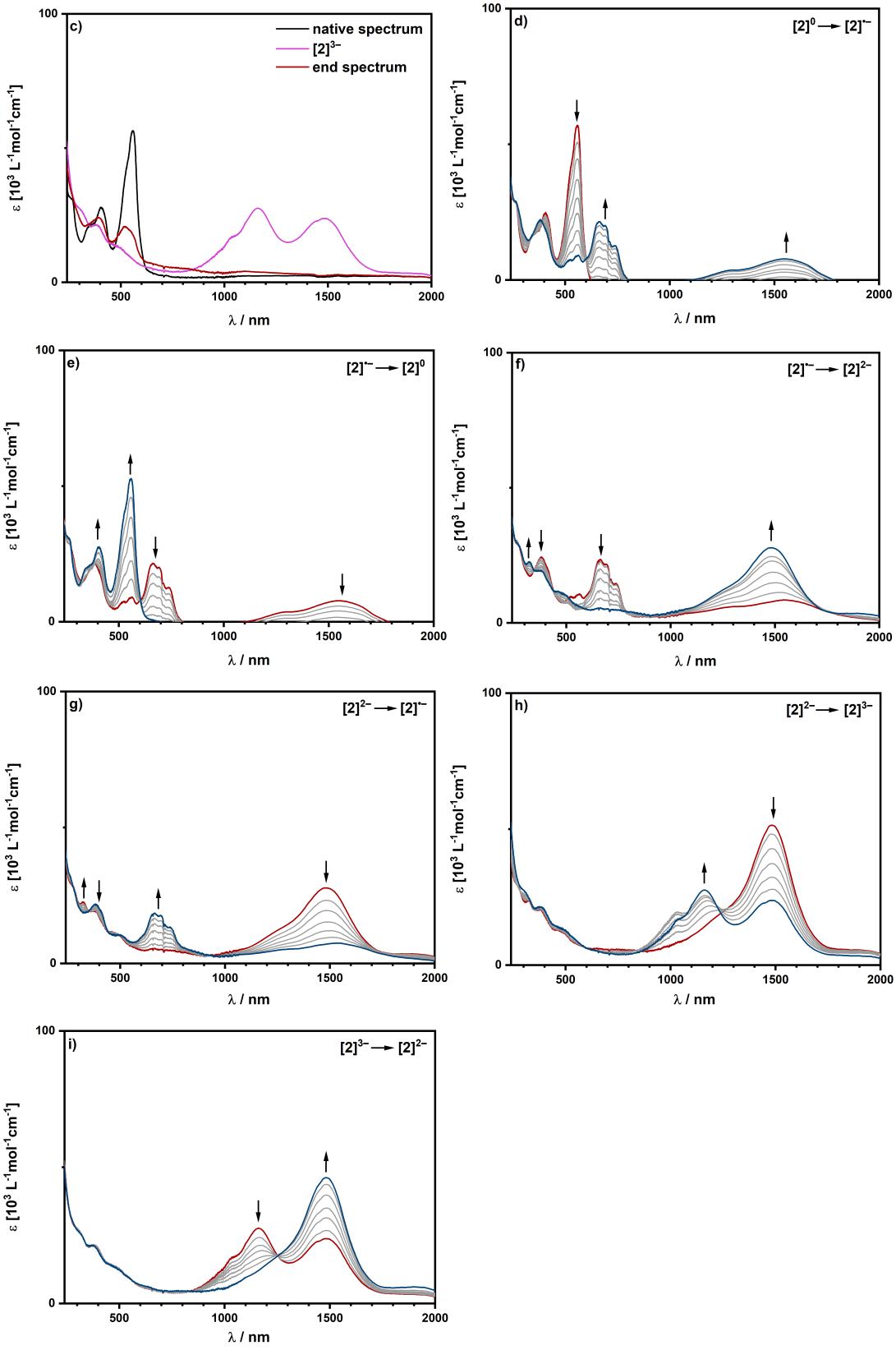

Figure S 47: UV/Vis/NIR SEC spectra of complex **2** in THF/NBu_4PF_6 measured with a gold working electrode.

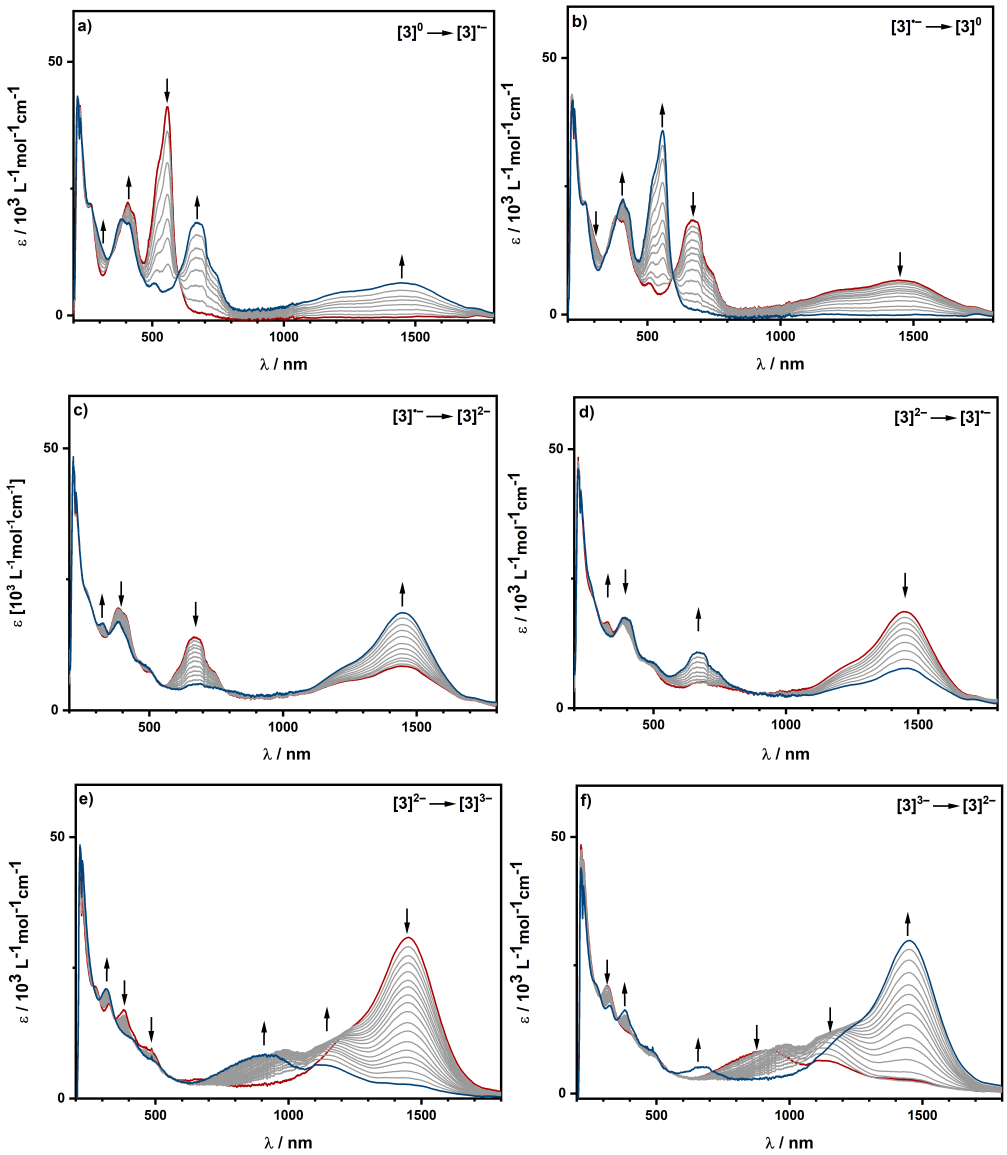

Figure S 48: UV/Vis/NIR SEC spectra of complex **3** in THF/NBu_4PF_6 measured with a gold working electrode.

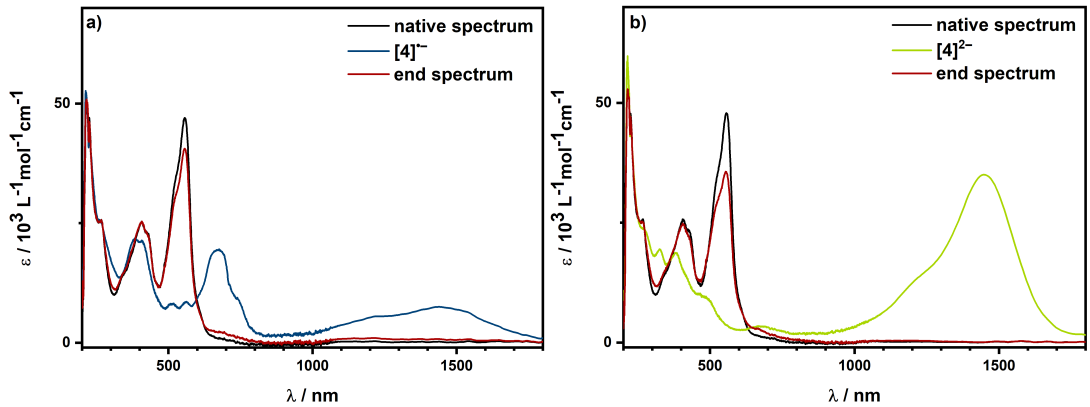

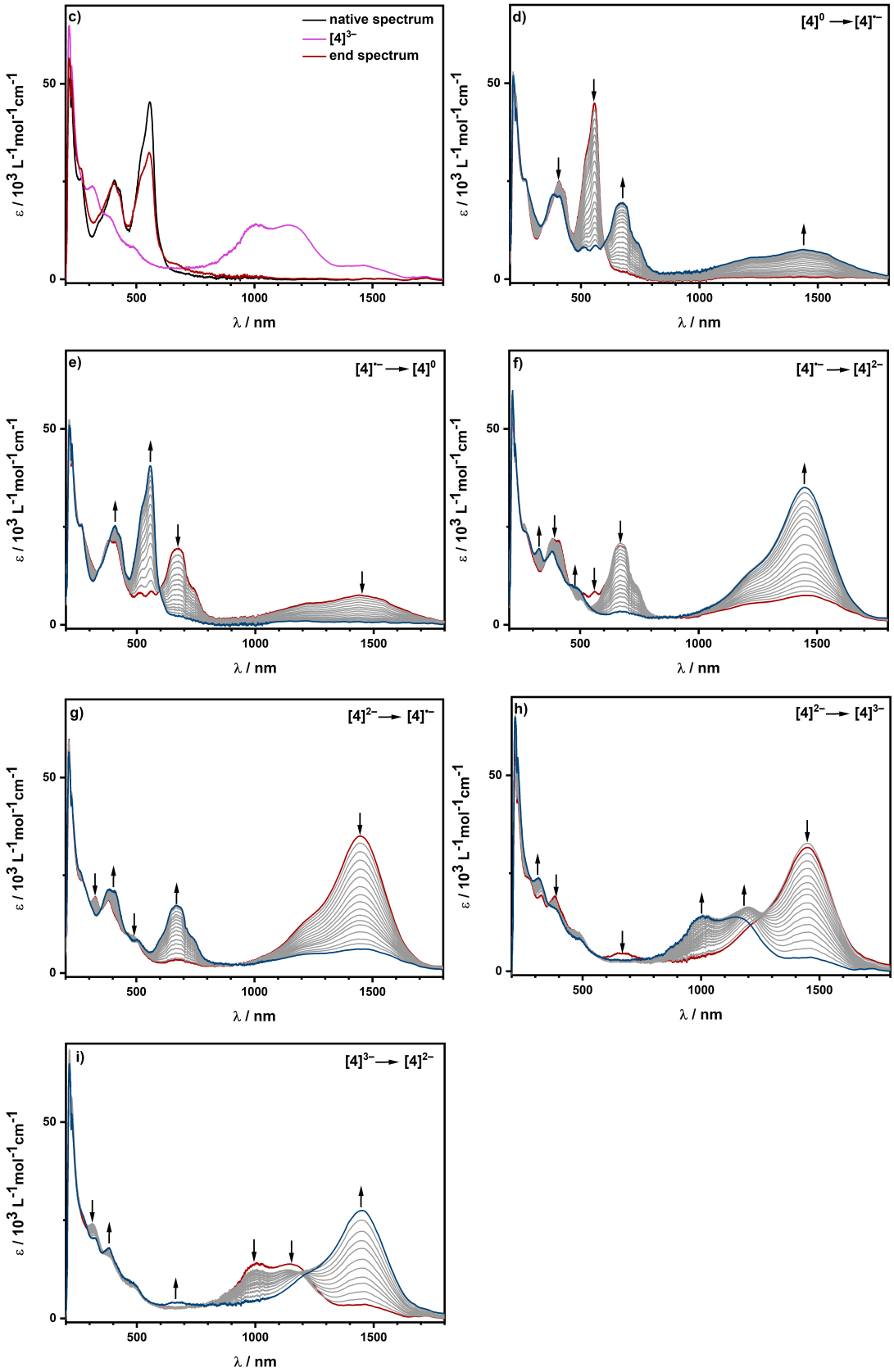

Figure S 49: UV/Vis/NIR SEC spectra of complex **4** in THF/NBu_4PF_6 measured with a gold working electrode.

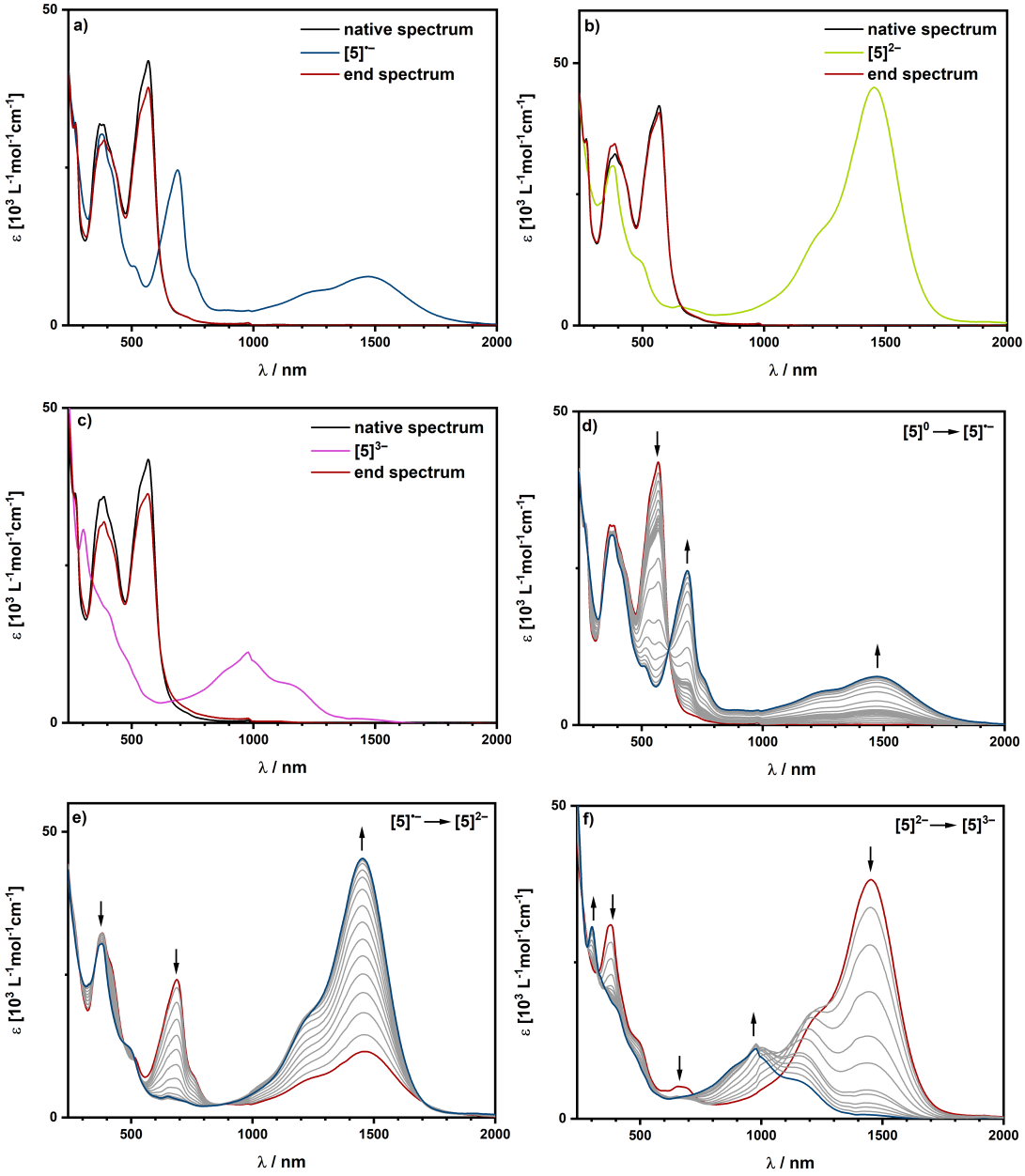

Figure S 50: UV/Vis/NIR SEC spectra of complex **5** in THF/NBu_4PF_6 measured with a gold working electrode.

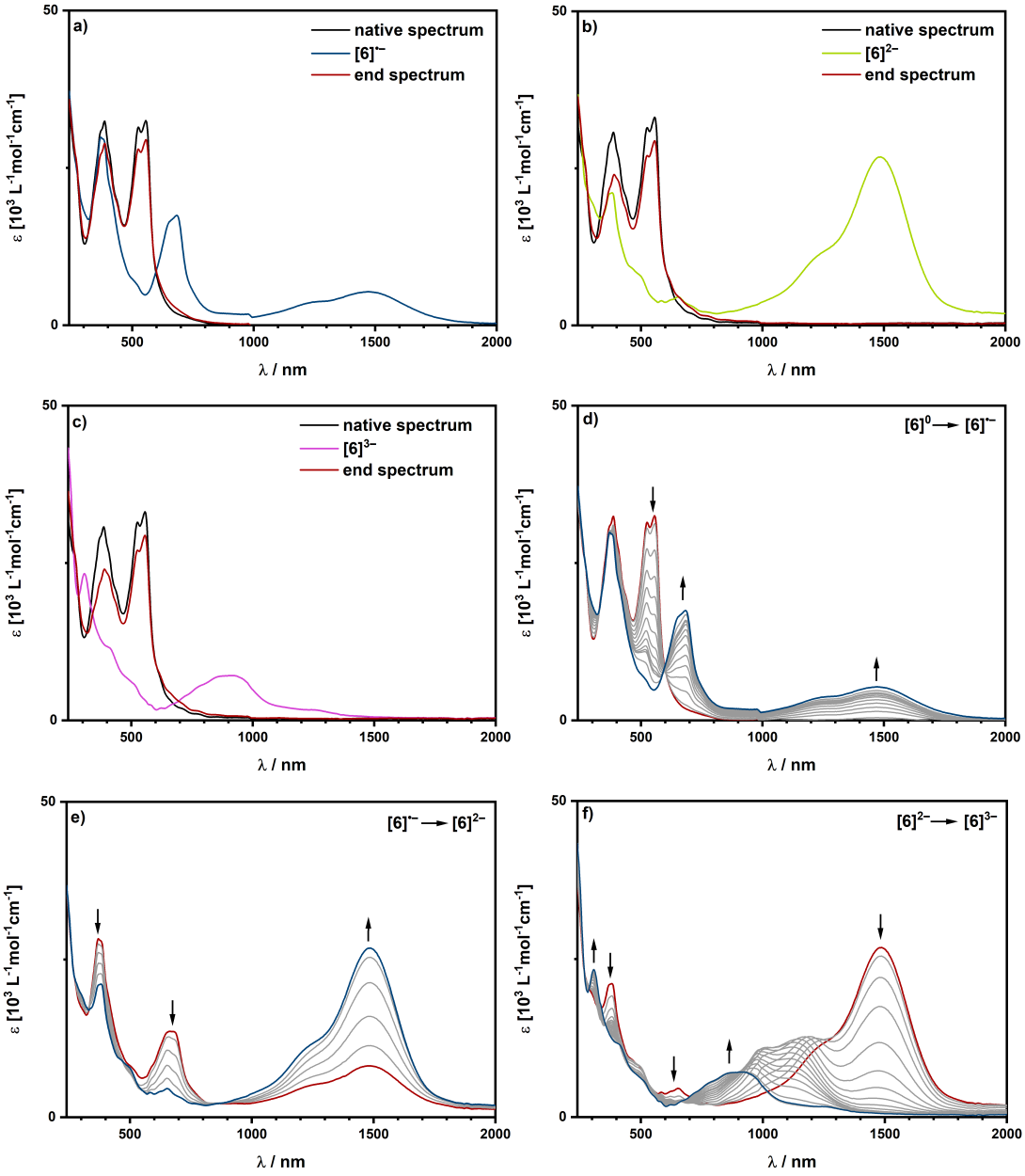

Figure S 51: UV/Vis/NIR SEC spectra of complex **6** in THF/NBu_4PF_6 measured with a gold working electrode.

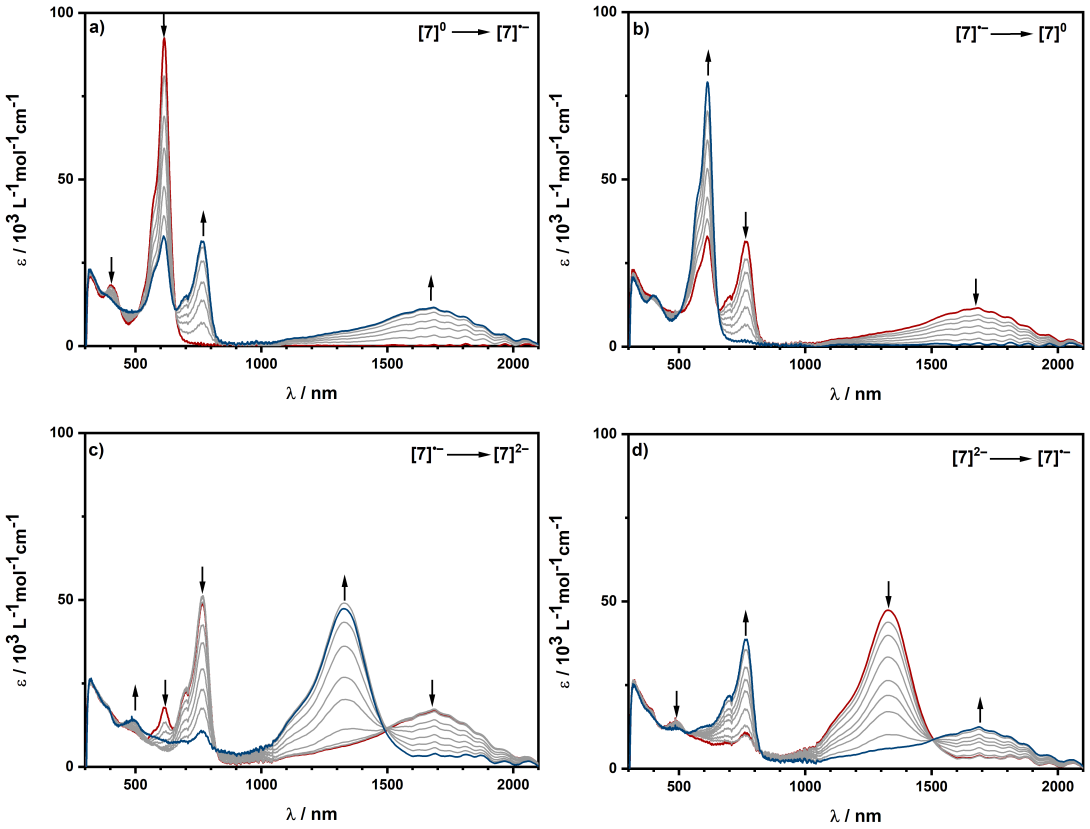

Figure S 52: UV/Vis/NIR SEC spectra of complex **7** in CH_2Cl_2/NBu_4PF_6 measured with a gold working electrode.

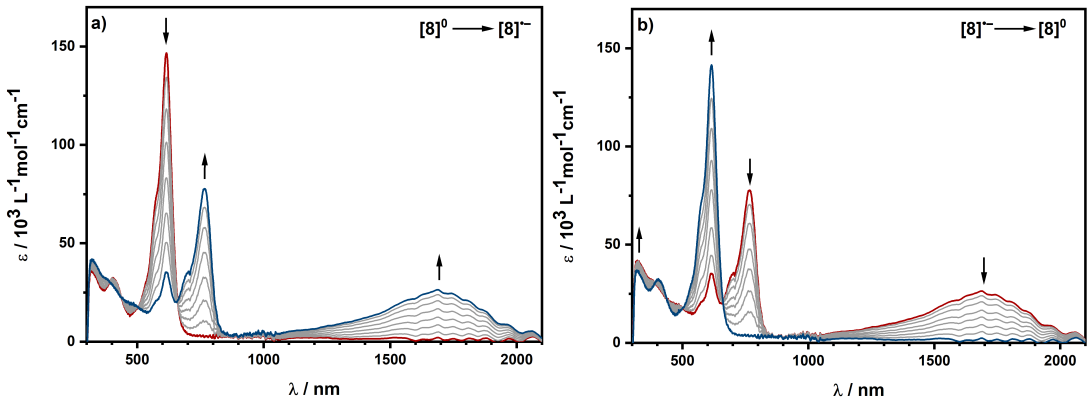

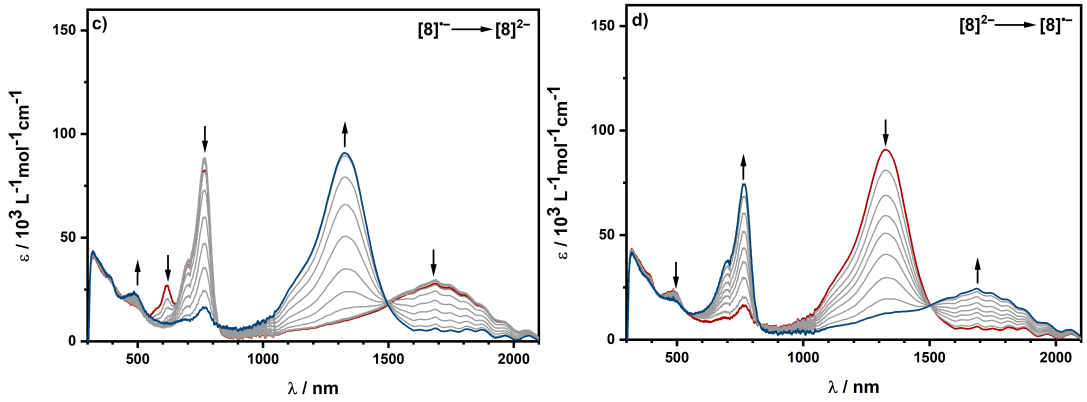

Figure S 53: UV/Vis/NIR SEC spectra of complex **8** in CH_2Cl_2/NBu_4PF_6 measured with a gold working electrode.

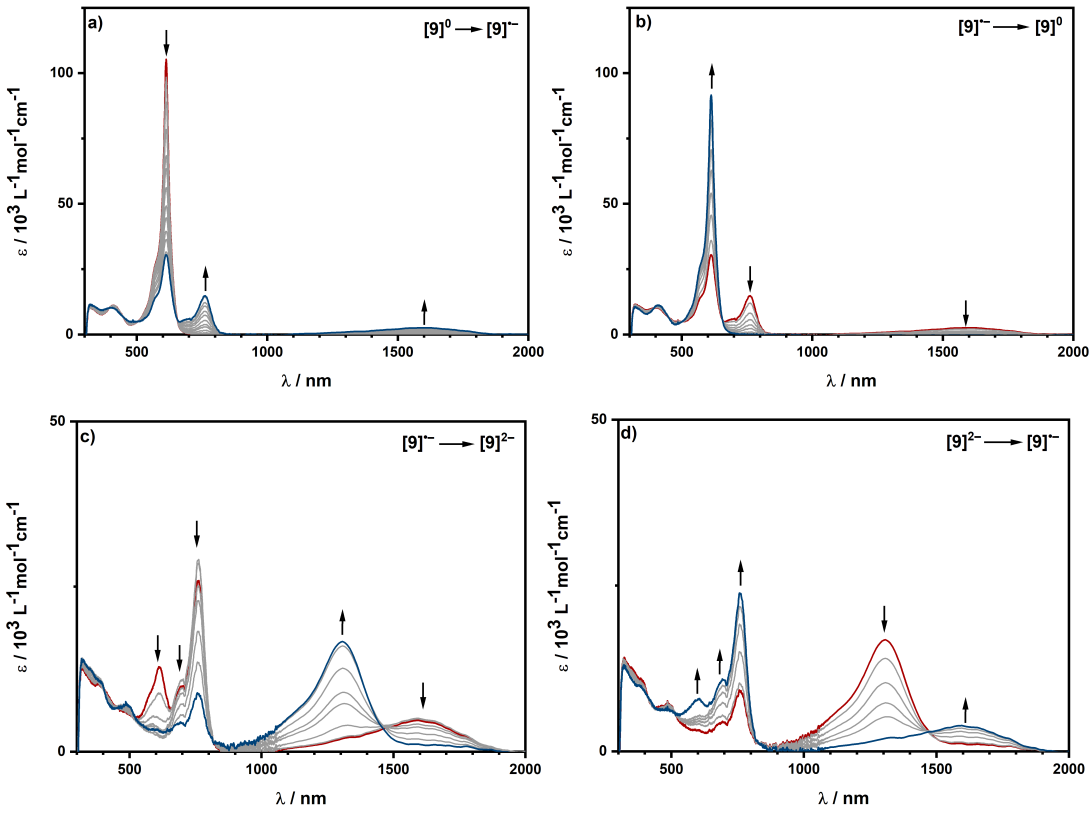

Figure S 54: UV/Vis/NIR SEC spectra of complex **9** in CH_2Cl_2/NBu_4PF_6 measured with a gold working electrode.

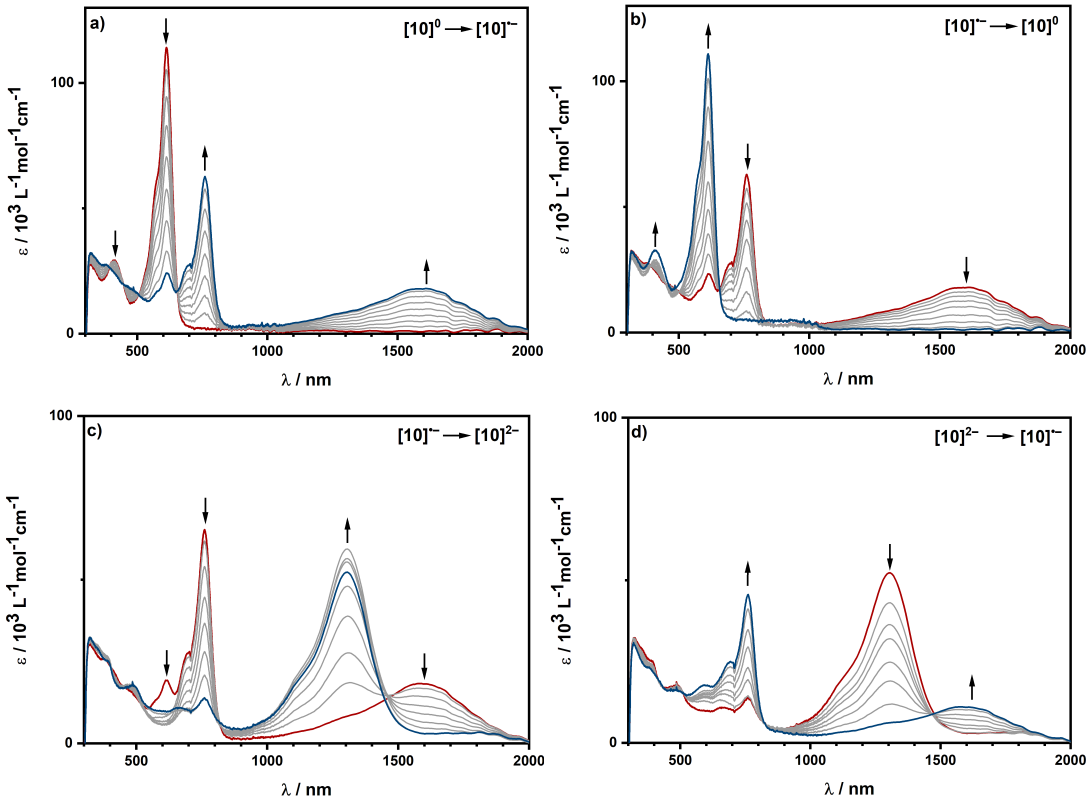

Figure S 55: UV/Vis/NIR SEC spectra of complex **10** in CH_2Cl_2/NBu_4PF_6 measured with a gold working electrode.

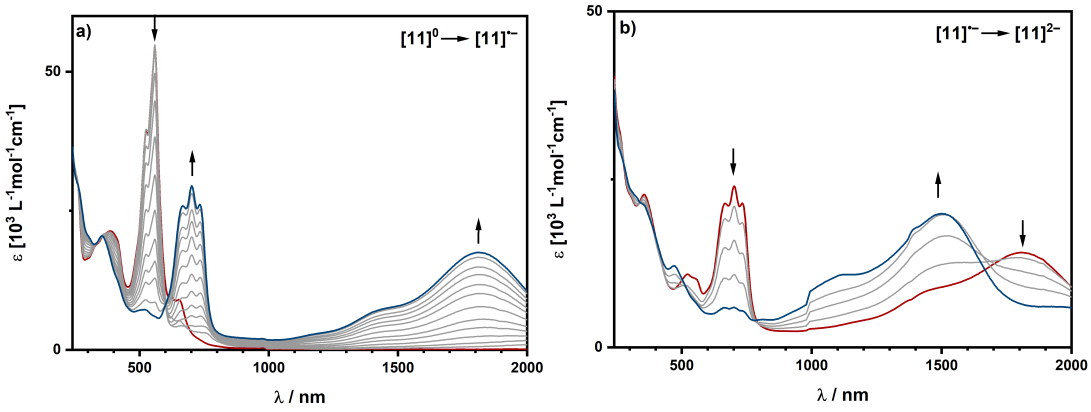

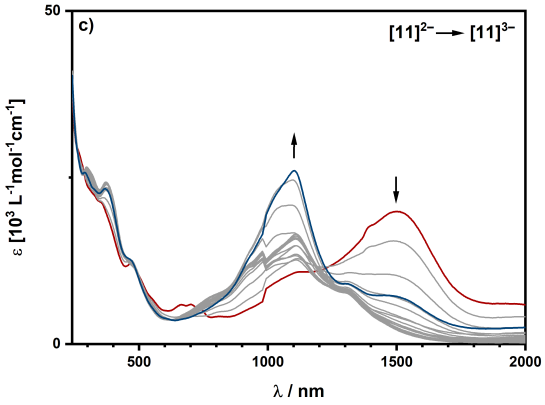

Figure S 56: UV/Vis/NIR SEC spectra of complex **11** in CH_2Cl_2/NBu_4PF_6 measured with a gold working electrode.

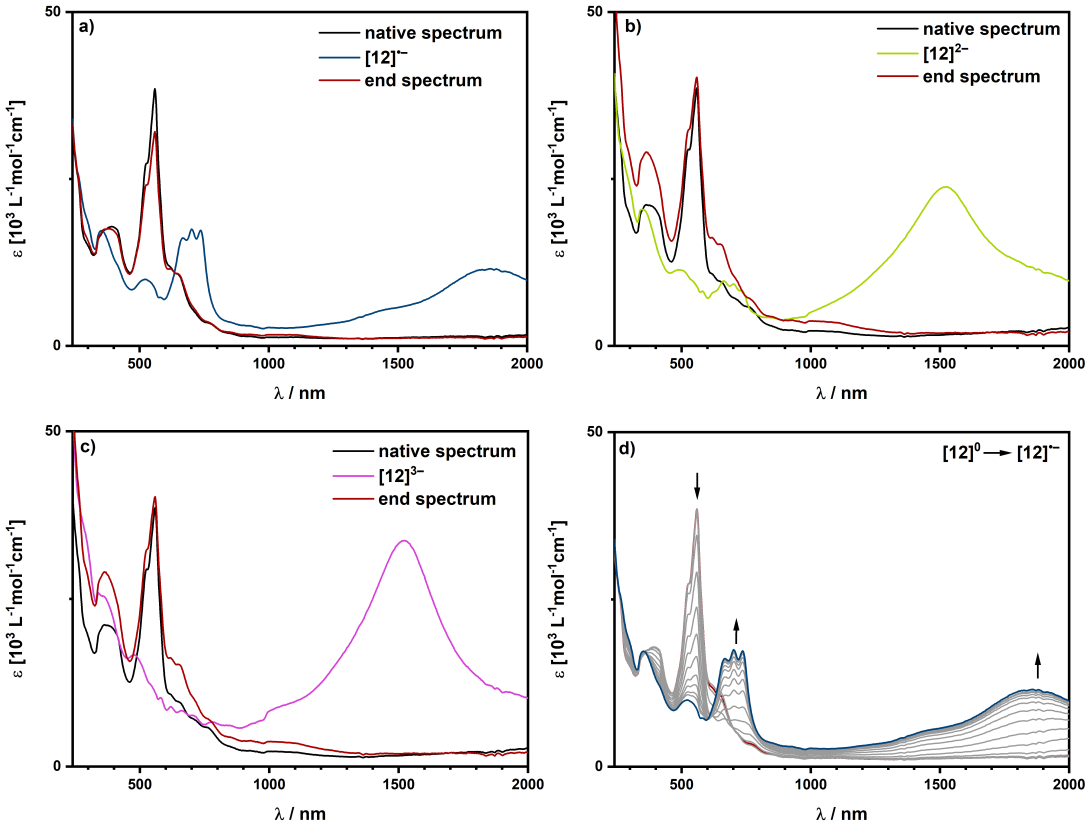

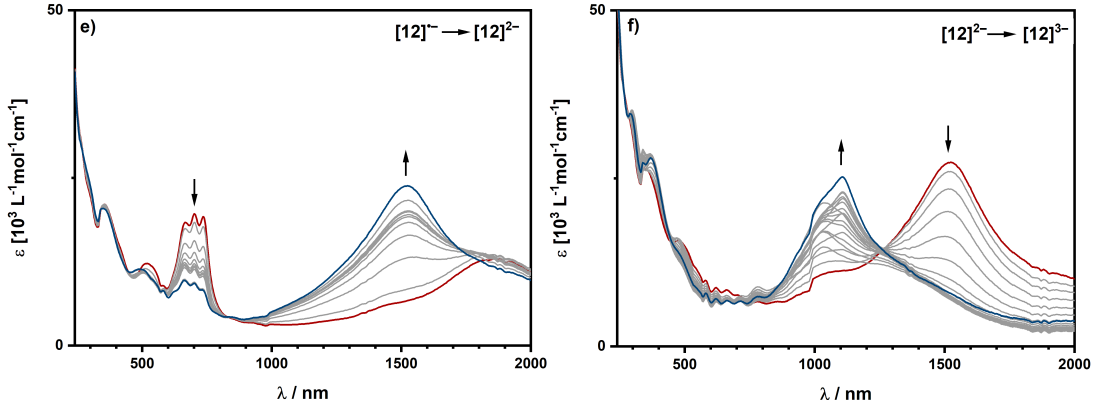

Figure S 57: UV/Vis/NIR SEC spectra of complex **12** in CH_2Cl_2/NBu_4PF_6 measured with a gold working electrode.

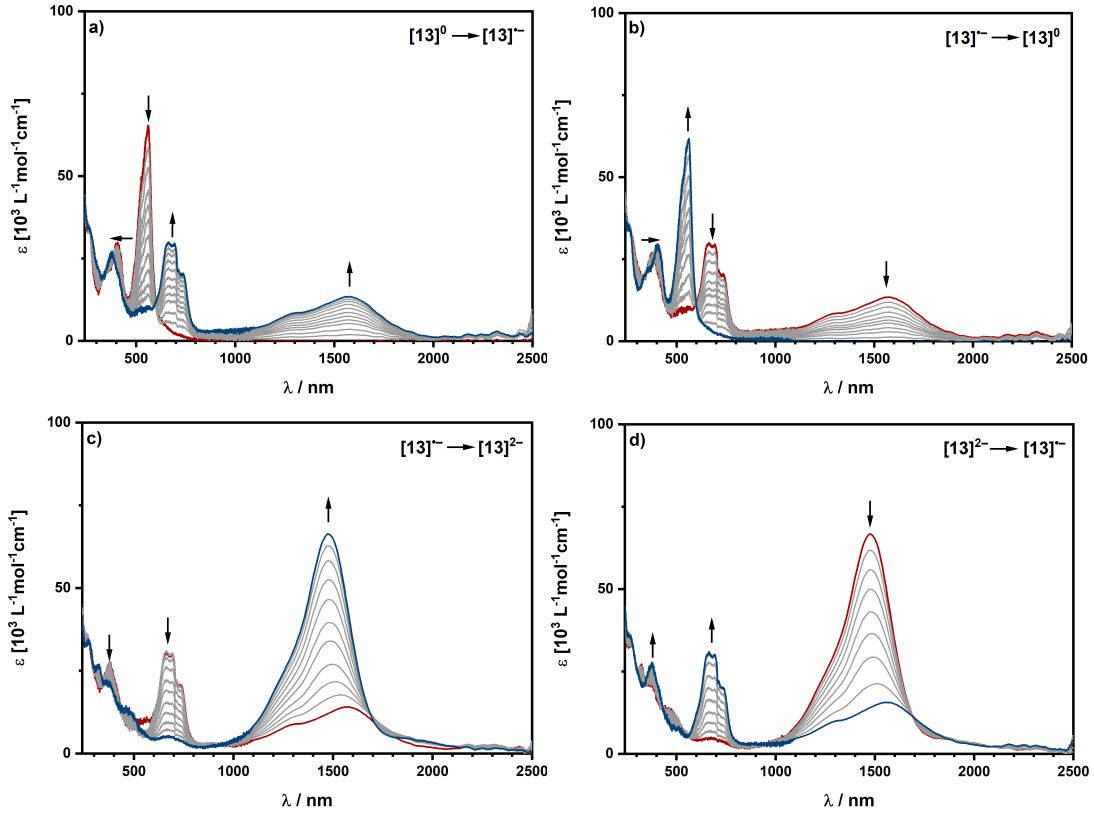

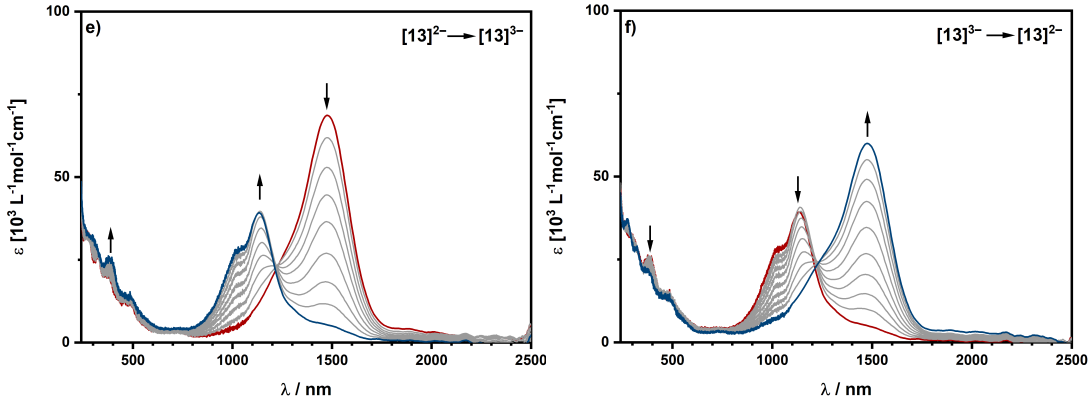

Figure S 58: UV/Vis/NIR SEC spectra of complex **13** in THF/NBu_4PF_6 measured with a gold working electrode.

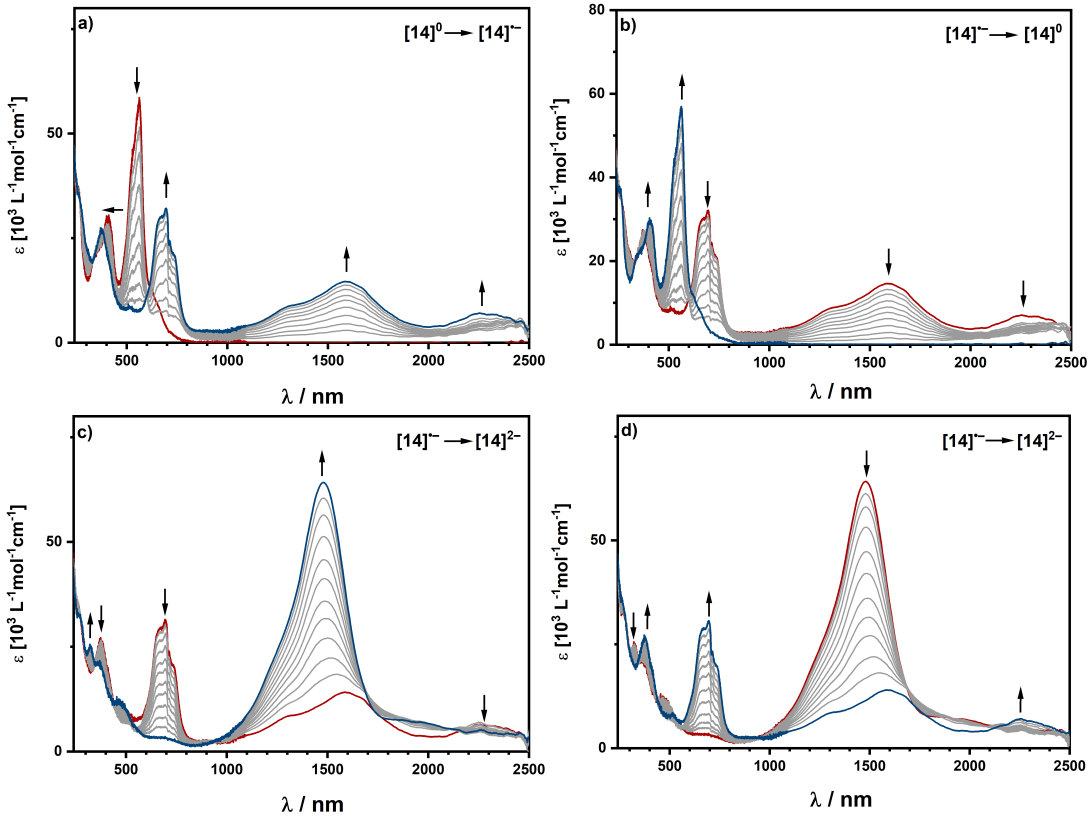

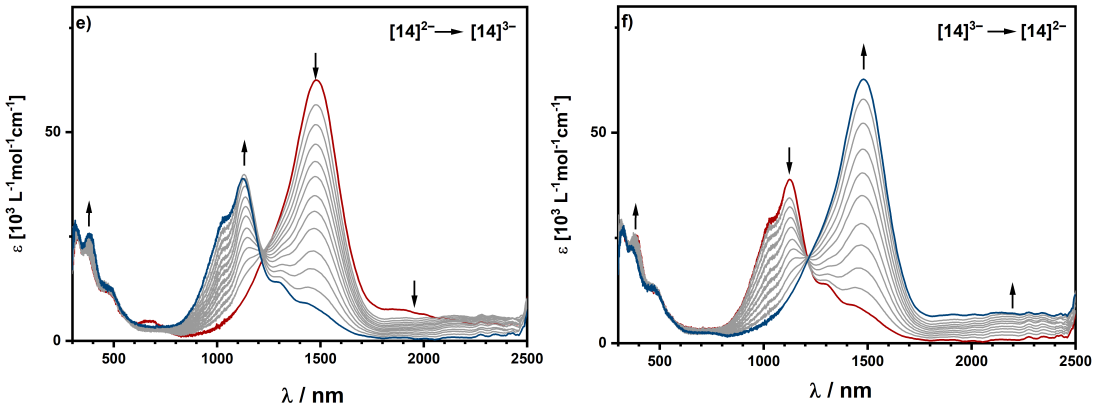

Figure S 59: UV/Vis/NIR SEC spectra of complex **14** in THF/NBu_4PF_6 measured with a gold working electrode.

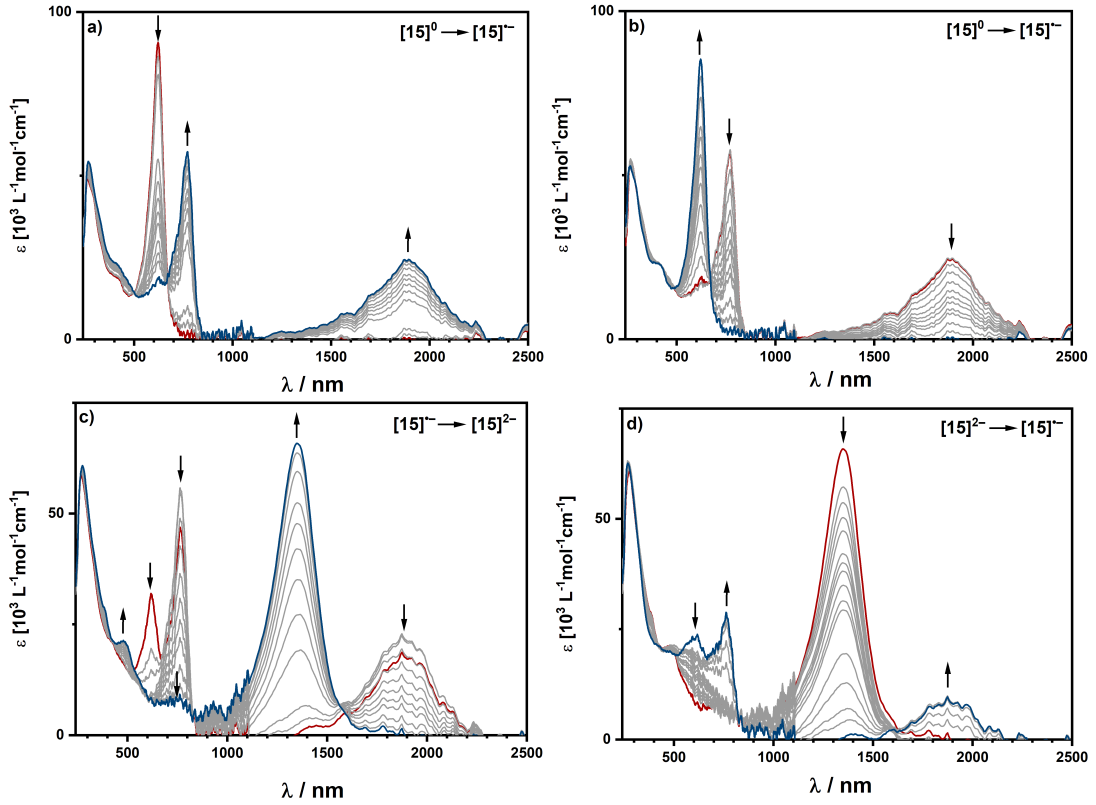

Figure S 60: UV/Vis/NIR SEC spectra of complex **15** in DCM/NBu_4PF_6 measured with a gold working electrode.

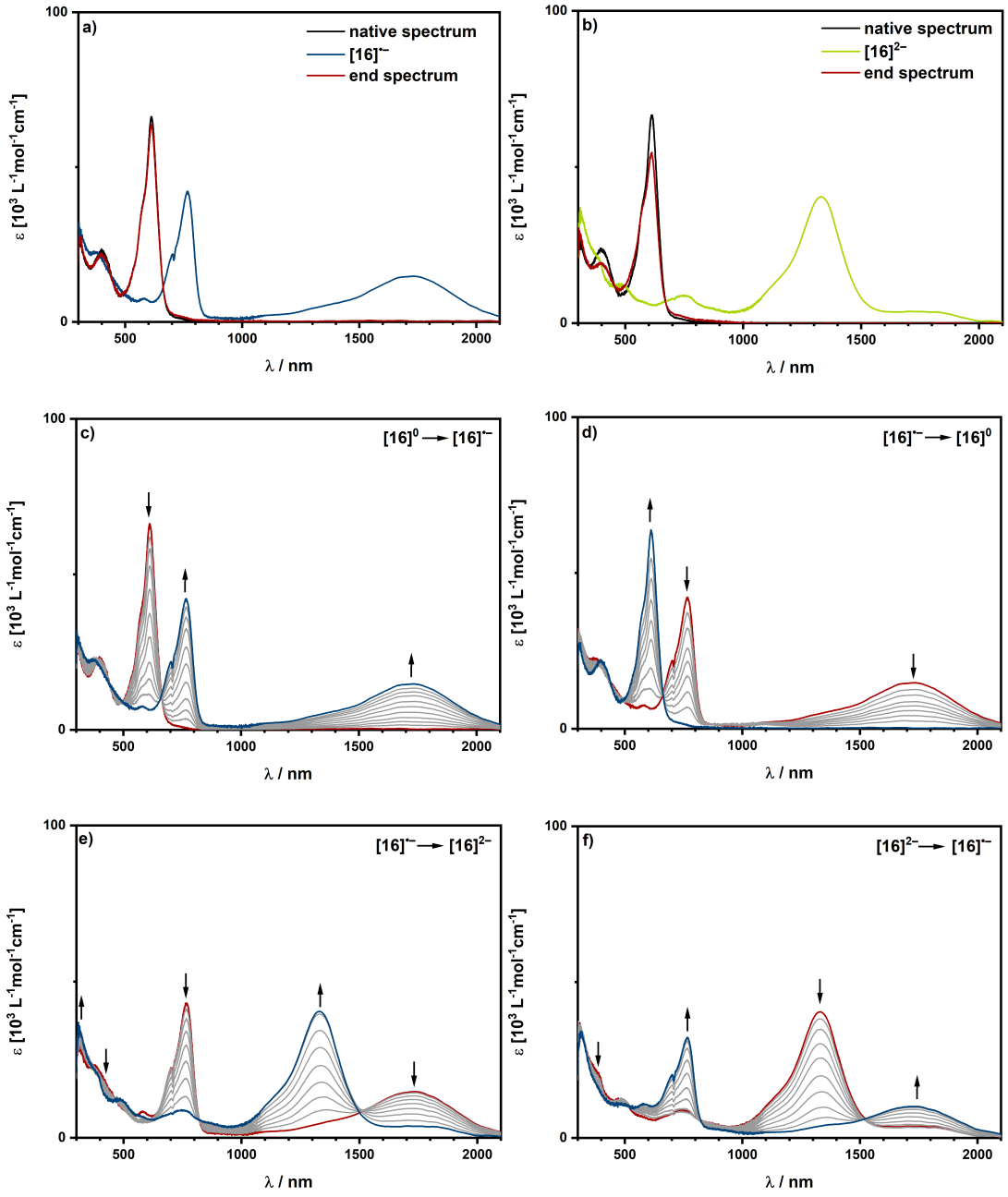

Figure S 61: UV/Vis/NIR SEC spectra of complex **16** in DCM/NBu_4PF_6 measured with a gold working electrode.

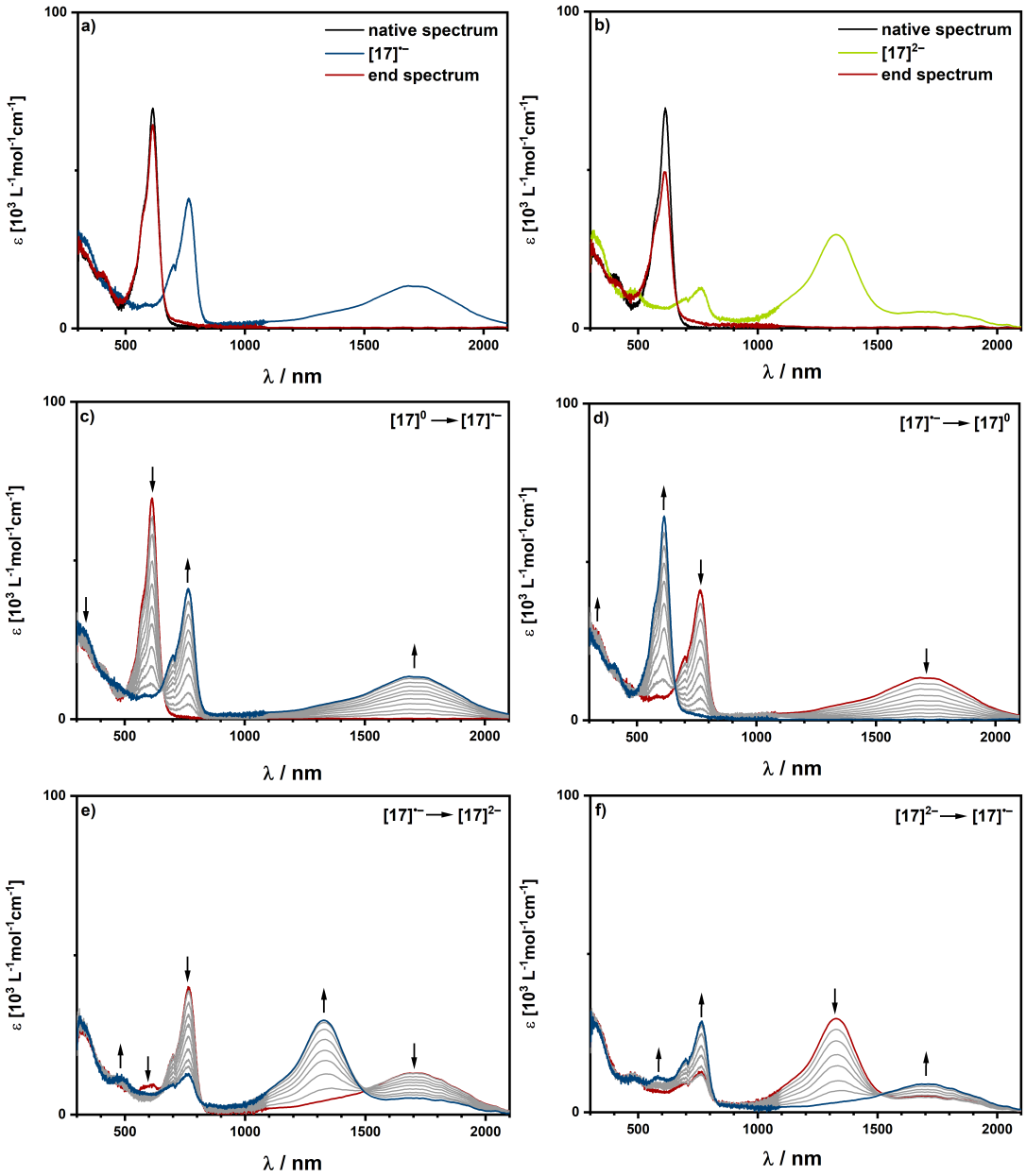

Figure S 62: UV/Vis/NIR SEC spectra of complex **17** in DCM/NBu_4PF_6 measured with a gold working electrode.

Table S 2: Data of the UV/Vis/NIR spectra during electrochemistry.

	λ / nm (ε / $10^3 M^{-1}cm^{-1}$)
$[1]^0$ start	217 (69.3), 225 (61.2), 266 sh, 348 sh, 404 (30.0), 530 sh, 559 (62.4)
$[1]^{\bullet-}$ Reduction	214 (72.4), 225 (58.6), 270 sh, 379 (27.2), 516 (9.4), 568 (9.5), 662 (29.1), 691 (27.4), 741 (18.2), 1300 sh, 1551 (12.8)
$[1]^{2-}$ Reduction	215 (79.1), 225 (63.3), 271 sh, 325 (25.4), 323 (21.2), 480 sh, 1027 sh,

	1479 (34.4)
$[1]^{3-}$ Reduction	214 (89.7), 225 (73.3), 301 sh, 385 (21.9), 476 (13.1), 1020 (18.6), 1158 (17.5), 1479 (16.3)
$[1]^{2-}$ Redoxidation	214 (87.0), 225 (69.0), 318 sh, 378 (20.8), 475 sh, 1008 sh, 1479 (23.6), 1920 (3.4)
$[1]^{\bullet-}$ Reoxidation	214 (76.7), 225 (62.0), 264 sh, 383 (25.2), 514 (12.6), 556 (11.7), 662 (21.6), 696 (20.4), 737 sh, 1551 (5.6)
$[1]^{0}$ end	217 (68.7),225 (62.7), 263 sh, 357 sh, 406 (29.9), 523 sh, 558 (58.6)
$[2]^{0}$ start	217 (61.2), 225 (55.8), 264 sh, 350 sh, 407 (24.5), 527 sh, 559 (56.4)
$[2]^{\bullet-}$ Reduction	213 (63.9), 225 (52.7), 264 sh, 382 (22.2), 523 (7.5), 563 (9.1), 664 (21.5), 693 (20.0), 741 (12.6), 1300 sh, 1551 (7.7)
$[2]^{2-}$ Reduction	214 (70.3), 224 (56.1), 268 sh, 325 (22.5), 382 sh, 470 sh, 1253 sh, 1486 (27.7)
$[2]^{3-}$ Reduction	216 (85.3); 225 (74.4), 309 sh, 385 (21.4), 487 sh, 1035 sh, 1158 (27.5), 1486 (23.7)
$[2]^{2-}$ Redoxidation	216 (84.0), 225 (71.4), 314 sh, 380 sh, 496 sh, 1246 sh, 1479 (46.1)
$[2]^{\bullet-}$ Reoxidation	214 (67.3), 224 (55.2), 274 sh, 381 (21.8), 501 sh, 664 (18.5), 694 (17.6), 738 sh, 1273 sh, 1538 (7.5)
$[2]^{0}$ end	216 (62.7), 225 (56.5), 268 sh, 354 sh, 405 (27.4), 528 sh, 556 (52.3)
$[3]^{0}$ start	217 (45.2), 225 (43.2), 267 (23.3), 407 (23.2), 428 sh, 523 sh, 557 (41.1)
$[3]^{\bullet-}$ Reduction	214 (45.8), 226 (40.1), 264 sh, 381 (19.5), 412 sh, 504 sh, 667 (14.0), 748 sh, 1253 sh, 1439 (8.4), 1722 sh
$[3]^{2-}$ Reduction	215 (48.4), 225 (41.6), 323 (16.6), 384 (16.9), 486 sh, 690 (5.1), 1233 sh, 1446 (18.6)
$[3]^{3-}$ Reduction	216 (48.5), 225 (45.4), 317 (21.0), 405 sh, 511 sh, 915 (8.5), 1110 (6.4), 1459 (2.7)
$[3]^{2-}$ Reoxidation	216 (44.0), 225 (40.4), 274 sh, 326 (17.2), 380 (16.3), 476 sh, 675 (5.2), 1219 sh, 1453 (29.8)
$[3]^{\bullet-}$ Reoxidation	216 (46.2), 226 (41.9), 389 (17.5), 496 sh, 675 (10.8), 746 sh, 1240 sh, 1459 (7.7)
$[3]^{0}$ end	218 (44.5), 226 (42.5), 264 sh, 405 (21.3), 521 sh, 557 (27.9), 380 (16.9), 480 sh, 685 (5.0), 1233 sh, 1446 (18.6)
$[4]^{0}$ start	216 (50.2), 225 (47.0), 267 (25.7), 347 sh, 407 (25.3), 431 sh, 524 sh,

S 35

	557 (47.0)
$[4]^{\bullet-}$ reduction	213 (52.7), 226 (43.7), 259 sh, 383 (21.8), 408 (21.4), 511 (8.1), 562 (8.6), 675 (19.4), 740 sh, 1233 sh, 1440 (7.5)
$[4]^{2-}$ reduction	214 (59.8), 225 (26.3), 274 sh, 328 (19.4), 380 (18.7), 486 sh, 677 (3.4), 1233 sh, 1446 (35.1)
$[4]^{3-}$ reduction	215 (64.9), 226 (8.7), 313.8 (23.8), 387 sh, 489 sh, 1008 (14.1), 1151 (13.8), 1466 sh
$[4]^{2-}$ reoxidation	214 (64.7), 225 (52.1), 320 sh, 382 (18.0), 476 sh, 670 (4.1), 1213 sh, 1453 (27.4)
$[4]^{\bullet-}$ reoxidation	214 (56.5), 225 (45.3), 264 sh, 386 (21.5), 410 (20.9), 504 (8.4), 671 (17.3), 738 sh, 1226 sh, 1460 (6.1)
$[4]^{0}$ end	216 (50.9), 226 (46.2), 266 (25.6), 344 sh, 407 (25.4), 432 sh, 524 sh, 557 (40.6)
$[5]^{0}$ start	269 (32.1), 369 (31.9), 383 (31.8), 441 sh, 535 sh, 369 (41.9)
$[5]^{\bullet-}$ Reduction	379 (30.3), 417 sh, 511 sh, 689 (24.6), 759 sh, 1243 sh, 1478 (7.7)
$[5]^{2-}$ Reduction	379 (30.4), 489 sh, 1237 sh, 1454 (45.3)
$[5]^{3-}$ Reduction	303 (30.7), 401 sh, 885 sh, 979 (11.2), 1013 sh, 1159 sh
$[5]^{0}$ end	269 (31.9), 369 sh, 387 (29.3), 413 sh, 541 (34.4), 569 (37.7)
$[6]^{0}$ start	371 sh, 387 (32.4), 439 sh, 525 (31.5), 557 (32.5),
$[6]^{\bullet-}$ Reduction	373 (29.8), 415 sh, 509 sh, 653 sh, 683 (17.4), 1253 sh, 1474 (5.3)
$[6]^{2-}$ Reduction	293 sh, 381 (21.1), 487 sh, 653 (4.5), 1241 sh, 1486 (26.8)
$[6]^{3-}$ Reduction	307 (23.3), 413 sh, 499 sh, 915 (7.1), 1267 sh
$[6]^{0}$ end	269 sh, 367 sh, 387 (28.9), 407 sh, 433 sh, 525 (28.0), 557 (29.5)
$[7]^{0}$ start	323 (21.3), 404 (18.3), 574 sh, 615 (92.4)
$[7]^{\bullet-}$ Reduction	321 (23.0), 387 sh, 575 sh, 612 (33.0), 695 sh, 769 (31.4), 1685 (11.6)
$[7]^{2-}$ Reduction	324 (26.5), 393 sh, 487 (14.3), 760 (10.9), 1138 sh, 1327 (47.4)
$[7]^{\bullet-}$ Reoxidation	322 (25.0), 379 sh, 493 (12.3), 604 sh, 695 sh, 769 (38.6), 1691 (12.5)
$[7]^{0}$ end	320 (20.8), 400 (15.4), 574 sh, 612 (79.1)
$[8]^{0}$ start	320 (35.8), 404 (32.5), 576 sh, 615 (146.6)
$[8]^{\bullet-}$ Reduction	321 (42.0), 384 sh, 486 sh, 574 sh, 617 (35.3), 702 sh, 766 (77.8), 1685 (26.4)
$[8]^{2-}$ Reduction	321 (43.5), 388 sh, 486 (24.2), 680 sh, 771 (16.5), 1124 sh, 1327 (90.9)
$[8]^{\bullet-}$ Reoxidation	321 (41.6), 381 sh, 486 sh, 702 sh, 766 (74.4), 1685 (24.4)
$[8]^{0}$ end	321 (36.5), 404 (32.6), 574 (71.0), 615 (141.5)

S 36

$[9]^{0}$ start	322 (10.4), 410 (11.2), 571 sh, 613 (105.3)
$[9]^{\bullet-}$ Reduction	322 (11.6), 404 (10.2), 569 sh, 613 (30.5), 762 (14.8), 1608 (2.5)
$[9]^{2-}$ Reduction	325 (14.0), 398 sh, 486 (7.6), 679 sh, 762 (8.8), 1307 (16.7)
$[9]^{\bullet-}$ Reoxidation	322 (13.3), 388 sh, 601 (8.1), 693 (10.8), 757 (23.7), 1602 (3.8)
$[9]^{0}$ end	321 (10.6), 409 (11.2), 571 (26.5), 613 (91.6)
$[10]^{0}$ start	320 (28.0), 411 (29.2), 574 sh, 612 (114.1)
$[10]^{\bullet-}$ Reduction	324 (32.2), 379 (27.6), 474 sh, 575 sh, 615 (24.1), 702 sh, 760 (62.7), 1602 (17.9)
$[10]^{2-}$ Reduction	323 (32.3), 395 sh, 491 (17.7), 660 (10.9), 761 (13.9), 1124 sh, 1307 (52.3)
$[10]^{\bullet-}$ Reoxidation	321 (30.8), 380 sh, 485 sh, 594 (17.8), 692 (24.9), 761 (45.6), 1327 sh, 1596 (11.0)
$[10]^{0}$ end	321 (32.9), 410 (33.4), 572 sh, 612 (111.9)
$[11]^{0}$ start	261 sh, 331 sh, 361 sh, 391 (21.0), 525 sh, 559 (52.8), 623 sh, 653 (8.8)
$[11]^{\bullet-}$ Reduction	265 sh, 353 (20.5), 521 (7.2), 667 (25.9), 701 (29.4), 733 (26.1), 1424 sh, 1816 (17.5)
$[11]^{2-}$ Reduction	273 sh, 355 sh, 473 (12.1), 665 (5.9), 701 (5.9), 739 (5.3), 1109 sh, 1508 (19.8)
$[11]^{3-}$ Reduction	293 (25.7), 369 (23.3), 469 (12.6), 1019 sh, 1103 (26.0), 1313 sh, 1498 sh
$[11]^{0}$ end	259 sh, 335 sh, 365 sh, 389 (21.3), 525 sh, 559 (54.4), 623 sh, 653 (9.0)
$[12]^{0}$ start	263 sh, 391 (17.9), 523 sh, 559 (38.5), 657 sh, 769 sh
$[12]^{\bullet-}$ Reduction	353 (17.2), 519 (9.9), 667 (16.1), 701 (17.4), 737 (17.3), 1850 (11.5)
$[12]^{2-}$ Reduction	351 (20.4), 489 (11.4), 661 (9.7), 703 (9.2), 733 sh, 1524 (23.8)
$[12]^{3-}$ Reduction	291 sh, 339 (25.9), 367 sh, 477 (16.7), 1031 sh, 1520 (33.6)
$[12]^{0}$ end	263 sh, 383 (17.5), 525 sh, 559 (32.1), 651 sh, 765 sh
$[13]^{0}$ start	262 sh, 347 sh, 407 (29.9), 558 (65.3)
$[13]^{\bullet-}$ Reduction	268 sh, 380 (27.1), 662 (30.0), 693 (29.6), 741 sh, 1287 sh, 1570 (13.4)
$[13]^{2-}$ Reduction	270 (34.6), 325 (27.0), 363 (22.3), 476 sh, 675 (5.4), 1472 (66.3)
$[13]^{3-}$ Reoduction	297 sh, 377 (26.1), 490 sh, 1016 sh, 1138 (39.1), 1479 sh
$[13]^{2-}$ Reoxidation	275 (37.2), 323 (29.0), 377 sh, 486 sh, 1472 (60.0)
$[13]^{\bullet-}$ Reoxidation	270 sh, 377 (27.7), 664 (30.9), 694 (30.0), 737 sh, 1300 sh, 1557 (15.6)
$[13]^{0}$ end	265 sh, 358 sh, 402 (29.7), 530 (48.9), 562 (61.7)
$[14]^{0}$ start	252 (37.5), 353 sh, 410 (30.5), 562 (58.6)

S 37

$[14]^{\bullet-}$ Reduction	264 sh, 370 (27.5), 665 sh, 696 (32.1), 737 sh, 1307 sh, 1589 (14.6), 2253 (7.1)
$[14]^{2-}$ Reduction	268 sh, 321 (25.6), 370 (21.7), 469 (12.5), 1233 sh, 1479 (64.2)
$[14]^{3-}$ Reduction	301 sh, 382 (25.7), 493 sh, 1021 sh, 1124 (34.1), 1294 sh
$[14]^{2-}$ Reoxidation	275 sh, 318 (28.2), 370 (23.1), 471 (14.8), 1246 sh, 1479 (54.0)
$[14]^{\bullet-}$ Reoxidation	265 sh, 372 (27.2), 663 sh, 696 (30.6), 743 sh, 1300 sh, 1589 (14.0), 2253 (7.1)
$[14]^{0}$ end	256 sh, 341 sh, 405 (30.3), 562 (56.9),
$[15]^{0}$ start	262 (49.4), 299 sh, 417 sh, 622 (90.7)
$[15]^{\bullet-}$ Reduction	268 (54.4), 415 sh, 627 (19.1), 771 (57.3), 1582 sh, 1893 (24.4)
$[15]^{2-}$ Reduction	276 (60.8), 479 (21.4), 762 (9.2), 931 (7.7), 1352 (65.8)
$[15]^{\bullet-}$ Reoxidation	268 (62.6), 618 (23.8), 762 (28.8), 1397 (1.1), 1874 (9.6)
$[15]^{0}$ end	266 (52.8), 409 sh, 622 (85.3)
$[16]^{0}$ start	398 (23.5), 572 sh, 611 (66.3)
$[16]^{\bullet-}$ Reduction	376 (22.6), 583 (7.6), 703 sh, 767 (42.1), 1729 (14.7)
$[16]^{2-}$ Reduction	380 sh, 483 (12.6), 745 (8.9), 1151 sh, 1334 (40.4), 1816 sh
$[16]^{\bullet-}$ Reoxidation	485 sh, 586 (10.7), 698 sh, 766 (32.2), 1360 sh, 1729 (10.1)
$[16]^{0}$ end	395 (22.1), 574 sh, 613 (63.5)
$[17]^{0}$ start	340 sh, 401 (17.4), 572 sh, 614 (69.7)
$[17]^{\bullet-}$ Reduction	328 (29.0), 700 sh, 764 (41.1), 1710 (13.3)
$[17]^{2-}$ Reduction	330 sh, 486 (12.5), 690 sh, 762 (12.6), 1130 sh, 1327 (29.5), 1748 (5.0)
$[17]^{\bullet-}$ Reoxidation	327 (28.1), 473 (11.5), 583 (11.6), 698 sh, 765 (28.7), 1716 (8.9)
$[17]^{0}$ end	342 sh, 405 (18.1), 570 sh, 614 (64.4)

S 38

6. NMR Spectra

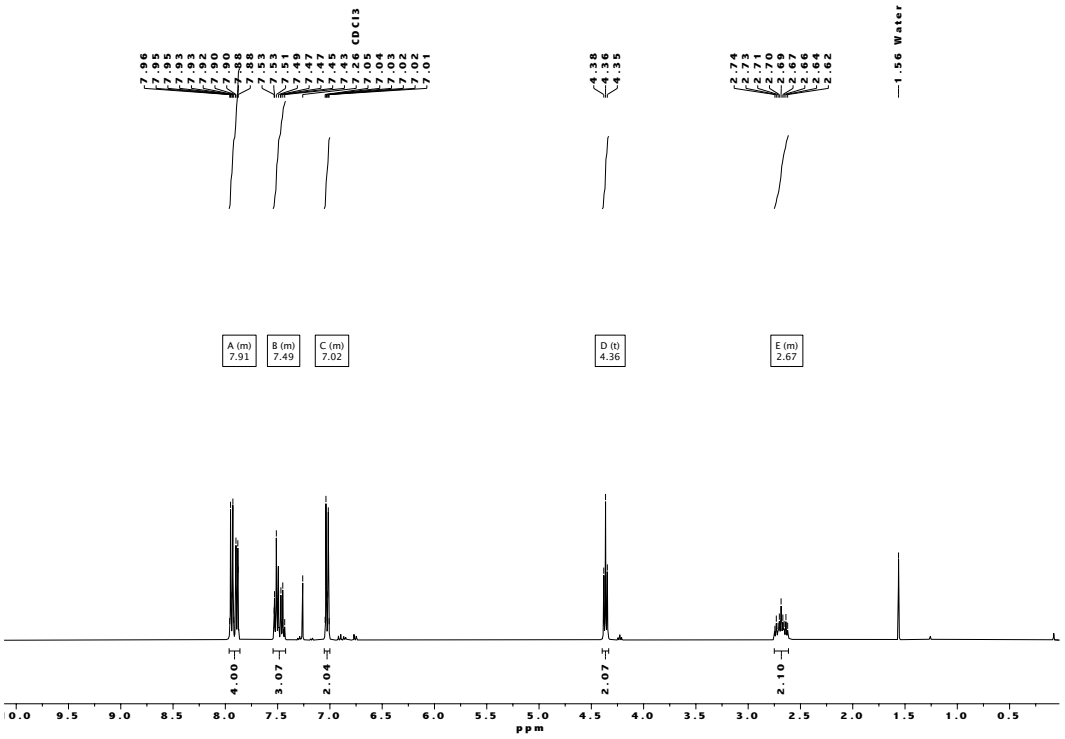

Figure S 63: ^{1}H NMR Spectrum of **L8**.

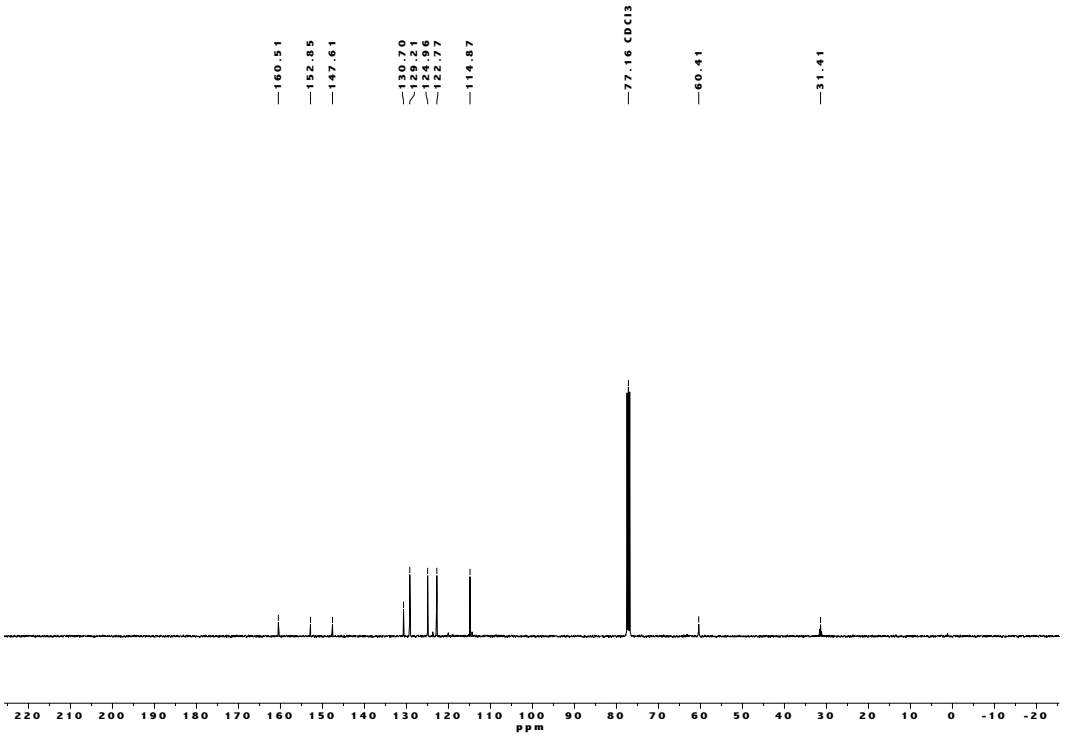

Figure S 64: ^{13}C NMR Spectrum of **L8**.

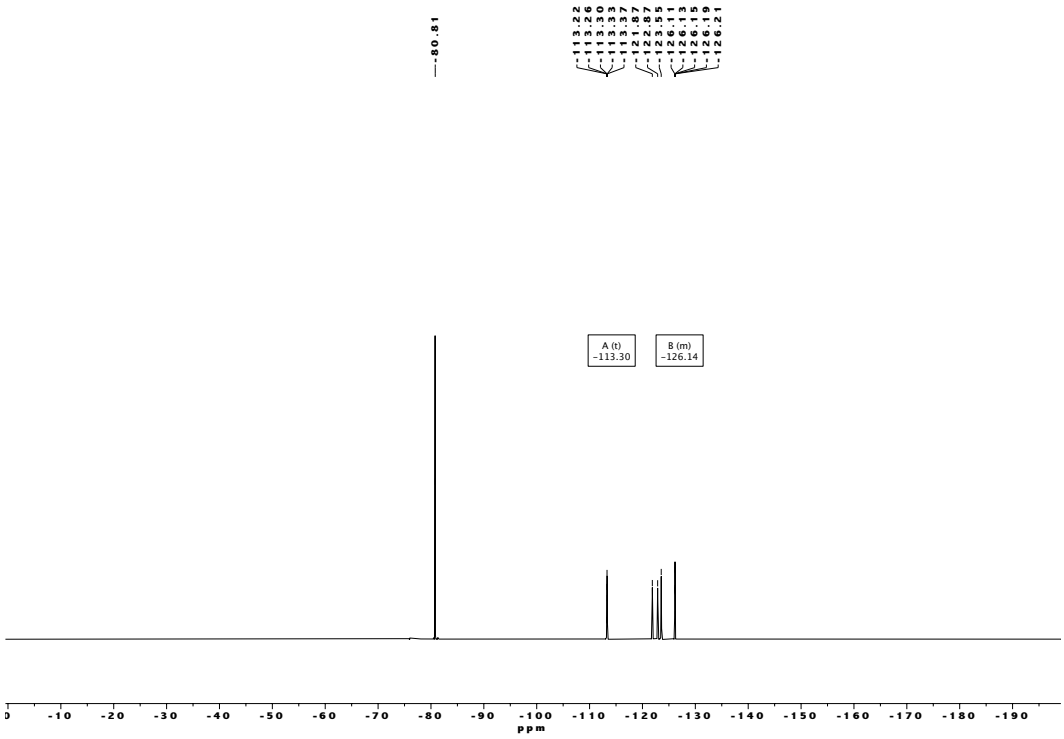

Figure S 65: ^{19}F NMR Spectrum of **L8**.

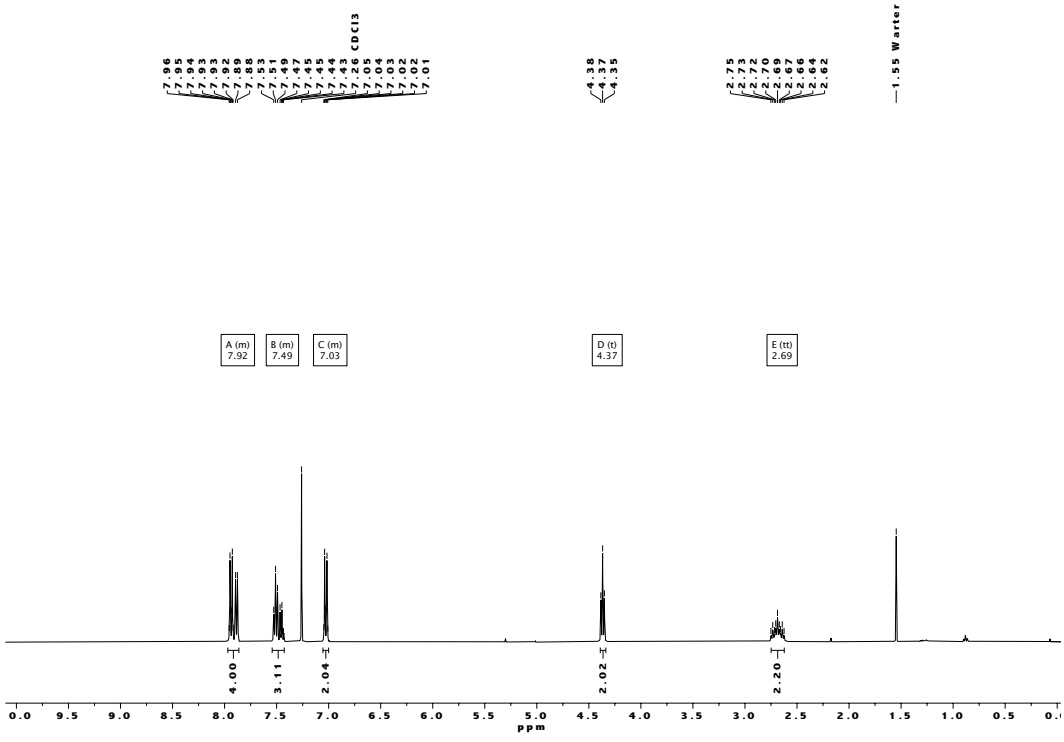

Figure S 66: ^{1}H NMR Spectrum of **L9**.

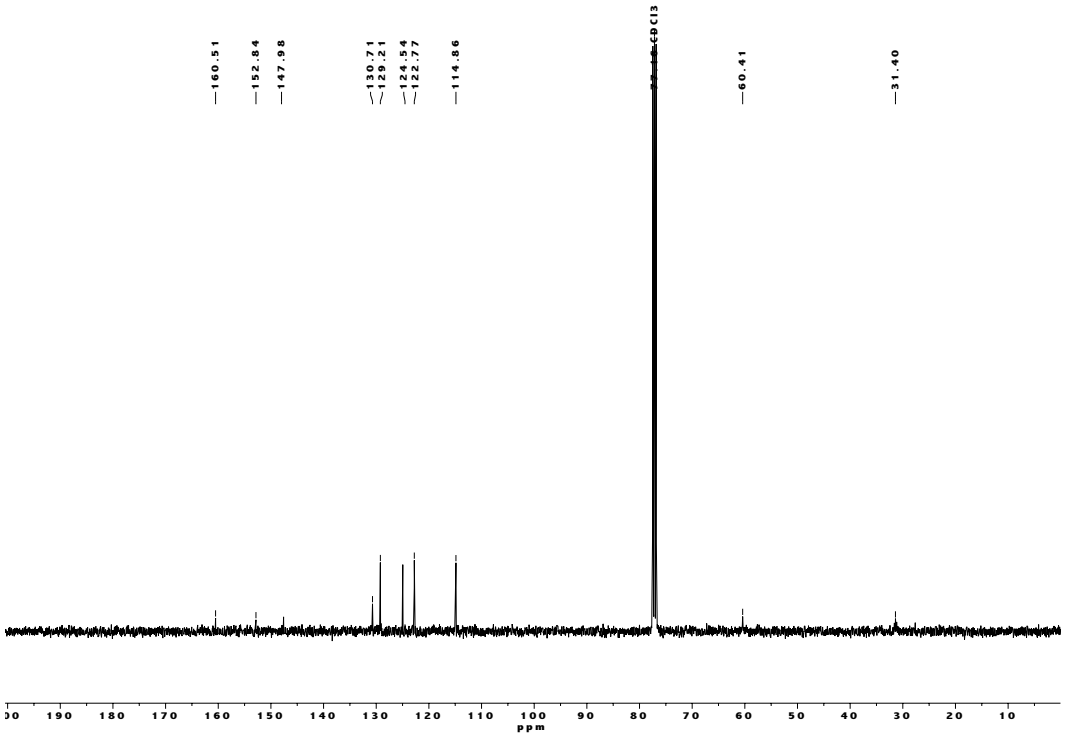

Figure S 67: ^{13}C NMR Spectrum of **L9**.

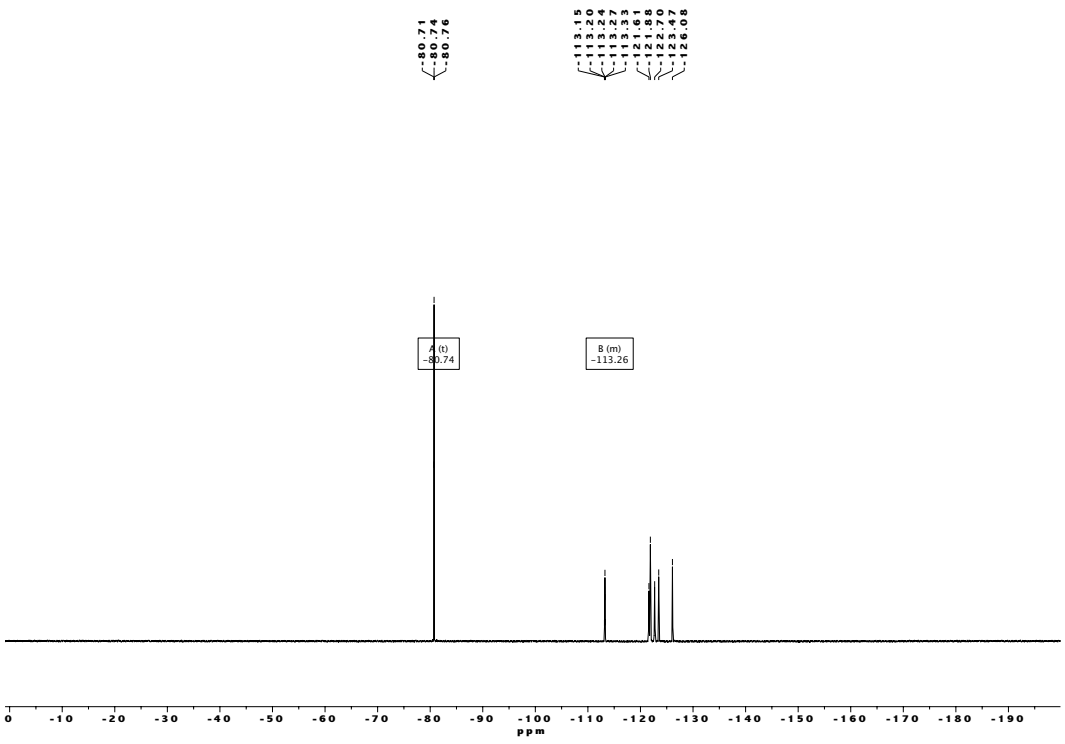

Figure S 68: ^{19}F NMR Spectrum of **L9**.

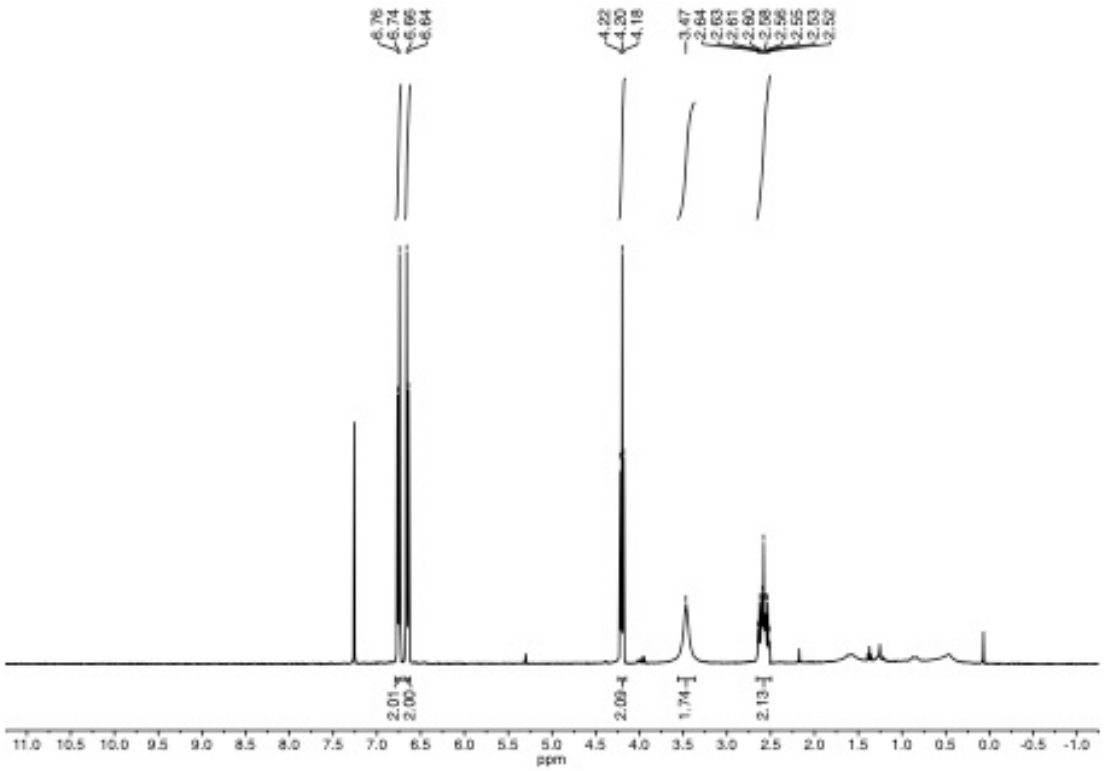

Figure S 69: ^{1}H NMR Spectrum of **L13**.

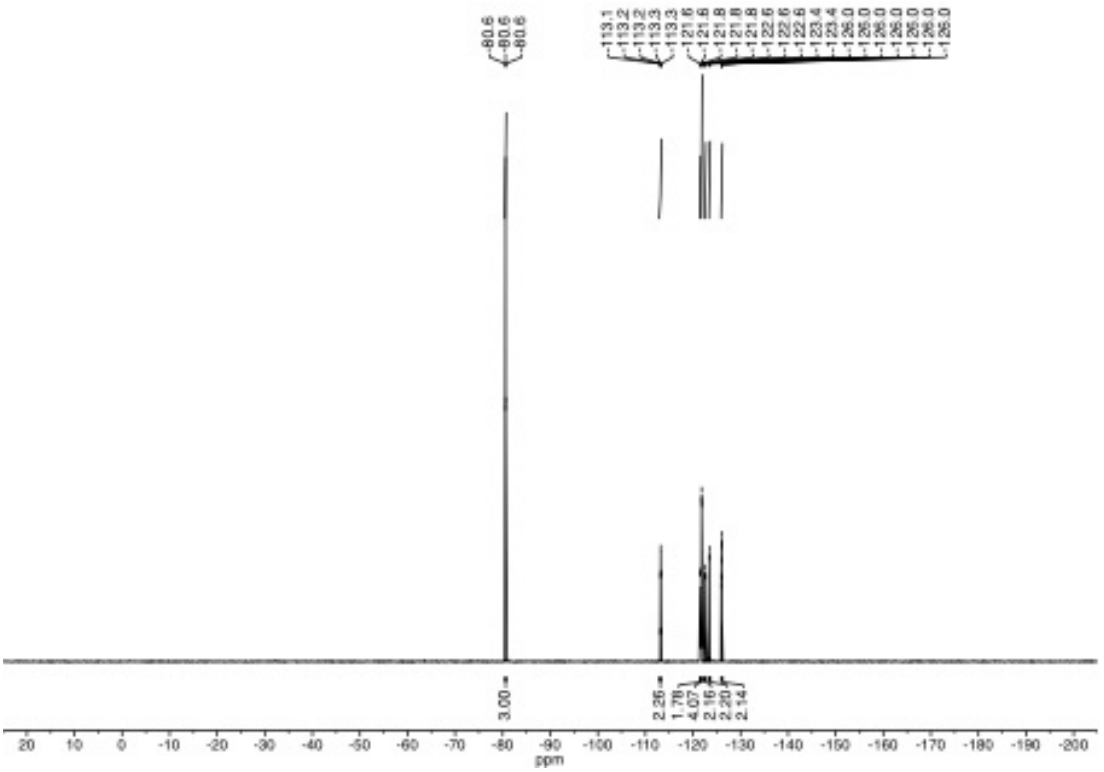

Figure S 70: ^{19}F NMR Spectrum of **L13**.

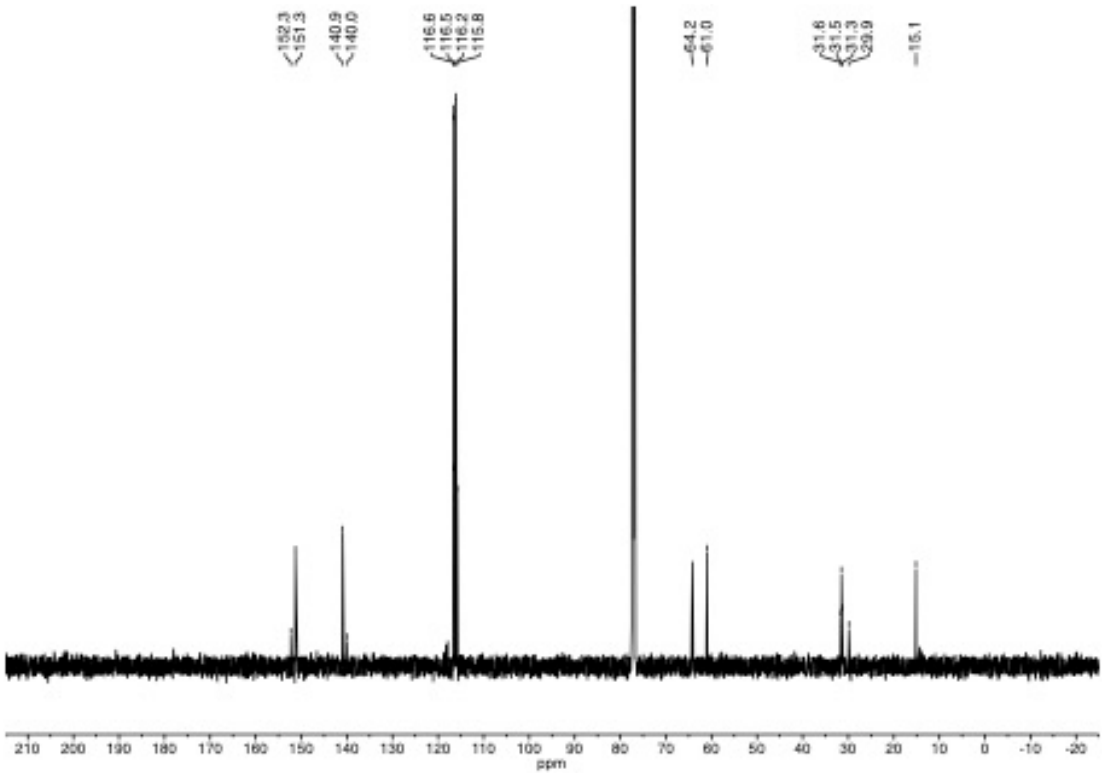

Figure S 71: ^{13}C NMR Spectrum of **L13**.

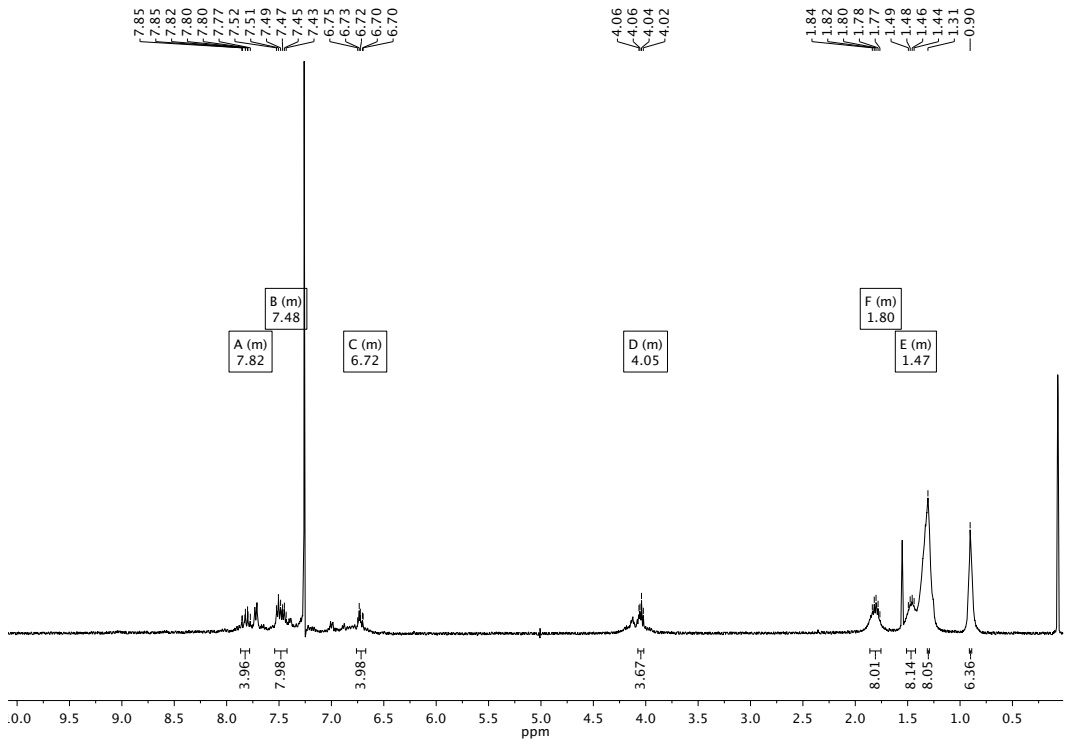

Figure S 72: ^{1}H NMR Spectrum of **P1.**

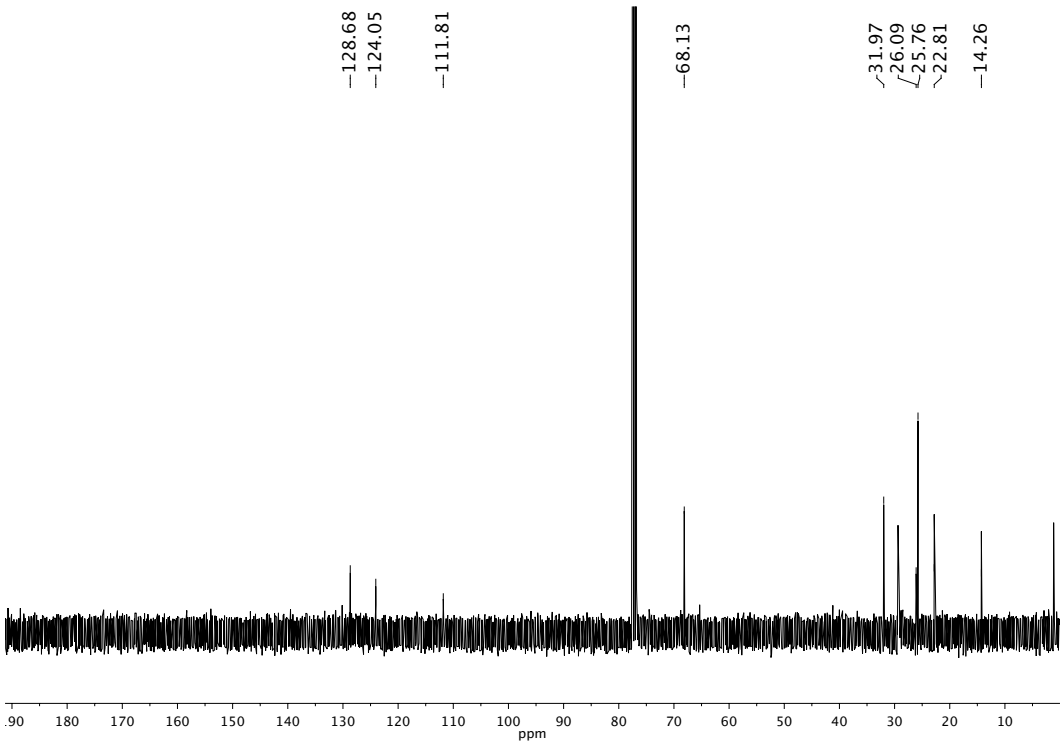

Figure S 73: ^{13}C NMR Spectrum of **P1.**

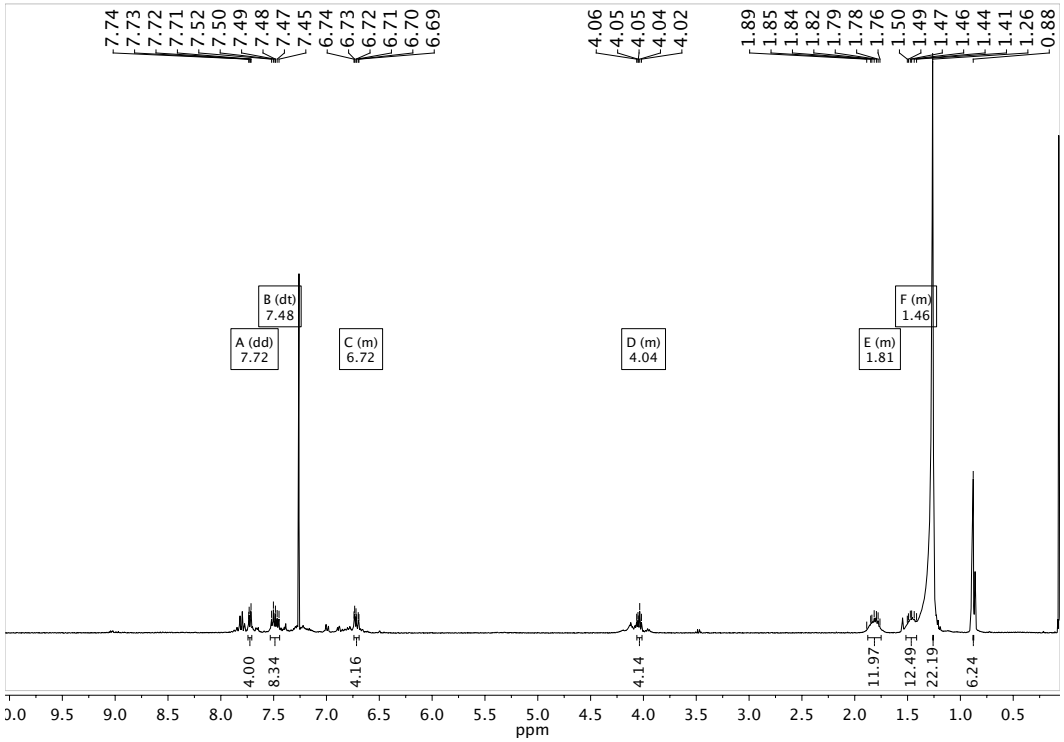

Figure S 74: ^{1}H NMR Spectrum of **P2**.

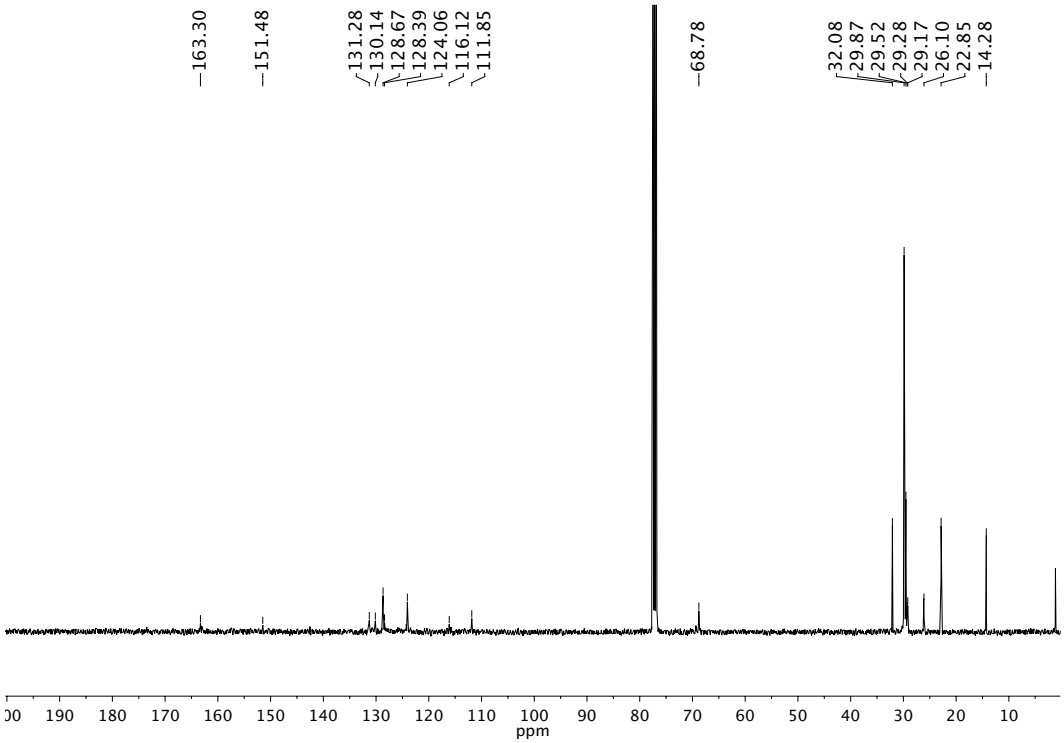

Figure S 75: ^{13}C NMR Spectrum of **P2.**

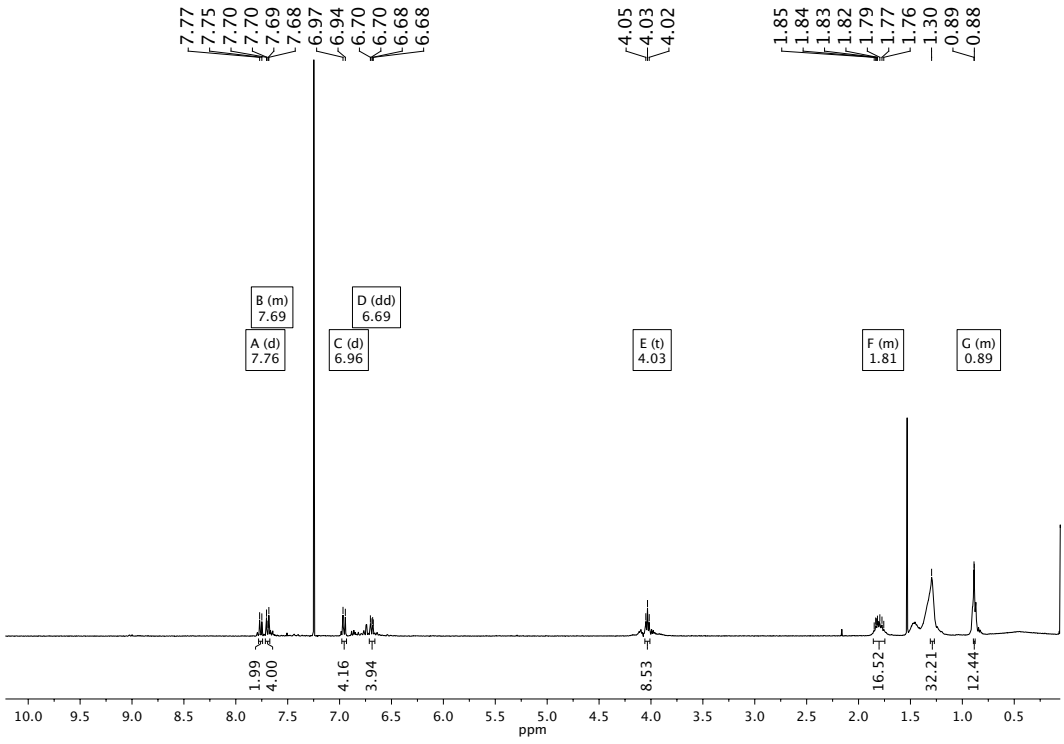

Figure S 76: ^{1}H NMR Spectrum of **P3.**

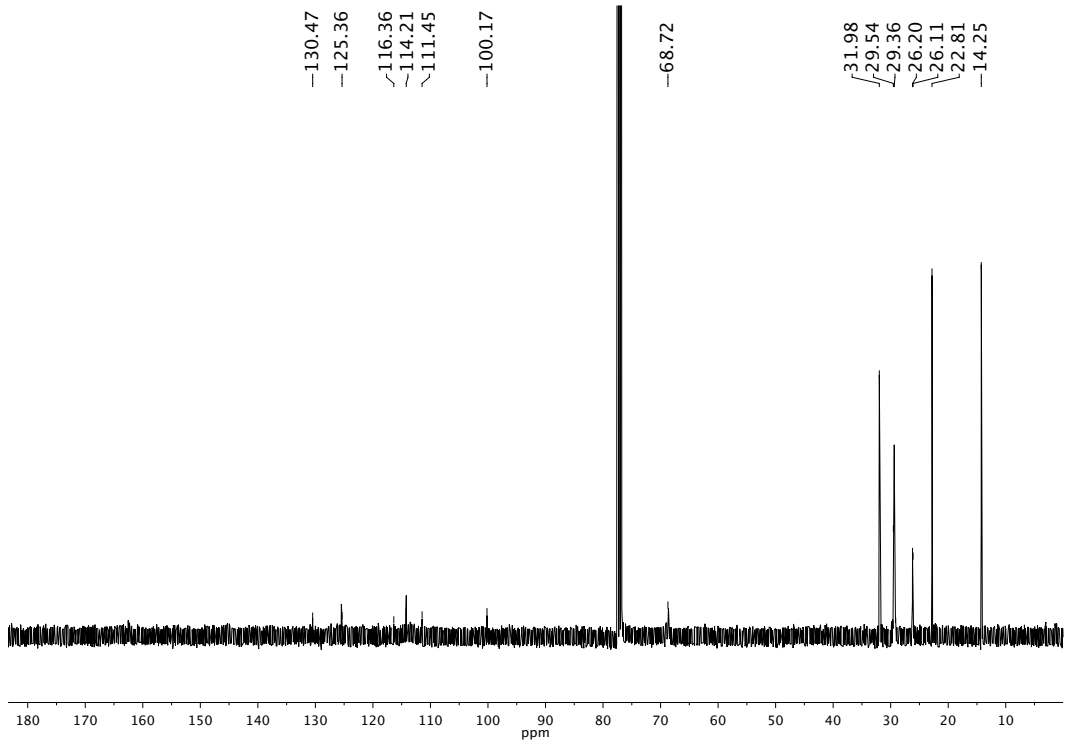

Figure S 77: ^{13}C NMR Spectrum of **P3.**

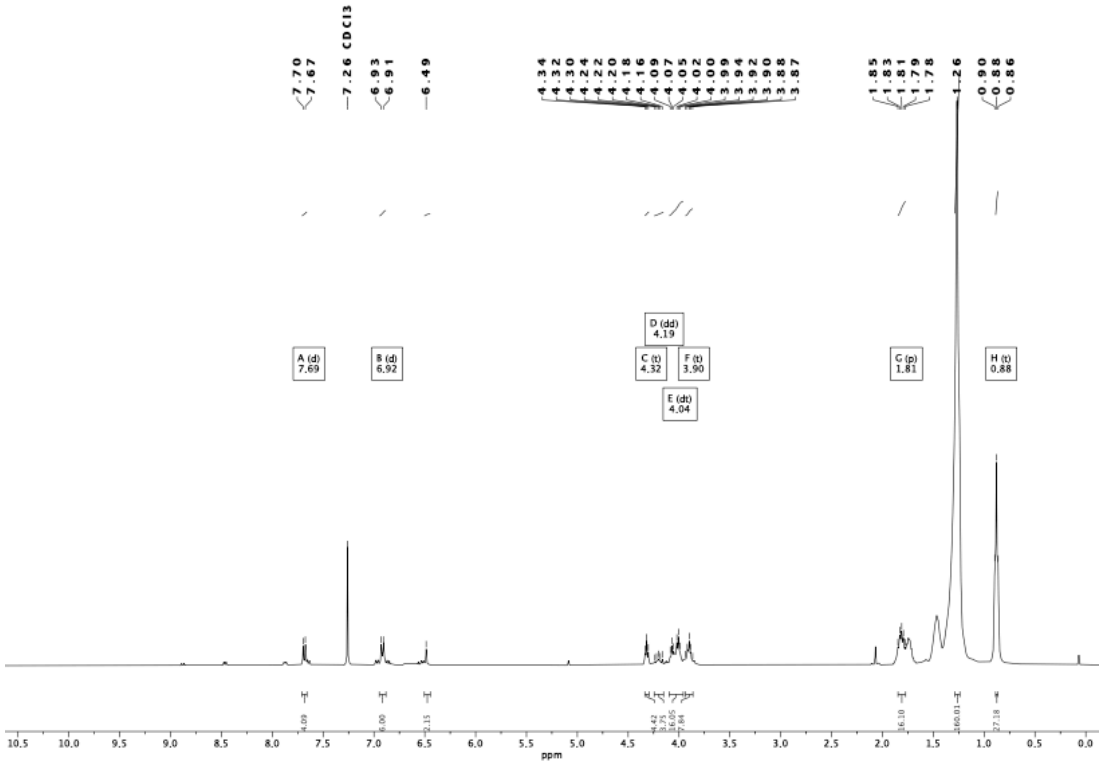

Figure S 78: ^{1}H NMR Spectrum of **P5.**

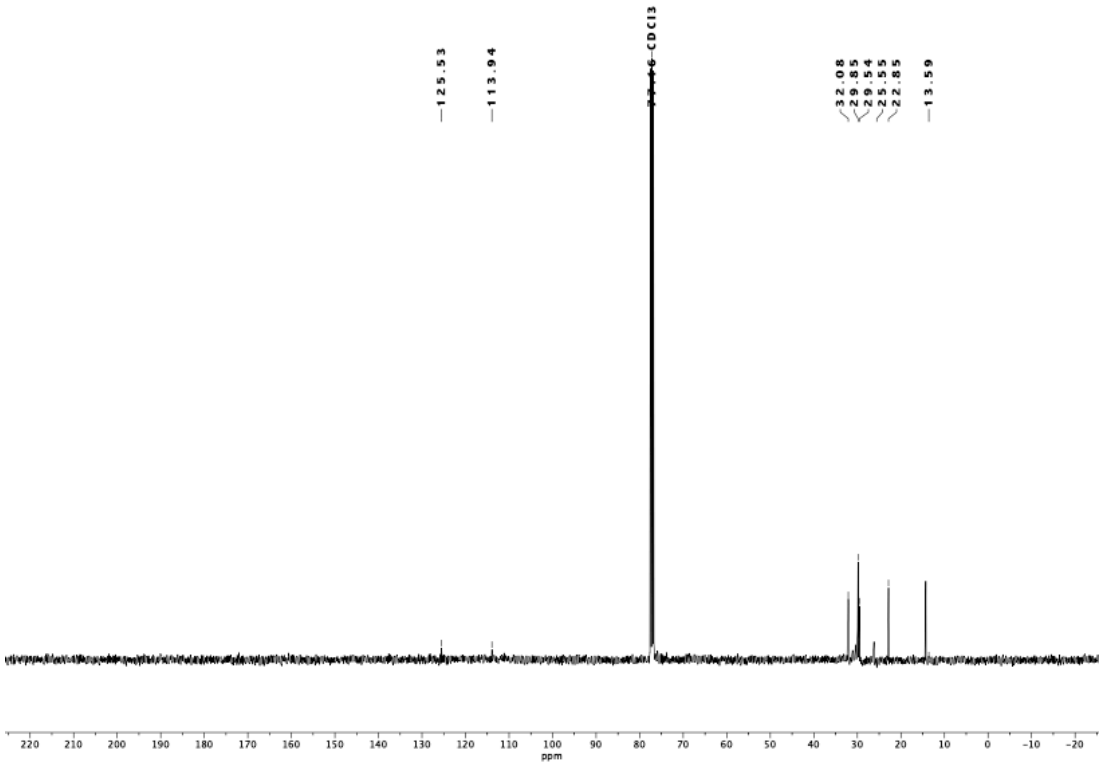

Figure S 79: ^{13}C NMR Spectrum of **P5.**

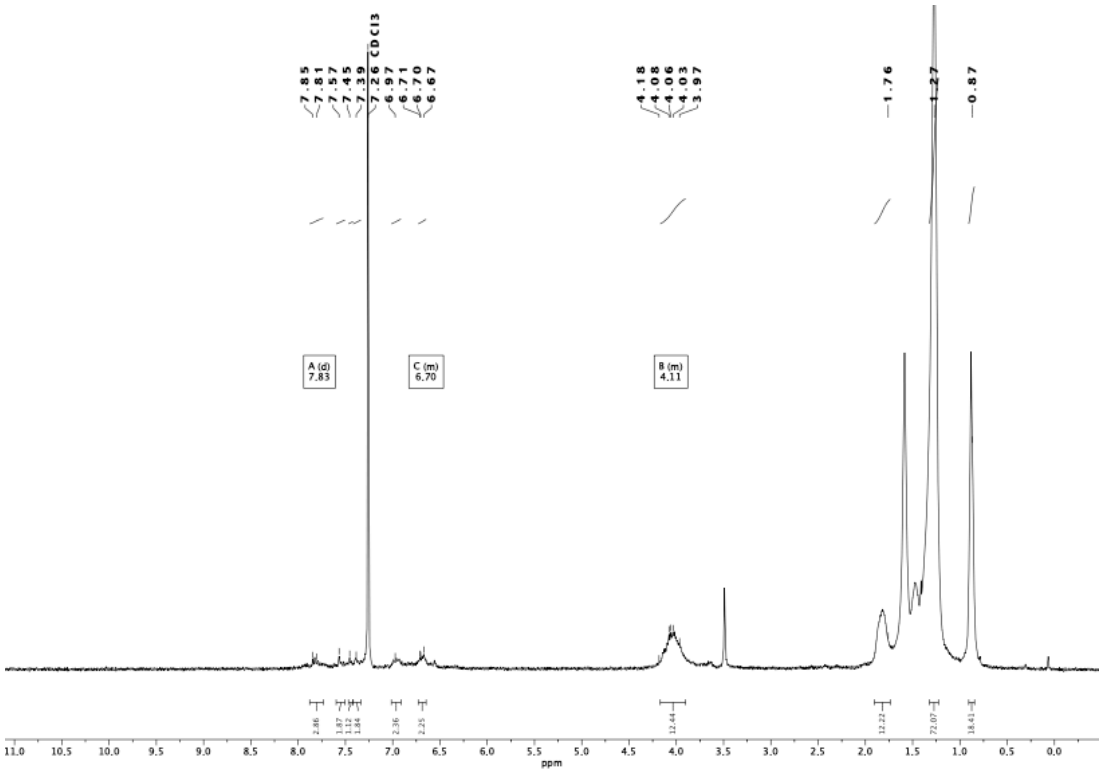

Figure S 80: ^{1}H NMR Spectrum of **P6.**

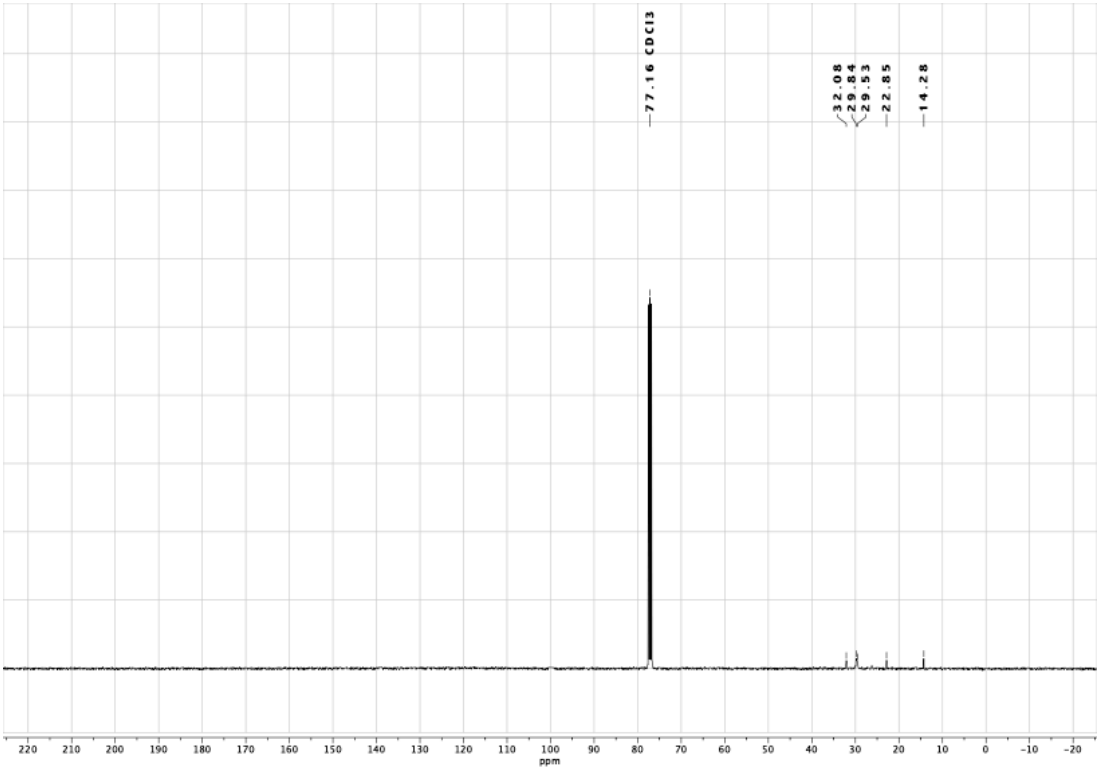

Figure S 81: ^{13}C NMR Spectrum of **P6.**

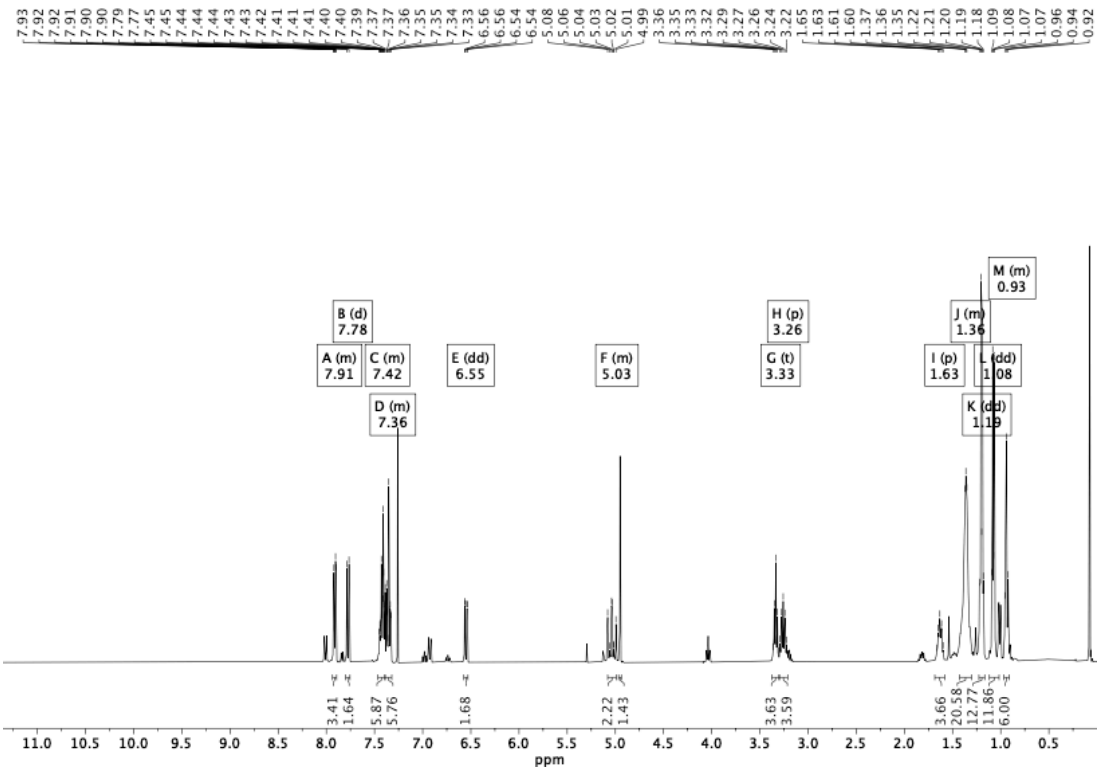

Figure S 82: ^{1}H NMR Spectrum of **1.**

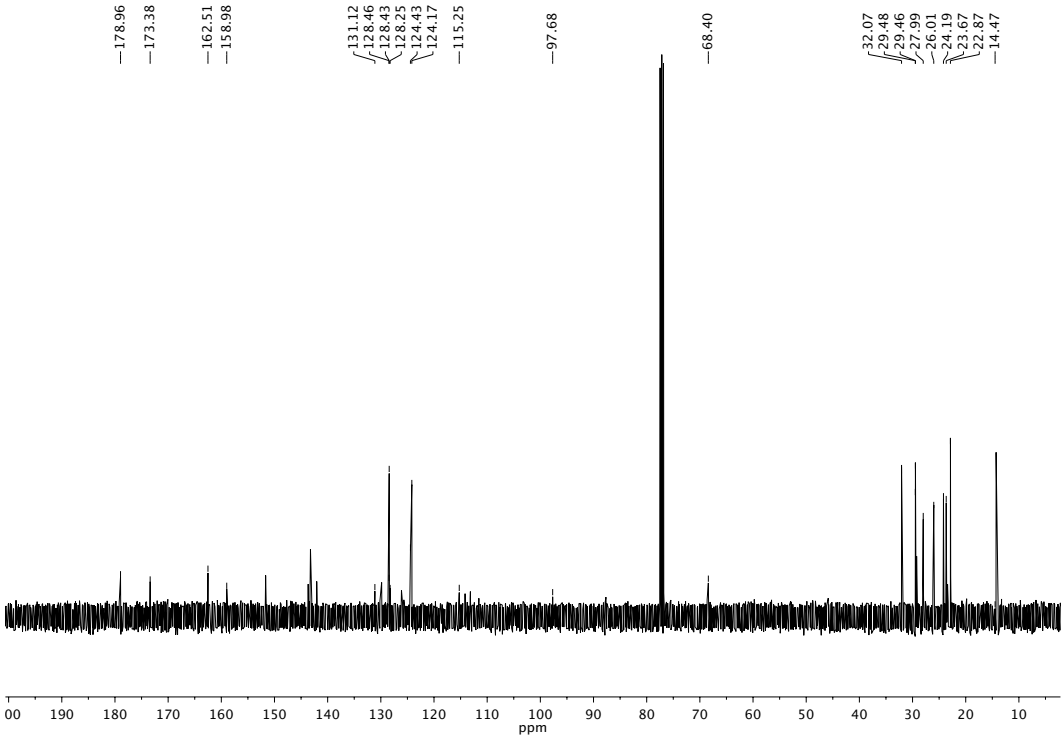

Figure S 83: ^{13}C NMR Spectrum of **1**.

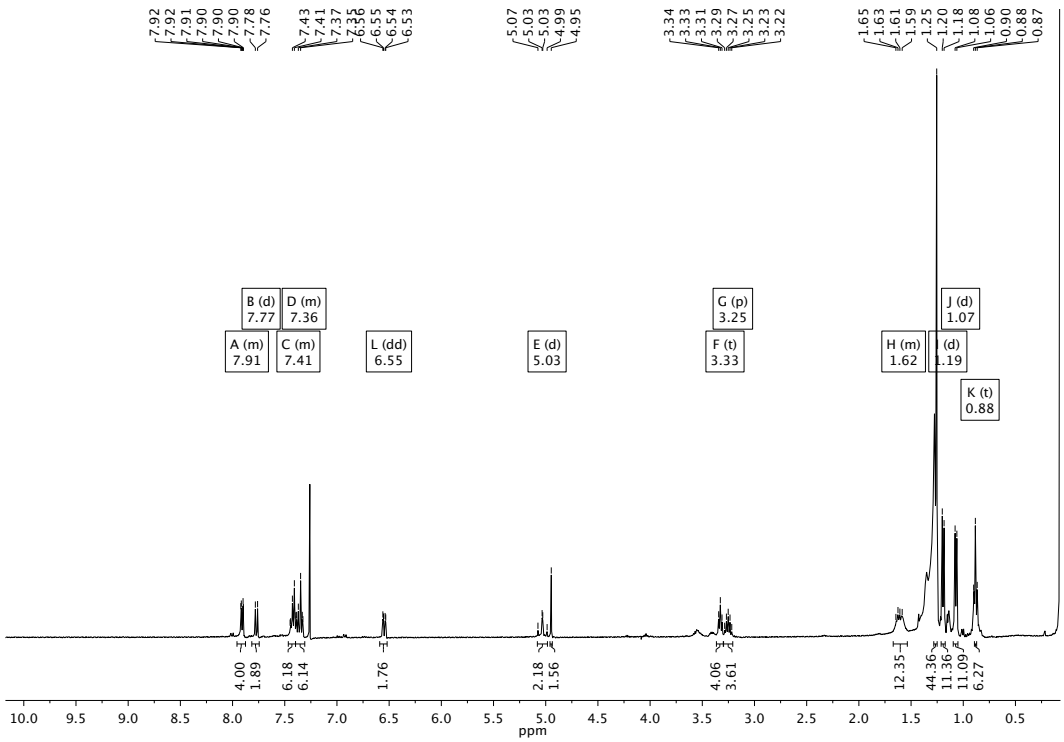

Figure S 84: ^{1}H NMR Spectrum of **2.**

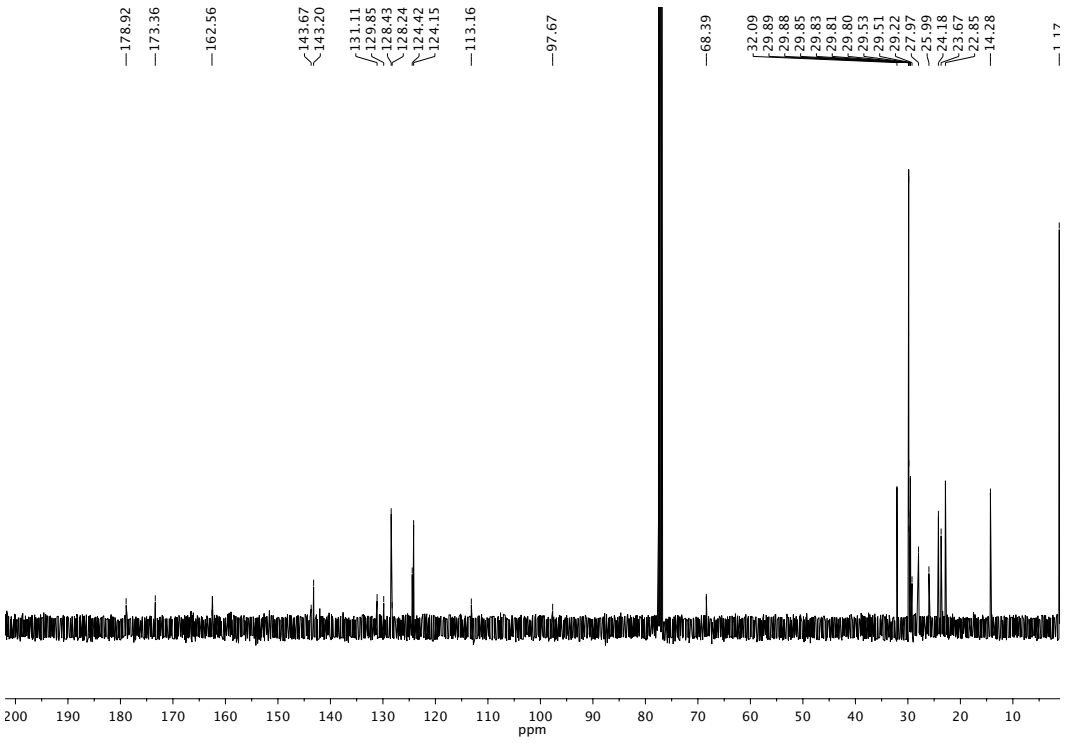

Figure S 85: ^{13}C NMR Spectrum of **2.**

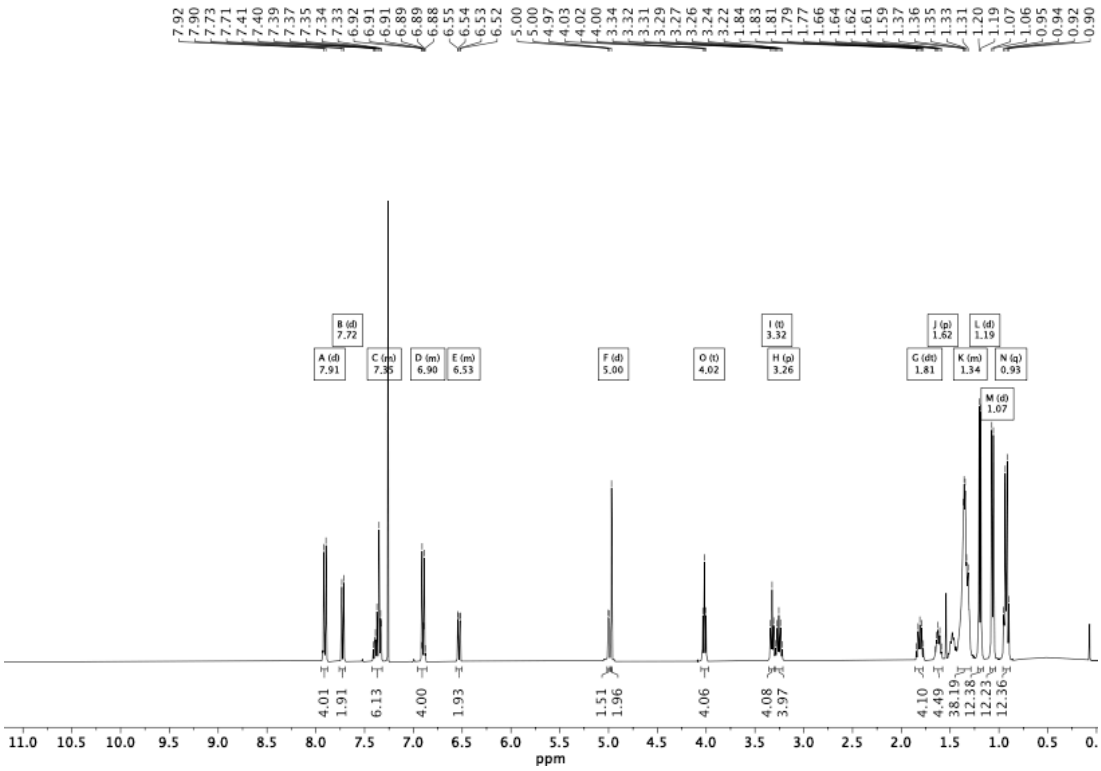

Figure S 86: ^{1}H NMR Spectrum of **3.**

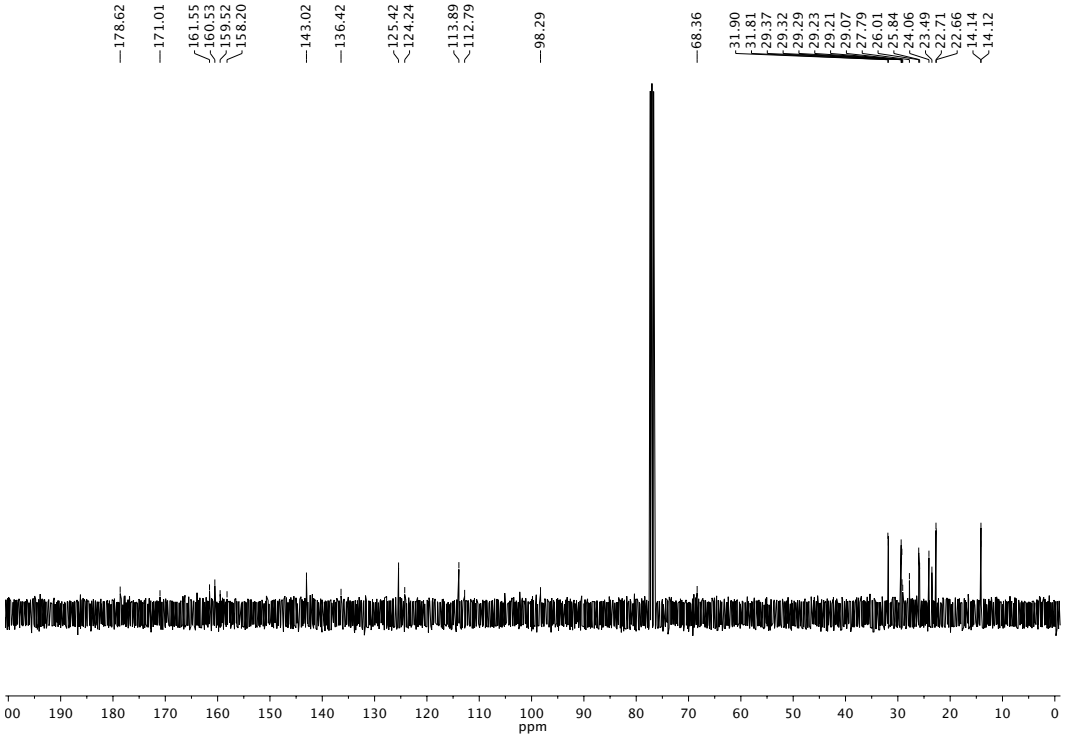

Figure S 87: ^{13}C NMR Spectrum of **3.**

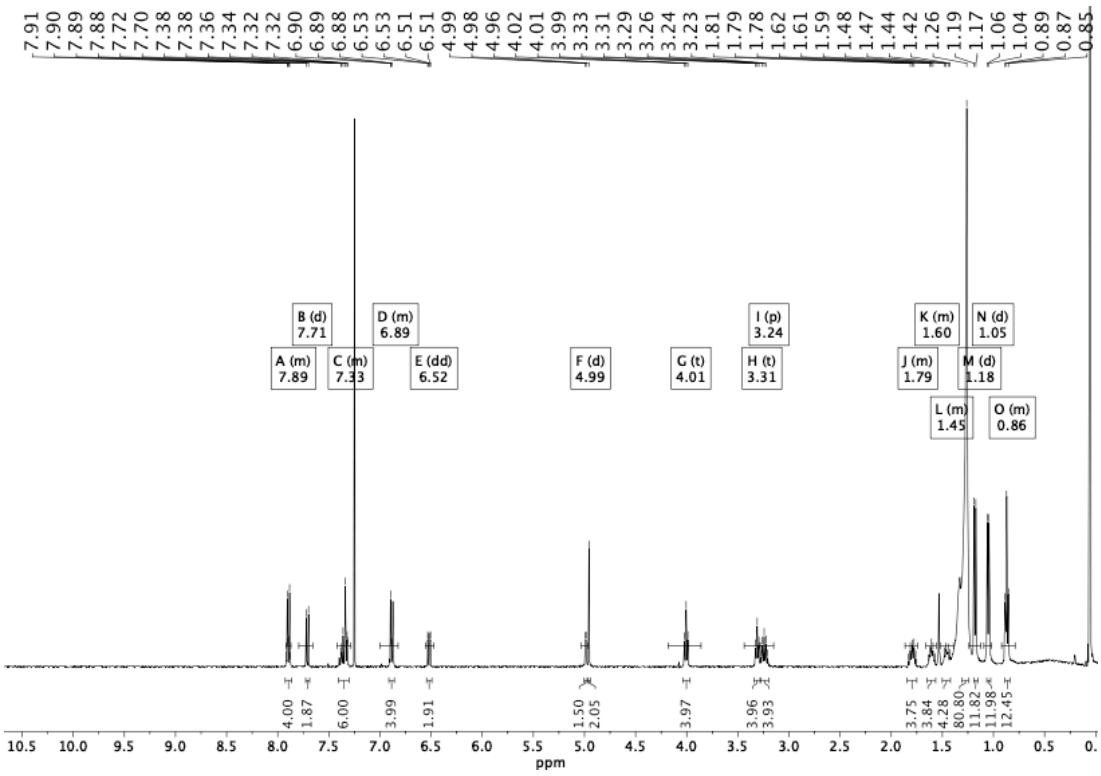

Figure S 88: ^{1}H NMR Spectrum of **4.**

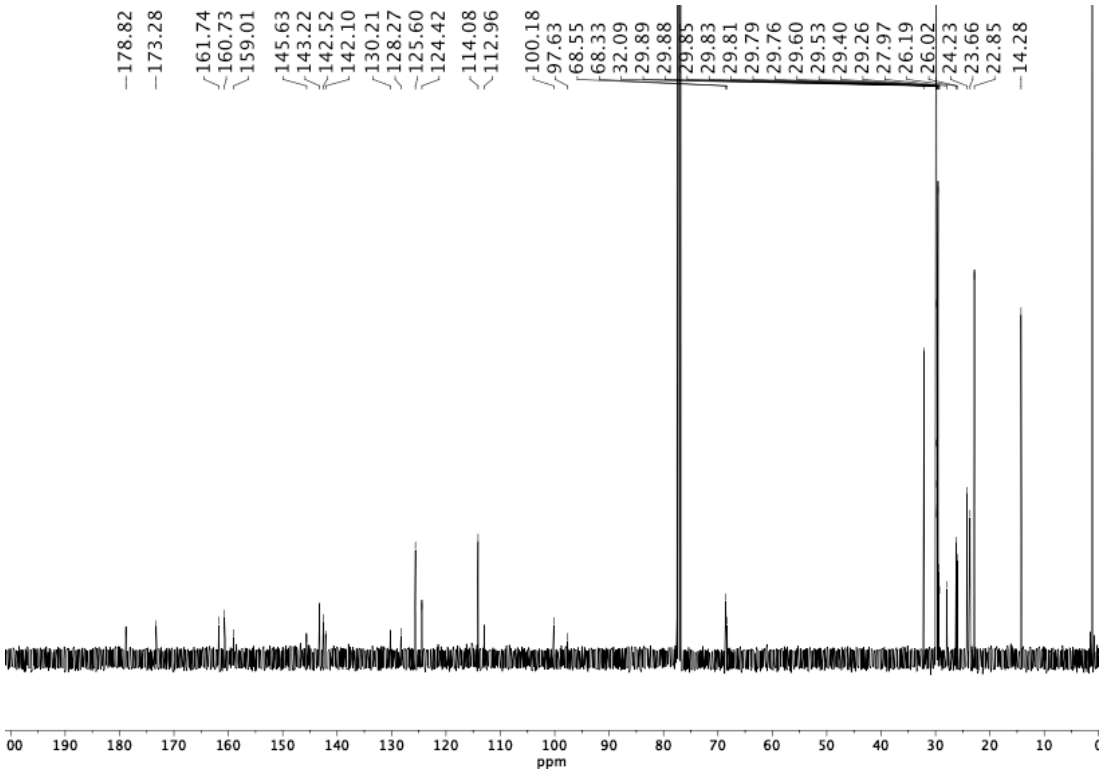

Figure S 89: ^{13}C NMR Spectrum of **4.**

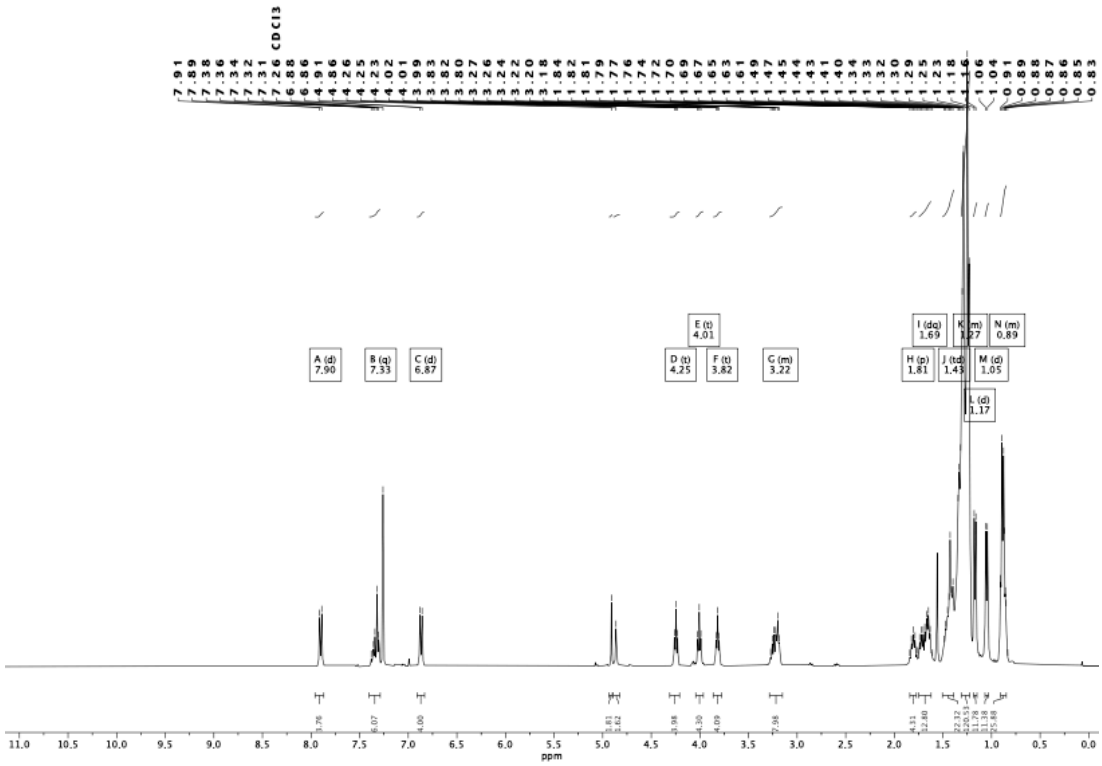

Figure S 90: ^{1}H NMR Spectrum of **5.**

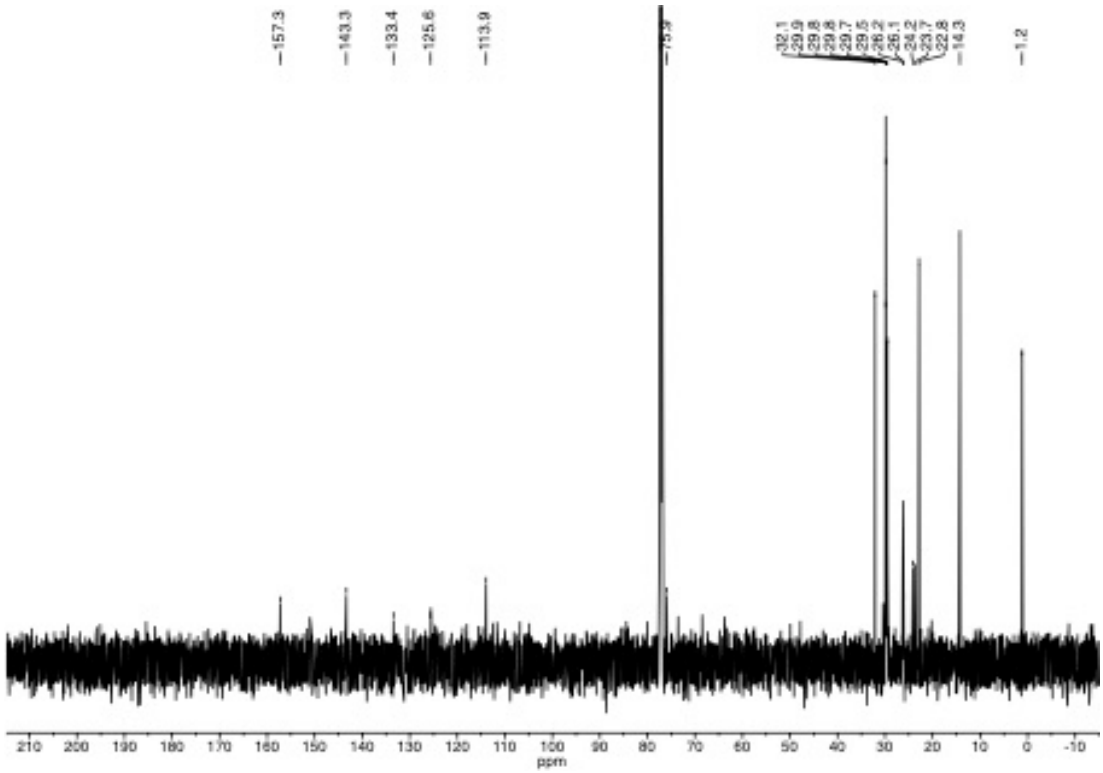

Figure S 91: ^{13}C NMR Spectrum of **5.**

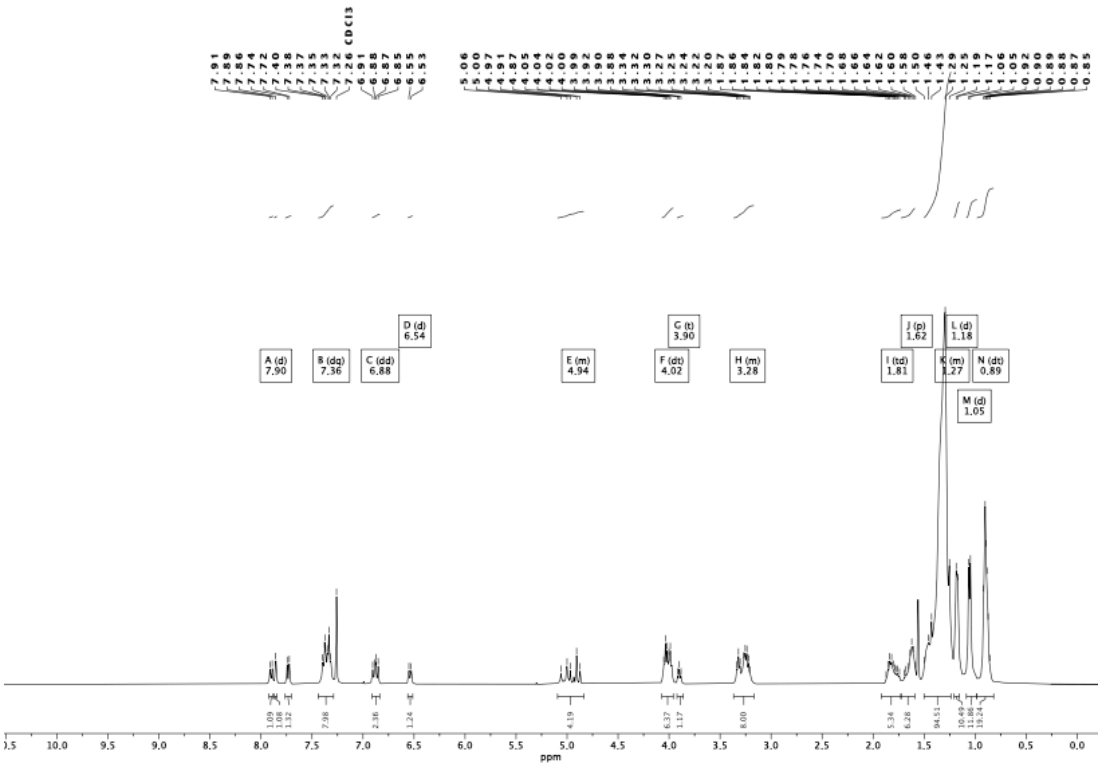

Figure S 92: ^{1}H NMR Spectrum of **6**.

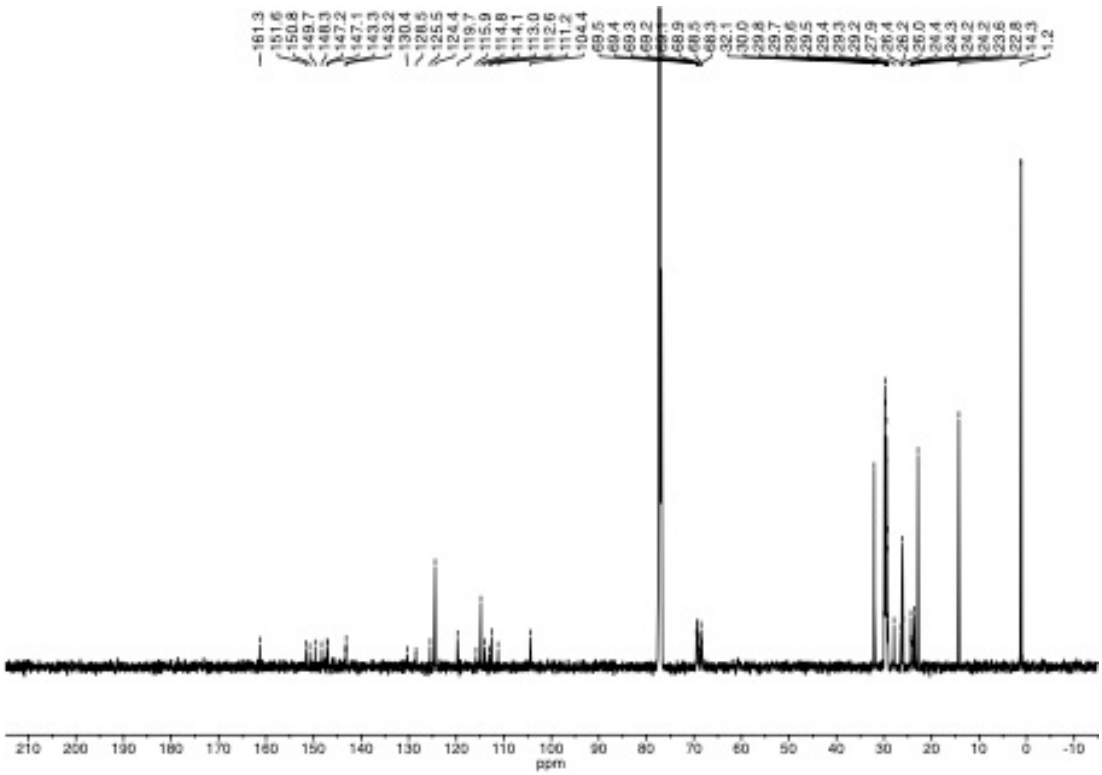

Figure S 93: ^{13}C NMR Spectrum of **6.**

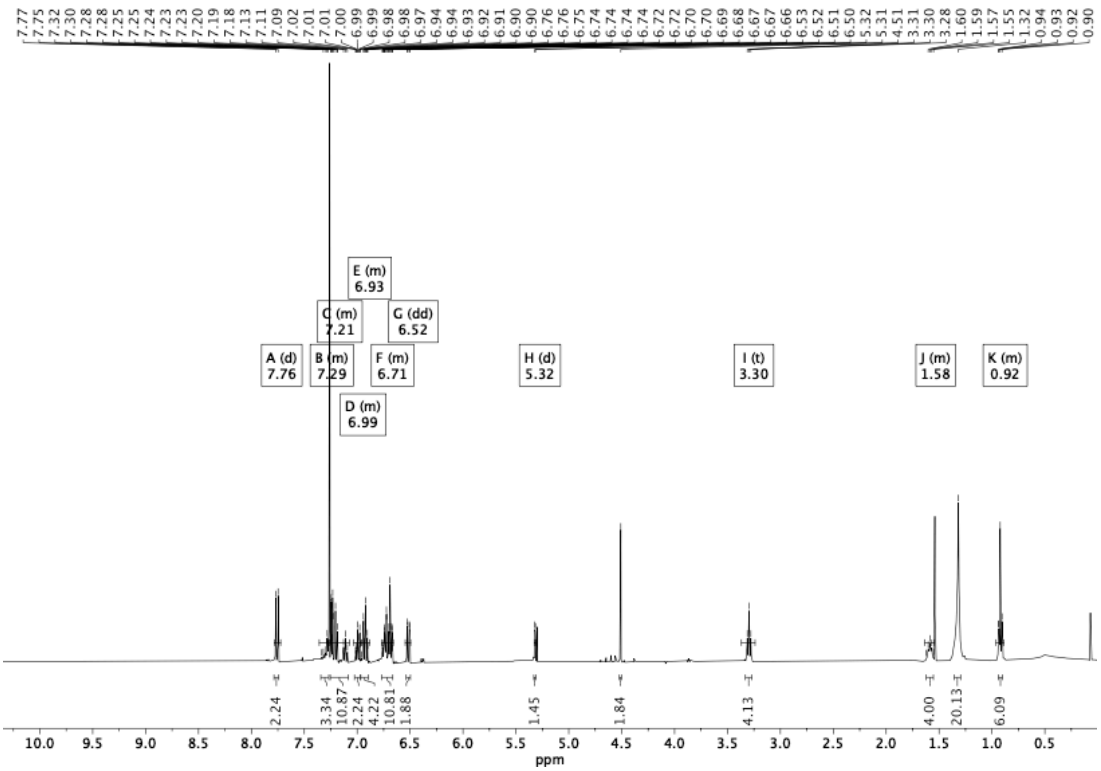

Figure S 94: ^{1}H NMR Spectrum of **7.**

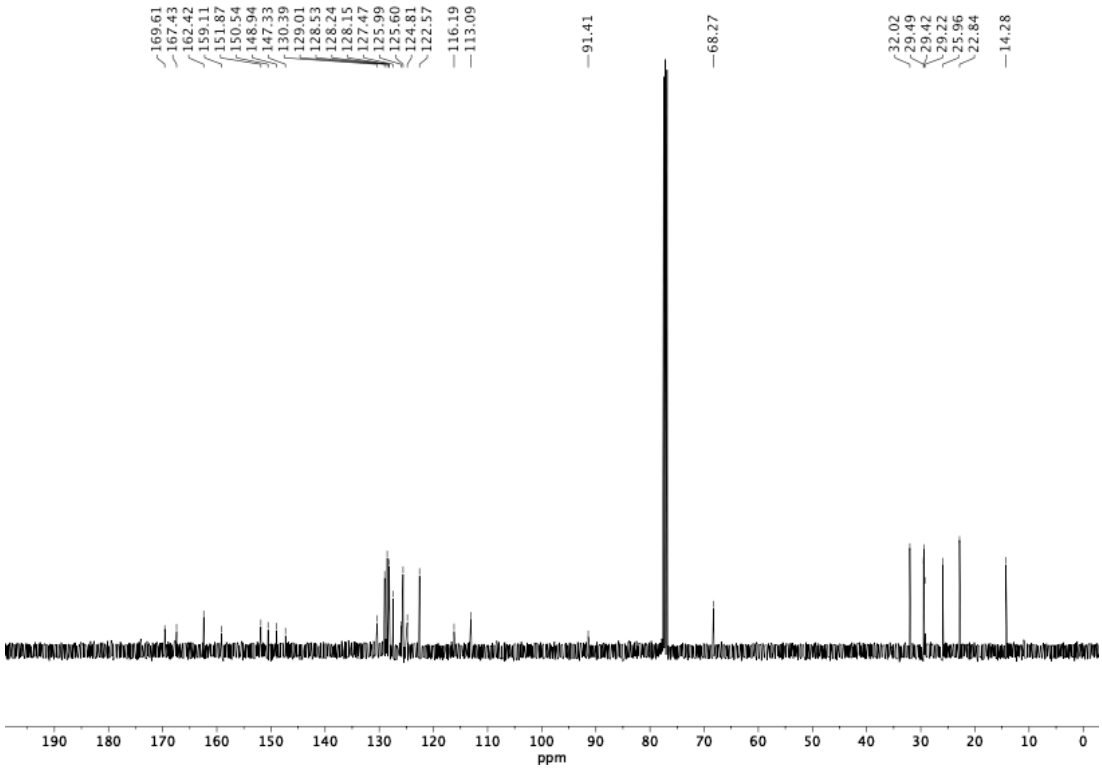

Figure S 95: ^{13}C NMR Spectrum of **7.**

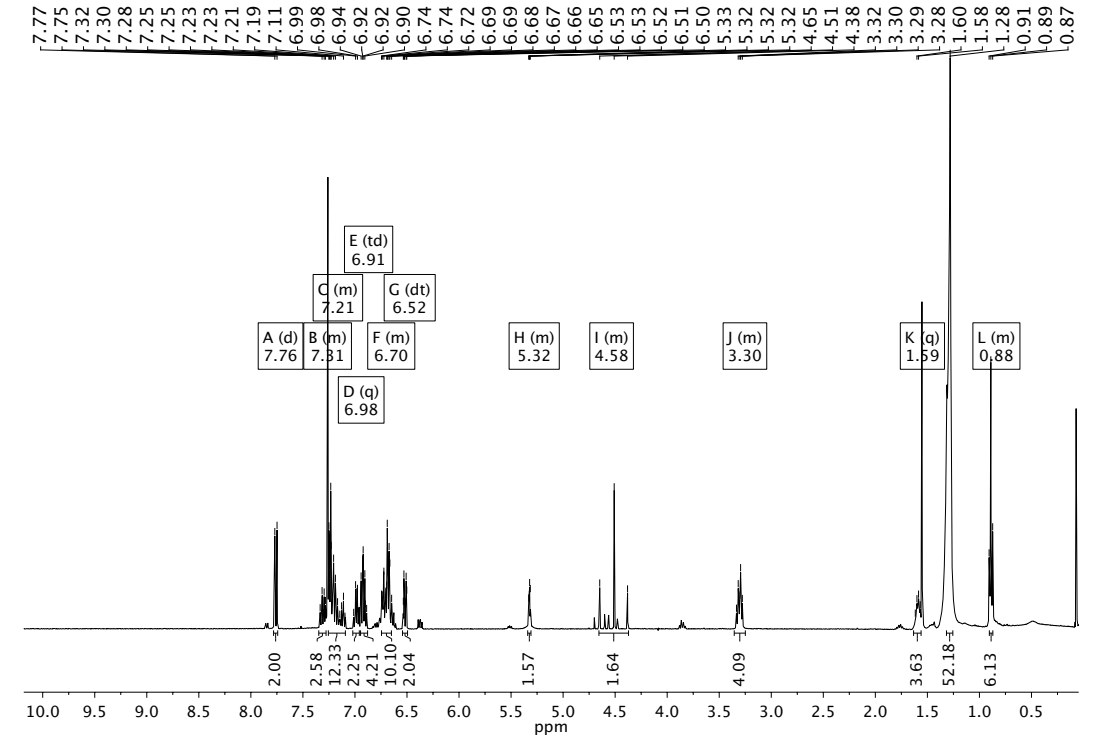

Figure S 96: ^{1}H NMR Spectrum of **8.**

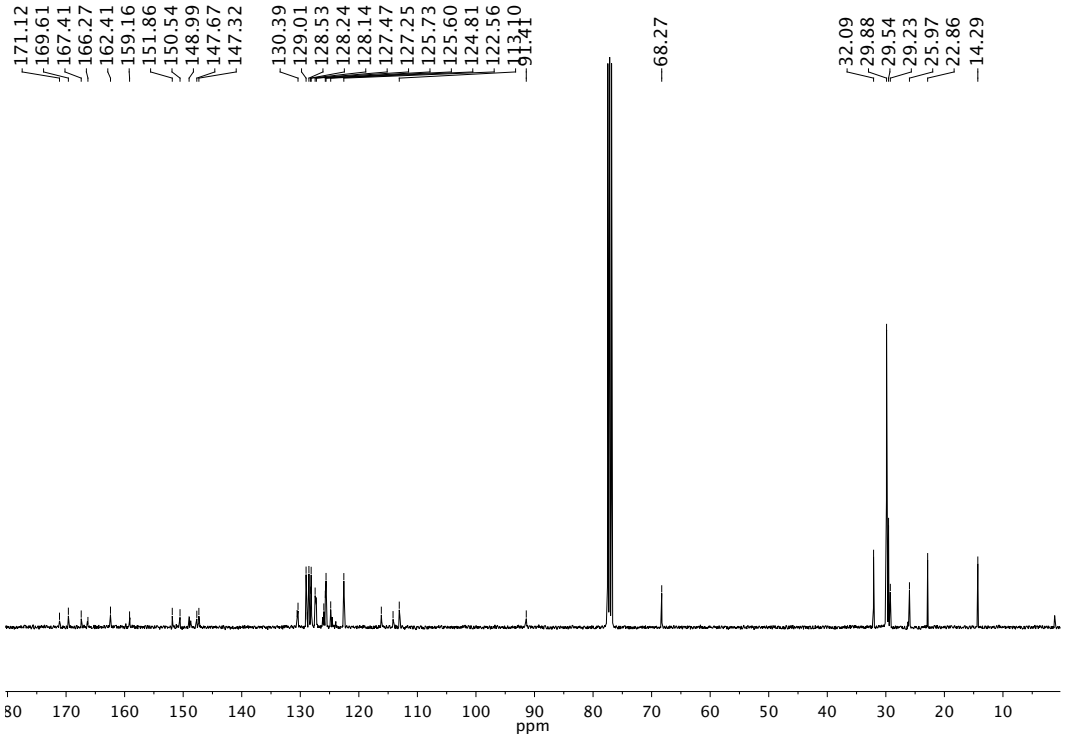

Figure S 97: ^{13}C NMR Spectrum of **8.**

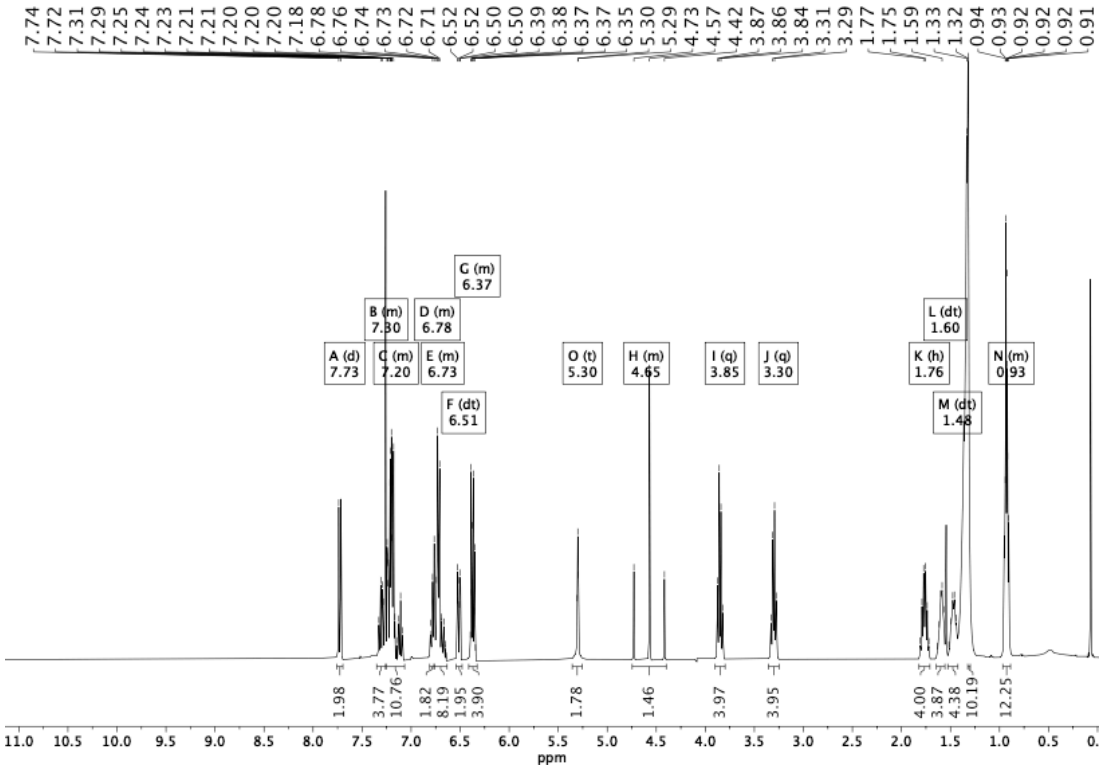

Figure S 98: ^{1}H NMR Spectrum of **9.**

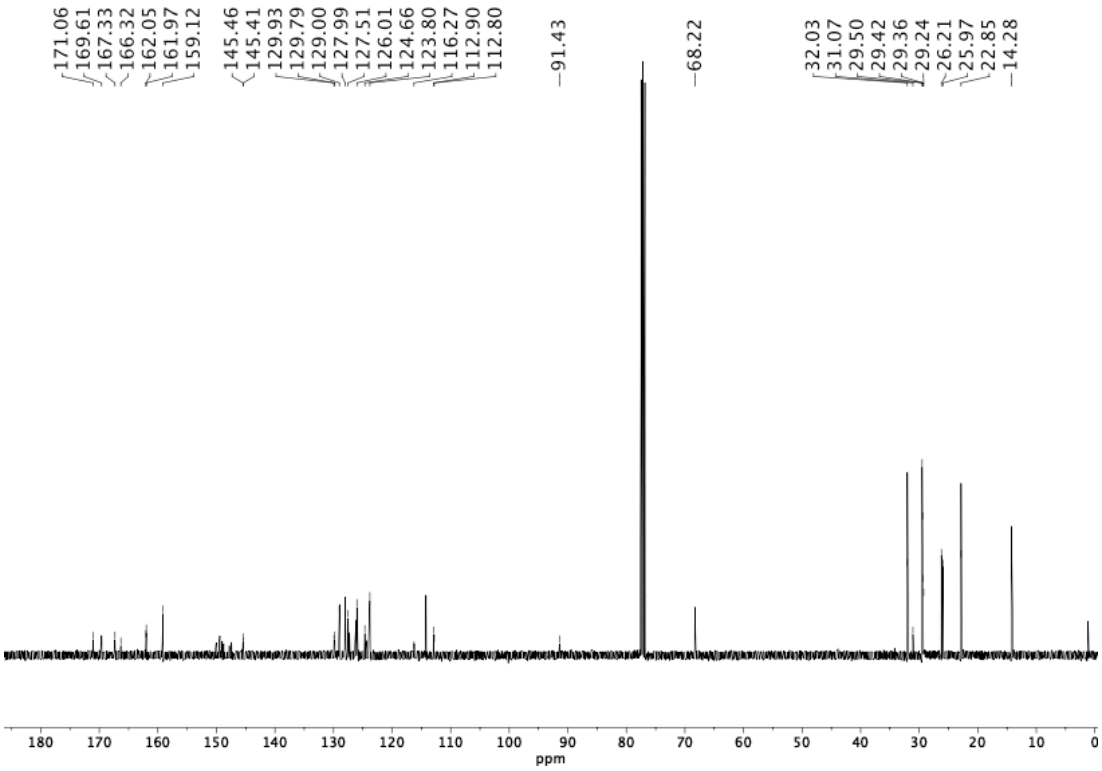

Figure S 99: ^{13}C NMR Spectrum of **9.**

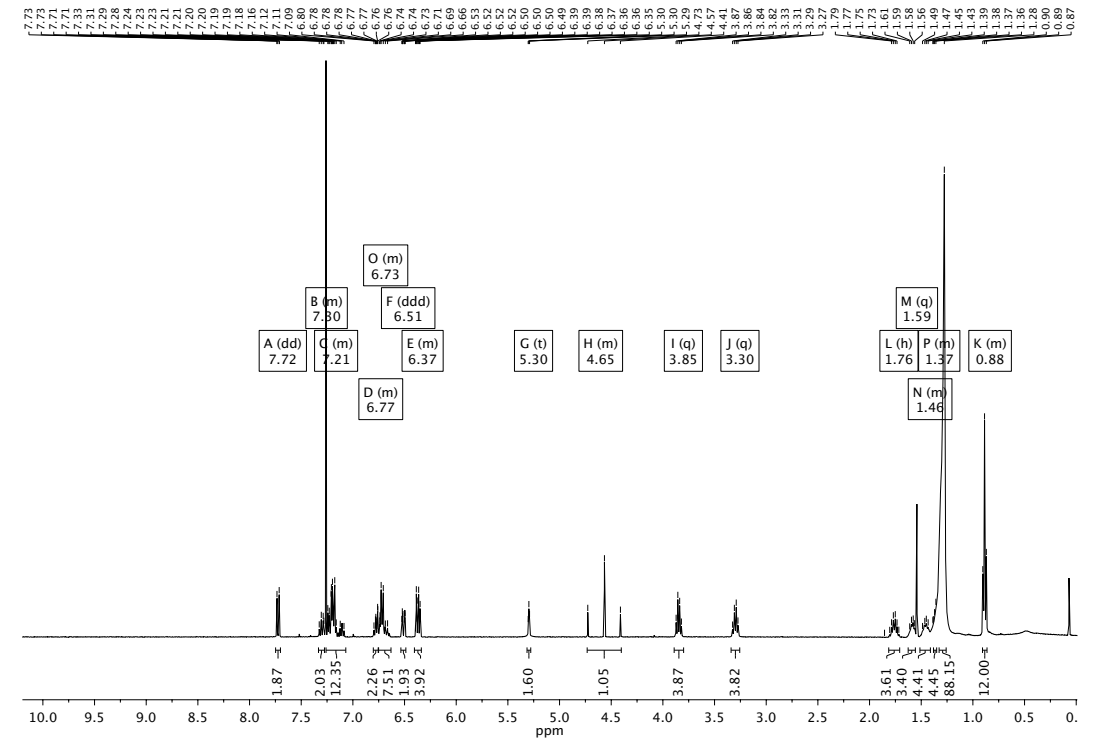

Figure S 100: ^{1}H NMR Spectrum of **10.**

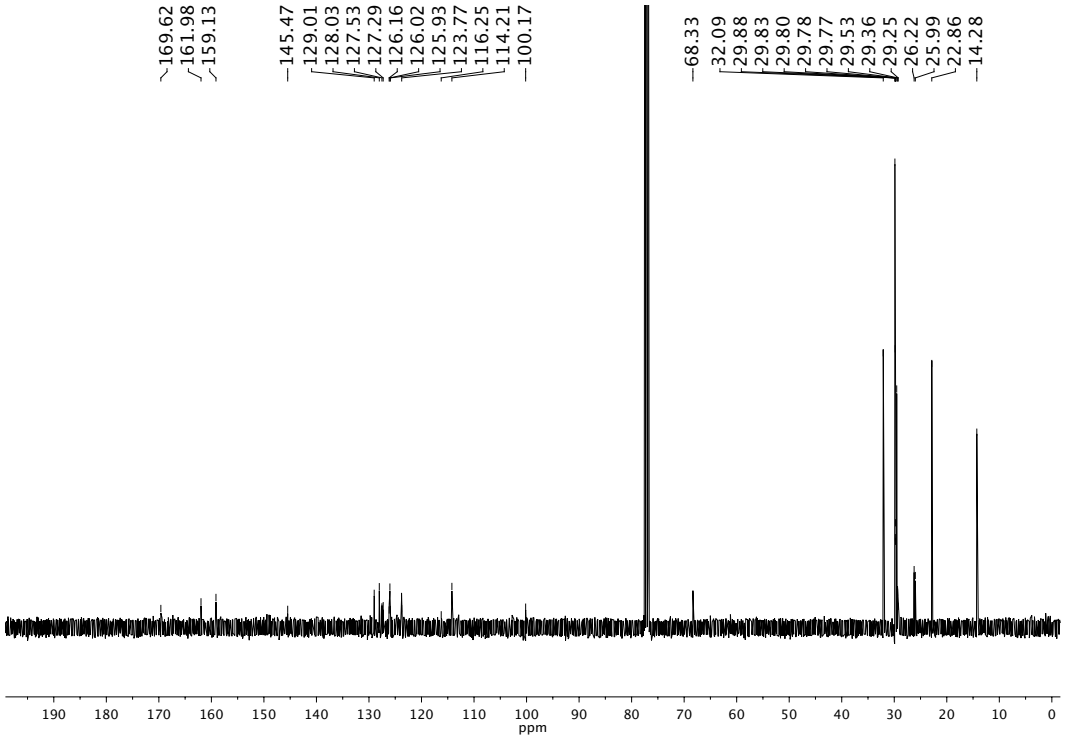

Figure S 101: ^{13}C NMR Spectrum of **10.**

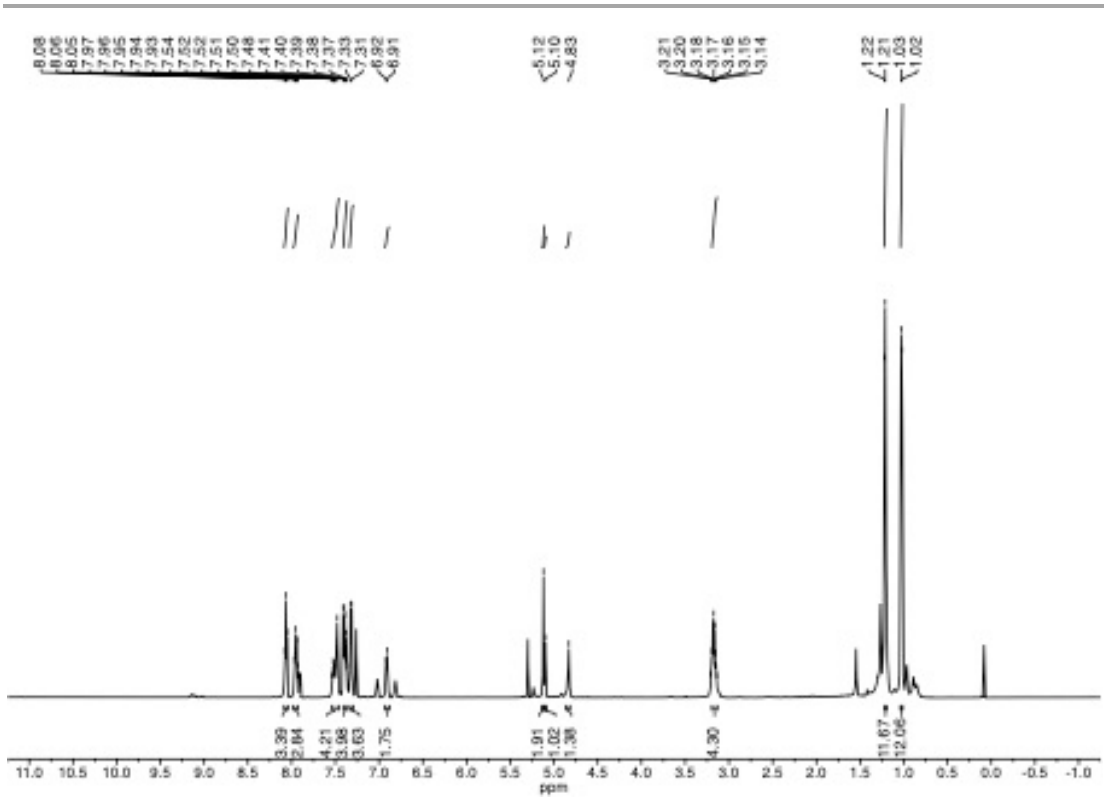

Figure S 102: ^{1}H NMR Spectrum of **11**.

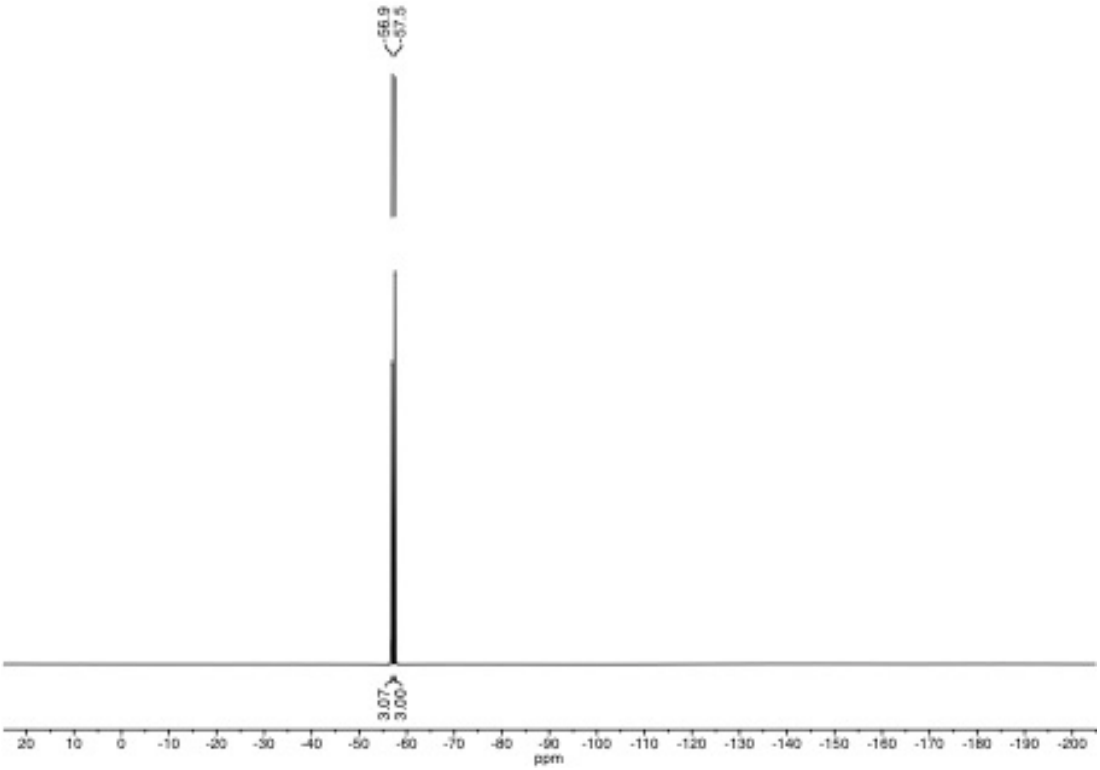

Figure S 103: ^{19}F NMR Spectrum of **11**.

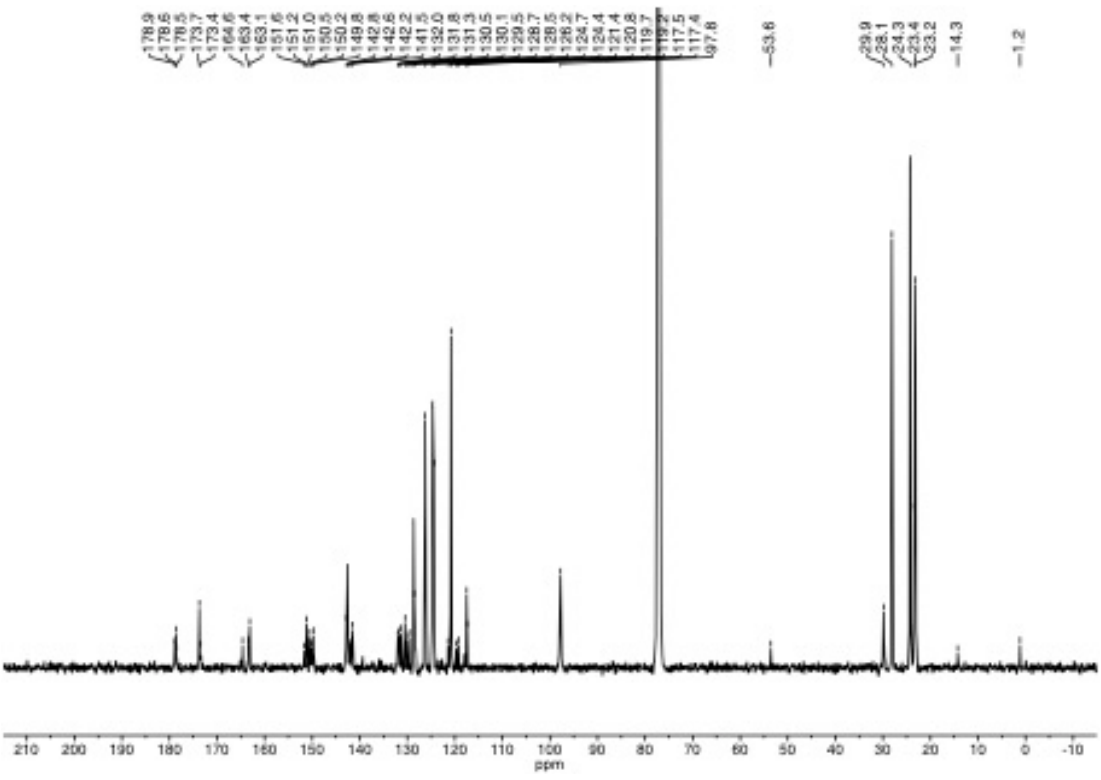

Figure S 104: ^{13}C NMR Spectrum of **11**.

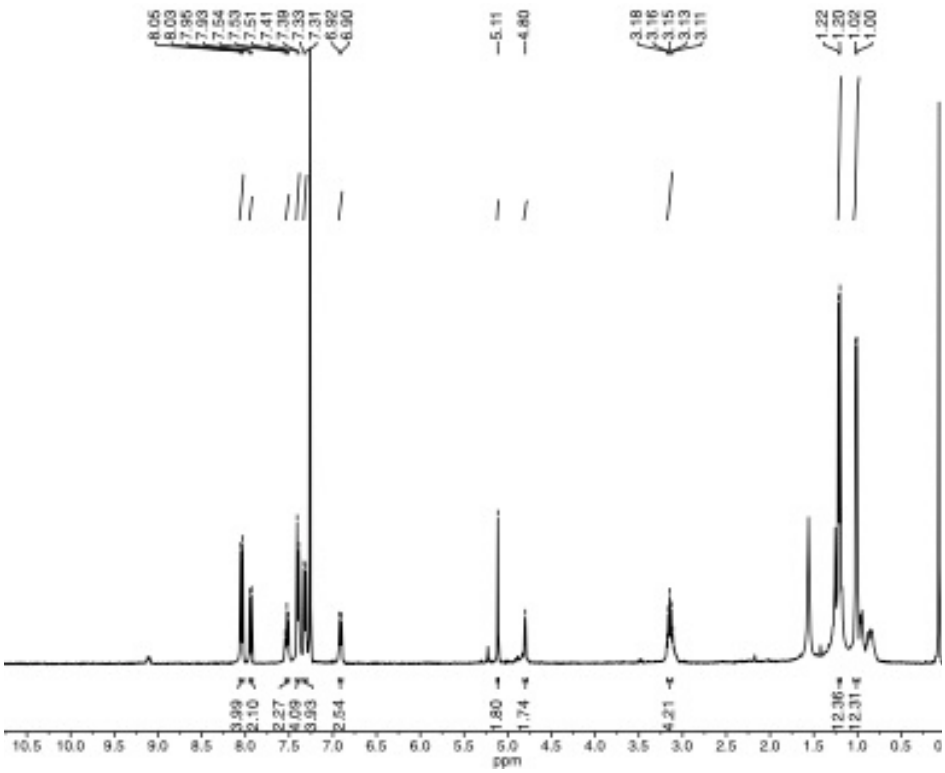

Figure S 105: ^{1}H NMR Spectrum of **12**.

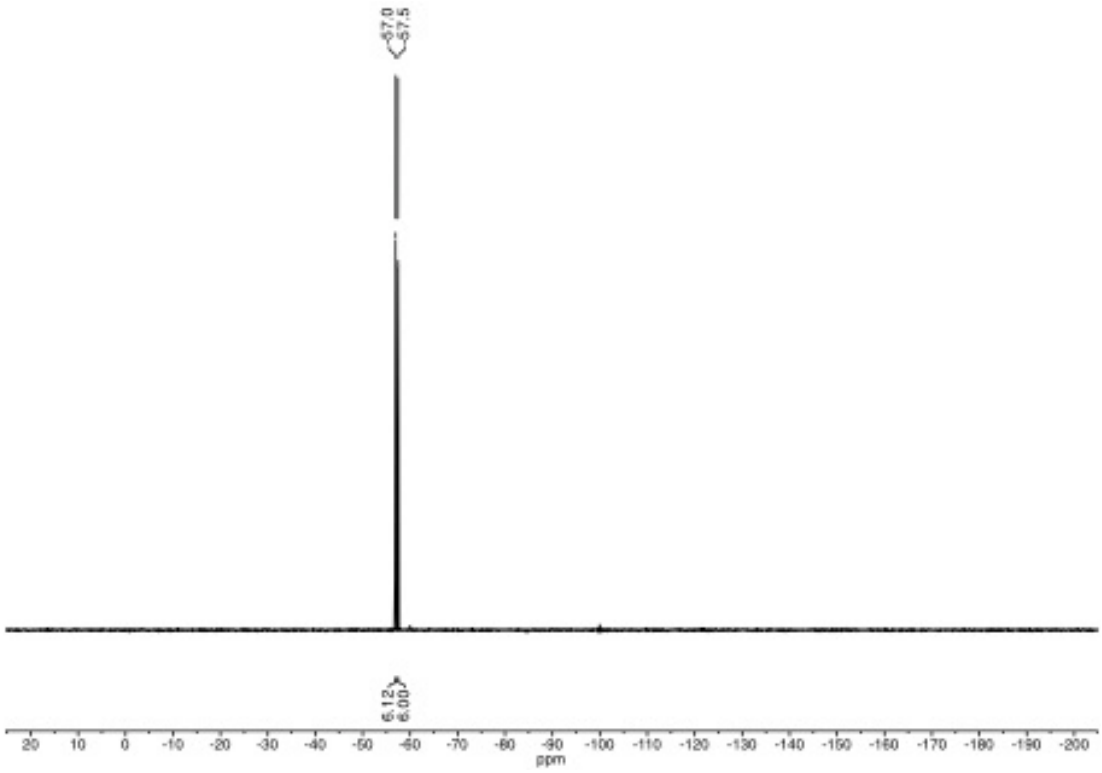

Figure S 106: ^{19}F NMR Spectrum of **12**.

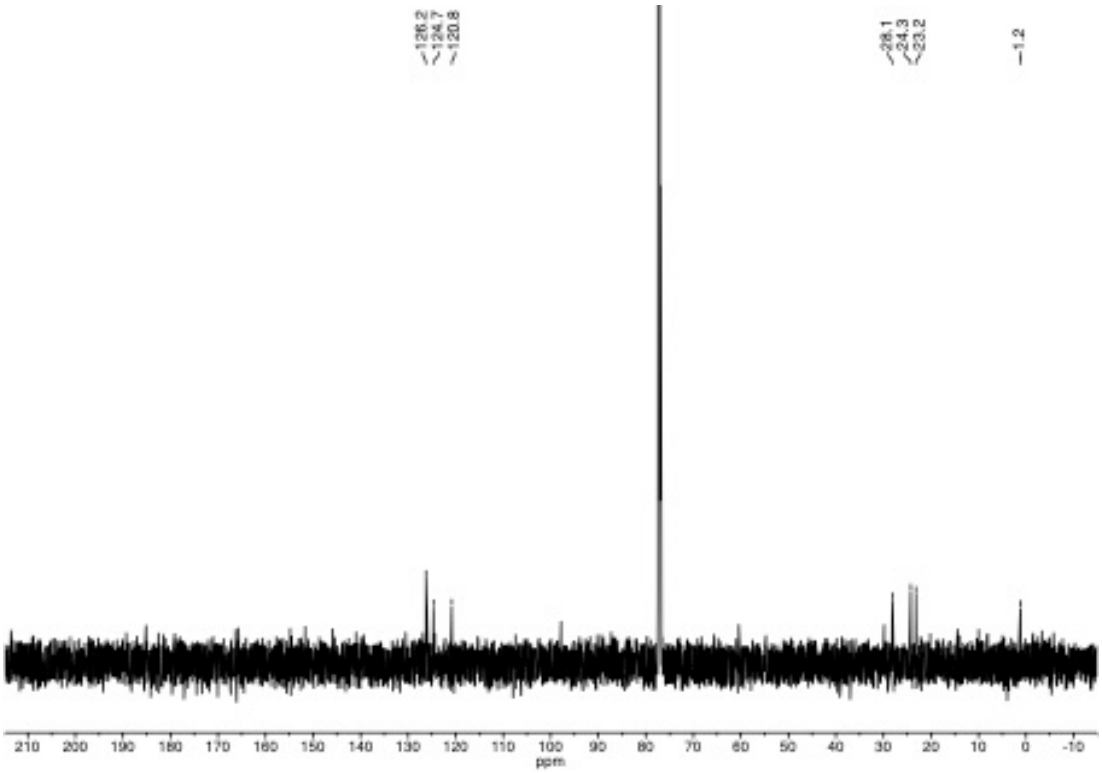

Figure S 107: ^{13}C NMR Spectrum of **12**.

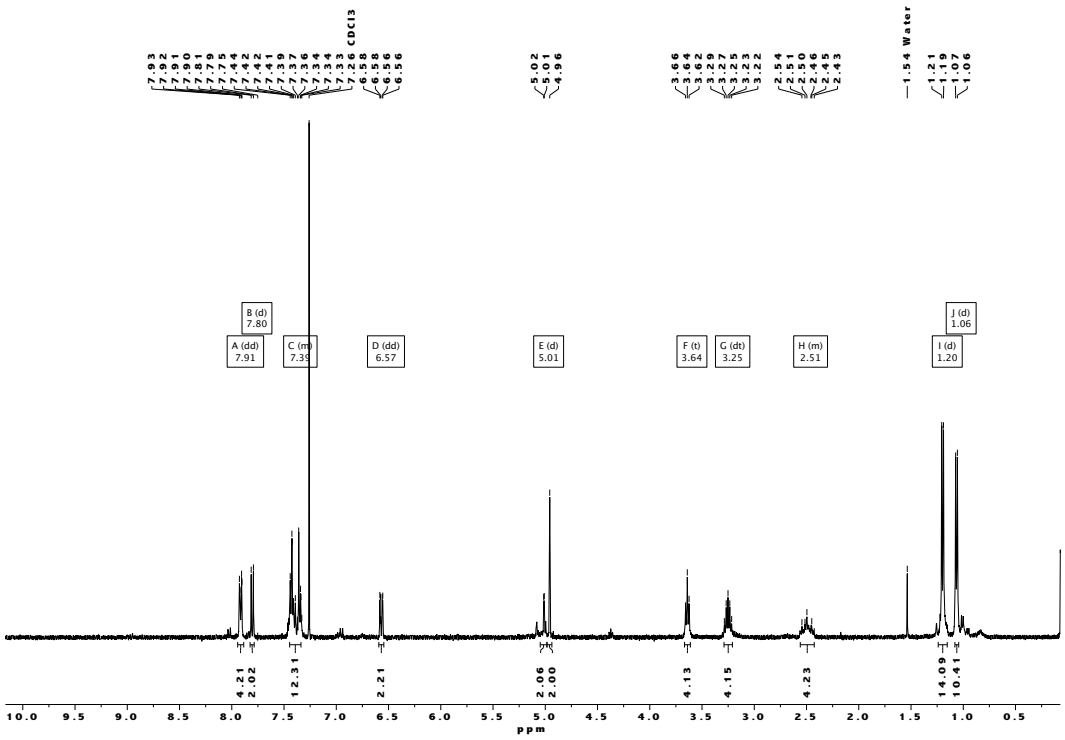

Figure S 108: ^{1}H NMR Spectrum of **13**.

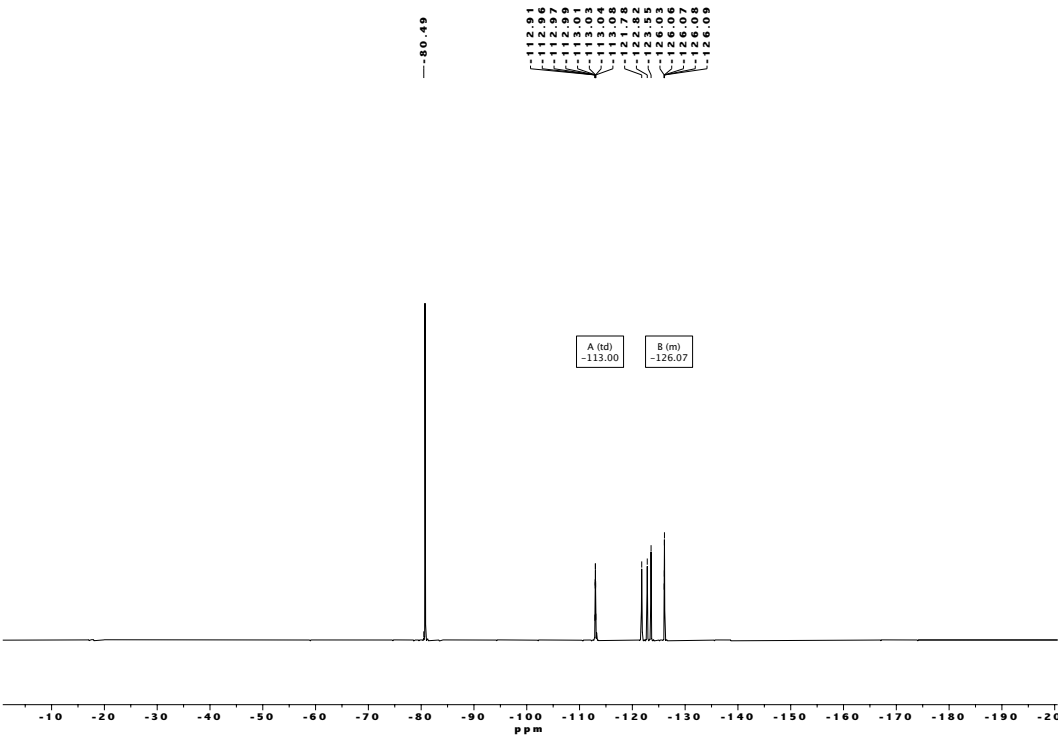

Figure S 109: ^{19}F NMR Spectrum of **13**.

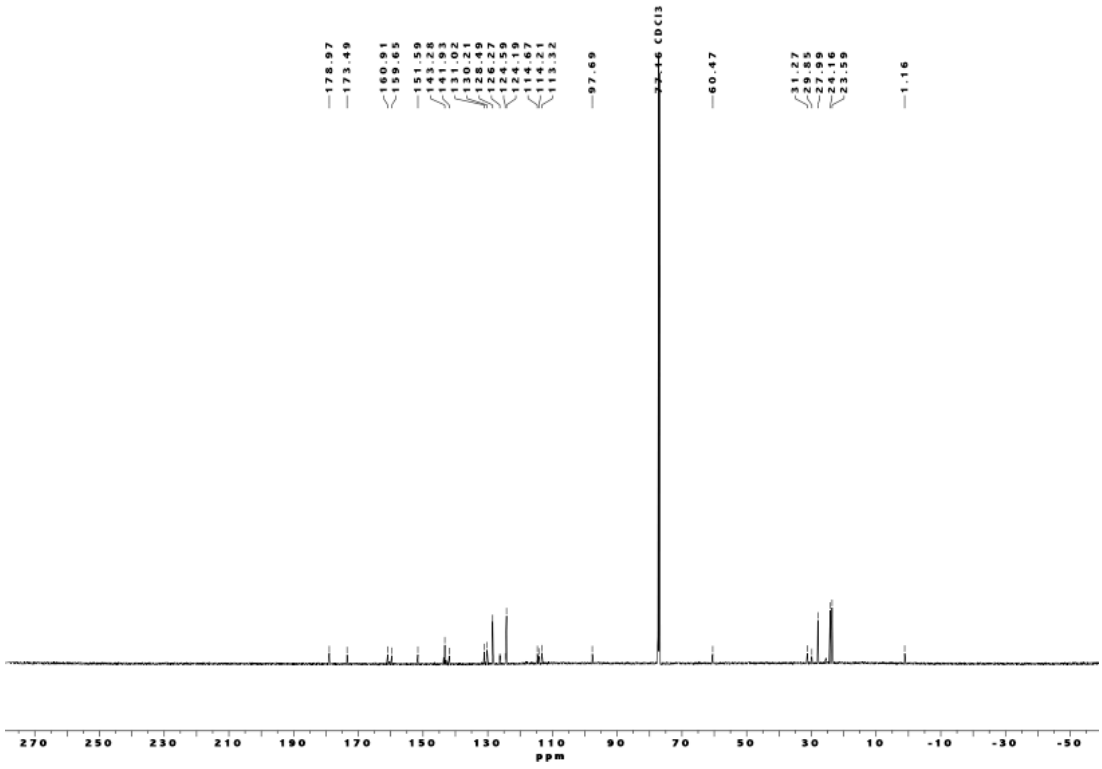

Figure S 110: ^{13}C NMR Spectrum of **13**.

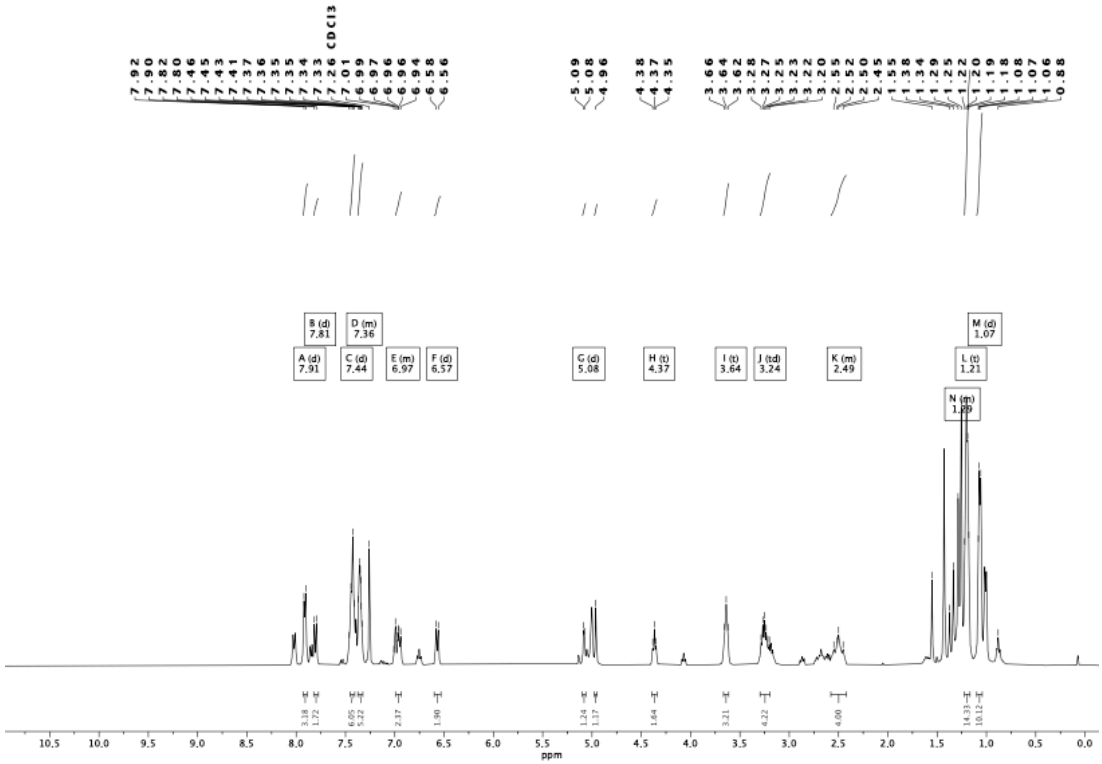

Figure S 111: ^{1}H NMR Spectrum of **14**.

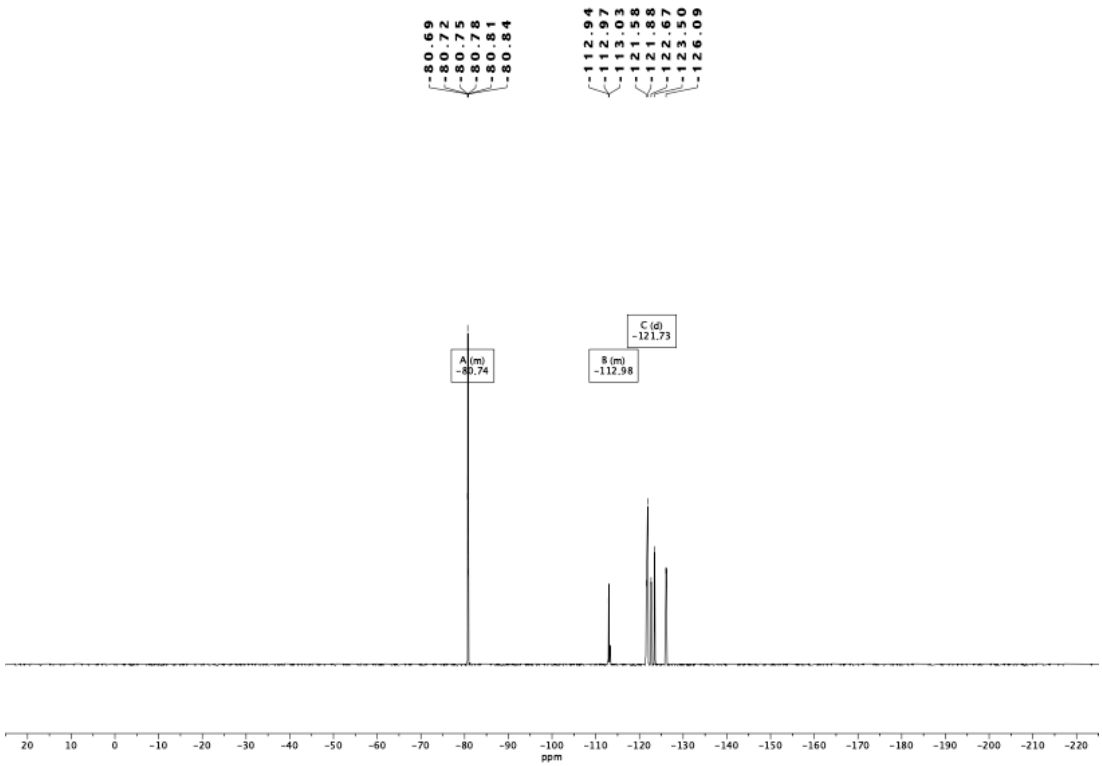

Figure S 112: ^{19}F NMR Spectrum of **14**.

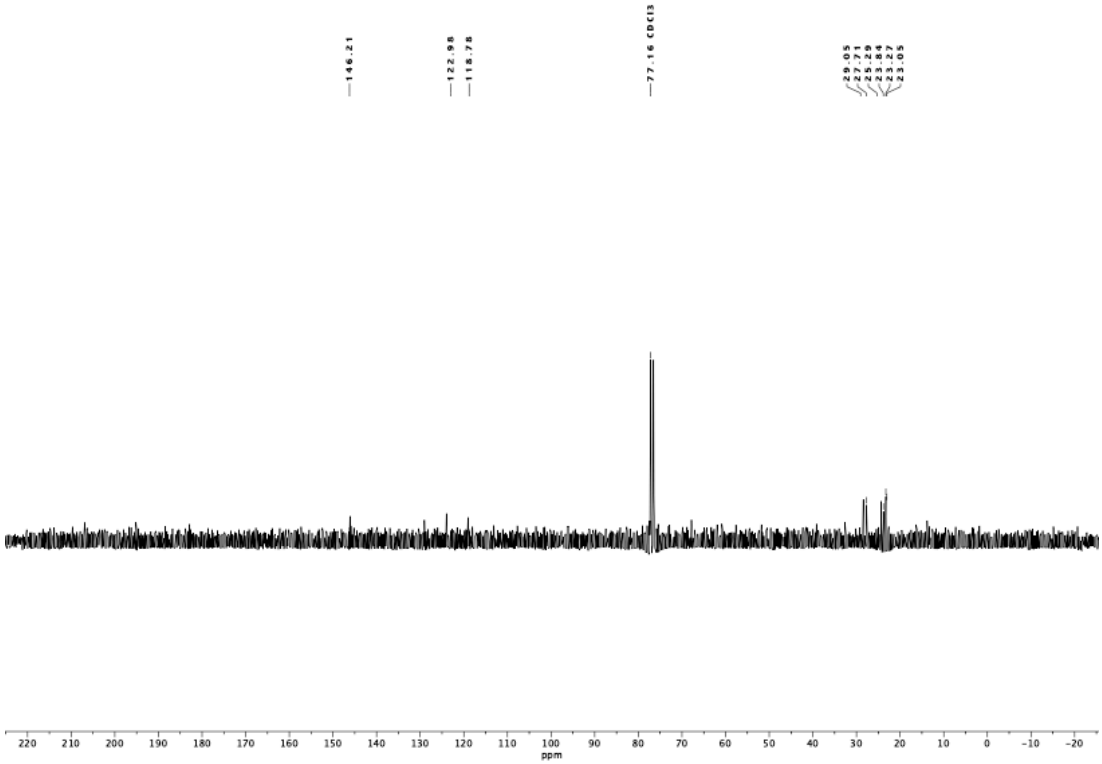

Figure S 113: ^{13}C NMR Spectrum of **14**.

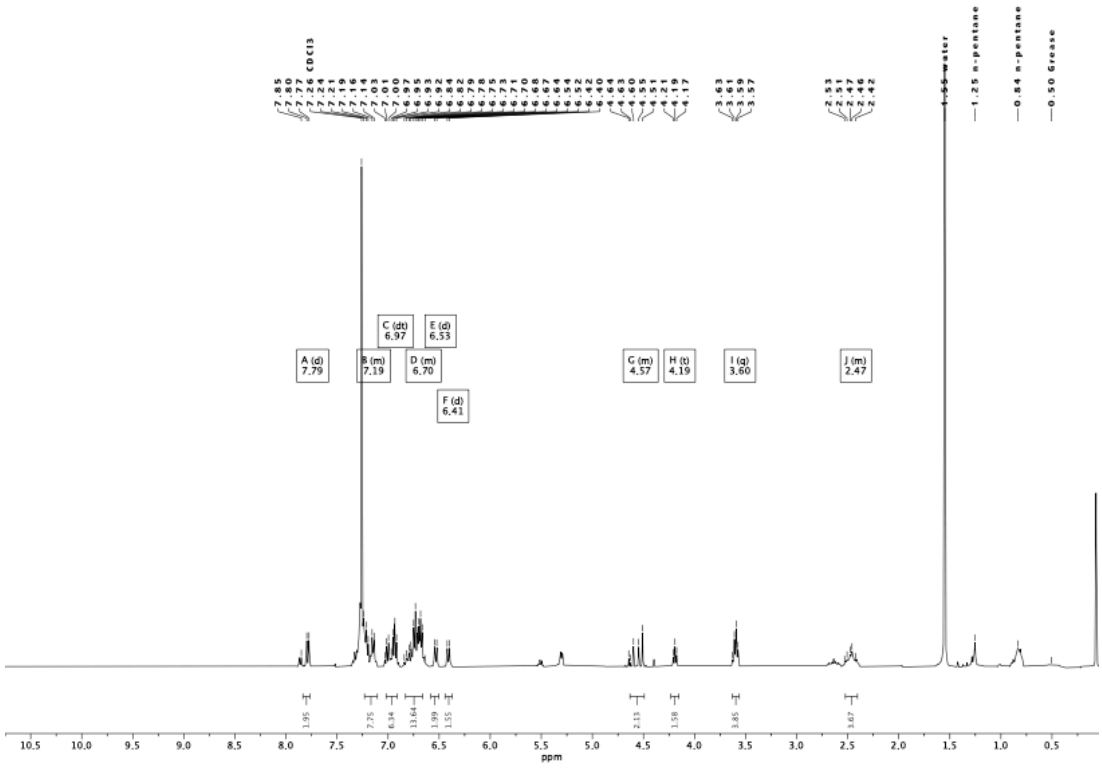

Figure S 114: ^{1}H NMR Spectrum of **15**.

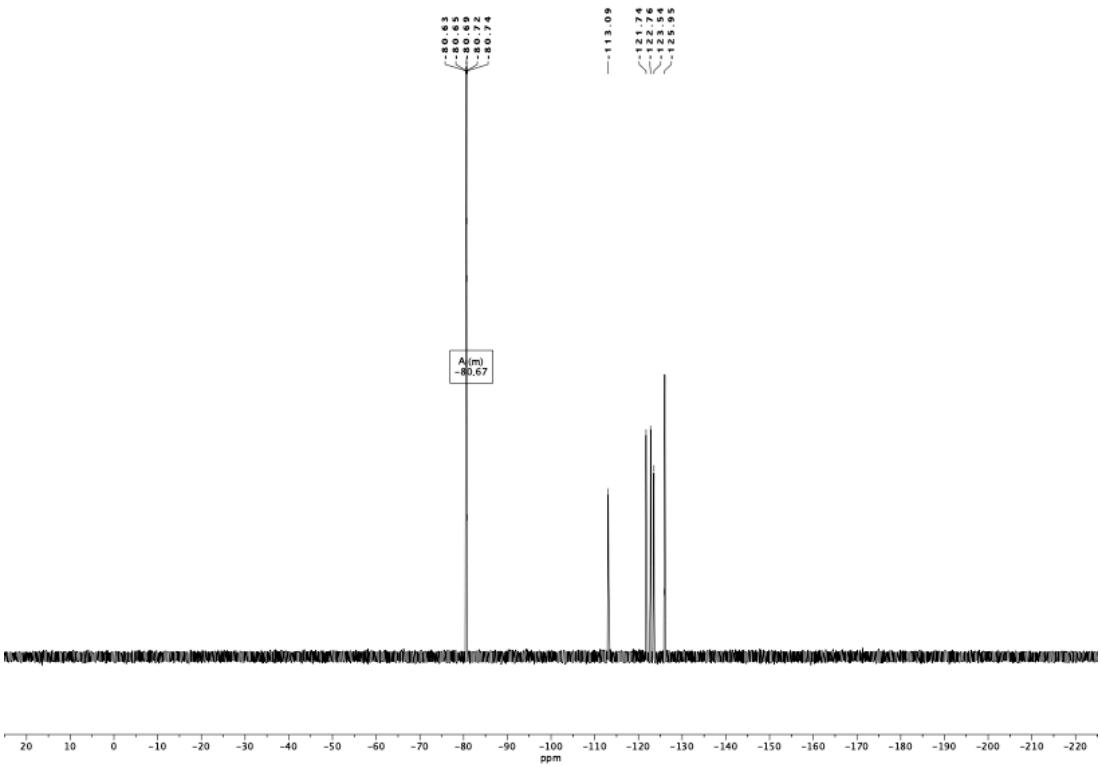

Figure S 115: ^{19}F NMR Spectrum of **14**.

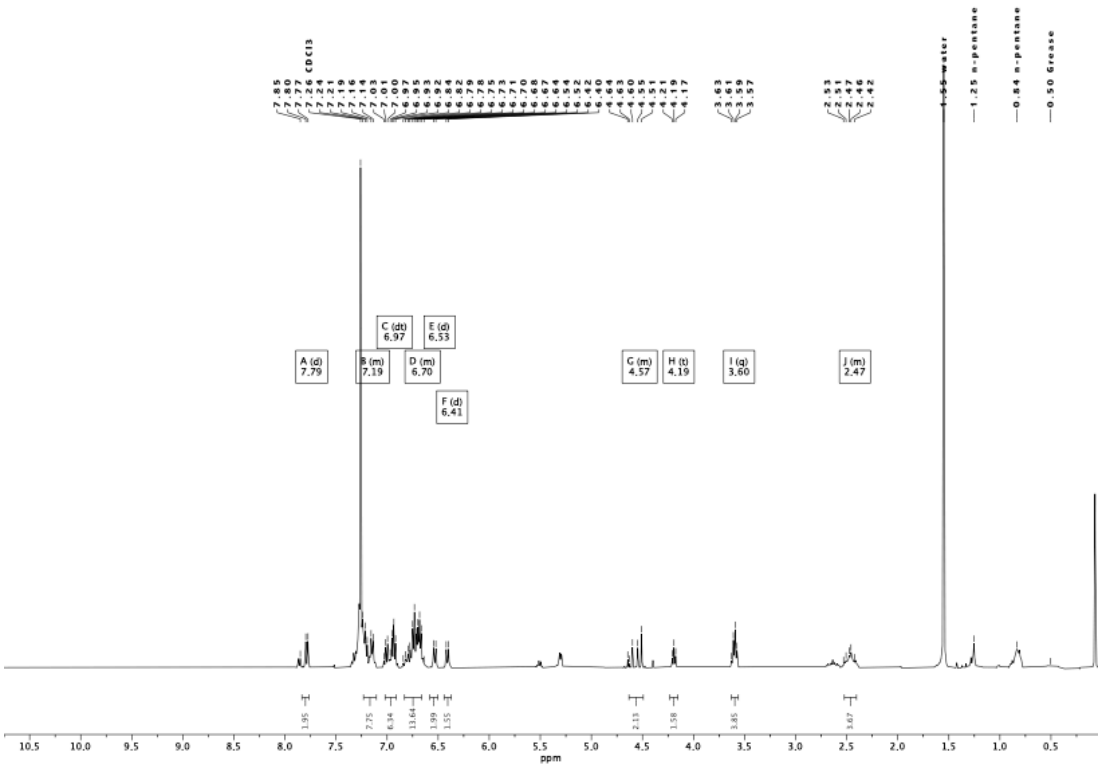

Figure S 116: ^{1}H NMR Spectrum of **16**.

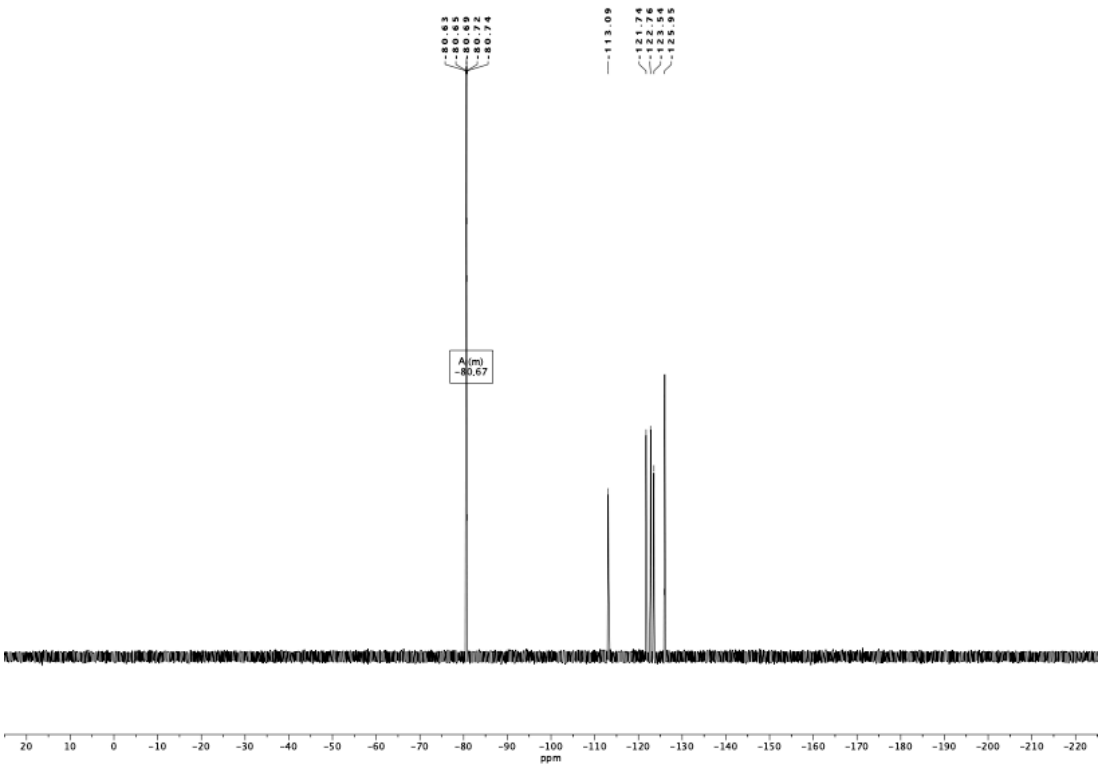

Figure S 117: ^{19}F NMR Spectrum of **16**.

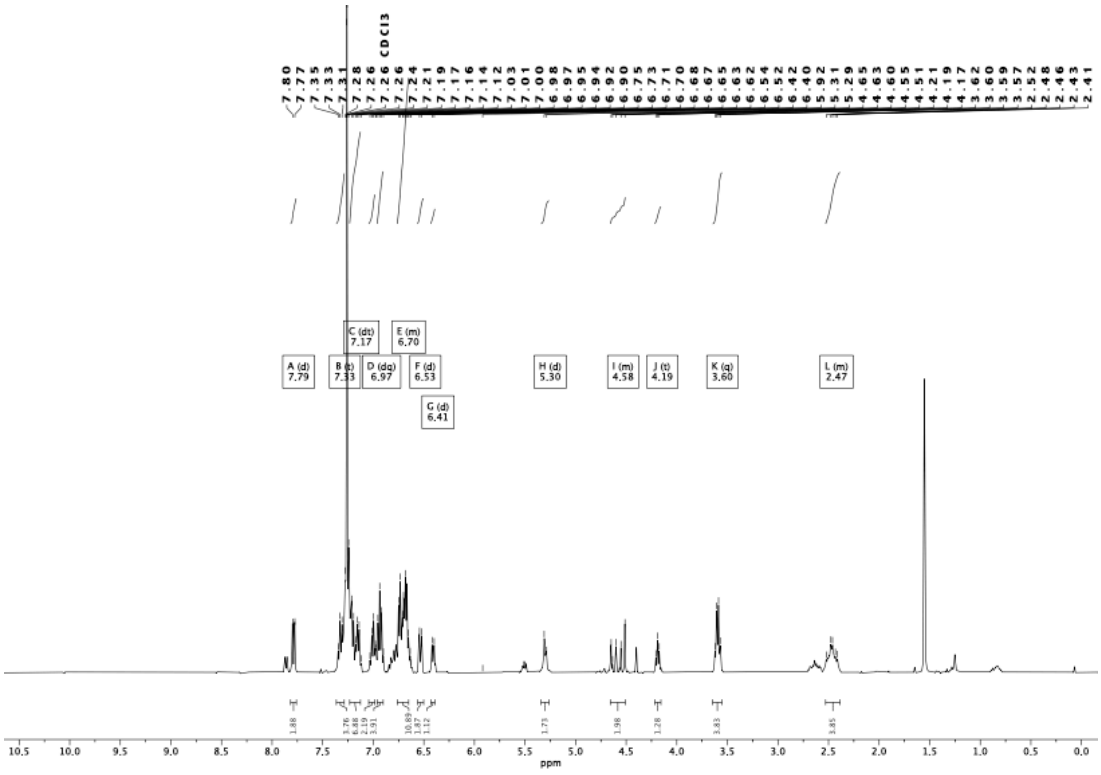

Figure S 118: ^{1}H NMR Spectrum of **17**.

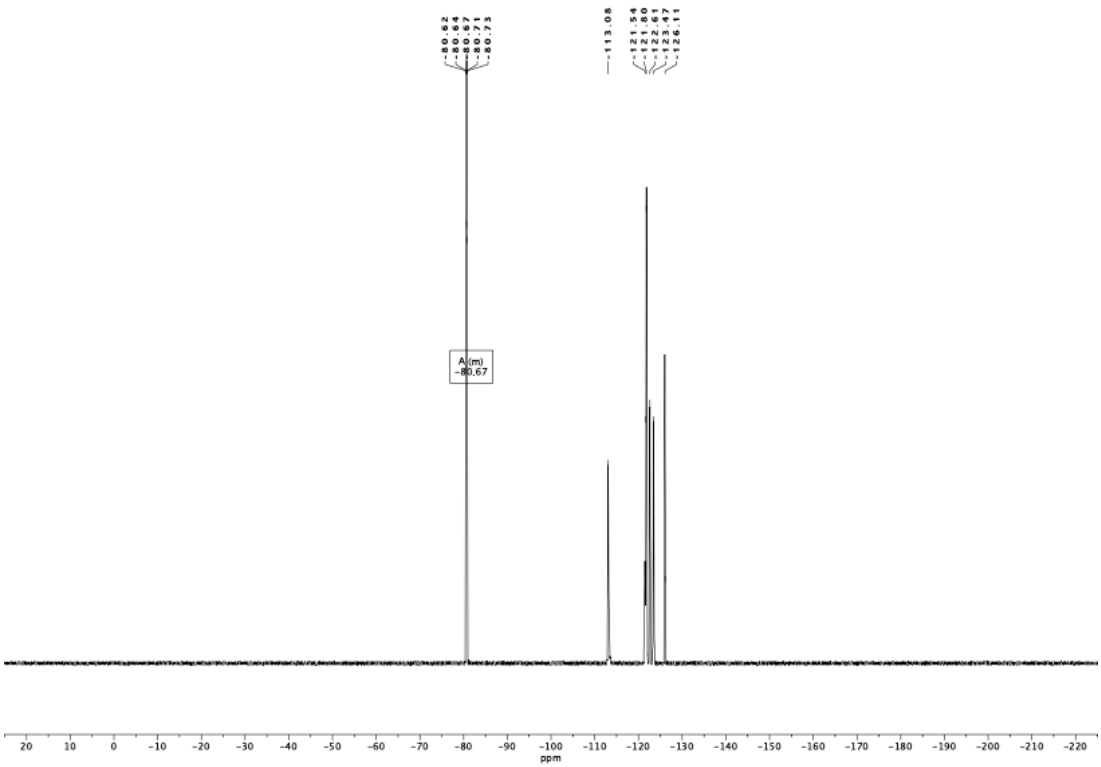

Figure S 119: ^{19}F NMR Spectrum of **17**.

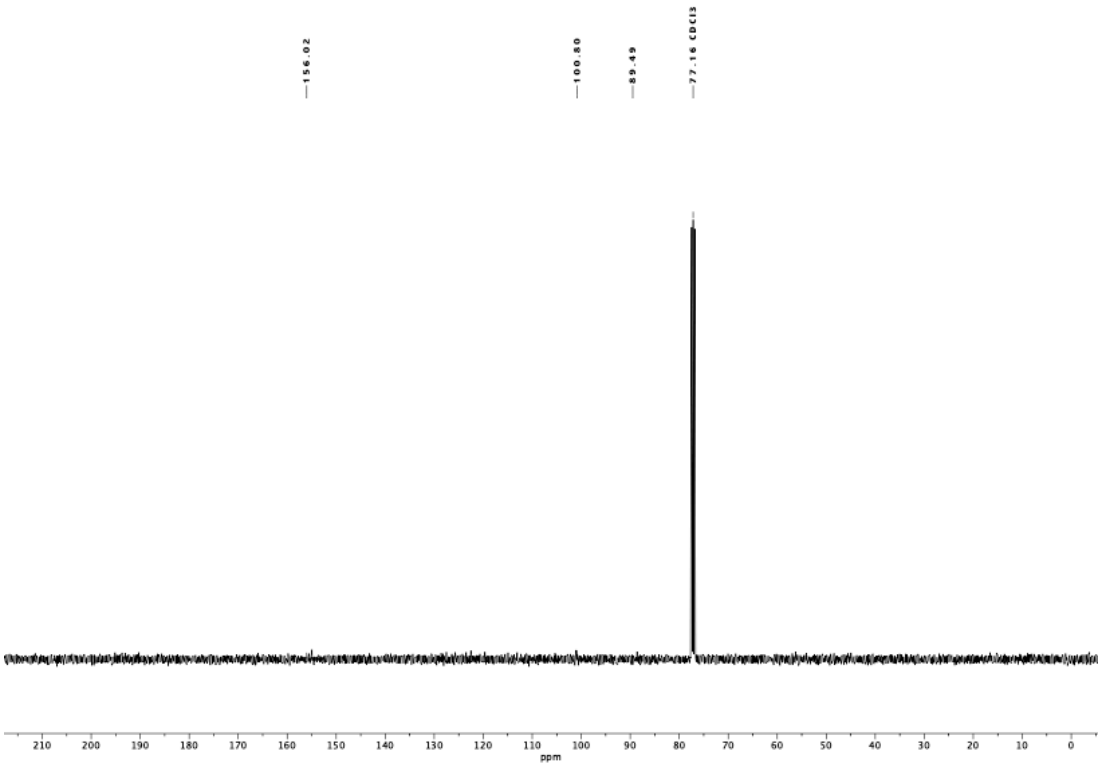

Figure S 120: ^{13}C NMR Spectrum of **17**.

4. Conclusion

In this dissertation, the synthesis of various fluorinated ligand systems and complexes with different transition metal centers was carried out and the magnetic properties and electrochemical behavior of the complexes were investigated

In the first part the influence of fluorine specific interactions in the secondary coordination sphere on the magnetic properties of the central metal ion was investigated. For this purpose, several fluorinated tripodal ligands were prepared and coordinated to cobalt(II) and iron(II) centers, resulting in homoleptic complexes, where the ligands coordinate in a tridentate fashion, while one arm remains uncoordinated. The investigations show that the fluorine-specific interactions and non-covalent interactions (NCIs) have an impact on the spin state of the metal center, which depends on the degree of fluorination on the benzyl ring and the co-crystallizing solvent. In most complexes with the tf_5ta ligand, the fluorine-specific interactions hinder the energetically favorable $\pi \cdots \pi$ stacking, leading to an edge-to-face stacking. Depending on the co-crystallizing solvent, the cobalt(II) center is either locked in the HS state or coexists in the LS and HS species. This is also the case for the complex with the unsymmetrically substituted tripodal ligand $mbdf_5ta$ and the one with the tf_3ta ligand. In case of the cobalt complexes with tfta, the NCIs in the secondary coordination sphere seem to be stronger than the ones observed for the non-fluorinated ligand tbta as the intramolecular interactions are not hindered by co-crystallization of solvent molecules. Even though both complexes show similar NCIs only one of them displays a partial SCO, which was further confirmed by EPR measurements. Furthermore, the iron complex with tf_5ta shows an edge-to-face stacking, while for the complex with tfta, an arene face-to-face interaction between the 4-fluorophenyl substituents was observed. Both iron complexes display a complete spin crossover (SCO). Therefore, the metal center, the different fluorinated ligands and the used solvent do have an impact on the NCIs and on the spin state (Figure 44). However, the manner, in which the sample is prepared for SQUID measurements, plays an important role, since the magnetic properties are impacted through grinding. All in all, fluorination of the secondary coordination sphere of metal complexes is a viable way to generate NCIs and to control their spin state.

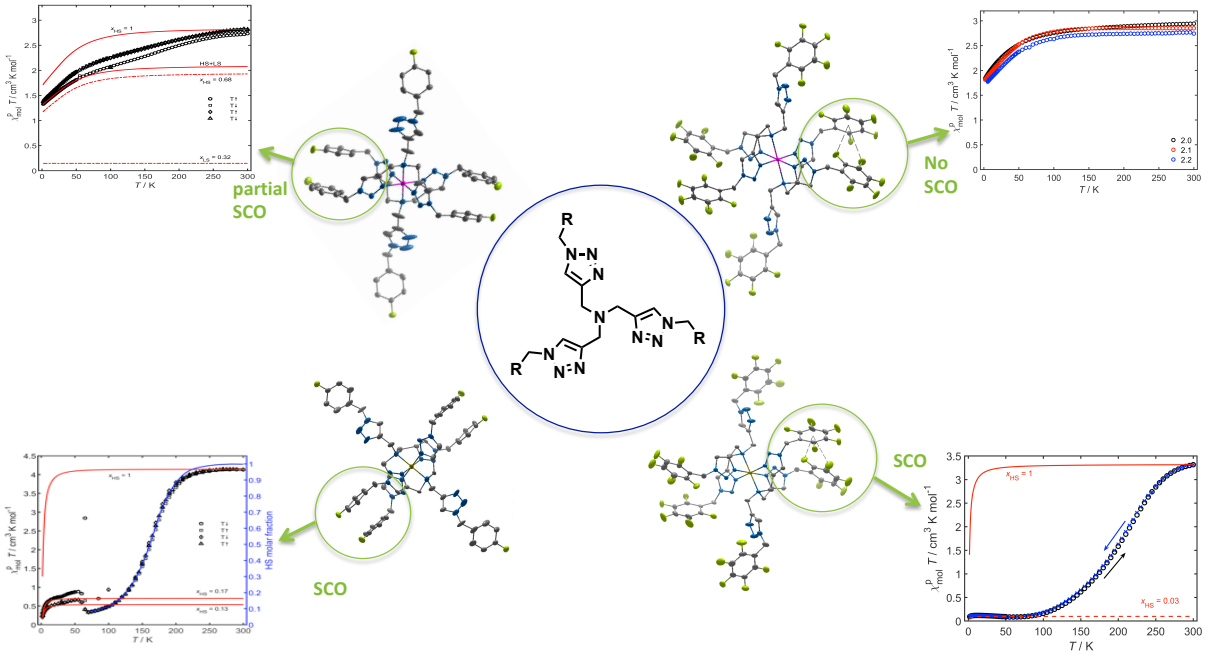

Figure 44: SCO behavior of cobalt(II) (top) and iron(II) (bottom) complexes with tfta (left) and tf_5ta (right).

The second part deals with various cobalt(II) and iron(II) tpy-based complexes containing different fluorinated substituents on the backbone of the tpy moieties. Using cyclic voltammetry, the redox processes of the complexes were investigated and further studied with UV/Vis-NIR spectroelectrochemistry. With SQUID magnetometry measurements, the spin state of the metal centers was evaluated. Most cobalt complexes show an incomplete SCO, while one sample contains molecules in the HS as well as in the LS state. The iron complexes remain in the LS state over the measured temperature range, which was also confirmed by ^{1}H NMR spectroscopy. The potential use as liquid crystalline (LC) material was studies by POM measurements, but as all samples remained solid over the measured temperature range, no LC properties could be identified. Since complexes with non-fluorinated alkyl chains on the tpy backbone show such behavior, the introduction of fluorine seems to have a large impact in this regard. Furthermore, the cobalt(II) complexes were probed by EPR spectroscopy, which revealed an interesting exchange narrowing for the complexes that contain a long fluorinated alkyl chain. This exchange narrowing is induced by the fluorine specific interactions of the chains. With the addition of perfluorooctanol, the exchange narrowing was inhibited, which led to resolved hyperfine splitting (Figure 45). Moreover, four mixed ruthenium(II) complexes containing a tpy and a mesoionic carbene moiety were synthesized and the possible application in electrocatalytic CO_2 reduction with TFE as proton source was investigated. A high selectivity towards the formation of CO is found. The best case exhibits a turnover frequency of 14.07 s^{-1} and a faradaic efficiency of

92%. Furthermore, the impact of the electronic effects of the ligand on the onset potential and catalytic efficiency is demonstrated. Further studies will focus on the combination of different MIC ligands with tpy, to achieve a better understanding of the potential progress in catalytic activity.

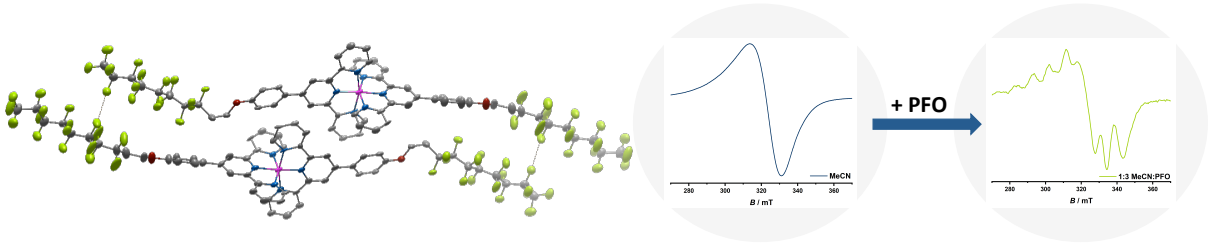

Figure 45: Tpy-based metal complexes used in this thesis.

In the last part, a series of novel platinum(II)-based donor acceptor systems has been prepared. For this purpose, various substituted azobenzene stoppers and two different quinone bridging ligands have been used (Figure 46). First, the influence of alkyl chains on azobenzene was investigated towards their possible application as LC material and later, perfluorinated alkyl chains were introduced on the azobenzene moieties. Almost none of the azobenzene ligands or the complexes show LC behavior. Even the introduction of a higher number of long alkyl chains on the azobenzene moiety does not lead to such behavior, therefore, further studies may be targeted to obtain LC behavior by, e.g., the introduction of long alkyl chains on the bridging ligands. The electrochemical studies showed that the substitution on the azobenzene has only a marginal influence on the redox potentials, which are mostly dependent on the used solvent. During UV/Vis/NIR spectroelectrochemical measurements, the observed bands of the complexes are similar to each other, but in comparison to the known complex with unsubstituted azobenzene, a loss in the extinction coefficient was observed. In EPR spectroelectrochemistry studies only the first reduction could be investigated, where a ligand-centered spin is observed.

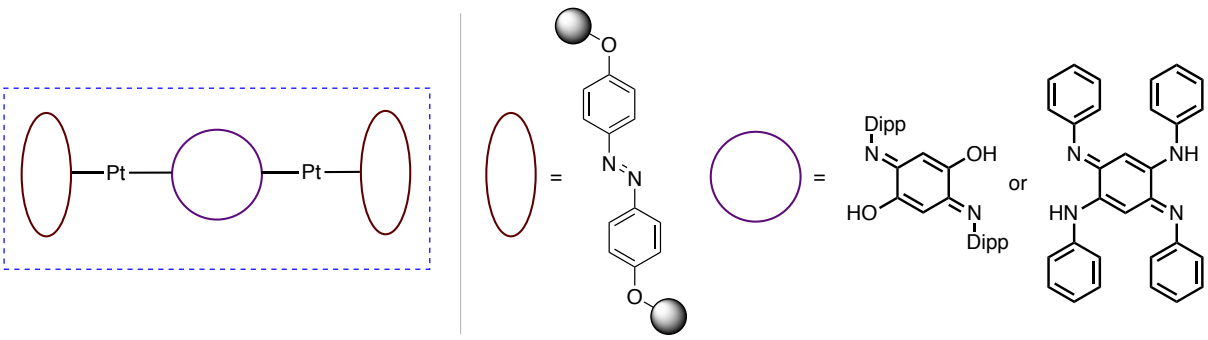

Figure 46: Schematic presentation of the building blocks for platinum(II)-based azobenzene complexes, bridged over a quinone ligand.

In conclusion, the presented thesis highlights the effect of the introduction of fluorine on different ligand systems used in coordination chemistry. A strong focus was put on the investigation of fluorine specific interactions in the secondary coordination sphere, to gain further insights into the design of suitable tripodal ligand systems and their NCIs that affect the spin state of the metal centers. Additionally, fluorination of tpy ligand backbones has a strong influence on the magnetic properties and leads to highly stable materials that do not exhibit LC behavior. Furthermore, fluorine specific interactions could be confirmed by EPR spectroscopy. Lastly, the introduction of long (perfluorinated) alkyl chains on azobenzene showed the influence on optical properties of the corresponding dinuclear platinum(II) complexes bearing quinone bridging ligands.

An overview over the prepared complexes and their most interesting properties is given in figure 47.

Taking all the data into account, this thesis can help to understand the fundamentals of fluorine specific interactions between tripodal ligand systems in the secondary coordination sphere. This should increase the understanding how to directly design complexes that exhibit SCO behavior. Moreover, the results contribute to provide the optimization of future target compounds suitable for redox-active LC material.

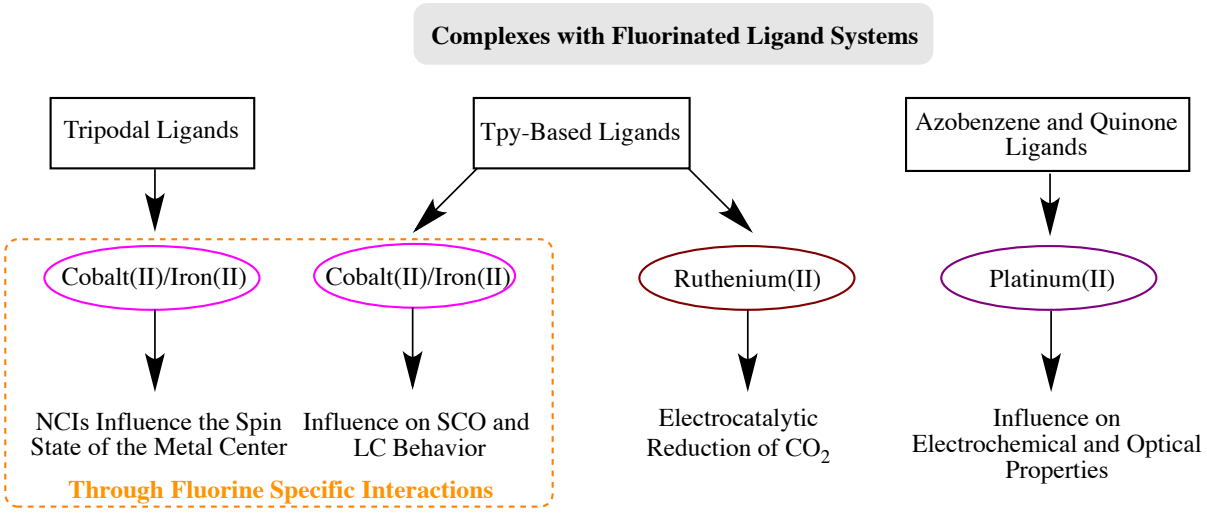

Figure 47: Summary of the presented metal complexes and their main results.